APPLICATION OF THE FMCW METHOD TO QUASI-DISTRIBUTED ABSORPTION SENSORS

A thesis submitted to the Department of Electrical and Electronic Engineering of Strathclyde University for the degree of Doctor of Philosophy by

MIHA ZAVRŠNIK

Optoelectronics Division

Department of Electronic and Electrical Engineering

Royal College Building

204 George Street

G1 1XW Glasgow

Scotland

UK

March 2000

Declaration

The copyright of this thesis belongs to the author under the terms of the United Kingdom Copyright Acts as qualified by the University of Strathclyde Regulation 3.49. Due acknowledgement must always be made of the use of any material contained in, or derived from, this thesis.

Acknowledgements

First I would like to sincerely thank my supervisors Dr. George Stewart and Prof. Brian Culshaw for their understanding, help and encouragement. Thanks to Prof. Brian Culshaw for making the study possible and for fighting with the bureaucracy.

Very special thank to Dr. George Stewart for his unlimited support and guidance. Thanks for numerous e-mails, faxes, helpful discussions and motivation during the difficult periods of the study. I very much appreciate all visits to Slovenia and the special time during the visits.

Finally, thanks to my co-workers in the Laboratory for Electro-Optics and Sensor Systems at the University of Maribor in Slovenia for their friendship and help.

Abstract

We report on different addressing mechanisms for quasi-distributed absorption sensors based on the frequency modulated continuous wave (FMCW) method. The sensor units consist of open-path micro-optic cells constructed from GRIN lenses, each of differing lengths.

Guided by initial simulations, two approaches are experimentally investigated and evaluated, namely reference arm addressing and coherence addressing. Reference arm addressing is accomplished by the selection of different length reference arms in a Michelson configuration where each reference arm corresponds to a certain sensing unit. Coherence addressing is achieved by the interferometric mixing of two signals originating from each cell (from the glass/air interfaces). For each method, we show theoretically and experimentally how individual cells can be addressed and the measured signals obtained by suitable choice of cell length, proper modulation of the source and appropriate signal processing.

In order to improve sensitivity we present the theoretical analysis of a new scheme based on combining the (FMCW) technique with frequency modulation spectroscopy (FMS). Here we arrange for only one sideband of the rf-modulation

to be attenuated by the absorption feature and a new signal, proportional to the absorbance, appears in the output spectrum at a frequency corresponding to the difference between the rf-modulation frequency and the beat frequency of a cell. The method is highly sensitive and applicable to a variety of chemical species with narrow absorption lines, such as in trace gas analysis. We present the mathematical analysis of the proposed method for single and multiple cell systems, using methane detection as an example.

Table of content

1. Introduction

Modern technologies are becoming more and more important for chemical and environmental sensing, efficient pollution prevention and cost effective industrial process control. The field of fibre optic sensors has expanded rapidly in the last decade. During this period optical fibre based sensors have been developed for measurement of a variety of physical and chemical parameters including temperature, pressure, flow, strain, position, thickness, rotation rate, humidity, pH, particle size, chemical reaction rates, fluorescence, chemical concentrations and characterisation of chemical species present in mixtures.

Fibre optic sensors offer unique capabilities when configured in a distributed nature or arranged in a multiplexing network. Distributed or multiplexed systems allow sensing at a large number of points by combining fibre-sensing methodologies with fibre telemetry. Applications of the technology include civil structural monitoring (smart structures), military systems (underwater acoustic arrays), industrial applications (process control sensor networks), chemical sensing and security monitoring, to mention just the most important fields.

In each of these areas, the ability to implement multiple sensors in passive networks can be advantageous with regard to a number of system aspects, including reduced component cost and low intrinsic susceptibility to the effect of electromagnetic interference.

In general multisensor systems can be formed in a number of ways. First a number of discrete sensors designed to operate as a point sensor can be arranged in a network or array configuration. Alternatively the inherent distributed sensing nature of intrinsic fibre optic sensors can be used to create unique forms of sensors for which in general there may be no counterpart based on conventional sensor technology.

For a *quasi-distributed sensor configuration*, the measurand is not monitored continuously along the fibre path, but at a finite number of locations. This is accomplished either by sensitising the fibre locally to a particular field of interest or by using extrinsic bulk sensing elements. Application areas for this form of sensors include those previously mentioned and various multimeasurand or/and multipoint applications such as those found in chemical industries.

In this work "*Application of the FMCW method to quasi-distributed absorption sensors*", different methods of addressing quasi-distributed sensor units, consisting of open-path micro-optic cells constructed from GRIN lenses will be discussed and evaluated. We will propose and evaluate new addressing methods for quasi-distributed absorption based fibre optic chemical sensors. Since the primary emphasis in designing a sensor array is the method of separating individual sensor signals, a combination of coherence addressing and the frequency modulated continuous wave method (FMCW) to distinguish between different sensing units arranged in series will be presented. In order to find the most appropriate scheme five different addressing mechanisms will be introduced and evaluated:

- Coherent FMCW with reference arm addressing
- FMCW with coherence addressing
- Forward FMCW
- FMCW White light reference arm addressing
- FMCW White light coherence addressing

For all the proposed addressing mechanisms a theoretical model will be determined and extensive simulations will be presented.

According to the simulation experiments two basic approaches called "*reference arm addressing*" and "*coherence addressing*" will be evaluated. For both addressing schemes we show theoretically and experimentally how individual cells can be addressed and the measured signals obtained by suitable choice of cell length, proper modulation of the source and appropriate signal processing.

For experimental evaluation an optical test system including a DFB source, three microoptic sensing cells and the corresponding driving and detecting units including a spectrum analyser has been constructed. In the final stage a micro-controller signal processing, driving and calibration system is implemented. Using a small graphics LCD display, with a 4-key keypad and menu driven commands, a simple and effective user interface is introduced.

Finally we report the theoretical analysis of a quasi-distributed sensor system for absorption measurements based on the frequency-modulated continuous wave (FMCW) technique combined with frequency modulation spectroscopy (FMS). The laser diode injection current is sawtooth modulated to provide a linear scan of the output over a certain frequency/wavelength range and the output is also externally modulated at radio frequencies. By arranging for only one sideband of the modulation to be attenuated by the absorption feature, a new signal, proportional to the absorbance, appears in the output spectrum at a frequency corresponding to the difference between the rf-modulation frequency and the beat frequency of a cell. The method is highly sensitive and applicable to a variety of

chemical species with narrow absorption lines, such as in trace gas analysis. We present the mathematical analysis of the proposed method for single and multiple cell systems, using methane detection as an example.

2. Overview of Chemical and Environmental sensing

Optical fibres have revolutionised a variety of fields. They carry images through endoscopes, voices through telephone lines, data and video through cable networks and, more recently physical and chemical information through sensors.

The field of fibre optic sensors has expanded rapidly in the last decade. Optical fibre based sensors have been developed for the measurement of a variety of physical and chemical parameters.

The detection of chemical analytes and gases in real time is very difficult to perform. However, its importance in industrial process control, industrial safety and environmental protection has necessitated the development of robust, inexpensive chemical sensor systems capable of remote deployment. Ideally these systems should be capable of making distributed measurements of any given analyte or gas which may be mapped over a domain extending from meters to kilo-meters, depending on the application. An ideal chemical sensor should fulfil the following requirements:

- small enough and able to monitor at several locations
- remote placement possible
- cheap to produce and maintain
- enable real time monitoring for immediate results
- accurate

One of the possible and very promising technologies which would provide a solution to this problem is the use of optical fibre techniques [2.1], [2.2], [2.3].

Fibre optic sensors represent a technology base that can be applied to a multitude of sensing applications. The following are some characteristic advantages of fibre optics that make their use especially attractive for chemical sensors:

- **nonelectrical** - fibre optic chemical sensors are much safer in explosive environments compared with traditional sensors involving electrical signals where a spark may trigger a gas explosion - **explosion proof**
- **measurements without direct contact possible**
- **remote location of sensor head** - optical fibres can transmit light over large distances with low loss allowing a sensor to be placed remotely
- **small size and weight** - allows access to areas that would otherwise be difficult to reach
- **potentially easy to install**
- **immune to** radio frequency interference (**RFI**) and electromagnetic interference (**EMI**)
- **high accuracy**
- **can be interfaced with data communication systems**
- **secure data transmission**
- **potentially resistant to ionising radiation**

However fibre optic sensors have also some disadvantages. They are often sensitive to parameters other then the desired measurand (e.g. temperature sensitive, or vibration sensitive). This requires special referencing or isolation from disturbances. When chemical sensors are considered, possible cross-sensitivity to other chemical analytes and gases must be taken into account.

2.1. Basic physical principles of fibre optic chemical sensors

Some of the basic physical principles which will be discussed in the next sections are already known from other scientific disciplines and have been used for sensing purposes before even fibre optics were introduced. The fibre optic chemical sensor of today is therefore a synthesis of well known principles and optical fibres or other optic assembles. Together they form a unique system fulfilling most of the requirements for an ideal chemical sensor, as presented in the preceding section.

2.1.1. Absorption sensors

Absorption is the process whereby the intensity of a beam of electromagnetic radiation is attenuated in passing through a medium by conversion of the energy of the radiation to an equivalent amount of energy which appears within the medium; the radiant energy is converted into heat or some other form of molecular energy. In general the absorption of electromagnetic radiation by a medium is defined as:

$$E_2 - E_1 = \frac{hc}{\lambda} = hf \tag{2.1}$$

where E_2-E_1 is the difference in energy levels of a molecular transition, hf is the photon energy required to induce the transition, h is the Planck's constant

($6.62 \cdot 10^{-34}$ Js), c free space speed of light and λ the wavelength at which the absorption takes place.

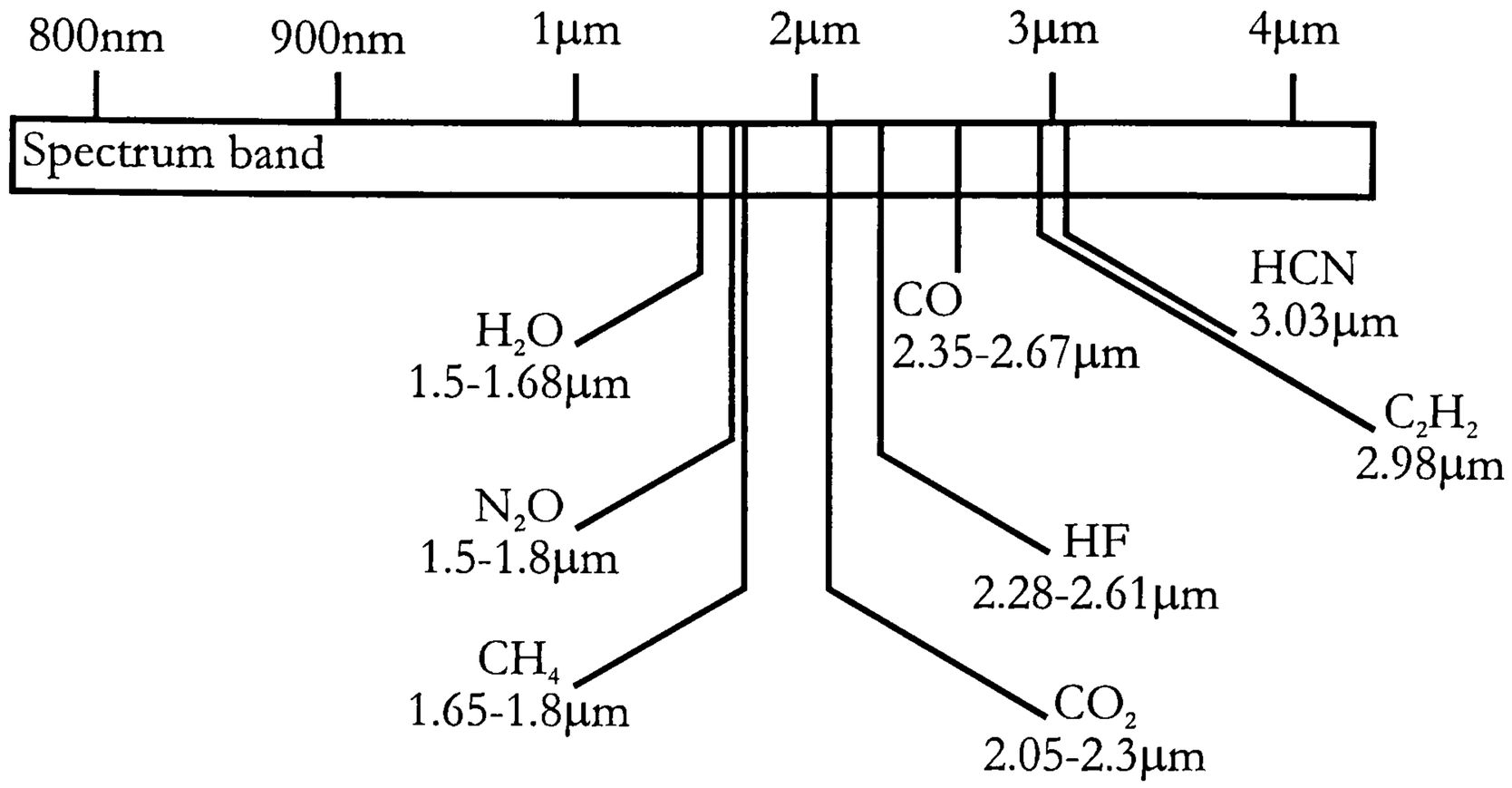

Figure 2.1: *Absorption lines*

A medium which absorbs a relatively wide range of wavelengths is said to exhibit general absorption, while a medium which absorbs only restricted wavelength regions of no great range exhibits selective absorption for those particular spectral regions. With selective absorption, the absorption spectrum serves as a "fingerprint" identification of the medium. The actual wavelength at which absorption takes place depends on the transition involved. Electron transitions within atoms occur at short wavelengths (high photon energy) corresponding to the UV-visible region of the spectrum, whereas transitions in vibrational or rotational levels (molecules) occur at energies corresponding to the near and mid-infrared band of the spectrum [2.14]. Figure 2.1 illustrates absorption lines of some common gases in the near-IR.

The effect of concentration of the absorbing medium, that is, the mass of absorbing material per unit of volume is expressed through the Beer-Lambert law. This relation is of prime importance in describing the absorption of an absorbing species, since the solute's concentration may be varied over wide limits, or the absorption of gases, the concentration of which depends on the pressure.

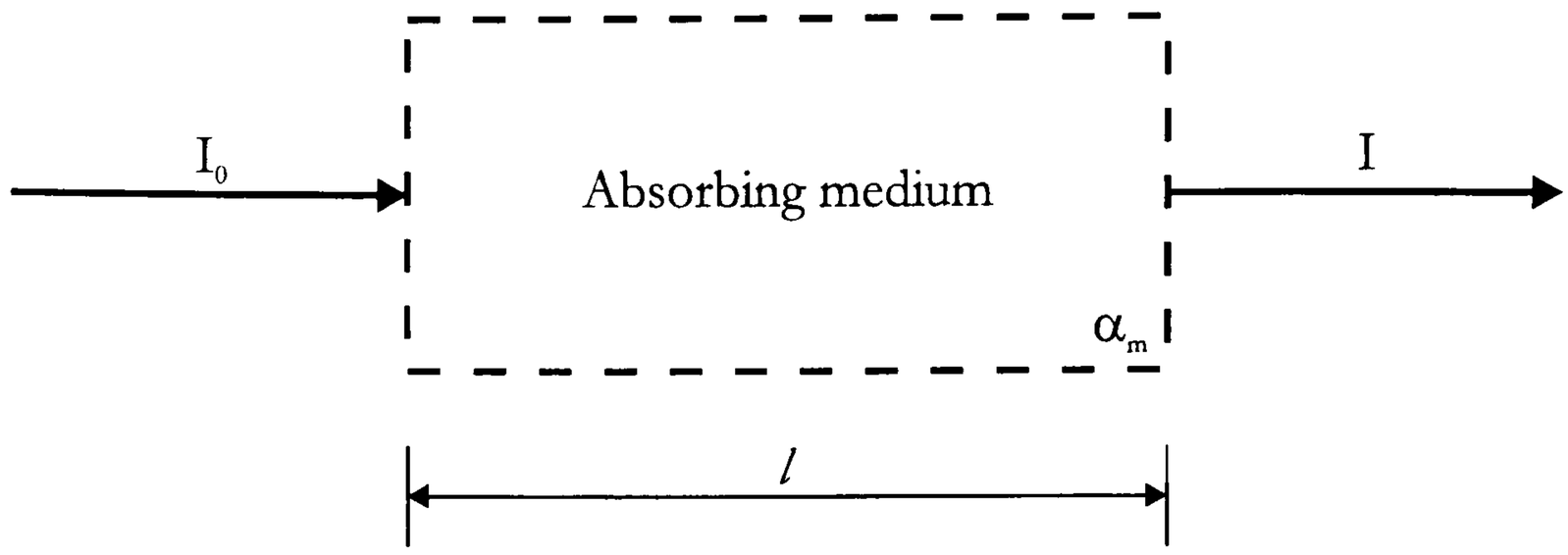

Figure 2.2: *For monocromatic radiation, absorbance is directly proportional to the path length through the medium and the concentration of the absorbing species*

According to the Beer-Lambert law, each individual molecule of the absorbing material absorbs the same fraction of the radiation incident upon it, no matter whether the molecules are closely packed in a concentrated solution or highly dispersed in a dilute solution. If I is the intensity to which a monochromatic parallel beam is attenuated after traversing a thickness l of the medium, and I_0 is the initial intensity (Figure 2.2), then [2.4]:

$$I = I_0 e^{-\alpha_m lC} \tag{2.2}$$

where α_m is the (molar) absorption coefficient and C is the chemical concentration. In logarithms the relation becomes

$$\log_{10}\left(\frac{I_0}{I}\right) = \left(\frac{\alpha_m}{2.303}\right)Cl = \varepsilon Cl \tag{2.3}$$

If the concentration is expressed in moles per litre, the constant ε is called the molar extinction coefficient. The quantity $log_{10}(I_0/I)$ is often called the optical density or the *absorbance* of the medium. The spectral absorption $A(\lambda)$ and the spectral transmission $T(\lambda)$ at a given wavelength are defines as follows:

$$A(\lambda) = \frac{I_0(\lambda) - I(\lambda)}{I_0(\lambda)} \tag{2.4}$$

$$T(\lambda) = \frac{I(\lambda)}{I_0(\lambda)}$$

and characterise the fraction of monochromatic radiation absorbed by a given medium.

2.1.1.1.Potential for gas monitoring

The first recognition of the potential for fibre optic remote gas sensing was reported 1979. A research group at Tohoku University, Japan, pointed out the large number of spectral absorption lines, which lie within the transmission window of a typical silica based optical fibre.

The intrinsic absorption of many gases can be measured directly with optical fibers serving as simple light guides. In particular, alkanes such as **methane** are important to monitor because of their safety risk [2.7], [2.8].

Methane is an all too common greenhouse gas, found where natural gas is present and occurs naturally around plant matter where anaerobic decomposition is taking place, such as in landfills and farms. Concentrations of 5 to 15 percent by volume can explode when ignited, where first concentration presents the lower explosion level (LEL) and the second concentration the upper explosion level (UEL). The LEL and UEL for some hydrocarbon gases are given in Table 2.1 [2.9].

Table 2.1: *Lower explosion and upper explosion limit of some Hydrocarbon Gases*

Gas	LEL (% by volume)	UEL (% by volume)	λ (nm)
Acetylene	2.50	80.00	1520
Ethane	3.00	12.5	1685
Ethylene	2.75	28.60	1619
Methane	5.00	15.00	1666
Propane	2.12	9.35	1696

A beneficiary of explosive gas-related fibre optic sensor technology is the petrochemical industry. Natural gas pipe lines emit methane and other "fugitive" hydrocarbons from petroleum distillates. Refineries rely on chemical or spectroscopic methods to measure these hydrocarbons, but the price for such equipment is very high and it is susceptible to degradation and breakdown.

Fibre optic is the only technology that offers onsite real-time measurements of contaminants and is mass-producible, which lowers the cost per sensor.

The first experiments demonstrated the remote determination of CH_4 and other alkanes with silica optical fibre links. The absorption lines in the NIR are weaker than at longer wavelengths (mid IR), hence the detection limits obtained are around 2000ppm (about 4% of the LEL) at 1330nm and 400ppm at 1666nm and 300ppm at 3390nm [2.9], [2.10].

To get a good "feel" for the chemical the source linewidth must be narrower than the absorption line. The smaller the ratio between laser linewidth and chemical absorption linewidth, the better the chance for identification [2.14]. A 1500nm laser beam has an optical frequency of 187.5 THz. A pressure broadened gas absorption line has a linewidth of a few GHz. The upshot of these numbers is that to detect gas molecules, the frequency of a laser must be controlled to within aproximatelly one part in a milion. Pollutants absorb strongly in the IR and UV. Because the semiconductor technology has yet to make serious inroads into the

UV, most diode-laser based gas sensing systems use telecommunication-grade diode lasers as the radiation source (mostly DFB laser diodes are used) [2.14], [2.15].

Distributed-feedback telecommunication lasers have several characteristics important to both open-path and flow-cell gas detection, including single mode continuous wave >100mW operation at room temperature. These power levels are more than sufficient for gas sensing. Although open-path systems lose a considerable amount of power, typical detectors and other receivers easily detect nano and picowatt optical signals.

Single frequency distributed feedback laser diodes have a very narrow linewidth (50MHz → 0.000375nm for 1500nm wavelength), less than the width of a single gas absorption line, wavelength modulation through injection-current modulation and thermal tuning of wavelength (by a TEC). However, injection current modulation also produces amplitude modulation in the output.

2.1.2. Sensing through indicator dyes

Sometimes the chemical properties of a solute may not be measured directly through absorption spectroscopy. The light sources may not be available or are to expensive for that particular wavelength of interest. In this cases an intermediate material or indicator is used.

Indicators are synthetic dyes that undergo colour changes on interaction with chemical species. The purpose of using so-called indicator chemistry (a dye in or on a polymeric support) in optical sensing is to relate the concentration of a chemical analyte into a measurable optical signal. The indicator acts as a transducer for chemical species that frequently can not be determined directly by optical means. On exposure to the chemical of interest the optical properties of the dye change through a chemical reaction and the optical change is monitored in the sensor.

The indicator is immobilised at the tip of either a bifurcated fibre-optic bundle or a single optical fibre. A bifurcated bundle of optical fibres can be used where the

indicator chemistry is immobilised as a layer at the tip of the common end. Large bundles of fibre are used to bring light to this sensing region and to carry the light to the detector optics. The size of this bundle represents both the major attraction and the primary limitation of this approach. The large bundle size of the fibre optic probe is easy to interface with the source and detector optics. High optical throughput can be achieved easily because of the large number of fibres involved. Higher optical throughput translates directly to greater signal to noise ratios, thereby providing superior analytical signals. However a typical bifurcated probe is several millimetres in diameter, which results in a relatively large sensing tip that is to big for certain applications. Alternatively we can use single optical fibres where the indicator chemistry is immobilised at the distal tip of the single fibre. Small sensors can be constructed in this manner. The principal drawback to this approach are the limited optical throughput and the low reagent loading capacity, since a single fibre offers a limited surface area to which the indicator can be attached.

2.1.3. Fluorescence sensors

Fluorescence is the phenomenon of light emission from a material which is excited by some form of electromagnetic radiation incident in the ultraviolet, visible, or infrared regions of the spectrum. Such emission is the release of the energy gained from the absorption of the incident photon energy. Normally the excitation spectrum is of a higher photon energy (and thus shorter wavelength) than that of the corresponding fluorescence.

Measurement of fluorescence is an extremely sensitive technique capable of detecting very low analyte concentrations. It is well suited for optical sensing, since the optical fibre can carry both the exciting and fluorescent light. The wavelength of the emitted luminescence is different from that of the exciting radiation.

The initial persistence of fluorescent emission following the removal of excitation depends on the lifetime of the excited state. The emission usually decays in a

manner that can be categorised by a time constant often termed the fluorescence decay time. Fibre optic sensors based on fluorescence make use of changes in either the intensity or lifetime of the fluorescence emission to monitor the chemical parameter of interest.

A method of assessing the degree of luminescence is to use a pulsed source and to look at the changes in the lifetime as a function of chemical concentration (Figure 2.3). When the concentration is zero this gives the simple exponential decay of the luminescence species with its characteristic lifetime. For other concentrations the luminescence half-life of the luminescent species is reduced.

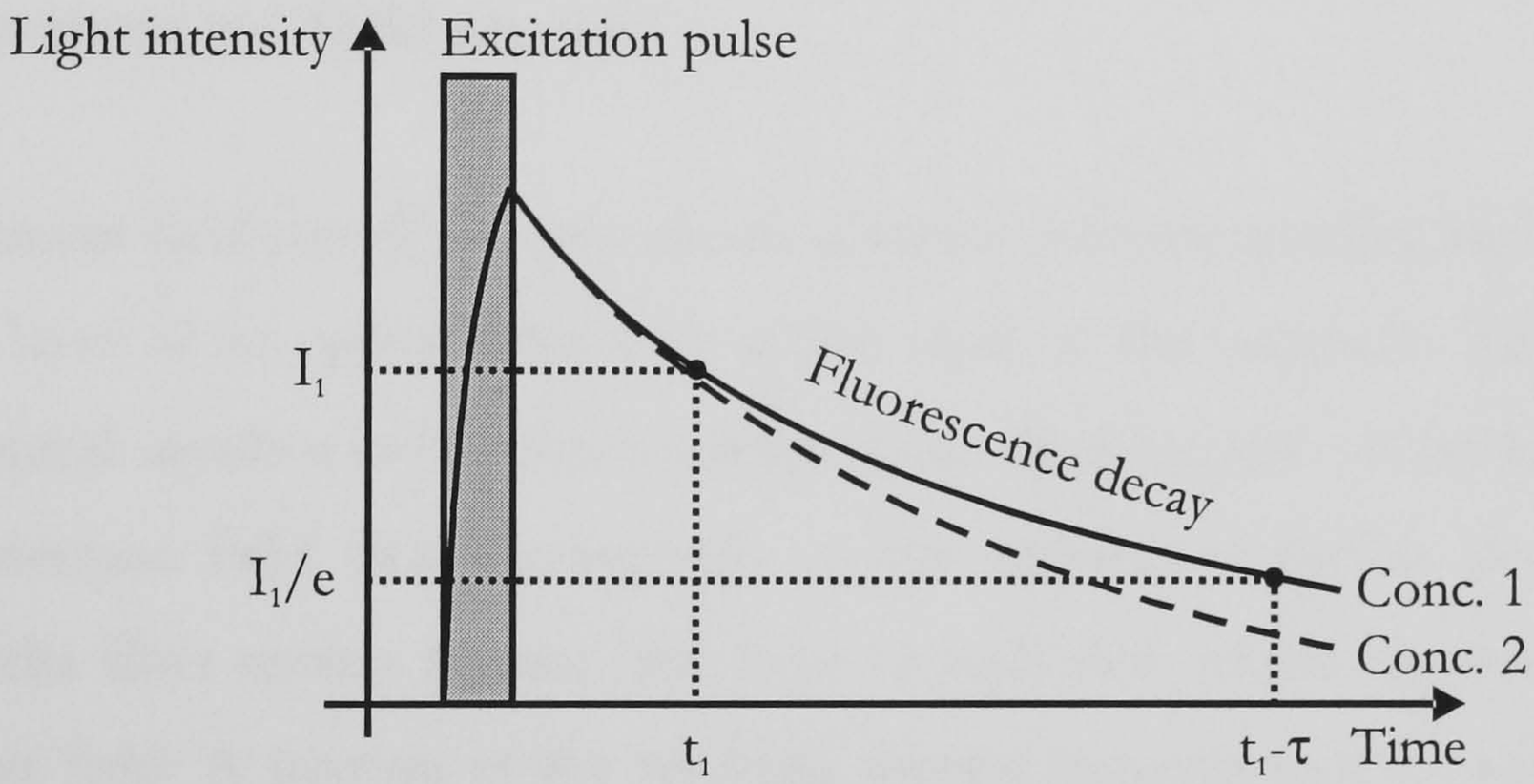

Figure 2.3: *Temporal decay of the intensity for fluorescence based chemical sensors*

This technique involves comparing the luminescence intensity at various times following excitation. Consequently, it is self-referencing, and compensates for factors like efficiency of the source, detector or electronics, which gives the technique a large advantage over simple intensity measurements. However it does require an increased capital cost for the controller electronics.

Another method for fluorescence lifetime measurement is to use a sinusoidally modulated excitation light. As shown in Figure 2.4, the phase shift which is related to the lifetime is measured relative to the excitation.

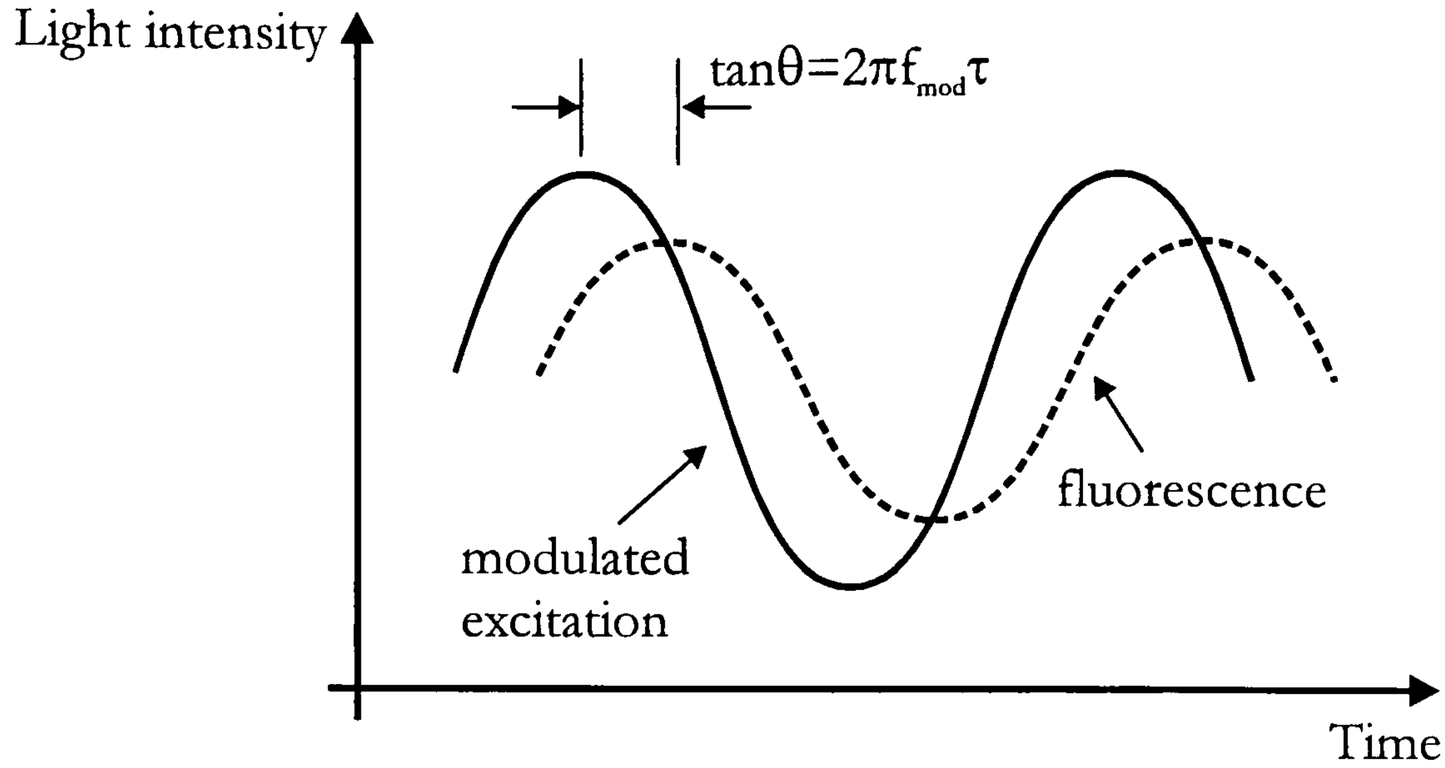

Figure 2.4: *Phase shift method for fluorescence lifetime measurement*

2.1.4. Evanescent field sensors

An evanescent field-type fibre optic chemical sensor is constructed by replacing the cladding layer of an optical fibre with a thin layer of the indicator. The sensing region typical involves only a short section of the fibre (typical ~10cm in length). The evanescent field that corresponds to the incident radiation propagating through the fibre excites reagent molecules immobilised within the zone of the evanescent field. A portion of the resulting reagent luminescence is coupled into the fibre through the same mechanism that generated the original evanescent wave [2.8], [2.11], [2.12].

One possible sensor configurations is that the incident radiation is launched into one end of the fibre, and then passes the evanescent filed sensing section of the fibre and interacts with the substance of interest. At the other end of the fibre the radiation attenuation or reagent luminescence properties are monitored.

The basic advantages of evanescent filed sensors are fast response and the possibility for distributed sensing, whereas the disadvantage is low sensitivity due to small fraction of power in the evanescent field and surface contamination during the sensing process.

2.2. Chemical sensors construction types

Fibre optic chemical sensors can be divided into two major categories (in the same manner as those for measuring physical parameters), i.e.

- **intrinsic sensors** - where the fibre, often in some modified form, is the sensing transducer
- **extrinsic sensors** - where the optical fibre merely acts as a light guiding link between the measuring point and the interrogation and display system;

For intrinsic fibre optic chemical sensors the basic methods involve fibre optrodes (or optodes) where the sensing medium is formed directly on the fibre tip. Fibre optrodes are particularly suitable for sensors based on indicator dye absorption or fluorescence. The second group of intrinsic sensors includes evanescent wave sensors. In this case the fibre is directly involved in the sensing process. For evanescent field sensors it is usually necessary to immobilise the indicator in a suitable host matrix that is then coated onto the exposed evanescent region of the fibre [2.4].

With extrinsic fibre optic chemical sensors the light is transferred to and from the sensing cell. The fibre provides access to the cell but has no influence on the sensing process. There are a variety of possible construction types for fibre optic sensing cells. For the work presented, absorption cells constructed with the use of GRIN lens have been implemented, therefore a short description of GRIN lens cells will be given in the next section.

2.2.1. Chemical sensors using gradient index lens

Within the communication area, most optical devices for manipulating and processing optical signals in optical fibre transmission systems include lenses, and for most of these devices GRIN lenses have a number of advantages over

conventional lenses, such as small size, light weight, low cost, short focal distance, easy mounting and adjustment etc. A GRIN lens can carry out typical functions such as on-axis imaging, collimating and focusing.

GRIN lenses are also important for fibre optic sensors. Using GRIN lenses, a variety of intensity modulated fibre optic sensors can be constructed. The basic set-up including GRIN lenses which is applicable for absorption type chemical sensors is presented in Figure 2.5.

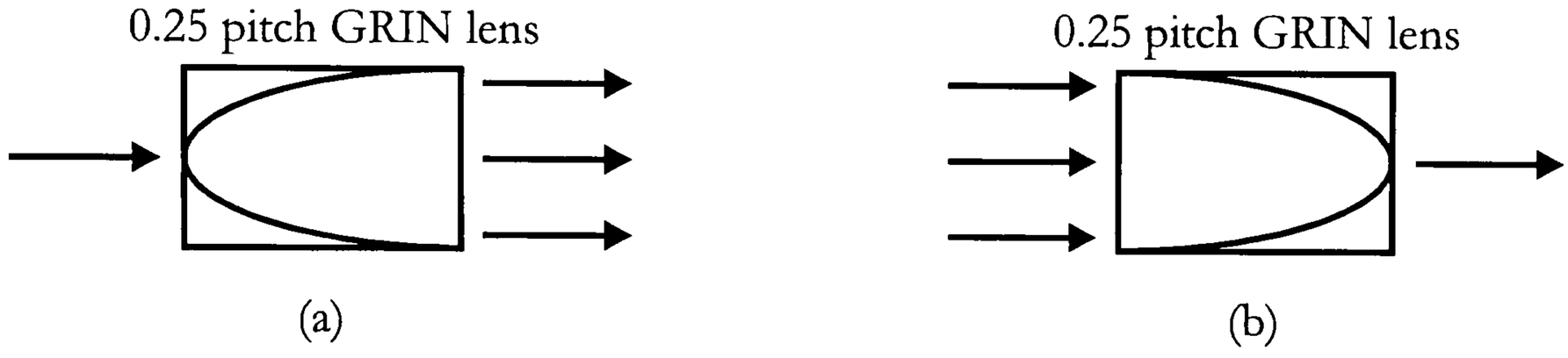

Figure 2.5: *A quarter-pitch lens (a) collimates or (b) focuses incoming light*

Using the quarter-pitch lens the output from a small light source such as diode laser, LED or a single mode optical fibre can be collimated and focused on another optical fibre or detector [2.9], [2.13].

A sensing cell can be constructed if two optical fibres are maintained at fixed position to each other, each adjacent to a quarter-pitch selfoc rod lens. For gas sensors, where gas concentration is measured through absorption in the near-IR, a lens is used to collimate the output light from the fibre end, and then after passage through the cell, a second lens focuses the light into the output fibre. The cell may typically be 1-50cm in length and is designed to allow the gas to penetrate into the cell volume (Figure 2.6) [2.4], [2.5], [2.6].

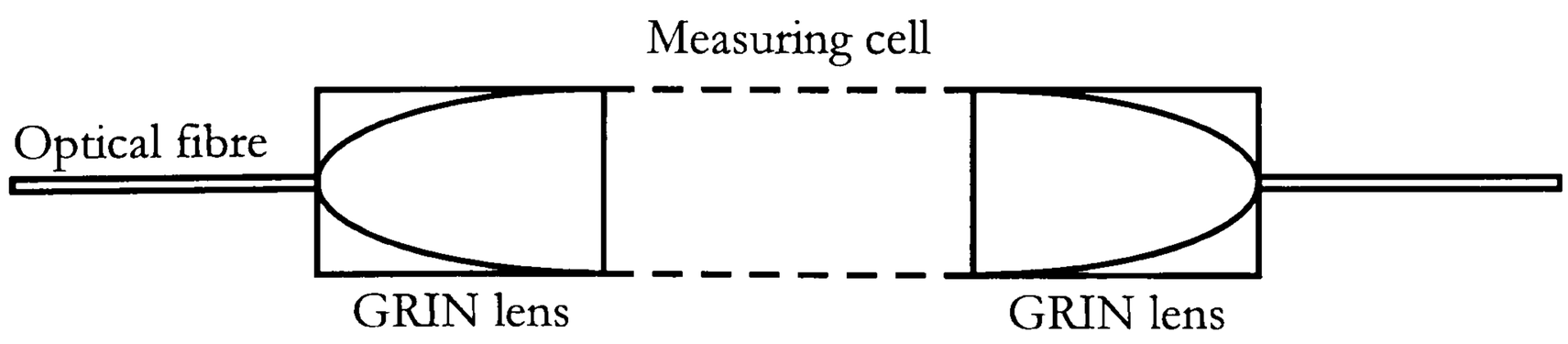

Figure 2.6: *Absorption cell using GRIN lenses*

The most attractive advantage of using GRIN rod lenses in a modulated intensity sensor is that they can be used for increasing sensor sensitivity by improving the coupling efficiency, reducing misalignments and therefore producing a stable sensing structure.

The chemical sensors constructed using GRIN lenses are especially suitable for gas monitoring applications. Since the gas can penetrate between the lenses (also if we use gas permeable walls to protect the cell from other environmental influences, but allow the gas to enter the cell) no special care has to be taken to ensure a good contact between the measurement unit and the measured analyte. Additionally we prefer to use the GRIN lenses, due to the reflectivity of the flat surface. The sensing cells which will be used in the work presented all base upon the structure shown in Figure 2.6 with some minor modifications.

2.3. Summary and Conclusion

One may find out that fibre optic chemical sensor inherently fulfil many of the demanding requirements (small size, remote displacement, ...). The absorption type of fibre optic sensor which will be used in this thesis represents one of the basis sensing principles for chemical detection. Using the measurand property (i.e. any gas or gas mixture of interest) to absorb light at restricted wavelength, differential absorption is used to detect concentration changes based on the Beer-Lambert law. Since the line-width of the source used must be narrower than the absorption line a distributed-feedback laser diode will be used as the light source. Because of relatively high single mode continuous wave power output and good coherence properties combined with injection current modulation possibilities it is the source of choice.

Even if intrinsic type of sensors (like evanescent sensors) with proper indicator coatings enable fast responses and possible distributed measurement, they are usually less sensitive due to small power in the evanescent field and the requirements for regular cleaning of the large evanescent filed region. The additional disadvantage of evanescent filed sensors is their manufacturing, since

chemical etching or polishing of the fibre and coating of the evanescent field region is necessary.

With extrinsic open path chemical sensors we have higher sensitivity due to more optical power inside the measuring cell and the construction using GRIN lenses is much more simple and reproducible. The main difficult here lies in the assembling precision, since alignment of measuring unit parts is critical.

Comparing the sensor type properties, especially with the emphasis on distributed or quasi distributed configurations we have decided to use an open path extrinsic type sensing cell constructed using GRIN lenses. This type of sensing cell is relatively easy to assemble and additionally offers opto/mechanical properties necessary for quasi distributed sensing unit addressing.

References

[2.1] M. Campbell, Y. Yang, P.A. Wallace, A.S. Holmes-Smith, "A Multipoint Quasi-Distributed Optical Fiber pH Sensor", Optical Review, Vol. 4, No. 1A, pp. 111-113, 1997

[2.2] J.A. Ferguson, D.R. Walt, "Optical fibers make sense of chemicals", Photonics Spectra, pp. 108-114, March 1997

[2.3] R.W. Hardin, "Eco-Optics: Remote Sensing Keeps Industry Clean", Photonics Spectra, pp. 102-109, April 1998

[2.4] G. Stewart, "Fibre optic sensors", Sensor Systems for Environmental Monitoring, Volume One: Sensor Technologies, Blackie Academic & Professional, 1997

[2.5] G. Stewart, A. Mencaglia, W. Philip, W. Jin, "Interferometric Signals in Fiber Optic Methane Sensors with Wavelength Modulation of the DF Laser Source", Journal of Lightwave technology, Vol. 16, No. 1, January 1998

[2.6] G. Stewart, "Fibre Optic Methane Sensor", Invited lecture at the University of Maribor, Faculty of Electrical Engineering and Computer Sciences, October 1997

[2.7] N. Yamazoe, N. Miurata, "Environmental gas sensing", Sensors and Actuators B, Vol. 20, pp. 95-102, 1994

[2.8] G. Dotzlaw, "Fiber Optic Chemical Sensors Monitor Bilge-Water Toxins", Photonics Spectra, pp. 20-21, April 1996

[2.9] G. Boisde, A. Harmer, "Chemical and Biochemical Sensing with Optical Fibers and Waveguides", Artech House, London 1996

[2.10] E.J. Lerner, "Fiberoptic sensors monitor environmental conditions", Laser Focus World, pp. 107-111, September 1997

[2.11] V. Ruddy, J. Maguire, "Chemical detection using pulse narrowing in evanescent wave sensors", Sensors and Actuators A, Vol. 41-42, pp. 525-528, 1994

[2.12] G. Stewart, W. Jin, B. Culshaw, "Prospects for fibre-optic evanescent-field gas sensors using absorption in the near infra red", Sensors and Actuators, No. B 38-39, pp. 42-47, 1997

[2.13] D. A. Landis, C. J. Seliskar, W. R. Heineman, "Fiber-optic-graded-index-lens absorbance sensor with wavelength-scanning capability", Applied Optics, Vol. 33, No. 16, pp. 3432-3439, June 1994

[2.14] R.W. Hardin, "Diode Lasers Pinpoint Pollutants", Photonics Spectra, pp. 110-114, April 1998

[2.15] K.G. Tatterson, "Pullutants Can't Hide from Fiber Optic Sensors", Photonics Spectra, pp. 116-118, April 1998

3. Distributed and Multiplexed Fibre Optic Sensors

The unique capabilities of fibre optic sensors when configured in distributed or quasi-distributed nature and multiplexed networks, make them very attractive for any modern sensor system. Such systems allow sensing at a large number of points by combining fibre-sensing methodologies with fibre telemetry. In the last 10 to 20 years fibre optic sensor technology has made a considerable impact in various fields including civil structural monitoring (smart structures), military systems (underwater acoustic arrays), industrial applications (process control sensor networks), chemical sensing, security monitoring, etc.

In each of these areas, the ability to multiplex sensors in passive networks can be advantageous with regard to a number of system aspects, including reduced component cost and low intrinsic susceptibility to the effect of electromagnetic interference [3.1].

In general multisensor systems can be formed in a number of ways [3.2]. First a number of discrete sensors designed to operate as a point sensor can be arranged in a network or array configuration. Alternatively the inherent distributed sensing nature of intrinsic fibre optic sensors can be used to create unique forms of sensors for which in general there may be no counterpart based on conventional sensor technology.

Intrinsic distributed sensors are particular attractive for use in applications where monitoring of a single measurand at a large number of points or continuously over the path of the fibre is required [3.2].

For extrinsic distributed sensors the number of measuring points is usually smaller. They are especially important for sensing applications where absorption or spectrographic measurements are included.

In a quasi-distributed sensor configuration, the measurand is not monitored continuously along the fibre path, but at a finite number of locations [3.1]. This is accomplished either by sensitising the fibre locally to a particular field of interest or by using extrinsic bulk sensing elements. Application areas for this form of sensor include various multimeasurand or/and multipoint applications such as those found in chemical industries.

3.1. Basic concepts of distributed and multiplexed sensors

A range of techniques for distributed and multiplexed fibre sensors have been developed, ranging from simple serial arrays of sensors based on optical time domain reflectometry (OTDR) processing concepts, to highly sophisticated interferometric fibre sensors using time or frequency-division concepts. In the

following sections a brief presentation of basic concepts of distributed and multiplexed sensors will be given, trying to highlight the advantages, disadvantages and possible area of application for each method presented.

3.1.1. Optical Time Domain Reflectometry

Optical time domain reflectometry (OTDR) systems are widely used for analysing and surveying fibre systems.

When light is guided by an optical fibre, loss occurs due to Rayleigh scattering which arises as a result of random microscopic variations in the index of refraction of the fibre core and, to a lesser extent, the clading. A fraction of the light is backscattered and is recaptured by the fibre and returned toward the source. If a short light pulse is coupled into a fibre, the arrival time of the backscatter light indicates the position along the fibre and its distribution the local attenuation [3.4]. The basic optical time domain reflectometer operation principle is illustrated in Figure 3.1.

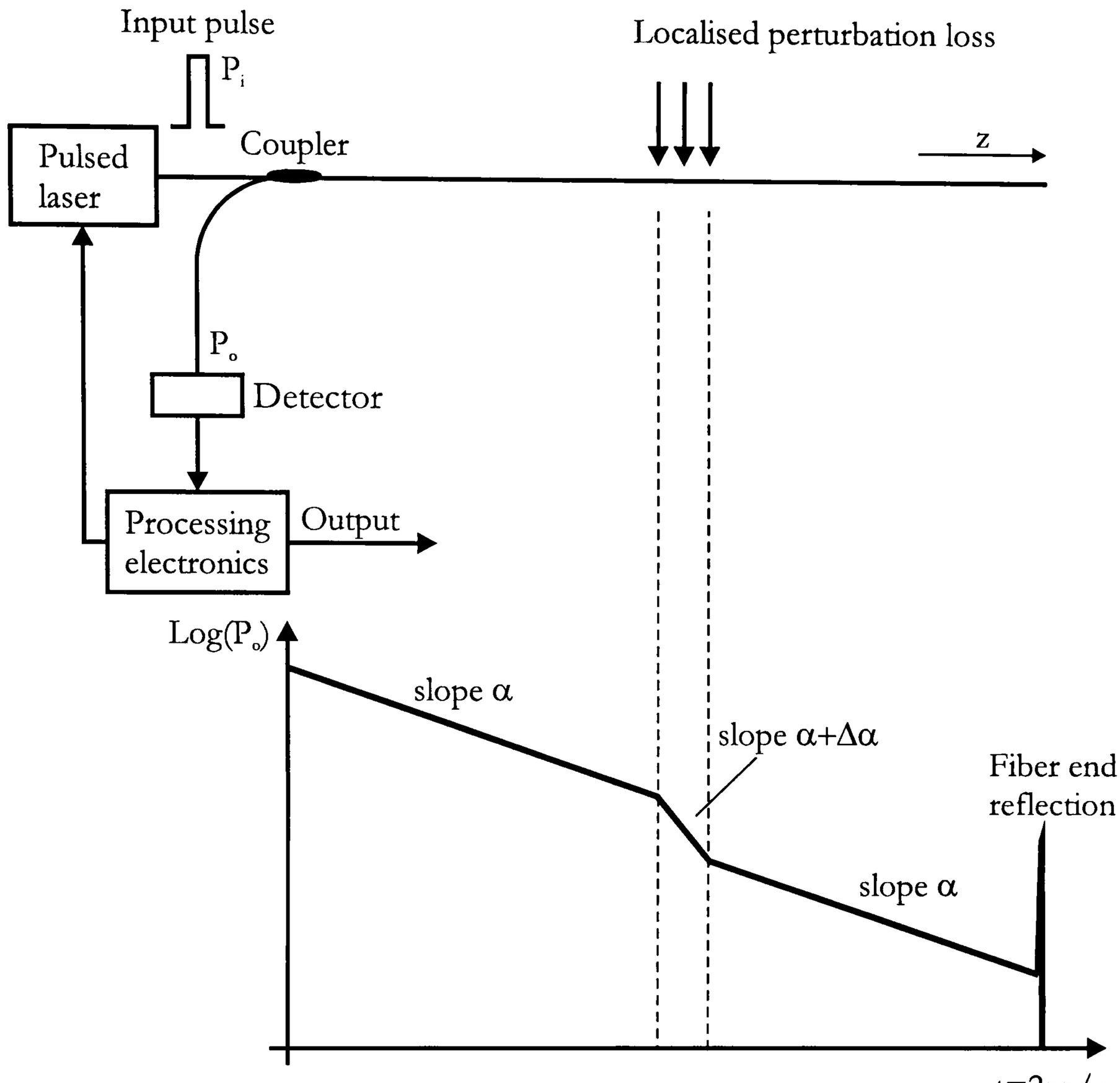

Figure 3.1: *Principle of OTDR operation*

In the simplest quasi distributed sensor set-up, modified sections or bulk devices with connecting fibres are spliced into a long fibre, to provide localised variations in the loss, backscatter intensity, polarisation, etc.. Loss mechanism can be introduced with force, pressure, displacement and hence enable the measurements of various variables.

Figure 3.2 schematically represents a quasi distributed sensor concept where discrete extrinsic type nonfibre sensor elements, which vary in transmitance and reflectance with the measurand field, are incorporated in the fibre line.

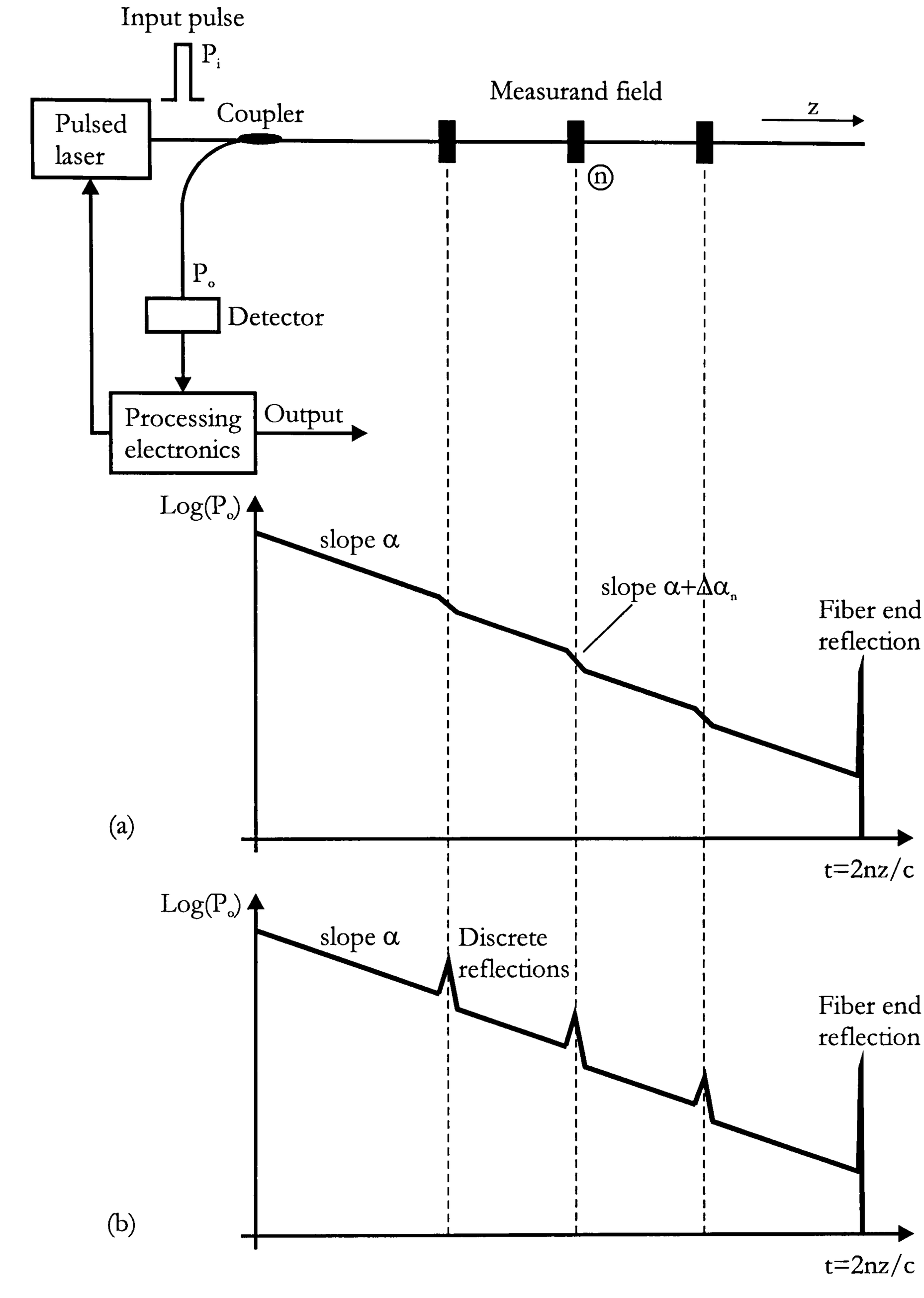

Figure 3.2: *Principle of quasi distributed sensing based on: (a) absorptive and (b) reflective elements*

The logarithm of the backscattered optical signal yields a linear dependence with time, corresponding to the scattering distance along the fibre. The slope of this

OTDR curve depends on the loss of the fibre. To achieve high spatial resolution a short duration optical pulse in the OTDR system is required. The spatial resolution of an OTDR instrument is the smallest distance between two scatters that can be resolved and is determined by the input pulse width according to:

$$\Delta z_{\min} = \frac{c\tau}{2n} \tag{3.1}$$

For a pulse width of $\tau = 10$ns a spatial resolution of ~ 1m is obtained.
Unfortunately shorter input pulses provide lower launched optical energies into the fibre and the signal to noise ratio of the output is reduced for continuous measurements. Often this results in the requirement for significant signal averaging for multiple input pulses.

Although quasi-distributed sensor configurations allow the measurand to be monitored at only a finite number of locations and not continuously along the fibre path, the approach has some distinct advantages over intrinsic distributed sensing. Due to the fact that sensor locations are defined, very short pulse OTDR operation is not necessary, and consequently, improved signal to noise performance can be achieved.

3.1.2. Basic networking principles

The servicing of a large number of sensors along common input/output fibre telemetry links is desirable in a wide range of possible application areas, where single or multiple measurands are monitored at different locations. The advantages of networking include:

- component cost: reduced number of lasers, detectors, etc., are required to support a given number of sensor elements
- reduced weight and cabling

Some basic networking concepts are presented in Figure 3.3.

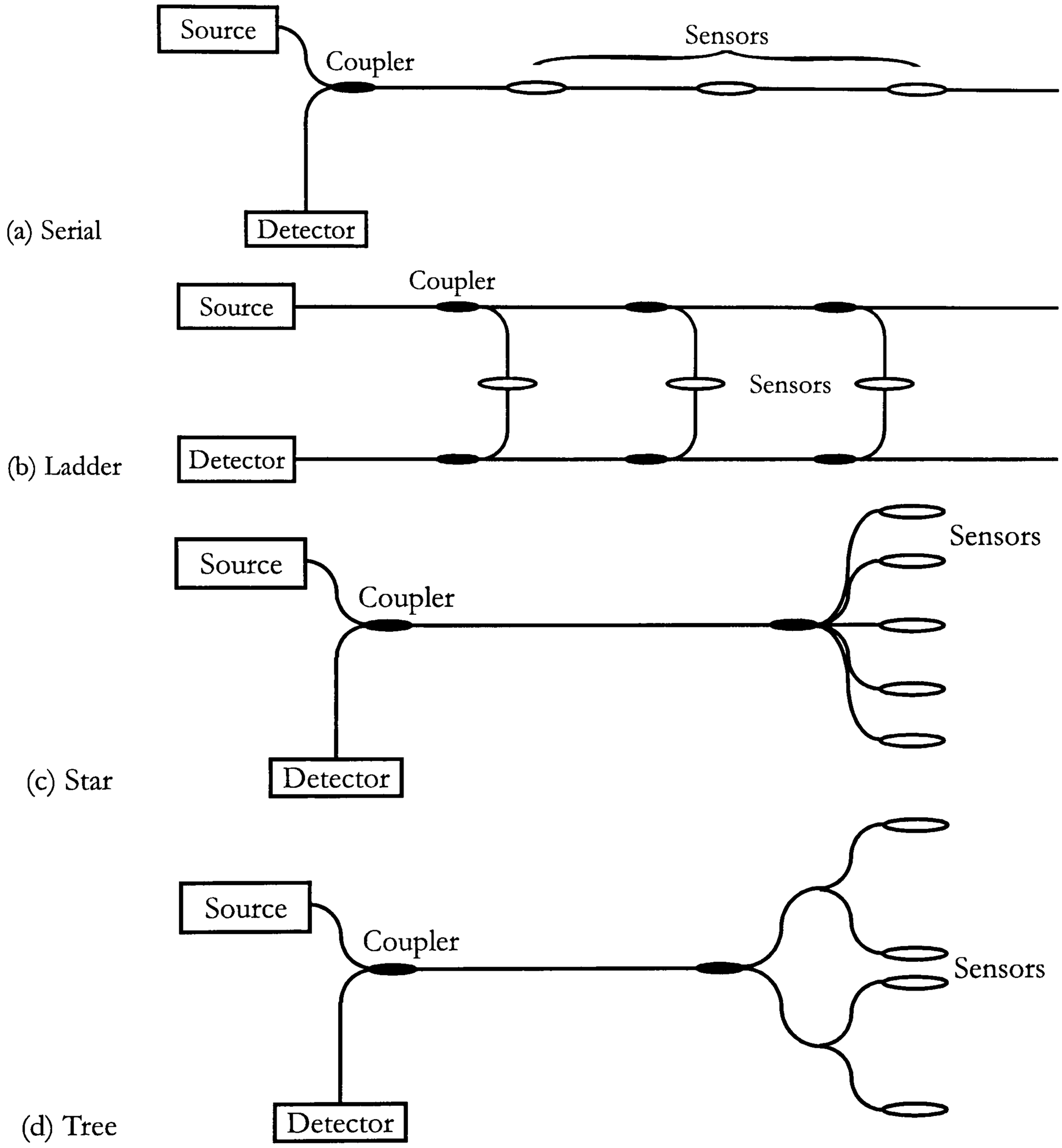

Figure 3.3: *Basic wiring methods for distributed and multiplexed fibre optic sensors*

In addition to these physical fibre wiring diagrams, methods for encoding the sensor signal are required to distinguish individual sensors and address them in one of the possible configurations. These methods include time, frequency, code,

wavelength and polarisation-division multiplexing [3.2]. The various multiplexing/addressing schemes are presented in Figure 3.4.

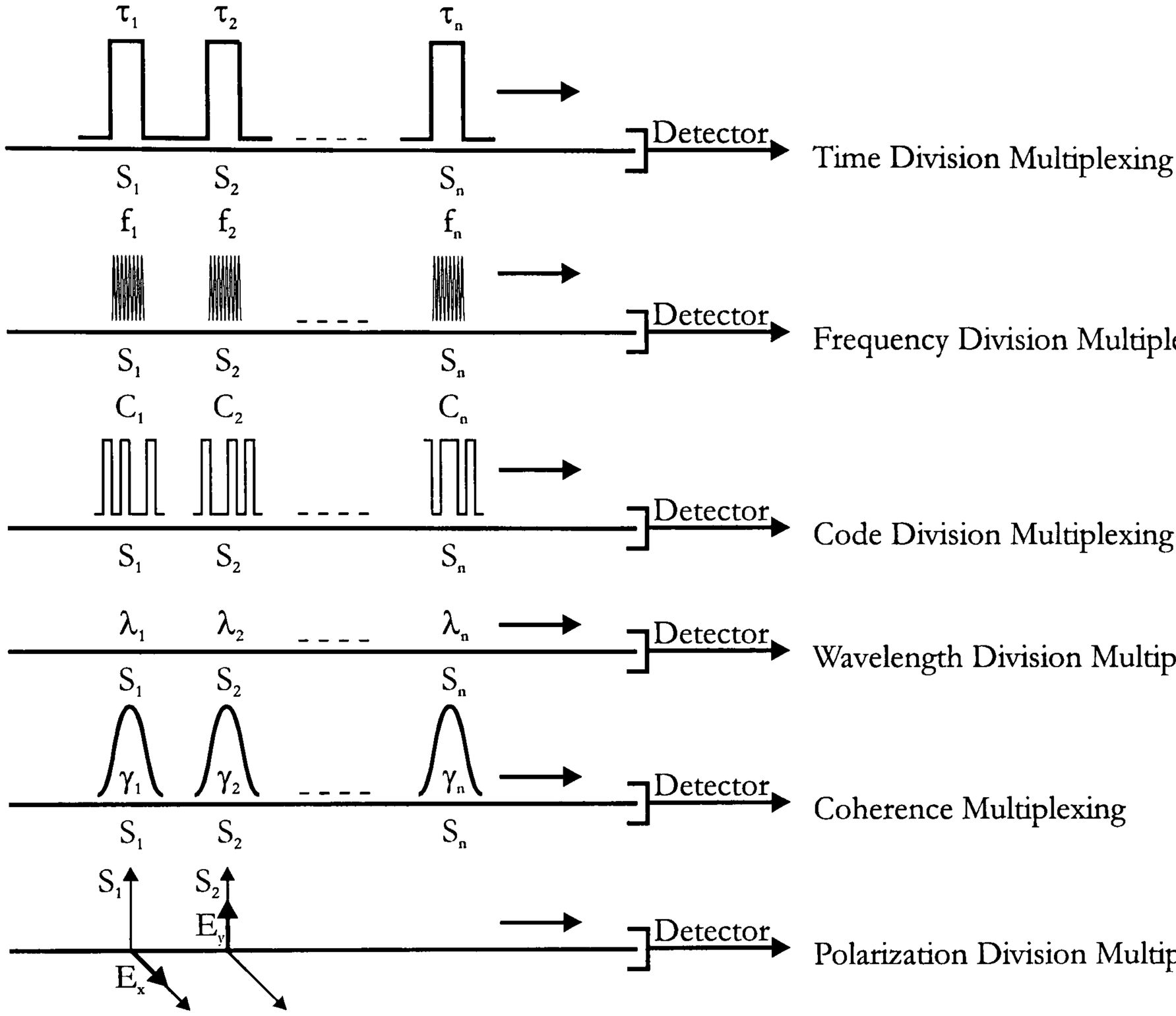

Figure 3.4: *Graphical representation of multiplexing techniques*

Time division multiplexing (TDM). Sensor information is allocated to a particular time slot within a repetitive transmission period (i.e. time samples of the sensor outputs are interleaved in time sequence to produce a pulse train).

Frequency division multiplexing (FDM). Sensor information is allocated on a particular frequency space (sensor data are encoded on carriers - amplitude or frequency modulated, of different frequencies).

Code division multiplexing (CDM). Code division multiplexing is based on the use of signal-encoding, typically binary, sequences which posses noiselike properties. In the FDM case, the sensor information is carried as sidebands of the

subcarrier frequency, but in CDM the sensor signals are spread over the wide bandwidth of the code sequence.

Wavelength division multiplexing (WDM). Sensor information is allocated to a particular optical wavelength (sensor data are encoded on optical carriers of different wavelengths).

Coherence multiplexing [3.5], [3.6]. Sensor information is differentially encoded on components of the optical carrier which have different degrees of mutual coherence with respect to some reference carrier.

Polarisation division multiplexing. Sensor information is encoded on orthogonal polarisation components of the optical carrier.

3.1.3. Interferometric sensor multiplexing

Interferometric fibre sensors offer extremely high sensitivity to weak measurand fields and have been widely researched for use in a range of application areas. In the multiplexing of interferometric sensors two main objectives are perceived. First, the reduction of the number of connecting fibres between the sensor array and the processing electronics and second, compatibility with demodulation techniques for processing the interferometric signals. For interferometric sensors all the previously described addressing mechanisms are feasible.

3.1.3.1.Time division multiplexing

The most straightforward approach on the time division multiplexing of interferometric sensors involves the interrogation of a number of Mach-Zehnder or Michelson interferometers using a pulsed or gated continuous wave source including appropriate optical delays between the sensors [3.5], [3.7].

One of the ways to implement interferometric time division multiplexing is presented in Figure 3.5.

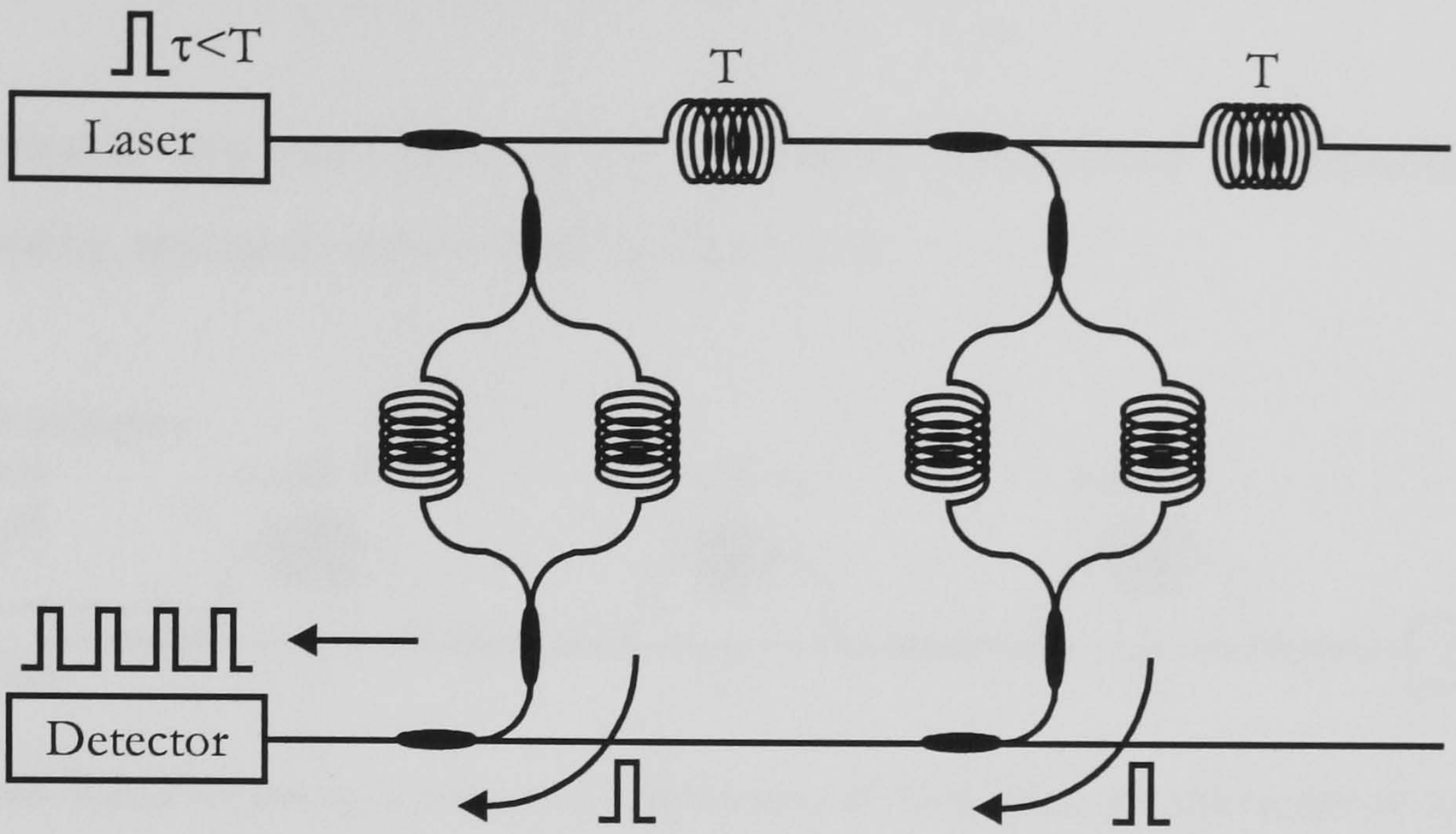

Figure 3.5: *Time division multiplexing of interferometric sensors (coils in the Mach-Zehnder arms are used just to highlight the interferometric setup)*

The input optical pulse width τ is set to $\tau \leq T$ (delay in the fibre coils) such that at the output of the N-sensor array a series of N output pulses is generated for each input pulse. As the path imbalance in the sensor is small, the pulses from the sensor and reference arms overlap and interfere at the output of each interferometer, and the output pulse train simply represents samples of the individual interferometer outputs interleaved in time sequence.

This topology does not lead to direct optical crosstalk between the sensor elements, and phase detection sensitivities comparable to those obtained in single sensor systems have been achieved.

3.1.3.2. Frequency division multiplexing

Frequency division multiplexing of interferometric fibre optic sensors relies on the use of frequency modulated laser source in conjunction with a network of

unbalanced sensor interferometers, to produce phase carrier output signals which are either amplitude or frequency (phase) modulated by the interferometer phase shift [3.7].

A schematic representation of a frequency modulated continuous wave multiplexing approach is presented in Figure 3.6.

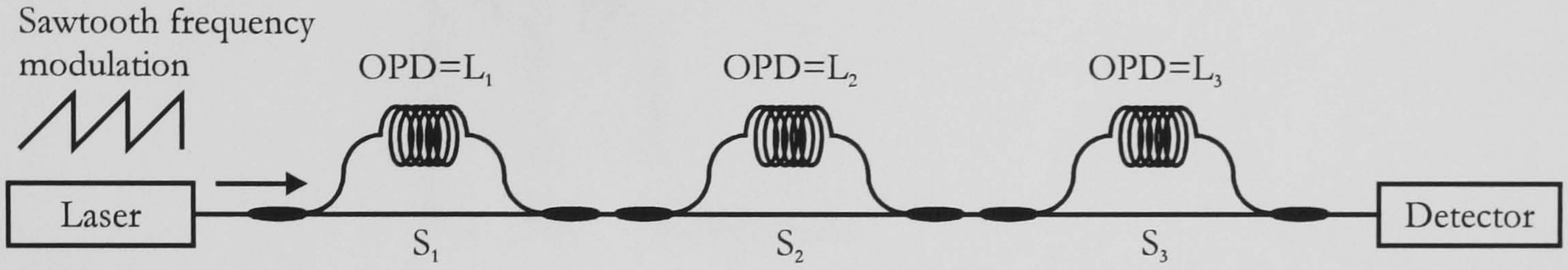

Figure 3.6: *Frequency division multiplexing of fibre optic interferometric sensors*

The laser induced phase shift produces output beat frequencies, which correspond to a particular sensor.

A more detailed description of the FMCW technique will be given in Chapter 4.

3.1.3.3.Coherence multiplexing

Outputs of a number of interferometric fibre optic sensors can be multiplexed onto a single optical fibre by using the coherence properties of light from a relatively short coherence length source [3.8], [3.10]. By choosing the optical delays in a sensor array appropriately, so that returns from the various sensors are mutually incoherent, one can ensure that the return signals do not interfere with one another.

The signals from an individual sensor can be recovered in the receiver by arranging for light associated with the sensor of interest to interfere coherently with its own reference beam. A coherence multiplexed system is presented in Figure 3.7.

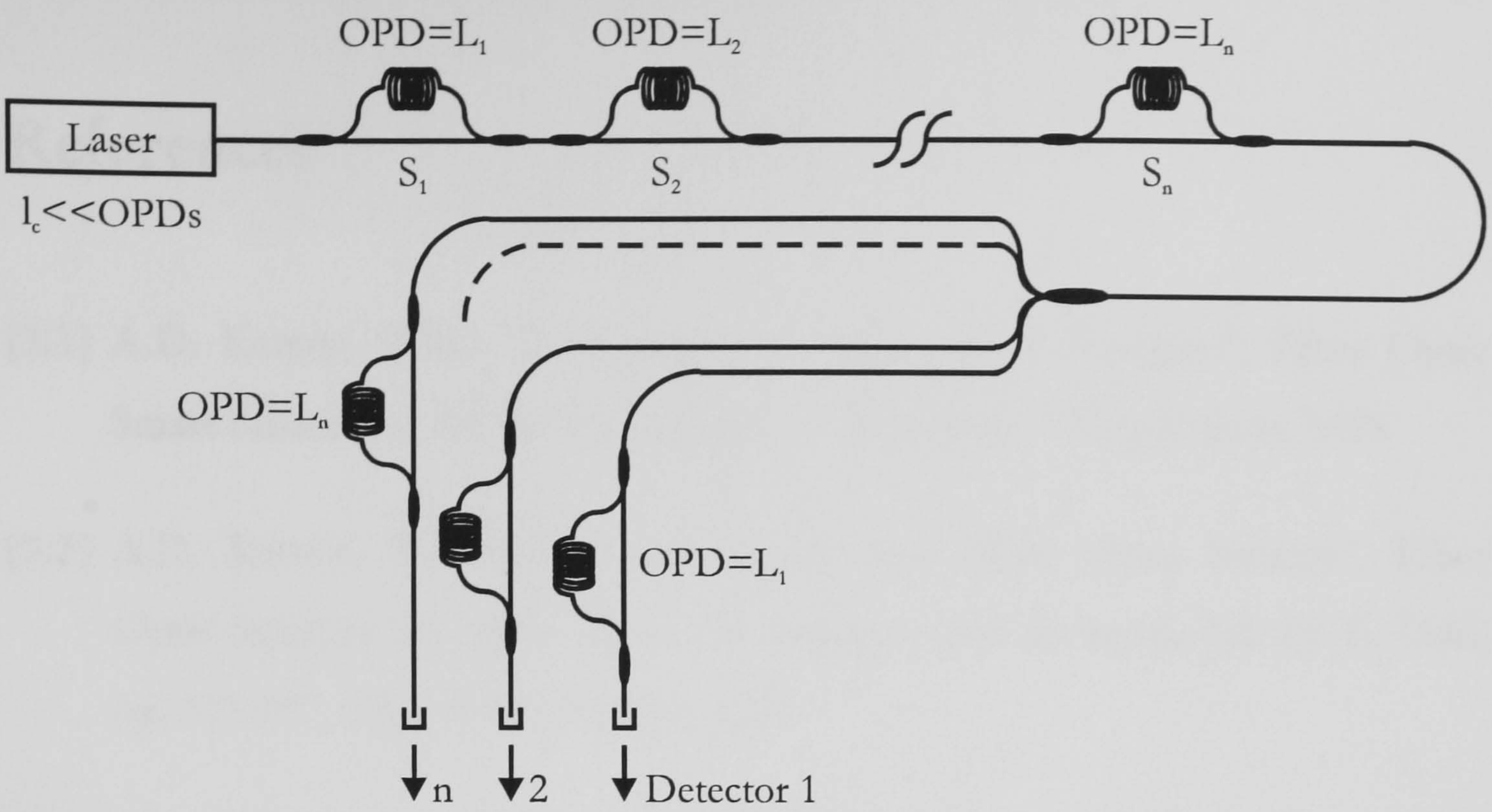

Figure 3.7: *Coherence multiplexed interferometric fibre optic sensors*

Each sensing interferometer has a unique differential path delay, chosen so that no sum or difference of differential path delays from more than one sensing interferometer can duplicate the differential delay of a single interferometer to within a few coherence times. After light passes through the sensor chain, it is split among various receiving interferometers each having a differential delay matched to that of one of the sensing interferometers. Each receiving interferometer produces an interference signal that depends only on the phase of the corresponding sensor.

A variety of other approaches to the multiplexing of sensors or sensor transducers have been described in the literature but are omitted here. Only the basic formalism for some methods which will be used in later chapters is given.
The OTDR principle was presented because it forms the basic and most extensively developed tool for distributed and multiplexed sensing. Later a comparison between the OTDR and FMCW principle will be presented.

References

[3.1] A.D. Kersey, "Fiber Optic Sensor Multiplexing Techniques", Fiber Optic Smart Structures, Ed. by E. Udd, pp. 409-443, John Wiley & Sons, 1995

[3.2] A.D. Kersey, "Distributed and Multiplexed Fiber Optic Sensors", Fiber Optic Sensors: *An introduction for Engineers and Scientists*, Ed. by E. Udd, pp. 325-367, John Wiley & Sons, 1991

[3.3] J.P. Dakin, "Distributed Optical Fiber Sensors", Fiber Optic Smart Structures, Ed. by E. Udd, pp. 372-409, John Wiley & Sons, 1995

[3.4] J. Niewisch, H. Bartelt, "Optical fiber sensor array for dynamic variables", Sensors and Actuators A, No. 41-42, pp. 562-566, 1994

[3.5] A.R. Nelson, D.H. McMahon, R.L. Gravel, "Passive multiplexing system for fiber-optic sensors", Applied Optics, Vol. 19, No. 17, pp. 2917-2920, September 1980

[3.6] G.J. Pendock, D.D. Sampson, "Noise in coherence-multiplexed optical fiber systems", Applied Optics, Vol. 36, No. 36, pp. 9536-9540, December 1997

[3.7] K. Blotekjaer, R. Wentworth, H.J. Shaw, "Choosing Relative Optical Path Delays in Series-Topology Interferometric Sensor Arrays", Journal of Lightwave Technology, Vol. LT-5, No. 2, pp. 229-235, February 1987

[3.8] R.H. Wentworth, "Theoretical Noise Performance of Coherence-Multiplexed Interferometric Sensors", Journal of Lightwave Technology, Vol. 7, No. 6, pp. 941-956, June 1989

[3.9] J.L. Santos, D.A. Jackson, "Coherence sensing of time-addressed optical-fiber sensors illuminated by a multimode laser diode", Applied Optics, Vol. 30, No. 34, pp. 5068-5076, December 1991

[3.10] J.L. Brooks, R.H. Wentworth, R.C. Youngquist, M. Tur, B.Y. Kim, H.J. Shaw, "Coherence Multiplexing of Fiber-Optic Interferometric Sensors", Journal of Lightwave Technology, Vol. LT-3, No. 5, pp. 1062-1071, October 1985

4. Frequency Modulated Continuous Wave Technique

Frequency-Modulated Continuous Wave reflectometry, also known as optical-frequency domain reflectometry is an alternative technique to the well known optical time domain reflectometry (OTDR) [4.1].

The FMCW Technique consists of analysing the beat signal produced by the optical interference between a fixed reference reflection, called local oscillator and difference reflections coming from the device (sensor) under observation. The technique was first introduced by Hymans and Lait [4.2] in the 1960's for radar range discrimination.

The interference signal is obtained with an interferometer for which the reflections at the end of one of the arms gives the reference signal, or local oscillator. The device (in further cases this should be a sensing unit) is connected to the other arm [4.3]. Figure 4.1 represents the basic experimental set-up for FMCW measurement.

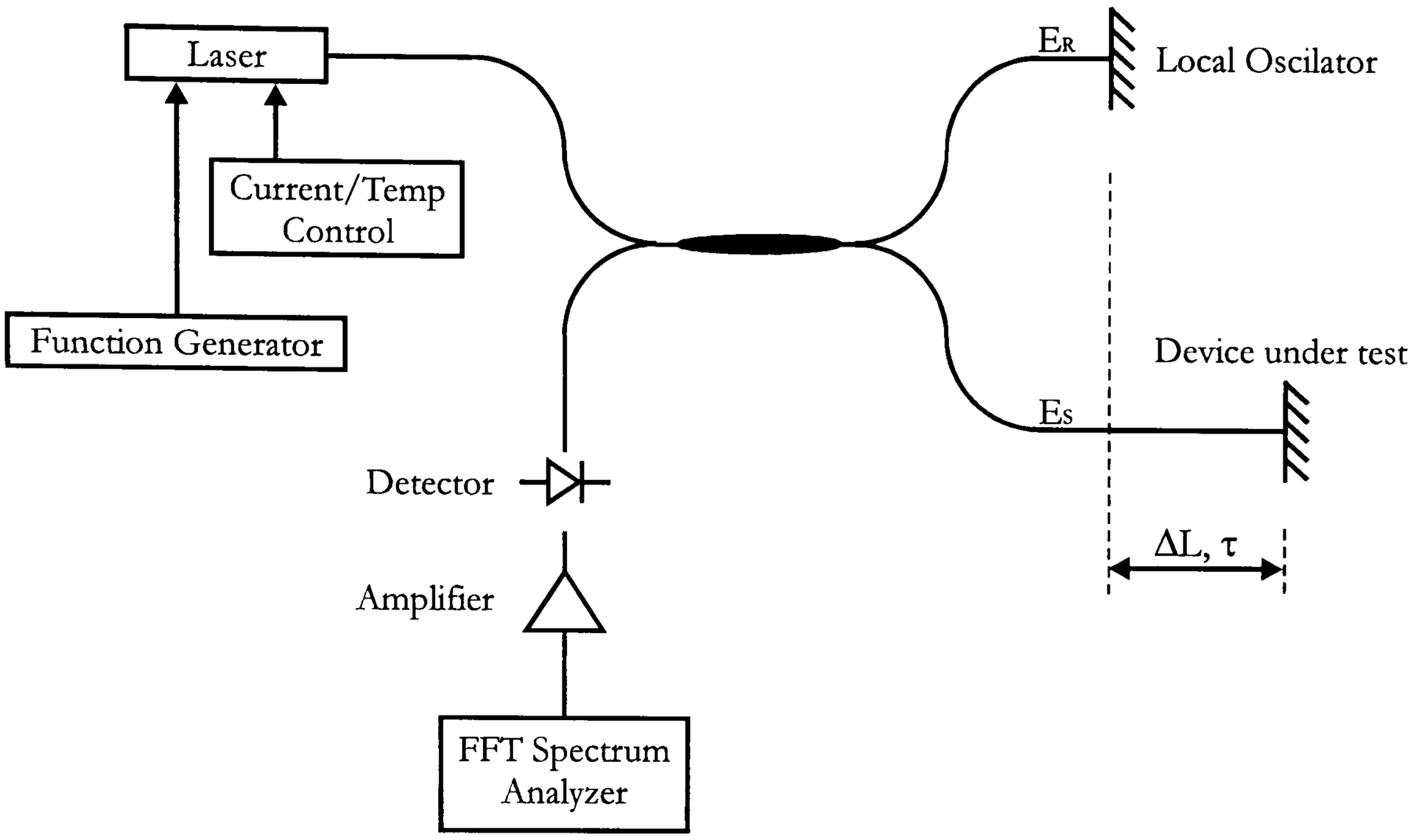

Figure 4.1: *Basic experimental set-up for FMCW measurement*

The optical frequency of the laser source is swept linearly and the light is launched at the input arm of a Michelson interferometer. Because of the linearity of the optical frequency sweep the beat frequency is proportional to the distance between the local oscillator and the reflection point while the reflection intensity is given by the squared amplitude of the beat signal.

Since the direct current modulation of a single longitudinal mode semiconductor laser can cause a dynamic shift of the peak wavelength emitted from the device, the frequency output of the laser diode is varied in a linear fashion, by driving the laser diode with a linear current ramp. Two effects contribute to the change in frequency, the change in temperature that follows from the change in the drive current and the change in the carrier concentration. Temperature effects both the refractive index and the cavity length. The carrier concentration affects both the refractive index and the gain coefficient. Hence, even small changes in carrier density will result in a phase shift of the optical field, giving an associated change in the resonance frequency within both Fabry-Perot and DFB laser structures.

Since the thermal time constant is rather large the thermal effect is important for modulation frequencies up to 10MHz whereas for larger modulation frequencies only the carrier effect may be considered. For the proposed FMCW system very low modulation frequency (< 100Hz) is applied, hence the source wavelength is changed mainly due to the thermal effect.

Commercially available semiconductor laser sources suitable for these FMCW experiments are DFB lasers, which may be purchased including fibre pigtail, optical isolator and temperature control with build in peltier elements and thermistor. Typically the output frequency excursion obtained from a DFB laser diode at modulation frequency of a few hundred hertz is few GHz per mA of injection current change.

The desired frequency modulation is however accompanied by intensity modulation, because the output power is injection current dependent [4.4]. However the principal features of the FMCW technique could be derived assuming that the output intensity remains unchanged. Figure 4.2 illustrates the operation of an ideal FMCW system.

The solid line represents the reference frequency varying with time in a sawtooth manner, while the broken line represents the same waveform which has been subject to a delay τ caused by the path length difference of the interferometer. The resulting instantaneous difference or beat frequency is also shown in Figure 4.2b as a function of time. The signal is generated by coherently mixing the output signal from the reference arm in Figure 4.1 with the delayed optical signal returning from the sensor at the photodetector surface. The value of the beat frequency is dependent on the delay τ and the rate of the change of the absolute frequency of the laser. Figure 4.2c shows the time dependence of the beat signal. As the scanning range is finite it is found that two beat frequencies are generated [4.2], the lower and upper beat frequency respectively. The bandwidth of the signal processing is normally chosen such that the upper beat frequency is not processed.

In this case, only the lower beat frequency henceforth referred as the beat frequency is detected.

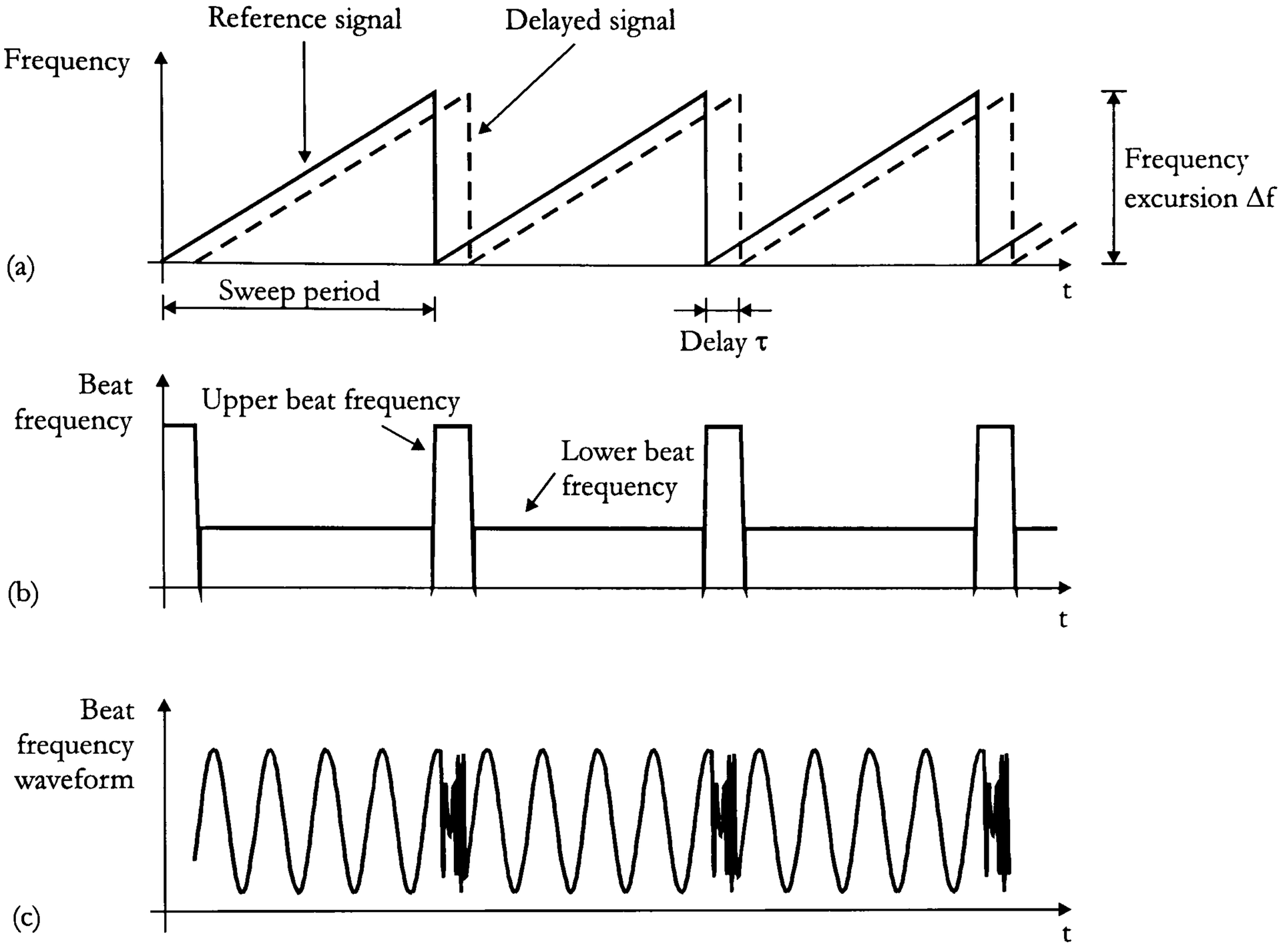

Figure 4.2: *Operation of an ideal FMCW system; (a) reference and delayed signal, (b) beat frequency, (c) beat frequency wave form*

In order to analyse the optical FMCW system the basic experimental set-up in Figure 4.1 will be used. Let the fields which interfere be E_R and E_S representing the reference and delayed sensor fields respectively:

$$E_R(t) = E_0 e^{j\left(\omega_0 t + \gamma t^2 + \Phi(t)\right)} \tag{4.1}$$

$$E_S(t) = rE_0 e^{j\left(\omega_0 (t-\tau) + \gamma (t-\tau)^2 + \Phi(t-\tau)\right)}$$

where γ is the Frequency sweep rate of the linear frequency excursion (Figure 4.3), ω_0 is the initial optical frequency and $\Phi(t)$ is the randomly fluctuating optical phase at time *t*.

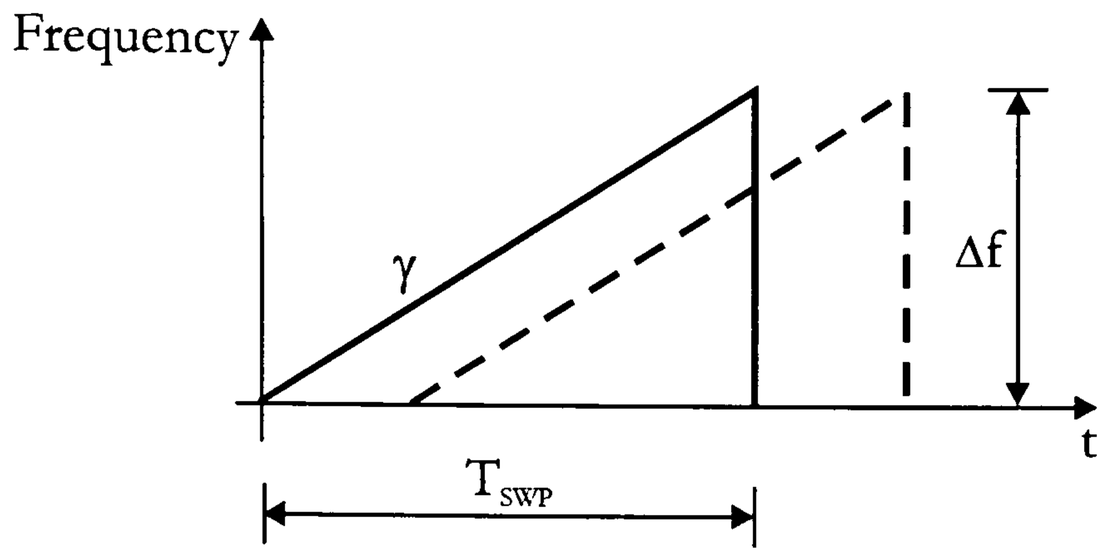

Figure 4.3: *Linear frequency excursion*

The frequency sweep rate is defined using sweep time T_{SWP} and the frequency excursion Δf as:

$$\gamma = \frac{\Delta f}{T_{SWP}} \tag{4.2}$$

The photocurrent *I(t)* is proportional to the optical intensity incident on the photodetector. Assuming a 3dB coupler as depicted in Figure 4.1 with reflection factors of unity in the reference arm and *r* in the sensing arm *I(t)* is calculated by taking the first order correlation of the total optical field *E(t)*, where

$$E(t) = E_R(t) + E_S(t) \tag{4.3}$$

The output photocurrent is then

$$I(t) = \left\langle E(t) \cdot E(t)^* \right\rangle \tag{4.4}$$

Equation (4.4) may be further derived as:

$$I(t) = \left\langle \begin{bmatrix} E_0 e^{j\left(\omega_0 t + \gamma t^2 + \Phi(t)\right)} + r E_0 e^{j\left(\omega_0 (t-\tau) + \gamma (t-\tau)^2 + \Phi(t-\tau)\right)} \end{bmatrix} \cdot \begin{bmatrix} E_0 e^{-j\left(\omega_0 t + \gamma t^2 + \Phi(t)\right)} + r E_0 e^{-j\left(\omega_0 (t-\tau) + \gamma (t-\tau)^2 + \Phi(t-\tau)\right)} \end{bmatrix} \right\rangle \tag{4.5}$$

$$= \left\langle E_0^2 + r^2 E_0^2 + r E_0^2 \cdot 2\cos\left[\gamma t^2 + \omega_0 \tau - \gamma (t-\tau)^2 + \Phi(t) - \Phi(t-\tau)\right] \right\rangle$$

$$= \left\langle E_0^2 + r^2 E_0^2 + 2 r E_0^2 \cos\left[\omega_0 \tau + 2\gamma \tau t - \gamma \tau^2 + \Delta\Phi(\tau)\right] \right\rangle$$

where $\Delta\Phi(\tau)$ is the source optical phase change over a time τ. Since the phase changes $\Delta\Phi(\tau)$ are introduced by a large number of random noise events due to spontaneous emission [4.11], $\Delta\Phi(\tau)$ may be considered to follow a Gaussian probability density distribution and (4.5) can be written as:

$$I(t) = E_0^2 + r^2 E_0^2 + 2 r E_0^2 \cos\left[\omega_0 \tau + \omega_b \left(t - \frac{\tau}{2}\right)\right] \cdot e^{-\frac{1}{2}\left\langle \Delta\Phi(\tau)^2 \right\rangle} \tag{4.6}$$

where $\omega_b = 2\pi\gamma\tau$ is the beat frequency. If we further assume that the phase fluctuations are caused by the frequency fluctuations of a Lorentzian lineshape source, we can express the phase change $\Delta\Phi(\tau)$ over a time period τ in terms of the laser linewidth $\Delta\nu_0$ or the source coherence time t_c using:

$$\left\langle \Delta\Phi(\tau)^2 \right\rangle = \left\langle \left[\Phi(t) - \Phi(t-\tau)\right]^2 \right\rangle = \frac{2\pi|\tau|}{\Delta\nu_0} \tag{4.7}$$

where

$$\Delta\nu_0 \equiv \frac{1}{\pi t_c} \tag{4.8}$$

Substituting (4.7) and (4.8) into (4.6) we obtain our final expression for the detector photocurrent:

$$I(t) = E_0^2 + r^2 E_0^2 + 2rE_0^2 \cos\left[\omega_0 \tau + \omega_b\left(t - \frac{\tau}{2}\right)\right] \cdot e^{-\frac{|\tau|}{t_c}} \tag{4.9}$$

Considering a single reflection from the device under test (Figure 4.1) with a displacement of ΔL, the displacement between the reference and sensing unit is related to the beat frequency ω_b using a frequency sweep rate as follows:

$$\Delta L = \frac{c\omega_b}{4\pi n\gamma} \tag{4.10}$$

Using the frequency sweep rate (4.2), equation (4.10) could be rearranged as:

$$\Delta L = \frac{c\omega_b T_{SWP}}{4\pi n\,\Delta f} \tag{4.11}$$

From (4.11) it is seen that the resolution increases with source frequency excursion. This should be considered for resolution enhancement when working with continuous backreflections from the sensing fibre. In cases where quasi distributed units are located along the sensing fibre a limited frequency excursion is not the limiting factor.

4.1. Output spectrum

To calculate the output spectrum of the FMCW system a Fourier transform of the detected signal has to be performed. The Fourier transform is defined as:

$$F(j\omega) = \int_{-\infty}^{\infty} f(t) e^{-j\omega t} dt \tag{4.12}$$

Assuming a sample time window [-T,T] equation (4.12) becomes:

$$F(j\omega) = \int_{-T}^{T} f(t) e^{-j\omega t} dt \tag{4.13}$$

Using (4.13) and (4.9) the output spectrum of the detected signal reads as follows:

$$I(j\omega) = \int_{-T}^{T} \underbrace{E_0^2 + rE_0^2}_{FIRST\ PART} + \underbrace{2rE_0^2 \cos\left(\omega_b t + \omega_0 \tau - \frac{1}{2}\omega_b \tau\right) e^{-\frac{2|\tau|}{t_c}}}_{SECOND\ PART} \tag{4.14}$$

The transform may be separated into two parts. First the Fourier transform of a constant term and then the Fourier transform of the cosine function have to be calculated:

$$I_1(j\omega) = \int_{-T}^{T} \left(E_0^2 + rE_0^2\right) e^{-j\omega t} dt = E_0^2(1+r) \frac{1}{-j\omega} e^{-j\omega t} \Bigg|_{-T}^{T} \tag{4.15}$$

$$= E_0^2(1+r)\left[\frac{e^{-j\omega T} - e^{j\omega T}}{-j\omega}\right] = 2E_0^2(1+r)T\frac{\sin\omega T}{\omega T}$$

where $I_1(j\omega)$ is the Fourier transform of the constant part. To perform the Fourier transform of the cosine function, first the cosine function has to be decomposed into the exponential function using the Euler formula:

$$\cos(x) = \frac{1}{2}\left[e^{jx} + e^{-jx}\right] \tag{4.16}$$

The transform of the cosine part is then made in two steps:

$$(i)\quad FT\left\{\frac{1}{2}e^{-\frac{2|\tau|}{t_c}}e^{j(\omega_b t+\alpha)}\right\}=Te^{j\alpha}e^{-\frac{2|\tau|}{t_c}}\frac{\sin\left[(\omega_b-\omega)T\right]}{(\omega_b-\omega)T} \tag{4.17}$$

$$(ii)\quad FT\left\{\frac{1}{2}e^{-\frac{2|\tau|}{t_c}}e^{-j(\omega_b t+\alpha)}\right\}=Te^{-j\alpha}e^{-\frac{2|\tau|}{t_c}}\frac{\sin\left[(\omega_b+\omega)T\right]}{(\omega_b+\omega)T}$$

where $\alpha=\omega_0\tau$-$0.5\omega_b\tau$. Equations (4.17)(i) and (4.17)(ii) combine to:

$$I_2(j\omega)=2rE_0^2Te^{-\frac{2|\tau|}{t_c}}\left\{\frac{\sin\left[(\omega_b-\omega)T\right]}{(\omega_b-\omega)T}e^{j\left(\omega_0\tau-\frac{1}{2}\omega_b\tau\right)}+\frac{\sin\left[(\omega_b+\omega)T\right]}{(\omega_b+\omega)T}e^{-j\left(\omega_0\tau-\frac{1}{2}\omega_b\tau\right)}\right\} \tag{4.18}$$

Combining (4.15) and (4.18) the Fourier transform of the detected signal is:

$$\begin{aligned}I(j\omega)&=I_1(j\omega)+I_2(j\omega)\\&=2E_0^2T(1+r)\frac{\sin\omega T}{\omega T}+\\&\quad 2rE_0^2Te^{-\frac{2|\tau|}{t_c}}\left\{\frac{\sin\left[(\omega_b-\omega)T\right]}{(\omega_b-\omega)T}e^{j\left(\omega_0\tau-\frac{1}{2}\omega_b\tau\right)}+\frac{\sin\left[(\omega_b+\omega)T\right]}{(\omega_b+\omega)T}e^{-j\left(\omega_0\tau-\frac{1}{2}\omega_b\tau\right)}\right\}\end{aligned} \tag{4.19}$$

To represent the power of the frequency components the power spectrum has to be calculated. By the autocorrelation theorem (a form of the Wiener-Khintchine theorem) the power spectrum is the Fourier transform of the autocorrelation function, whereby autocorrelating corresponds to squaring (the modulus) of its transform [4.12]:

$$P(\omega)=\left|I(j\omega)\right|^2 \tag{4.20}$$

Using equations (4.19) and (4.20) the power spectrum of the detected signal may be written as:

$$P(\omega) = 4E_0^4(1+r)^2T^2\frac{\sin^2\omega T}{(\omega T)^2} + 4r^2E_0^4T^2e^{-\frac{4|\tau|^2}{t_c^2}}\cdot\left[\frac{\sin^2[(\omega_b-\omega)T]}{[(\omega_b-\omega)T]^2}+\frac{\sin^2[(\omega_b+\omega)T]}{[(\omega_b+\omega)T]^2}\right] \tag{4.21}$$

$$+8E_0^4r(1+r)T^2e^{-\frac{2|\tau|}{t_c}}\frac{\sin\omega T}{\omega T}\cdot\left[\frac{\sin[(\omega_b-\omega)T]}{(\omega_b-\omega)T}+\frac{\sin[(\omega_b+\omega)T]}{(\omega_b+\omega)T}\right]\cdot\cos\left(\omega_0\tau-\frac{1}{2}\omega_b\tau\right)$$

$$+8E_0^4r^2T^2e^{-\frac{4|\tau|^2}{t_c^2}}\cdot\frac{\sin[(\omega_b-\omega)T]}{(\omega_b-\omega)T}\cdot\frac{\sin[(\omega_b+\omega)T]}{(\omega_b+\omega)T}\cdot\cos(2\omega_0\tau-\omega_b\tau)$$

To show how the sample time window affects the shape of the Fourier transform let us first consider the Fourier transform of an ideal offset cosinus signal $f(t)=a+b^*Cos(\omega_b t)$. The Fourier transform is composed of Dirac function at zero frequency representing the constant time domain term and additional Dirac functions corresponding to the frequency of the cosine part (Figure 4.4a).

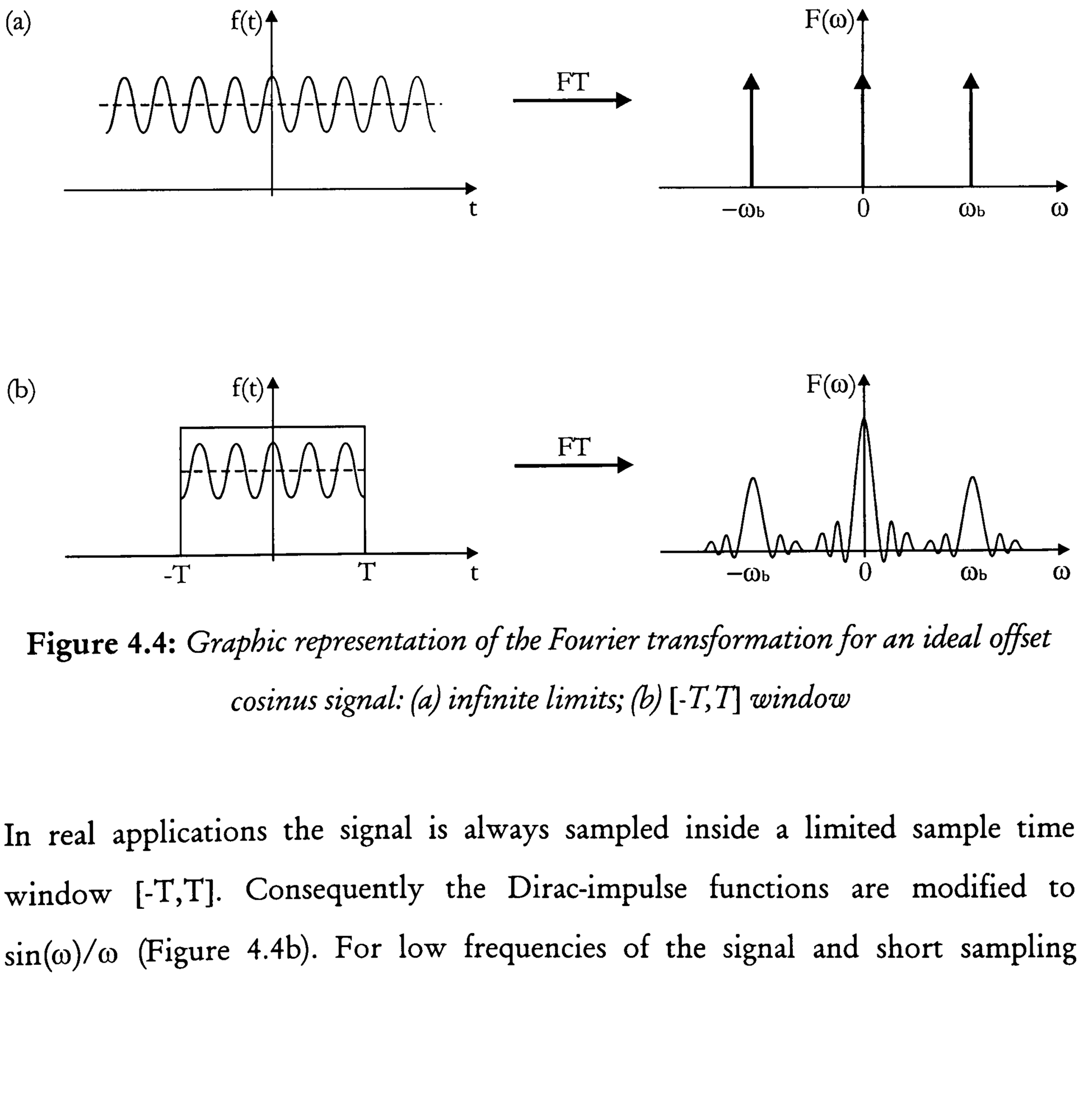

Figure 4.4: *Graphic representation of the Fourier transformation for an ideal offset cosinus signal: (a) infinite limits; (b)* [*-T,T*] *window*

In real applications the signal is always sampled inside a limited sample time window [-T,T]. Consequently the Dirac-impulse functions are modified to $\sin(\omega)/\omega$ (Figure 4.4b). For low frequencies of the signal and short sampling

windows the spectrums of the constant and alternating signal components may overlap in the frequency domain. To minimise this one may increase the sampling window width, whereby the sinc spectral peaks gradually transform to Dirac functions.

The graphic presentation of the FMCW power spectrum for different sample time windows is shown in Figure 4.5. As the width of the window increases the sinc spectrum shape is transformed to impulse function centred around the beat frequency.

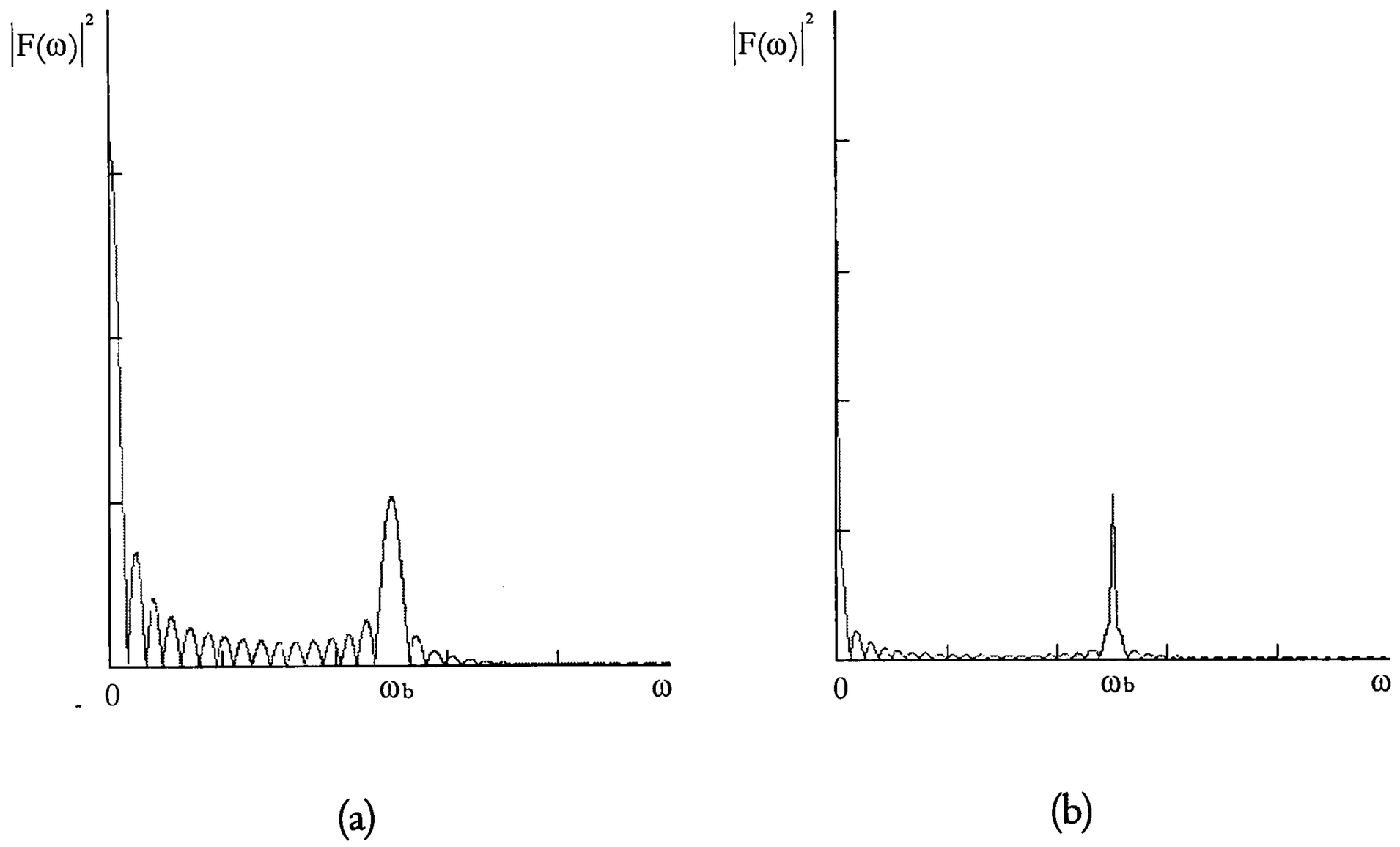

Figure 4.5: *Power spectrum of the FMCW signal (4.14); (a) T=100ms; (b) T=500ms*

Since in real applications the continuous Fourier transform is replaced by its discrete equivalent the power spectrums shown in Figure 4.4 represents the envelope inside which discrete frequency components are spaced at a certain fundamental frequency determined by the sampling time and the number of sampling points. Consequently it is not necessary that the beat frequency of the

FMCW system matches one of the discrete frequency components. In this case the beat frequency peak corresponds to the nearest frequency component.

4.2. Comparison between the FMCW and OTDR Technique

The optical frequency modulation technique has several application areas [4.6], [4.7], [4.8], [4.9], [4.10] and will be used through this work for optical sensors addressing as described later. Although the main advantage of FMCW over OTDR techniques is the potential high resolution available, this is not the deciding factor in using it for sensing system applications.

Compared with the time domain reflectometer the frequency modulation system has further advantages. First there is continuous operation of the system, where the optical power produced is determined by the bias current. Comparing this to the pulsed technique, much greater peak pulse powers would be required to produce the same average power [4.4]. Whereas with OTDR the receiver bandwidth is inversely proportional to the pulse rise time resulting in gigahertz receiver bandwidths, with FMCW the receiver bandwidth is determined by the difference between the local oscillator and the device under test, the modulation period and frequency excursion of the source. This combines to a few megahertz receiver bandwidth for the FMCW system.

The high average power and low receiver bandwidth for the FMCW system therefore improve the signal to noise ratio. For standard FMCW applications where a continuous scan of the device under test (usually an optical fibre) is realised, the major disadvantage of the FMCW system is the limited range over which measurements can be made and is determined by the coherence properties of the source used. However this can be mitigated by using some modifications

where local coherence over a wide range is attained (more detailed description of this follows in the next chapter).

4.3. Basic options for a fibre optic quasi-distributed measuring system using FMCW technique

The FMCW technique proves to be a practical technique for interrogating a sensor system. The high average power due to continuous wave system operation and the possibility of using relatively low receiver bandwidth allows a high sensitivity with a relatively low power laser and makes it a good candidate for further evaluation and implementation.

In a quasi-distributed sensor configuration, the measurand is not monitored continuously along the fibre path, but at a finite number of locations. This is accomplished either by sensitising the fibre locally to a particular field of interest or by using extrinsic bulk sensing elements.

In this work different methods of addressing quasi distributed sensor units using the Frequency modulated continuous wave technique will be proposed and evaluated. A combination of coherence addressing and FMCW method is presented to address different sensing units arranged in series.

Together five different addressing and signal resolving mechanisms will be presented (all schemes are outlined in Figure 4.6):

- **Coherent FMCW with reference arm addressing**
- **Coherent addressed quasi-distributed absorption based sensor system implementing the FMCW method (FMCW with Coherence addressing)**
- **Forward addressed system applying FMCW**
- **FMCW White light reference arm addressing**
- **FMCW White light coherence addressing**

Since for all addressing and resolving schemes frequency modulated continuous wave technology is implemented the laser diode output is changed in a linear fashion by driving the laser diode with a linear current ramp. The basis of the coherent FMCW interferometry is the interferometric mixing of two signals for each cell, one signal following a test path, while the other follows a reference path. Any time delays between the signals reflected back along the test path and the signal from the reference reflection give rise to beat frequencies in the mixed output.

With all addressing schemes the microoptic cell is used as the basic sensing and addressing element. Depending on the type of addressing the cell provides the sensing signal and for 4 of 5 addressing schemes the cell also provides the reference signal. The basic novelty of those addressing mechanisms is in the realisation of the signal paths, where apart from the cell length, both reflected beams from each cell travel the same path and experience the same perturbations, hence conventional interferometer problems are minimised.

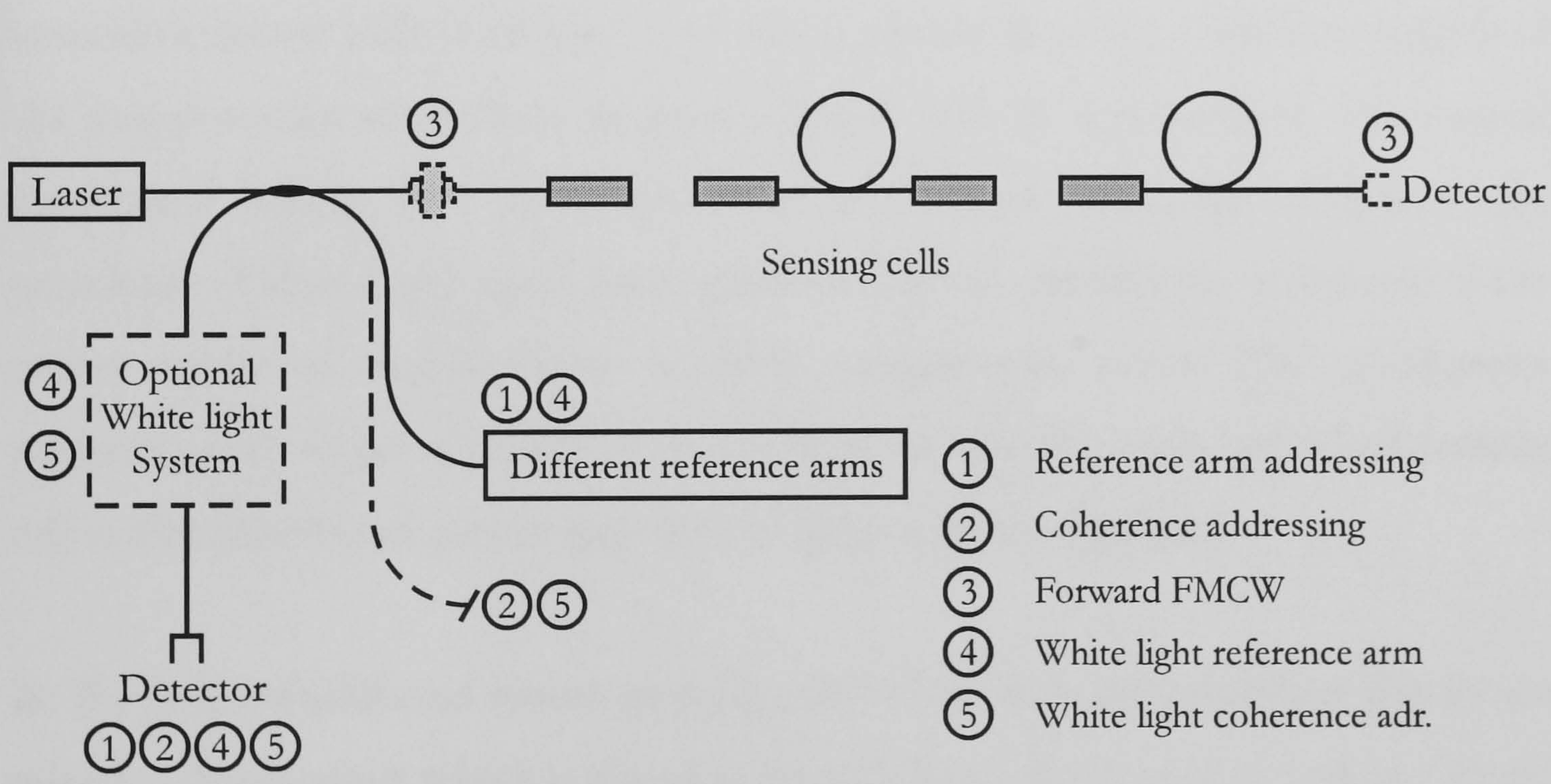

Figure 4.6: *Diagram illustrating all five addressing schemes*

The coherent FMCW with reference arm addressing uses different reference arms to address individual sensing units. The source signal is divided into the reference

arm line and the sensing arm line. In the reference arm line fibres of different length are alternately switched to and from the line. The optical path for each reference is chosen to match the appropriate sensing unit in the sensing line within the coherence length of the source. Two backreflected signals, first signal arising form the reference arm and the second signal first passing the sensing cell which is then reflected back from the second GRIN lens of the cell interfere at the detector. Due to different path mismatch and the modulation of the source each sensing unit has its unique beat frequency in the frequency spectrum of the interference signal.

For the *Coherent addressed quasi-distributed absorption based sensor system* only one fibre line is used where the reference and measuring signals travel almost the same optical path. Coherence addressing of the cells using FMCW is achieved by the interferometric mixing of two signals originating from each cell (from the glass/air interfaces). The time delay between the two reflections, along with the linear frequency ramp of the source, gives rise to beat frequencies in the mixed output which are different for each cell. The connecting fibre length between two successive sensor cells is chosen to be much greater than the coherence length of the source so that the reflections from different cells do not interfere. The optical absorbance which is a characteristic of a chemical substance attenuates the amplitude of the optical signal passing the sensing cell, resulting in a decrease of the power spectrum amplitude for a given measurement point. The interference patterns of all sensor cells add up at the detector whereby each individual sensing cell is identified by its power spectrum in the frequency domain.

In *The forward addressed system applying FMCW* the forward travelling signals are mixed at the detector which is placed at the distal end of the sensing system. To get two forward travelling signals for each sensing unit some additional reflection points are provided using air gap connectors. In the system interference pattern each sensing unit and its appropriate reflection point is presented with its beat amplitude in the frequency domain.

Both *white light addressing schemes* just extend the reference arm and coherence method with the white light resolving system if appropriate.

References

[4.1] R. Passy, N. Gisin, J.P. von der Weid, H.H. Gilgen, "Experimental and Theoretical Investigations of Coherent OFDR with Semiconductor Laser Sources", Journal of Lightwave Technology, Vol. 12, No. 9, pp. 1622-1630, September 1994

[4.2] A.J. Hymans, J. Lait, "Analysis of a frequency-modulated continuous ranging system", The Institution of Electrical Engineers, Paper No. 3264 E, pp. 365-372, July 1960

[4.3] J.P. von der Weid, R. Passy, G. Mussi, N. Gisin, "On the Characterisation of Optical Fibre Network Components with Optical Frequency Domain Reflectometry", Journal of Lightwave Technology, Vol. 15, No. 7, pp. 1131-1141, July 1997

[4.4] D. Uttam, B. Culshaw, "Precision Time Domain Reflectometry in Optical Fibre Systems Using a Frequency Modulated Continuous Wave Ranging Technique", Journal of Lightwave Technology, Vol. LT-3, No. 5, pp. 971-977, October 1985

[4.5] S. Venkatesh, W.V. Sorin, "Phase Noise Considerations in Coherent Optical FMCW Reflectometry", Journal of Lightwave Technology, Vol. 11, No. 10, pp. 1694-1700, October 1993

[4.6] G. Beheim, K. Fritsch, "Remote displacement measurement using a laser diode", Electronics Letters, Vol. 21, No. 3, pp. 93-94, January 1985

[4.7] K. Tsuji, K. Shimizu, T. Horiguchi, "Coherent Optical Frequency Domain Reflectometry Using Phase-Decorrelated Reflected and Reference Lightwaves", Journal of Lightwave Technology, Vol. 15, No. 7, pp. 1102-1109, July 1997

[4.8] I.P. Giles, D. Uttam, B. Culshaw, D.E.N. Davies, "Coherent optical-fibre sensors with modulated laser sources", Electronics Letters, Vol. 19, No. 1, pp. 14-15, January 1983

[4.9] C.A. Wade, A.D. Kersey, A. Dandridge, "Temperature sensor based on a fibre-optic differential delay RF filter", Electronics Letters, Vol. 24, No. 21, pp.1305-1307, October 1988

[4.10] R.I. MacDonald, "Frequency domain optical reflectometer", Applied Optics, Vol. 20, No. 10, pp. 1840-1844, May 1981

[4.11] K. Petermann, "Laser Diode Modulation and Noise", Kluwer Academic Publishers, The Netherlands, 1988

[4.12] R.N. Bracewell, "The Fourier Transform and Its Applications", McGraw-Hill Book Company, Singapore 1986

5. Mathematical Modelling and Simulation

In previous chapters an overall assessment of chemical and environmental sensing has been presented and some common multiplexing and distributed sensing topologies have been reviewed.

In the following chapter on mathematical modelling and simulation a detailed mathematical analysis for five in Chapter 4.3. presented fibre optic quasi-distributed measuring systems using FMCW technique will be given. For all proposed schemes a mathematical model will be derived and reviewed. The discussion will start by evaluating the one sensor configuration with all influential parameters, and then continue with mathematical modelling and analysis of multiple sensing unit system according to the specific configuration implemented.

5.1. Single Sensor Coherent FMCW

The basic principle of the coherent FMCW system will be explained using the single sensor set-up shown in Figure 5.1.

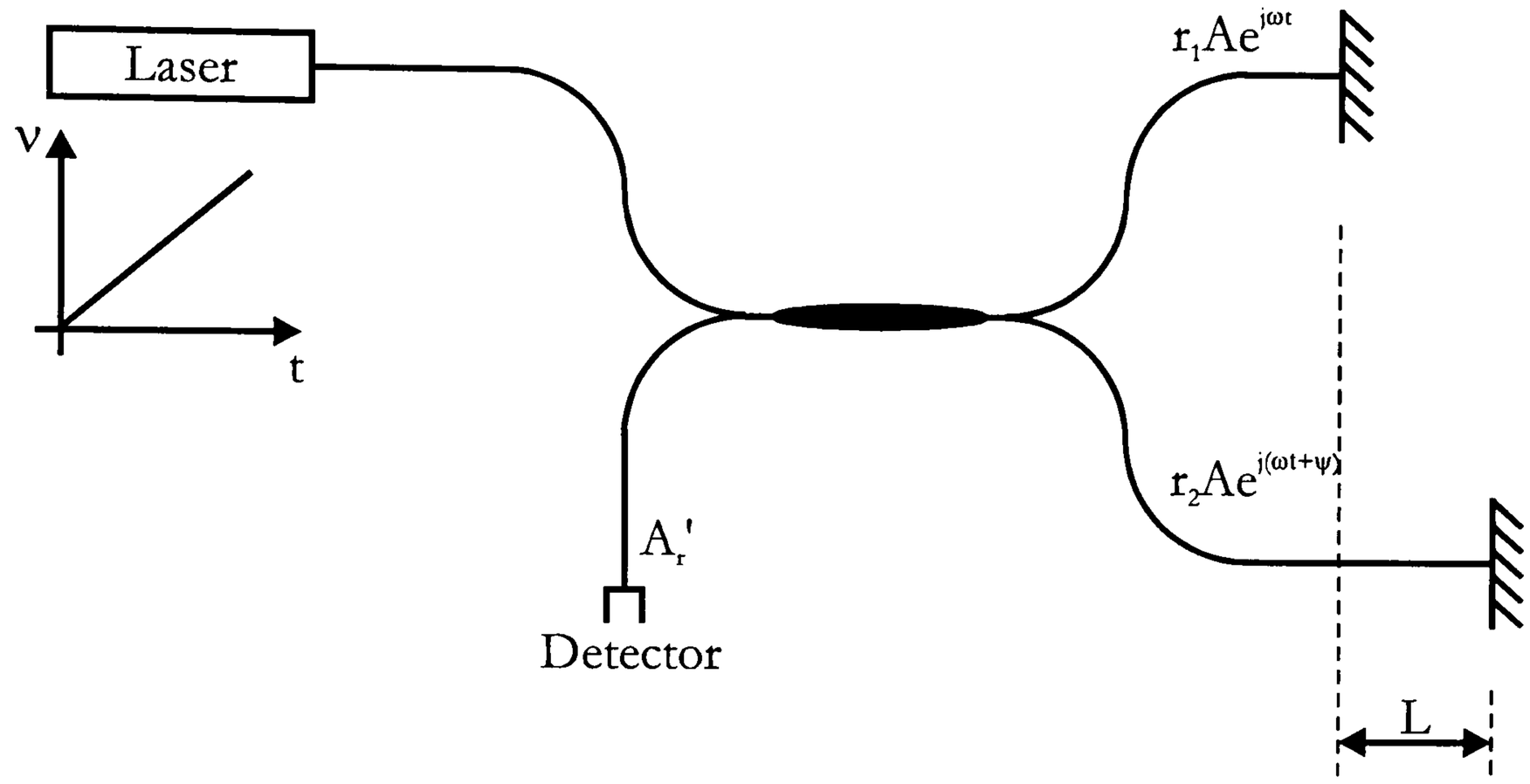

Figure 5.1: *FMCW configuration of the Michelson interferometer*

The frequency output of the laser diode is varied in a linear fashion, by driving the laser diode with a linear current ramp.

The basis of coherent FMCW is the interferometric mixing of two signals, one signal following a test path, while the other follows a reference path. Any time delays between the signals reflected back along the test path and the signal from the reference reflection give rise to beat frequencies in the mixed output.

A perfectly time linear slope of the frequency change is assumed. A single reflection from the test arm of the interferometer, occurring at the end of the length of fibre at a distance L further than the length of the reference arm is considered. Consequently a total time delay experienced by the test signal relative to the reference signal is $\tau = 2n_eL/c$ where c/n_e is the phase velocity of light in fibre. According to Figure 5.1 the returning light A_r' is:

$$A'_R = r_1 A e^{j\omega t} + r_2 A e^{j(\omega t+\psi)} \tag{5.1}$$

where ω is the angular frequency which equals $2\pi c/\lambda_0$, λ_0 is the free space wavelength of light, c is the velocity of light in vacuum and ψ is the phase shift superimposed due to the time delay. A, r_1 and r_2 are constants. The imposition of a dynamic shift in the frequency of the laser light Δω, due to the driving of the laser with a current ramp results in a dynamic shift of the phase ψ. ψ increases from a value of $2\pi\left[\frac{2n_eL}{\lambda_0}\right]$ by a factor Δψ which equals $2\pi[2n_eL]\frac{\Delta\lambda}{\lambda_0^2}$ and L is the optical path difference.

Thus the total phase shift which occurs due to the sum of the static phase shift and the additional component due to current ramping of the laser source is given by ψ + Δψ where

$$\psi + \Delta\psi = 2\pi\frac{2n_eL}{\lambda_0} + 2\pi 2n_eL\frac{\Delta\lambda}{\lambda_0^2} = \frac{2\pi}{\lambda_0}\left(\frac{2n_eL}{\lambda_0}\right)(\lambda_0 + \Delta\lambda) \tag{5.2}$$

However current ramping of the laser diode results not only in a change in the output light frequency but also in a change in the amplitude of the output light A_r'. Under this condition, this may be represented as

$$A'_R = r_1\sqrt{(A+Bt)}e^{j\omega t} + r_2\sqrt{(A+B(t-\tau))}e^{j(\omega t+\psi+\Delta\psi)} \tag{5.3}$$

Where A, B, r_1 and r_2 are constants and Bt represents the change in amplitude of the light signal due to current ramping.

Hence the light intensity measured at the detector from the receiving end of the fibre is given by

$$
\begin{aligned}
I_{out} &\propto \left\langle A'_R \cdot A'^{*}_R \right\rangle \qquad (5.4)\\
&= \left[r_1 \sqrt{(A+Bt)} e^{j\omega t} + r_2 \sqrt{\left(A+B(t-\tau)\right)} e^{j(\omega t+\psi+\Delta\psi)} \right] \cdot \\
&\quad \left[r_1 \sqrt{(A+Bt)} e^{-j\omega t} + r_2 \sqrt{\left(A+B(t-\tau)\right)} e^{-j(\omega t+\psi+\Delta\psi)} \right] \\
&= r_1^2 \left(A+Bt\right) + r_2^2 \left(A+B(t-\tau)\right) + r_1 r_2 \sqrt{\left(A+Bt\right)\left(A+B(t-\tau)\right)} \left[e^{j(\psi+\Delta\psi)} + e^{-j(\psi+\Delta\psi)} \right] \\
&= r_1^2 \left(A+Bt\right) + r_2^2 \left(A+B(t-\tau)\right) + 2 r_1 r_2 \sqrt{\left(A+Bt\right)\left(A+B(t-\tau)\right)} \cos(\psi+\Delta\psi)
\end{aligned}
$$

If we assume that amplitude changes are small then $B(t-\tau) \approx B(t)$ and equation (5.4) may be simplified to

$$
I_{out} = (A+Bt)\left[r_1^2 + r_2^2 + 2 r_1 r_2 \cos(\psi+\Delta\psi) \right] \qquad (5.5)
$$

Using the expression for phase ψ and phase change $\Delta\psi$, (5.5) can be rewritten as

$$
I_{out} = (A+Bt)^2 \left[r_1^2 + r_2^2 + 2 r_1 r_2 \cos\left(\frac{2\pi}{\lambda_0} \left[\frac{2 n_e L}{\lambda_0} \right] (\lambda_0 + \Delta\lambda) \right) \right] \qquad (5.6)
$$

For sensing applications, variations in the OPD of the Michelson interferometer are measured. They are caused by either changes in L or n.

5.1.1. The Microoptic Sensing Cell

The fibre microoptic sensing cell is constructed using two capillaries, two GRIN lenses and a supporting V-groove alignment block.

The placement of the optical fibre relative to the GRIN lens position is critical. Any displacement of the fibre off the optical axis of the lens would cause the light emergent from the GRIN lens not to be centrosymmetrically distributed around the sensor optical axis, and thus the reflection from the second GRIN lens would not re-enter the GRIN lens in a manner that would allow it to be collected by the fibre. Therefore on both ends of the microoptic cell capillaries are used to fix the fibre and align it to the centre of the subsequent GRIN lens. As shown in Figure 5.1 the capillary and GRIN lens are carefully aligned to minimise the air gap between them. Because the air gap could cause undesirable backreflections the gap is usually filed with index matching oil or gel.

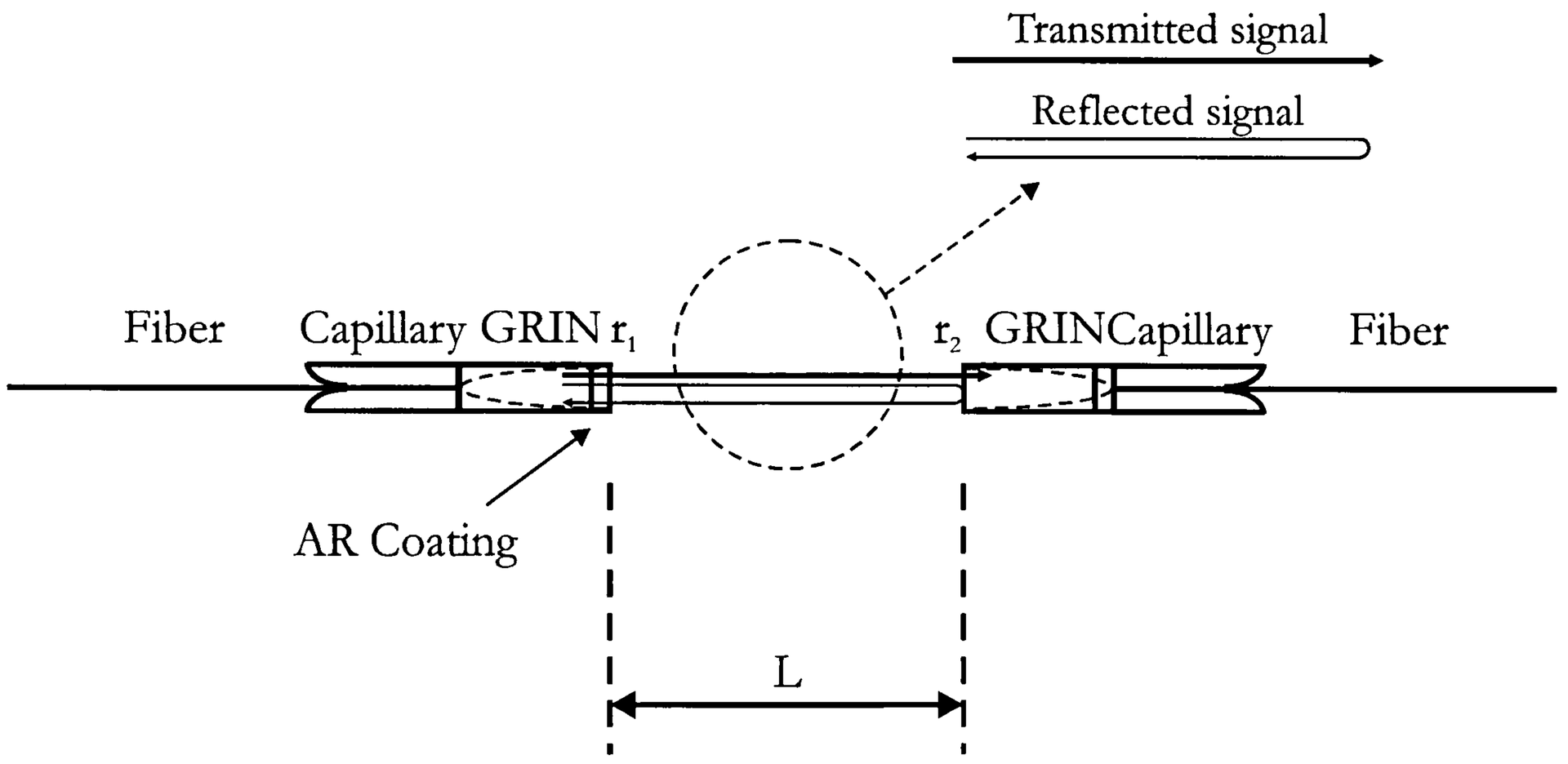

Figure 5.2: *Structure of the microoptic sensing cell*

For some of the proposed sensor systems the first GRIN lens is turned with the antireflection coating facing the non antireflection coated side of the second GRIN lens. Using such a set-up the backreflection from the first GRIN lens is minimised compared to the second GRIN lens. The main signal passes through the cell and is partially reflected from the second lens. The reflected signal passes the cell once again and is coupled into the input fibre. Typical values for r_1^2 and r_2^2 are 0.1% and 4% respectively.

5.1.2. Parasitic reflections inside the microoptic sensing cell

With parasitic reflections inside the microoptic cell the output signal at the receiving end of the fibre is composed of the original interference signal and the interference due to parasitic reflections (Figure 5.3).

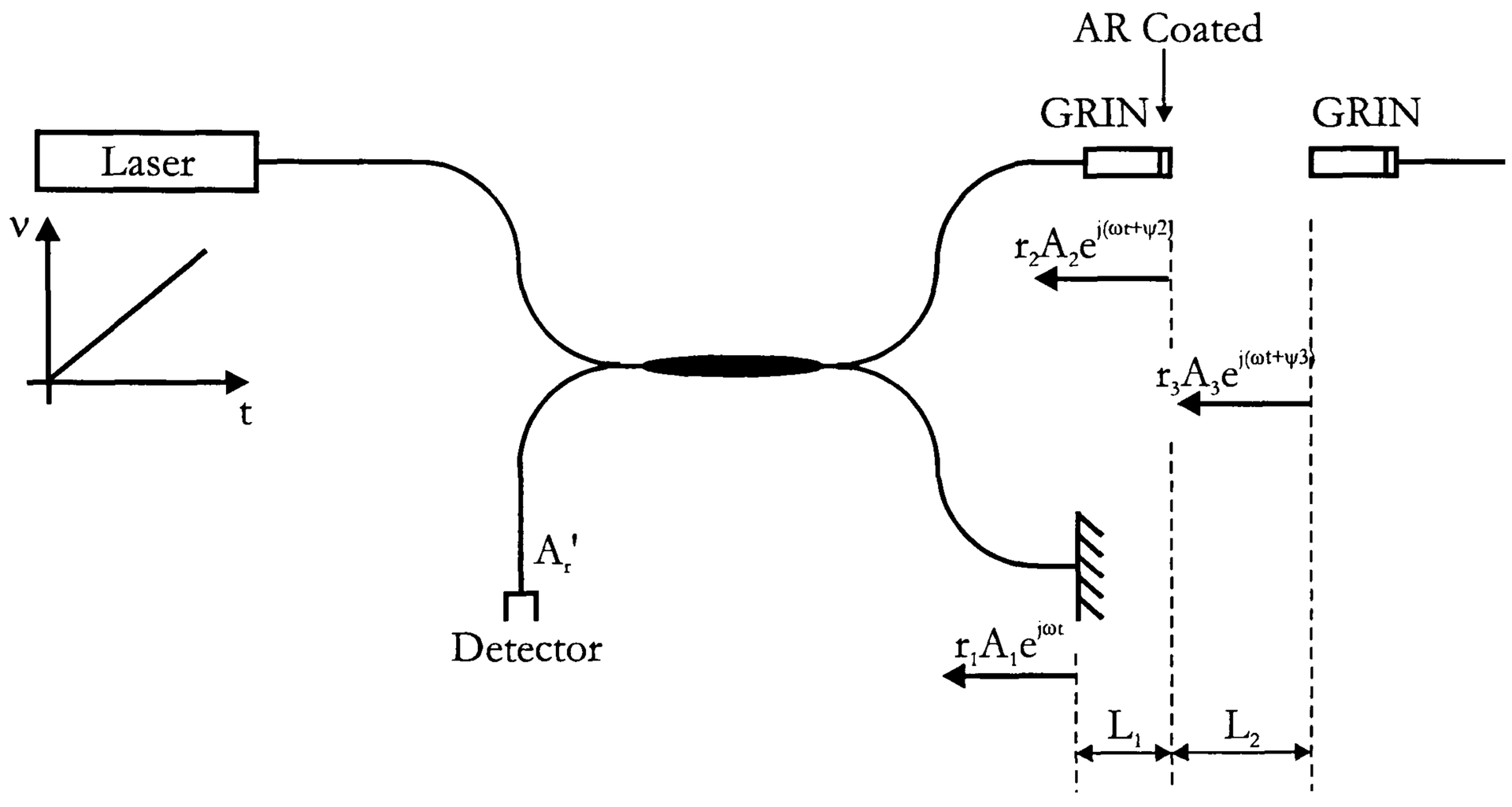

Figure 5.3: *FMCW configuration of the Michelson interferometer considering parasitic backreflections*

Major parasitic backreflection is caused by the first glass to air interface. Inspite of anti reflection coating on the GRIN lens, approximately 0.2% of incident light is backreflected. Equation (5.4) has to be rewritten in the following form

$$\Gamma_{out} \propto \left\langle A'_R \cdot A'^{*}_R \right\rangle \tag{5.7}$$

where

$$A'_R = r_1\sqrt{\left(A_1 + B_1 t\right)}e^{j\omega t} + r_2\sqrt{\left(A_2 + B_2 t\right)}e^{j(\omega t+\psi_2)} + r_3\sqrt{\left(A_3 + B_3 t\right)}e^{j(\omega t+\psi_3)} \tag{5.8}$$

The light intensity measured at the detector is:

$$I'_{out} = \left[r_1\sqrt{(A_1+B_1t)}e^{j\omega t} + r_2\sqrt{(A_2+B_2t)}e^{j(\omega t+\psi_2)} + r_3t_2t_2'\sqrt{(A_3+B_3t)}e^{j(\omega t+\psi_3)}\right]. \tag{5.9}$$

$$\left[r_1\sqrt{(A_1+B_1t)}e^{-j\omega t} + r_2\sqrt{(A_2+B_2t)}e^{-j(\omega t+\psi_2)} + r_3t_2t_2'\sqrt{(A_3+B_3t)}e^{-j(\omega t+\psi_3)}\right]$$

$$= r_1^2(A_1+B_1t) + r_2^2(A_2+B_2t) + r_3^2t_2^2t_2'^2(A_3+B_3t) +$$

$$2r_1r_2\sqrt{(A_1+B_1t)(A_2+B_2t)}\cos(\psi_2+\Delta\psi_2) +$$

$$2r_1r_3t_2t_2'\sqrt{(A_1+B_1t)(A_3+B_3t)}\cos(\psi_3+\Delta\psi_3) +$$

$$2r_2r_3t_2t_2'\sqrt{(A_2+B_2t)(A_3+B_3t)}\cos((\psi_2+\Delta\psi_2)-(\psi_3+\Delta\psi_3))$$

where

$$\psi_2+\Delta\psi_2 = \frac{2\pi}{\lambda_0}\left[\frac{2n_eL_1}{\lambda_0}\right](\lambda_0+\Delta\lambda) \tag{5.10}$$

$$\psi_3+\Delta\psi_3 = \frac{2\pi}{\lambda_0}\left[\frac{2n_eL_1}{\lambda_0}\right](\lambda_0+\Delta\lambda) + \frac{2\pi}{\lambda_0}\left[\frac{2n_{air}L_2}{\lambda_0}\right](\lambda_0+\Delta\lambda)$$

$$= \frac{2\pi}{\lambda_0}(\lambda_0+\Delta\lambda)\frac{2}{\lambda_0}\left[n_eL_1+n_{air}L_2\right]$$

The constants r_1, r_2 and r_3 represent reflection coefficients and t_2, t_2' transmission coefficients in each direction at the glass/air interface of the first GRIN lens. Here r_1 represents the reflection at the end of the reference arm and could be set arbitrary, and r_2 and r_3 are determined with the GRIN lenses inside the microoptic cell.

5.1.3. Microoptic cell absorption

When using the microoptic cell for sensing applications there are three major influences which cause variations of the output power. Previously derived expression for the output signal already includes modelling of the length of the cell and refractive index perturbations (5.9). Additional when radiation passes through

a layer of solid, liquid, or gas, certain frequencies may be selectively removed by *absorption*, a process in which electromagnetic energy is transferred to the atoms, ions, or molecules composing the sample. In general the absorption across a layer of length l is described using:

$$\mathrm{Out} = \mathrm{In} \cdot e^{-\alpha C \cdot l} \tag{5.11}$$

where *In* is the input signal, *Out* is the output signal, α is the absorption coefficient, C is concentration and l is the length of the absorption cell.

In accordance to (5.11) we have to modify the equation (5.9) and include the absorption term. Thus (5.9) becomes:

$$\begin{aligned} I'_{out} = {} & r_1^2(A_1 + B_1 t) + r_2^2(A_2 + B_2 t) + r_3^2 t_2^2 t_2'^2 (A_3 + B_3 t) e^{-2\alpha C L_2} + \\ & 2 r_1 r_2 \sqrt{(A_1 + B_1 t)(A_2 + B_2 t)} \cos(\psi_2 + \Delta\psi_2) + \\ & 2 r_1 r_3 t_2 t_2' \sqrt{(A_1 + B_1 t)(A_3 + B_3 t)} e^{-\alpha C L_2} \cos(\psi_3 + \Delta\psi_3) + \\ & 2 r_2 r_3 t_2 t_2' \sqrt{(A_2 + B_2 t)(A_3 + B_3 t)} e^{-\alpha C L_2} \cos((\psi_2 + \Delta\psi_2) - (\psi_3 + \Delta\psi_3)) \end{aligned} \tag{5.12}$$

5.1.4. Parameter examination for one sensor coherent FMCW

To obtain a detailed overview of how parameters such as reflection coefficients, cell length, modulation frequency etc. influence the output interference signal and the corresponding power spectrum a number of simulations have been accomplished using the *Mathematica* program for math analysis. For single sensor set-up the following parameters have been investigated:

- individual reflection coefficients
- cell length
- modulation frequency of the laser source

- wavelength change due to modulation
- change in the amplitude of the output light due to current modulation
- absorption inside the microoptic cell
- shape of the current modulation

To compare individual results within single sensor parameter investigation a "reference" interferometer signal and its spectrum were obtained using the following parameters: $L_2 = 20mm$, $L_1 = 10mm$, $\Delta\lambda = 0.7nm$, linear ramp $f_{mod} = 20Hz$, $r_1^2 = 0.9$, $r_2^2 = 0.005$ and $r_3^2 = 0.1$, $\lambda_0 = 1300nm$ and constant $B = 1$. The output in time and frequency domain is shown in Figure 5.4.

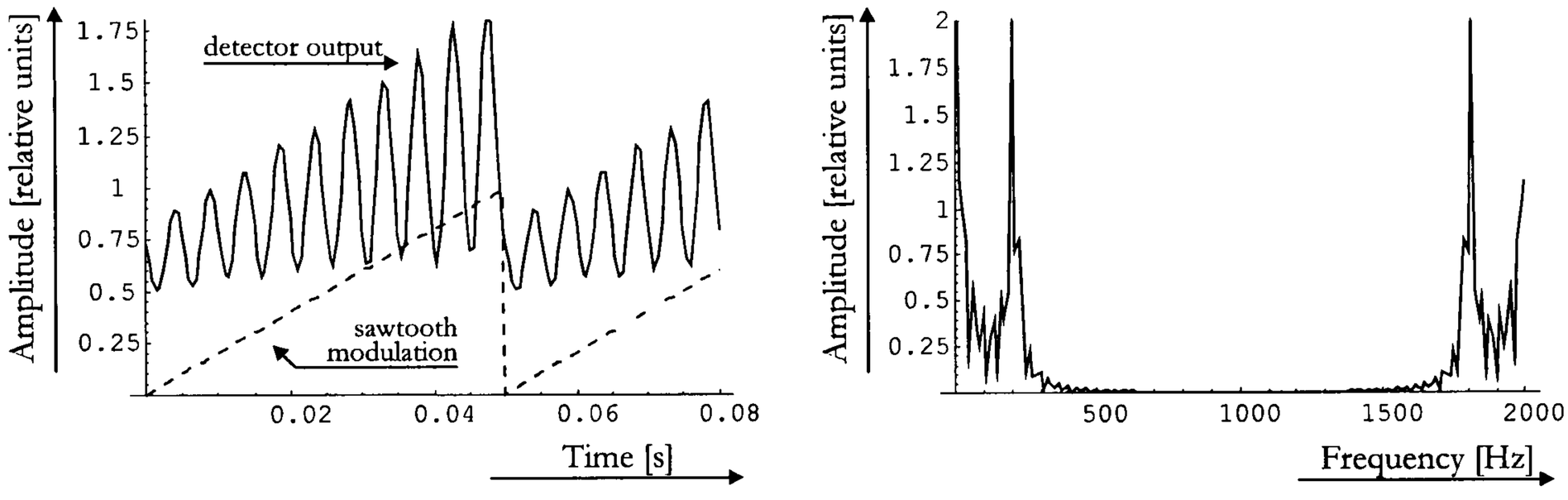

Figure 5.4: *Reference interferometer signal: (a) detector output and sawtooth signal versus time; (b) output power spectrum*

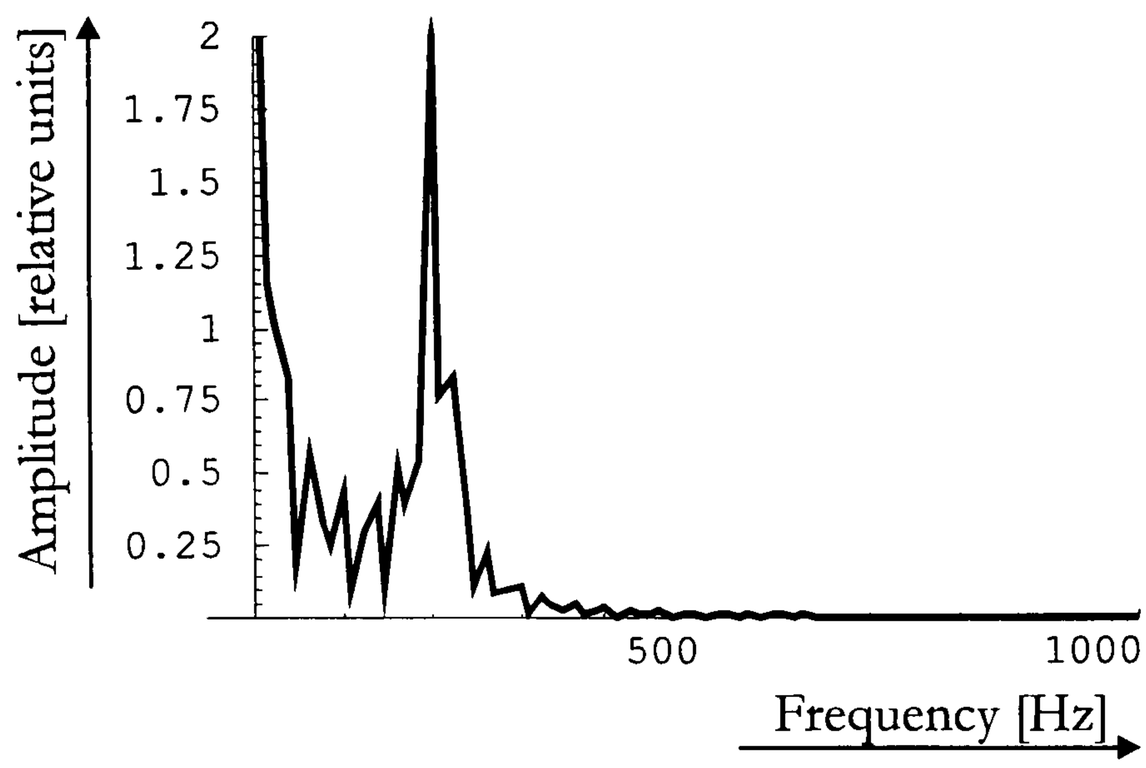

Figure 5.5: *Correct interferometer spectrum representation*

Due to the digital Fourier transformation the spectral output has a symmetric shape across the frequency axis (Figure 5.4b). The discrete Fourier transform (DFT) is performed in 160 points with a sampling time of 0.0005s which corresponds to a maximum frequency of 2000Hz. For the analysis only the first half of the spectrum is representative. The reason that the number of frequencies is only half is that if the values of f(t) are real (as usually when we record physical quantities) there are N real data values. Now the transform has N complex values which would require 2N real numbers to specify, except that F(0) and F(N) have no imaginary part and half the remaining values of F(η) are complex conjugate of the other half. This is because f(t) is real. Due to that the relevant part of the power DFT spectrum is only the first half, since the modulus of the conjugate part is the same. The correct interferometer spectrum is presented in Figure 5.5.

Although that subsequent power spectrums will be presented as shown in Figure 5.4b we have to keep in mind that only the first half is relevant for the analysis. Ordinate and abscise axes on next graphs do not have special legends, however they all correspond to legends as presented in Figure 5.4. Pictures on the left side represent the signal on the detector in time domain, and pictures on the right represent the power spectrum of the detector signal in frequency domain.

5.1.4.1.Influence of reflection coefficients

For the first set of simulations the reference arm backreflection coefficient was changed while the other two where held constant. From Figure 5.6 we can see, that the shape of the interference and spectrum signals remained almost unchanged, only with reference arm backreflection reduction the amplitude of both signals is decreasing.

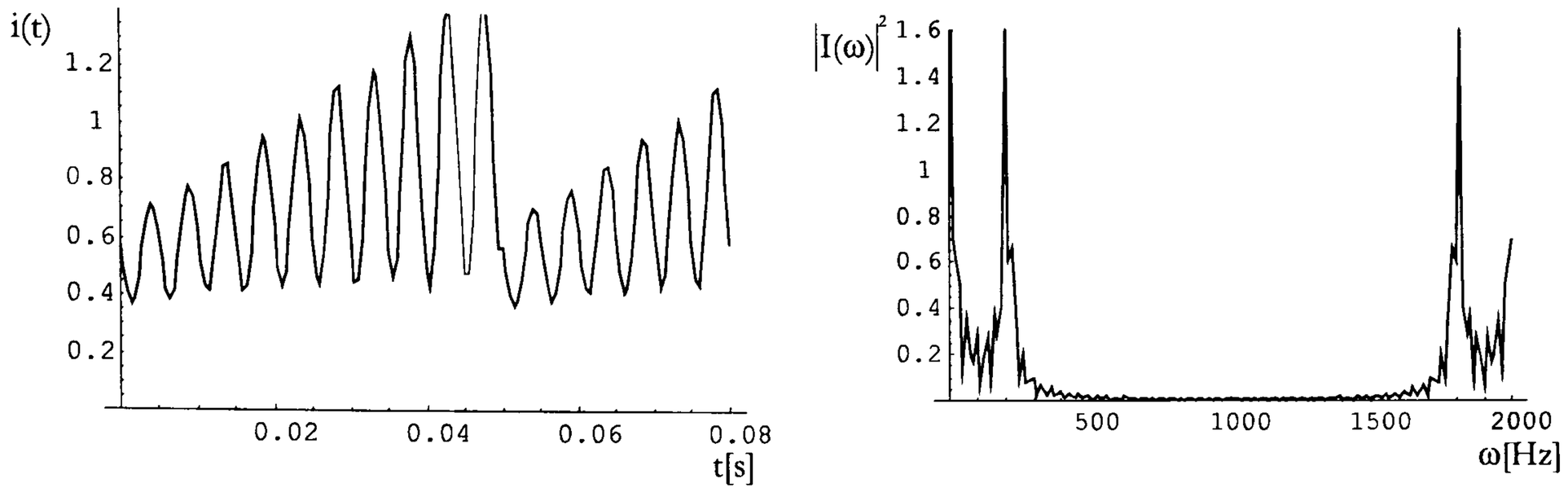

$r_1^2=0.7,\ r_2^2=0.005,\ r_3^2=0.1$

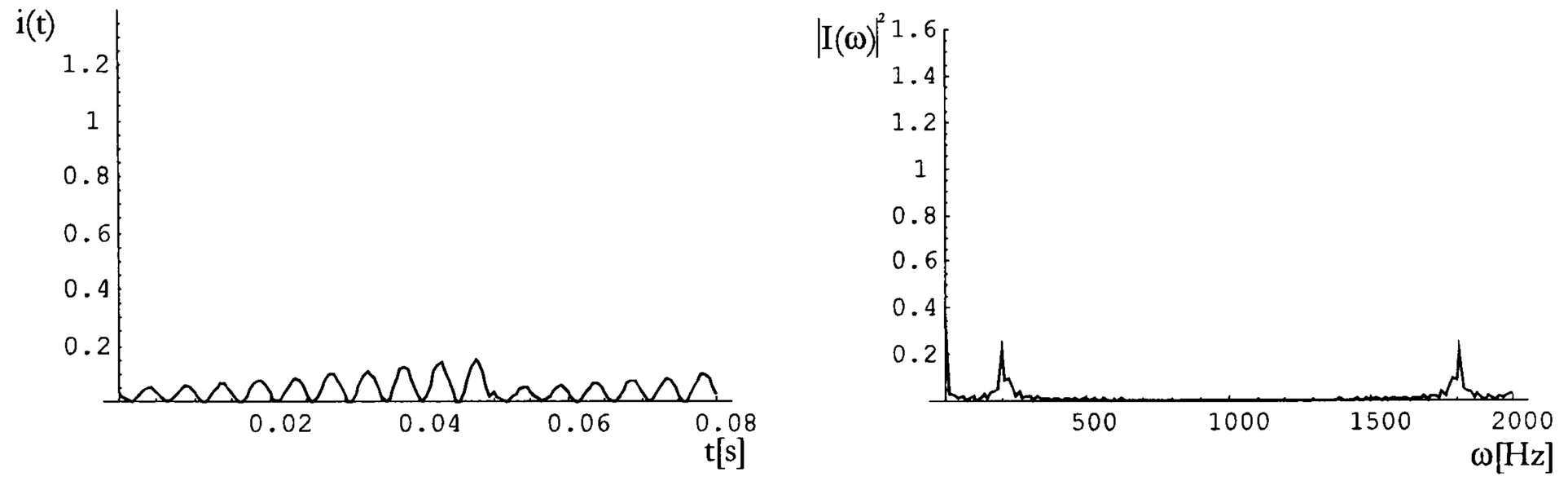

$r_1^2=0.1,\ r_2^2=0.005,\ r_3^2=0.1$

Figure 5.6: *Output versus time (left) and corresponding power spectrum in frequency domain (right) for reference arm backreflection reduction*

In the next set the reference arm backreflection was changed back to the reference level and the backreflection of the first GRIN lens was altered. From Figure 5.7 a new spectral component from the frequency as well as time domain is observed. Due to first GRIN lens backreflection enlargement an additional interferometer is introduced.

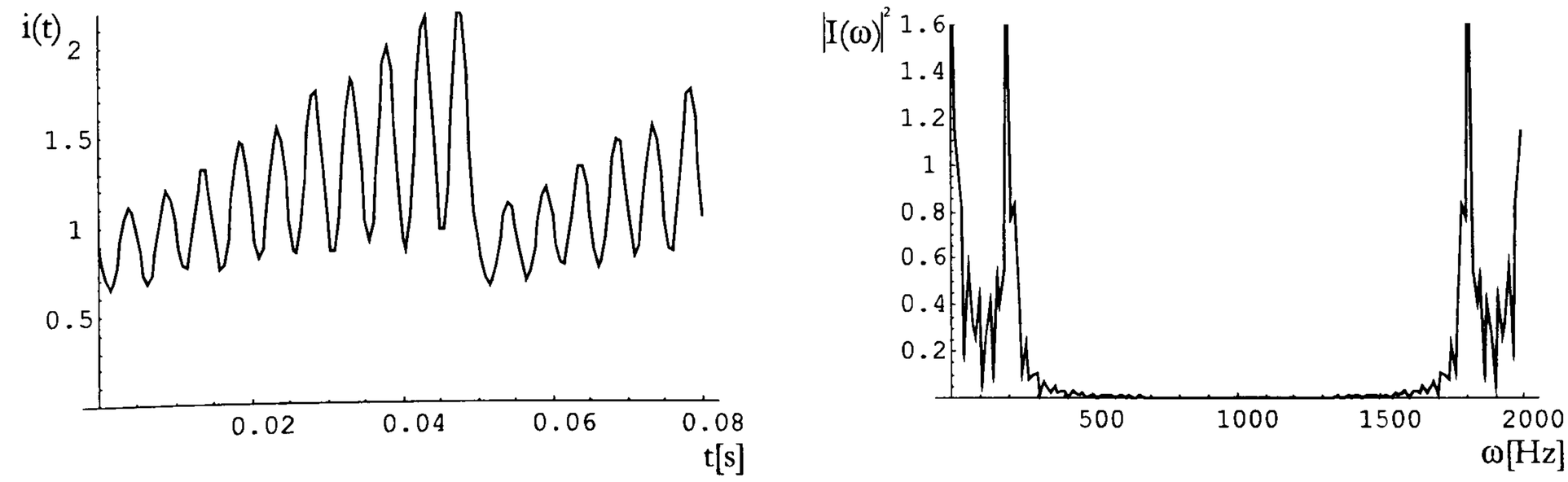

$r_1^2=0.9,\ r_2^2=0.009,\ r_3^2=0.1$

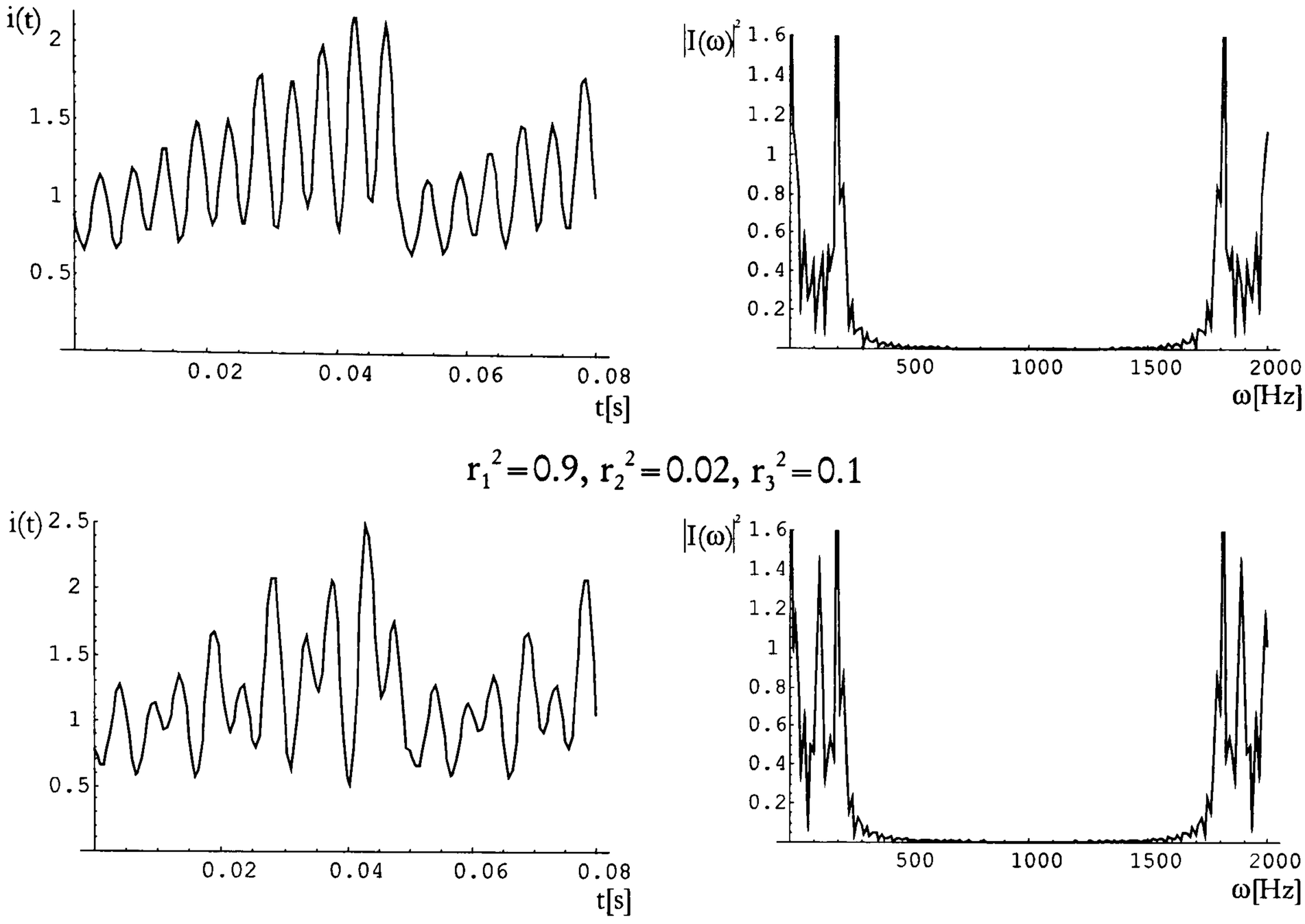

Figure 5.7: *Output versus time (left) and corresponding power spectrum in frequency domain (right) for first GRIN lens backreflection enlargement*

The first GRIN lens backreflection enlargement gives rise to a new interferometer which is presented as an additional spectral peak in the last spectral response in Figure 5.7. To avoid these ghost signals in final sensor set-up (for one of the possible configuration, i.e. reference arm configuration) the backreflection of the first GRIN lens must be maintained as low as possible.

For final simulation examination of reflection coefficients, again the reflection from the reference arm and the reflection for the first GRIN lens were kept constant and the backreflection of the second GRIN lens has been reduced. Figure 5.8 shows the appropriate time and frequency signals. With the backreflection reduction of the second GRIN lens the interference term is vanishing and is almost totally lost for values around $r_3^2=0.01$ (second power spectrum in Figure 5.8).

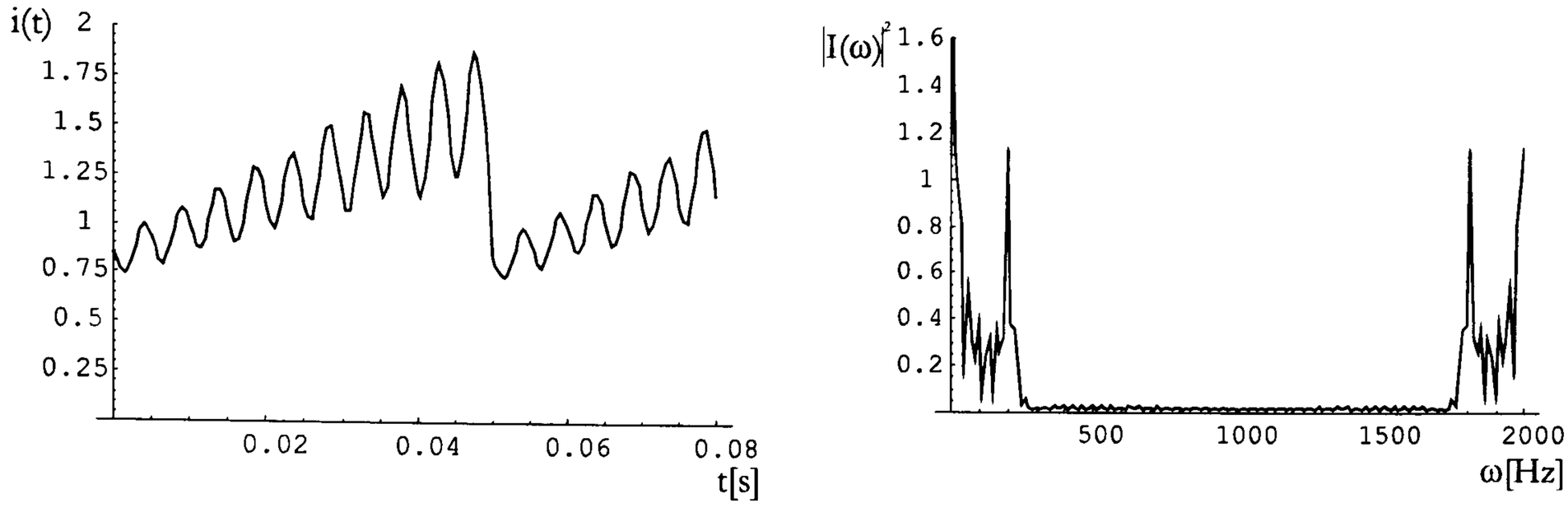

$r_1^2=0.9$, $r_2^2=0.005$, $r_3^2=0.05$

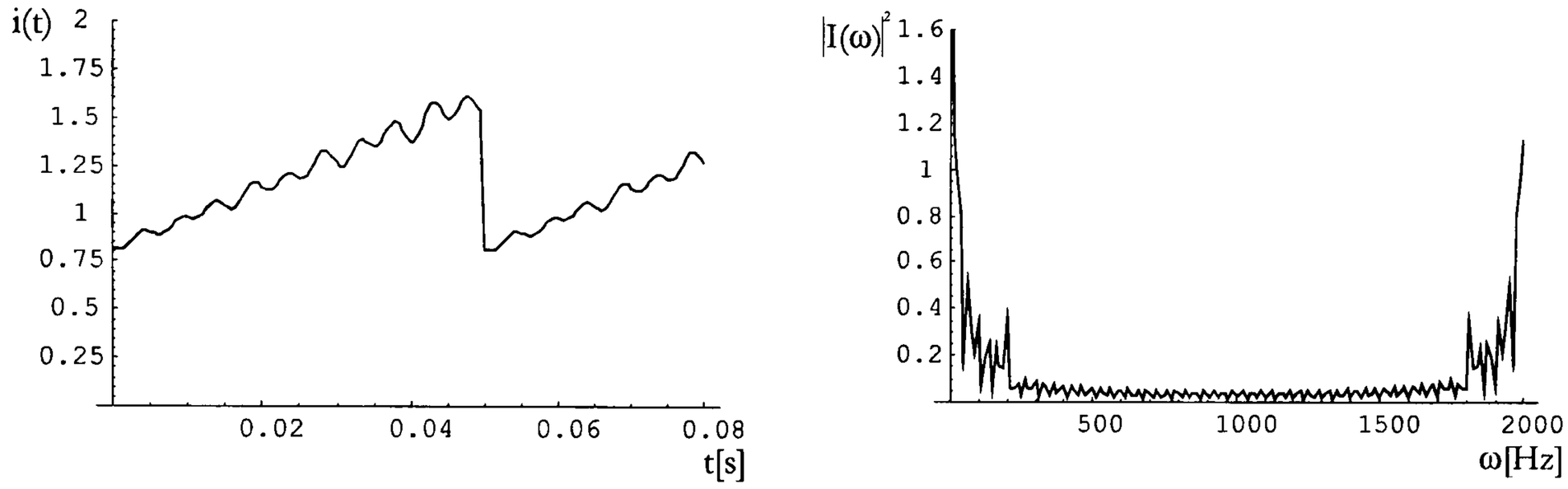

$r_1^2=0.9$, $r_2^2=0.005$, $r_3^2=0.01$

Figure 5.8: *Output versus time (left) and corresponding power spectrum in frequency domain (right) for second GRIN lens backreflection reduction*

5.1.4.2.Influence of cell length (separation between both GRIN lenses)

The length of the sensing microoptic cell depends on the final system configuration and sensitivity requirements. For the simulations the reflection coefficients were set to the "reference" level ($r_1^2=0.9$, $r_2^2=0.005$ and $r_3^2=0.1$) and the distance between the GRIN lenses was increased. According to the equation (4.9) the beat frequency is increasing. The same can be observed from time and frequency responses shown in Figure 5.9.

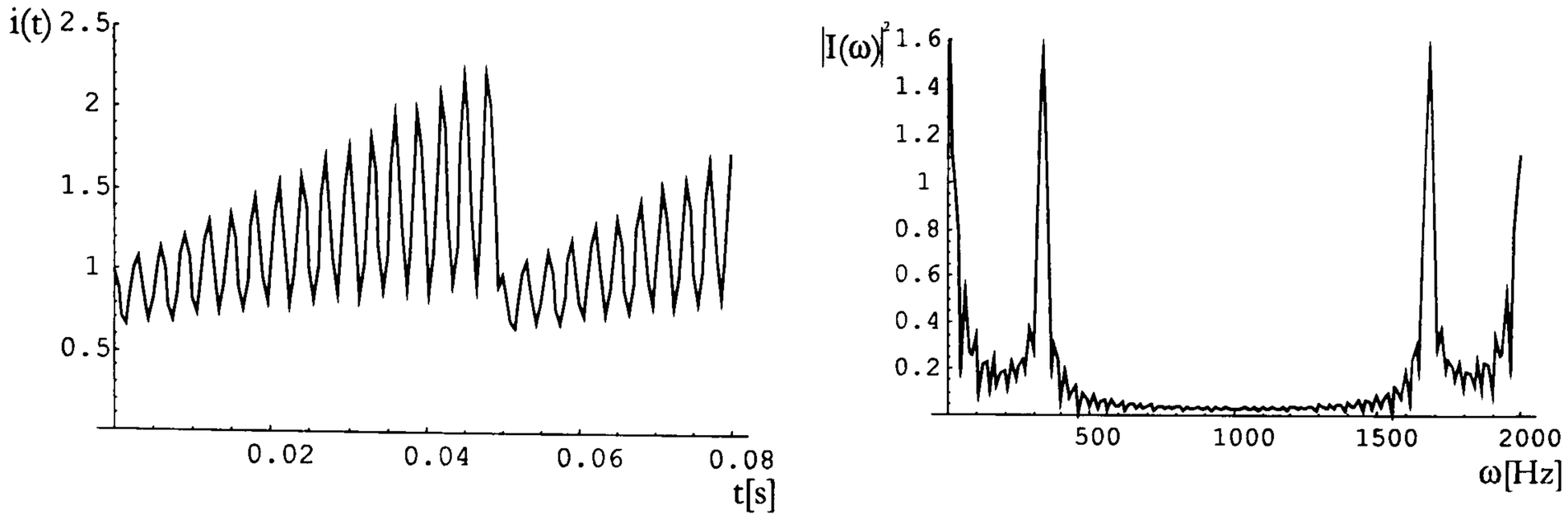

$L_2 = 20\text{mm}, f_{beat} = 331\text{Hz}$

$L_2 = 30\text{mm}, f_{beat} = 497\text{Hz}$

$L_2 = 40\text{mm}, f_{beat} = 662\text{Hz}$

Figure 5.9: *Output versus time (left) and corresponding power spectrum in frequency domain (right) for different separations between the GRIN lenses*

Due to the increase in cell length the beat frequency increases and the peak is shifted to the right. This phenomena will be further used later for coherence addressing, when different techniques of cell addressing are proposed.

5.1.4.3.Change in the modulation frequency of the laser source

In the previous chapter we have derived equation (4.6) which determines the beat frequency in a FMCW system. Since the ramping frequency of the laser source is one of the variables used in (4.6) here influences of the modulation frequency on the output will be presented. For the final sensing system where spectral analysis detection will be used, low values of the beat frequency are desirable in order to build a simple and inexpensive device. Low modulation frequencies together with a small distance between the GRIN lenses enable simple detection with beat frequencies under 5kHz.

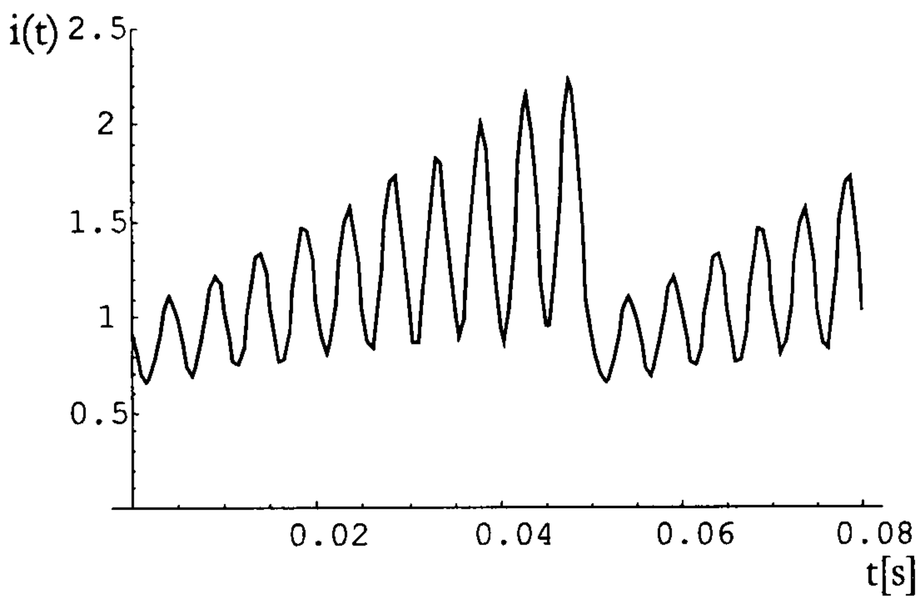

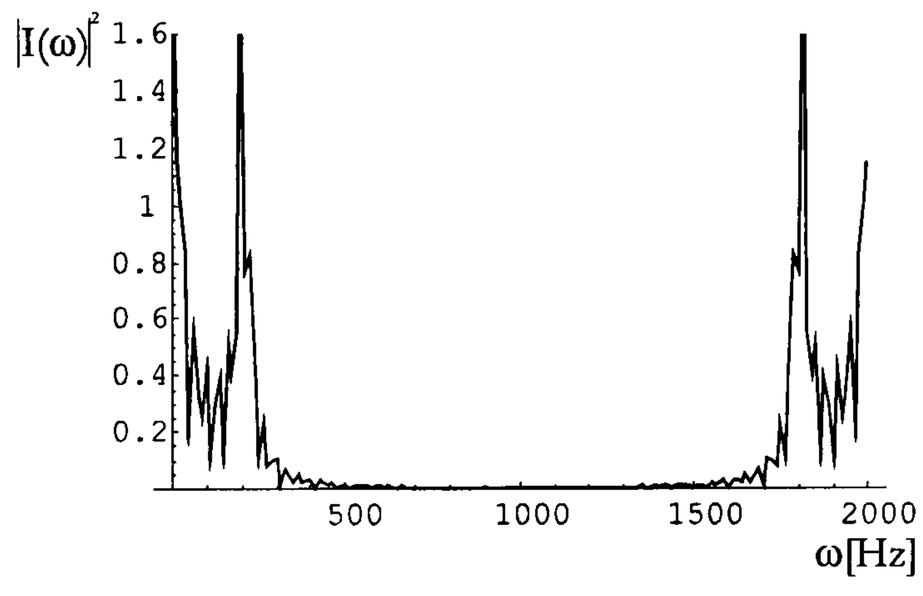

$f_{mod} = 20Hz$

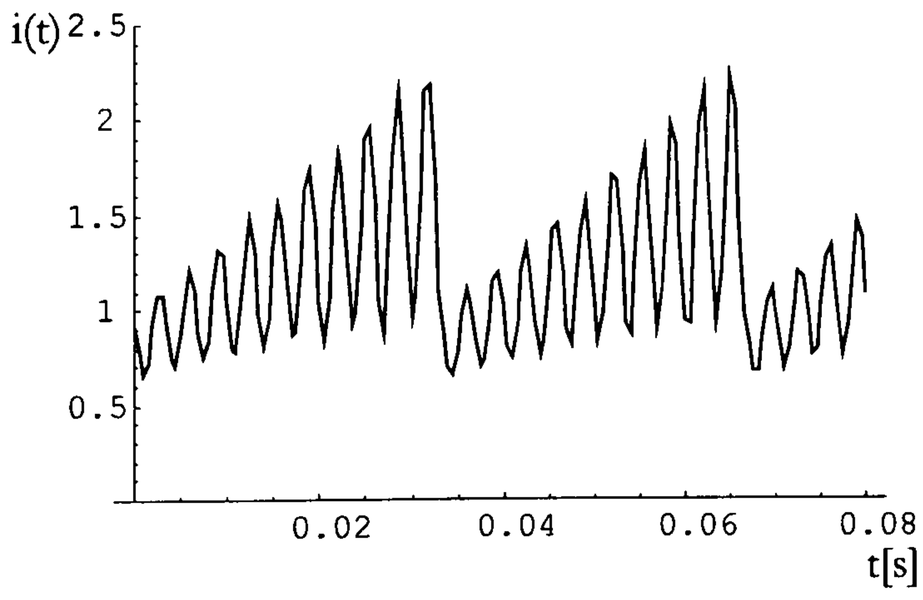

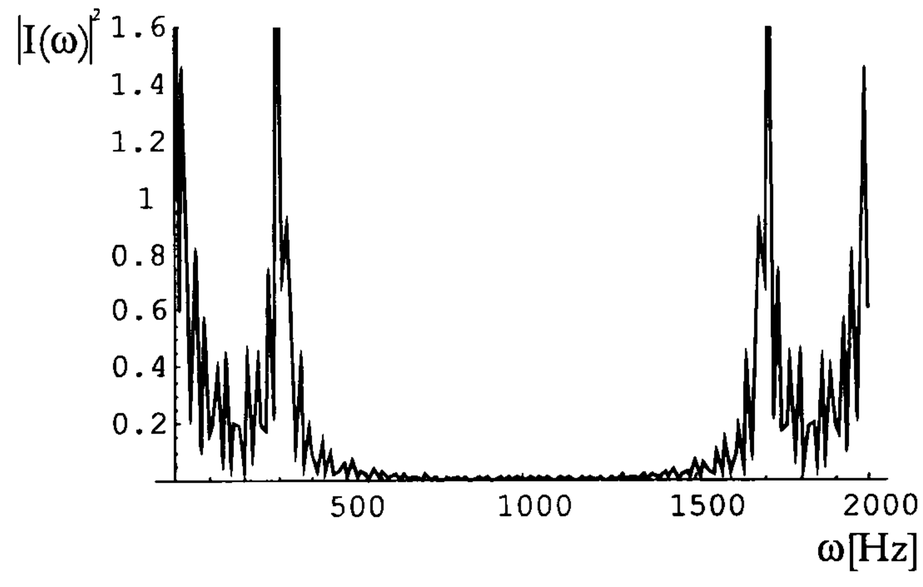

$f_{mod} = 30Hz$

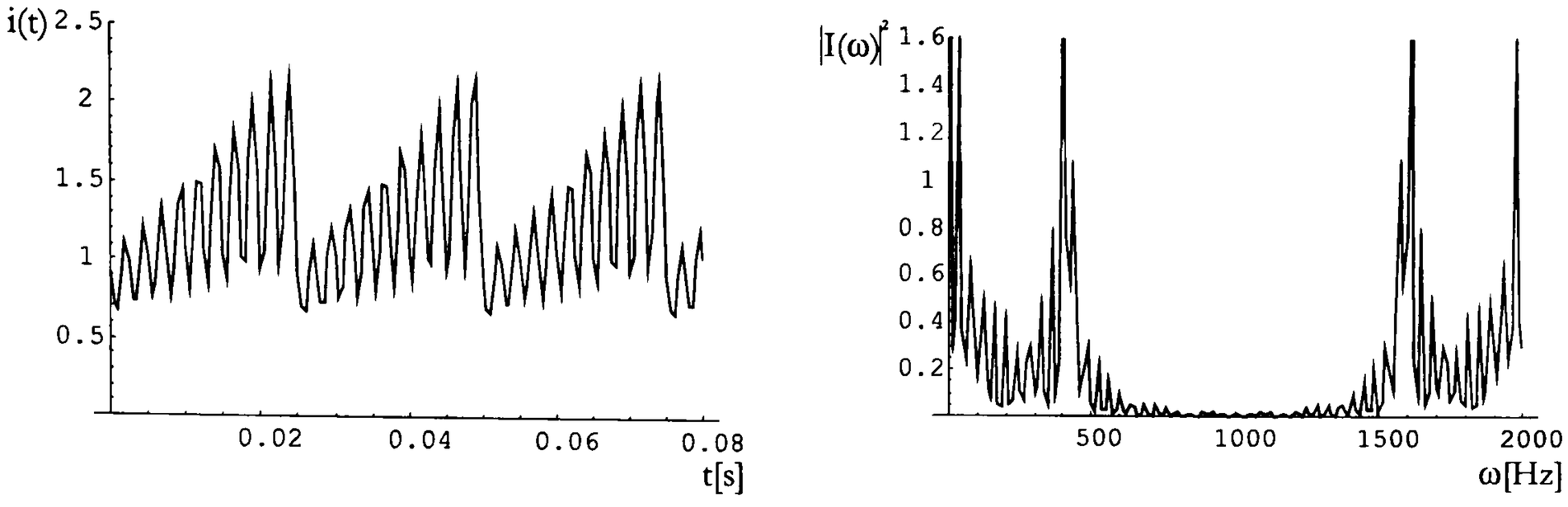

$$f_{mod} = 40Hz$$

Figure 5.10 *Output versus time (left) and corresponding power spectrum in frequency domain (right) using different laser modulation frequency*

Figure 5.10 represents time and frequency domain outputs using different laser modulation frequency. The parameters are set as $L_2 = 20mm$, $L_1 = 10mm$, $\Delta\lambda = 0.7nm$, $r_1^2 = 0.9$, $r_2^2 = 0.005$ and $r_3^2 = 0.1$, $\lambda_0 = 1300nm$ and constant $B = 1$.

As expected the beat frequency shifts to higher frequencies as the modulation frequency is increased.

5.1.4.4. Wavelength change due to modulation

When the laser diode is current modulated the wavelength changes according to the depth of the current modulation. For simulations the wavelength change due to modulation has been altered from 0.1nm to 1nm. The results are shown in Figure 5.11.

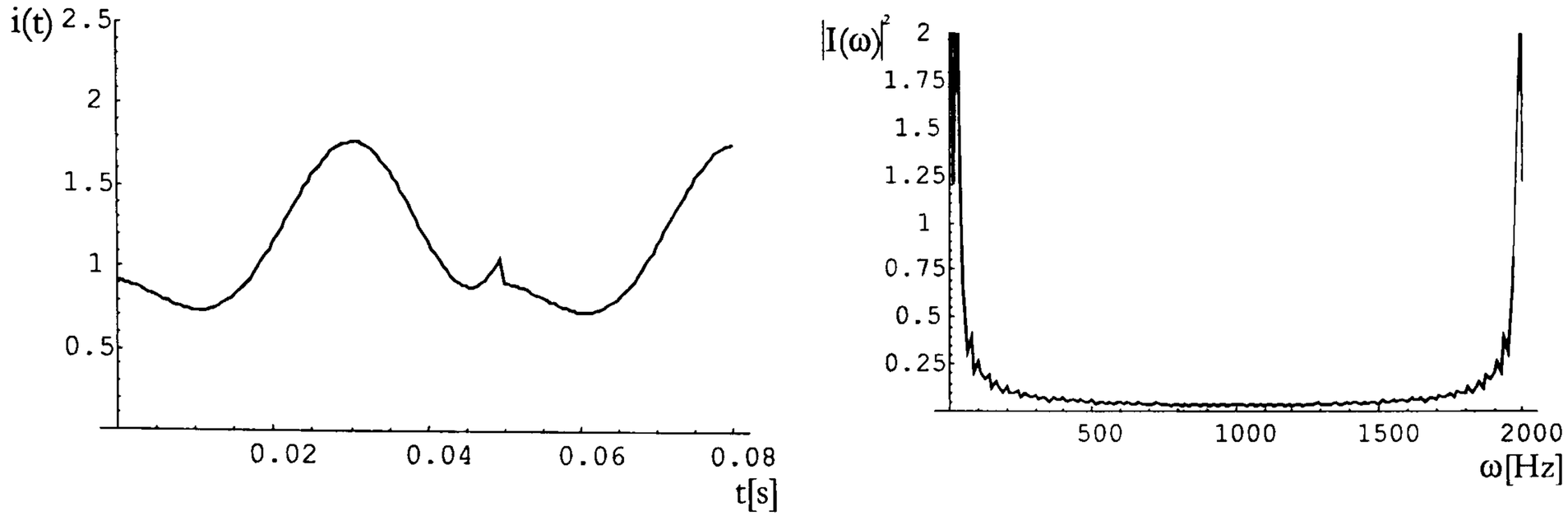

Figure 5.11 *Output versus time (left) and corresponding power spectrum in frequency domain (right) for different wavelength changes due to modulation*

The peak of the beat frequency shifts to higher frequencies when the depth of the current modulation is increased. To minimize the amplitude change one might choose small current modulation, but increase f_{mod} to give a sufficient high beat frequency.

5.1.4.5.Change in the amplitude of the output light due to current modulation

As stated with (5.3) current ramping of the laser diode results not only in a change in the output light frequency but also in the output light amplitude A_r change. Under this conditions a set of simulation experiments has been accomplished to show the influence of laser diode amplitude change (Figure 5.12). Here the constant B represents the change in amplitude of the light signal due to current ramping.

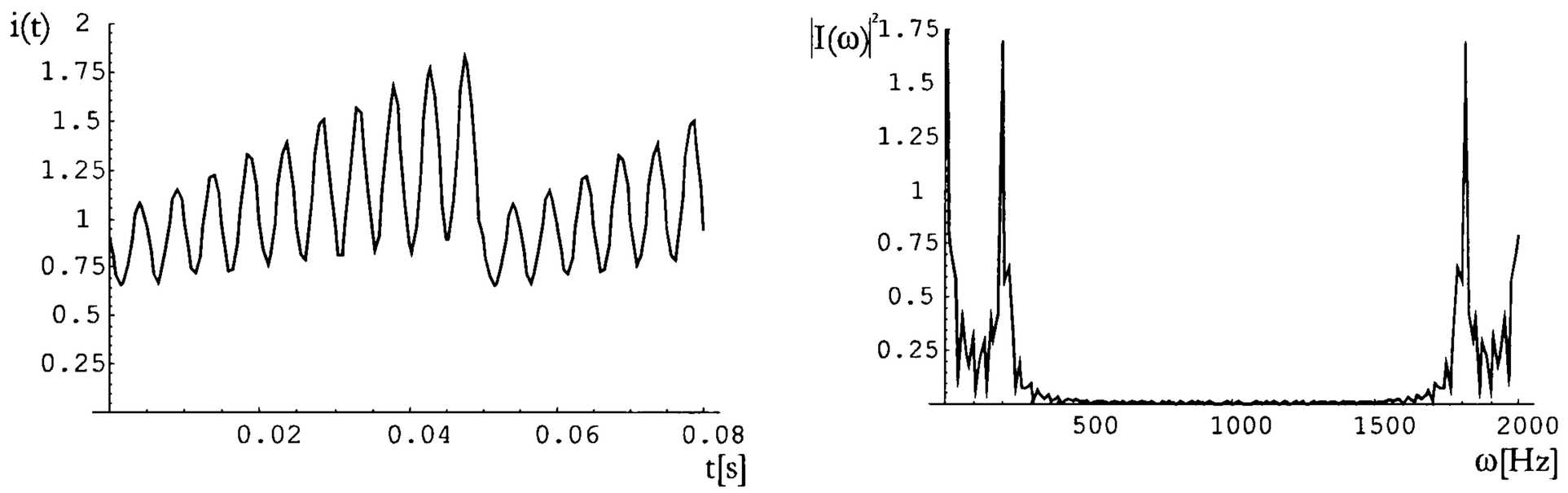

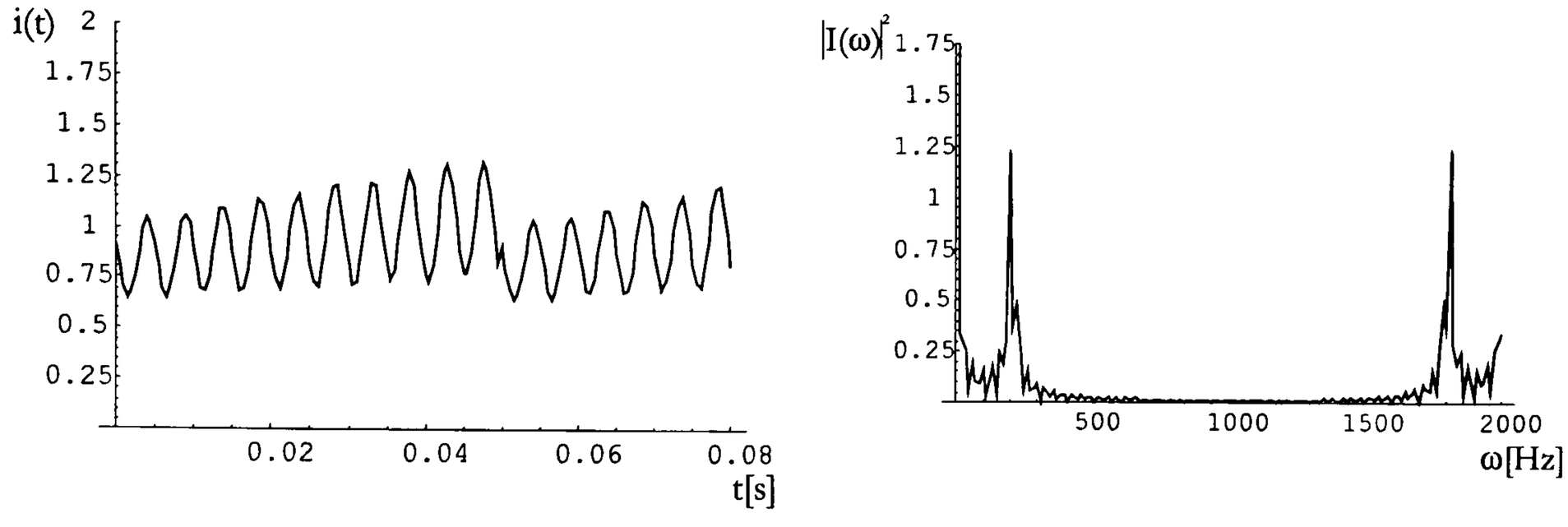

Figure 5.12: *Output versus time (left) and corresponding power spectrum in frequency domain (right) for different values of change in amplitude of the light signal due to current ramping (B)*

The influence of the current modulation on the laser diode output amplitude has almost no influence on the spectral characteristics and could be neglected. The spectrum remains almost constant with small amplitude drops for reduced change in amplitude of the light signal due to current ramping.

5.1.4.6.Absorption inside the microoptic cell

The absorption inside the microoptic cell should influence the spectral amplitude of the beat frequency. To compare a cell with and without absorption, additional to previous simulations the spectrum difference between the "reference" cell (the power spectrum for the "reference" cell without absorption has been presented in Figure 5.4b) and sensing cell (measured absorption) has been included (Figure 5.13).

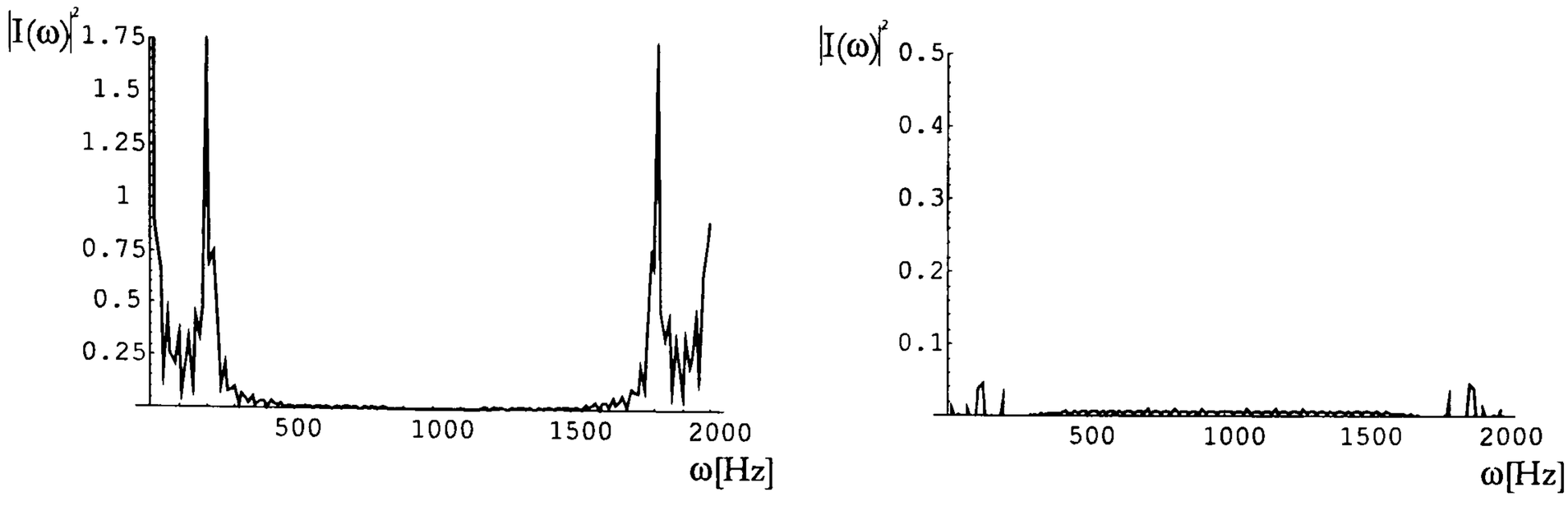

Absorbtion = 0.01%

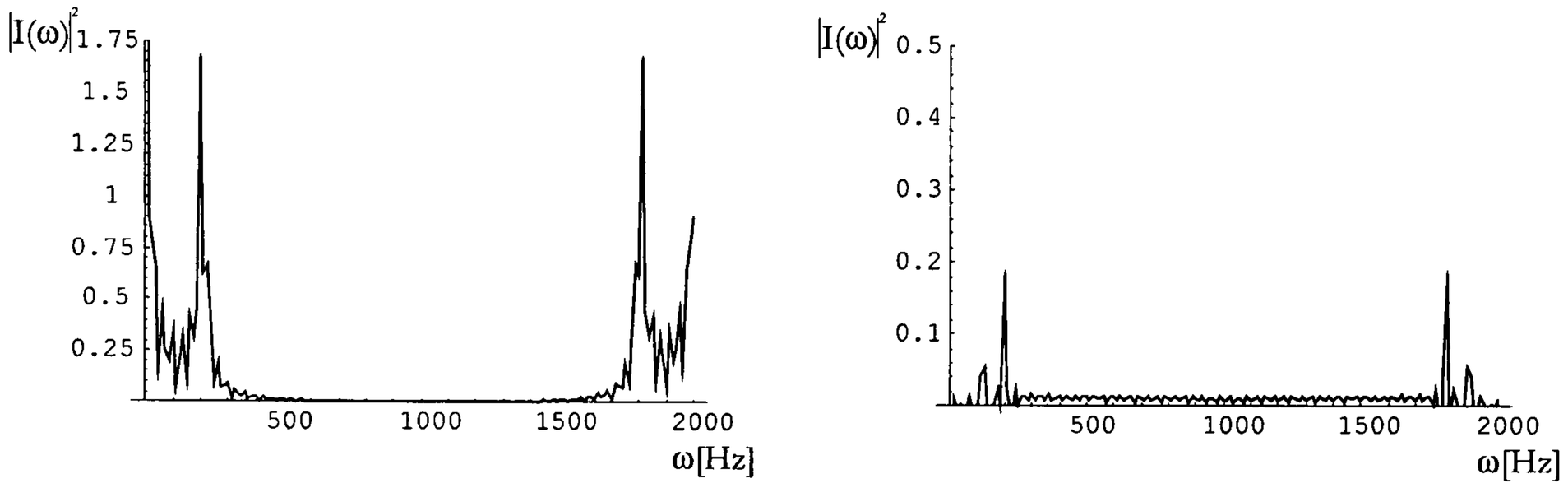

Absorbtion = 0.1%

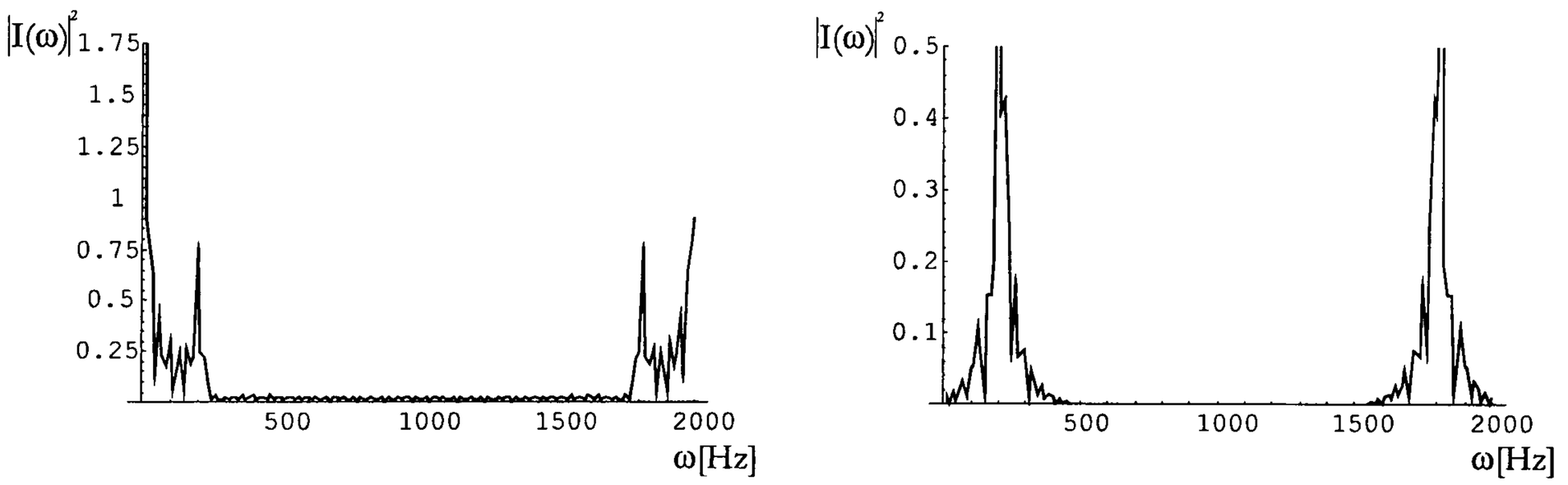

Absorbtion = 1%

Figure 5.13 *Measured power spectrums for different levels of absorption; output power spectrum with absorption (left), difference between the output spectrum without absorption and current measured power spectrum (right)*

As expected, with increase of the absorption the amplitude of the difference between the reference and measured spectrum is increasing. The shape remains identical and is not absorption dependent.

5.1.4.7. Shape of the current modulation

Thermally induced contributions to an optical-frequency variation with injection current is dominant at low-frequency modulation (< 1MHz), with the maximum value in the current-modulation transfer function [5.1]. Since the laser current modulation must be limited between the threshold and the maximum current by power dissipation, the given optical modulation must be limited accordingly. A linear sweep must be obtained either by sawtooth-shaped or triangular modulation. The discontinuity of the current modulation produces high-frequency harmonics. The direct effect of the sweep rate variation is the broadening of the peak produced by reflection in the Fourier transform of the signal. For all preceding evaluations a saw tooth modulation of the laser current has been used. The other possibility to obtain a linear sweep could be the use of triangular current modulation. In the simulation experiments both modulations were tested in order to get an insight on how modulation affects the spectral distribution. For comparison with the linear sweep, a nonlinear sweep was introduced using sinusoidal current modulation. The results are presented in Figure 5.14.

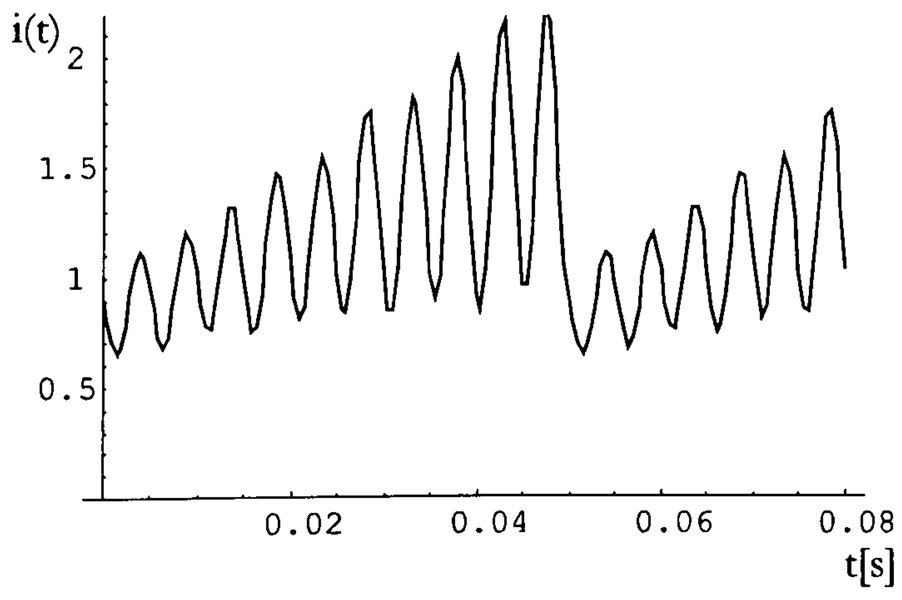

(a) sawtooth modulation, f_{mod} = 20Hz

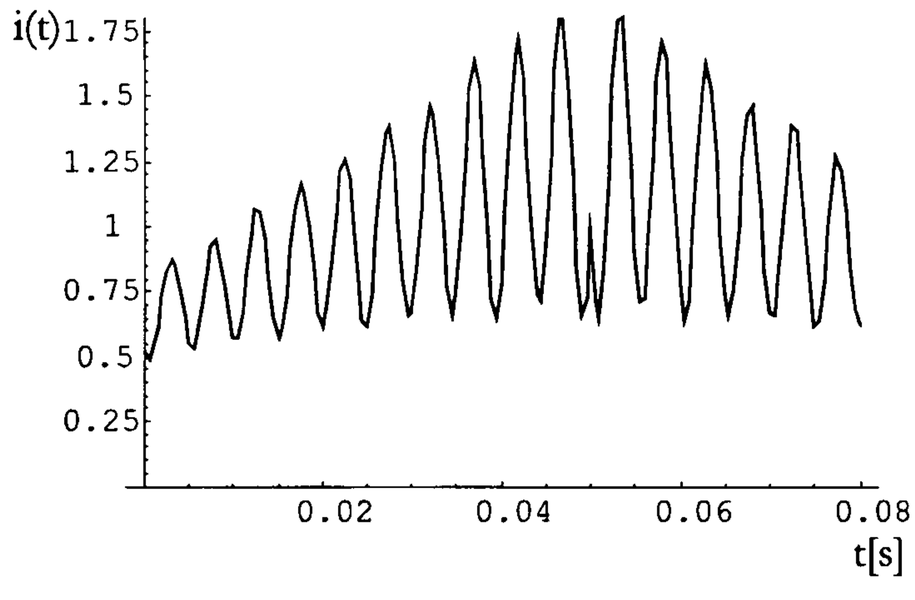

(a) triangular modulation, f_{mod} = 20Hz

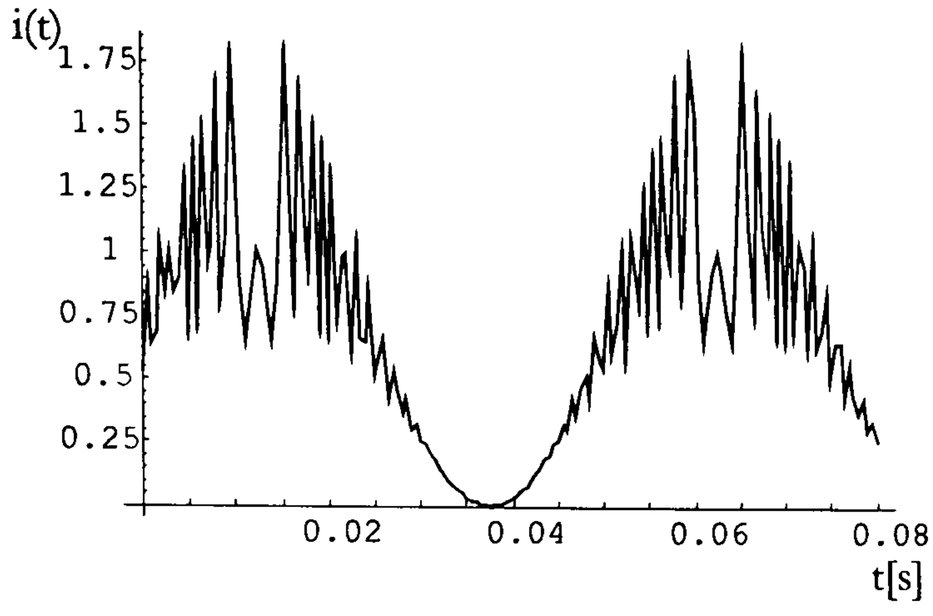

(a) sinusoidal modulation, f_{mod}=20Hz

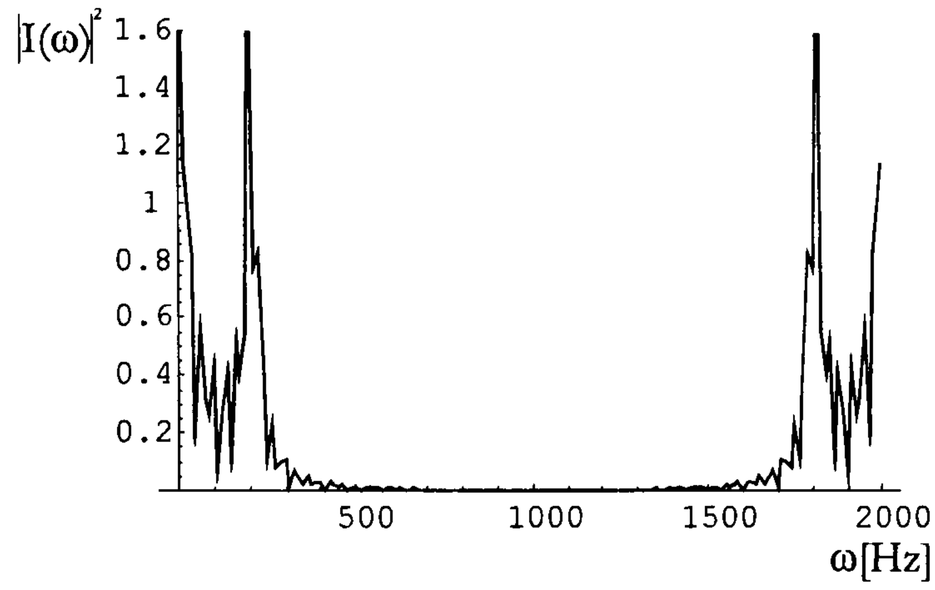

(b) sawtooth modulation, f_{mod}=20Hz

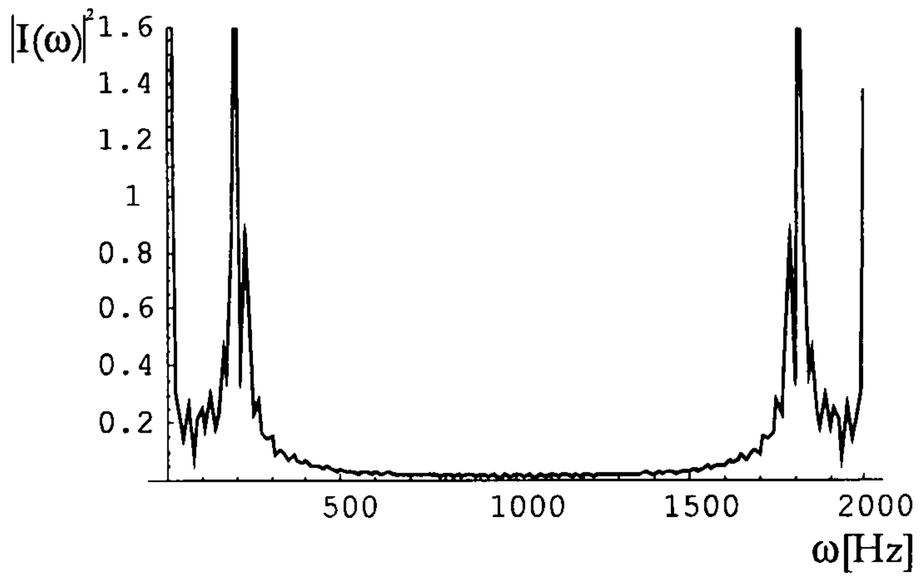

(b) triangular modulation, f_{mod}=20Hz

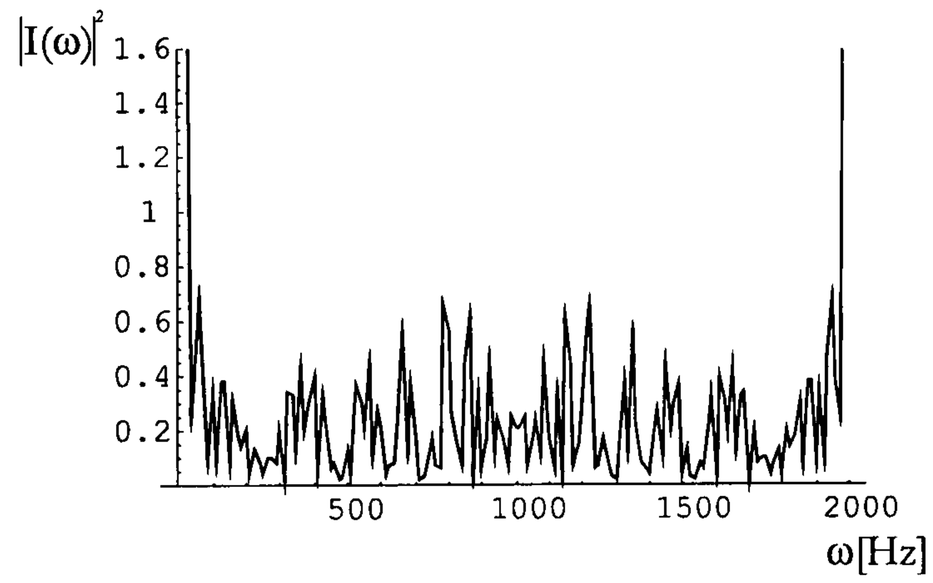

(b) sinusoidal modulation, f_{mod}=20Hz

Figure 5.14: *(a) output versus time and (b) corresponding power spectrum in frequency time for different shapes of current modulation*

The results for the sawtooth and triangular modulation are very similar. Both techniques enable a good signal to noise level. Comparing the spectrum difference between the reference cell without absorption and sensing cell with some absorption, the triangular modulated system has a slightly smoother signal difference, probably because of the smaller discontinuity of the current modulation signal. Regardless of that, both linear modulations could be used for

further system design without any hesitation. For non-linear modulation of the laser source we were not able to obtain any results of practical significance.

In practice, the sawtooth (or triangular) modulation will not be perfectly linear. To determine the tolerable nonlinearity simulations for a diversity of maximum differences and hence nonlinearities have been accomplish. The driving current was modified as presented in Figure 5.15.

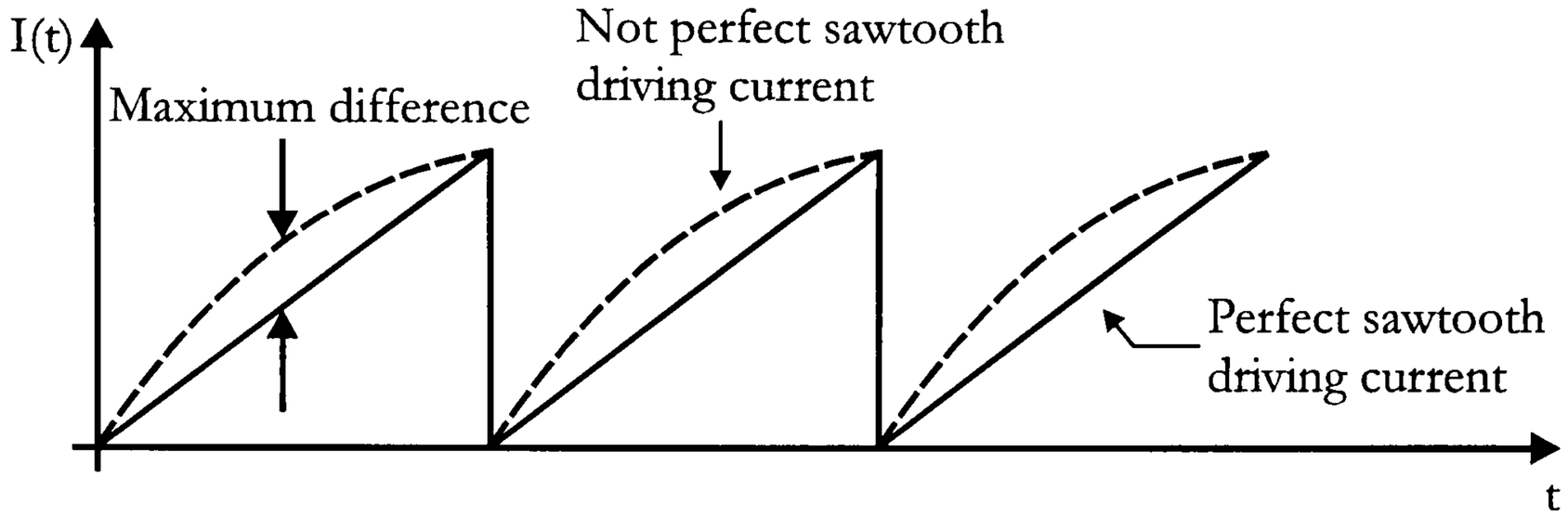

Figure 5.15: *Non perfectly linear sawtooth modulation*

The maximum difference between the perfect and non perfect sawtooth modulation (MDSM) was changed between 0.1% and 30% of the ideal half period value. The corresponding sawtooth shape in the time domain and the interferometer power spectrum are shown in Figure 5.16.

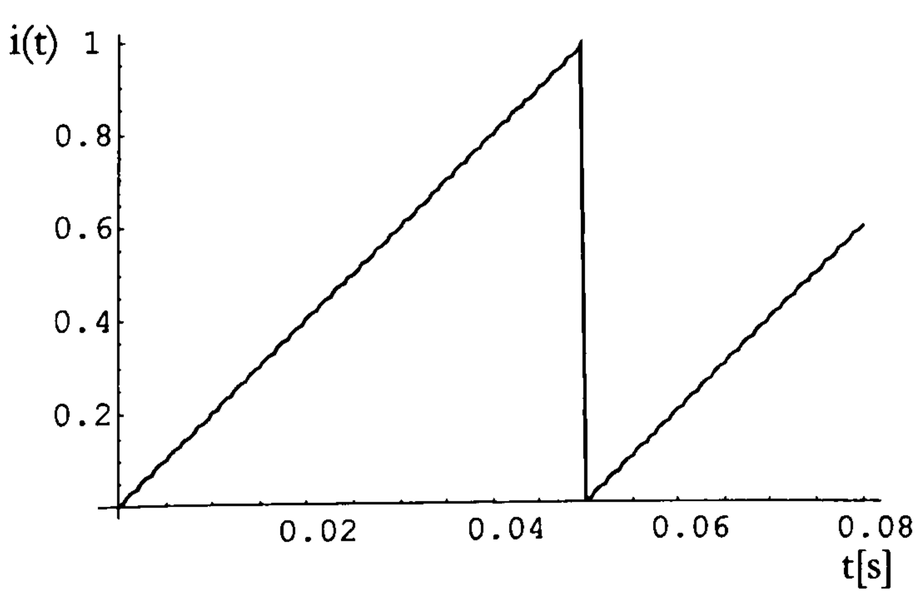

sawtooth shape in time domain

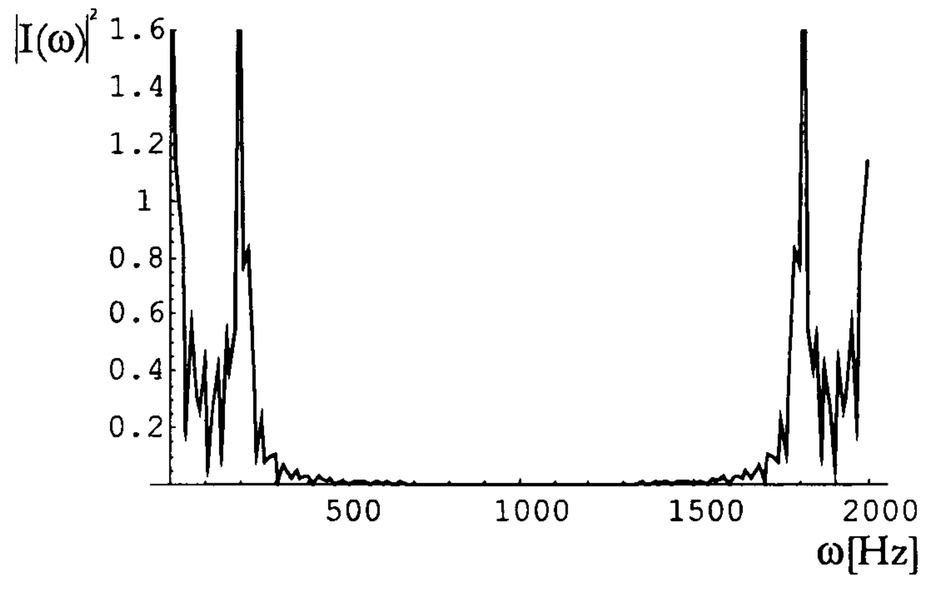

interferometer spectral response

MDSM = 0, ideal case

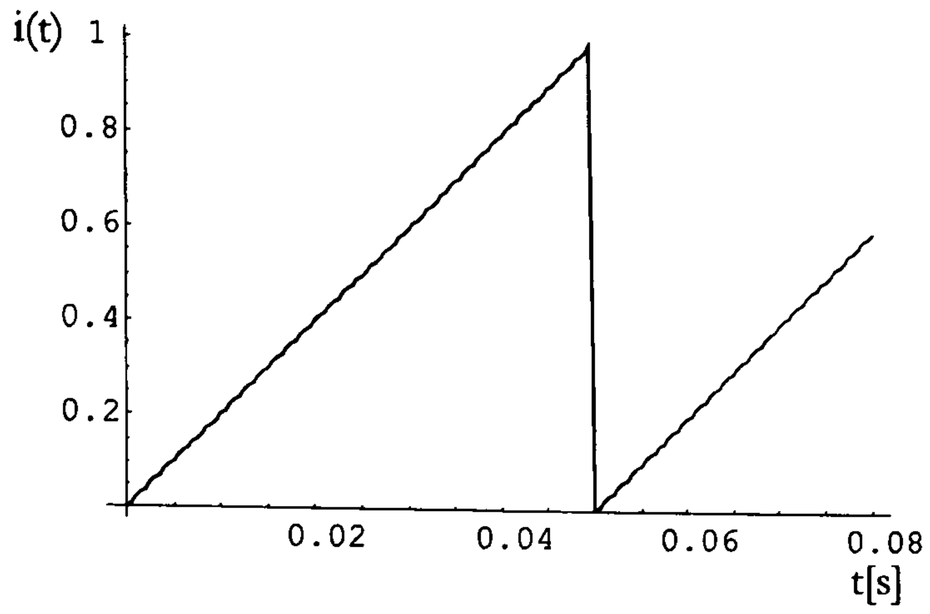

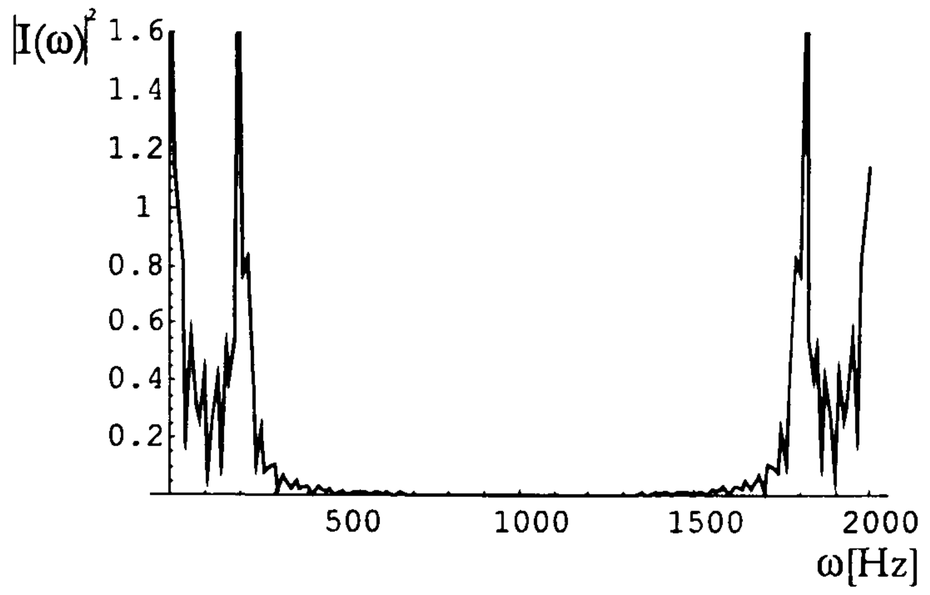

MDSM = 0.1%

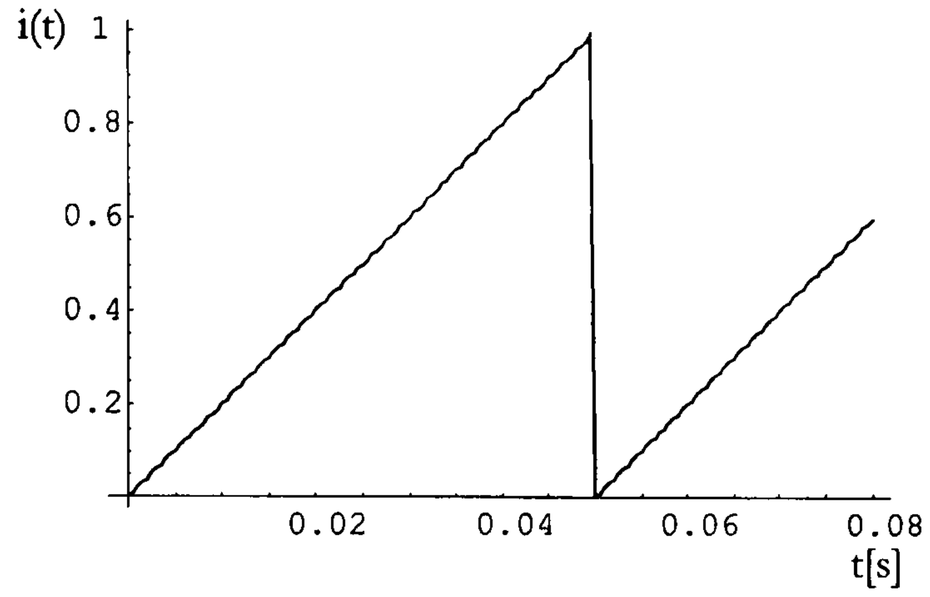

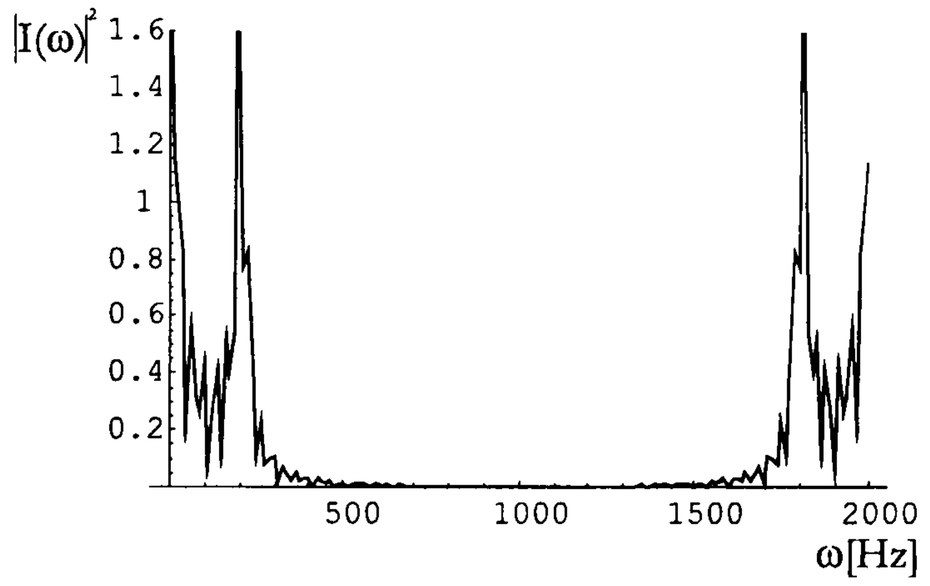

MDSM = 1%

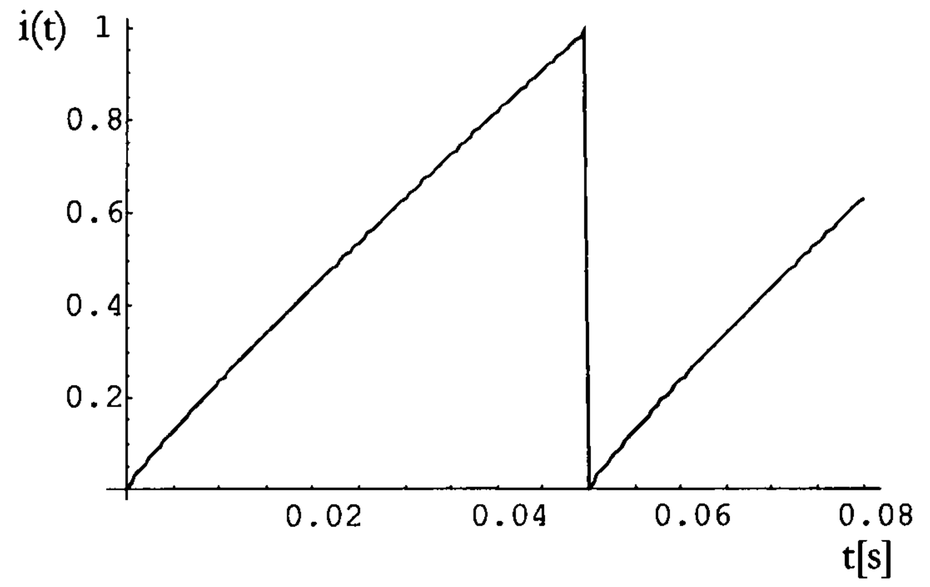

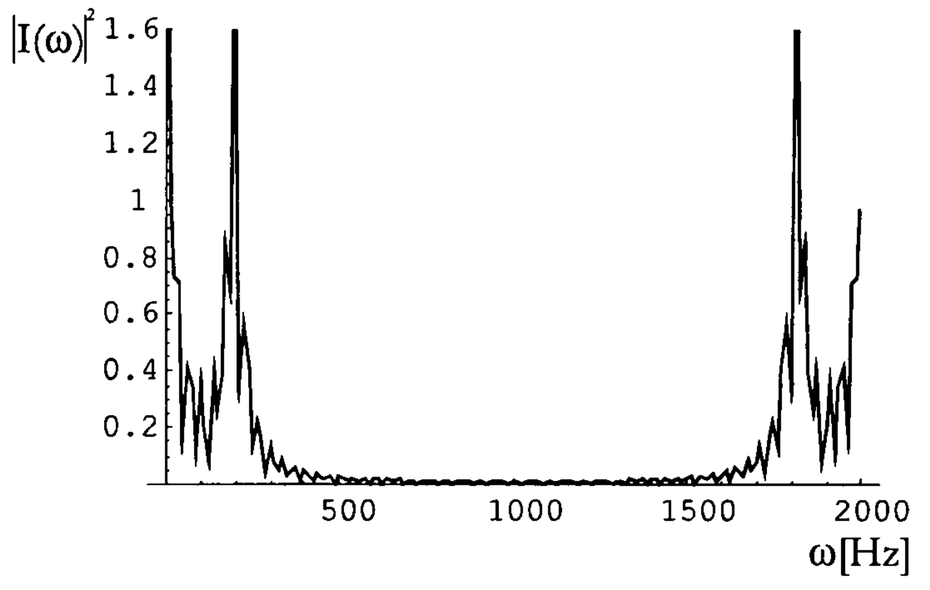

MDSM = 10%

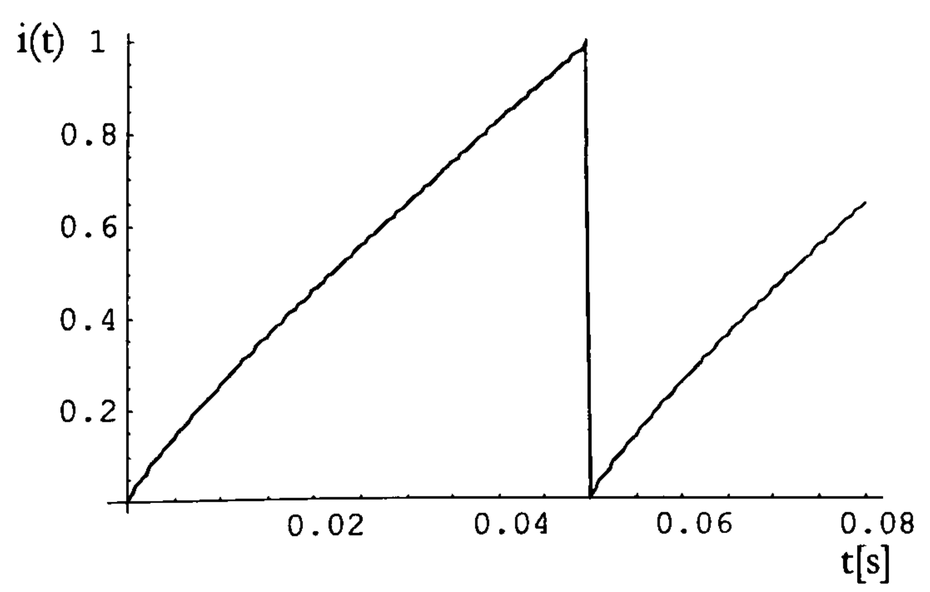

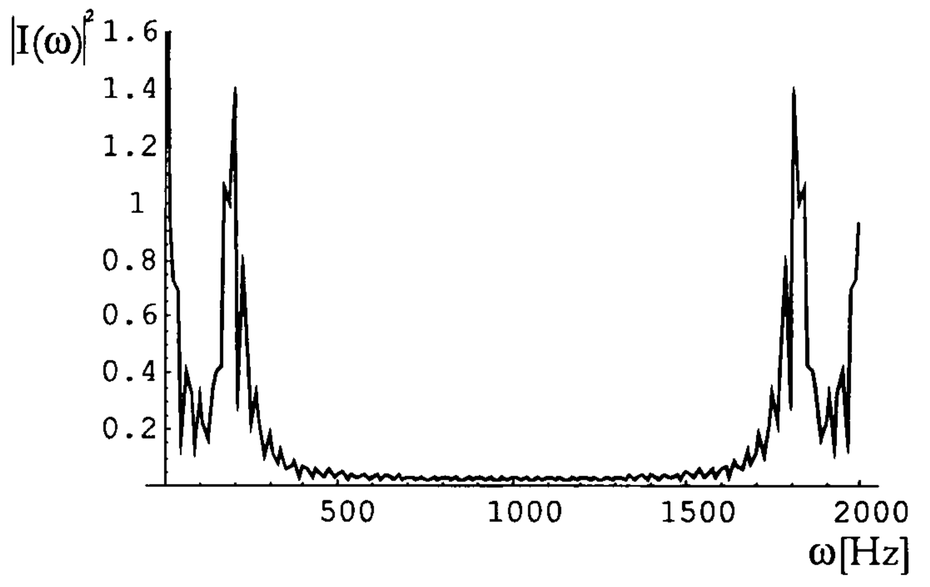

MDSM = 15%

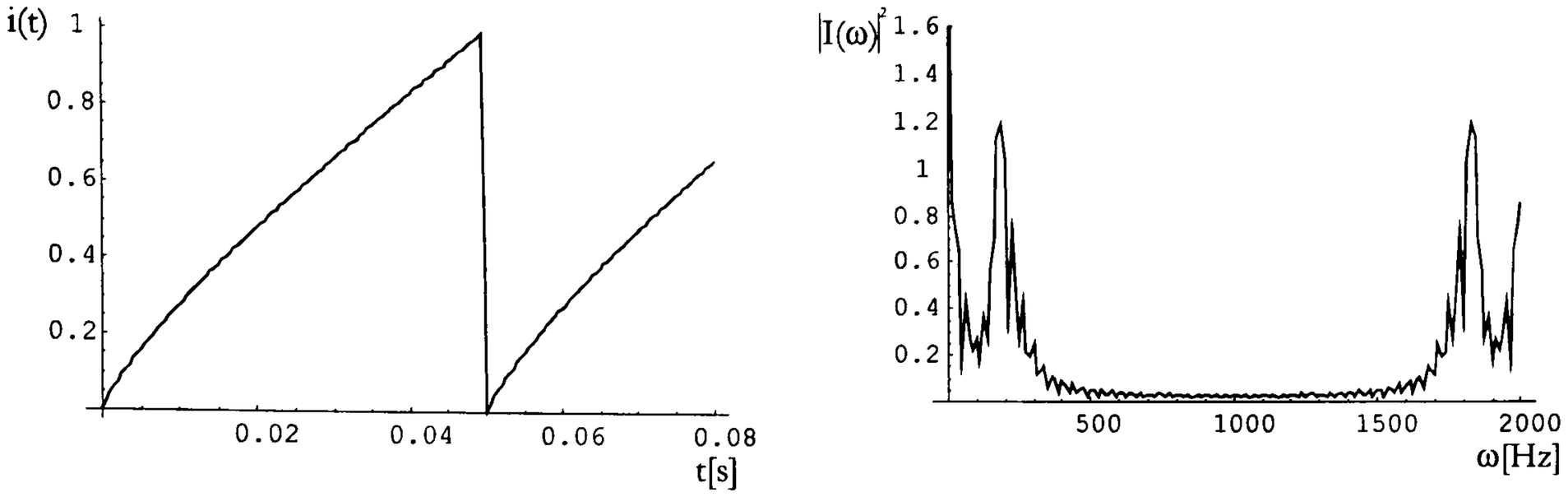

MDSM = 20%

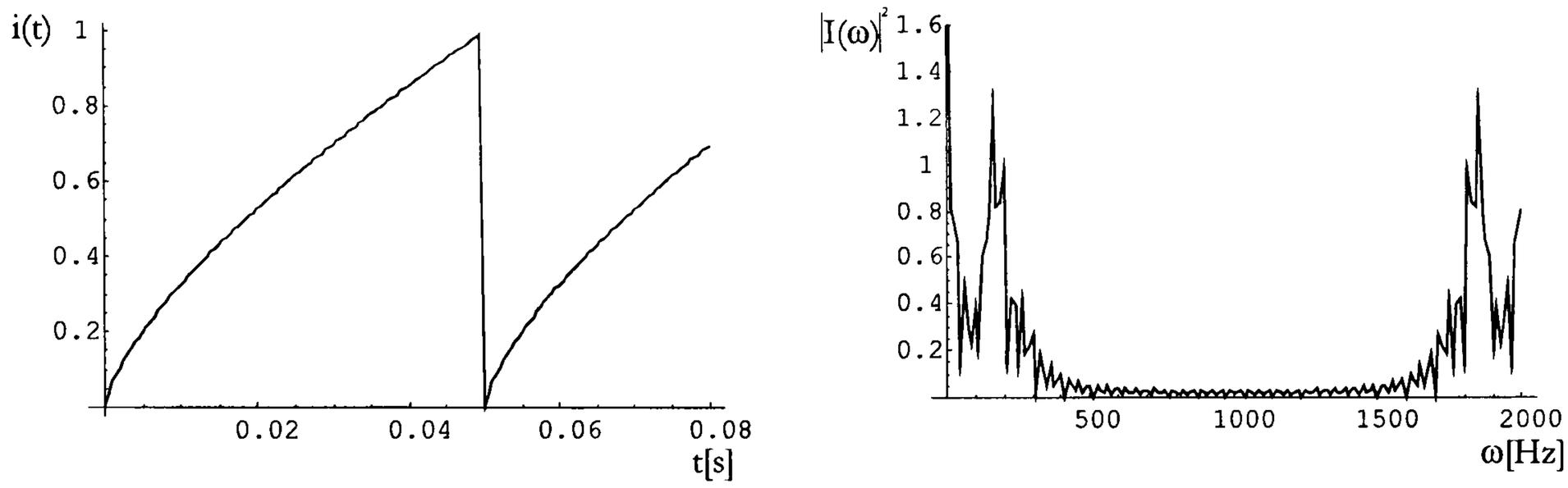

MDSM = 30%

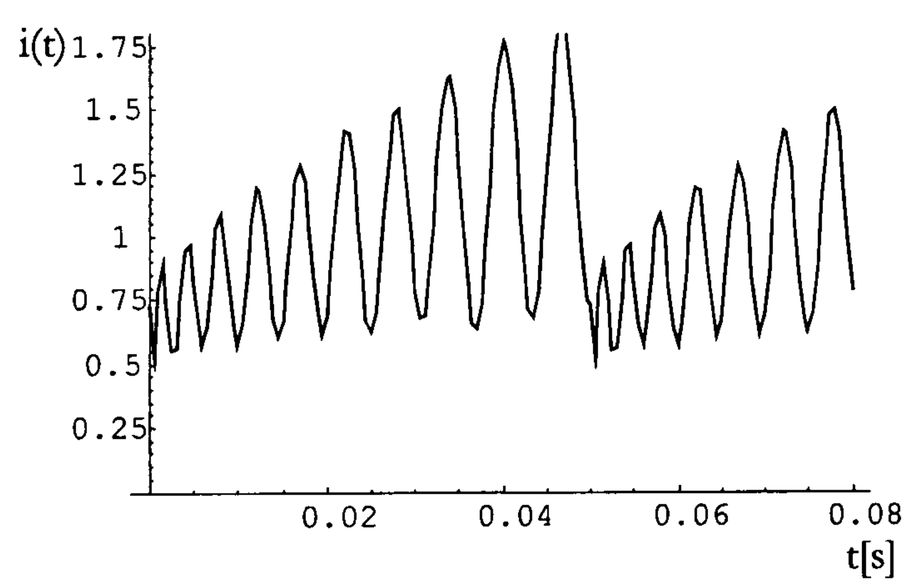

output time response for difference between the perfect and non perfect sawtooth modulation MSDM = 30%

Figure 5.16: *Time responses of the modulating current and corresponding interferometer power spectrums for different levels of non-perfect linear sawtooth modulation*

Comparing the spectral responses for different maximum differences between the perfect and non-perfect modulation one can conclude, that a 10%-15% change of

the ideal value are tolerable. After those values the spectrum includes new peaks and/or the peak amplitude is decreasing due to the nonlinearity of the modulation.

5.1.5. Conclusions on parameter examination for single sensor coherent FMCW

To build a well defined and effective sensing system incorporating many sensing units which are connected in a serial manner, in first step we have to choose the GRIN lenses. Whether a reference addressing or coherence addressing scheme will be used (different proposed multiplexing strategies will be covered in the next section of this chapter) the backreflection coefficients influence the transmission and reflection signal levels as well as the maximum number of sensing units which the system is capable of handling. The sensing cell length has to be chosen such that the beat frequencies are in the range of simple process electronics (under 10KHz), but still long enough so that the absorption is perceived.

The same is valid for the modulation frequency and shape. To observe interference effects the depth of the current modulation must assure sufficient wavelength change, regardless of whether sawtooth or triangular modulation is used.

In the next sections, several different addressing schemes for quasi distributed chemical sensing using FMCW will be introduced and evaluated.

5.2. Coherent FMCW with reference arm addressing

In order to construct a quasi distributed sensing system, where the sensing units are connected in series we have to be able to address each cell individually. In the

literature many distributed addressing schemes have been presented and a short overview was given in Chapter 3.

Here a novel addressing mechanism is presented which combines the Frequency Modulated Continuous Wave technique with the reference arm addressing. The connecting fibres between two successive sensing cell are always much greater then the coherence length of the source and the beams from two different cells do not interfere. With the appropriate selection of the length (switch between different lengths) of the reference arm in the Michelson configuration the sensing cell is addressed. Each reference arm corresponds to a certain sensing unit and the optical path distance between the reference and sensing part is within the coherence length of the source. We refer to this scheme as *Coherent FMCW with reference arm addressing.*

The reference arm addressing system will be initially analysed using mathematical simulations. To demonstrate the principle and to consider all parameters a quasi distributed system made up of three sensing microoptic cells will be implemented. In further analysis approximate real values for the reflection and transmission coefficients will be used. In practice $r_2, r_3 << r_1$ therefore equation (5.12) becomes:

$$I'_{out} = r_1^2(A_1 + B_1 t) + \underbrace{2r_1 r_2\sqrt{(A_1 + B_1 t)(A_2 + B_2 t)}\cos(\psi_2 + \Delta\psi_2)}_{\text{interference between reference and first GRIN lens}} + \underbrace{2r_1 r_3 t_2 t_2^{'}\sqrt{(A_1 + B_1 t)(A_3 + B_3 t)}\cos(\psi_3 + \Delta\psi_3)}_{\text{interference between reference and second GRIN lens}} \tag{5.13}$$

(tipically $r_1^2 = 0.8$, $r_2^2 = 0.005$ and $r_3^2 = 0.1$)

For the serial sensing cell arrangement the transmission factor of each microoptic cell has to be included. The transmission coefficient is the product of the transmission coefficients for each GRIN lens (Figure 5.17):

$$t_i = t_{2i} t_{2i}^{'} \cdot t_{3i} t_{3i}^{'} \tag{5.14}$$

where t_{2i} and t_{2i}' are the transmission coefficient of the first GRIN lens in both directions and t_{3i} and t_{3i}' are the transmission coefficient for the second GRIN lens of the of the i-th sensing cell.

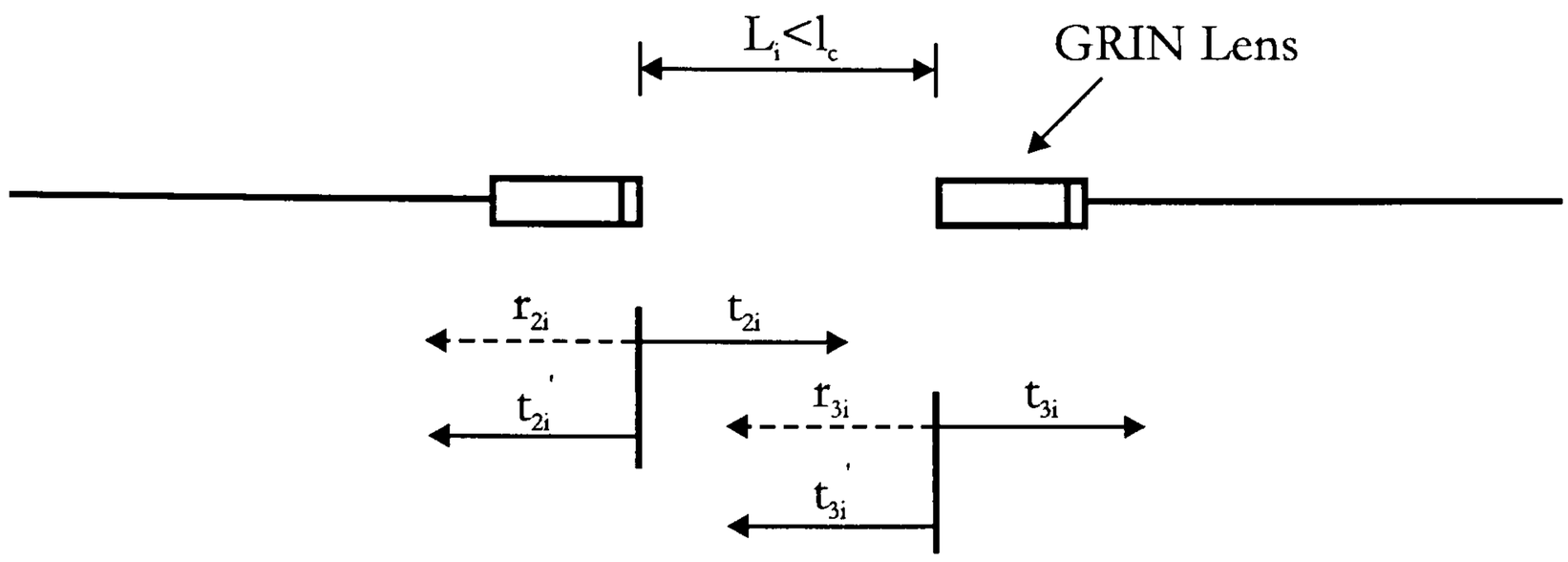

Figure 5.17: *The transmission coefficient for the microoptic cell*

Considering the absorption inside sensing cells the total transmitted power through the i-th cell is

$$P_i = P_{i-1} \cdot t_i \cdot e^{-(\alpha_i C_i L_i)} \tag{5.15}$$

Using three microoptic cells connected in series the output of each cell (if addressing it using the reference arm method) reads as:

$$I_{out}^1 = r_{11}^2(A_1 + B_1 t) + 2r_{11}r_{21}\sqrt{(A_1 + B_1 t)(A_2 + B_2 t)}\cos(\psi_{21} + \Delta\psi_{21}) + 2r_{11}r_{31}t_{21}t_{21}'\sqrt{(A_1 + B_1 t)(A_2 + B_2 t)}e^{-(\alpha_1 C_1 2 L_{21})}\cos(\psi_{31} + \Delta\psi_{31}) \tag{5.16}$$

$$I_{out}^2 = r_{12}^2(A_1 + B_1 t) + 2r_{12}r_{22}t_1^2\sqrt{(A_1 + B_1 t)(A_2 + B_2 t)}e^{-(\alpha_1 C_1 2 L_{21})}\cos(\psi_{22} + \Delta\psi_{22}) + 2r_{12}r_{32}t_1^2 t_{22}t_{22}'\sqrt{(A_1 + B_1 t)(A_2 + B_2 t)}e^{-(\alpha_1 C_1 2 L_{21} + \alpha_2 C_2 2 L_{22})}\cos(\psi_{32} + \Delta\psi_{32}) \tag{5.17}$$

$$I_{out}^{3} = r_{13}^{2}(A_1 + B_1 t) + \qquad (5.18)$$
$$2r_{13}r_{23}t_1^2 t_2^2 \sqrt{(A_1 + B_1 t)(A_2 + B_2 t)}\, e^{-(\alpha_1 C_1 2 L_{21} + \alpha_2 C_2 2 L_{22})} \cos(\psi_{23} + \Delta\psi_{23}) +$$
$$2r_{13}r_{33}t_1^2 t_2^2 t_{23} t_{23}' \sqrt{(A_1 + B_1 t)(A_2 + B_2 t)} \cdot$$
$$e^{-(\alpha_1 C_1 2 L_{21} + \alpha_2 C_2 2 L_{22} + \alpha_3 C_3 2 L_{23})} \cos(\psi_{33} + \Delta\psi_{33})$$

The coherence FMCW system using reference arm addressing is presented in Figure 5.18.

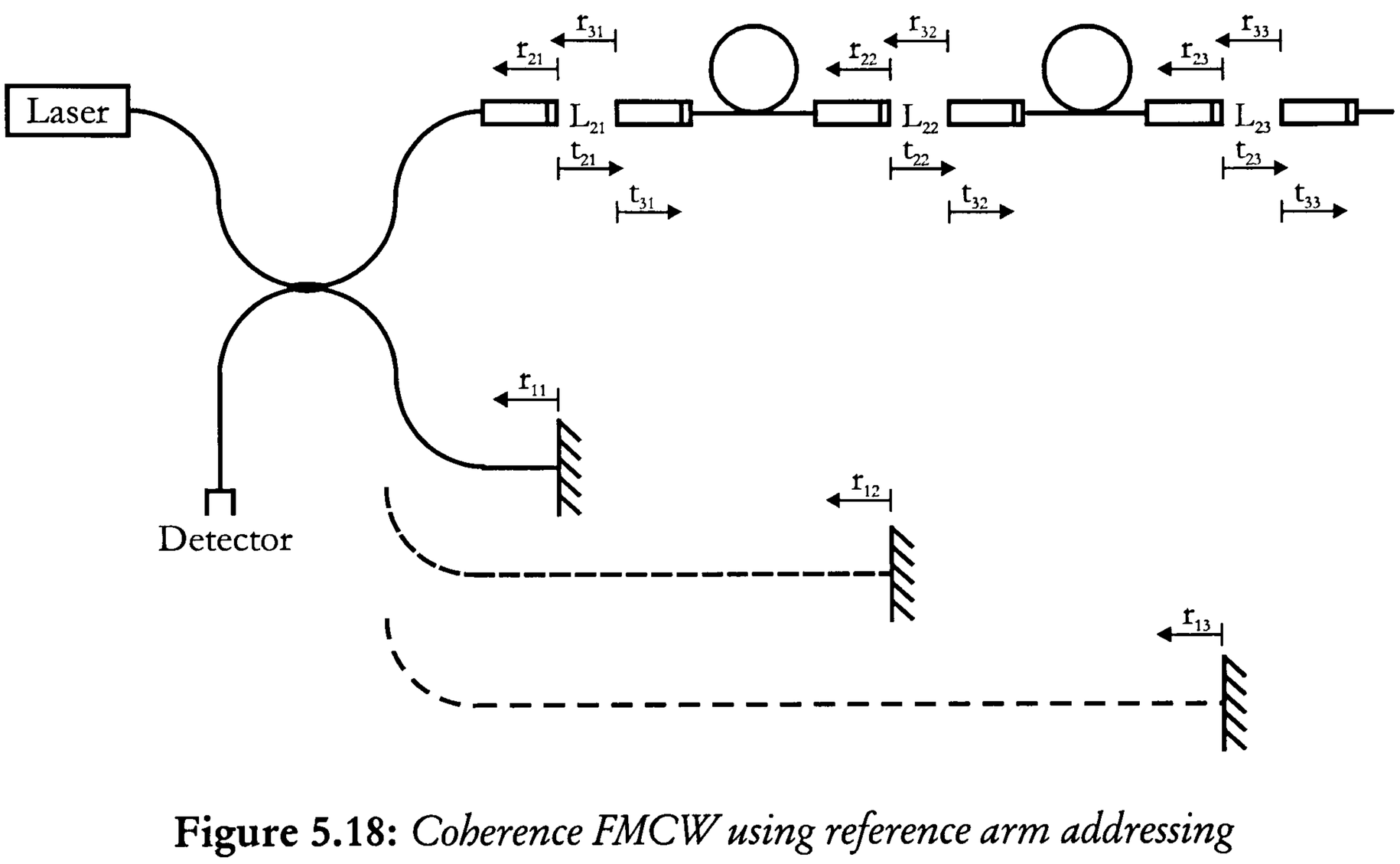

Figure 5.18: *Coherence FMCW using reference arm addressing*

To generalise the formula for a set-up involving *n* sensing units (5.18) becomes:

$$I_{out}^{n} = r_{1n}^{2}(A_1 + B_1 t) + \qquad (5.19)$$
$$2r_{1n}r_{2n}t_1^2 t_2^2 \cdots t_{n-1}^2 \cdot$$
$$\sqrt{(A_1 + B_1 t)(A_2 + B_2 t)}\, e^{-\left(\alpha_1 C_1 2 L_{21} + \alpha_2 C_2 2 L_{22} + \ldots + \alpha_{(n-1)} C_{(n-1)} 2 L_{2(n-1)}\right)} \cos(\psi_{2n} + \Delta\psi_{2n}) +$$
$$2r_{1n}r_{3n}t_1^2 t_2^2 \cdots t_{n-1}^2 t_{2n} t_{2n}' \cdot$$
$$\sqrt{(A_1 + B_1 t)(A_2 + B_2 t)}\, e^{-(\alpha_1 C_1 2 L_{21} + \alpha_2 C_2 2 L_{22} + \ldots + \alpha_n C_n 2 L_{2n})} \cos(\psi_{3n} + \Delta\psi_{3n})$$

5.2.1. Parameter examination for multiple sensor coherent FMCW using reference arm addressing

To obtain an overview of how parameters of the sensing cell influence the output signal and the corresponding power spectrum, a number of simulations has been performed. The results were obtained by implementing equations (5.16), (5.17) and (5.18) in the math program *Mathematica*. For multiple sensor coherence FMCW with reference arm addressing, the analysis has focused on:

- cell length
- absorption inside the microoptic cell
- change in transmission and reflection coefficients
- signal level decrease with increase of the number of sensing units

5.2.1.1.Cell length influence in a serial sensor setup

For cell length analysis the lengths of all three sensing units have been altered. The reference values for the modulation frequency, wavelength change and reflection coefficients were set as follows: $\Delta\lambda=0.7$nm, $f_{mod}=20$Hz, $r_1^2=0.9$, $r_2^2=0.005$ and $r_3^2=0.1$. The difference between the reference arm and first GRIN was set to 10mm. For system analysis only time and frequency responses of the last (in this case the third) cell will be given. Although equations (5.13) (and equations (5.16)-(5.17)) show that we should obtain two beat frequencies, one corresponding to first GRIN and reference arm difference (Figure 5.19), the other to the second GRIN and the reference arm difference on the responses only one beat frequency is visible.

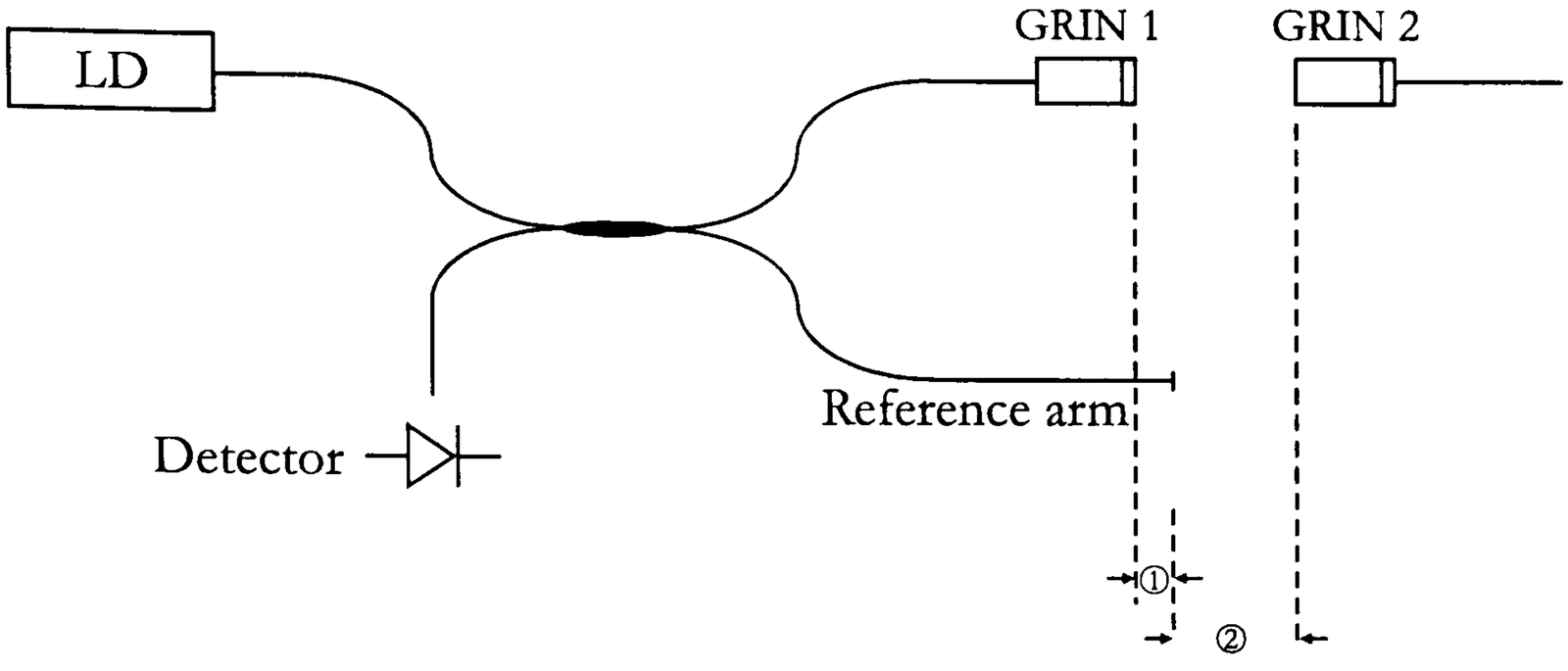

Figure 5.19: *Schematic diagram showing (1) difference between first GRIN and reference arm and (2) second GRIN and reference arm*

Since $r_1r_2 << r_1r_3$ the beat from the first GRIN to air interface is negligible to the beat from the second GRIN and hence only the beat corresponding to the second GRIN to reference arm difference is observed. The last cell is considered to be the most important in signal to noise evaluation, since the signal has to pass all proceeding sensing units before entering the last one. The time and frequency responses for the third sensing unit are presented in Figure 5.20.

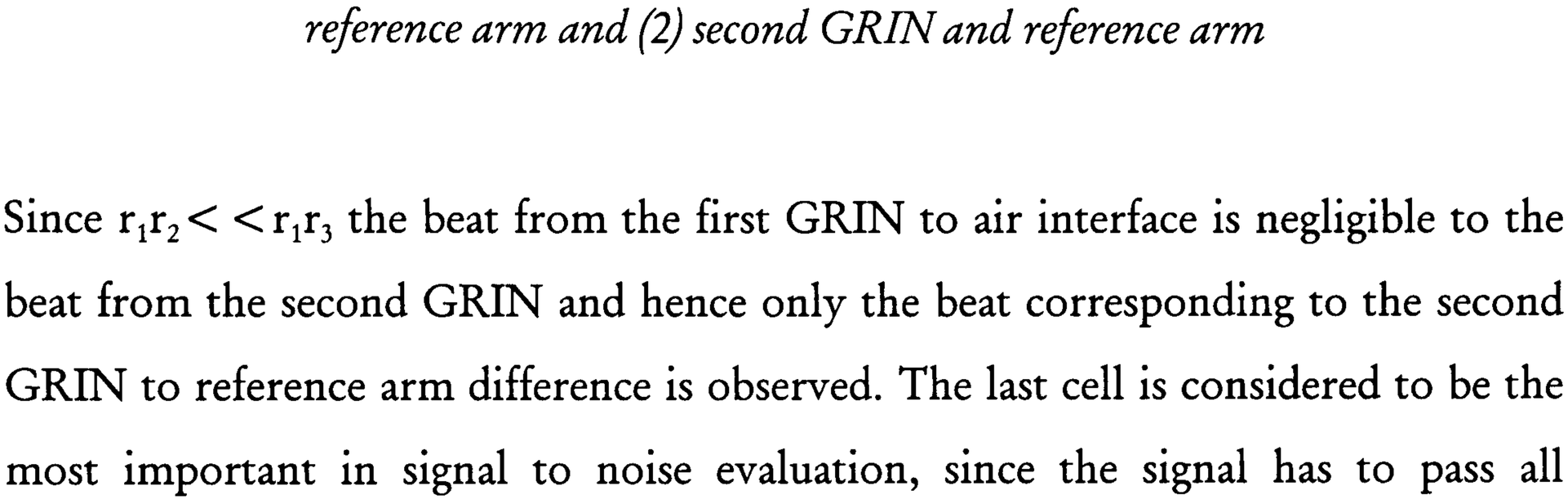

$L_{21}=30mm$, $L_{22}=30mm$, $L_{23}=30mm$, $\alpha C=0.502m^{-1}$

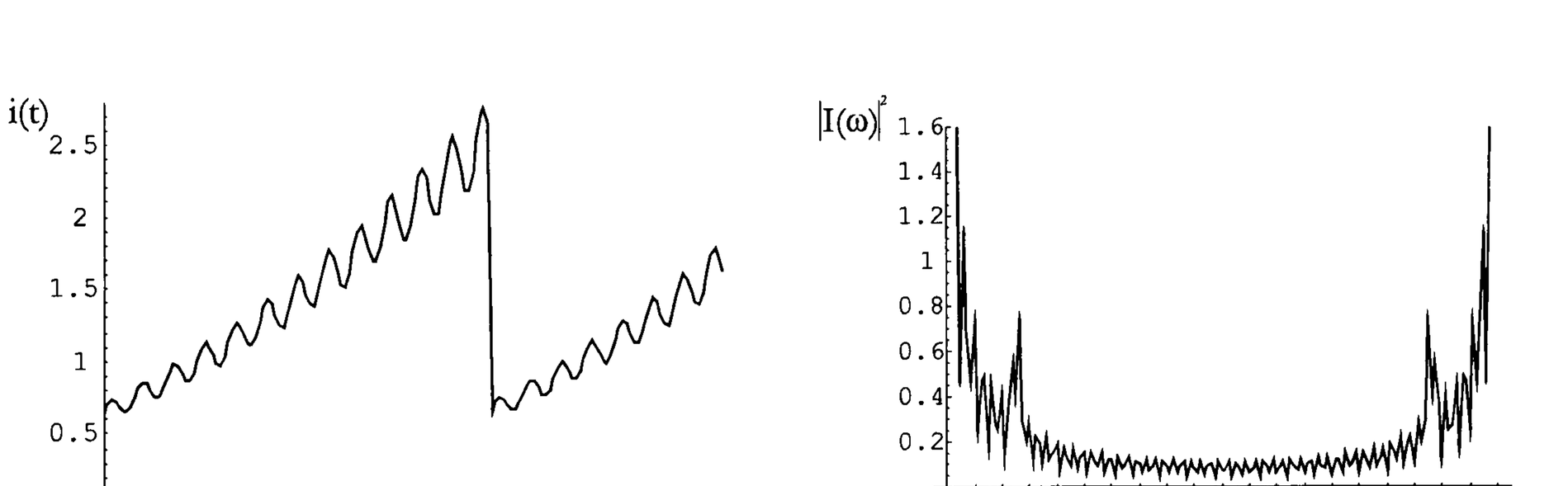

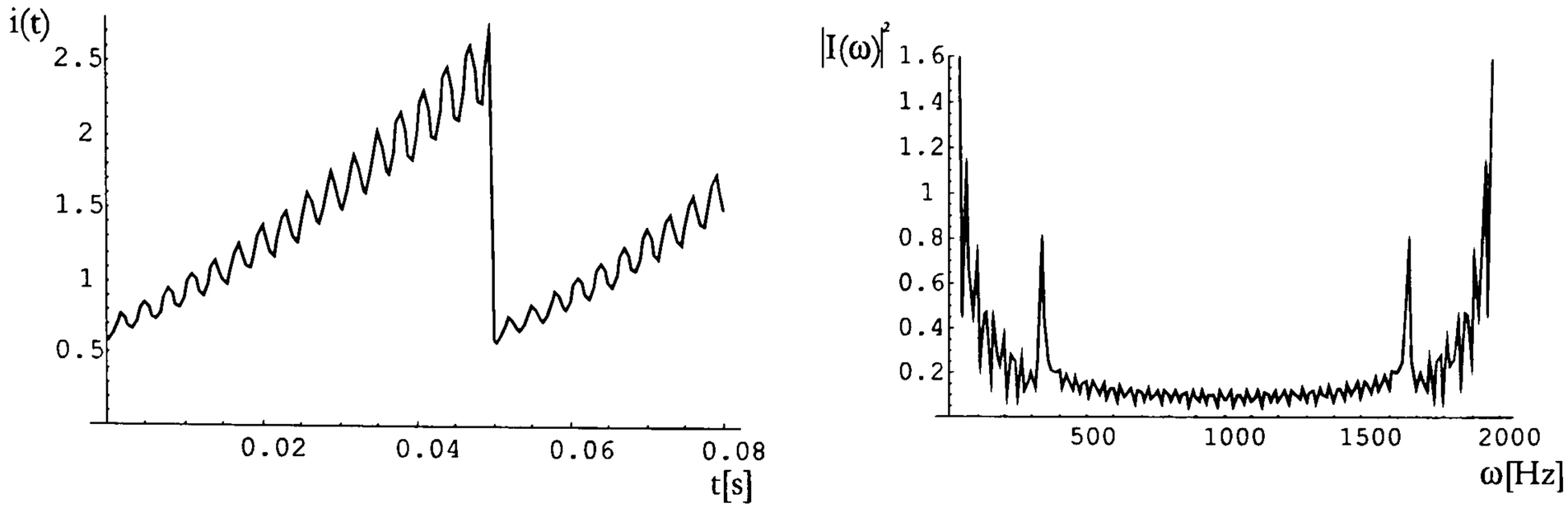

Figure 5.20: *Output versus time (left) and frequency response (right) for the third sensing unit applying different cell lengths*

To compare all three sensing units Figure 5.21 shows the time responses for the case of equal cell lengths, $L_{21}=L_{22}=L_{23}=30mm$ respectively.

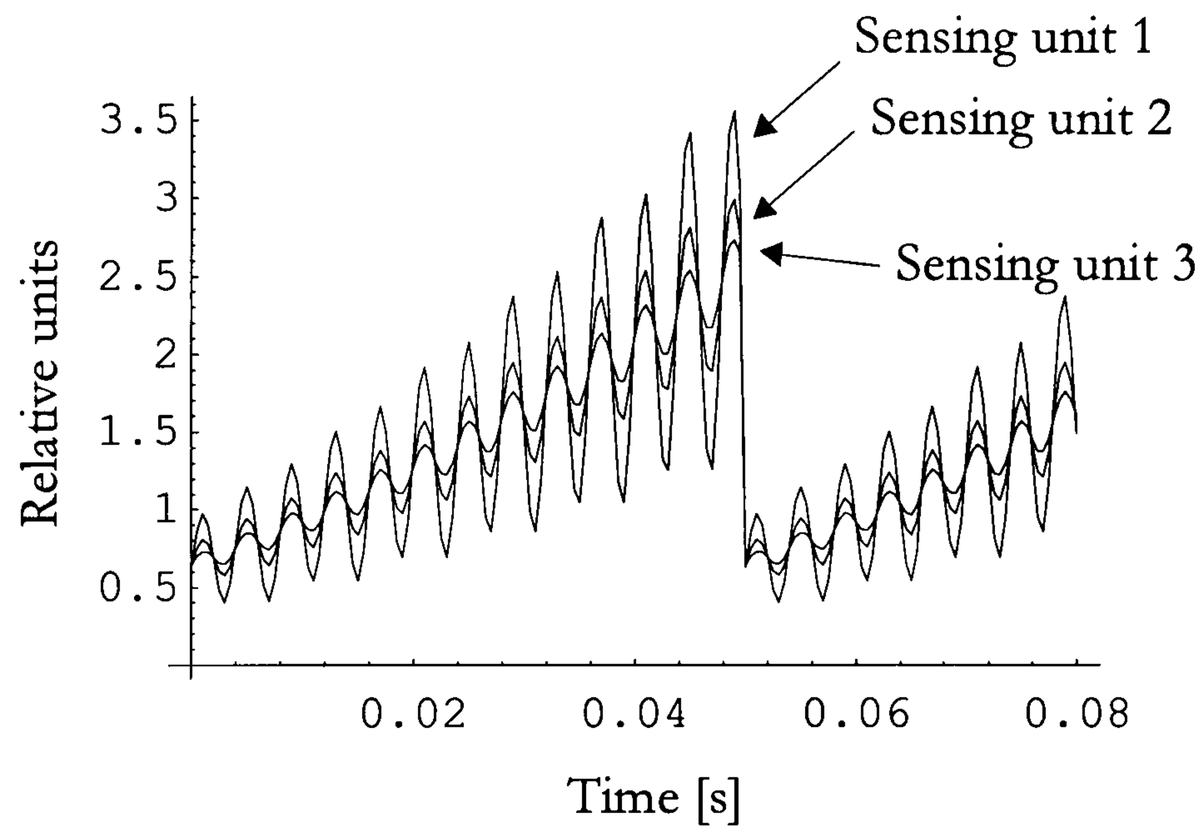

Figure 5.21: *Time response for all three sensing units*

From Figure 5.21 and Figure 5.20 one can observe that with increase in the number of sensing units and assuming the same amount of absorption in each unit the signal falls exponentially. In the case of equal sensing lengths we can also observe a drop in the amplitude of the spectrum and its broadening. This effect could be minimised (see Figure 5.20) using different sensing units lengths. One option would be to successively reduced the cell length, however by this also the sensitivity is reduced.

5.2.1.2.Influence of microoptic cell absorption for a serial sensing system setup

In the previous section the major emphasis was on the length of the sensing cell whereas the concentration has been considered constant. With further analysis we would like to get an insight on how different sensing cell absorption values influence the response of each cell.

To compare the cells with and without absorption we introduced the spectrum difference between the "reference" cell (the "reference" cell without absorption has been presented in Figure 5.4b) and sensing cell (arbitrary absorption). Additional a numerical value Δ_{rm} representing the difference between the amplitude of the reference and measured signal will be presented. The value rises as absorption increases (Figure 5.22).

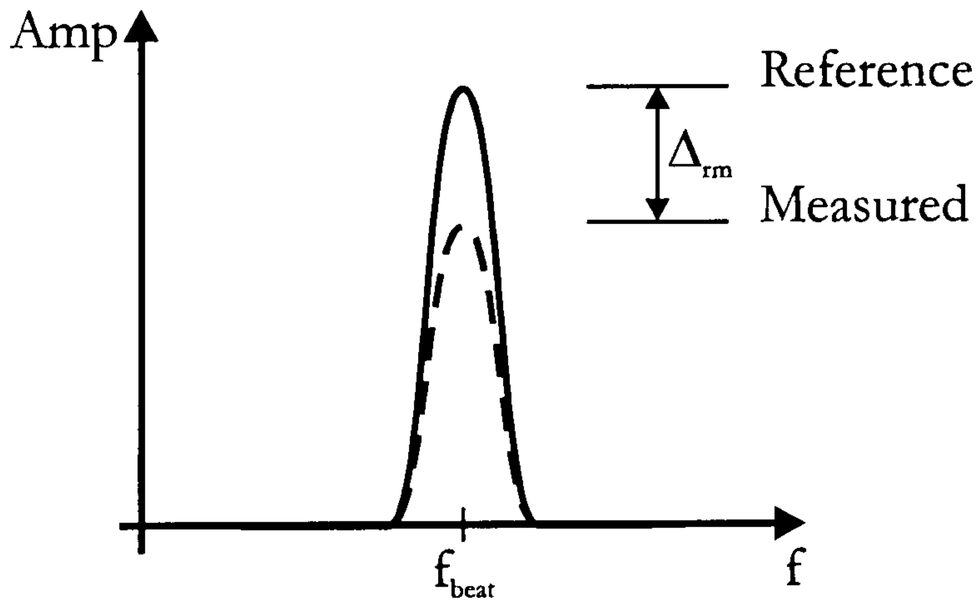

Figure 5.22: *Difference between the reference and absorption spectrum*

Spectral responses and appropriate differences for the last sensing cell for different values of absorption are presented in Figure 5.23. The sensing cells are chosen to have the same length of 30mm.

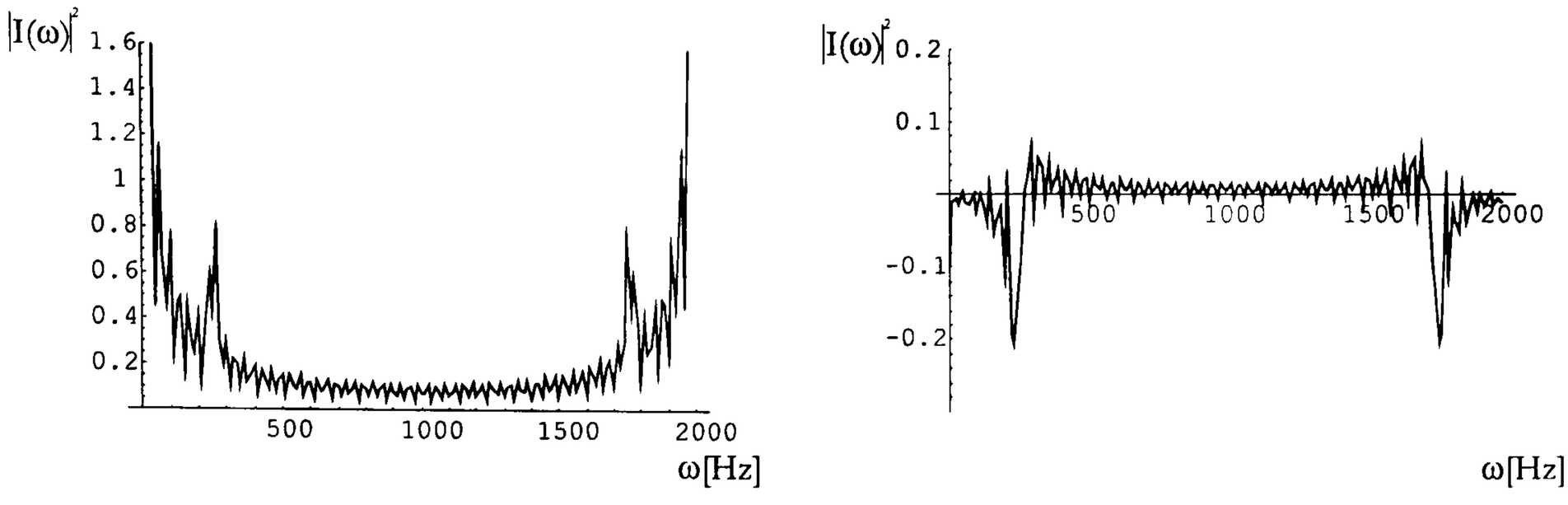

$\alpha_1 C_1 = 0.025 m^{-1}$ (0.05%), $\alpha_2 C_2 = 0.025 m^{-1}$ (0.05%), $\alpha_3 C_3 = 0.025 m^{-1}$ (0.05%),
$\Delta_{rm} = 0.06859$

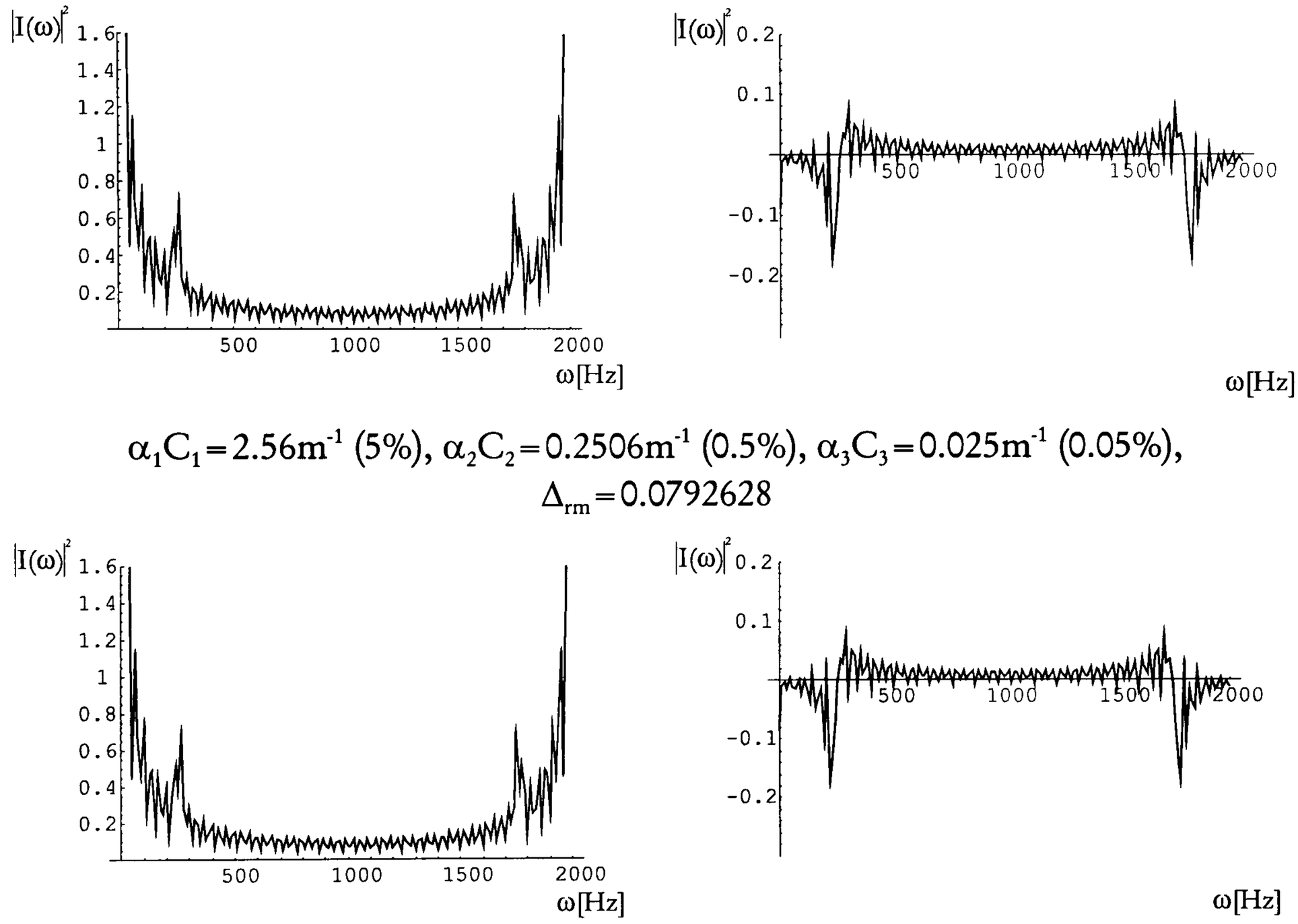

$\alpha_1 C_1 = 2.56 m^{-1}$ (5%), $\alpha_2 C_2 = 0.2506 m^{-1}$ (0.5%), $\alpha_3 C_3 = 0.025 m^{-1}$ (0.05%),
$\Delta_{rm} = 0.0792628$

$\alpha_1 C_1 = 0.025 m^{-1}$ (0.05%), $\alpha_2 C_2 = 0.2506 m^{-1}$ (0.5%), $\alpha_3 C_3 = 2.56 m^{-1}$ (5%),
$\Delta_{rm} = 0.0792556$

Figure 5.23: *Frequency response and difference between the "reference" and second sensing cell for different absorptions*

A visual comparison between spectral responses with and without absorption is very difficult. Therefore we have introduced the parameter Δ_{rm} representing the difference between the amplitude of the reference and measured signal. Comparing the first four responses we ascertain that Δ_{rm} increases (greater absorption)

although the absorption level remained constant. This is because in the second experiment the previous sensing cells experienced more absorption as in the first case. To overcome the problem of getting different values for the same amount of absorption extra measures have to be taken. In the process of scanning the system cell by cell using the reference arm method we have to keep track of all the Δ_{rm} from the previous cells. Using differences from previous cell and the difference from the current cell we can then calculate the proper absorption level.

5.2.1.3.Change in transmission and reflection coefficients

Although previously the influence of reflection coefficient on a single sensing cell has been extensively tested, there is no data on interactions between the units. Figure 5.24 presents two cases. First the reflection coefficients gradually increase with the number of sensing units, second they gradually decrease. The lengths of the cell are set to 30mm and the signal is attenuated with $\alpha C = 0.502 m^{-1}$ (1%).

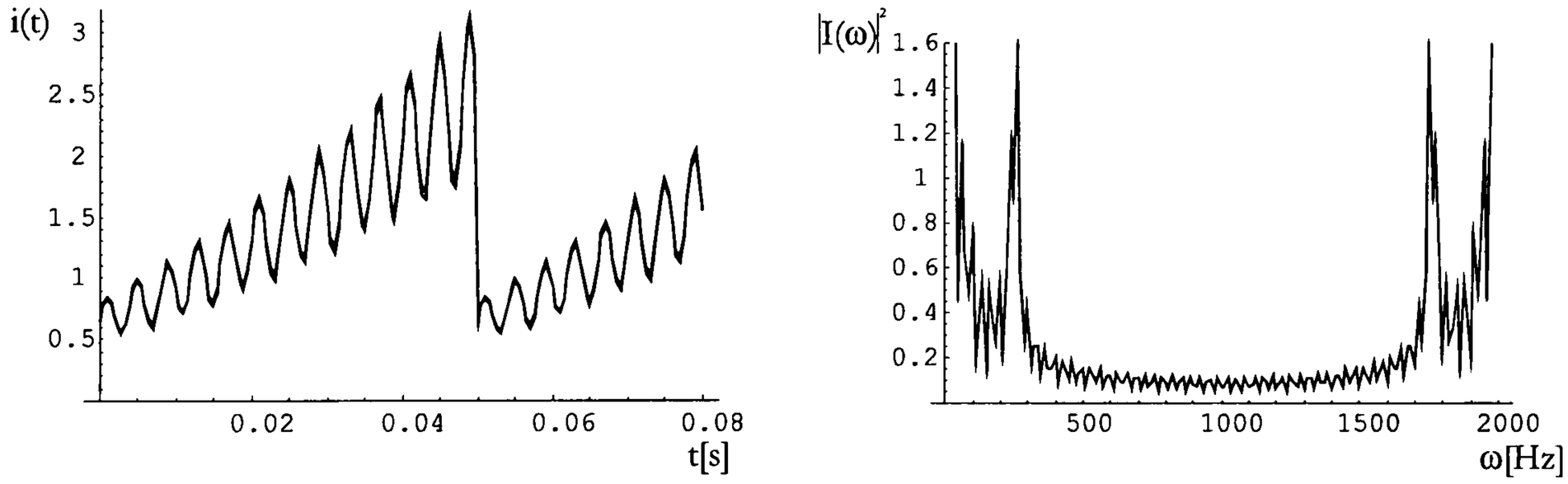

$r_{21}^2 = 0.005,\ r_{31}^2 = 0.1,\ r_{22}^2 = 0.01,\ r_{32}^2 = 0.15,\ r_{23}^2 = 0.015,\ r_{33}^2 = 0.2$

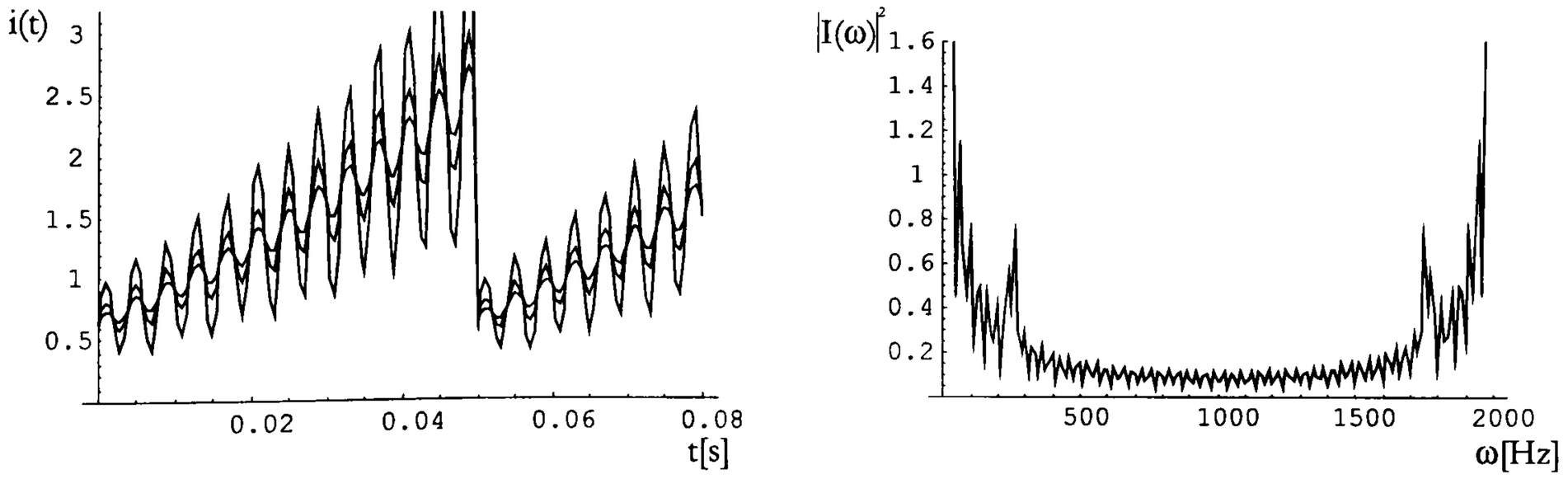

$r_{21}^2 = 0.015,\ r_{31}^2 = 0.2,\ r_{22}^2 = 0.01,\ r_{32}^2 = 0.15,\ r_{23}^2 = 0.005,\ r_{33}^2 = 0.1$

Figure 5.24: *Time responses for all three units and power spectrum for the third unit for different reflection coefficients*

In order to increase the signal to noise level for the most distant sensing units one of the solutions is to gradually increase the reflection coefficients in very small steps.

5.2.1.4.Signal level decrease because of the sensing unit number increase

The optical power available for each sensor is decreasing with the increasing number of sensors. The effect varies with the configuration used and will be evaluated with regard to the proposed addressing mechanism.

Through the previous simulations we have found out that the signal level decreases, while the number of units is increasing. Some alternative methods including cell length and reflection coefficient change have been shown to minimise the effect. To represent the signal level decrease a program has been written which calculates the output amplitude of the i-th cell. To simplify the calculation process, for all sensing units the same amounts of absorption (1%, 0.5%, 0.1% or 0.05%), same sensing cell lengths (30mm) and reflection coefficients (0.005 and 0.1) have been assumed. The signal level decay versus number of sensing units is shown in Figure 5.25.

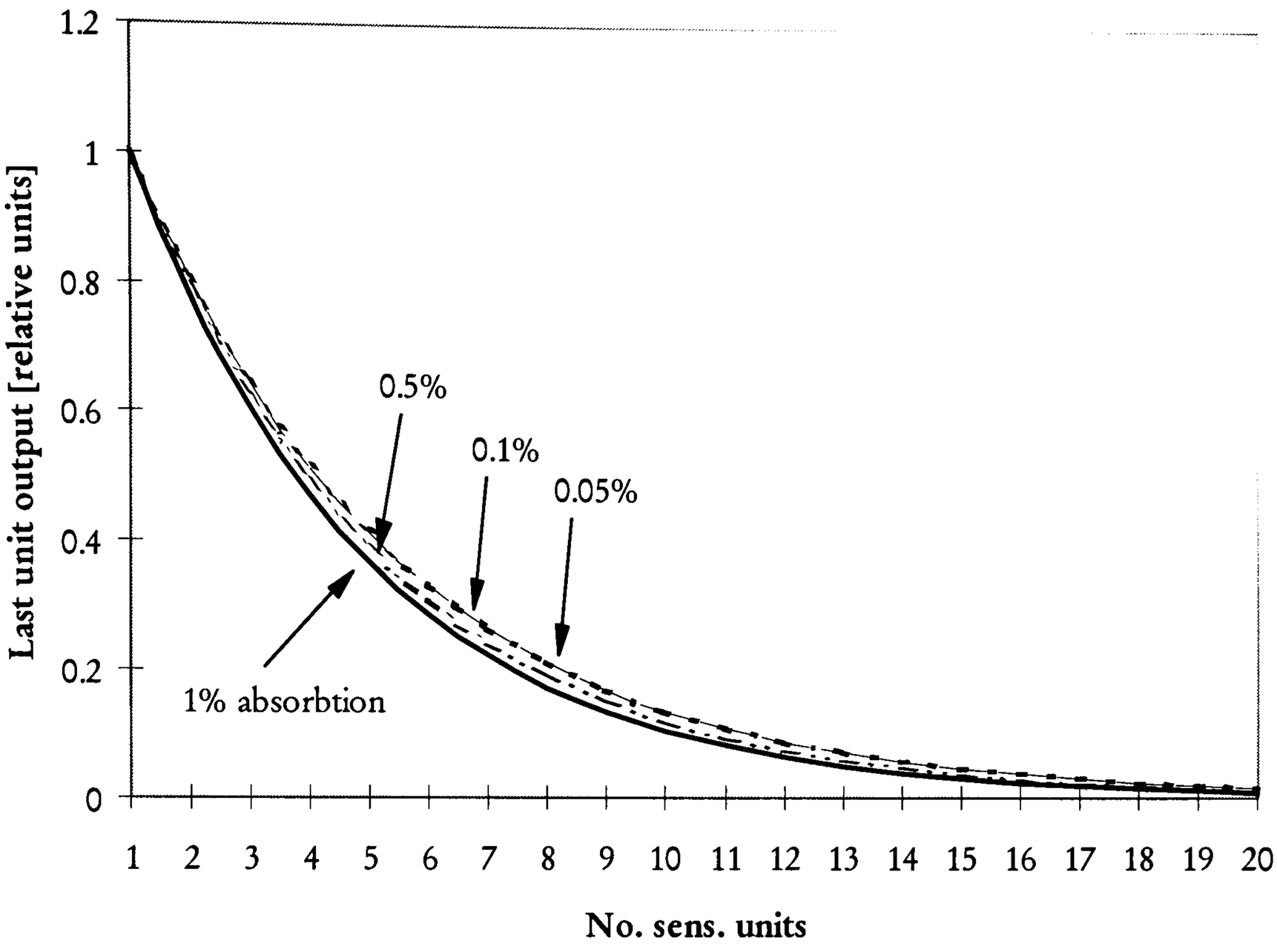

Figure 5.25: *Signal level decay versus number of sensing units*

The signal level declines exponentially with sensor number increase. From first to the tenth cell we have a 9.8dB decrease, from first to the fifteen a 15.25db and for 20 sensing units a 20.7db decrease in the output signal level. This gives approximately 1db for every sensing unit.

The coherent FMCW reference arm addressing method enables the use of approximately 10 to 15 sensing units (supposing 1% absorption in each cell) connected in series when no special attention to cell length or GRIN lens backreflection coefficients is taken.

5.2.2. FMCW reference arm method quasi-distributed absorption measurement - simulation results

A modelled test bed with three microoptic sensing cells was used to simulate quasi-distributed absorption based measurement with the FMCW reference arm method. The absorption in each cell was altered from 0% to 1% in 0,2% steps. Because the number of simulations would increase significant if every possible combination between the absorption levels for all three cells would be measured, only tests where one of the cells experiences zero absorption at the time were carried out. The output versus absorption characteristics are presented in Figure 5.26 to Figure 5.32.

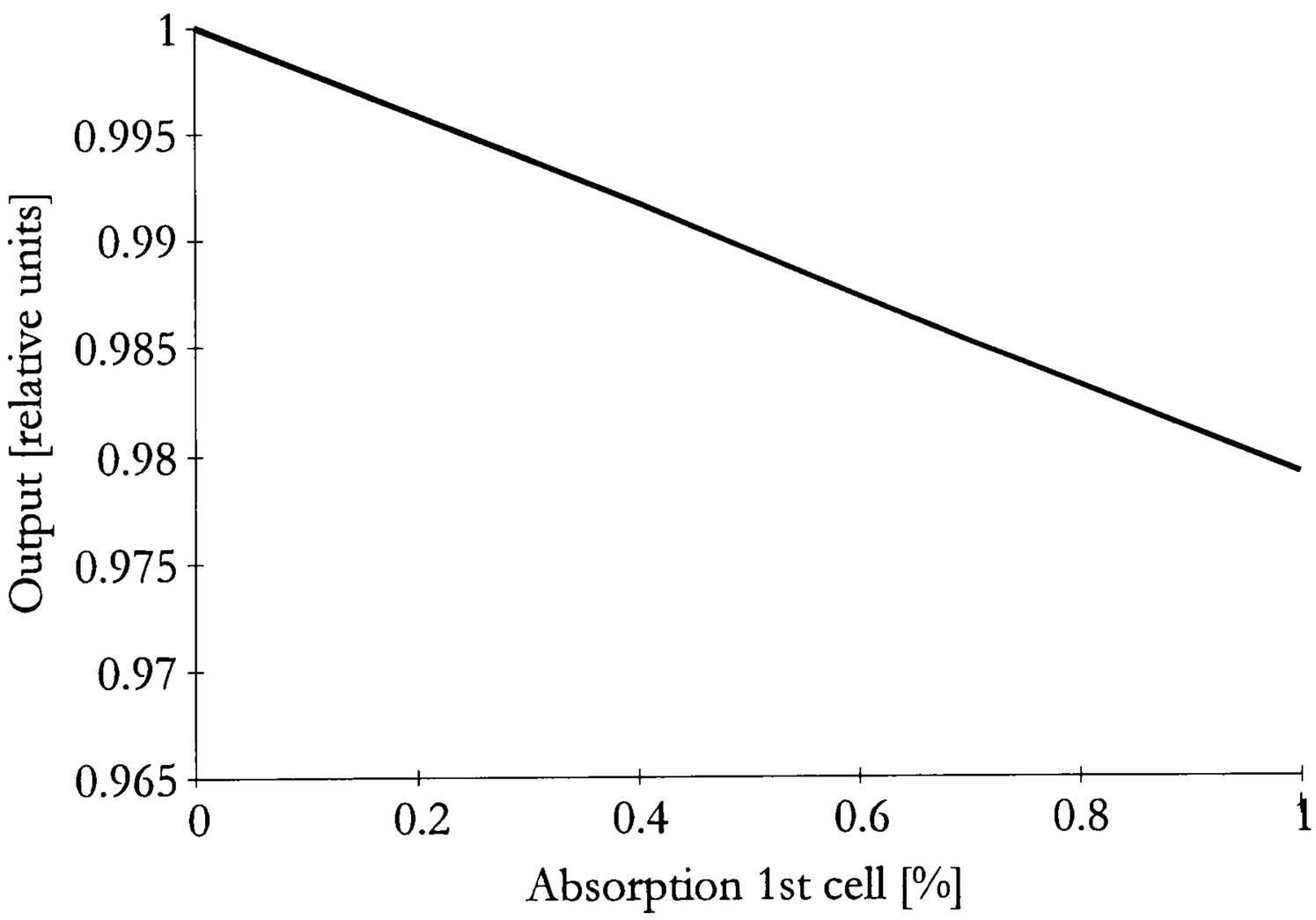

Figure 5.26: *Absorption in the first cell*

When absorption in the first cell is increased the output value determined by the spectral characteristics falls linear with the absorption (Figure 5.26). Because of the serial arrangement the influence from the first cell has impact on the following units (see Figure 5.27 and Figure 5.28).

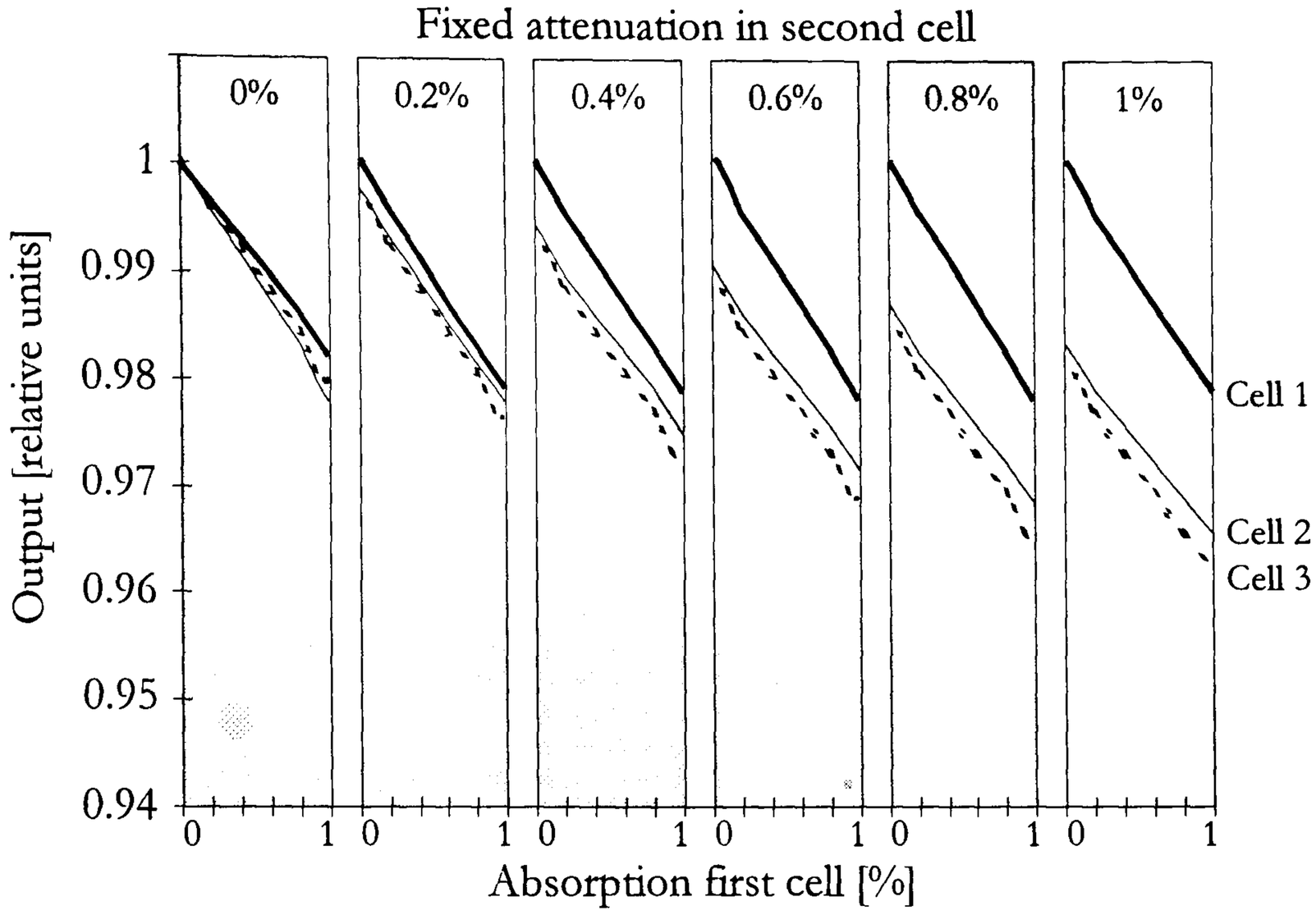

Figure 5.27: *Reference arm addressing - absorption in the second cell held at fixed shown*

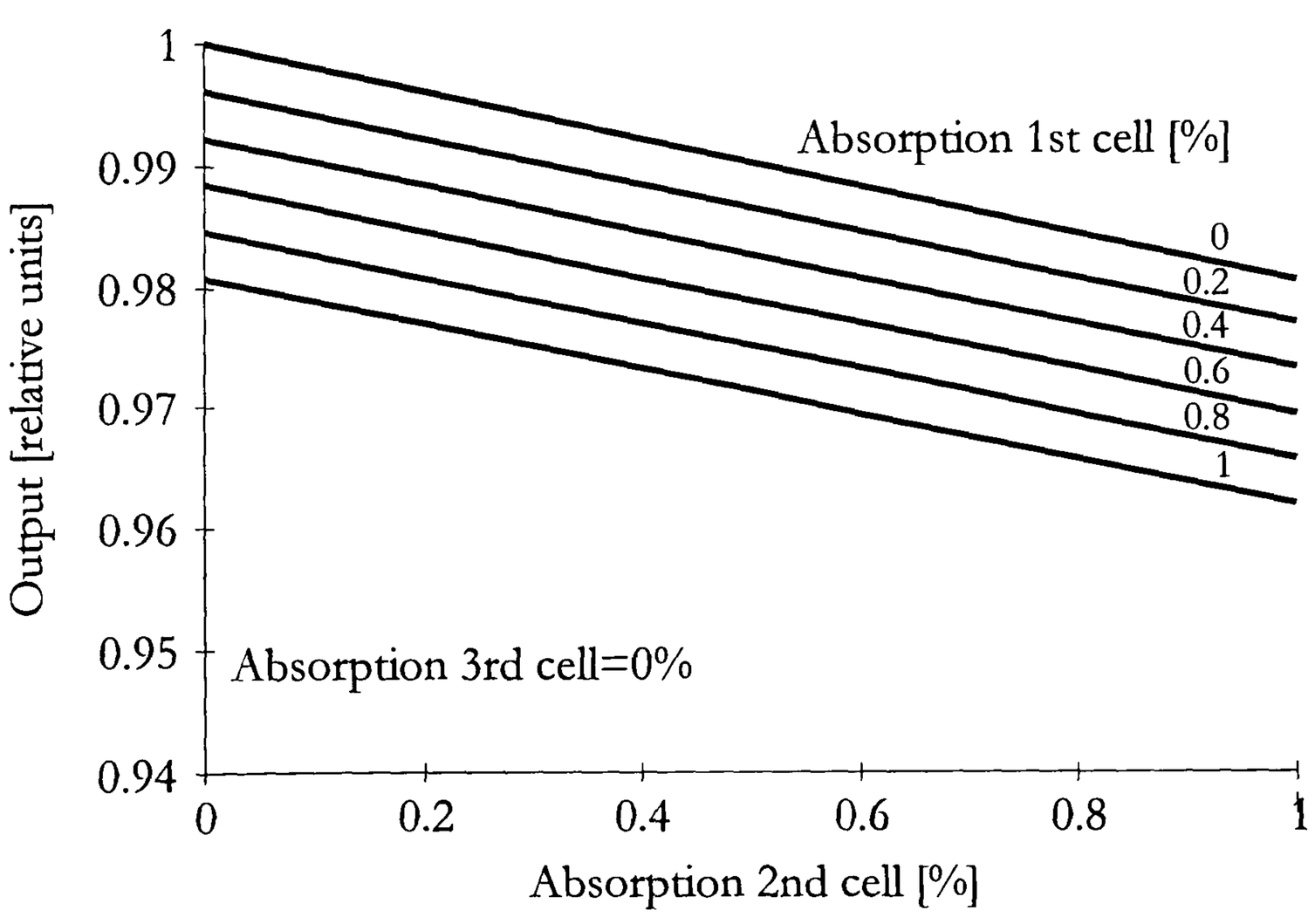

Figure 5.28: *Absorption of the second cell for different values of first cell absorption*

The additional absorption from the first cell (if present) causes that the second cell output characteristics is shifted downwards, but the sensitivity stays the same.

Because of the zero absorption in the third unit the third output follows the second one.

Similar results are obtained when observing the third sensing cell. Preceding cells cause the shift of the linear output characteristics (Figure 5.30). In this case the second cell absorption is set to zero, therefore the output curves for the first and second cell coincide (Figure 5.29).

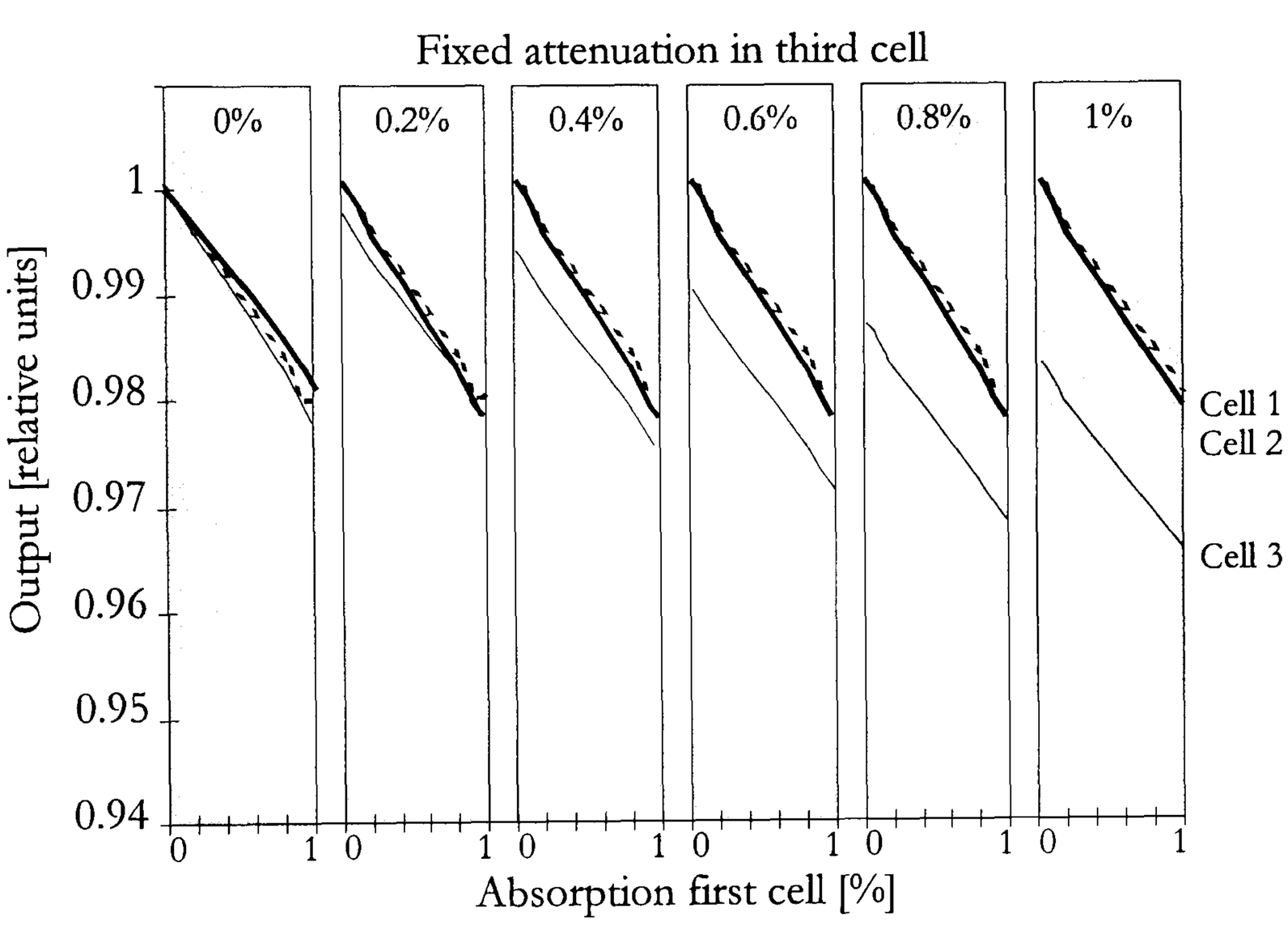

Figure 5.29: *Reference arm addressing - absorption in the third cell held at fixed shown*

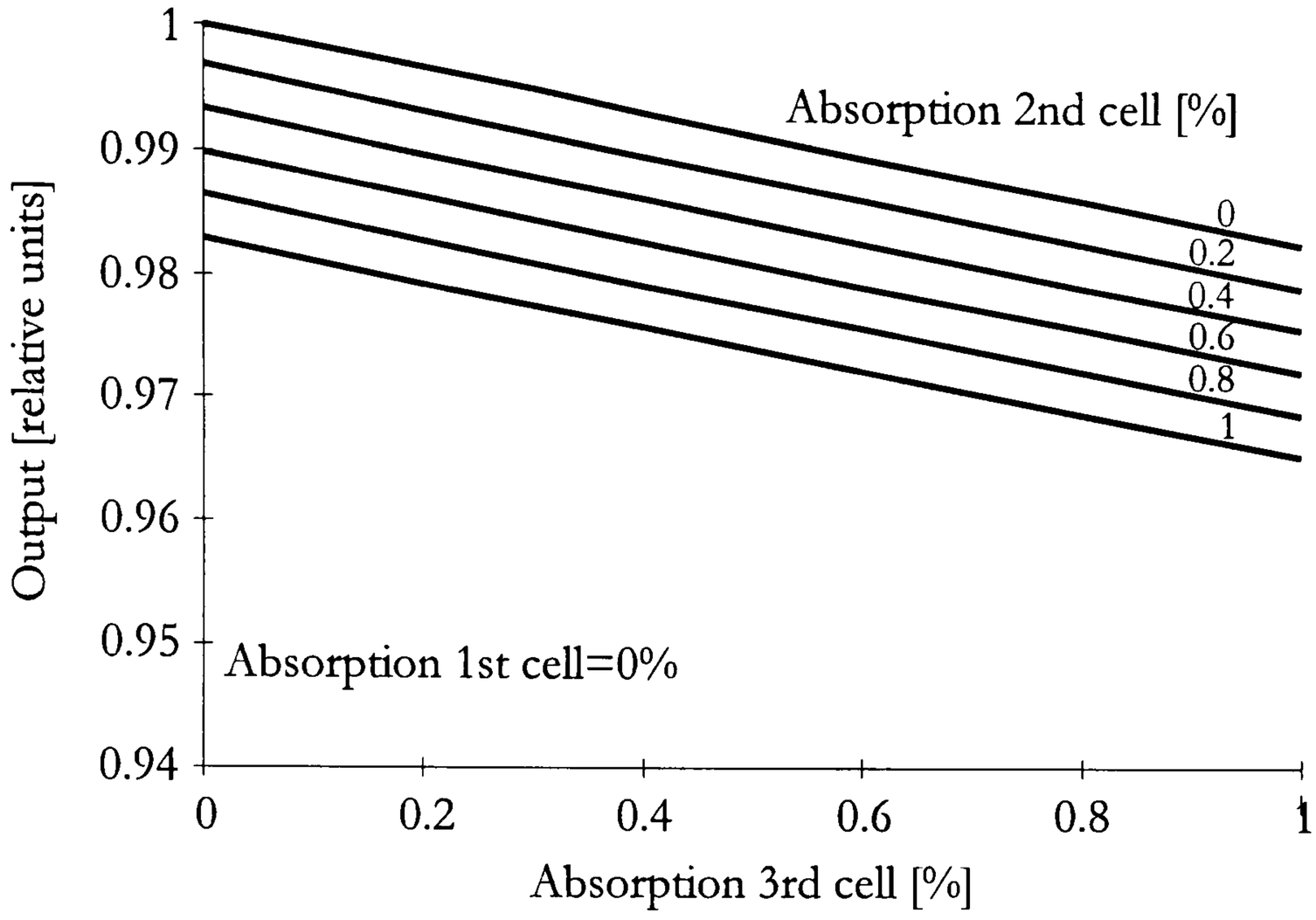

Figure 5.30: *Absorption of the third cell for different values of second cell absorption*

The linear output for the third cell is very similar to output characteristics for the second and first cell. Depending on the previously introduced absorption, one of the parallel shifted characteristics is appropriate (Figure 5.30).

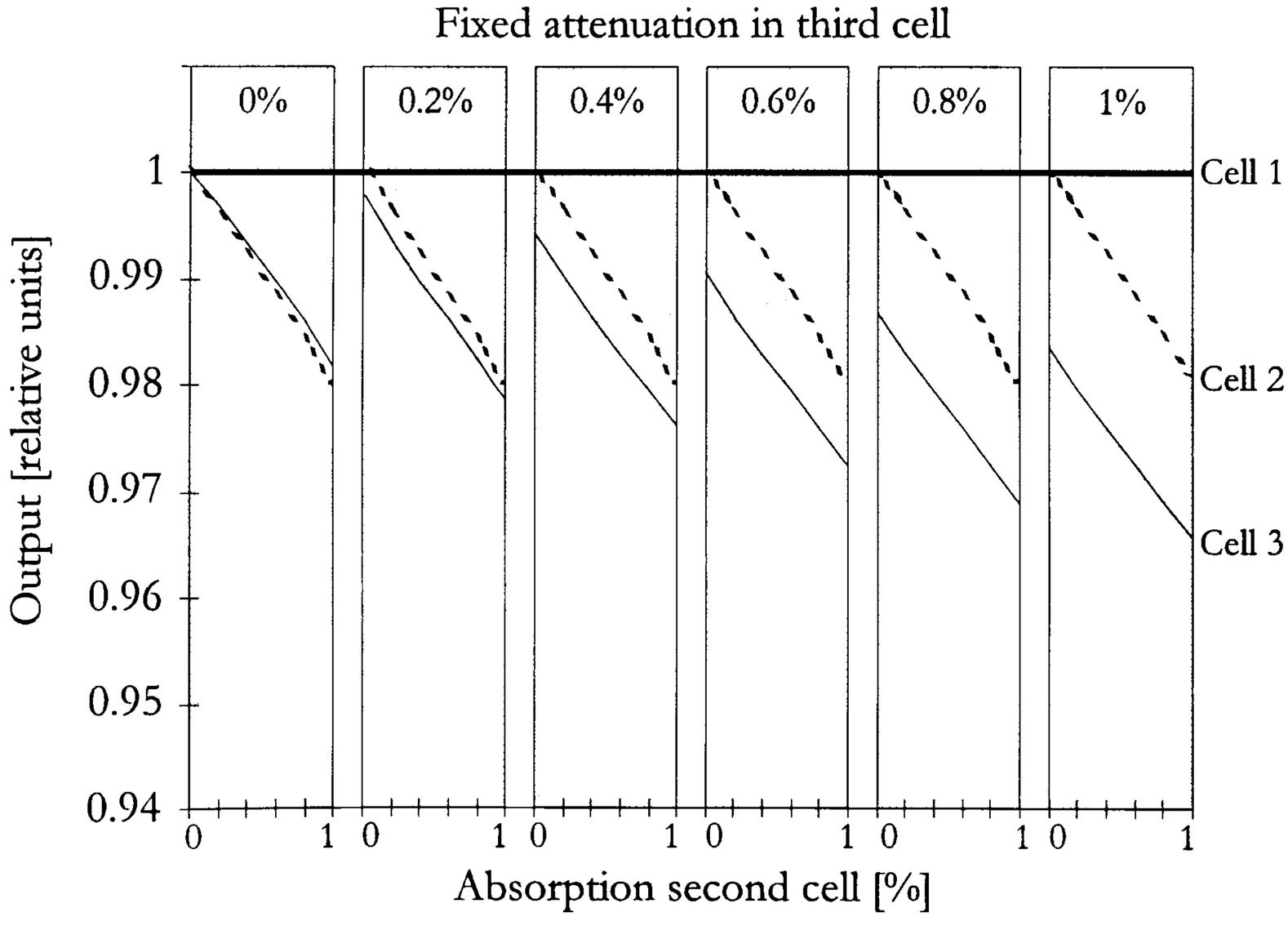

Figure 5.31: *Reference arm addressing - absorption in the third cell held at fixed shown*

In the case when there is no absorption in the first cell the system reduces the number of its members and the only influence of the first cell remains the signal loss due to microoptic cell construction.

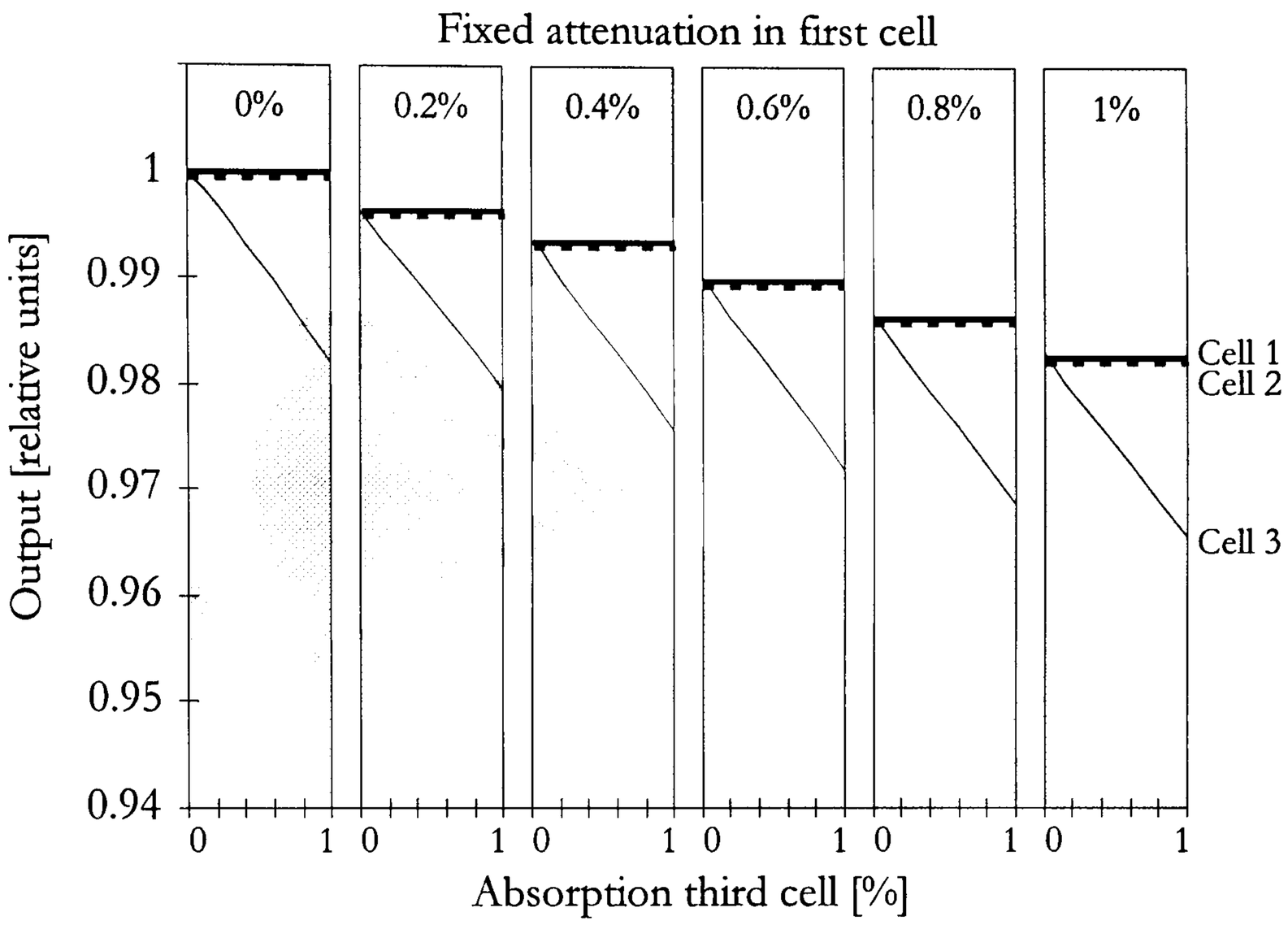

Figure 5.32: *Absorption in the first and third cell*

Figure 5.32 shows the outputs for all sensing cells when the absorption in the first cell is increased in steps, and for each step the absorption in the third cell is increased. The second cell absorption is set to zero. The absorption increases for the first and consequently for the second unit are reflected in the step like output, whereas the third output falls linear within the constant first cell absorption region.

Without regard to previous influences the sensitivity in each sensing unit is approximately the same. Because of the absorption the output's are only downwards shifted and the shift scale is depended on the preceding level of absorption.

5.3. FMCW with Coherence Addressing

The second proposed serial quasi distributed sensing system combines the Frequency Modulated Continuous Wave technique, coherence properties of the source and the optomechanical characteristics of the microoptic cell. As with previous addressing mechanism, the connecting fibres between two successive sensing cell are always much greater than the coherence length of the source and the beams from two different cells should not interfere. By modifying the initially introduced microoptic cell such that the first GRIN lens is turned with the anti reflection coating facing the capillary, we introduce an additional backreflected signal from the measuring cell (Figure 5.33).

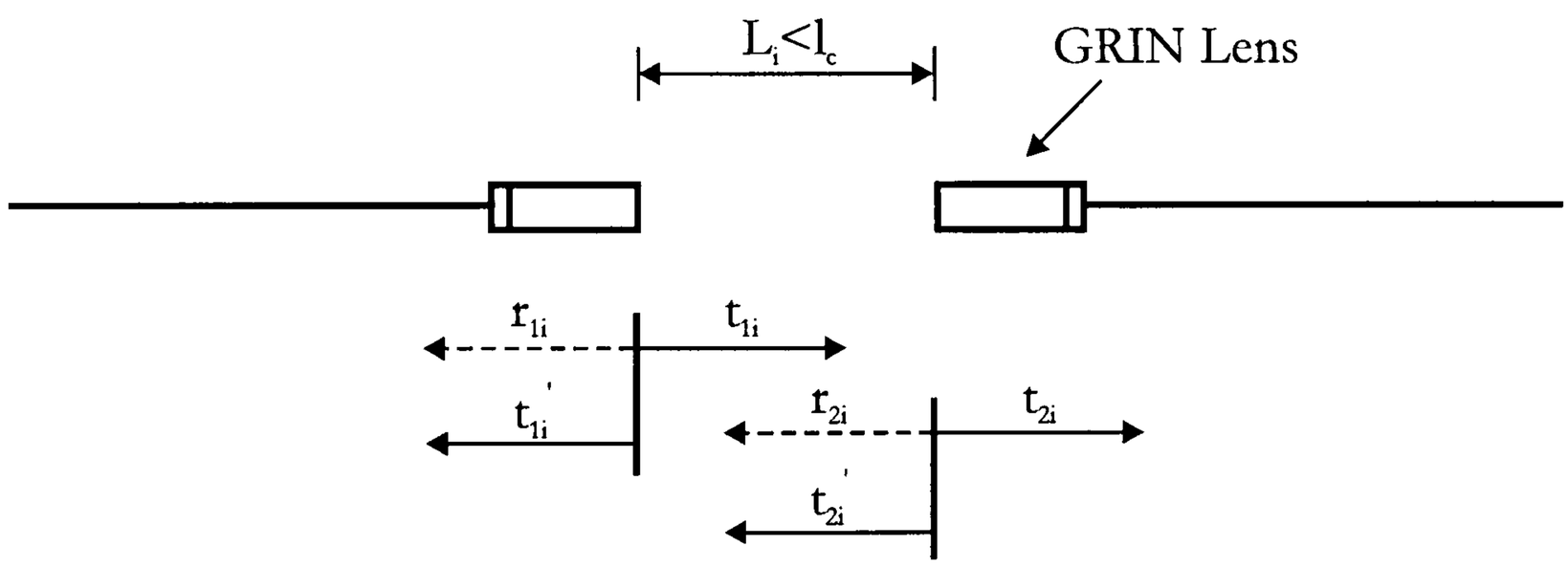

Figure 5.33: *Sensing unit used for coherence addressing of absorption sensors by the FMCW method*

If the separation between the GRIN lens is smaller than the coherence length of the source l_c, the backreflected signals will generate an interference pattern. We refer to this scheme as *FMCW with Coherence Addressing.*

In the same manner as for the reference arm method, a quasi-distributed system consisting of three microoptic sensing cells will be employed. The system configuration is shown in Figure 5.34.

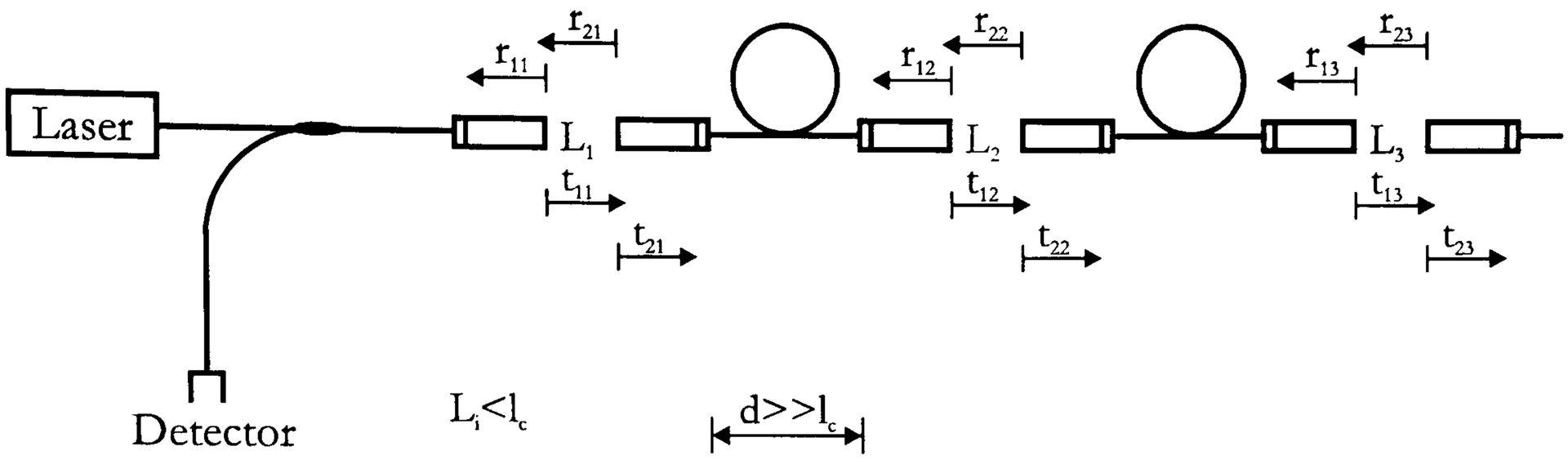

Figure 5.34: *FMCW with Coherence Addressing*

Since in this configuration the reference arm is omitted, standard problems associated with interferometers are not expected. Both signals from the cell experience almost the same optical path (apart from the cell length difference). Beginning with one sensing unit the output on the detector reads as:

$$I_{out}^{1} \propto \left\langle A_{out}^{1} \cdot A_{out}^{1\,*} \right\rangle = \left[r_{11}\sqrt{(A+Bt)}e^{j\omega} + r_{21}t_{11}t_{11}^{'}\sqrt{(A+Bt)}e^{-\alpha_1 C_1 2 L_1}e^{j(\omega t+\psi_1+\Delta\psi_1)} \right]. \qquad (5.20)$$

$$\left[r_{11}\sqrt{(A+Bt)}e^{-j\omega} + r_{21}t_{11}t_{11}^{'}\sqrt{(A+Bt)}e^{-\alpha_1 C_1 2 L_1}e^{-j(\omega t+\psi_1+\Delta\psi_1)} \right]$$

$$= r_{11}^{2}(A+Bt) + r_{21}^{2}t_{11}^{2}t_{11}^{2'}(A+Bt)e^{-\alpha_1 C_1 4 L_1} +$$

$$2r_{11}r_{21}t_{11}^{2}t_{11}^{2'}(A+Bt)e^{-\alpha_1 C_1 2 L_1}\cos(\psi_1+\Delta\psi_1)$$

The outputs for the second and third units are:

$$I_{out}^{2} = t_1^4 r_{12}^2 (A+Bt)e^{-\alpha_1 C_1 4 L_1} + t_1^4 t_{12}^2 t_{12}^{2'} r_{22}^2 (A+Bt)e^{-[\alpha_1 C_1 4 L_1+\alpha_2 C_2 4 L_2]} + \qquad (5.21)$$

$$2t_1^4 t_{12}t_{12}^{'} r_{12}r_{22}(A+Bt)e^{-[\alpha_1 C_1 4 L_1+\alpha_2 C_2 2 L_2]}\cos(\psi_2+\Delta\psi_2)$$

$$I_{out}^{3} = t_1^4 t_2^4 r_{13}^2 (A+Bt)e^{-[\alpha_1 C_1 4 L_1+\alpha_2 C_2 4 L_2]} + t_1^4 t_2^4 t_{13}^2 t_{13}^{2'} r_{23}^2 (A+Bt)e^{-[\alpha_1 C_1 4 L_1+\alpha_2 C_2 4 L_2+\alpha_3 C_3 4 L_3]} + \qquad (5.22)$$

$$2t_1^4 t_2^4 t_{13}t_{13}^{'} r_{13}r_{23}(A+Bt)e^{-[\alpha_1 C_1 4 L_1+\alpha_2 C_2 4 L_2+\alpha_3 C_3 2 L_3]}\cos(\psi_3+\Delta\psi_3)$$

here L_j is the length of the j-th sensing cell and α_j the j-th intensity attenuation coefficient. The quantity $t_i^2 = t_{1i}t_{2i}t_{1i}'t_{2i}' = (1-r_{1i}^2)(1-r_{2i}^2)$ and is the (power) transmission factor of cell (i).

According to (5.22) for a set-up involving n sensing units the output of the n-th cell reads as:

$$I_{out}^{n} = t_1^4 t_2^4 \cdot\ldots\cdot t_{n-1}^4 r_{1n}^2 (A+Bt) e^{-[\alpha_1 C_1 4 L_1 + \alpha_2 C_2 4 L_2 + \ldots + \alpha_{n-1} C_{n-1} 4 L_{n-1}]} + \quad (5.23)$$
$$t_1^4 t_2^4 \cdot\ldots\cdot t_{n-1}^4 t_{1n}^2 t_{1n}^{2'} r_{2n}^2 (A+Bt) e^{-[\alpha_1 C_1 4 L_1 + \alpha_2 C_2 4 L_2 + \ldots + \alpha_{n-1} C_{n-1} 4 L_{n-1}]} +$$
$$2 t_1^4 t_2^4 \cdot\ldots\cdot t_{n-1}^4 t_{1n} t_{1n}^{'} r_{1n} r_{2n} (A+Bt) e^{-[\alpha_1 C_1 4 L_1 + \alpha_2 C_2 4 L_2 + \ldots + \alpha_{n-1} C_{n-1} 4 L_{n-1} + \alpha_n C_n 2 L_n]} \cos(\psi_n + \Delta\psi_n)$$

The power on the detector is a sum of individual unit outputs:

$$I_{out} = I_{out}^1 + I_{out}^2 + \ldots + I_{out}^n \quad (5.24)$$

5.3.1. Parameter examination for multiple sensor FMCW using coherence addressing

To examine the parameter influence on the output signal and the corresponding power spectrum, a number of simulations have been performed. For simulation experiments equations (5.22) and (5.24) have been coded using the *Mathematica* program package and the influence of the following parameters has been investigated:

- changes in cell length
- changes in backreflection coefficients
- changes in absorption inside the microoptic cell
- signal level decrease with increase in number of sensing units

5.3.1.1.Cell length influence for FMCW Coherence addressing system

As for the FMCW Reference arm addressing system, the sensing unit lengths have been altered. The reference values for the modulation frequency and wavelength

change were set to: $f_{mod}=20Hz$ and $\Delta\lambda=0.7nm$. According to the description of the coherence addressing mechanism the backreflection coefficient of the first and second GRIN lens were set to $r_1^2=r_2^2=0.04$. The absorption inside all cell is set to a constant value of 1%.

For system analysis the joint time and frequency responses for all three sensing units will be given. The main purpose of this analysis is to find the minimal difference between the cell lengths, where the spectral peaks become evident. Here the middle sensing unit length was left unaltered, while the lengths of the remaining first and third unit were successively altered by 1mm (Figure 5.35).

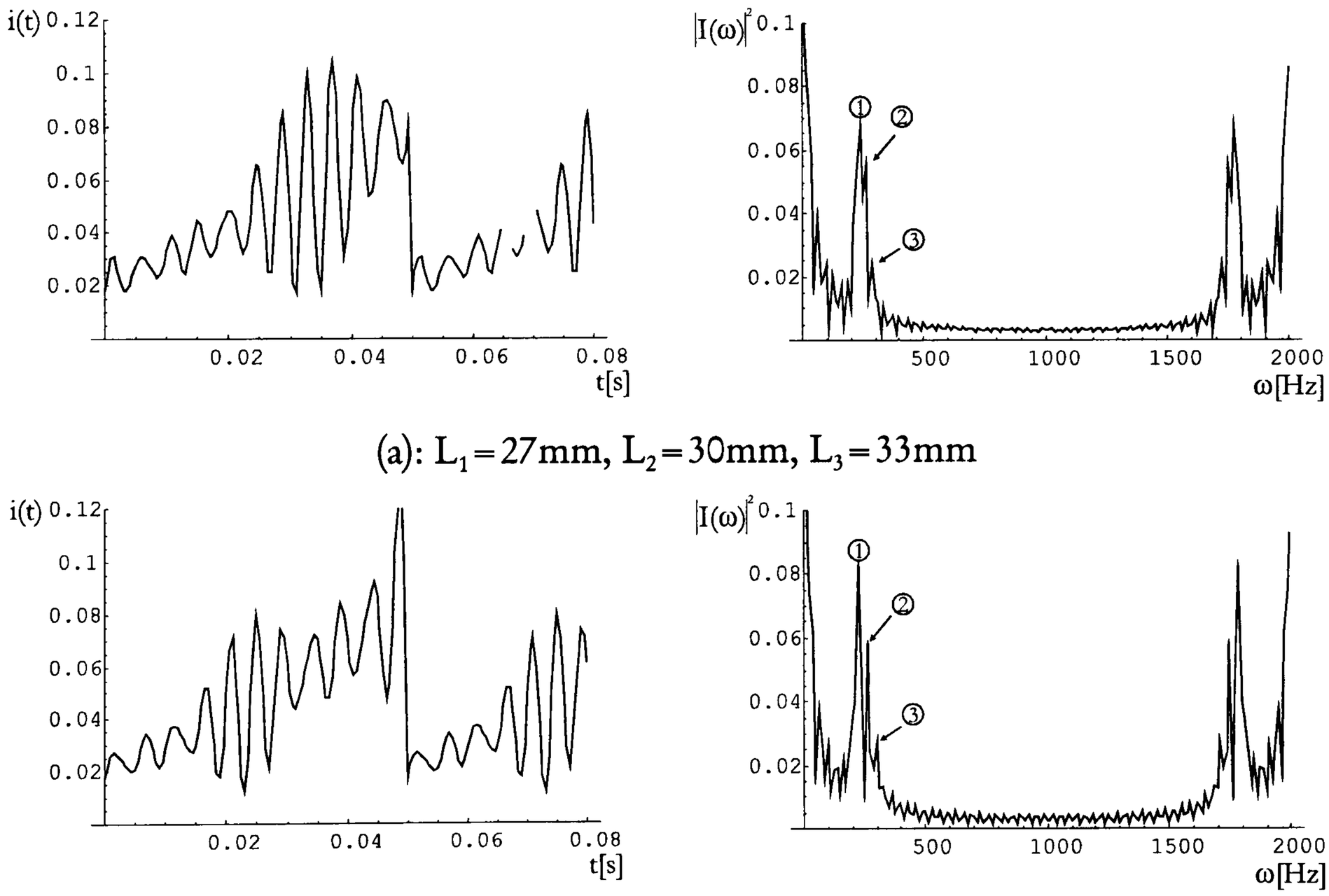

(a): $L_1=27mm$, $L_2=30mm$, $L_3=33mm$

(b): $L_1=26mm$, $L_2=30mm$, $L_3=34mm$

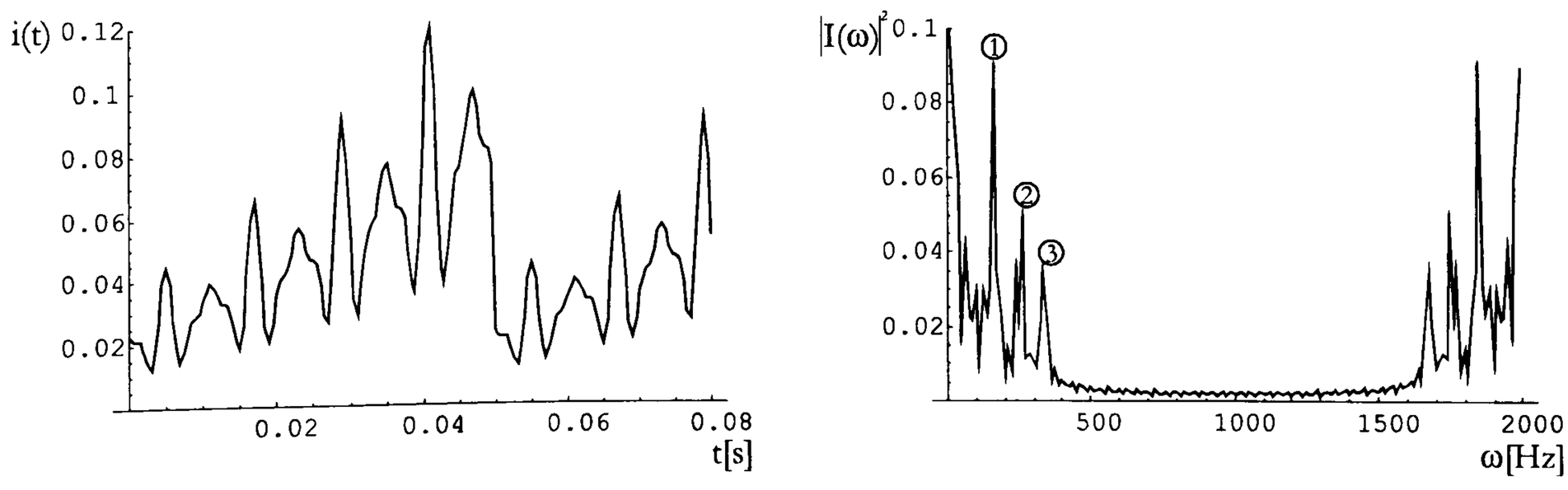

(c): $L_1 = 20mm$, $L_2 = 30mm$, $L_3 = 40mm$

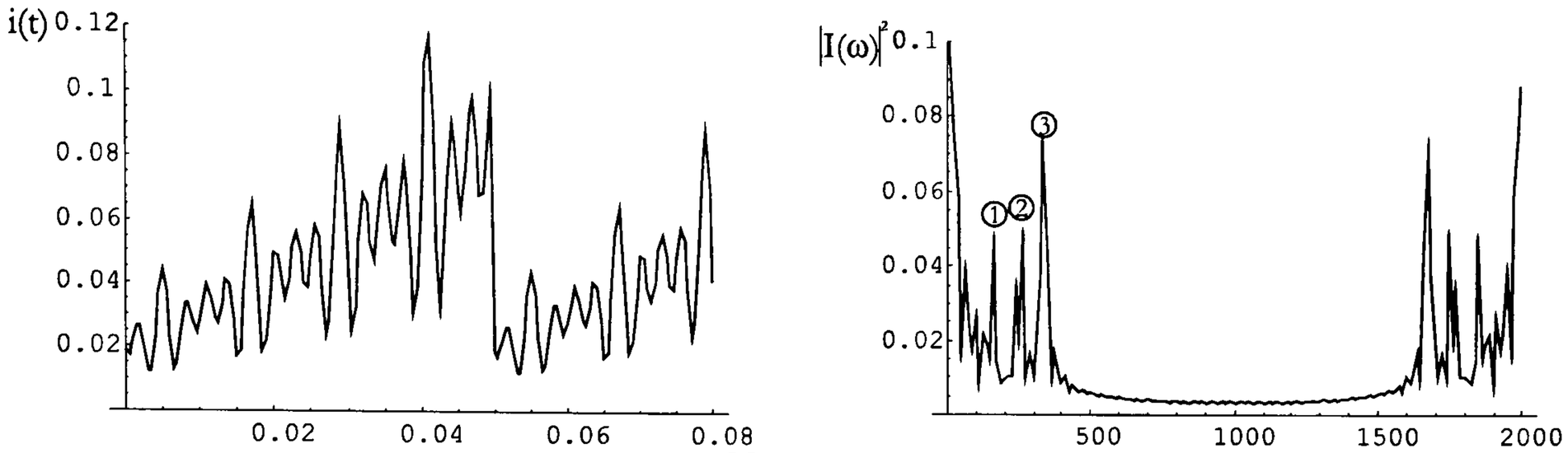

(d): $L_1 = 40mm$, $L_2 = 30mm$, $L_3 = 20mm$

Figure 5.35: *FMCW Coherence addressing: output versus time (left) and appropriate power spectrum (right) for different sensing lengths of the cells*

For a difference between the sensing units of about 3mm (case (a)) the spectral peaks corresponding to individual sensing units start to separate, and are well separated for a difference of 4mm or more. For the 10mm difference between cell lengths both arrangements, first the cells are arranged by starting with the shortest and finishing with the longest cell - case (c), whereas for case (d) the result for the reverse order are presented are presented. Using the reverse order the signal decay due to cell number increase is partially compensated and the spectrum peaks have approximately the same amplitude. With such a method, if using cell which lengths differ by minimum of 4 mm, a set-up of 10 serial sensing units with cell lengths from 50 mm to 10 mm could be incorporated. More emphasis on the number of sensing cells will be given in some of the next sections, where signal level decrease with increase in number of sensing units will be presented.

5.3.1.2. Influence of reflection coefficients on the coherence addressing of absorption sensors by the FMCW method

For the reflection coefficient influence analysis using FMCW Coherence addressing we suppose a 2.5% Methane concentration inside each cell. A set-up

with three sensing units with equal backreflection coefficient for both reflections inside the cell have been considered. The analysis includes two sets of simulation experiments. In the first set of simulations the cells lengths were 72mm, 60mm and 48mm for the first, second and third cell. For the second set we changed the cell length arrangement starting with the shortest and ending with the longest cell.

In both cases the backreflection coefficients for the first and last cell were changed in the range from 2% to 8%, whereas the second cell reflections were kept constant at 4%.

In order to evaluate the system and find the appropriate reflection coefficient and cell length distribution two output quantities have been observed. First, the output value of the last unit is interesting due to the signal decay in a serial arrangement of the system. The high of the signal amplitude signal effects the number of sensing cells which can be arranged in series. The second signal which has to be considered is the returning measuring optical signal. Since we would like to have a high output signal, but still maintain enough returning beat signal amplitude to detect and resolve individual measuring points we introduced a ratio between the last output signal amplitude and the returning signal amplitude.

The last unit output dependence on the backreflection coefficients in the first and last cell is shown in Figure 5.36 and the ration between the last output signal amplitude and the returning signal amplitude is presented in Figure 5.37.

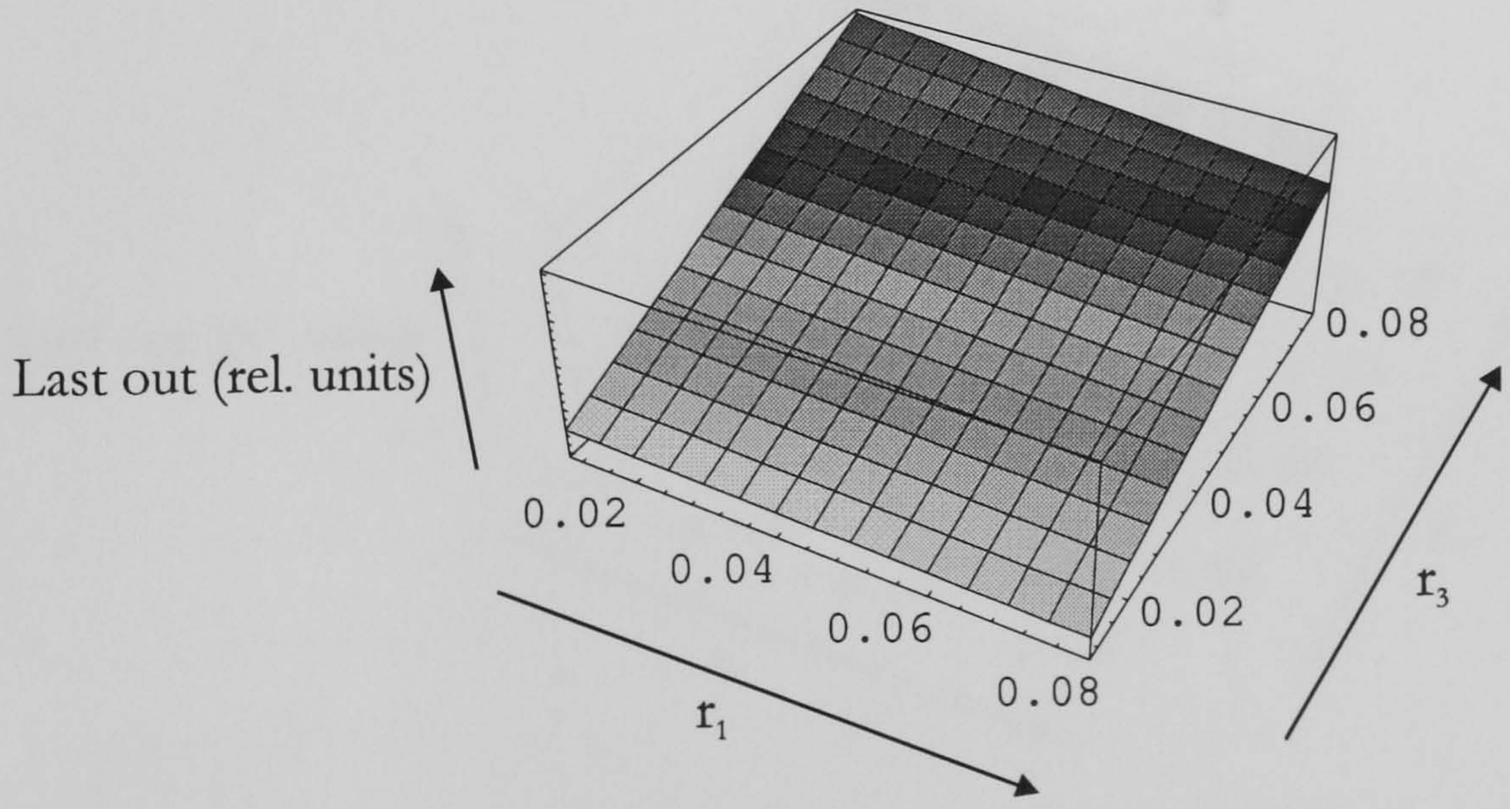

Figure 5.36: *Last unit output versus cell backreflection coefficients; L_1=72mm, L_2=60m and L_3=48mm*

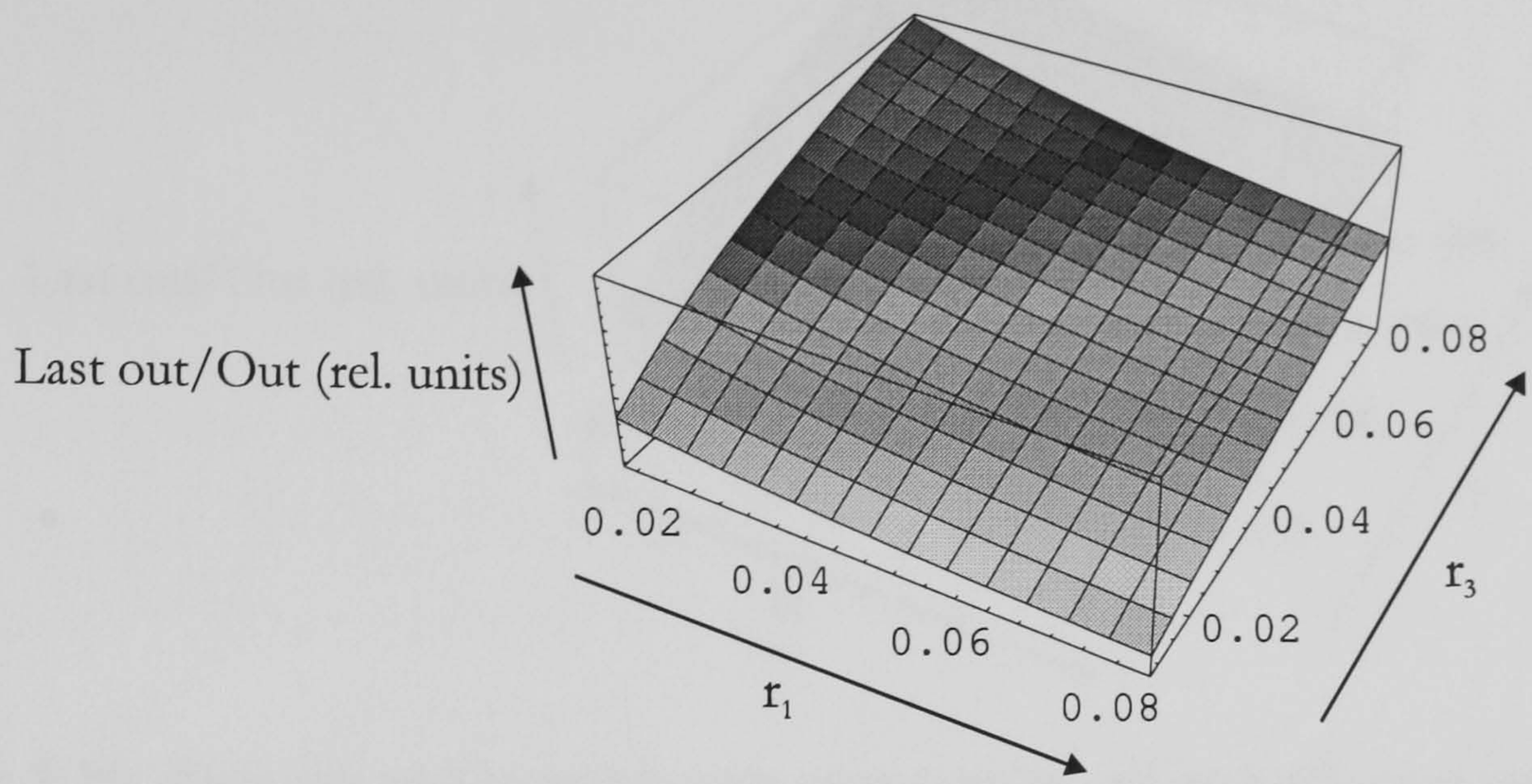

Figure 5.37: *Ratio last unit output/system output versus cell backreflection coefficient; L_1=72mm, L_2=60mm and L_3=48mm*

For both output values similar conclusions can be made. To ensure high last output amplitude and hence a high number of sensing units connected in series, together with enough returning power to detect and resolve individual measuring points the values of the backreflection coefficients should increase with the number of sensing units. Considering the surface graphs in Figure 5.36 and Figure 5.37 the values of 2%, 4% and 8% for the first, second and third cell would represent the best selection.

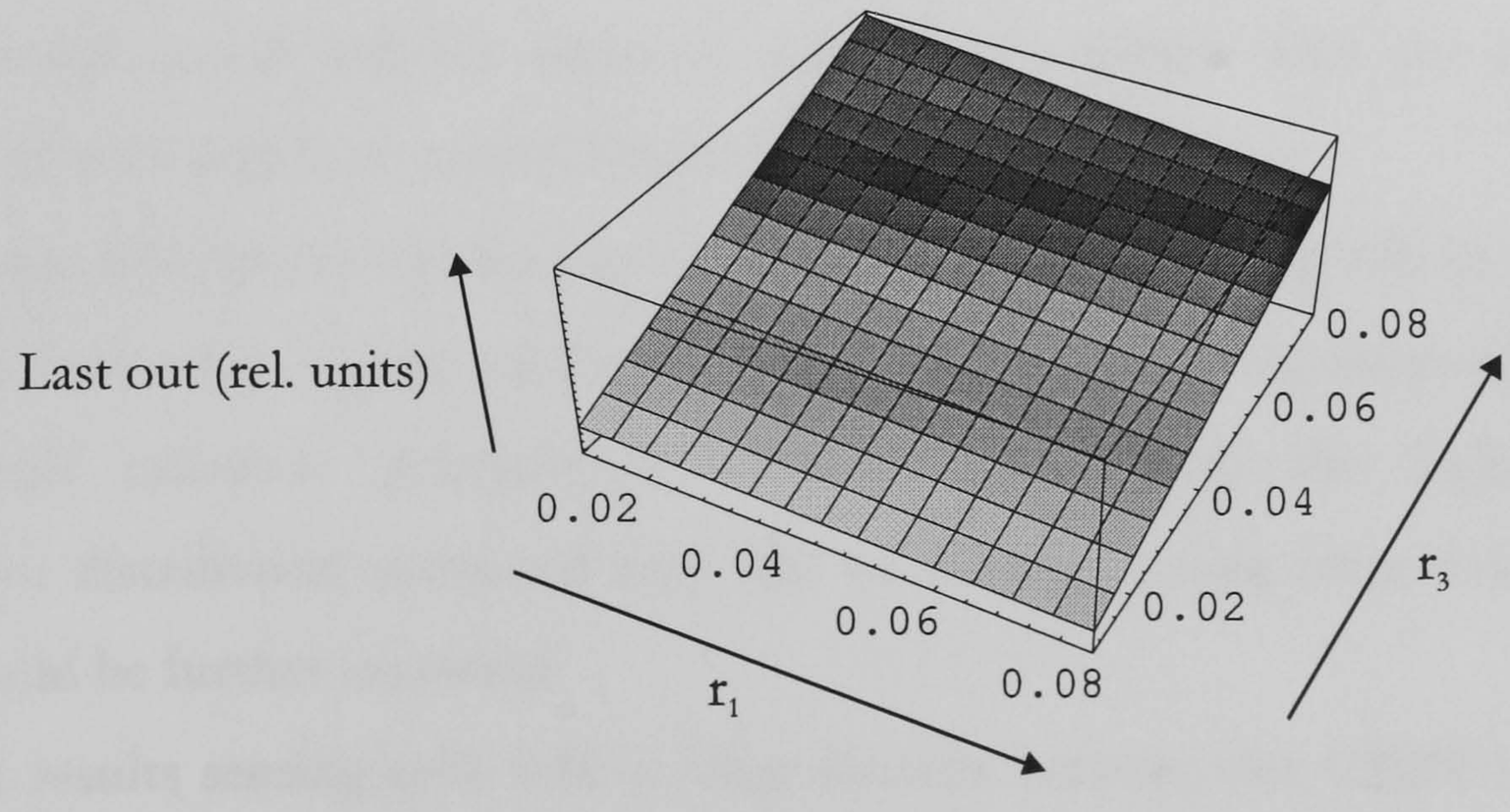

Figure 5.38: *Last unit output versus cell backreflection coefficients; L_1=48mm, L_2=60mm and L_3=72mm*

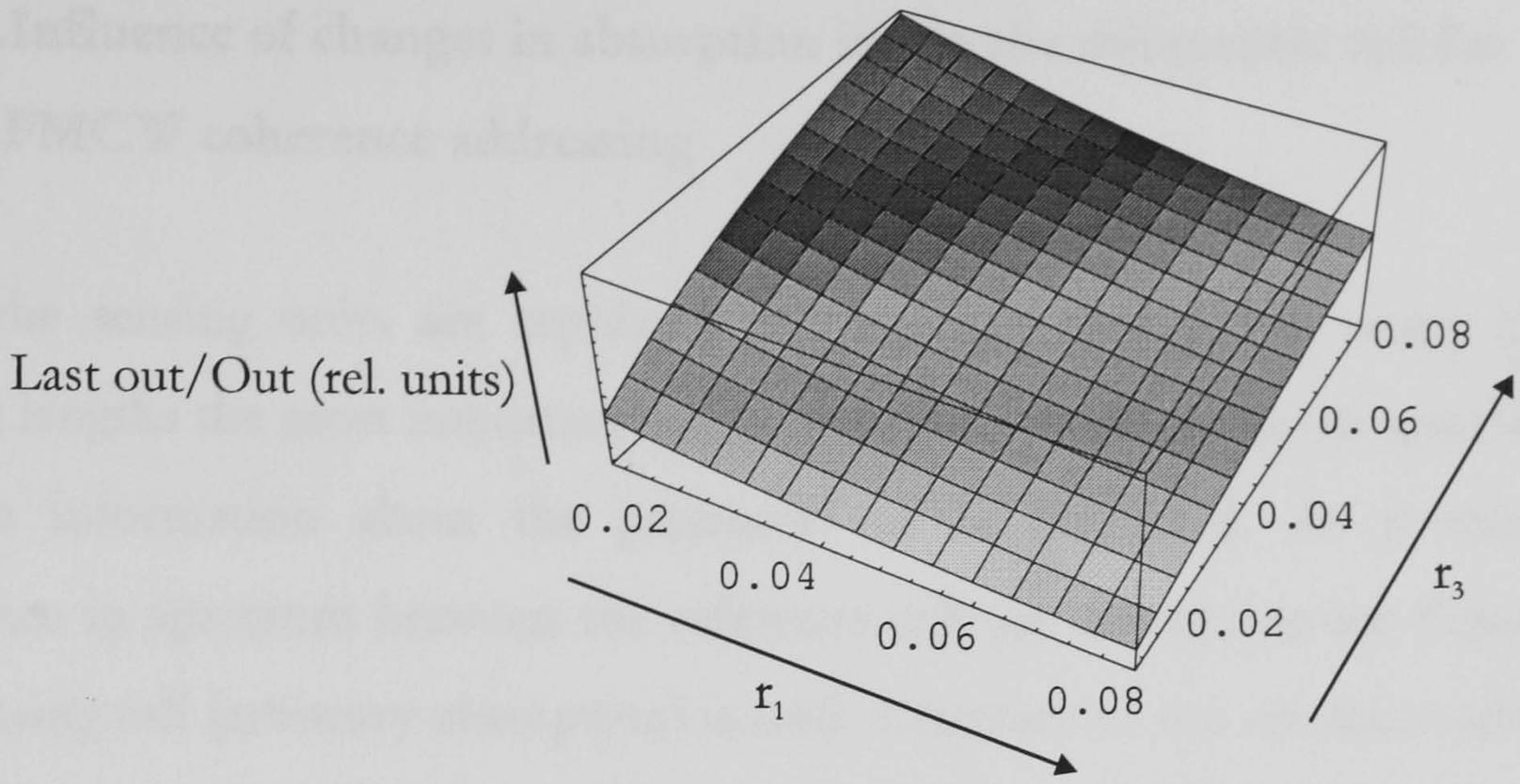

Figure 5.39: *Ratio last unit output/system output versus cell backreflection coefficient; L_1=48mm, L_2=60mm and L_3=72mm*

Almost identical conclusions can be made if observing the last unit output dependence and the ration between the last output signal amplitude and the returning signal amplitude shown in Figure 5.38 and Figure 5.39.

Focusing on the influence of the backreflection coefficients we may found out that to increase the number of sensing units and maintain enough returning power to detect and resolve individual measuring points the values of the backreflection coefficients have to gradually increase with each new sensing unit. The minimum, maximum values and the increase of the backreflections depend mostly on the input optical power and the signal to noise ratio together with the maximum number of cells which we would like to implement.

For current simulations the lengths of the cells did not play a significant role since we got very similar conclusions for both cases. When combining the results for the cell length influence presented in Chapter 5.1.4.2 with the backreflection coefficient distribution presented here, the number of sensing units connected in series could be further increased.

For best results sensing cells with a large distance between the GRIN lenses and low backreflection coefficient in the beginning and cells with short distance between GRIN lenses and larger backreflection coefficients for final measuring units should be used.

5.3.1.3.Influence of changes in absorption inside the microoptic cell for FMCW coherence addressing

After the sensing units are separated in frequency domain by using different sensing lengths the most important task is to measure the change in spectral peaks for the information about the parameter to be measured. As previously, a difference in spectrum between the reference cell (no absorption-see Figure 5.40) and sensing cell (arbitrary absorption) is used. Contrary to the reference addressing scheme, a spectral peak tracking has to be used. Because different peaks represent different sensing units we have to track each separately to determine the measured value as shown before in Figure 5.22.

In Figure 5.41 three cases are presented. First same absorption level of 0.05% is used for all sensing units, second the absorption is successively increased and third the absorption is successively decreased. Cell lengths are $L_1=20mm$, $L_2=30mm$ and $L_3=40mm$.

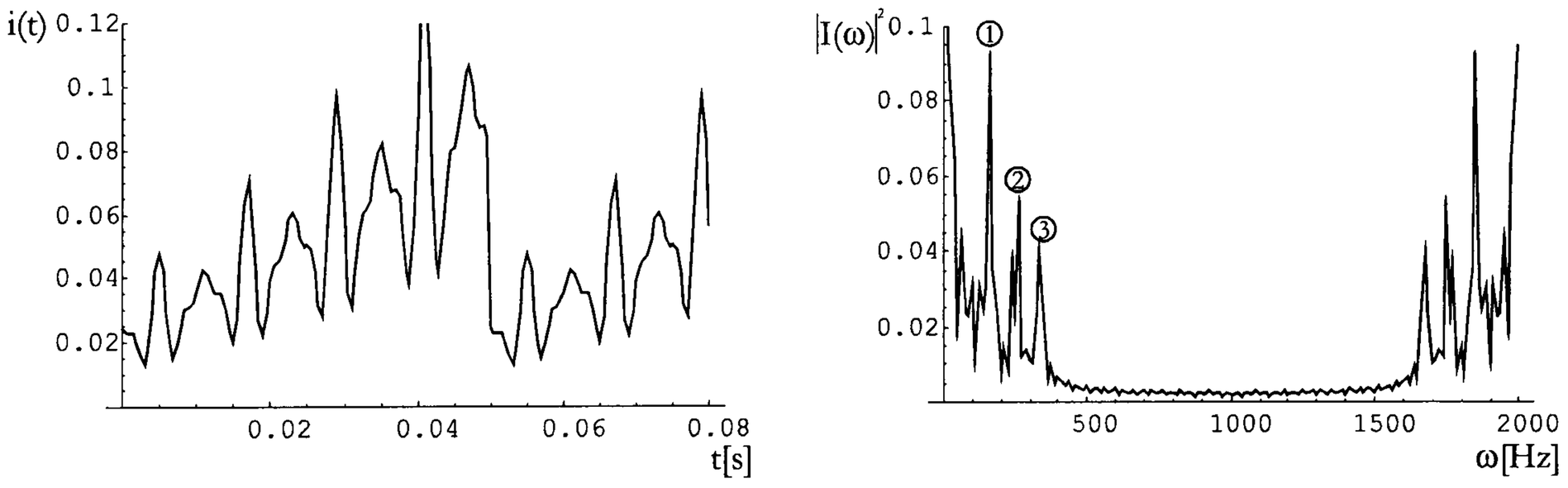

Figure 5.40: *Output time response (left) and power spectrum (right) used as a "reference" for further comparison; $L_1=20mm$, $L_2=30mm$ and $L_3=40mm$*

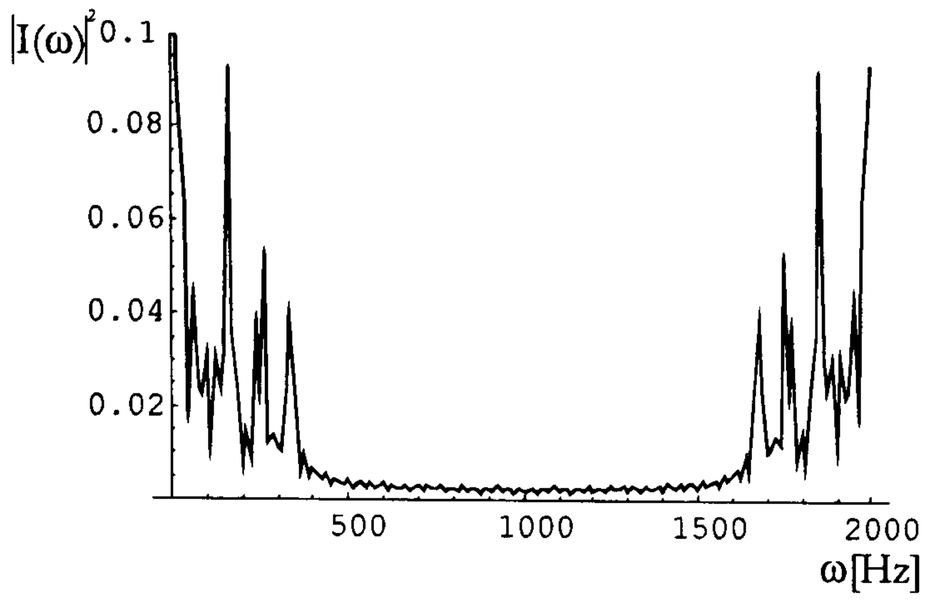

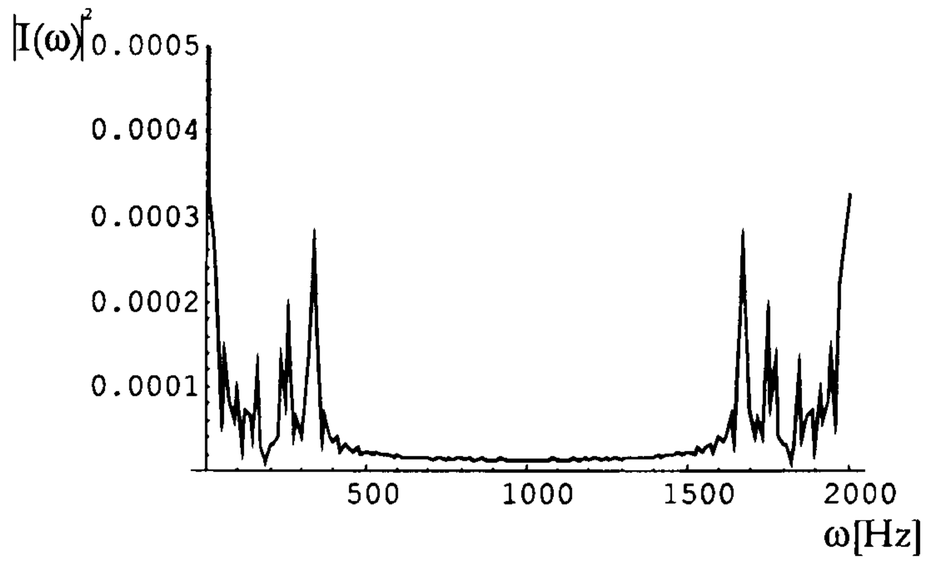

$\alpha_1 C_1 = 0.025 m^{-1}$ (0.05%), $\alpha_2 C_2 = 0.025 m^{-1}$ (0.05%), $\alpha_3 C_3 = 0.025 m^{-1}$ (0.05%)

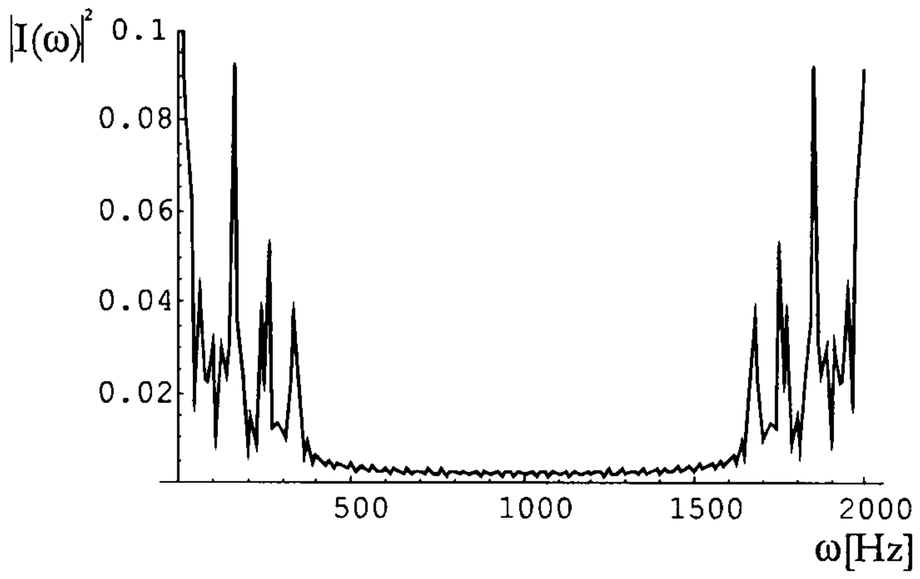

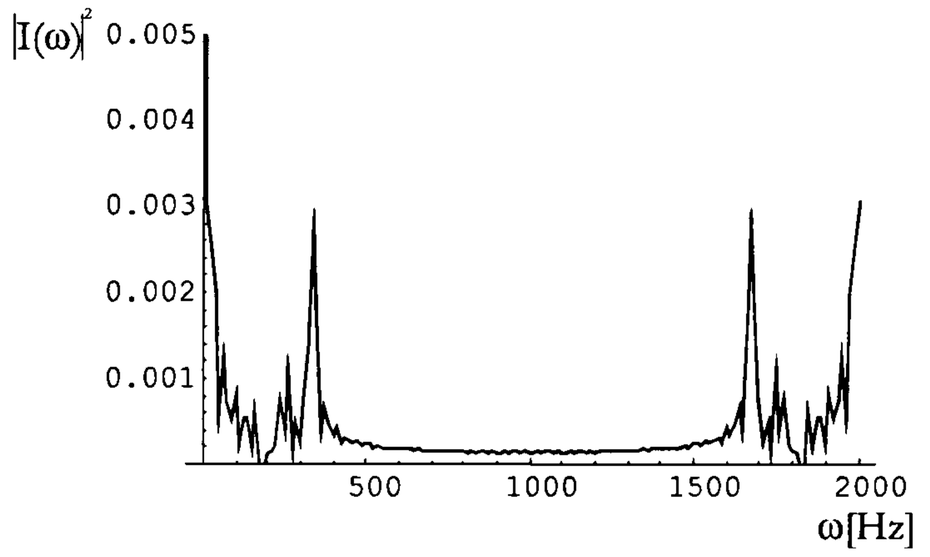

$\alpha_1 C_1 = 0.05 m^{-1}$ (0.1%), $\alpha_2 C_2 = 0.2506 m^{-1}$ (0.5%), $\alpha_3 C_3 = 0.502 m^{-1}$ (1%)

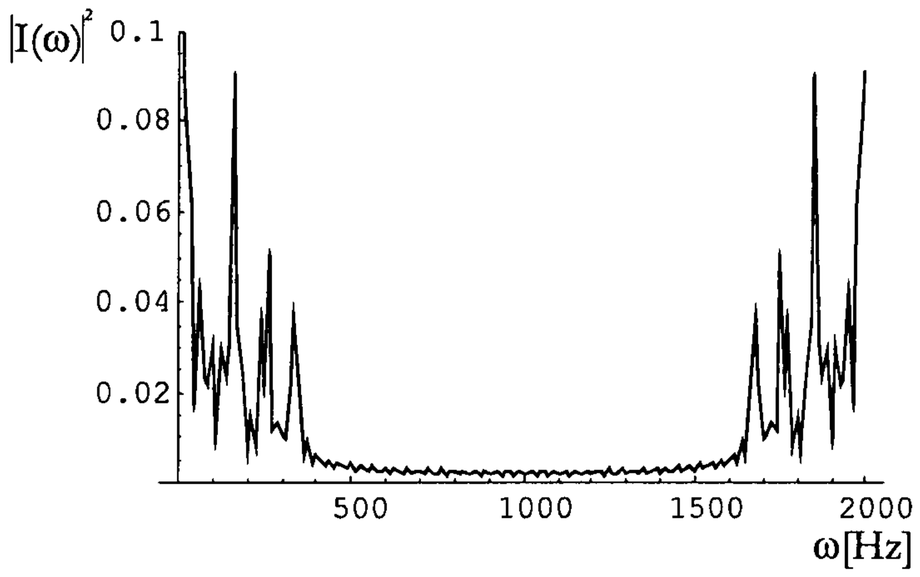

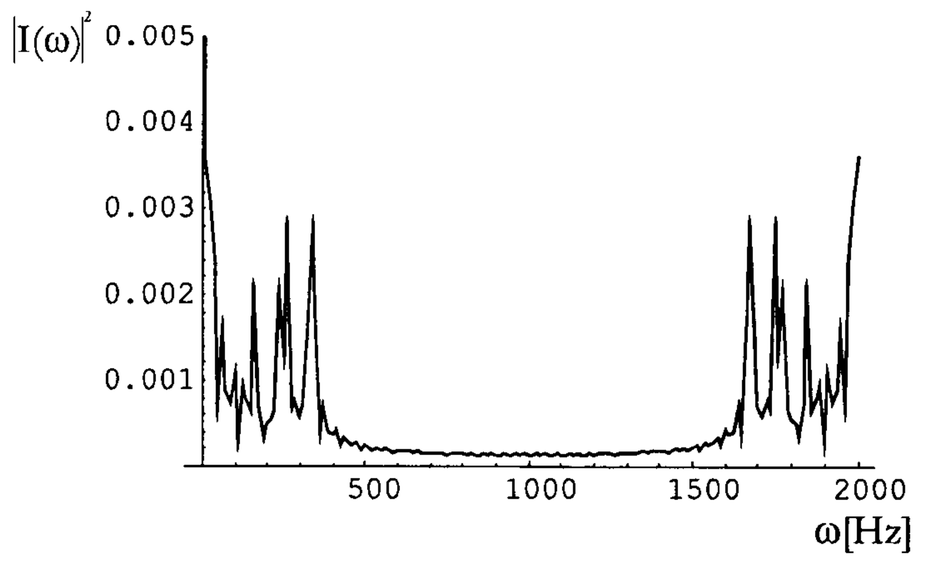

$\alpha_1 C_1 = 0.502 m^{-1}$ (0.1%), $\alpha_2 C_2 = 0.2506 m^{-1}$ (0.5%), $\alpha_3 C_3 = 0.05 m^{-1}$ (0.1%)

Figure 5.41: *Frequency response (left) and difference between the "reference" and sensing cell (right) for different levels of absorption*

As evident from the first experiment, all three measurands are very well defined if observing the difference between the reference and sensing cells. From the amplitude of each peak the absorption is determined. Greater absorption corresponds to smaller spectral amplitudes and vice versa. As in the case of cell length reduction with increase in number of sensing units, the spectral amplitudes become comparable when decreasing the absorption level downwards the serial link. Although there is no influence on the absorption distribution, this special

case of output could be used as an identification sign that the concentration is decreasing or increasing along the sensing system.

5.3.2. Signal power

Similar as in the case of Reference arm addressing the optical power used for each sensor is decreased if the number of sensors is increased.

If considering FMCW with coherence addressing the maximum number of sensors is limited by two factors: the available space in the frequency domain and the optical source power. The available space in the frequency domain is limited by the coherence length of the source. With the increase of the coherence length of the source also the optical path difference between both reflection from the microoptic sensing cell which interfere could be larger. To distinguish between different beat frequencies in the power spectrum at the detector, every sensing unit should have its own unique optical path difference. If the coherence length is large the number of unique optical path differences is increased and hence the total number of sensing cells connected in series is greater. The maximum number of sensors due to available frequency space N_{maxf} is calculated as:

$$N_{\text{maxf}} = \frac{\omega_c}{\Delta\omega} \tag{5.25}$$

where ω_c is the beat frequency corresponding to the coherence time of the source, hence the maximum beat frequency and $\Delta\omega$ is the minimum difference between two beat frequencies.

The second limitation for the maximum sensor number is the optical source power and the signal to noise ratio of the receiver. Because every glass/air reflection reduces the optical power, a minimum 0.35dB loss for every sensing cell is expected. A detailed SNR analysis will be presented in Chapter 9.6.

5.3.2.1.Signal level decrease because of the sensing unit number increase for FMCW coherence addressing

Similar to the reference arm addressing scheme the output signal amplitude decreases with number of sensing units. To represent this effect a program has been written which calculates the output amplitude of the i-th cell. For all sensing units the same amounts of absorption (1%, 0.5%, 0.1% or 0.05%), same sensing cell lengths (30mm) and reflection coefficients (0.04 and 0.1) have been assumed. The signal level versus unit number is shown in Figure 5.42.

With additional sensing units the signal is weakening exponentially as the number of sensors increases. From first to the tenth unit there is a 12.8dB decrease, from first to the fifteen a 20.4db and for 20 sensing units a 32.33db decrease.

The FMCW coherence addressing method enables the use of approximately 10 to 12 sensing units (supposing 1% absorption in each cell) connected in series.

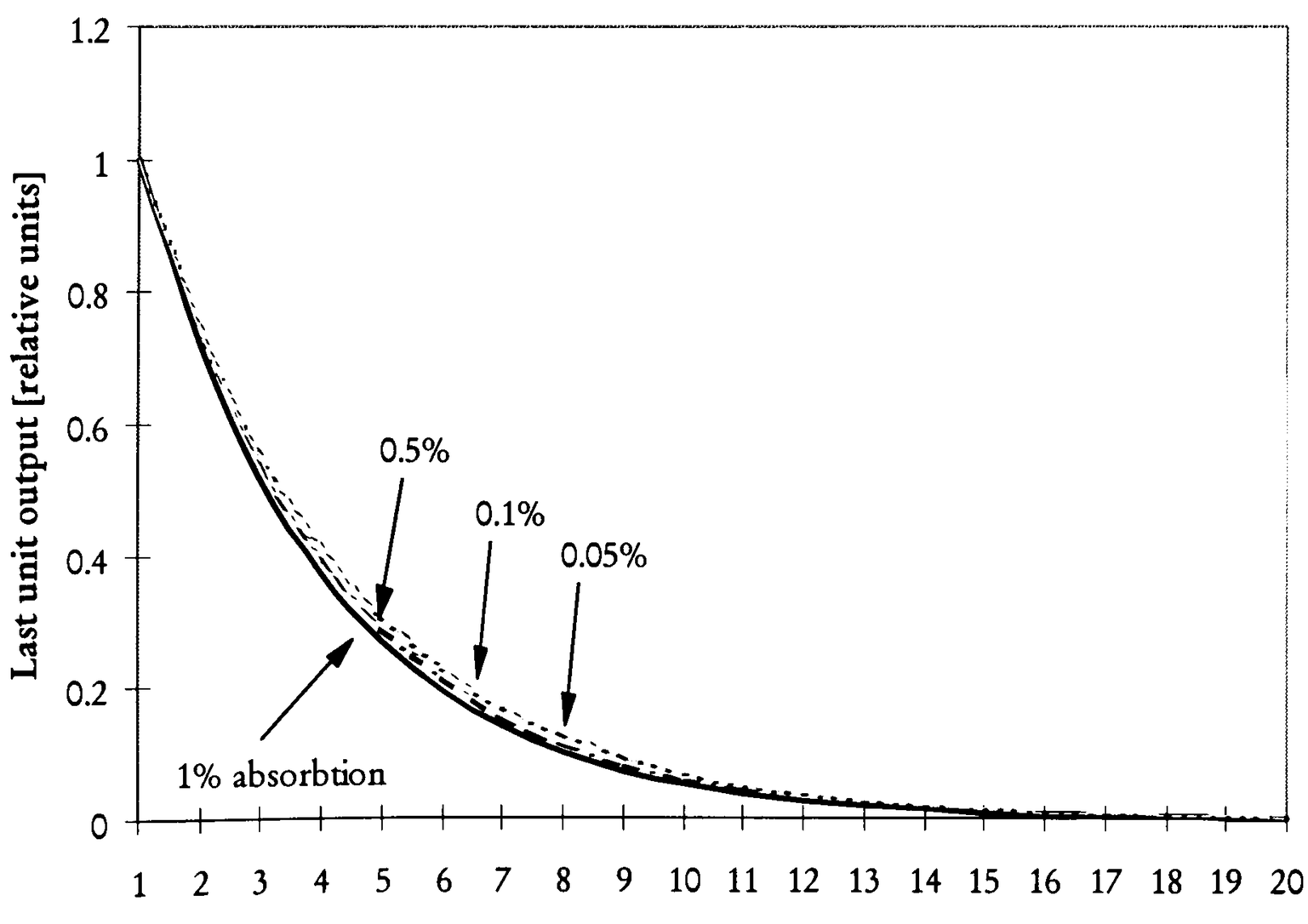

Figure 5.42: *Signal level versus number of sensing units for FMCW coherence addressing*

5.3.3. Coherence addressing of quasi-distributed absorption sensors by the FMCW method - simulation results

For the coherence addressed system with three microoptic sensing cells the same procedure as with the reference arm method was used to simulate quasi-distributed absorption measurement. To analyse the influence of different levels of absorption for subsequent cells and the overall system performance a range of possible combinations of sensing cell absorption has been evaluated. Attenuation in one of the cells increased in fixed steps (from block to block) whereas the other cell experiences the attenuation of 0-1% across each block in 0,2% steps. Only evaluations where one of the cells experiences zero absorption at the time were made. The output characteristics are shown in Figure 5.43 to Figure 5.48.

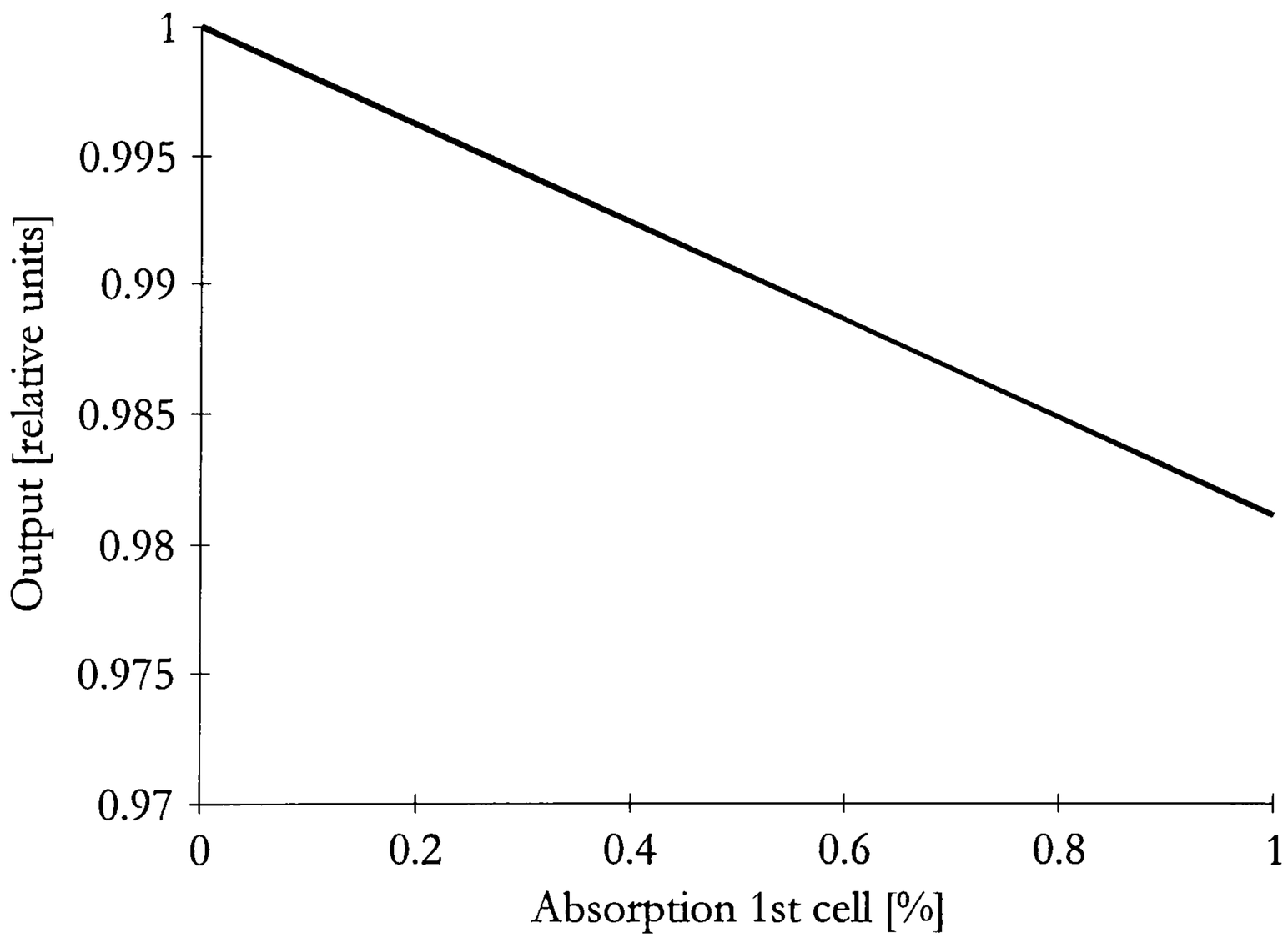

Figure 5.43: *Coherence addressing - absorption in the first cell*

With increased absorption in the first cell the output value, which is determined by the first peak of the power spectrum, falls linear with the absorption (Figure 5.43). Because of the successive arrangement of the sensing cells the influence from

the cells in the beginning is transferred to the subsequent cells. As shown in Figure 5.44 and Figure 5.45 the additional absorption causes the downward shift of the output characteristics, whereby the sensitivity stays the same. Because of the zero absorption in the third unit the third output is just following the second one.

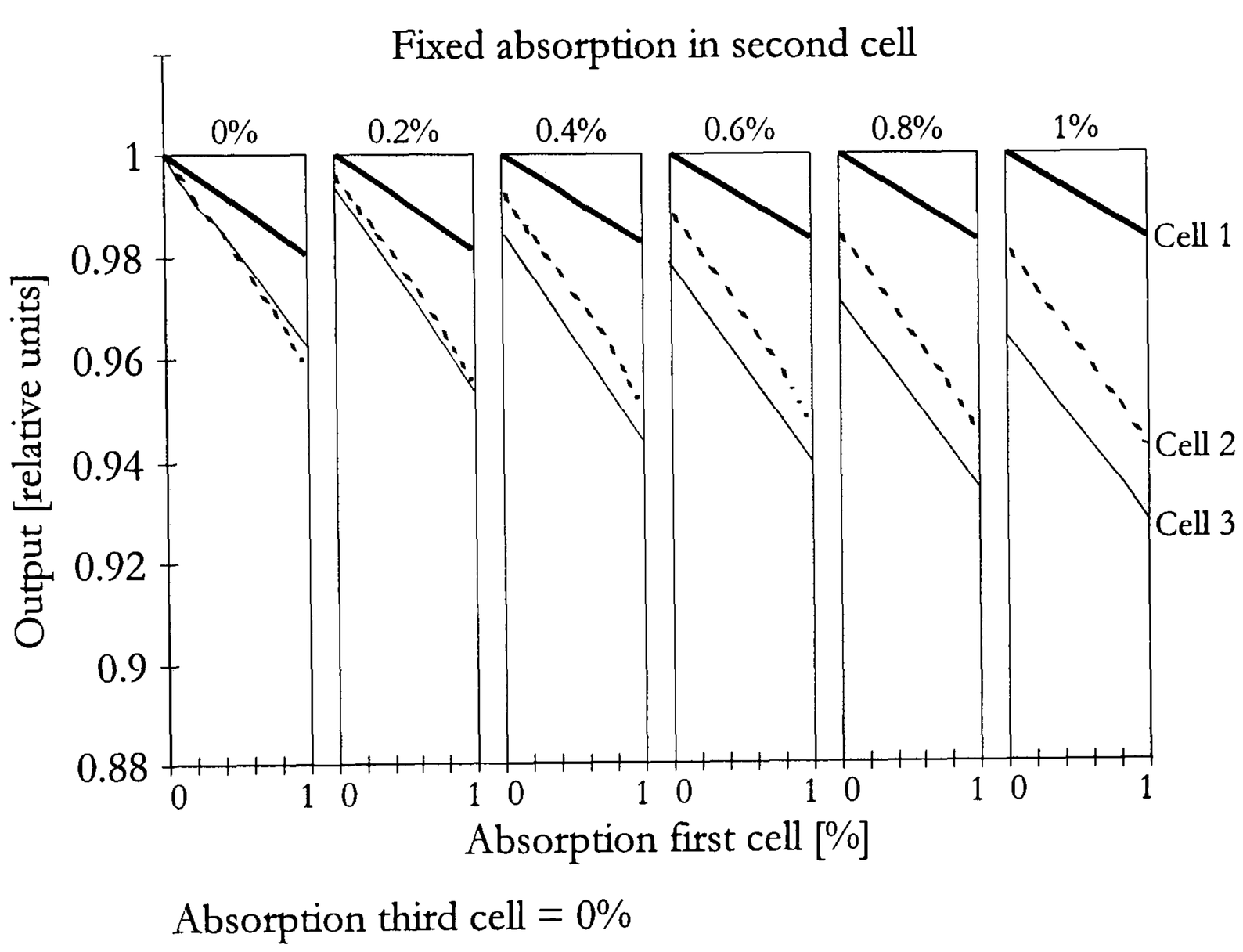

Figure 5.44: *Coherence addressing - absorption in the second cell held at fixed values shown*

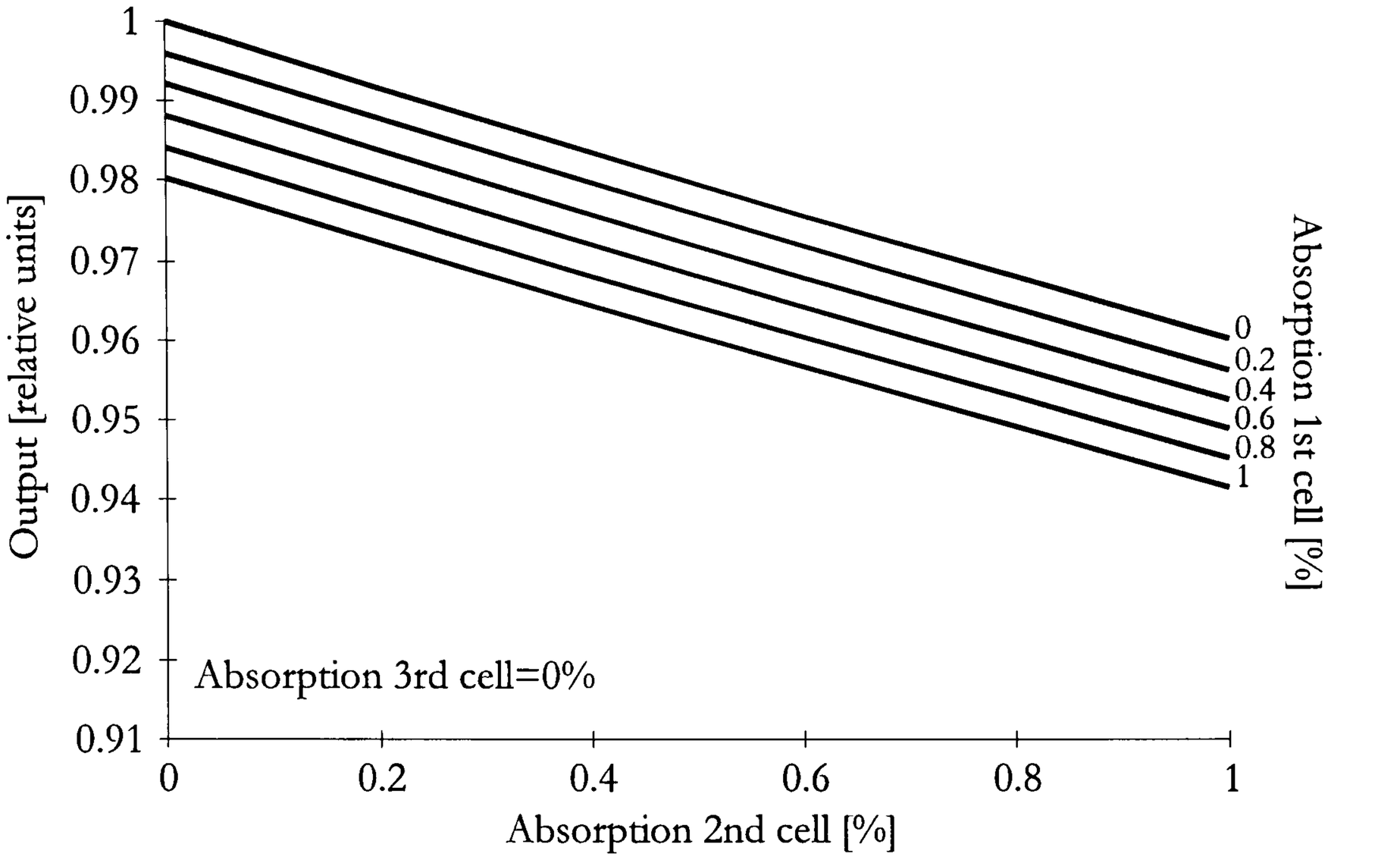

Figure 5.45: *Coherence addressing - absorption of the second cell for different values of first cell absorption*

Very similar results are obtained when observing the third cell output with a zero absorption in the second cell (Figure 5.46). The ratio between first and second stays constant and a linear regression of the third cell with increased absorption is present.

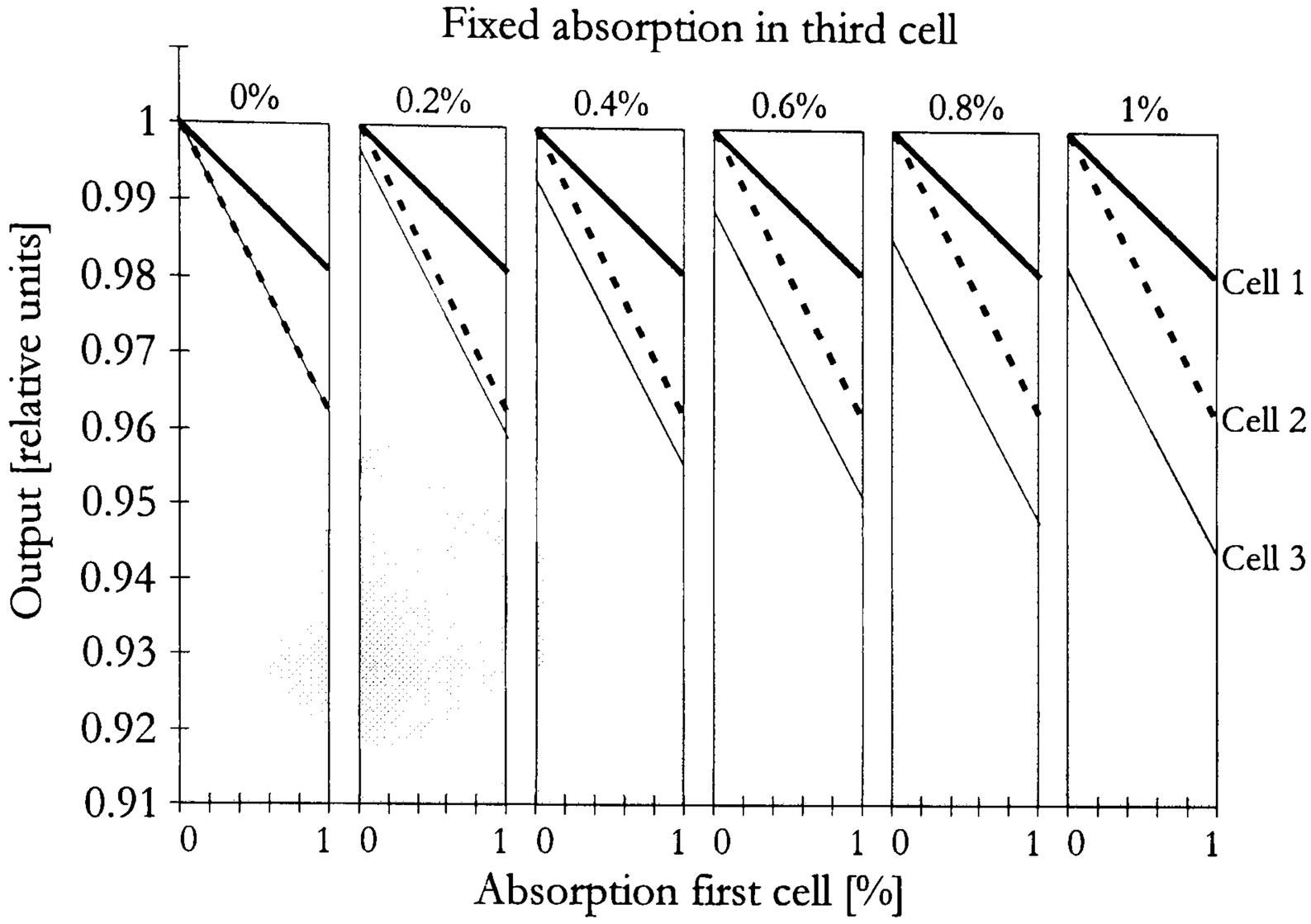

Figure 5.46: *Coherence addressing - absorption in the third cell held at fixed values shown*

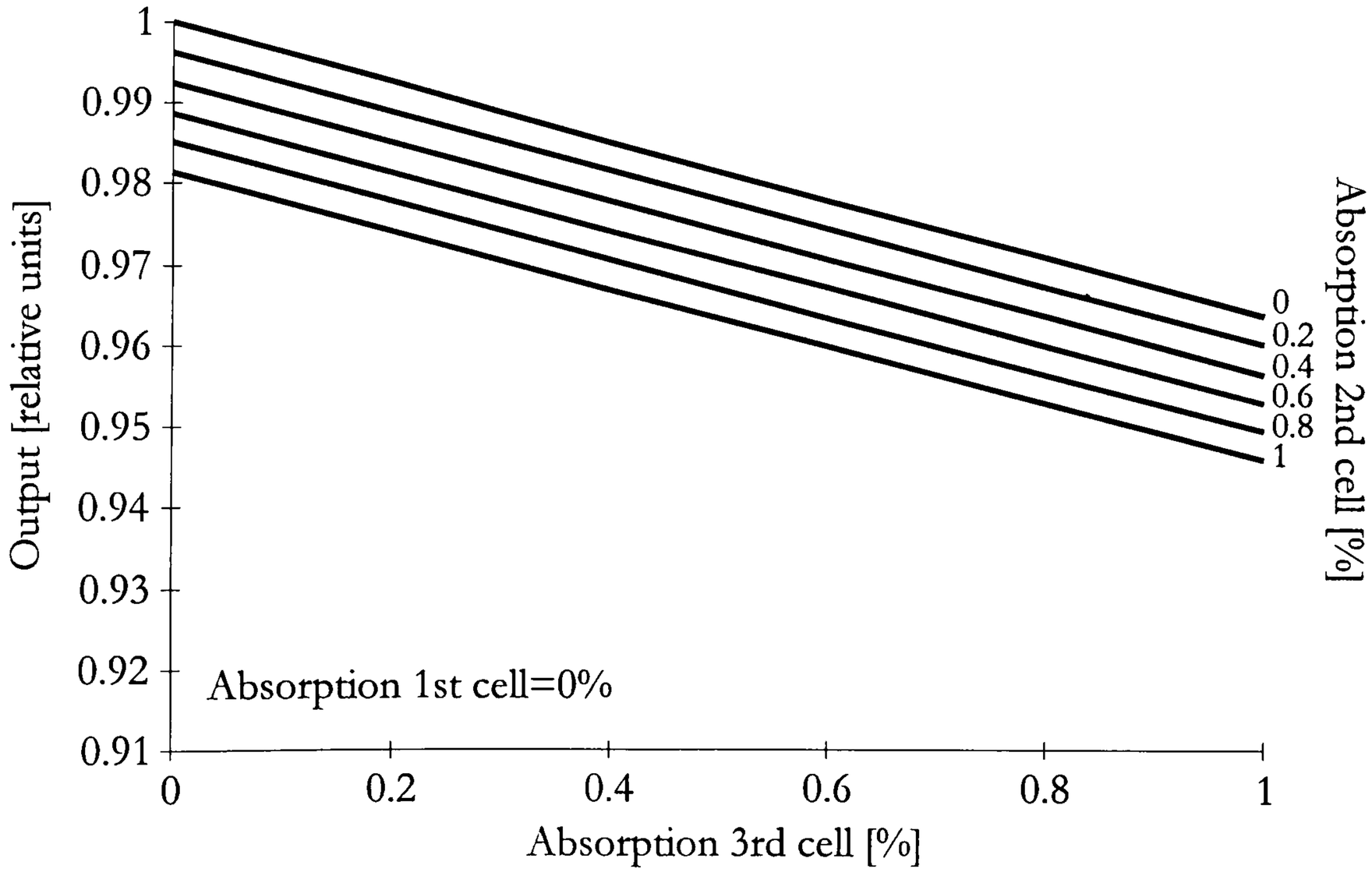

Figure 5.47: *Coherence addressing - absorption of the third cell for different values of second cell absorption*

For zero absorption values of the first cell this sensing unit can be abandoned and the linear characteristics of the third cell absorption is vertically shifted due to second cell influence (Figure 5.47).

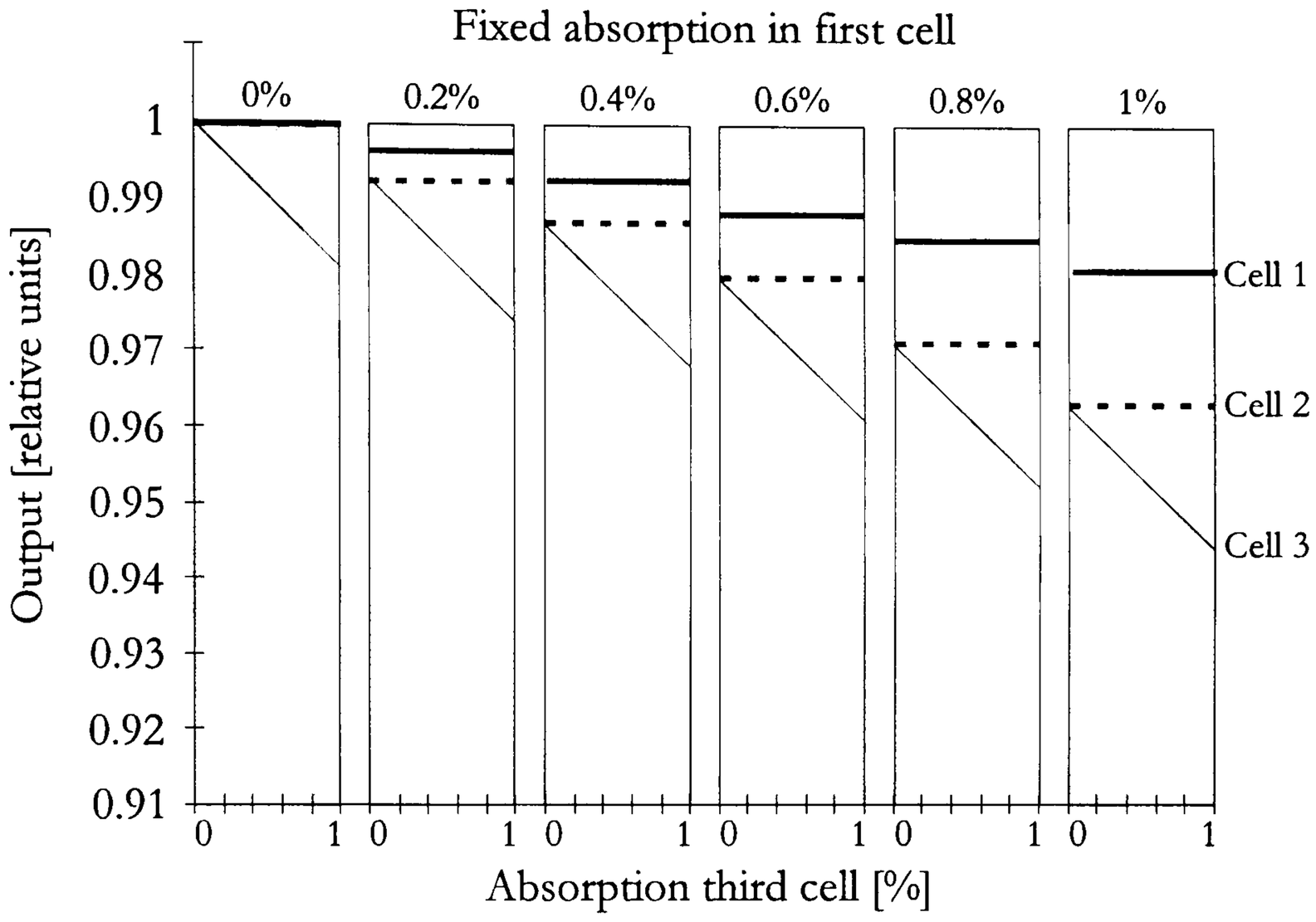

Figure 5.48: *Coherence addressing - absorption in the first cell held at fixed values shown*

Figure 5.48 represents the output curves for all cells for zero second cell absorption. The increase of the absorption in the first cell causes a step like response for the first and consequently second unit.

Without regard to preceding cells the sensitivity in each sensing unit is approximately the same and is mostly influenced by the length of the cell.

5.4. Forward FMCW

In both previously presented quasi distributed sensing schemes, the backreflection signals were used for the interference output. Another possibility is to use the forward travelling signals and a detector connected to the distal end of the sensing

system. As shown in Figure 5.49 some additional reflection points are used in order to get two forward travelling signals for each sensing unit which will interfere at the detector.

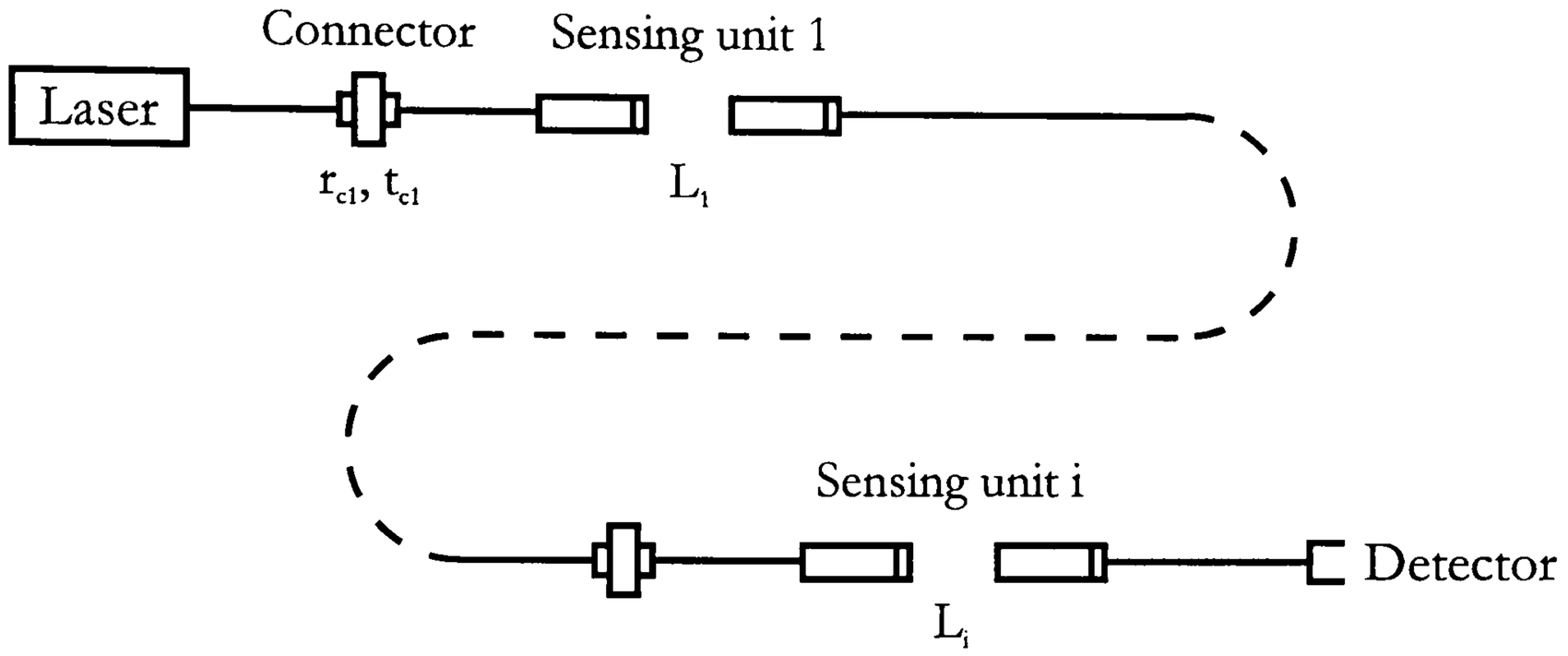

Figure 5.49: *Forward FMCW sensing system*

Additional reflections are provided using the air gap in a ordinary connector. One part of the light travels through the connector, is reflected from the second GRIN lens, travels back to the connector, is there reflected and passes the sensing cell once again before passing through the second GRIN and continuing towards the detector (Figure 5.50). The other part is reflected from the first GRIN, and continues the same way as the first part approaching the sensing region just once.

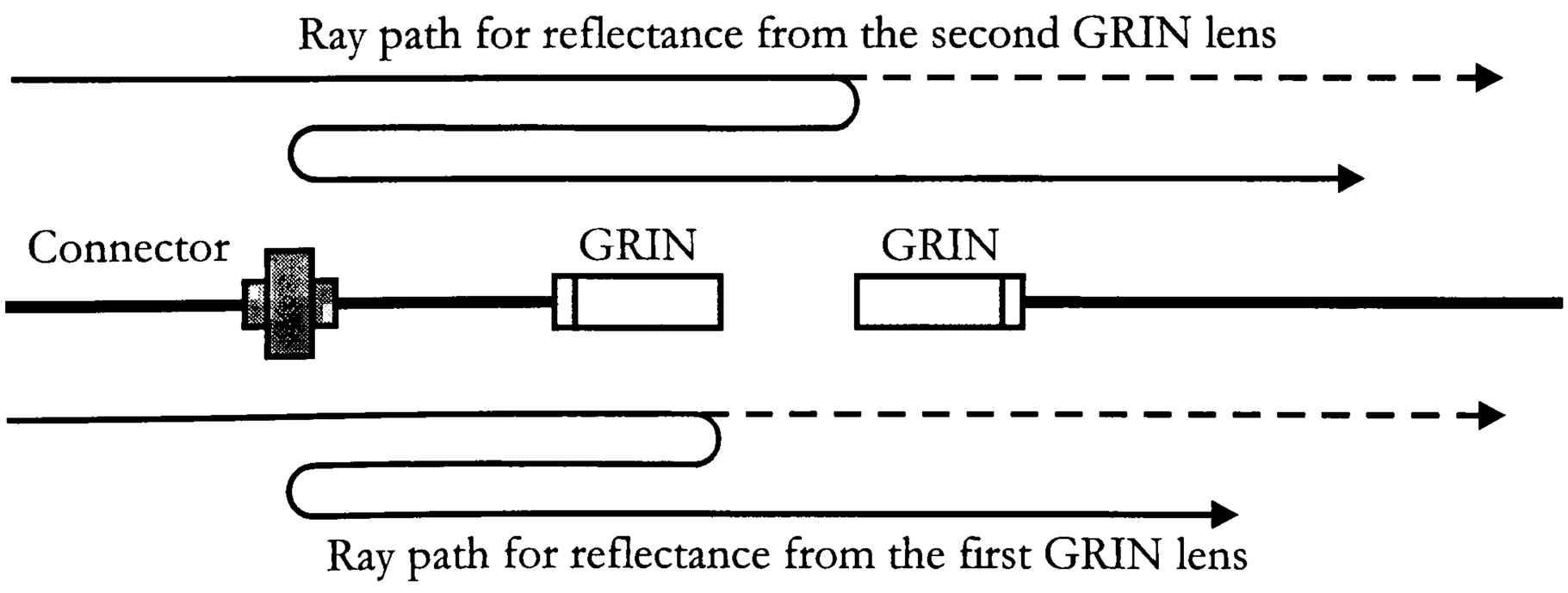

Figure 5.50: *Ray paths for one sensing unit using forward FMCW*

The path difference between both is therefore twice the length of the sensing region and is independent of the distance between the connector and sensing unit. To prevent inter-cell interference the connecting fibre length between two successive units is much greater then the coherence length of the source. To prevent self-interference (interference between the signal reflecting from the connector and the second GRIN signal partially reflecting from the first GRIN when travelling towards the connector) the optical path difference between both reflection points should also exceed the coherence of the source. The units are addressed using the coherence method, whereas the scheme is referred as *Forward FMCW*.

Using one microoptic cell with a connector connected in series the output of the cell reads as:

$$I_{out}^{1} = t_{c1}^{2} r_{c1}^{2} t_{11}^{2} r_{11}^{2} t_{21}^{2} (A+Bt) e^{-\alpha_1 C_1 2L_1} + t_{c1}^{2} r_{c1}^{2} t_{11}^{6} r_{21}^{2} t_{21}^{2} (A+Bt) e^{-\alpha_1 C_1 6L_1} + 2 t_{c1}^{2} r_{c1}^{2} t_{11}^{4} r_{11} r_{21} t_{21}^{2} (A+Bt) e^{-\alpha_1 C_1 4L_1} \cos(\psi_1 + \Delta\psi_1) \tag{5.26}$$

where t_{c1} and r_{c1} are the transmission and reflection coefficients of the connector. Further derivation of the output intensity gives the expression for the n-th cell in a forward FMCW system:

$$\begin{aligned} I_{out}^{n} = {} & t_{c1}^{2} r_{c1}^{2} t_{c2}^{2} r_{c2}^{2} \cdot \ldots \cdot t_{cn}^{2} r_{cn}^{2} \cdot t_{11}^{2} r_{11}^{2} t_{12}^{2} r_{12}^{2} \cdot \ldots \cdot t_{1n}^{2} r_{1n}^{2} \cdot t_{21}^{2} t_{22}^{2} \cdot \ldots \cdot t_{2n}^{2} (A+Bt) e^{-[\alpha_1 C_1 2L_1 + \ldots + \alpha_n C_n 2L_n]} + \\ & t_{c1}^{2} r_{c1}^{2} t_{c2}^{2} r_{c2}^{2} \cdot \ldots \cdot t_{cn}^{2} r_{cn}^{2} \cdot t_{11}^{6} t_{12}^{6} \cdot \ldots \cdot t_{1n}^{6} \cdot r_{21}^{2} t_{21}^{2} r_{22}^{2} t_{22}^{2} \cdot \ldots \cdot r_{2n}^{2} t_{2n}^{2} (A+Bt) e^{-[\alpha_1 C_1 6L_1 + \ldots + \alpha_n C_n 6L_n]} + \\ & 2 t_{c1}^{2} r_{c1}^{2} t_{c2}^{2} r_{c2}^{2} \cdot \ldots \cdot t_{cn}^{2} r_{cn}^{2} \cdot t_{11}^{4} t_{12}^{4} \cdot \ldots \cdot t_{1n}^{4} \cdot r_{11} r_{21} r_{12} r_{22} \cdot \ldots \cdot r_{1n} r_{2n} \cdot t_{21}^{2} t_{22}^{2} \cdot \ldots \cdot t_{2n}^{2} \cdot \\ & (A+Bt) e^{-[\alpha_1 C_1 4L_1 + \ldots + \alpha_n C_n 4L_n]} \cos(\psi_n + \Delta\psi_n) \end{aligned} \tag{5.27}$$

The major advantage of most forward travelling systems is their better signal to noise ratio. Although the forward FMCW system is general forward travelling, it has a lot of backreflecting sections. Therefore the signals pass the GRIN lens with

their transmitance and reflectance three to four times in each section. The total output signal of the system is therefore very weak. To compare it with other addressing mechanisms the output for a single sensing unit working in the forward regime is presented in Figure 5.51.

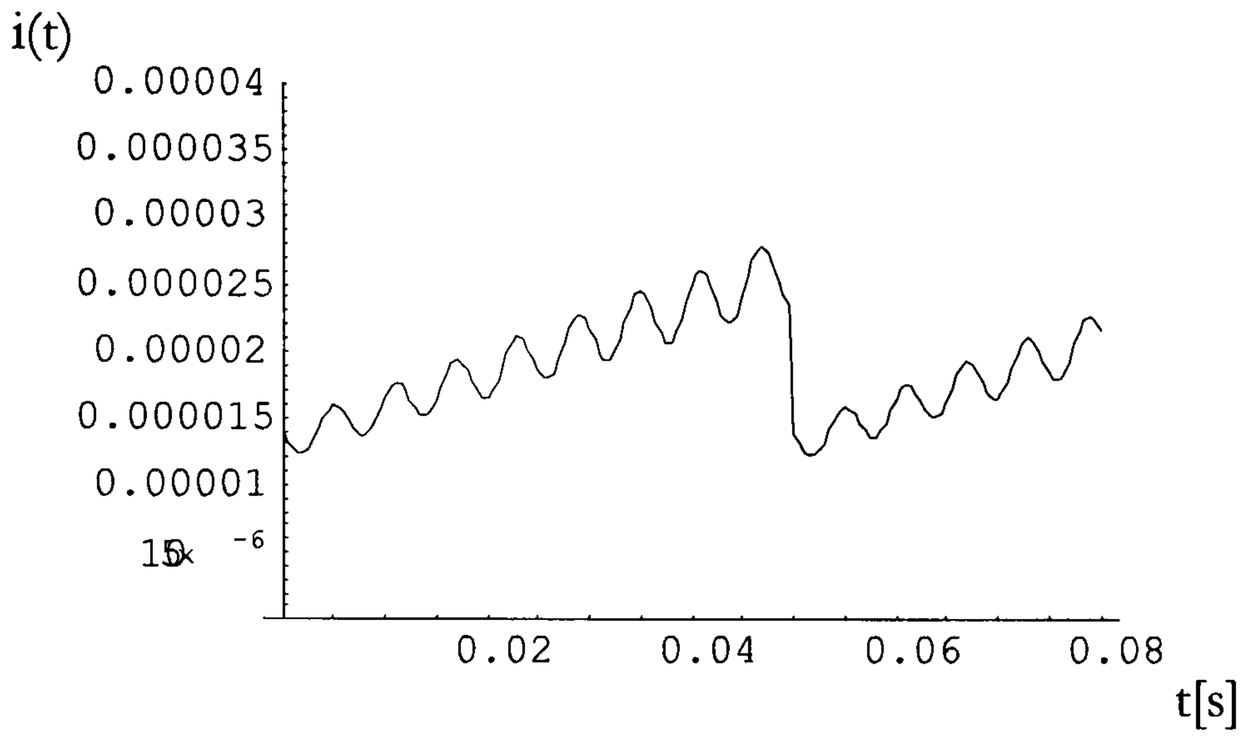

Figure 5.51: *Output of first sensing unit for forward FMCW*

The signal amplitude is insignificant compared to the other two previous presented addressing mechanisms, therefore no further analysis will be carried out. To show the drastic signal decline with sensing unit number increase similar program as before is used and the last unit output versus number of units is shown in Figure 5.52.

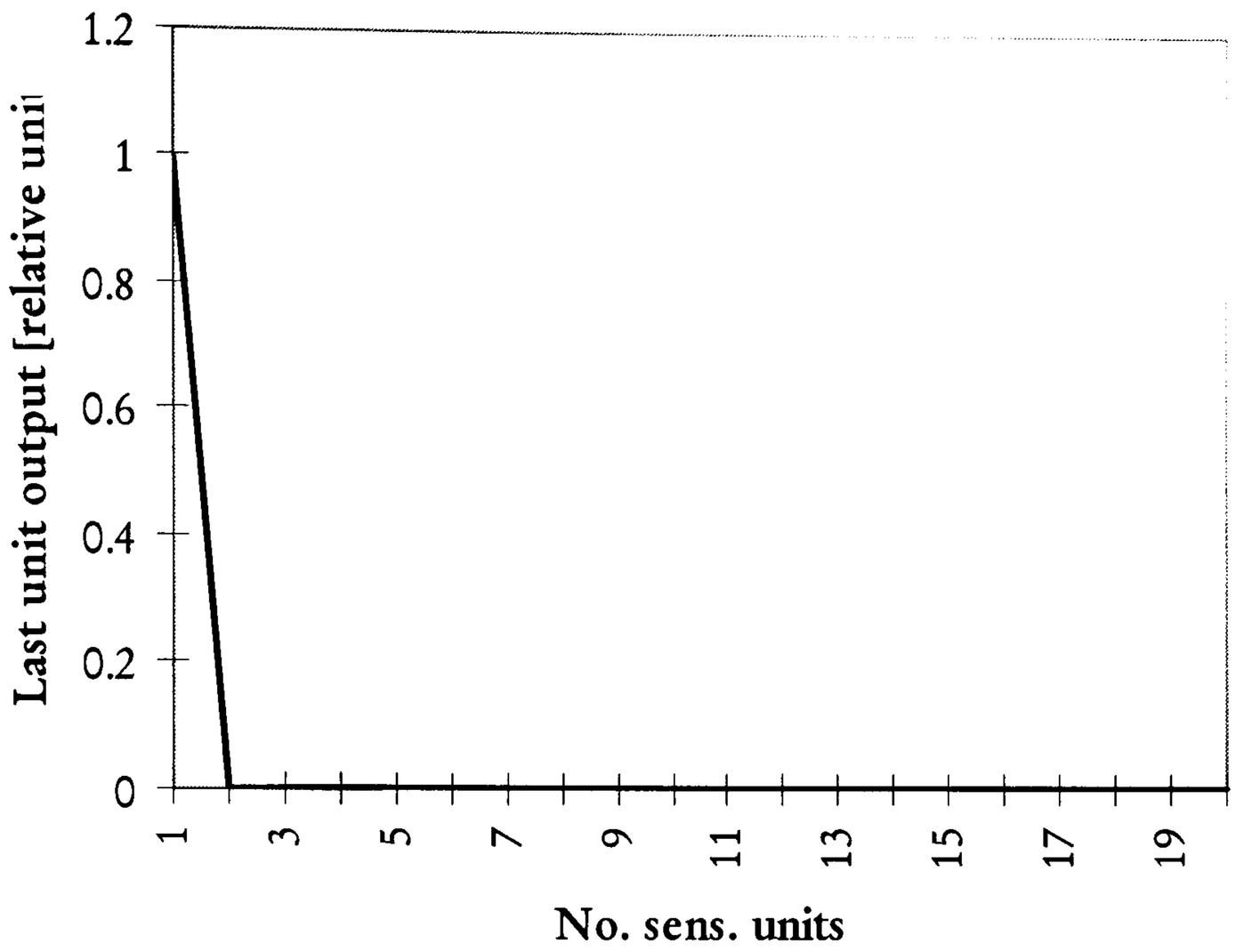

Figure 5.52: *Signal level versus number of sensing units for forward FMCW system*

For quasi-distributed sensing the proposed forward FMCW system is not applicable, since there is almost a total loss of signal after the first sensing unit. In some other modified form the forward system could be used just as single sensor system.

5.5. White Light FMCW Reference arm addressing

White light interferometry is mostly used as an alternative approach to the usual interferometry for overcoming some of the standard interferometric problems, to obtain unambiguous and absolute measurements. In its simplest form a white light interferometer is composed of two standard interferometers of any type; the first is referred to as the sensing interferometer and the second as the resolving interferometer. Light from a broadband light source is introduced into the sensing interferometer. The coherence length of the light source l_c is necessarily short, so if the path difference in the interferometer is greater then the coherence length no interference is observed at the output of the sensing interferometer. The output of

the sensing interferometer is then provided as input to the resolving interferometer. The optical path difference in this interferometer is scanned by moving one of the mirrors. Again, no interference will be observed at the output of the resolving interferometer unless the optical path difference in the resolving interferometer is equal, within the coherence length to the optical path difference in the sensing interferometer. In other words, the total OPD of the combined system is zero. At these exact positions a maximum in interference fringe contrast will be observed.

Using the white light approach with reference arm addressing, we obtain the system shown in Figure 5.53.

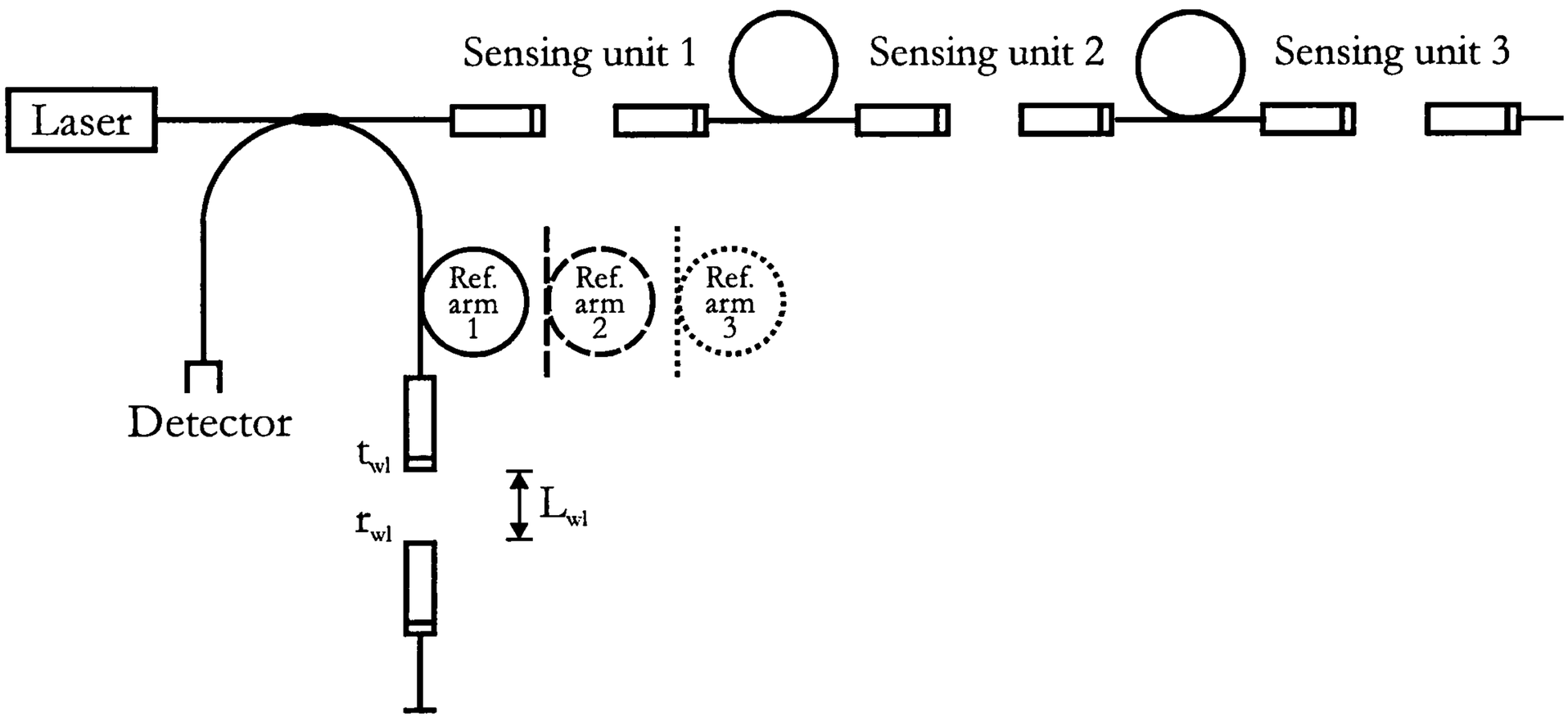

Figure 5.53: *White light FMCW reference arm addressing system*

For the FMCW reference arm system, a laser source with great coherence length was used to allow interference between the backreflecting signals. To cut down costs, a source with less coherence combined with the white light technique and the resolving cell could be introduced. Here the optical path mismatch is compensated using a resolving cell in which one of the GRINs is adjusted back and forth. To demonstrate the principle only the output of a single sensing unit system is given:

$$I_{out}^{1} = (A + Bt)\left[r_{wl}^{2} t_{wl}^{4} + r_{21}^{2} t_{11}^{4} e^{-\alpha_1 C_1 4 L_1} + 2 r_{21} t_{11}^{2} r_{wl} t_{wl}^{2} e^{-\alpha_1 C_1 2 L_1} e^{-\left(\frac{L_1 - L_{wl}}{l_c}\right)^2} \cos(\psi_1 + \Delta\psi_1) \right] \tag{5.28}$$

where r_{wl}, t_{wl} and L_{wl} are the white light resolving cells reflection, transmission coefficient and length respectively. No reflection from the AR coated input cell lens is assumed.

In simulations the second GRIN lens of the resolving cell was shifted to reduce the OPD. The response for three different OPDs approaching zero OPD in the middle, is shown in Figure 5.54.

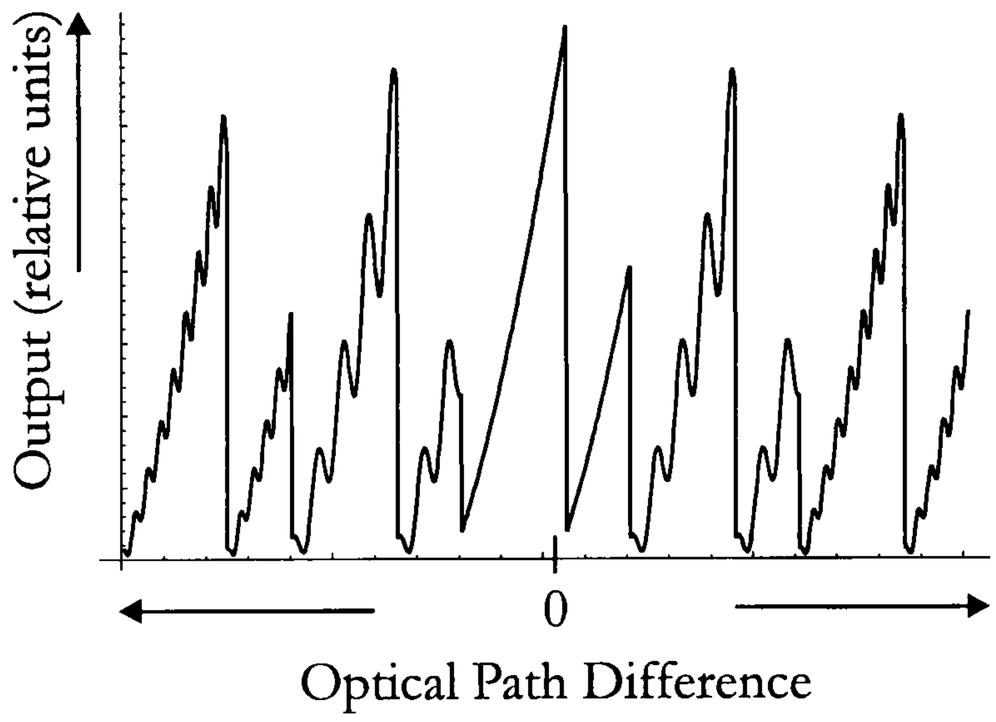

Figure 5.54: *Output (time domain) of the white light FMCW reference arm system for a single sensing unit*

The interference visibility is increased as the zero OPD is approached. The analysis of the system is omitted since all previous conclusions from the FMCW reference arm addressing method apply here also. The main disadvantages in this case is the necessity for an additional cell working as a resolving interferometer, and problems related to GRIN lens displacement (motors, piezo plates or some other techniques).

5.6. White Light FMCW Coherence addressing

Another possibility to introduce the white light system is to combine it with the FMCW coherence addressing mechanism. The resolving interferometer is appended in parallel to the existing system before the signals reach the detector. With white light FMCW coherence addressing the individual sensing cells are greater than the coherence length of the source used. The resolving white light part introduces an additional OPD, and enables the backreflected beams to interfere. The proposed system is shown in Figure 5.55.

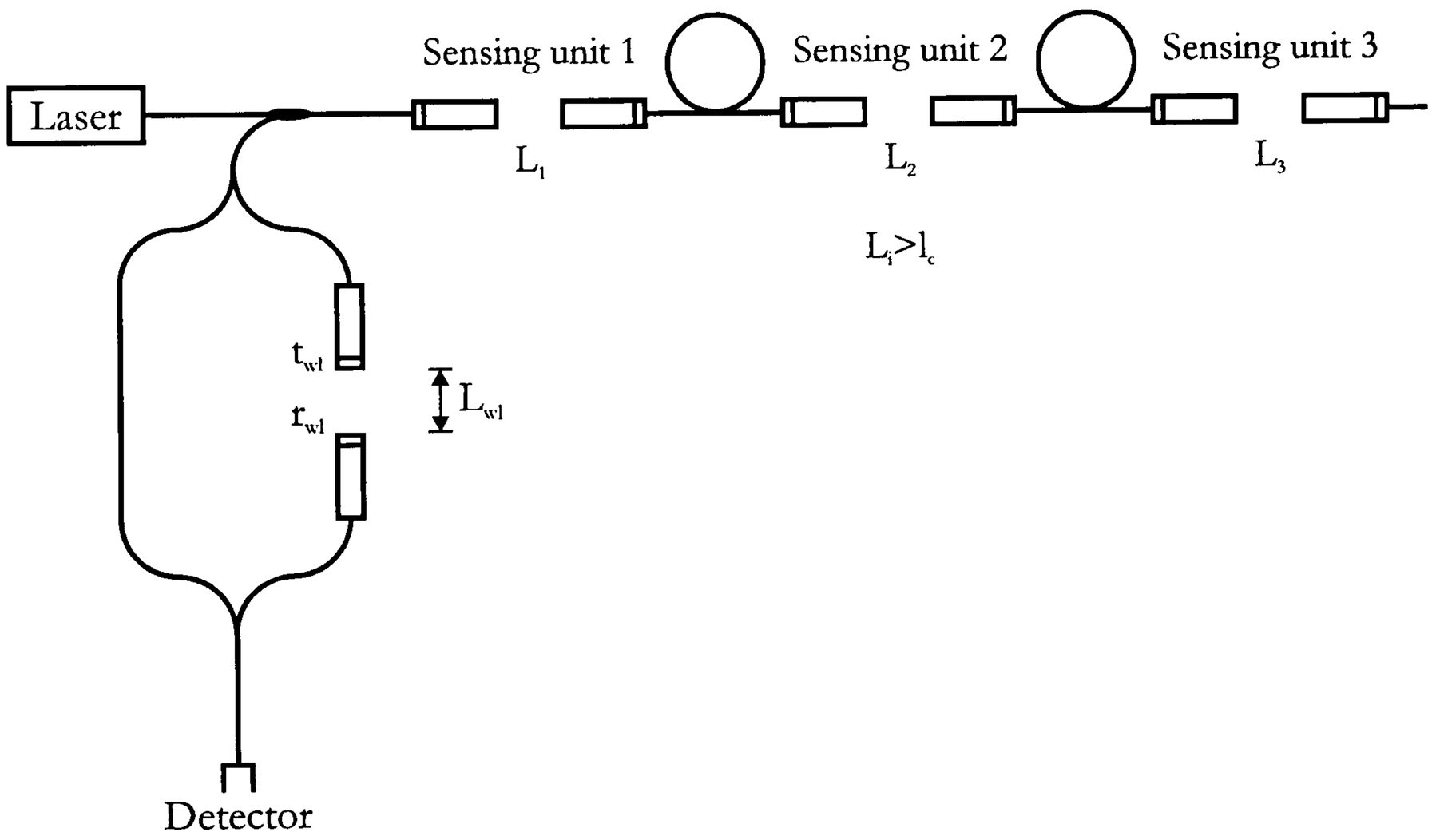

Figure 5.55: *White light FMCW coherence addressing system*

The output for a single unit reads as:

$$I_{out}^{1} = (A + Bt)\begin{bmatrix} r_{11}^{2}t_{wl}^{4} + r_{21}^{2}t_{11}^{4}e^{-\alpha_1 C_1 4L_1} \\ +2r_{11}r_{21}t_{11}^{2}t_{wl}^{2}e^{-\alpha_1 C_1 2L_1}e^{-\left(\frac{L_1 - L_{wl}}{l_c}\right)^2}\cos(\psi_1 + \Delta\psi_1) \end{bmatrix} \tag{5.29}$$

Using (5.29) the output intensity for three different OPD of the resolving unit is shown in Figure 5.56.

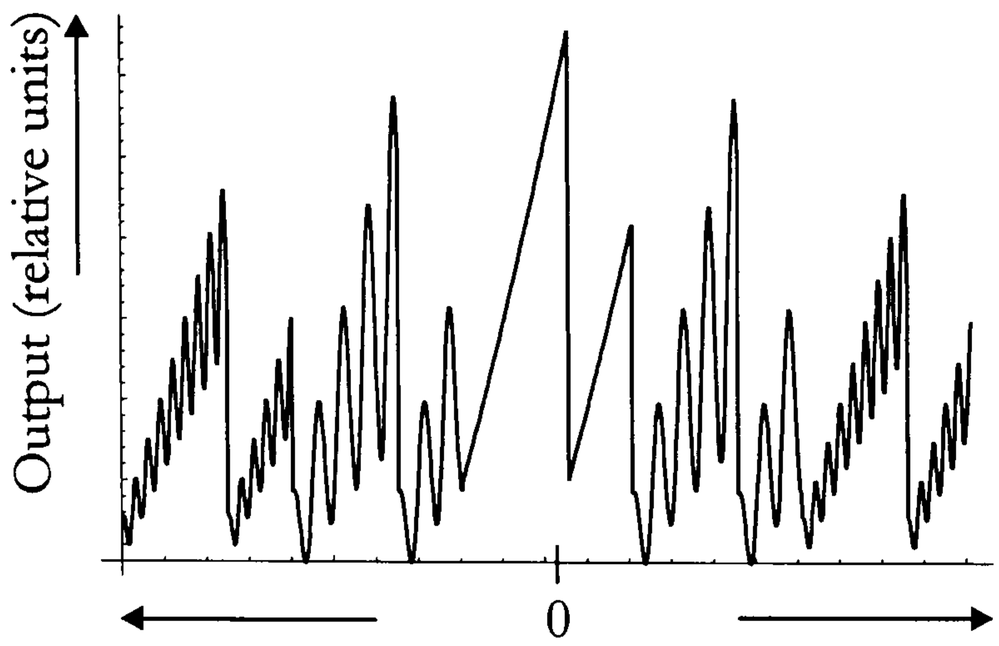

Figure 5.56: *Output (time domain) of the white light FMCW coherence addressing system for a single sensing unit*

Similar to the white light reference arm system, the visibility of the interference fringes is increased as zero total OPD is approached. Comparing the signal levels from both white light systems the same conclusions as with the reference arm and coherence addressing scheme can be made. A detailed comparison is presented in the next section.

5.7. Comparison of the proposed addressing mechanisms

For quasi distributed fibre optic measurements, five different addressing schemes have been proposed. First three are autonomous addressing mechanisms, while the last two combine the low coherence interferometry with the first two. All addressing schemes use the microoptic cell as the sensing element.

If comparing the structure of sensing cells for different addressing schemes all use identical components and therefore the same care in system assembling has to be maintained. Slight differences arises due to the method in which those sensing cells are being addressed. In the first we have to switch between different reference arms

which may cause some problems in the construction. For the third some additional components such as connectors are required. One of ways to determine which method for addressing quasi-distributed absortption sensors should be investigated further is to compare the signal drop with increase in number of sensors as shown in Figure 5.57.

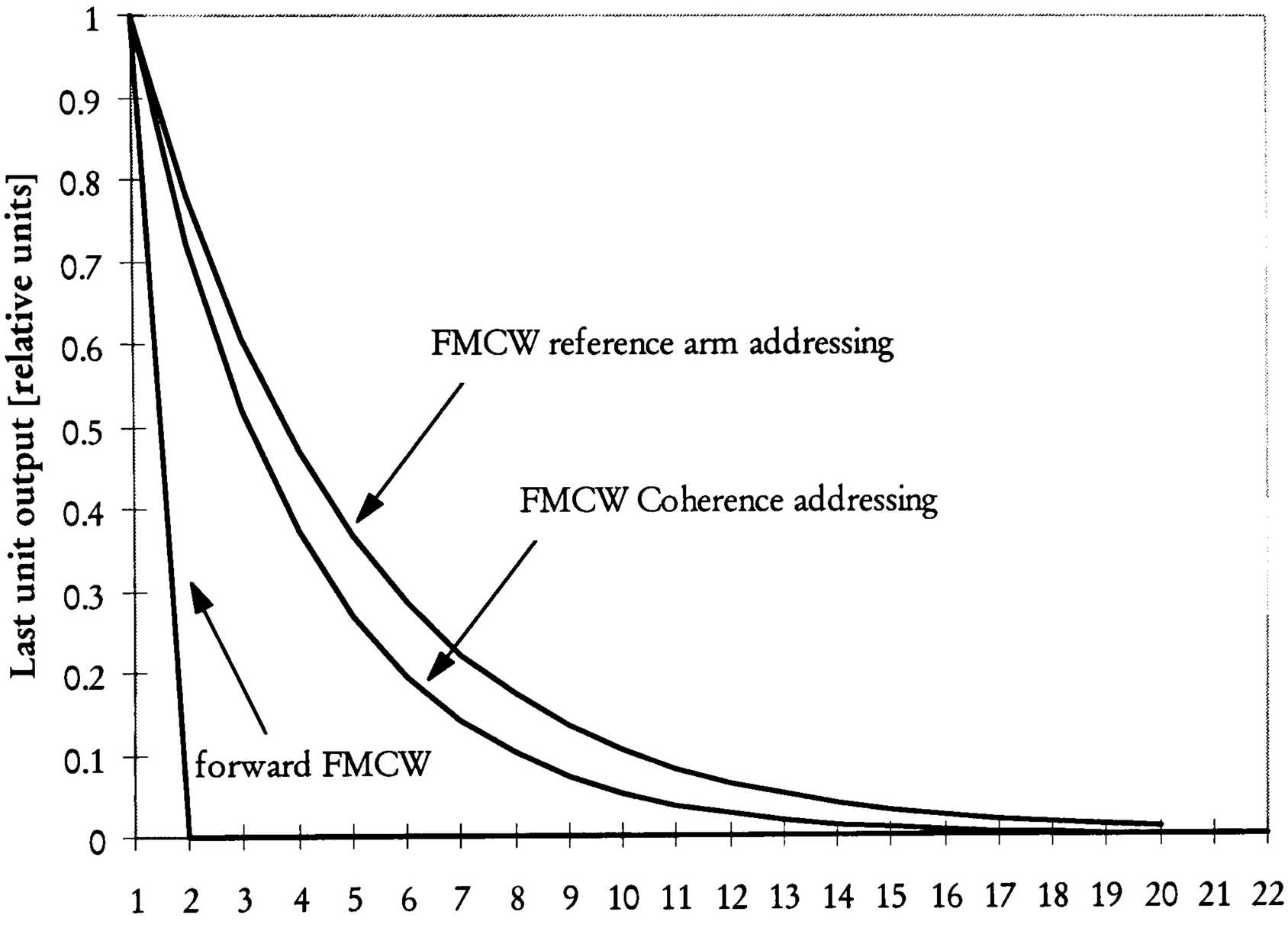

Figure 5.57: *Comparison of addressing mechanisms in regard to the number of sensing units*

Reference addressing and coherence addressing schemes are superior to the forward addressing mechanism considering the signal level after passing through a number of sensing units. Whereas the forward system is unsuitable for some real sensing applications, both the reference arm and the coherence method are feasible for quasi distributed measurements.

Table 5.1: *Signal level drop with regard to the number of sensing units for FMCW reference arm and FMCW coherence addressing*

No. sensing units	Reference arm	Coherence addr.	Difference
10	9.8dB	12.8dB	3dB
15	12.25dB	20.4dB	8.15dB
20	20.7dB	32.33dB	11.63dB

Irrespective of the fact that the reference method is better if considering the signal decay with number of sensors (as demonstrated using Figure 5.57 and Table 5.1) both methods roughly coincide for systems with up to 20 sensing units.

For both addressing schemes, methods to increase the signal level have been shown. For reference arm addressing one of the possibilities is to gradually increase the reflection coefficients of successive cells in very small steps. For coherence addressing similar could be achieved by gradually decreasing the cell length in order to compensate for signal reduction. In this case large signals would experience large changes and small signals would experience small changes, while the sensitivity remains constant.

For distributed sensing, forward FMCW system is not applicable, since there is almost a total loss of signal after the first sensing unit. Therefore the forward system will not be used in any of the following realisations.

The visibility of the white light reference arm and white light coherence system interference fringes is increased as approaching the zero total OPD, whereas the total signal drop with the number of sensing units is the same as with their non white light counterparts. Both methods could be used if the coherence property of the source is not compatible with the optical path differences used. Irrespective of that, even if we downgrade the source using the white light approach, the costs and complexity of the system increases because of additional scanning components.

The white light approach should therefore be used only if some special demands on signal processing or cell referencing are required.

According to the initial simulation results the reference arm and coherence addressing approach will be further experimentally investigated in the next sections.

References

[5.1] R. Passy, N. Gisin, J.P. von der Weid, H.H. Gilgen, "Experimental and Theoretical Investigations of Coherent OFDR with Semiconductor Laser Sources", Journal of Lightwave Technology, Vol.12, No. 9, September 1994

6. Theoretical analysis of Crosstalk

In the following chapter a short analysis of crosstalk between sensing cells will be presented. Individual sensor signals are allocated at different beat frequencies. Although the selection of different optical path differences, i.e. cell lengths enables the separation between sensor signals in the frequency domain, it does not completely ensure their separation from cross interferences which are the result of undesired interference between any two optical paths associated with more that one sensor in a system.

If the crosstalk is considered when designing the system, signals should be allocated so, that cross interferences do not coincide with any of the sensing beat signals in the frequency domain.

For the crosstalk analysis of both addressing schemes, a crosstalk factor will be introduced. We define the crosstalk factor from sensing cell (element) n to the sensing cell $(n+1)$ as the crosstalk level (CL) relative to the signal level (SL) at a given beat frequency:

$$CF_{n,(n+1)} = 10\log\frac{CL}{SL} \tag{6.1}$$

Here the crosstalk level is determined from the signal power spectrum amplitude when crosstalk is present and the signal level from the power spectrum for the same beat frequency without the crosstalk term. If cross-terms from neighbouring sensing units are present, then the signal level at the observed beat frequency raises compared to the case without cross-terms. When no crosstalk is observed the crosstalk level is equal to the signal level and the crosstalk factor is zero.

6.1. Reference arm method addressing crosstalk

The influence of cross interferences between successive sensors using the reference arm addressing mechanism will be analysed using the set-up shown in Figure 6.1.

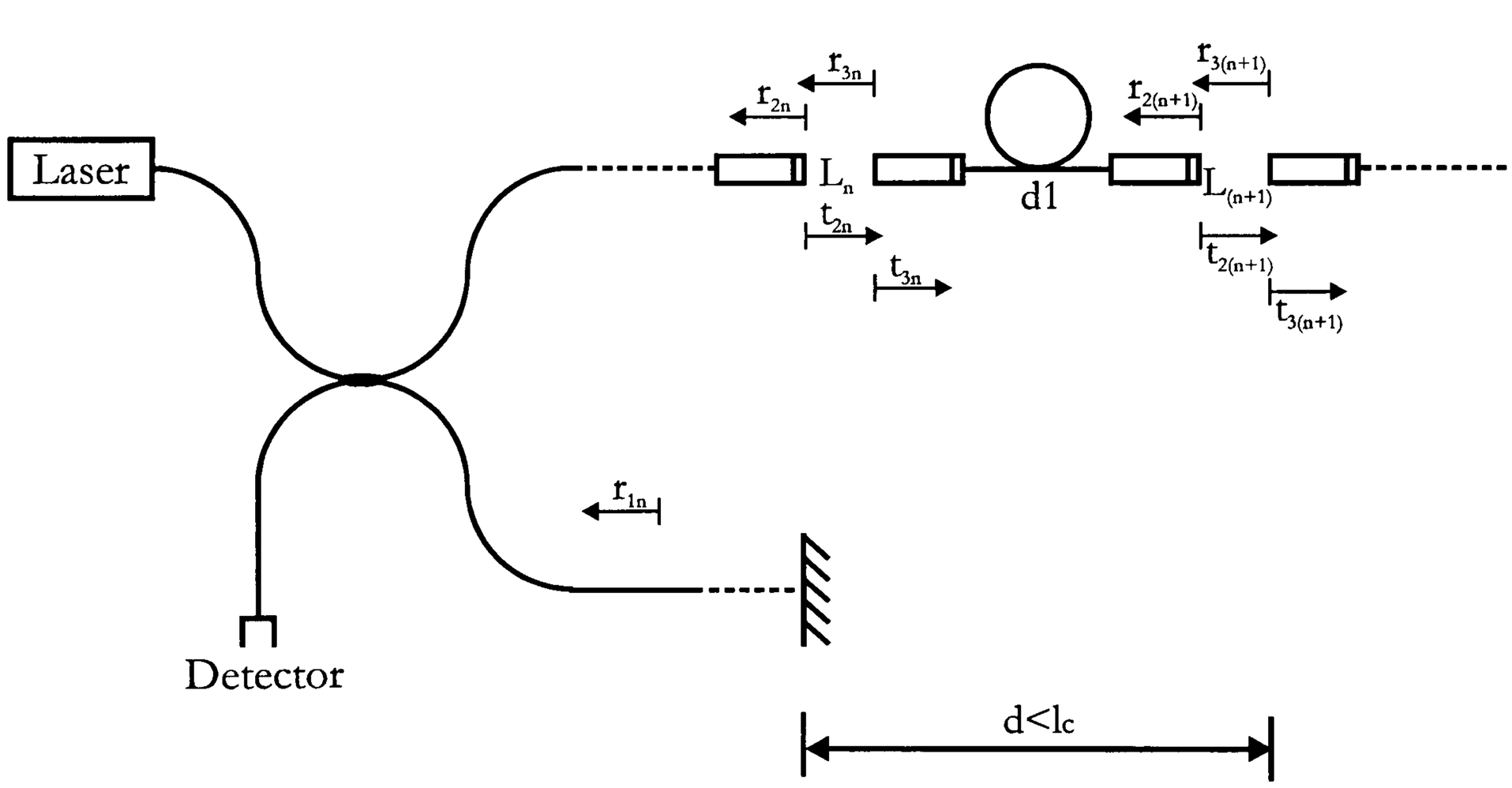

Figure 6.1: *Reference arm microoptic cell setup for the crosstalk analysis*

If we suppose that the influence of the backreflection from the antireflection coated GRIN lens can be neglected when cross interferences are presented and we

assume that the position of the reference mirror corresponds to the position of the first GRIN lens in the first cell, 3 interference terms in the output intensity can be observed. The first is the interference term between the reference arm and the reflected signal from the n-th sensing cell:

$$I_1 = (A + Bt) \cdot \left[r_{1n}^2 + r_{3n}^2 e^{-(\alpha_n C_n 4 L_n)} + 2 r_{1n} r_{3n} e^{-(\alpha_n C_n 4 L_n)} \cos(\psi_n + \Delta\psi_n) \right] \tag{6.2}$$

where

$$\psi_n + \Delta\psi_n = \frac{2\pi}{\lambda_0} \left[\frac{2 n_e L_n}{\lambda_o} \right] (\lambda_0 + \Delta\lambda) \tag{6.3}$$

Here the values $r_{ij}^2 = 4\%$ and $t_{ij}^2 = 96\%$. The wavelength is 1300nm.

The second term is the interference between the reference arm and the reflected signal from the (n+1)-th cell:

$$I_2 = (A + Bt) \cdot \begin{bmatrix} r_{1n}^2 + r_{3(n+1)}^2 t_{2n}^4 t_{3n}^4 e^{-\left(\alpha_n C_n 8 L_n + \alpha_{n+1} C_{n+1} 8 L_{(n+1)}\right)} + \\ 2 r_{1n} r_{3(n+1)} t_{2n}^2 t_{3n}^2 e^{-\left(\alpha_n C_n 4 L_n + \alpha_{n+1} C_{n+1} 4 L_{(n+1)}\right)} \cos(\psi_{n+1} + \Delta\psi_{n+1}) \end{bmatrix} \tag{6.4}$$

and

$$\psi_{n+1} + \Delta\psi_{n+1} = \frac{2\pi}{\lambda_0} \left[\frac{2\left(n_{cell} L_n + n_e d_1 + n_{cell} L_{(n+1)}\right)}{\lambda_o} \right] (\lambda_0 + \Delta\lambda) \tag{6.5}$$

The last is the interference between signals originating from the reflections from the n-th and (n+1)-th cells:

$$I_3 = (A + Bt) \cdot \begin{bmatrix} r_{3n}^2 e^{-(\alpha_n C_n 8 L_n)} + r_{3(n+1)}^2 t_{3n}^4 e^{-\left(\alpha_n C_n 8 L_n + \alpha_{n+1} C_{n+1} 8 L_{(n+1)}\right)} + \\ 2 r_{3n} r_{3(n+1)} t_{3n}^2 e^{-\left(\alpha_n C_n 4 L_n + \alpha_{n+1} C_{n+1} 4 L_{(n+1)}\right)} \cos(\psi_{n,n+1} + \Delta\psi_{n,n+1}) \end{bmatrix} \tag{6.6}$$

here

$$\psi_{n,n+1} + \Delta\psi_{n,n+1} = \frac{2\pi}{\lambda_0}\left[\frac{2\left(n_e d_1 + n_{cell} L_{(n+1)}\right)}{\lambda_o}\right](\lambda_0 + \Delta\lambda) \tag{6.7}$$

All three signals add up at the detector as:

$$I_{out} = I_1 + I_2 + I_3 \tag{6.8}$$

A typical power spectrum for the proposed system is shown in Figure 6.2.

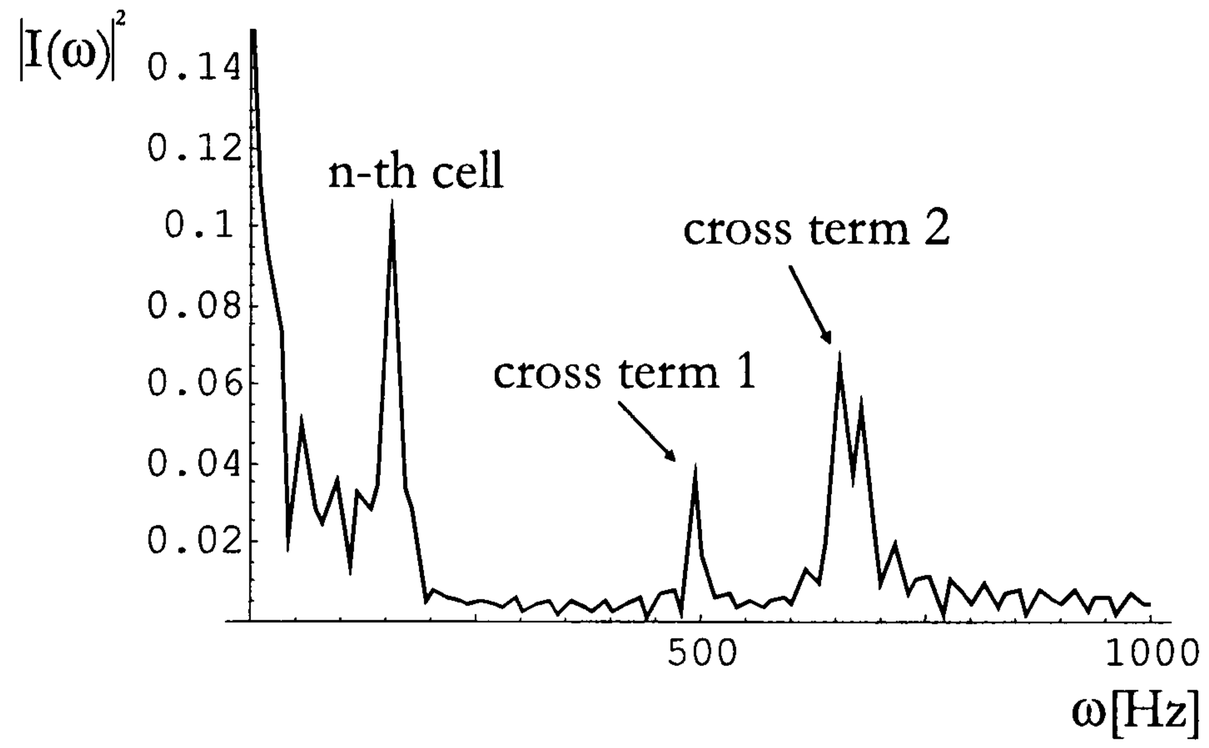

Figure 6.2: *Power spectrum for the reference arm method with additional cross interference signals; cross term 1 - cross interference between the n-th and (n+1)-th cell, cross term 2 - beat peak from the (n+1)-th cell*

The power spectrum for the n-th cell including cross interference signals has three distinctive peaks, each representing the interference terms (6.2), (6.4) and (6.6). Here 20mm and 30mm separation between the GRIN lenses in the n-th and (n+1)-th cell where used with a 30mm spacing between the cells. Therefore the first peak in the power spectrum corresponds to the n-th and the last one (highest beat frequency) to the (n+1)-th sensing cell. The middle peak is the result of the

interference between the reflections originating from the n-th and (n+1)-th GRIN lens. As shown in Figure 6.3 the middle and high peak is shifting according to the separation between the cells:

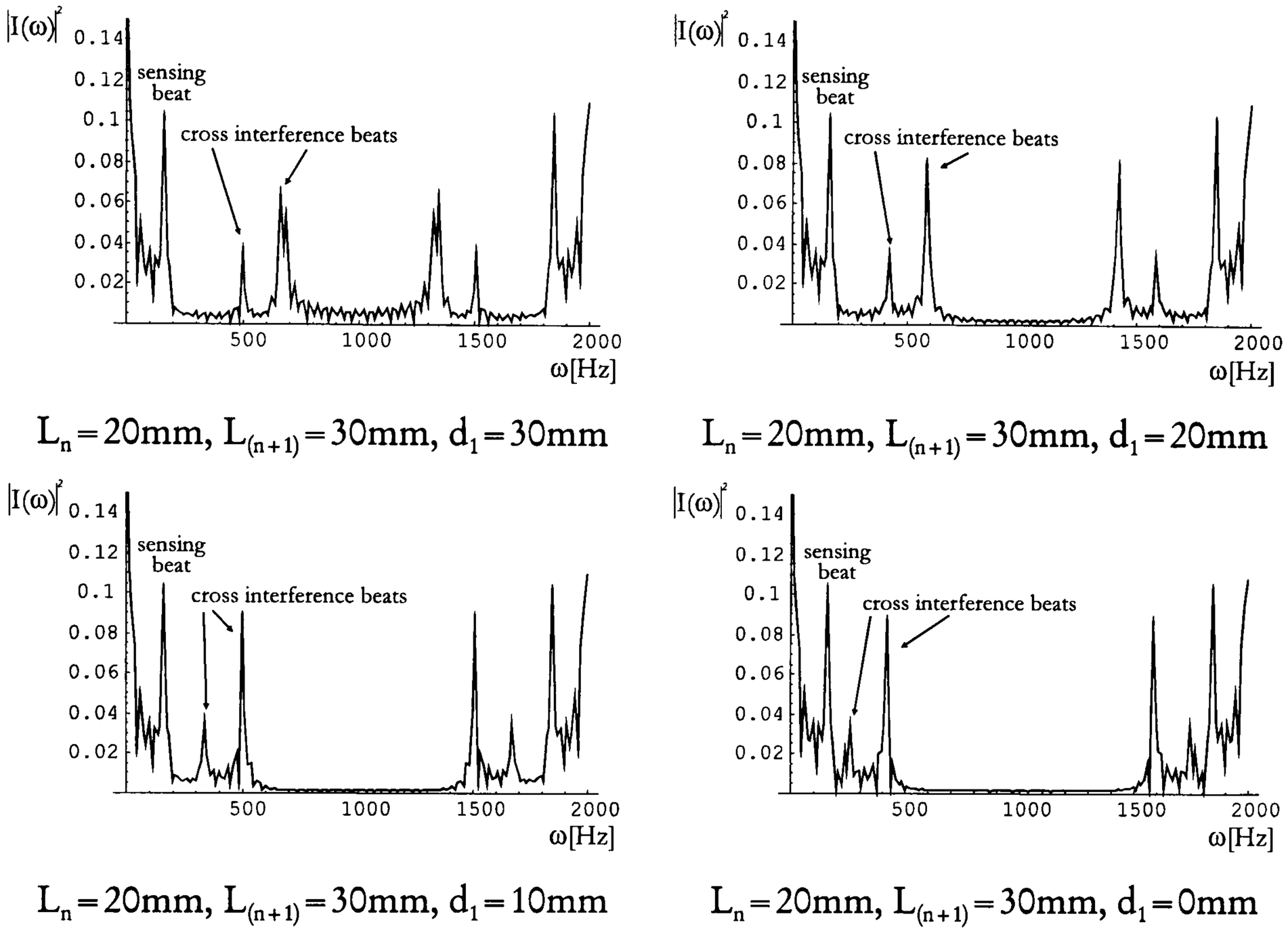

Figure 6.3: *Shift of the cross interference beats in the output power spectrum due to the change in the separation between the cells*

When considering the reference arm addressing crosstalk analysis the most noticeable difference are additional spectral peaks in the power spectrum. In the usual cases (the worst case possible will be discussed later) this does not present a major problem for the signal post processing, since during the calibration procedure, cells beat frequencies and amplitudes are assigned to the individual measuring units. In this case the signal processing is accomplished just by tracking the beat nodes as recorded. Any spurious beat peaks can therefore be ignored (if the cross interference appears at the different frequency from the beat frequency of

the sensors, the cross interference can be also eliminated by electric bandpass filtering).

The worst case for the reference arm method occurs when the beat signals from the n-th sensing cell and the beat signal originating from the GRIN reflections from neighbouring cells overlap. For a long coherence source this can happen when:

$$n_e d_1 = n_{cell}\left(L_n - L_{(n+1)}\right) \tag{6.9}$$

If we neglect different index within cells from fibre, i.e. optical path length, the reflections are overlapped when the spacing between cells is equal to length difference of adjacent cells:

$$d_1 = L_n - L_{(n+1)} \tag{6.10}$$

If all parameters except the optical path difference which determines the beat frequency are kept constant, the power spectrum overlap or crosstalk between neighbouring sensing cells will be determined by the lengths and spacing of the cells. As shown in equation (6.10), when the length of the n-th cell is matched with the sum of the length of the (n+1)-th cell and the spacing between them, the power spectrums overlap and signal resolving becomes difficult.

For those special cases the crosstalk factor analysis has been accomplished. The length of the n-th cell was set to 48mm, the (n+1)-th to 28mm and the distance d_1 was changed from 20mm (total overlap of the power spectrums) to 0 in powers of ten. For each case the crosstalk factor has been calculated. The worst case power spectrum is presented in Figure 6.4a and the calculated crosstalk factor curve in Figure 6.5.

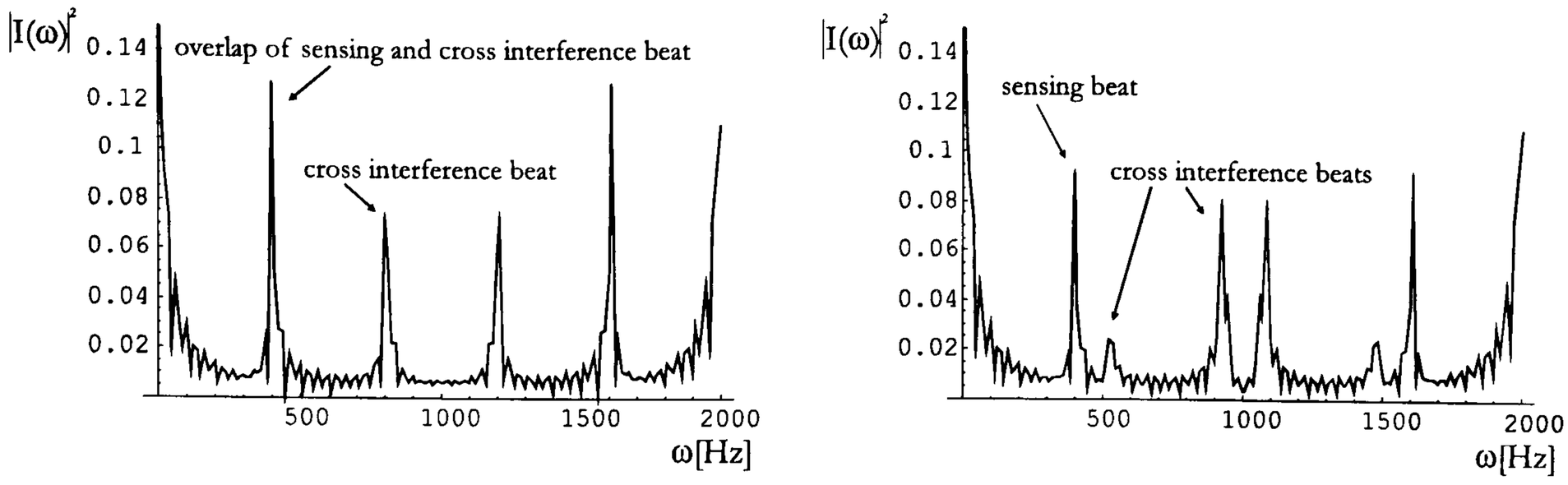

(a) CF = 1.402dB, d_1 = 20mm (b) CF = 0.018dB, d_1 = 35mm

Figure 6.4: *(a) Crosstalk - overlapping of the signals from the n-th cell and the cell to cell cross interference term; (b) all three interference beat terms are distinctive*

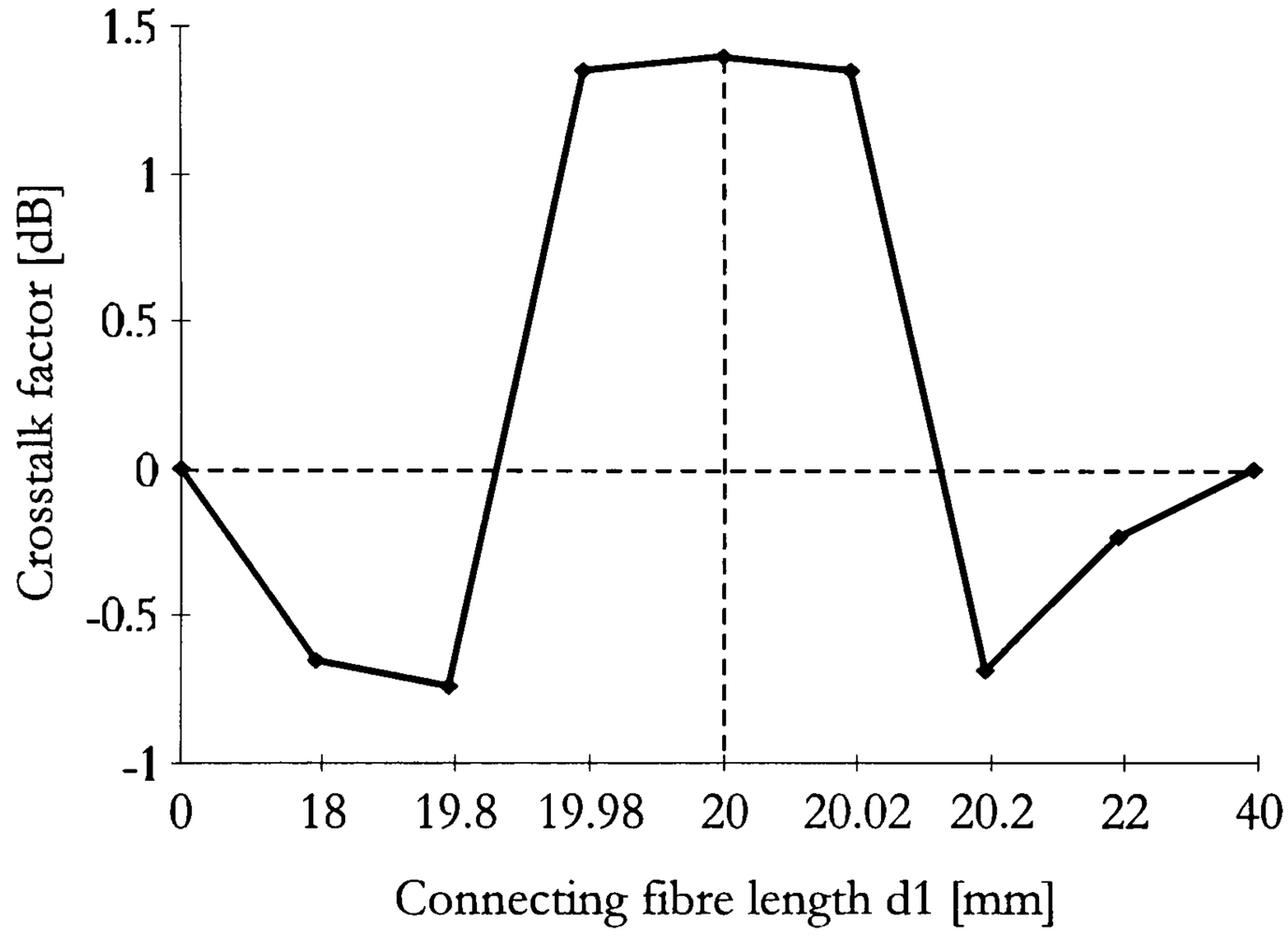

Figure 6.5: *The influence of the connecting fibre length on the crosstalk factor for reference arm addressing scheme*

6.1.1. Summary

The cross interference effect for the reference arm addressing scheme is evident through additional peaks in the power spectrum. Due to the interference between reflections from neighbouring cells the power spectrum peaks correspond to the

addressed cell, the nearest cells inside the coherence length and all mutual interactions.

In the usual case the additional peaks are not a problem since the proper beat frequencies are recorded during the calibration procedure. The only additional step is to use a similar locking mechanism as in the coherence addressing method. Once locked to the right peak, spurious reflections can be ignored, or electric bandpass filtering could be used.

When the worst case is considered, power spectrums overlap. A very simple and effective solution here is to use either sensing cells with equal length or to increase the length of the connecting fibre but within the coherence length. In both cases the spectrums will be separated and then previously mentioned measures could be applied.

When the cross interference effect for the reference arm method is considered two cases and suitable solutions can be presented:

1. the coherence length of the source is greater then the optical path difference between the sensing cells
    - presence of additional spectrum peaks and proper locking mechanism to avoid spurious peaks
    - to avoid spectrum overlapping equal cell lengths or connecting fibre which is longer than the separation between the cells should be used
2. the coherence length of the source is smaller then the optical path difference between the sensing cells
    - because the optical path difference is large enough no crosstalk effects can be observed
    - only secondery effects from the reflections from the AR coated GRIN lenses, connectors in the system, etc.

6.2. Coherence addressing crosstalk

The set-up for the FMCW Coherence addressing cross interference analysis is shown in Figure 6.6.

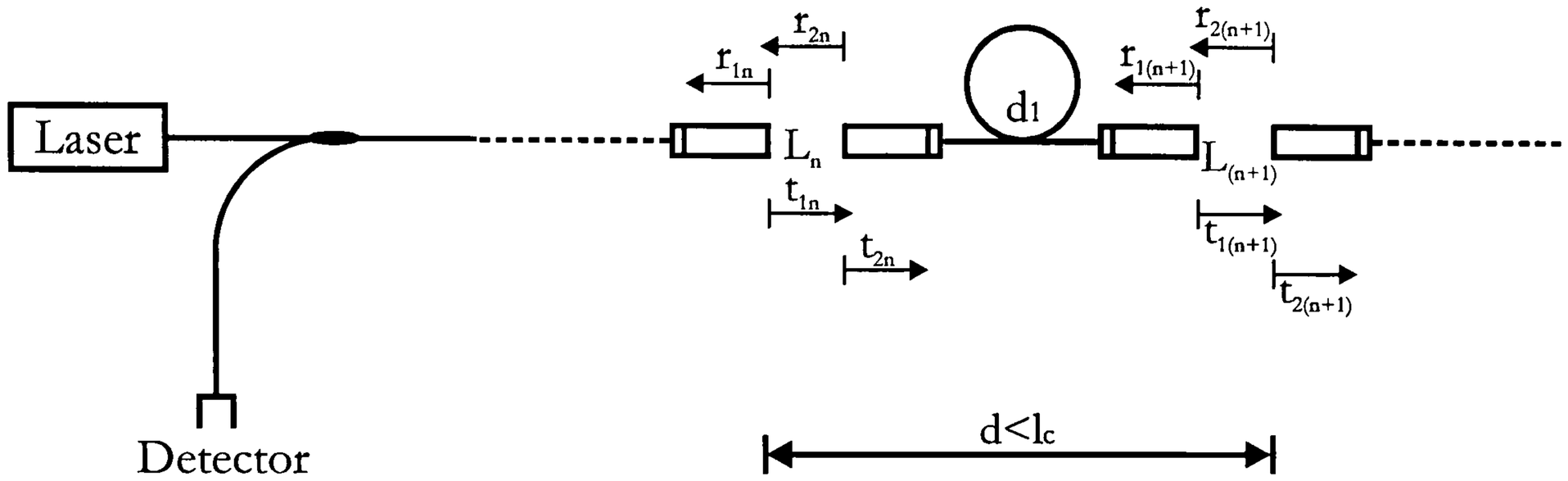

Figure 6.6: *Coherence addressing set-up for cross interference analysis*

Together with the interference from the sensing unit we get four additional interference terms resulting from the GRIN reflections in the neighboring sensing cells when cross interference is considered. The total output light intensity therefore includes six terms. First is the interference from reflections in the n-th sensing cell:

$$I_1 = (A + Bt) \cdot \left[r_{1n}^2 + r_{2n}^2 t_{1n}^4 e^{-(\alpha_n C_n 8 L_n)} + 2 r_{1n} r_{2n} t_{1n}^2 e^{-(\alpha_n C_n 4 L_n)} \cos(\psi_1 + \Delta\psi_1) \right] \tag{6.11}$$

where

$$\psi_1 + \Delta\psi_1 = \frac{2\pi}{\lambda_0} \left[\frac{2 n_{cell} L_n}{\lambda_o} \right] (\lambda_0 + \Delta\lambda) \tag{6.12}$$

The second term is the interference from GRIN reflections in the (n+1)-th cell:

$$I_1 = (A + Bt) \cdot \begin{bmatrix} r_{1(n+1)}^2 t_{1n}^4 t_{2n}^4 e^{-(\alpha_n C_n 8 L_n)} + r_{2(n+1)}^2 t_{1n}^4 t_{2n}^4 t_{1(n+1)}^4 e^{-(\alpha_n C_n 8 L_n + \alpha_{n+1} C_{n+1} 8 L_{n+1})} + \\ 2 r_{1(n+1)} r_{2(n+1)} t_{1n}^4 t_{2n}^4 t_{1(n+1)}^2 e^{-(\alpha_n C_n 8 L_n + \alpha_{n+1} C_{n+1} 4 L_{n+1})} \cos(\psi_2 + \Delta\psi_2) \end{bmatrix} \quad (6.13)$$

and

$$\psi_2 + \Delta\psi_2 = \frac{2\pi}{\lambda_0}\left[\frac{2 n_{cell}(L_{n+1})}{\lambda_o}\right](\lambda_0 + \Delta\lambda) \quad (6.14)$$

The third is the interference between signals originating from the reflections on the first GRIN in the n-th cell and the first GRIN lens of the (n+1)-th cell:

$$I_3 = (A + Bt) \cdot \left[r_{1n}^2 + r_{1(n+1)}^2 t_{1n}^4 t_{2n}^4 e^{-(\alpha_n C_n 8 L_n)} + 2 r_{1n} r_{1(n+1)} t_{1n}^2 t_{2n}^2 e^{-(\alpha_n C_n 4 L_n)} \cos(\psi_3 + \Delta\psi_3)\right] \quad (6.15)$$

here

$$\psi_3 + \Delta\psi_3 = \frac{2\pi}{\lambda_0}\left[\frac{2(n_{cell} L_n + n_e d_1)}{\lambda_o}\right](\lambda_0 + \Delta\lambda) \quad (6.16)$$

The fourth interference is between reflections on the first GRIN in the n-th cell and the second GRIN lens of the (n+1)-th cell:

$$I_4 = (A + Bt) \cdot \begin{bmatrix} r_{1n}^2 + r_{2(n+1)}^2 t_{1n}^4 t_{2n}^4 t_{1(n+1)}^4 e^{-(\alpha_n C_n 8 L_n + \alpha_{n+1} C_{n+1} 8 L_{n+1})} + \\ 2 r_{1n} r_{2(n+1)} t_{1n}^2 t_{2n}^2 t_{1(n+1)}^2 e^{-(\alpha_n C_n 4 L_n + \alpha_{n+1} C_{n+1} 4 L_{n+1})} \cos(\psi_4 + \Delta\psi_4) \end{bmatrix} \quad (6.17)$$

and

$$\psi_4 + \Delta\psi_4 = \frac{2\pi}{\lambda_0}\left[\frac{2(n_{cell} L_n + n_e d_1 + n_{cell} L_{n+1})}{\lambda_o}\right](\lambda_0 + \Delta\lambda) \quad (6.18)$$

The fifth term is the interference between reflections on the second GRIN in the n-th cell and the first GRIN lens of the (n+1)-th cell:

$$I_5 = (A + Bt) \cdot \left[\begin{array}{l} r_{2n}^2 t_{1n}^4 e^{-(\alpha_n C_n 8 L_n)} + r_{1(n+1)}^2 t_{1n}^4 t_{2n}^4 e^{-(\alpha_n C_n 8 L_n)} + \\ 2 r_{2n} r_{1(n+1)} t_{1n}^4 t_{2n}^2 e^{-(\alpha_n C_n 8 L_n)} \cos(\psi_5 + \Delta\psi_5) \end{array} \right] \tag{6.19}$$

and

$$\psi_5 + \Delta\psi_5 = \frac{2\pi}{\lambda_0} \left[\frac{2 n_e d_1}{\lambda_o} \right] (\lambda_0 + \Delta\lambda) \tag{6.20}$$

The last interference comes from reflections on the second GRIN in the n-th cell and the second GRIN lens of the (n+1)-th cell:

$$I_6 = (A + Bt) \cdot \left[\begin{array}{l} r_{2n}^2 t_{1n}^4 e^{-(\alpha_n C_n 8 L_n)} + r_{2(n+1)}^2 t_{1n}^4 t_{2n}^4 t_{1(n+1)}^4 e^{-(\alpha_n C_n 8 L_n + \alpha_{n+1} C_{n+1} 8 L_{n+1})} + \\ 2 r_{2n} r_{2(n+1)} t_{1n}^4 t_{2n}^2 t_{1(n+1)}^2 e^{-(\alpha_n C_n 8 L_n + \alpha_{n+1} C_{n+1} 4 L_{n+1})} \cos(\psi_6 + \Delta\psi_6) \end{array} \right] \tag{6.21}$$

where

$$\psi_6 + \Delta\psi_6 = \frac{2\pi}{\lambda_0} \left[\frac{2(n_e d_1 + n_{cell} L_{n+1})}{\lambda_o} \right] (\lambda_0 + \Delta\lambda) \tag{6.22}$$

All six signals add up at the detector as:

$$I_{out} = I_1 + I_2 + I_3 + I_4 + I_5 + I_6 \tag{6.23}$$

The power spectrum for the system is shown in Figure 6.7.

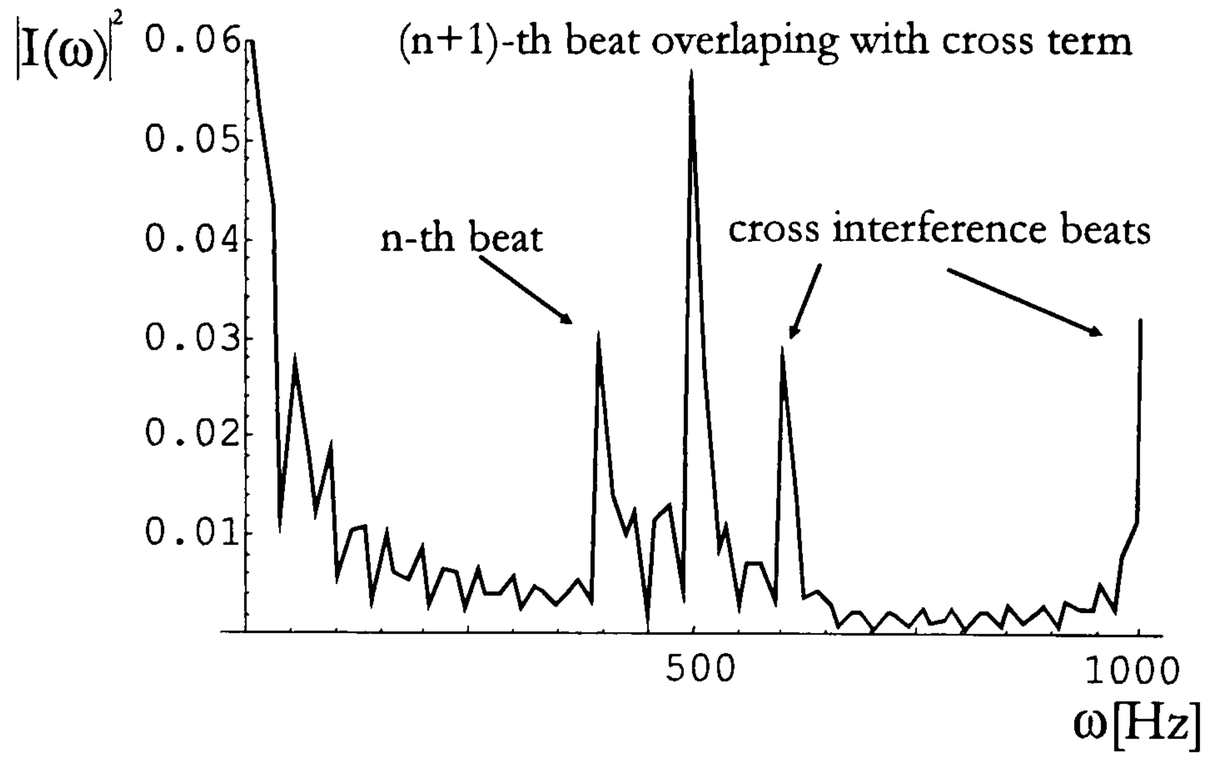

Figure 6.7: *Power spectrum for the coherence addressing scheme when cross interference between sensing units is present*

Because of the cross interference between sensing cells additional power spectrum peaks are visible. Their position along the frequency axis is dependent on the length of the cells used and the separation between them. In Figure 6.7, 48mm separation between the GRIN lenses for the n-th and 60mm for the (n+1)-th cell was used. The connecting fibre length d_1 (see Figure 6.6) has been chosen to have the critical length of 12mm. The cell lengths correspond to beat frequencies of 400Hz and 500Hz.

From equations (6.12), (6.14), (6.16), (6.18), (6.20) and (6.22) a crosstalk beat frequency will coincide with a cell's beat frequency if any one of the following conditions are satisfied (same as for the reference arm addressing we neglect different index within cells from fibre):

$$\begin{aligned} d_1 &= L_n \quad \text{or} \quad d_1 = L_{n+1} \\ d_1 &= (L_{n+1} - L_n) \quad \text{or} \quad d_1 = (L_n - L_{n+1}) \end{aligned} \tag{6.24}$$

i.e. if the spacing between the cells is either equal to a cell length, or the difference in length of two adjacent cells.

To obtain information about the crosstalk level, the crosstalk factor has been calculated as a function of connecting fibre lenght d_1. The results for cell length 48mm and 60mm are presented in Figure 6.8.

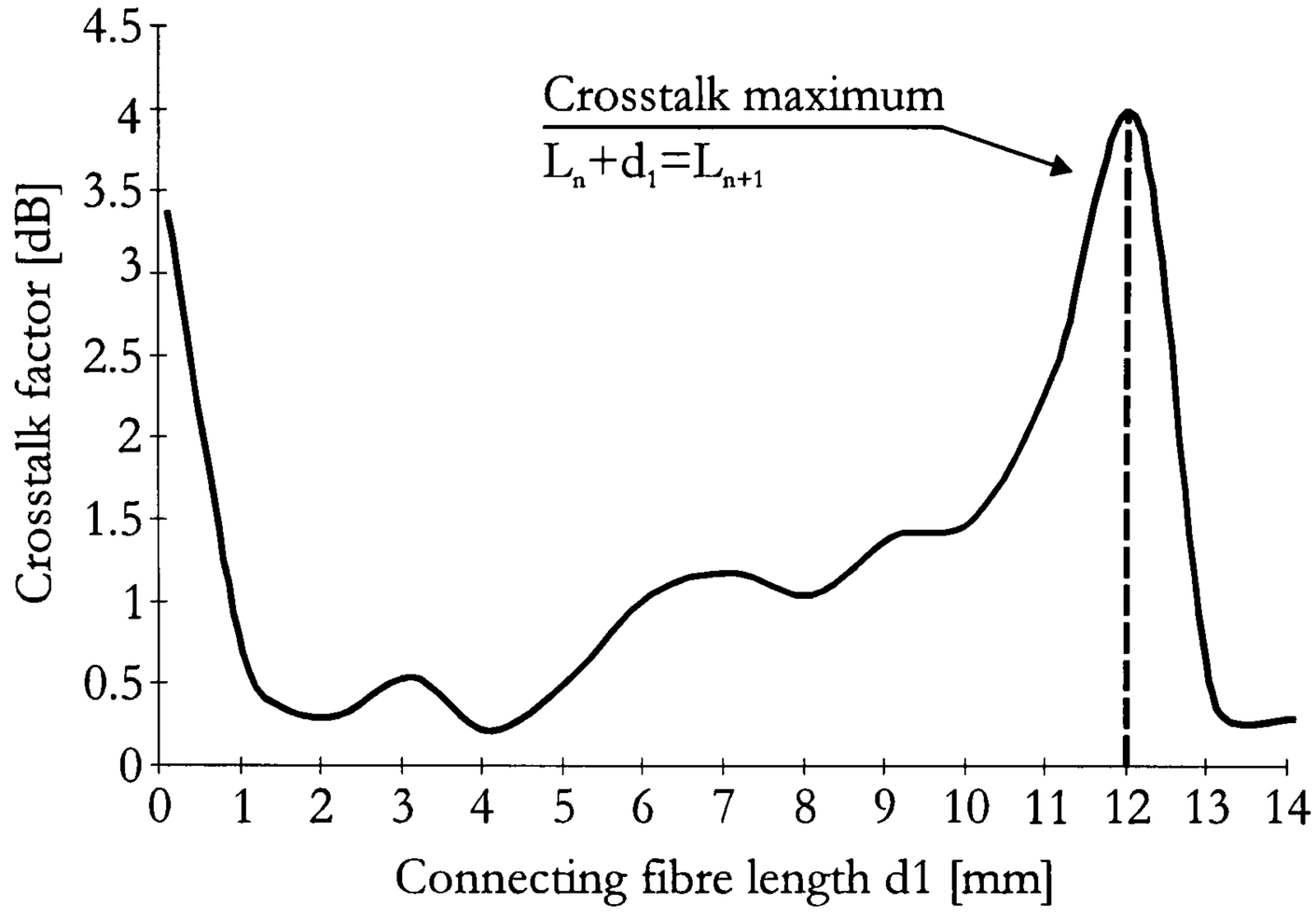

Figure 6.8: *The influence of the connecting fibre length on the crosstalk factor for the coherence addressing scheme*

In this case the maximum crosstalk factor is the point where the beat frequency corresponding to the separation between the sensing units is equal to the beat frequency difference of successive units. For 400Hz and 500Hz cell beat frequencies the separation is 100Hz, or 12mm in optical path difference (see Figure 6.8). The power spectrums for two different separations are presented in Figure 6.9.

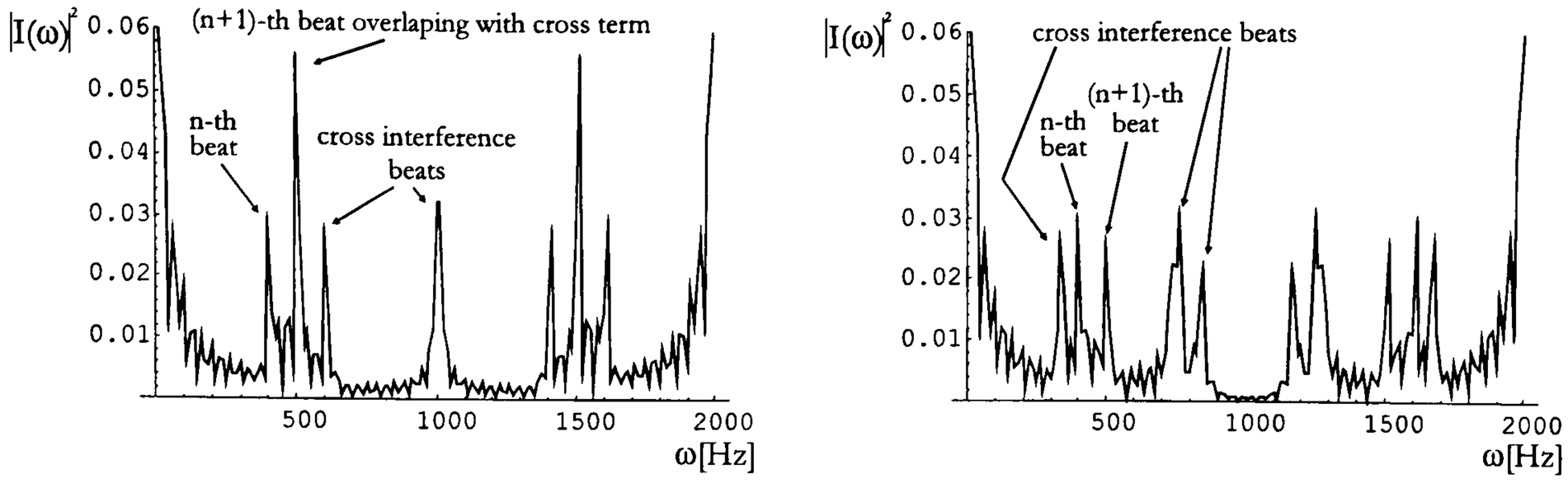

Figure 6.9: *Power spectrum for two distinctive distances d_1; (a) crosstalk - overlap of the sensor and cross interfernce signal at 500Hz, (b) separation of sensor and cross interference signals*

Figure 6.9a represents the worst case possible. Because the distance between the cells equals the difference in cell lengths the cross interference signal and the measured signal are overlapped.

In principle, if cross interference beat frequencies do not coincide with cell beat frequencies (see Figure 6.9b), then cross-talk is not a problem because measurements are taken by tracking the cell beat frequencies, or the cross interference frequencies may be eliminated by band pass filtering. In practice, however, because beat frequencies have a certain spectral width in the frequency domain (due to the finite time interval over which the signal is sampled by the spectrum analyser), crosstalk will still influence measurements if cross interference frequencies are sufficiently close to cell beat frequencies.

6.2.1. Summary

The crosstalk effect for the FMCW coherence addressing method can be summarised as follows:

Case 1: the coherence length of the source is greater then the optical path difference between the sensing cells

- presence of additional spectrum peaks and locking required to avoid cross-talk peaks

- to avoid spectrum overlapping:
  - * the separation between successive cells should be different from any cell length
  - * the sum an arbitrary number of cell lengths should not match another cell length
  - * the sum of arbitrary number of cell lengths plus the fibre connection length should be different from any other cell length within the coherence length.

Case 2: the simplest solution to avoid crosstalk between successive sensors is to make sensors incoherent with each other by introducing long time delays between sensors so that cross terms do not arise.

7. Construction and test of an experimental FMCW Reference arm system

During the stages of mathematical modelling and simulation we found out that only two of five proposed mechanism for quasi-distributed addressing of fibre optic chemical sensors are suitable for further experimental investigation and possible practical implementation. First method to be experimentally evaluated is the FMCW with reference arm addressing.

The experimental set-up for the FMCW reference arm method is presented in Figure 7.1. We used a NORTEL LC131-20A DFB laser diode operating at 1308nm with maximum 2mW output power and a coherence length l_c of approximately 22cm (the laser diode has been characterised to have a 0.0077818nm line-width applying 20Hz modulation and ~0.05nm/mA dynamic shift). The source had an internal optical isolator and Peltier elements for temperature control. The power spectrum was recorded with a Hawlett Packard Dynamic Spectrum Analyser

35660A (start frequency 0Hz, stop frequency 3.2kHz, 10k samples/s, 250ms record length, 80dB dynamic range). The laser diode was sawtooth modulated with a frequency of 20Hz and the experienced wavelength change was approximately 0.5nm.

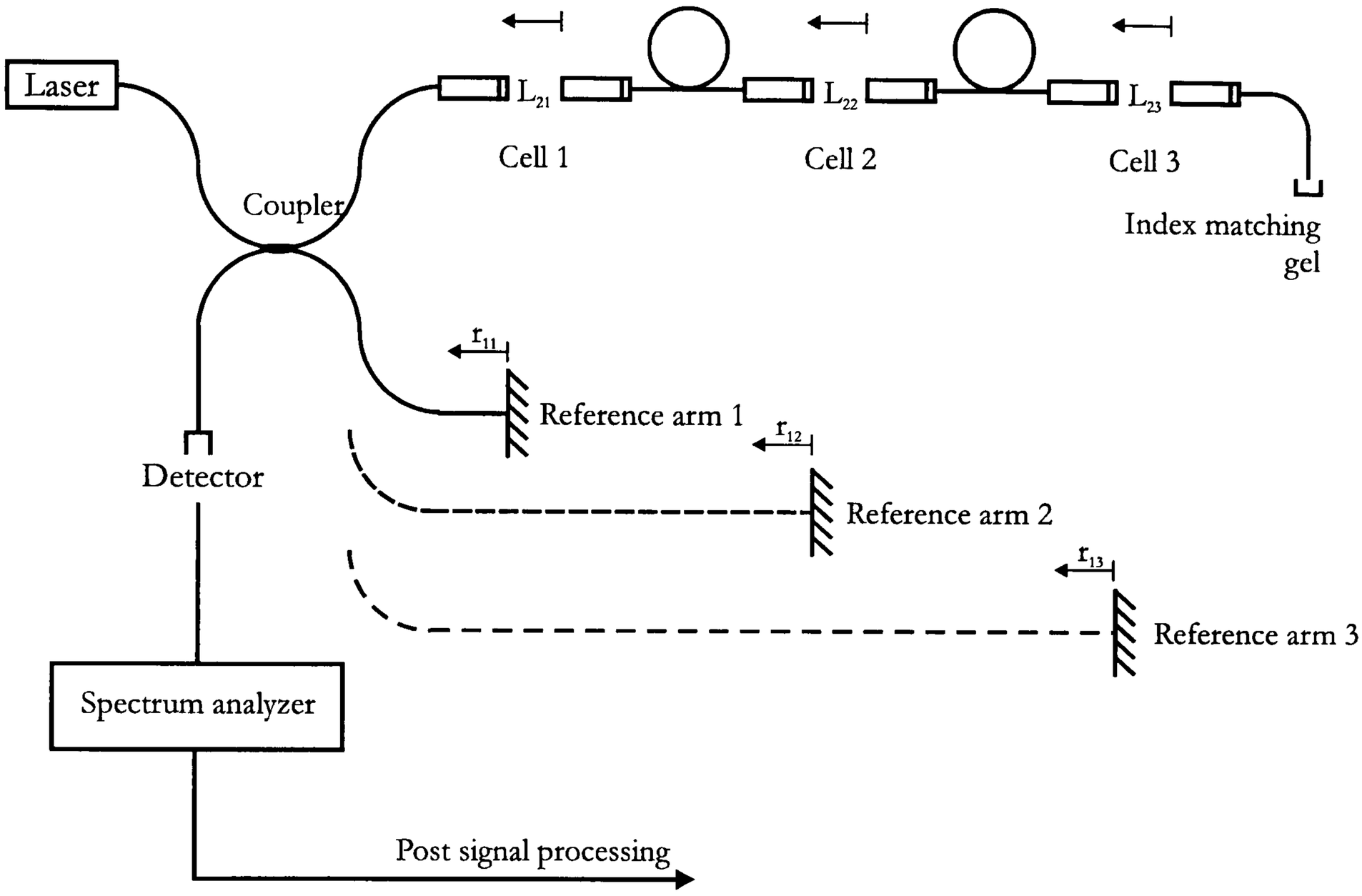

Figure 7.1: *Experimental setup for the FMCW reference arm method*

In order to compare the simulations and experimental results first a simple Michelson interferometer according to Figure 5.1 has been constructed. The time detector time response and appropriate power spectrum with the beat frequency corresponding to the difference between the reference and sensing arm are shown in Figure 7.2.

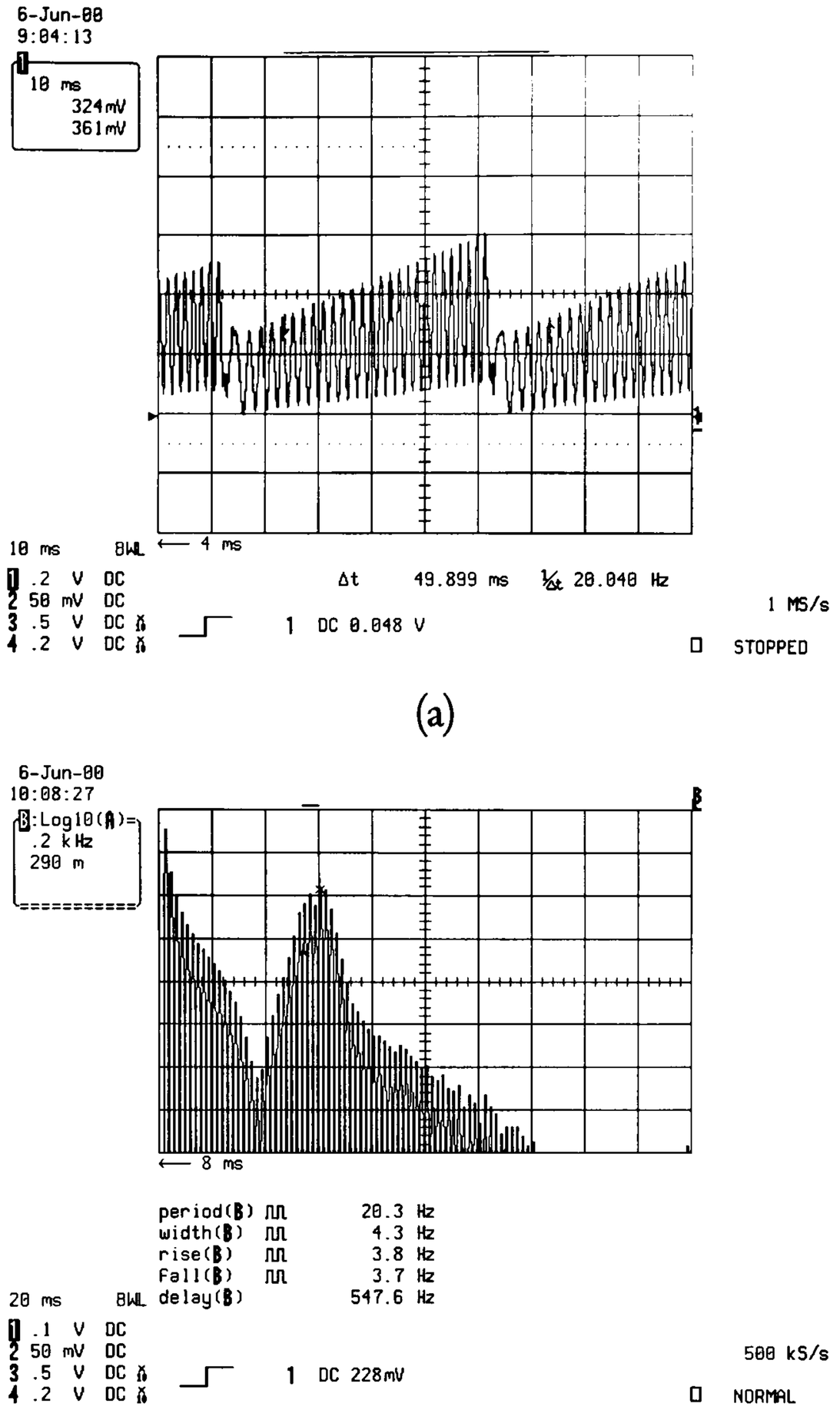

Figure 7.2: *FMCW operation of the Michelson interferometer: (a) time domain, (b) frequency domain*

Obtained experimental result are in agreement with the theoretical analysis of the FMCW reference arm method in Chapter 5 (time and frequency response of Figure 5.4).

After this verification experiment of the reference arm system, the cell was assembled in steps. Firs only the capillary and the first GRIN lens were put together and the backreflected signal interfering with the signal reflected from the

reference arm was observed. Figure 7.3 shows the interference signal with the sawtooth modulation envelope.

Although the first GRIN lens in each sensing cell is anti reflection coated a small portion of the light is still backreflected. Due to this a very small peak is observed in the power spectrum of the interference signal between the reference arm and the signal reflected from the first GRIN in the sensing cell (Figure 7.4).

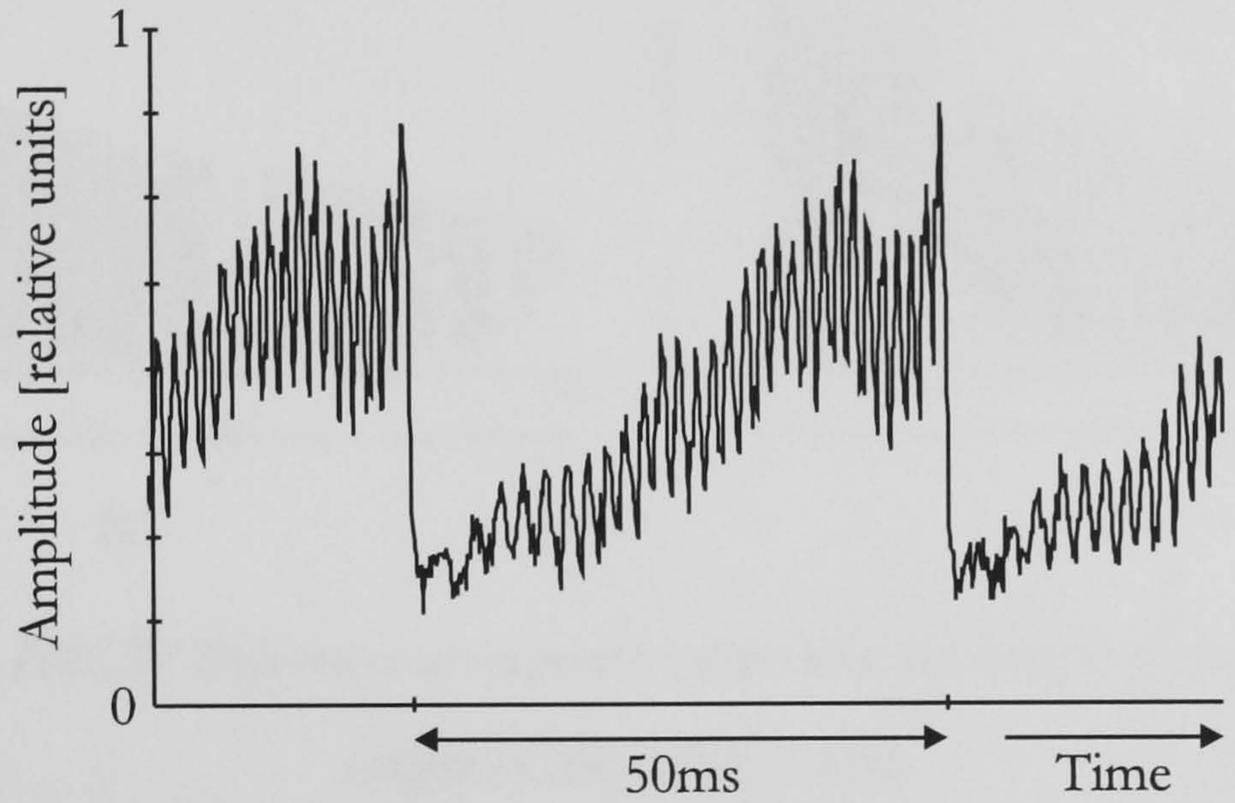

Figure 7.3: *FMCW reference arm method time response: first capillary GRIN lens backreflection*

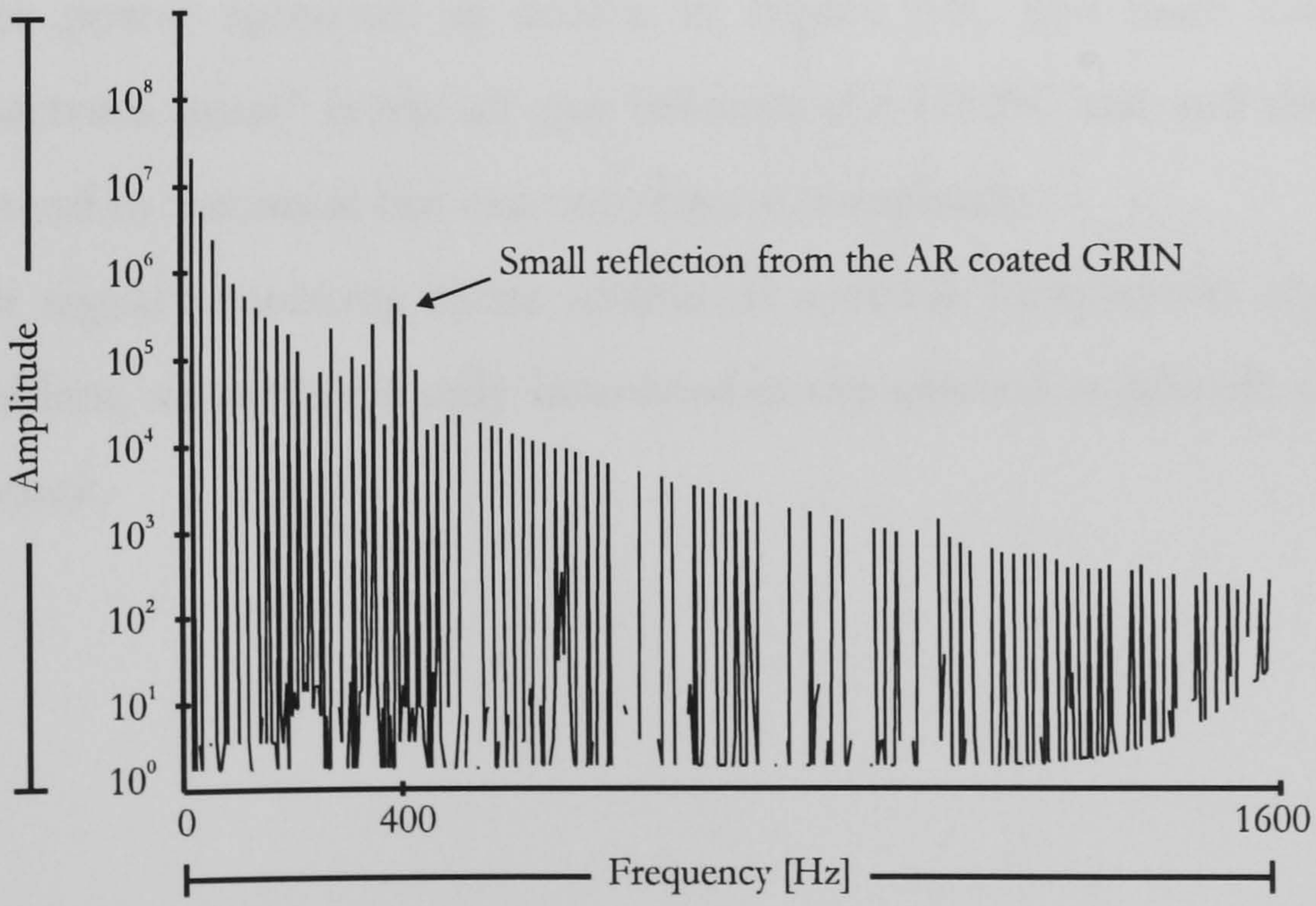

Figure 7.4: *Power spectrum; reflection from the first AR coated GRIN*

After another GRIN lens is added to the sensing cell the main reflection comes from these second GRIN lens. In Figure 7.5a and Figure 7.5b two different displacement between the GRIN lenses are presented. Because of the difference also the distance to the reference arm is changed and therefore the power spectrum maximum is shifted.

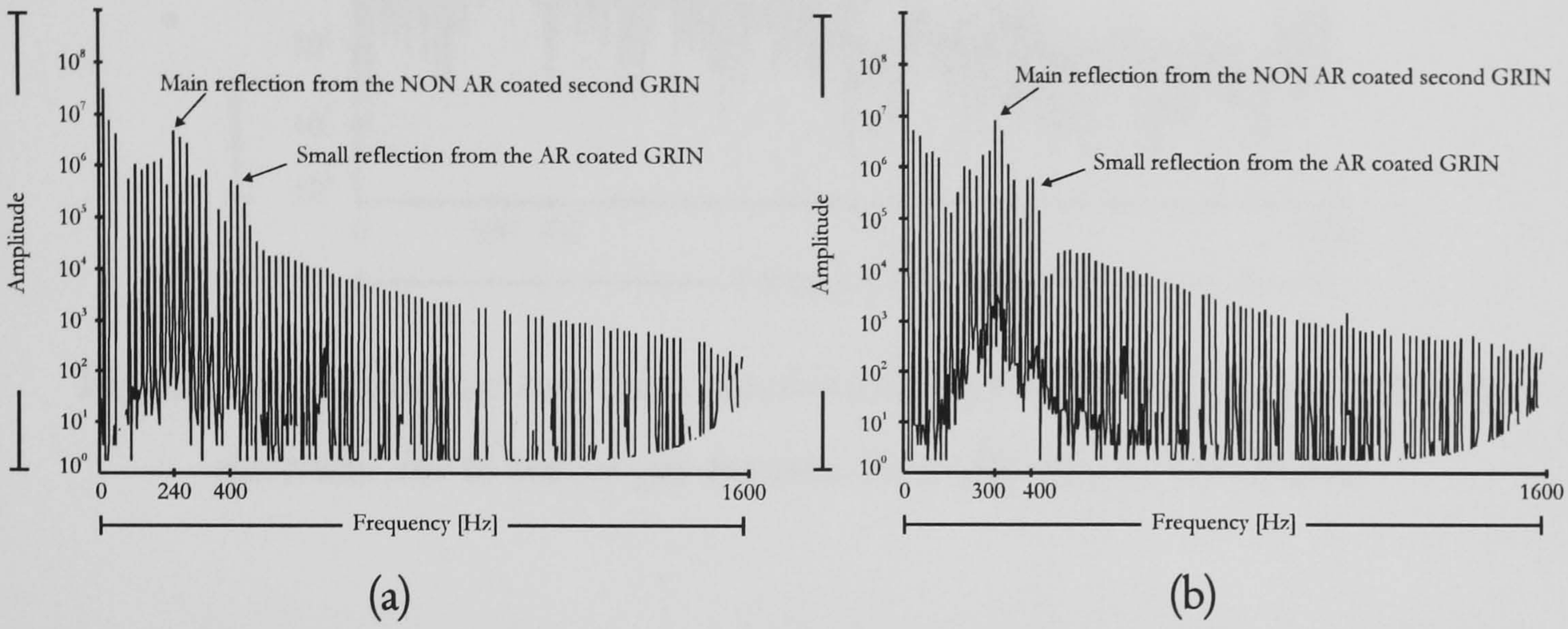

Figure 7.5: *FMCW Reference arm power spectrum: (a) length of the cell is 6mm, length of the cell is 12mm*

When the sensing cell is completely assembled, i.e. both capillaries and both GRIN lenses are properly aligned, some additional spectral components are added to the interference power spectrum as shown in Figure 7.6. The main cause of the "power spectrum noise" is the air gap between the GRIN lens and the capillary which we tend to minimise but can not remove completely.
Using post signal processing those additional spectral components represent no special problem, since we are only interested in the spectral amplitude at a specific beat frequency.

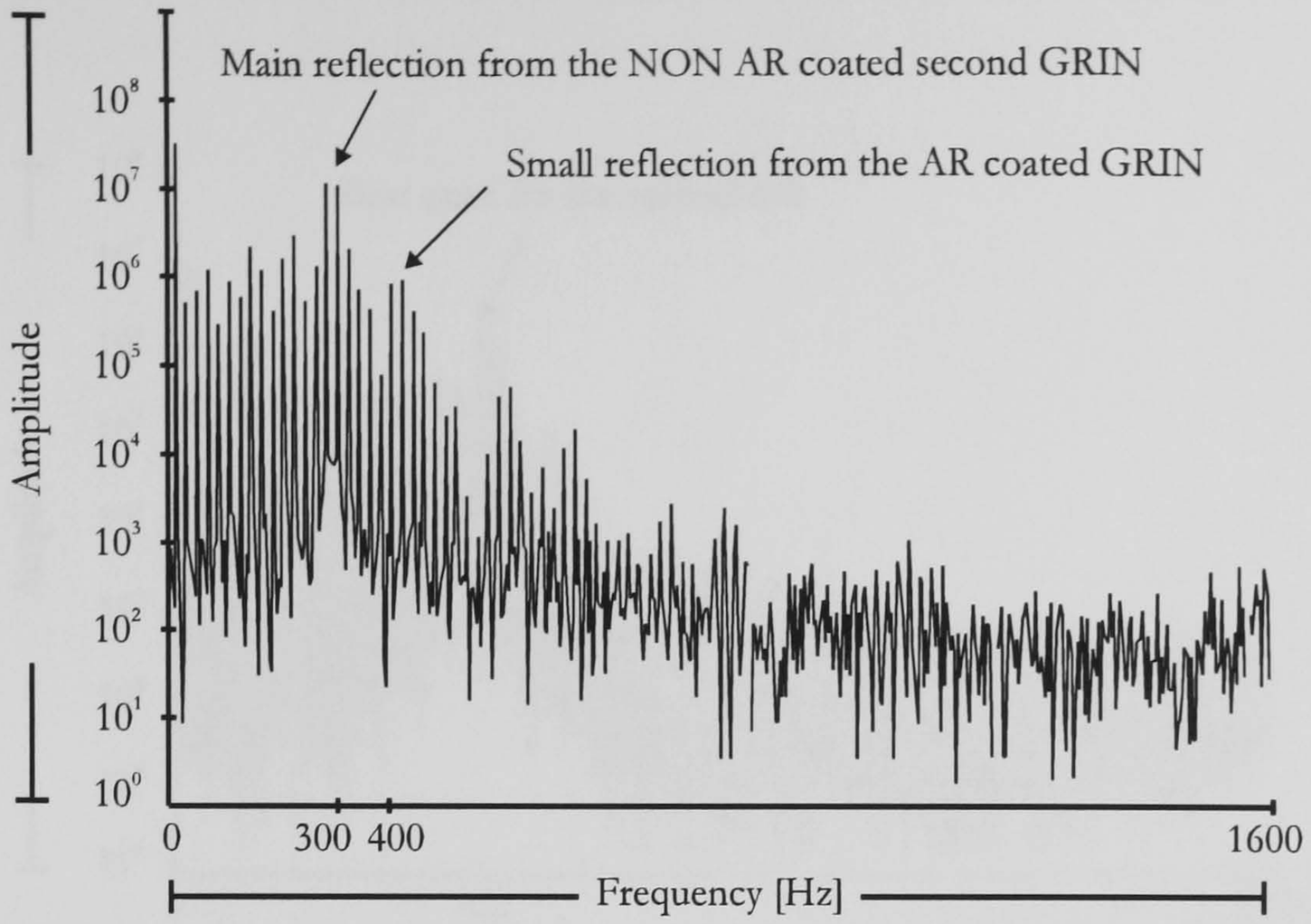

Figure 7.6: *Additional spectral components of the FMCW reference arm power spectrum due to the air gap between the capillary and GRIN lens*

The next step in system evaluation is the serial connection of two cells. When the proper length of the reference arm which ensures good interference fringe visibility is established, the second sensing cell is assembled in the same manner as the first one. After the capillaries and GRIN lenses are aligned with the supporting V-groove block, the interference for the second cell is observed as shown in Figure 7.7.

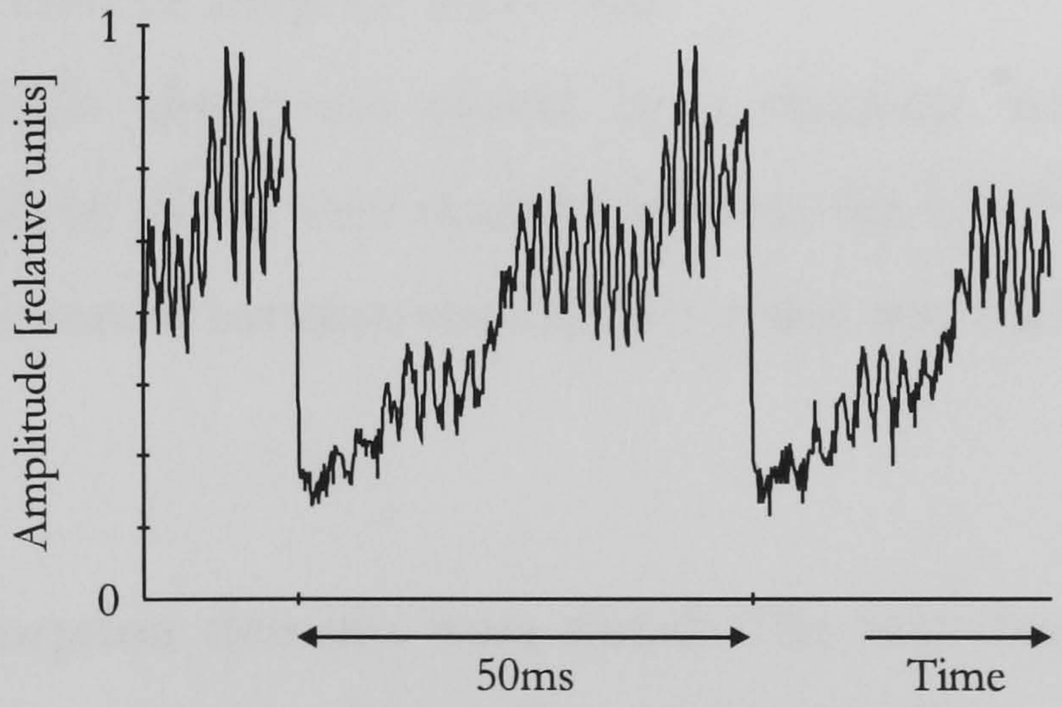

Figure 7.7: *Interference for the second sensing cell*

The appropriate power spectrum for the interference signal for the second cell is shown in Figure 7.8.

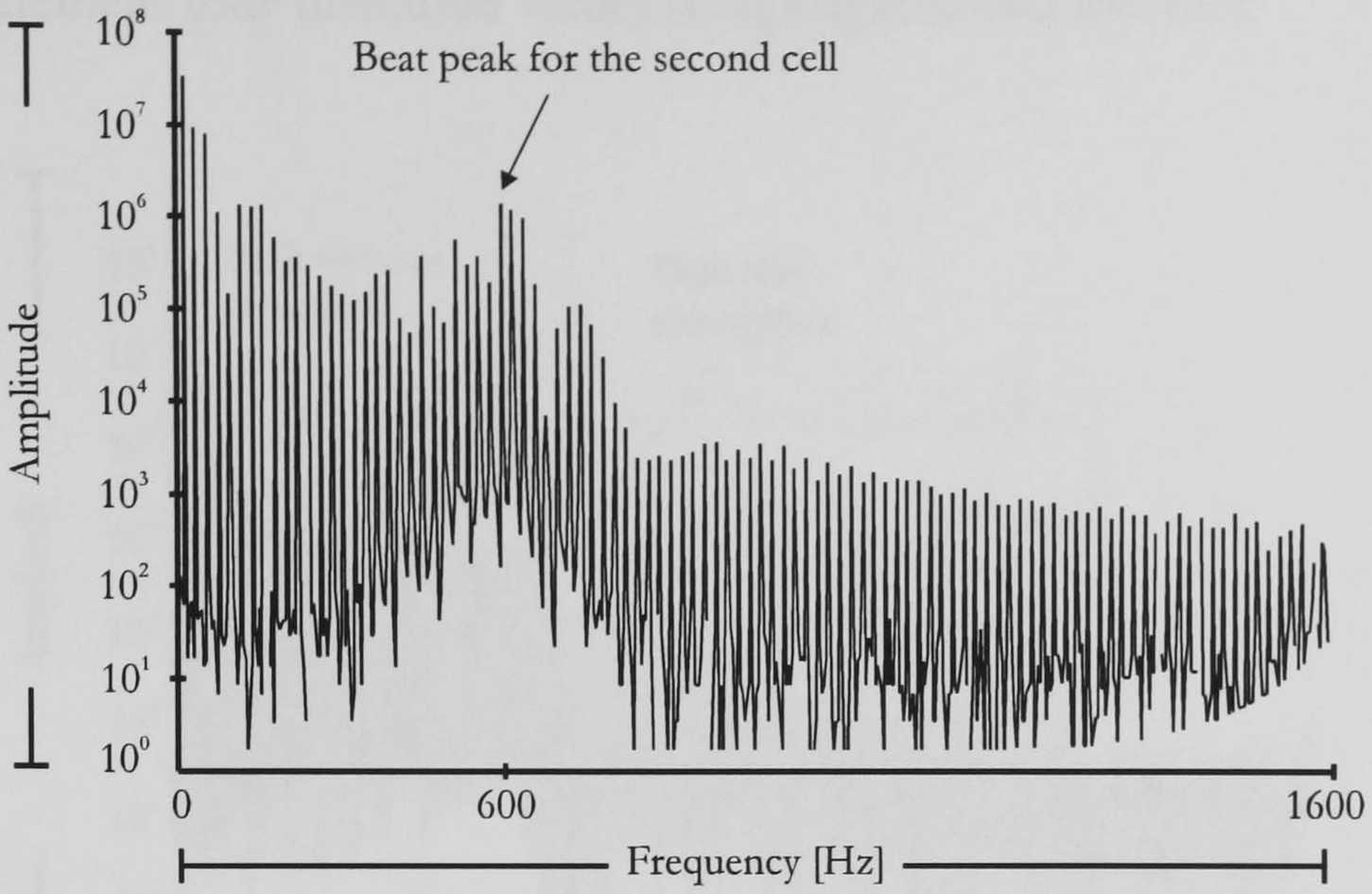

Figure 7.8: *Power spectrum for the second cell*

7.1. Absorption measurement with the second cell

Because in the time these experiments were made only few "home made" V-grooves for the alignment where available the absorption properties are evaluated for the second cell only, whereby the light passes through the first sensing unit. For future experiment special high purity aluminium V-grooves will be available and measurement could be made for more cells.

To simulate the light absorption caused by a chemical substance absorption elements (filters and/or slides) were inserted between the GRIN lenses. To enable the element to be inserted between the GRIN's a slot was made in the middle of the V-groove.

Four different absorption elements were tested. The first three were absorption filters F1 (99.9%), F2 (69%), F3 (40%) and F4 with 8% of absorption. As the fourth element we used an ordinary microscope slide. For each experiment the power spectrums with and without the absorption element were recorded and compared. The power spectrums are shown in Figure 7.9 to Figure 7.12. For each absorption

the difference in the amplitude of the beat frequency with and without the absorbing element (our measured value) is highlighted and marked.

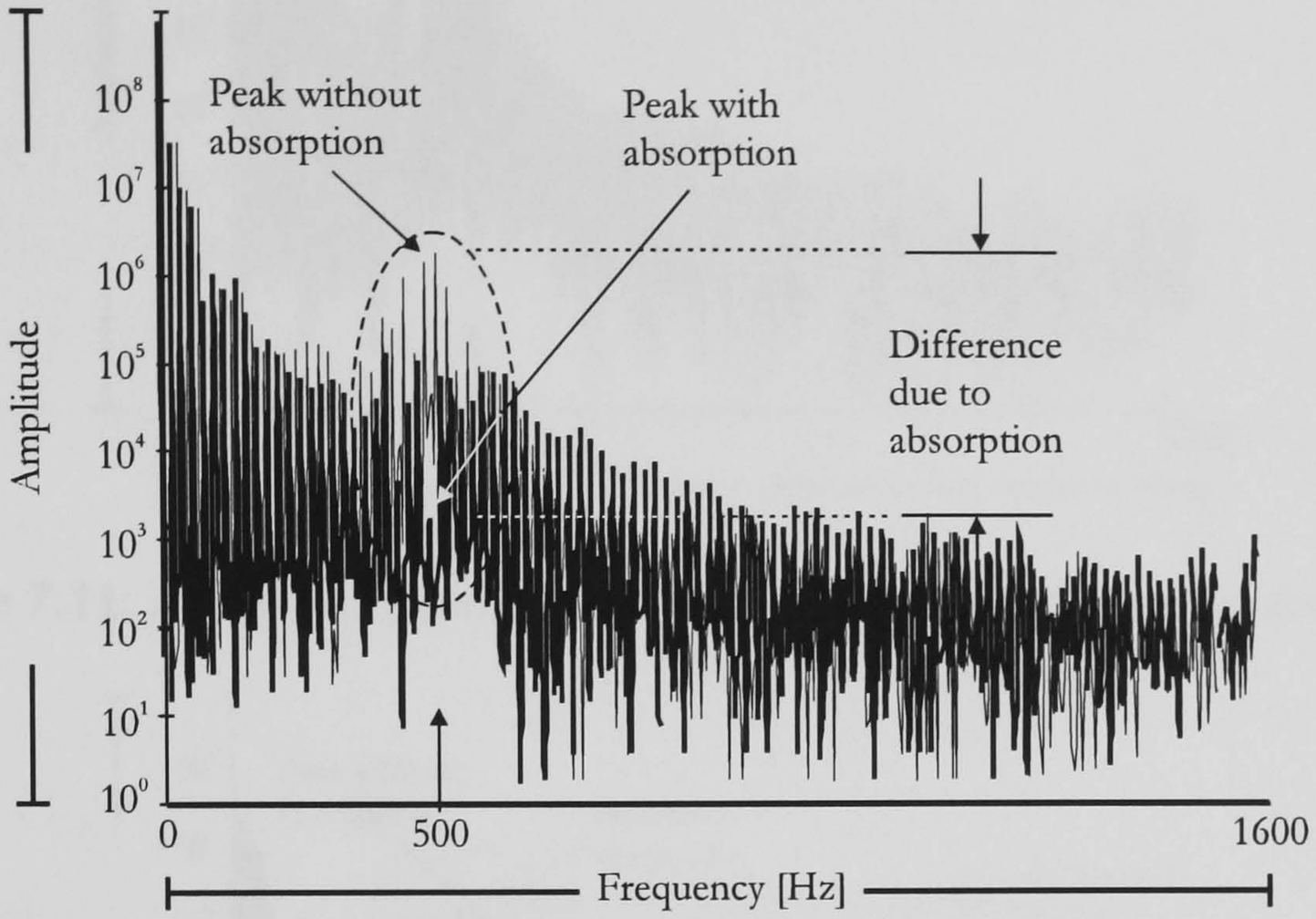

Figure 7.9: *Power spectrum of the second cell with the F1 absorption element*

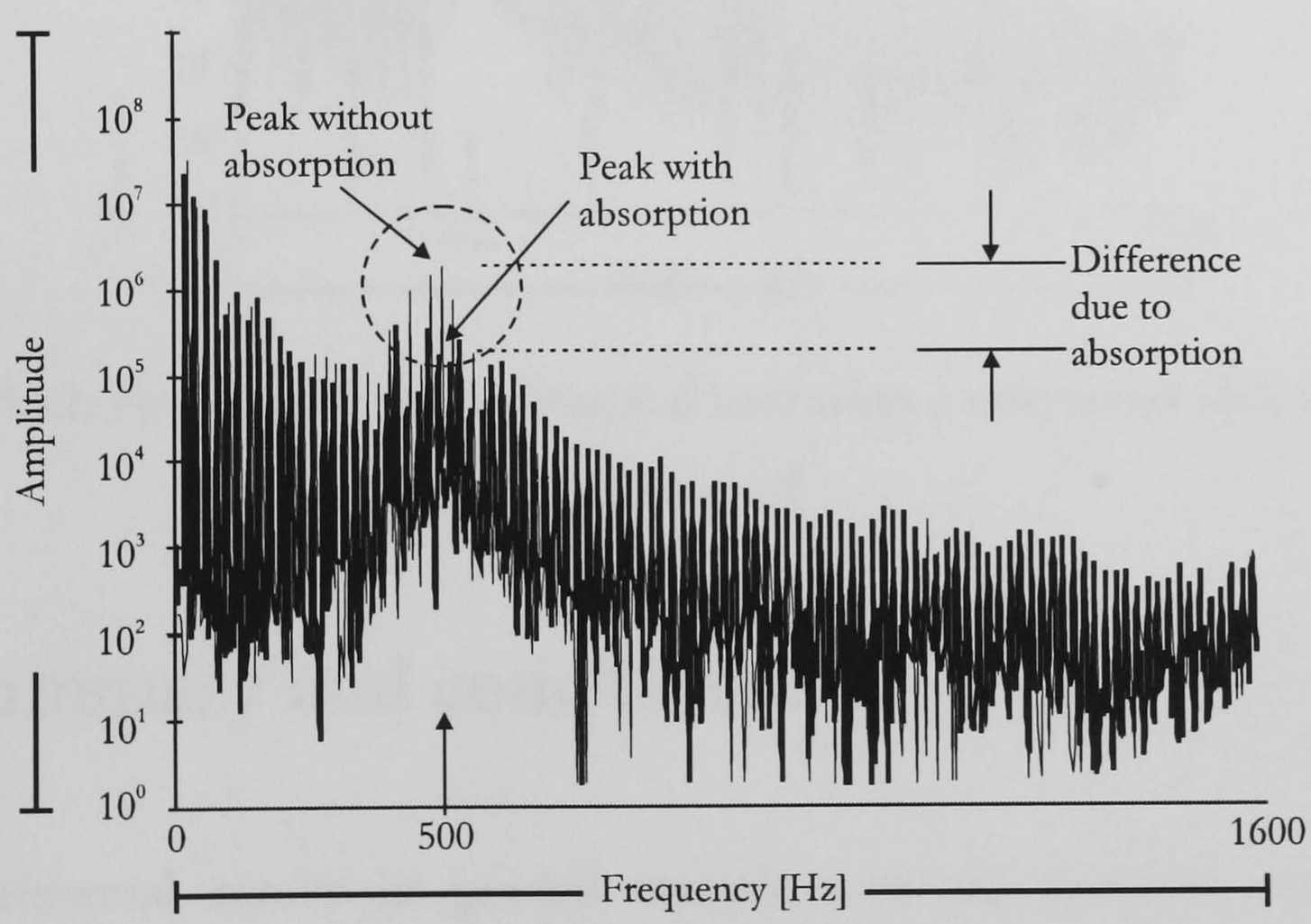

Figure 7.10: *Power spectrum of the second cell with the F2 absorption element*

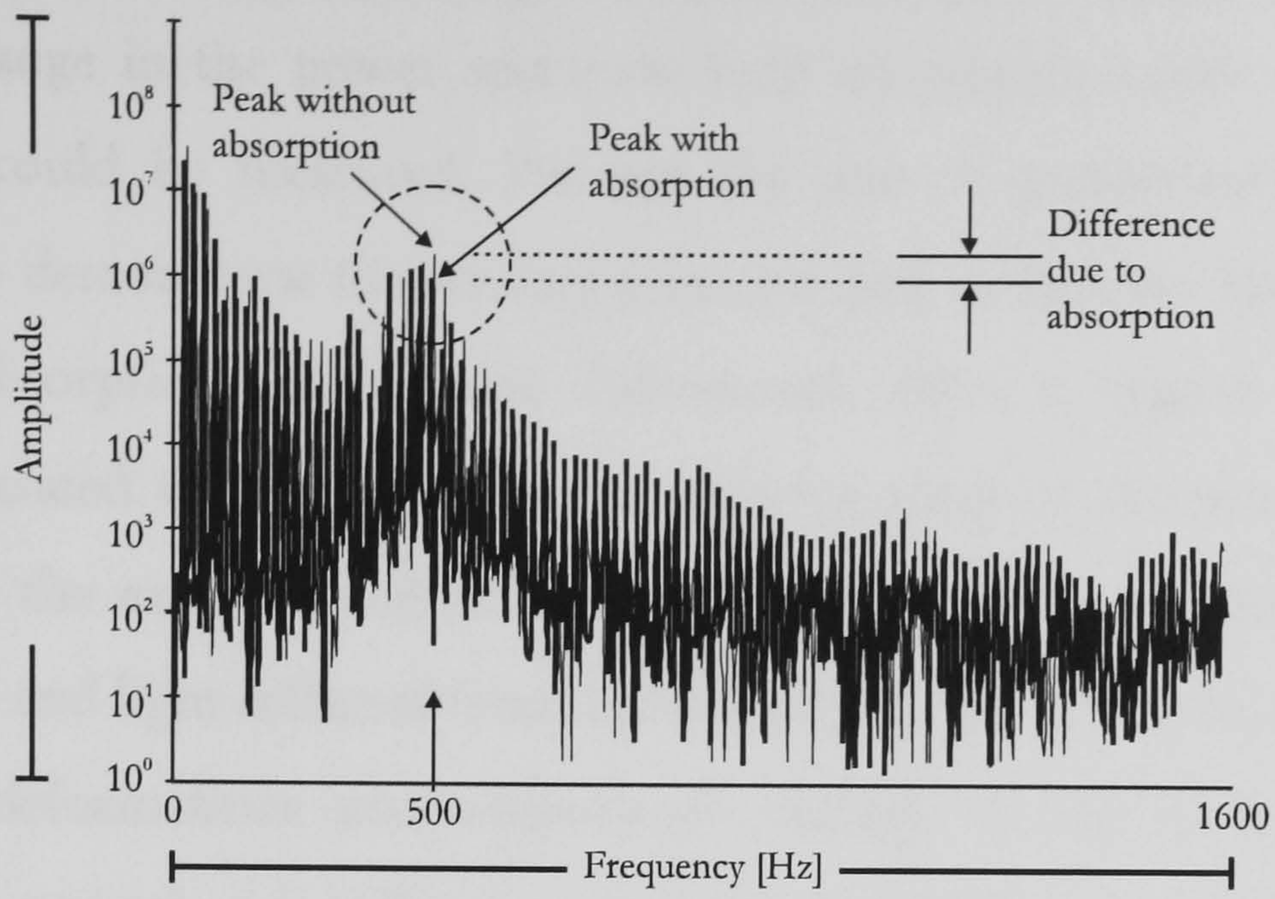

Figure 7.11: *Power spectrum of the second cell with the F3 absorption element*

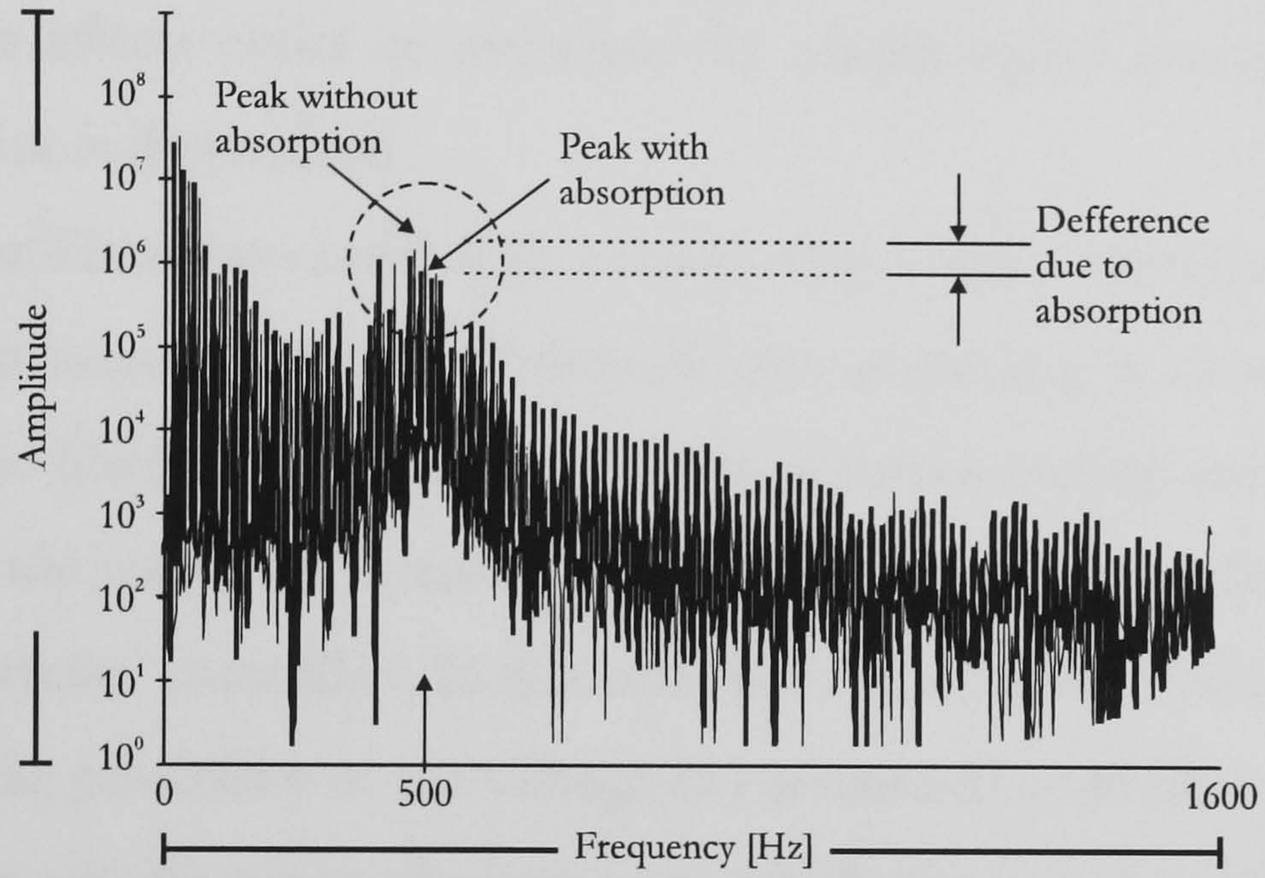

Figure 7.12: *Power spectrum of the second unit when a microscope slide is inserted inside the cell*

7.2. Summary and conclusions

The experimental results in general comply with the previous mathematical modelling and simulation experiments. The responses in the time domain for the real open path microoptic sensing cell are in accordance with those predicted from the simulations. The same is valid for the power spectrums of the interference signals from individual sensing cells, however we obtain some additional beat components due to cross interference effects because of the cell construction.

From the change in the power spectrum light absorption inside the microoptic sensing cell could be measured. Because the aim of preliminary experimental results was to demonstrate the sensing principle and to indicate the crucial points only large absorption values were introduced. Also a typical interferometer problem associated with the use of two different arms of the interferometer has arisen during the experimental investigations. Since the light reflected from the reference arm and light reflected from the microoptic cell travel in different optical fibres slight deformations and temperature changes in one of them causes the change in the optical path difference and thus a modification of the interference pattern. Therefore the interference power spectrum experienced small variations. Some of those effects could be overcome by proper signal averaging before the absorption value is determined.

The second problem associated with constructing a quasi distributed fibre optic sensing system based on FMCW Reference arm addressing is associated with the necessity to use fibre optic switches to address different sensing units. To have the possibility of the automatic control over all installed sensing cells the switching should be computer controlled. In this case more alternatives could be considered. First there is the possibility to use voltage or current activated fibre optic switches. Those switches usually use mechanical parts which are moved to align the fibre to be connected. Mostly this kind of mechanical voltage controlled switches are not suitable for the reference arm addressing mechanism because large backreflections and signal attenuations are present. The second possibility is to use interferometric fibre optic switches. Those would be adequate for the reference arm addressing scheme, but the application is limited because of the high price.

In conclusion, the experimental tests performed on the reference arm system confirm our initial feelings that this arrangement is not the best way of designing an FMCW system, and is therefore not worthy of further investigation here. In the remainder of the thesis, we focus solely on the coherence addressing technique, which avoids most of the problems described above.

8. Coherence addressing of Quasi-Distributed Absorption Sensors by the FMCW method

The second addressing mechanism for distributed fibre optic gas sensors which we would like to extensively evaluate experimentally is the Coherence addressing of quasi-distributed absorption sensors by the FMCW method.

The feasibility of the proposed addressing method will be demonstrated using a three-sensor system shown in Figure 8.1. The optical source is a 1308nm DFB laser diode produced by Nortel (l_c ~ 22cm, the laser diode has been characterised to have a 0.0077818nm line-width applying 20Hz modulation and ~0.05nm/mA dynamic shift). The output frequency of the laser diode is saw-tooth injection current modulated. The saw-tooth ramping frequency is 20Hz, and the corresponding frequency excursion of the laser diode due to current modulation is approximately 90GHz (the experienced wavelength change is approximately 0.5nm). In the design of the coherence addressed quasi-distributed absorption sensors by the FMCW

method, light emergent from the optical fibre is collimated by the GRIN lens, transmitted through the sample cavity, reflected at the second GRIN lens, and then returned to the first GRIN lens and the optical fibre. A Hawlett-Packard spectrum analyser is used to calculate the power spectrum (start frequency 0Hz, stop frequency 3.2kHz, 10k samples/s, 250ms record length, 80dB dynamic range) and a personal computer for post signal processing.

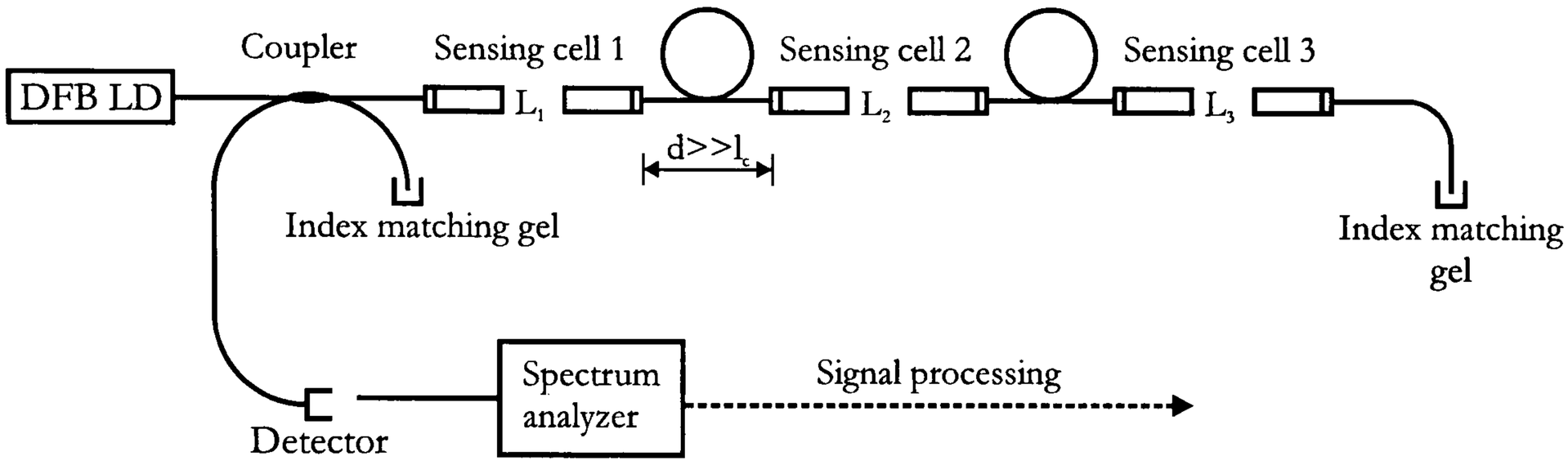

Figure 8.1: *Experimental set-up for the FMCW coherence addressing method*

The system will be evaluated in four steps. In first three steps each sensing cell will be investigated individually. After that the cells will be connected together and the system is going to be examined with regard to its properties for quasi distributed absorption based measurements.

8.1. Absorption measurement in the first cell (length 35mm)

The fibre micro-optic sensing cell used for FMCW Coherence addressing is constructed using two capillaries, two collimating GRIN lenses and a supporting V-groove alignment block. On both ends of the micro-optic cell the capillaries are used to fix the fibre and align it to the centre of the adjacent GRIN lens. As shown in Figure 8.2 the capillary and GRIN lens are carefully aligned to minimise the air gap between them. Because the air gap could cause undesirable backreflections the gap could be filed with index matching oil or gel.

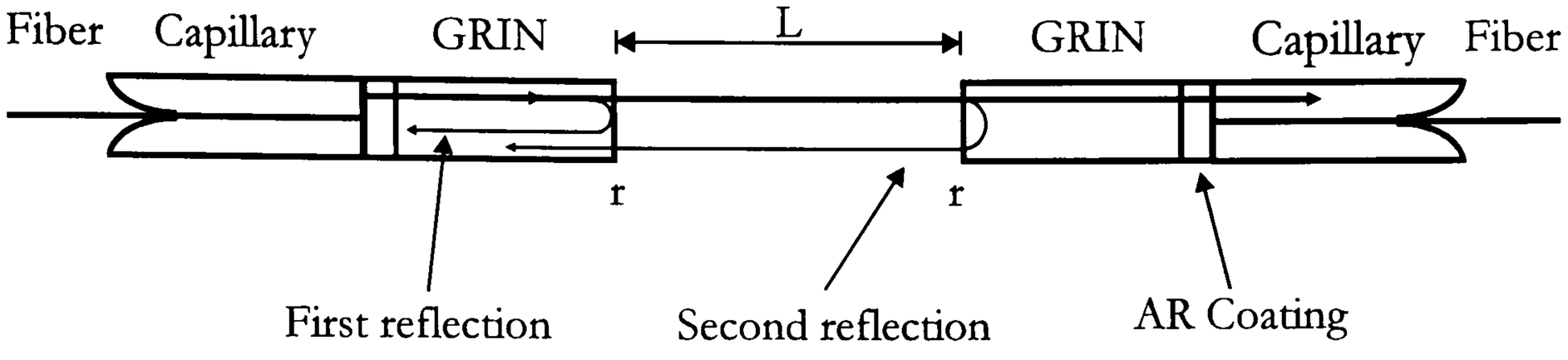

Figure 8.2: *Structure of the micro-optic sensing cell*

For the proposed sensor systems the collimating GRIN lenses are turned with the anti-reflection coating side facing the capillary. The main signal is partially reflected from the first lens, passes through the cell and is then partially reflected from the second lens. The reflected signal passes the cell once again and is coupled into the input fibre. The cell length is typically from few milimeters up to several cetimeters which is less then the coherence length of the laser source used. Typical values for $r_1^2 = r_2^2$ are 4%.

After the cell was assembled the time response shown in Figure 8.3 has been recorded.

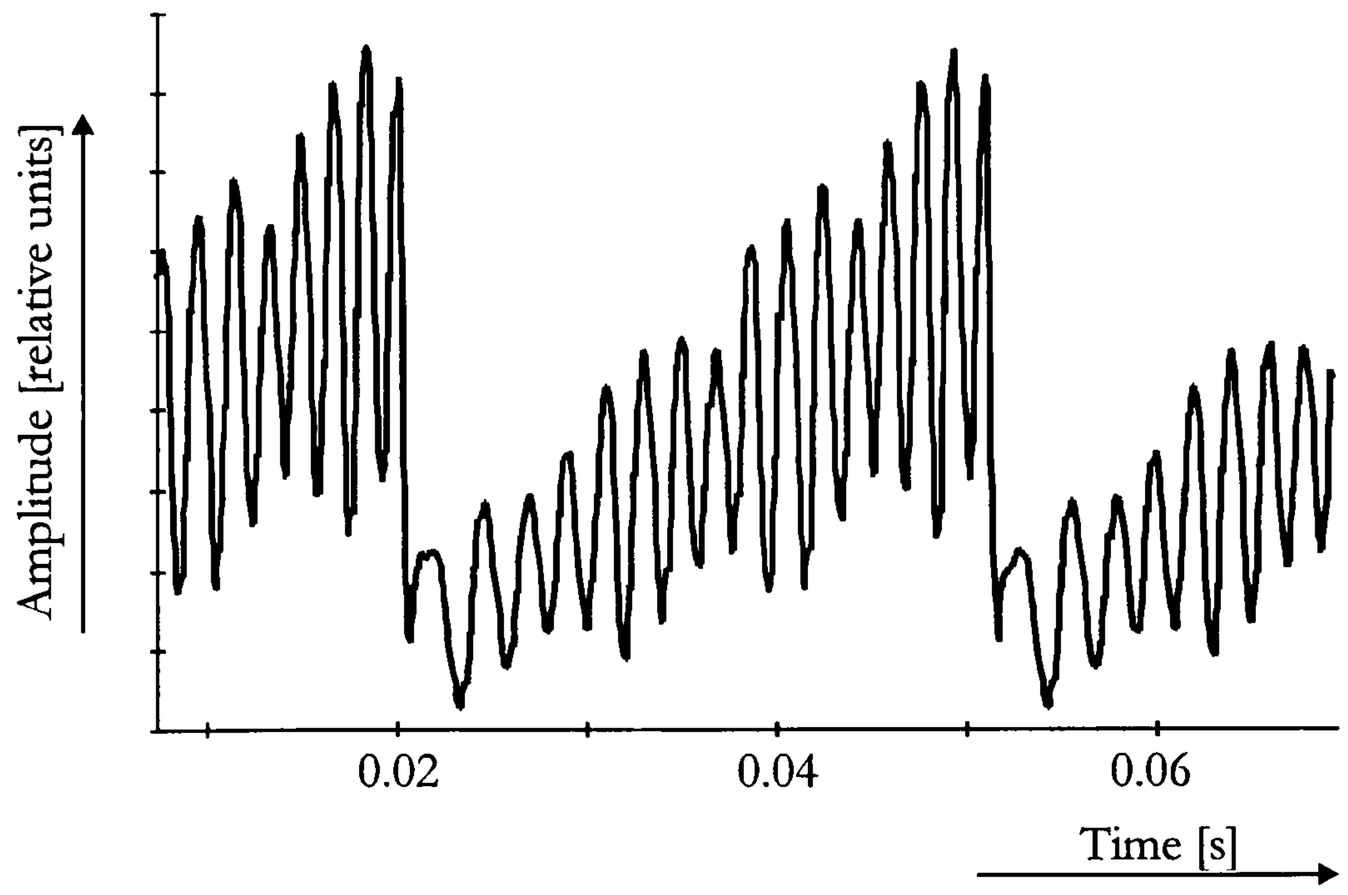

Figure 8.3: *Time response for the first sensing cell*

The observed time response is in accordance with the simulation results presented for a single cell in Figure 5.4. To examine the absorption properties of the measuring cell the experiments were accomplished in two steps.

First absorption filters F1 (99.9%), F2 (69%), F3 (40%) and F4 with 8% of absorption were placed inside the cell to simulate the broadband absorption of an analyte or gas and the power spectrum was observed. For each experiment the power spectrums with and without the absorption element were recorded and compared (Figure 8.4).

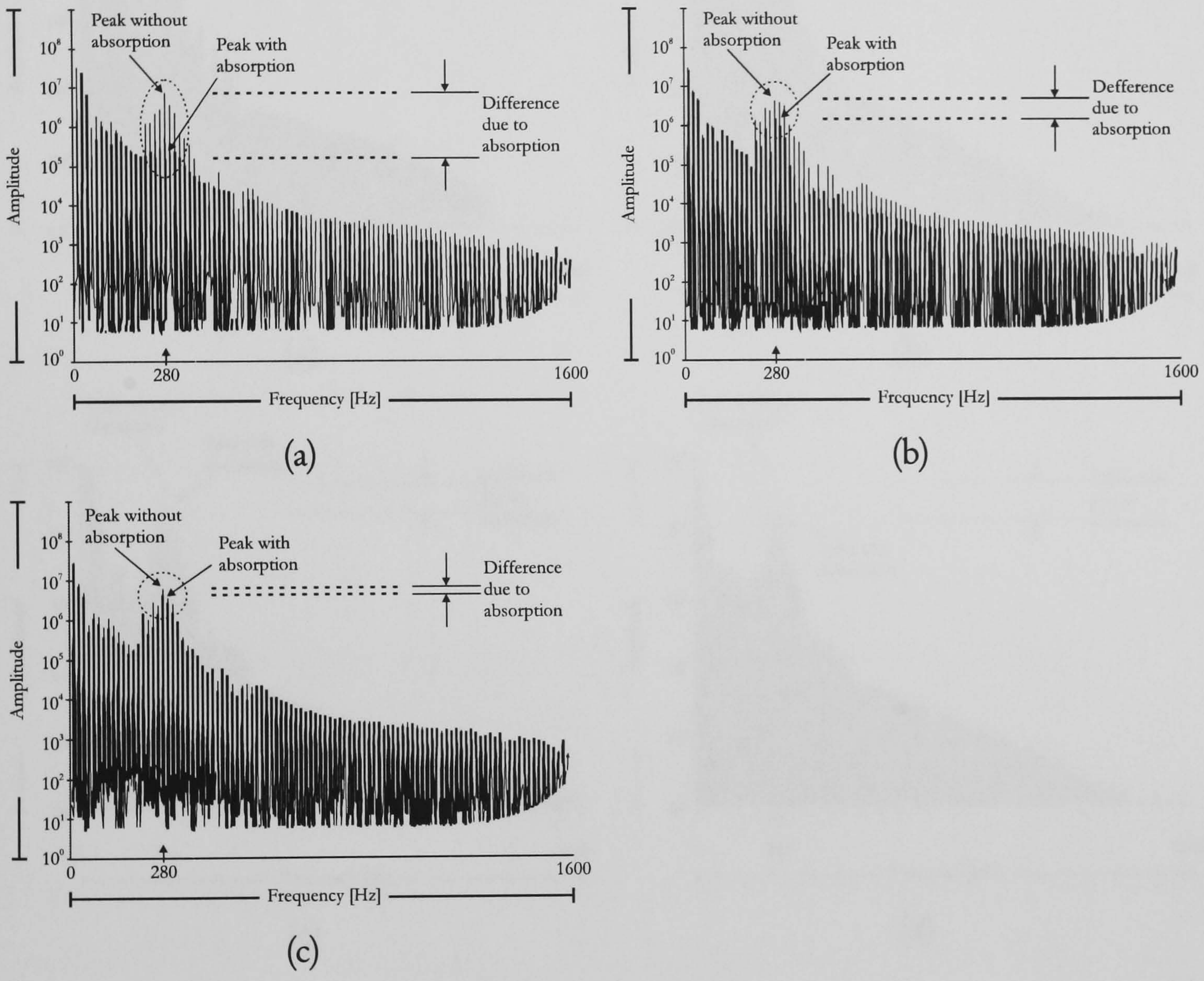

Figure 8.4: *Power spectrums of the first cell using FMCW Coherence addressing for different absorption elements: (a) F1; (b) F2; (c) F3*

Although the change in power spectrum amplitude at the beat frequency for a particular absorption element is clearly visible this type of measurement was carried out only for the first cell. Since filters which would enable a linear

absorption increase were not available we decided to use microscope slides to introduce different levels of absorption inside the sensing cell.

A maximum of four microscope slides was inserted in a cell, whereby introducing a 32% absorption span. Comparison between power spectra with and without absorption is presented in Figure 8.5.

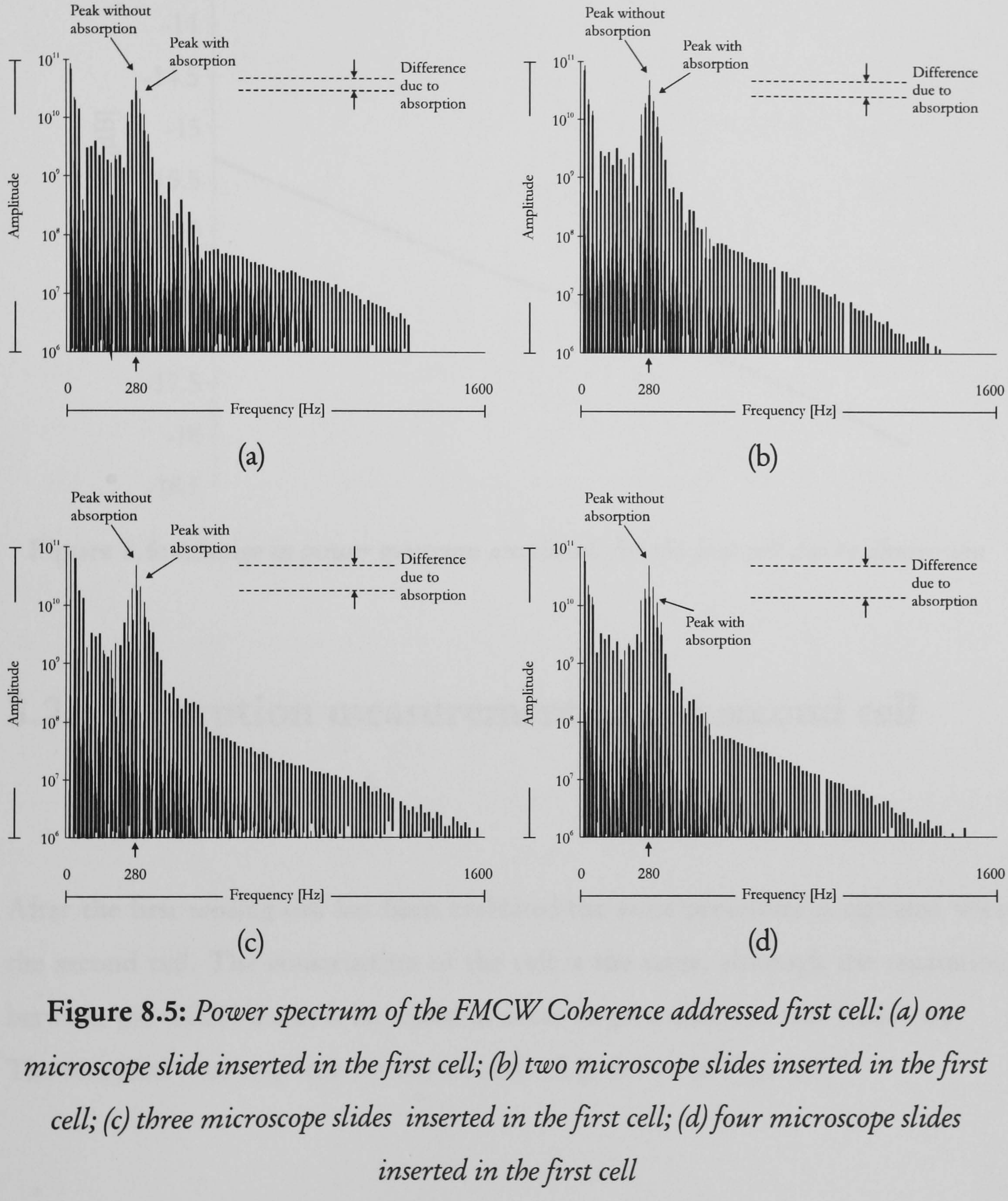

Figure 8.5: *Power spectrum of the FMCW Coherence addressed first cell: (a) one microscope slide inserted in the first cell; (b) two microscope slides inserted in the first cell; (c) three microscope slides inserted in the first cell; (d) four microscope slides inserted in the first cell*

As shown in Figure 8.5 the change in the power spectrum amplitude at the beat frequency due to increased absorption is clearly visible. The first beat amplitude decrease due to absorption is shown in Figure 8.6.

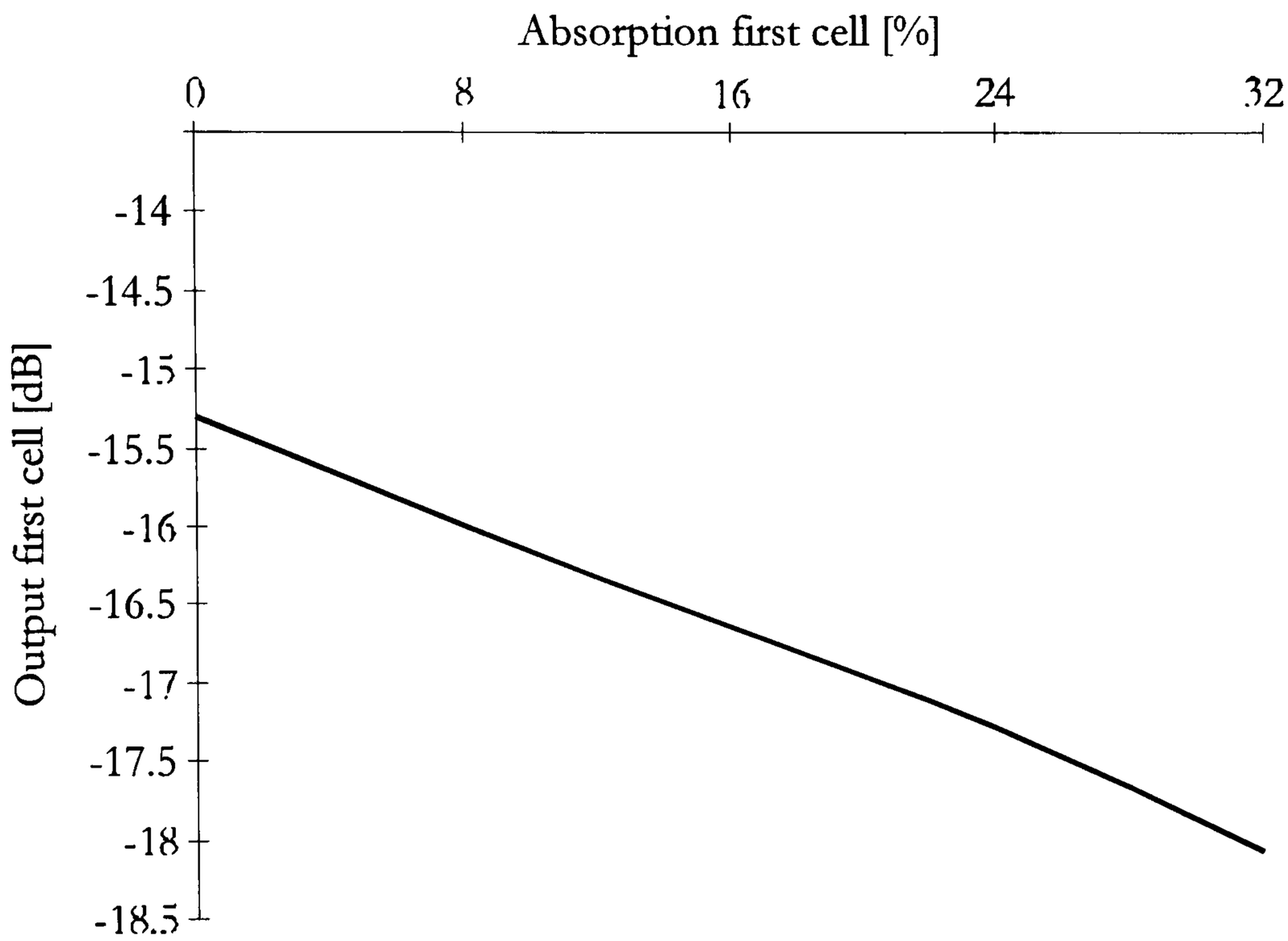

Figure 8.6: *Change in power spectrum amplitude for the first cell due to absorption*

8.2. Absorption measurement in the second cell (length 46mm)

After the first sensing cell has been evaluated the same procedure is repeated with the second cell. The construction of the cell is the same, although the separation between the GRIN lenses is increased in order to get a different beat frequency. The recorded time response for the second cell is shown in Figure 8.7.

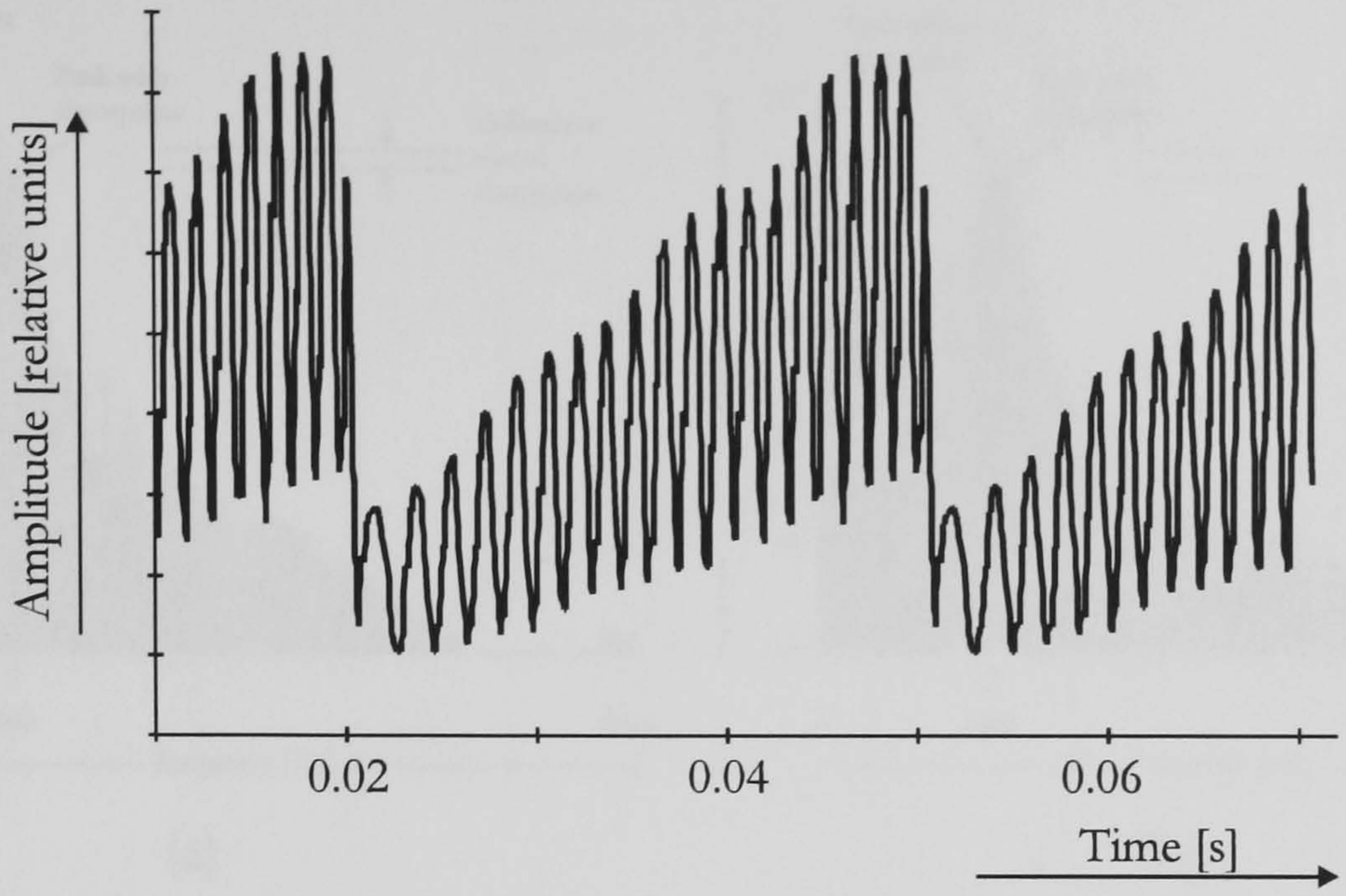

Figure 8.7: *Time response for the second cell using FMCW Coherence addressing*

One may wonder why the shape of the time response curve has some ripples in the cosine function. In reality the shape of the time response for the second cell is much clearer on the oscilloscope (without ripples on the cosine function), but due to the transfer from the oscilloscope to the computer the picture is worsen. In spite of that the response is in accordance with the simulation results presented in Chapter 5.

In the same manner as for the first cell the absorption experiments were accomplished using microscope slides. We omitted the use of absorption filters since filters with linear absorption increase were not available. The microscope slides were inserted inside the micro-optic cell to cause an absorption increase from 0 to 32%. For each experiment the power spectrum with and without the absorption element were recorded and compared. The appropriate change in power spectrum amplitude is presented in Figure 8.8.

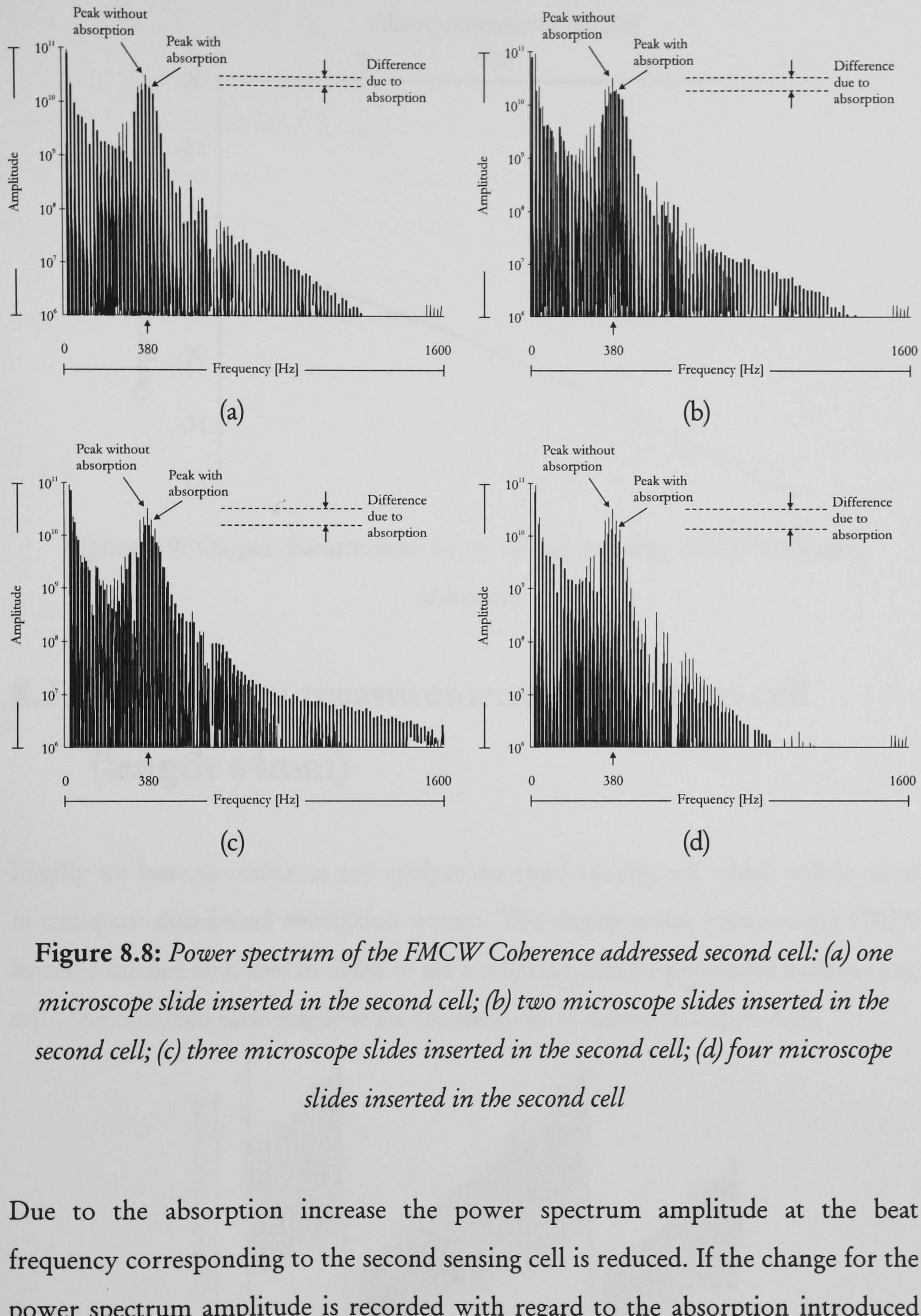

Figure 8.8: *Power spectrum of the FMCW Coherence addressed second cell: (a) one microscope slide inserted in the second cell; (b) two microscope slides inserted in the second cell; (c) three microscope slides inserted in the second cell; (d) four microscope slides inserted in the second cell*

Due to the absorption increase the power spectrum amplitude at the beat frequency corresponding to the second sensing cell is reduced. If the change for the power spectrum amplitude is recorded with regard to the absorption introduced the output characteristics for the second cell can be presented in Figure 8.9.

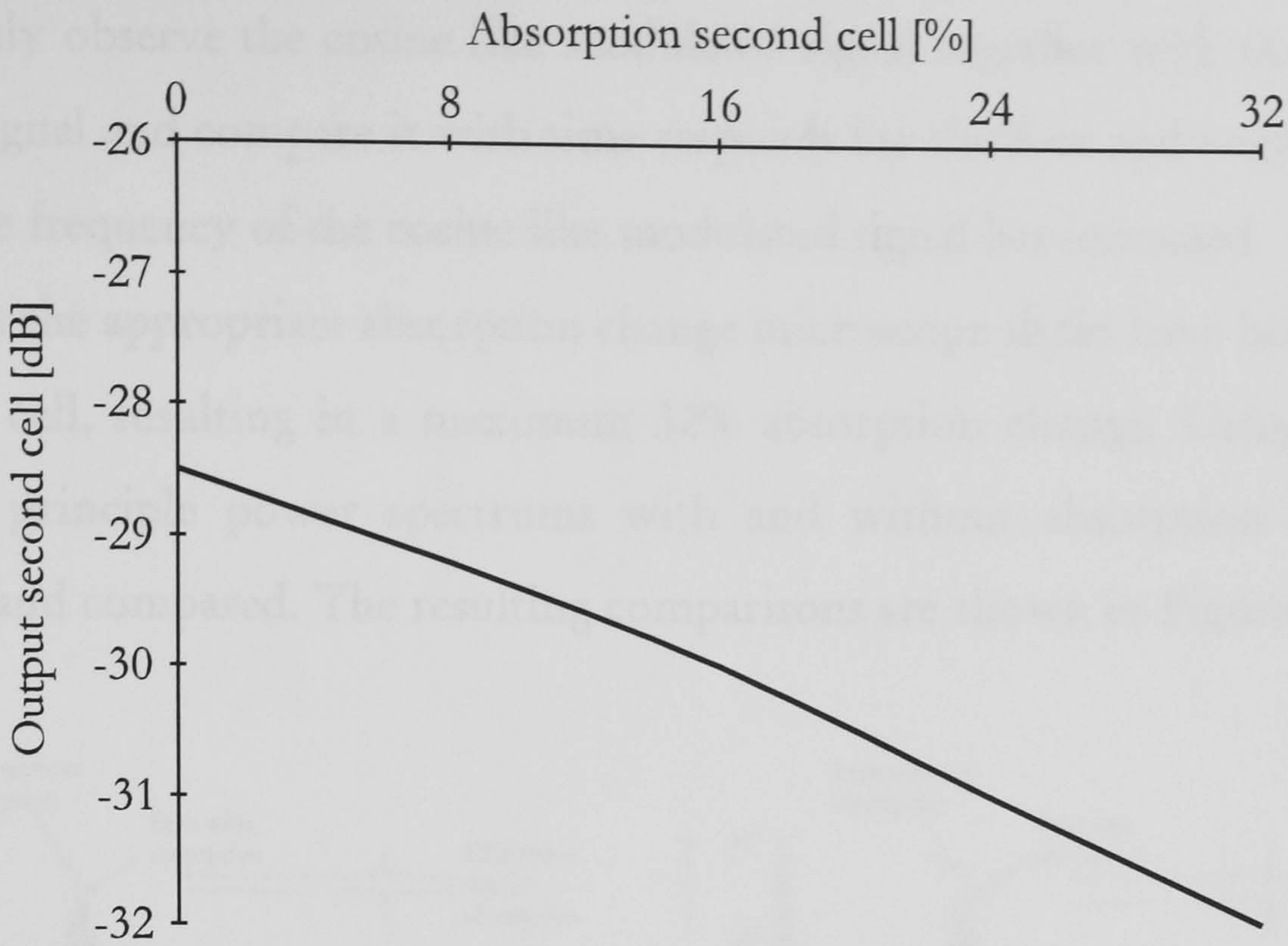

Figure 8.9: *Output characteristics for the second cell using FMCW Coherence addressing*

8.3. Absorption measurement in the third cell (length 64mm)

Finally we have to construct any analyse the third sensing cell which will be used in the quasi distributed absorption system. The displacement between the GRIN lenses is further increased in order to get a different beat frequency for each sensing cell. The observed time response for the third cell is shown in Figure 8.10.

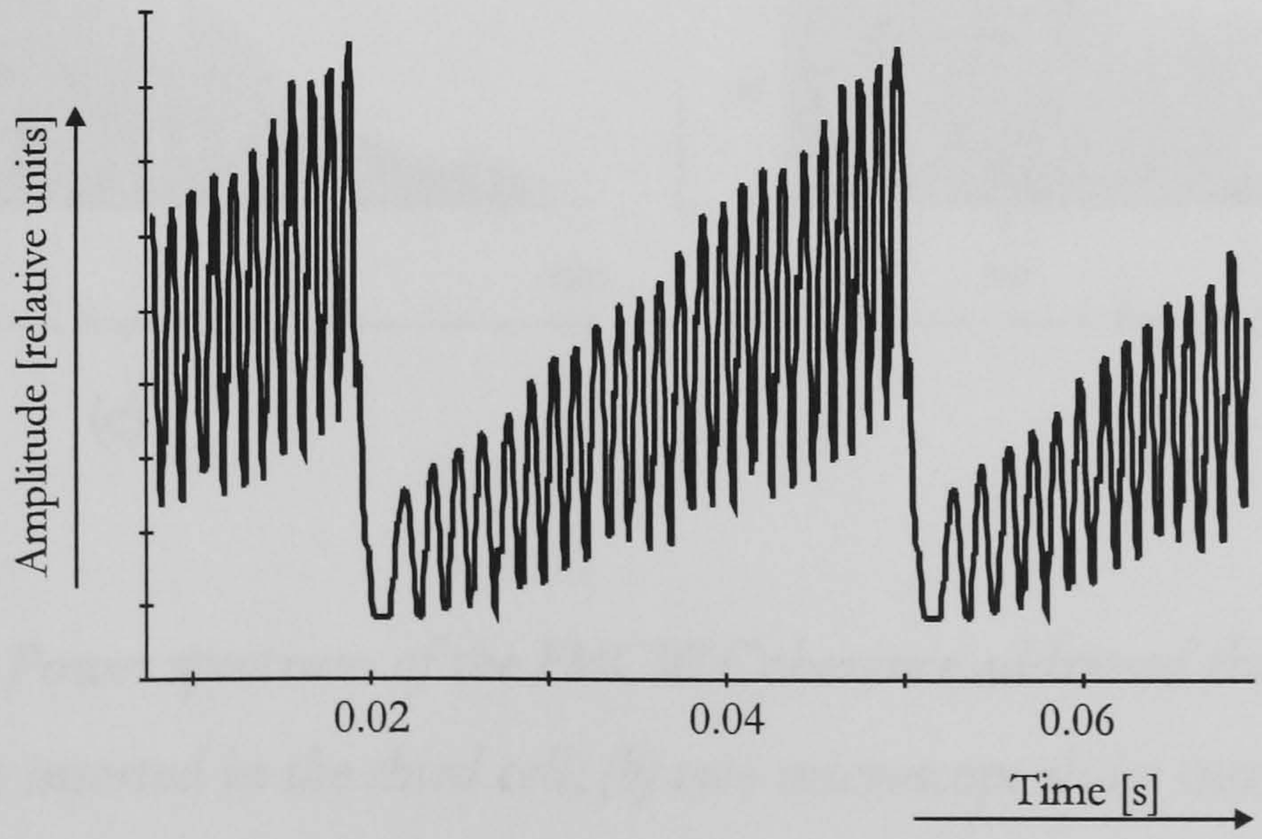

Figure 8.10: *Time response for the third cell using FMCW Coherence addressing*

If we closely observe the cosine like modulated signal together with the sawtooth carrying signal and compare it with time responds for the first and second cell, we see that the frequency of the cosine like modulated signal has increased.

To achieve the appropriate absorption change microscope slides have been inserted inside the cell, resulting in a maximum 32% absorption change. Using the same recording principle power spectrums with and without absorption have been measured and compared. The resulting comparisons are shown in Figure 8.11.

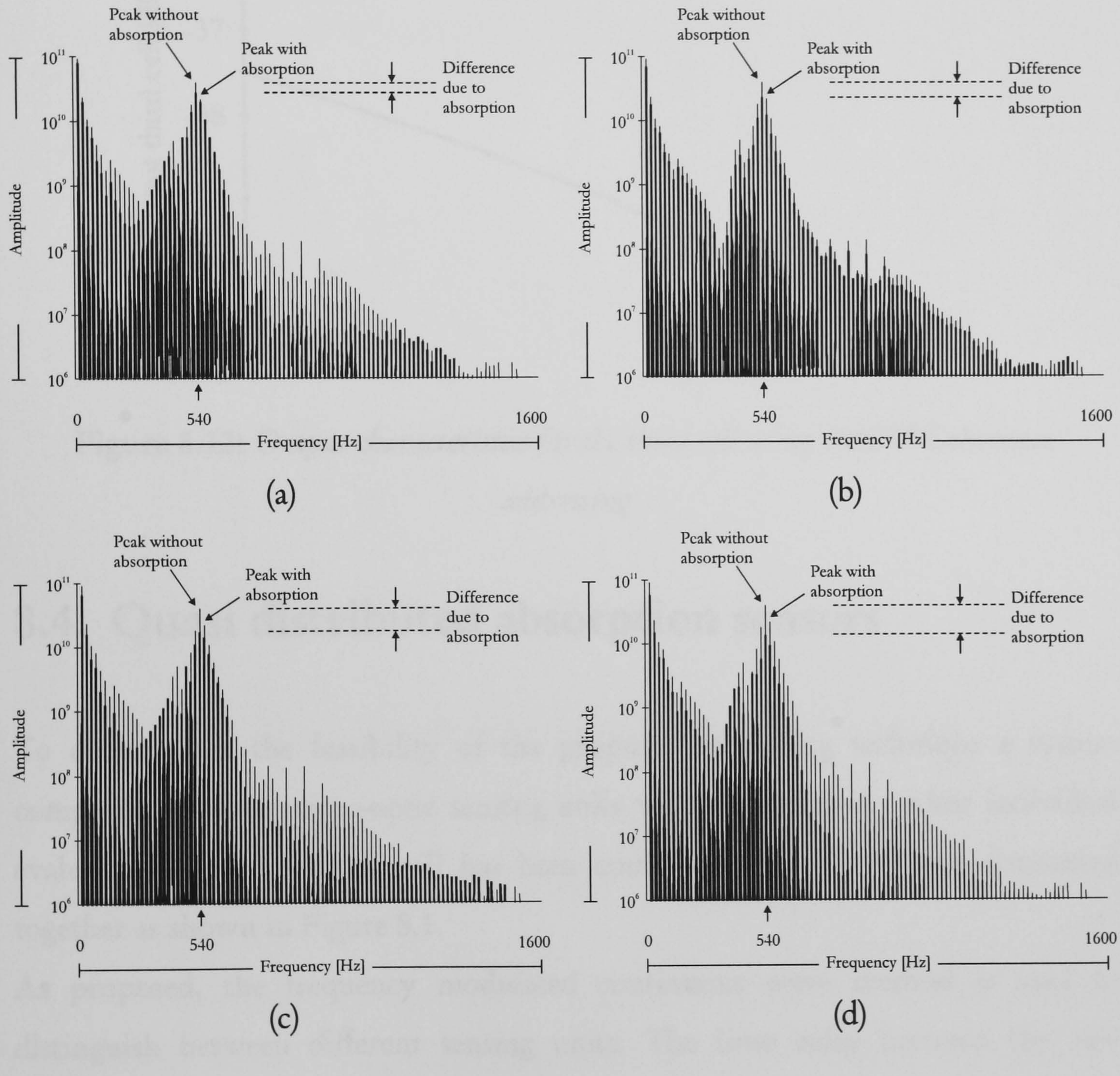

Figure 8.11: *Power spectrum of the FMCW Coherence addressed third cell: (a) one microscope slide inserted in the third cell; (b) two microscope slides inserted in the third cell; (c) three microscope slides inserted in the third cell; (d) four microscope slides inserted in the third cell*

The change in the power spectrum amplitude for the third cell beat frequency due to absorption increase is shown in Figure 8.12.

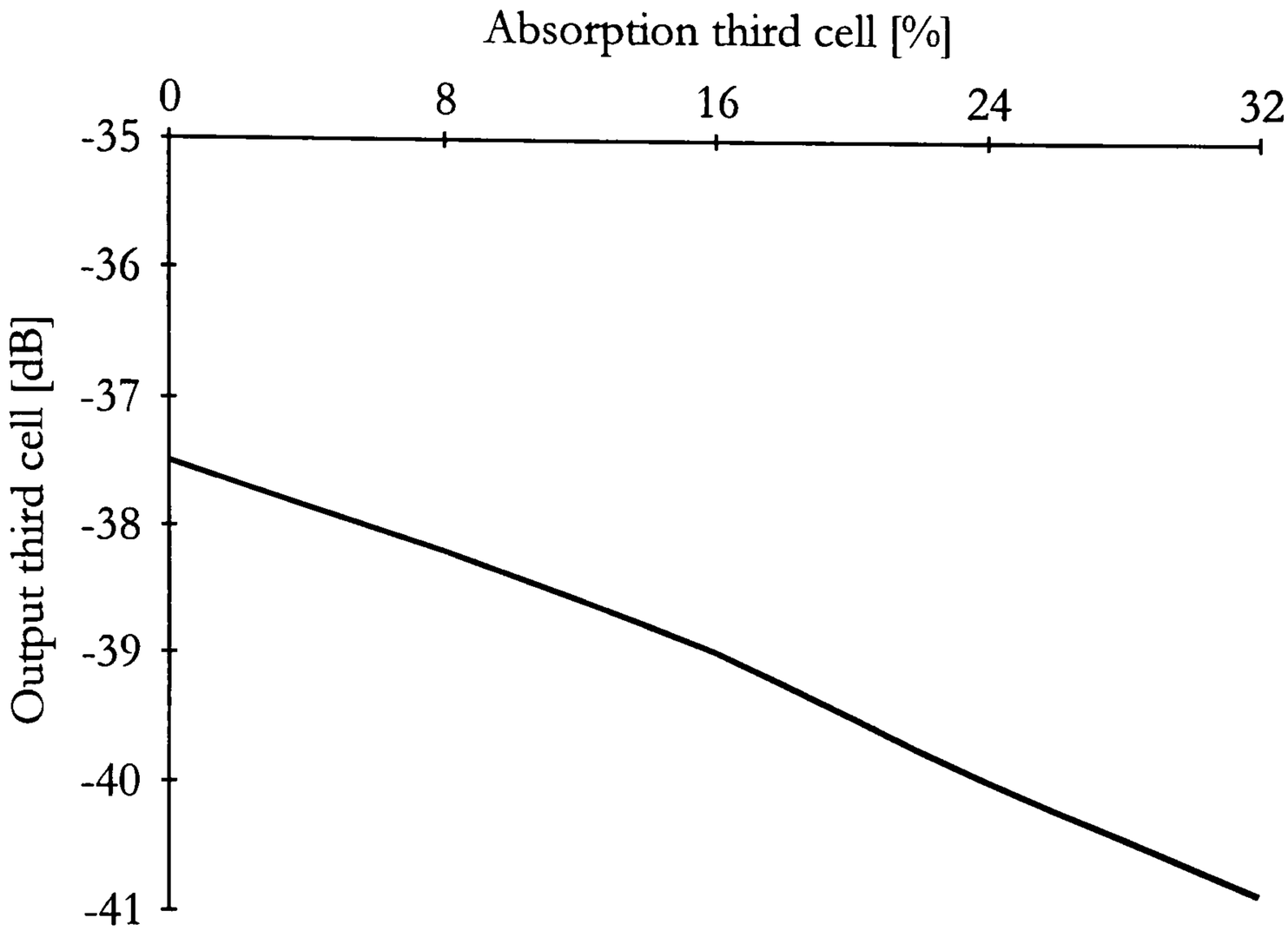

Figure 8.12: *Output characteristics for the third cell using FMCW Coherence addressing*

8.4. Quasi distributed absorption sensors

To demonstrate the feasibility of the proposed addressing technique a system composed of three micro-optic sensing units will be evaluated. After individual evaluation of each sensing cell has been completed, they have been connected together as shown in Figure 8.1.

As proposed, the frequency modulated continuous wave method is used to distinguish between different sensing units. The time delay between the two reflections, along with the linear frequency ramp of the source, gives rise to beat frequencies in the mixed output which are different for each of the three cells. The connecting fibre length between two successive sensor cells is chosen to be much greater than the coherence length of the source so that the reflections from

different cells do not interfere and the crosstalk between the units can be omitted. The optical absorbance which is a characteristic of a chemical substance attenuates the amplitude of the optical signal passing the sensing cell, resulting in a decrease of the power spectrum amplitude for a given measurement point. The interference patterns of all sensor cells add up at the detector whereby each individual sensing cell is identified by its power spectrum in the frequency domain.

After all three cells were connected together we could observe the time domain signal as shown in Figure 8.13. The general shape of the time response is well predicted by (5.24) and corresponds to the theoretical calculations shown in Figure 5.35d.

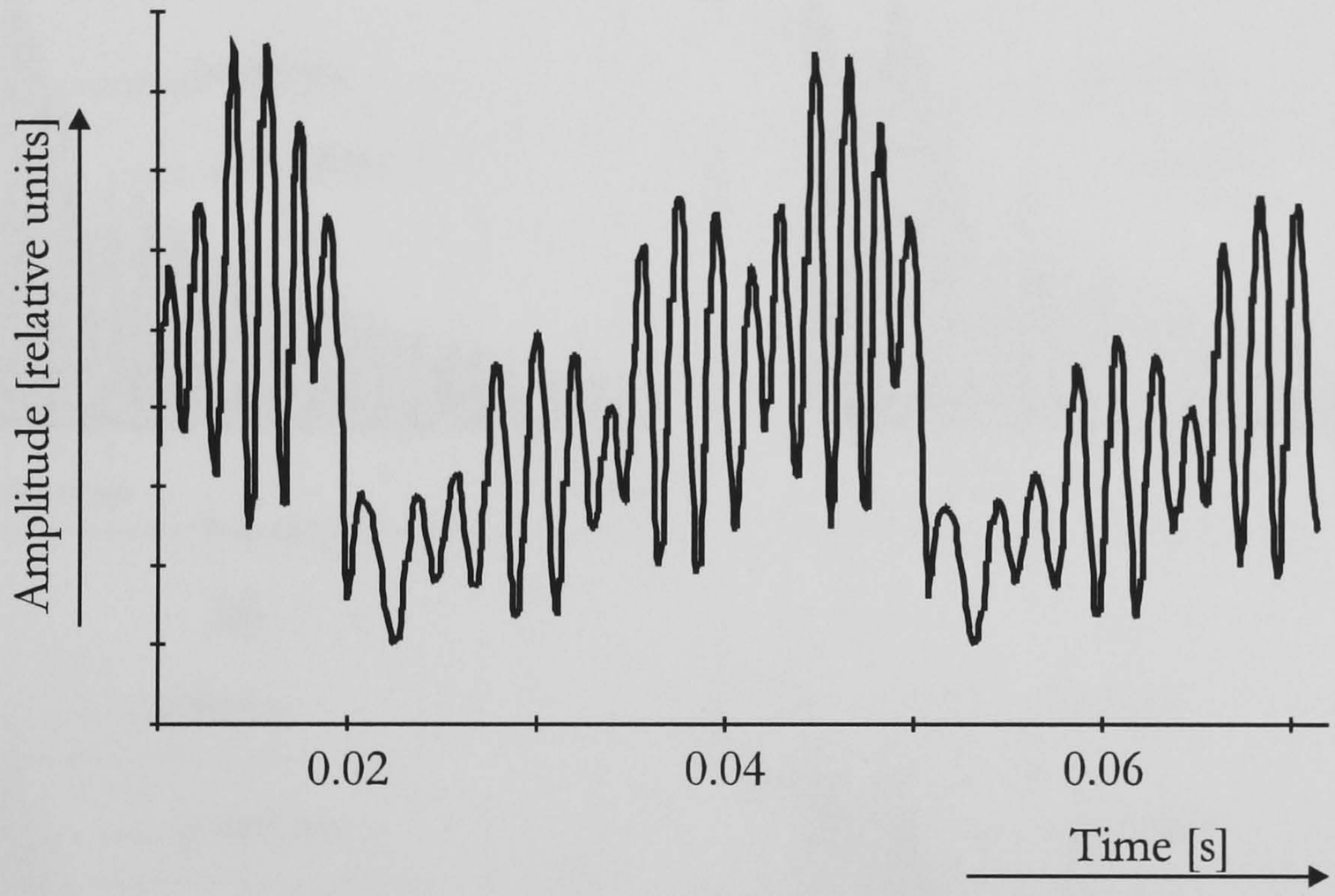

Figure 8.13: *Time response for the coherence addressed quasi-distributed absorption sensors*

8.4.1. Experimental power spectrum

Using the same method to increase the absorption inside a cell as for the single sensing unit evaluation the absorption was increased by inserting microscope slides between the GRIN's. The lengths of the sensing units are selected for a 280Hz, 380Hz and 540Hz beat frequency for the first, second and third cell. With proper tracking of the individual beat frequency and peak amplitude the level of absorption in the individual cell can be determined.

After the three sensing cells have been connected together one could observe three distinctive power spectrum peaks in the frequency domain, each representing an individual sensing cell. To analyse the changes in the power spectrum for every sensing unit when absorption is present in one of the cells we first introduce an increase of the absorption for the first, next for the second cell and finally for the third cell. For each step the power spectrum has been recorded and comparison with the power spectrum for zero absorption is given. The appropriate power spectrum images are presented in Figure 8.14, Figure 8.15 and Figure 8.16.

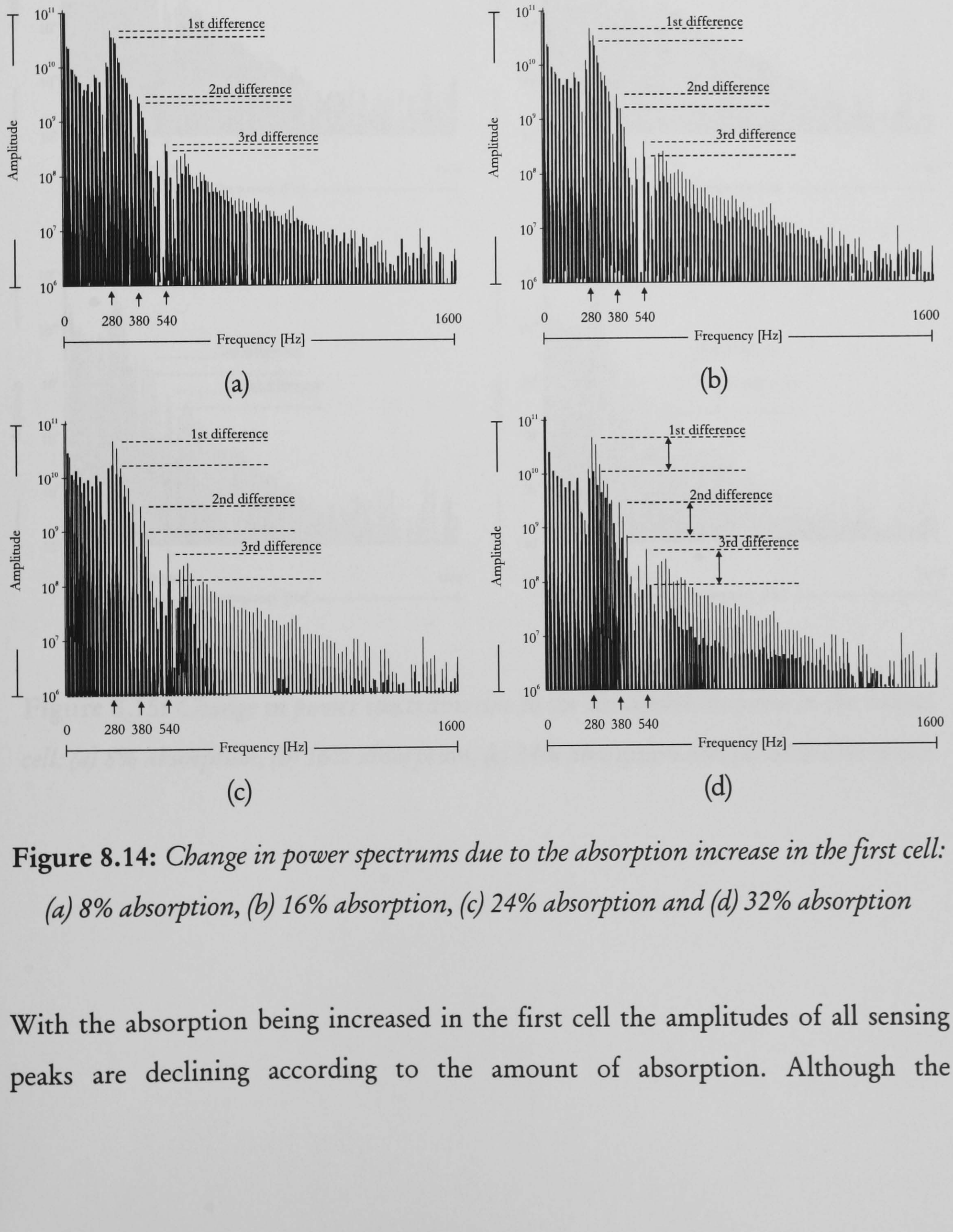

Figure 8.14: *Change in power spectrums due to the absorption increase in the first cell: (a) 8% absorption, (b) 16% absorption, (c) 24% absorption and (d) 32% absorption*

With the absorption being increased in the first cell the amplitudes of all sensing peaks are declining according to the amount of absorption. Although the

absorption is increased in the first cell, also the second and third cell are effected due to the serial arrangement of the sensing units.

The same could be observed if only the second cell is influenced. Here the previous cell is not effected whereas the spectrum amplitude representing subsequent cells is decreased.

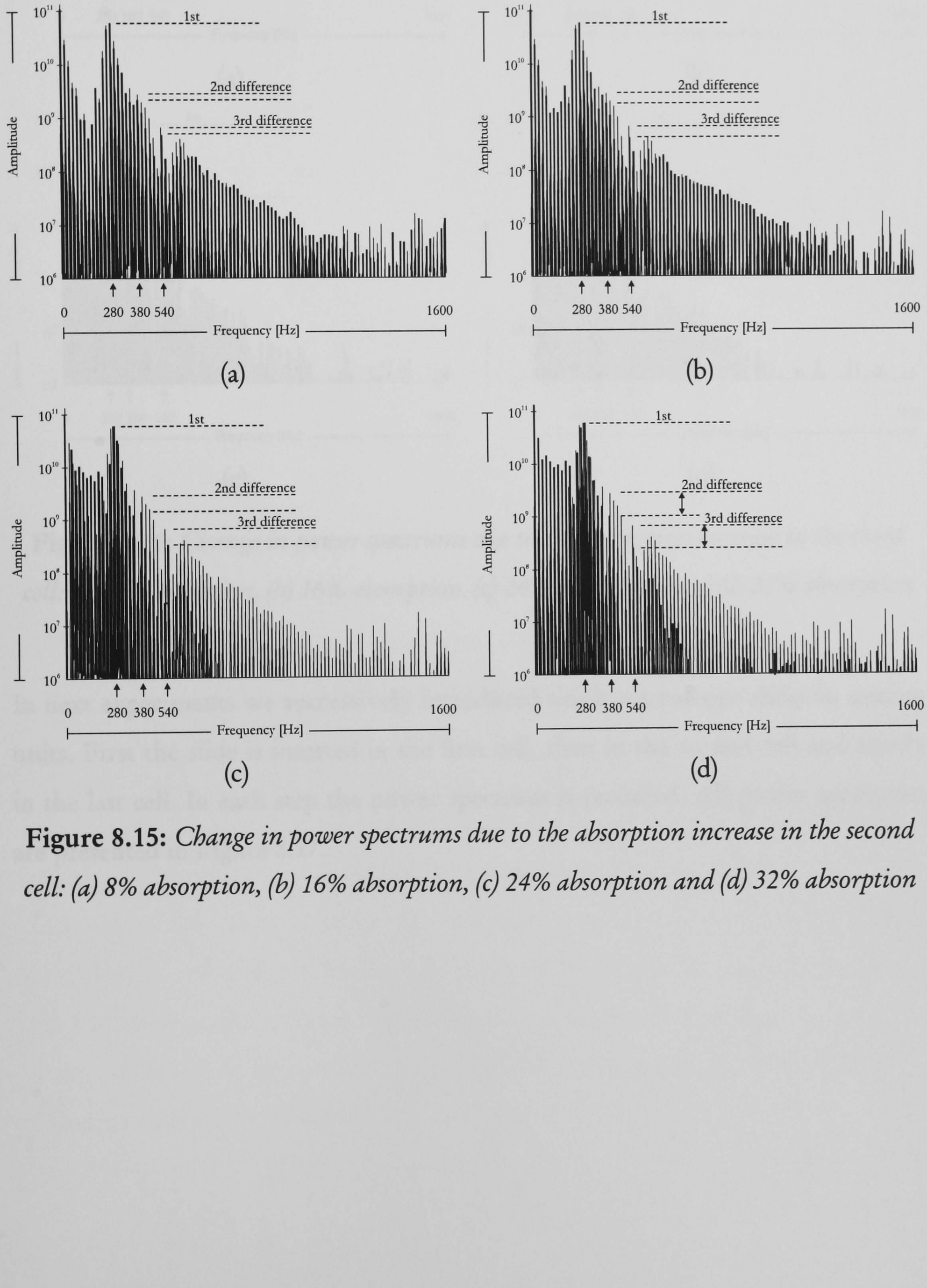

Figure 8.15: *Change in power spectrums due to the absorption increase in the second cell: (a) 8% absorption, (b) 16% absorption, (c) 24% absorption and (d) 32% absorption*

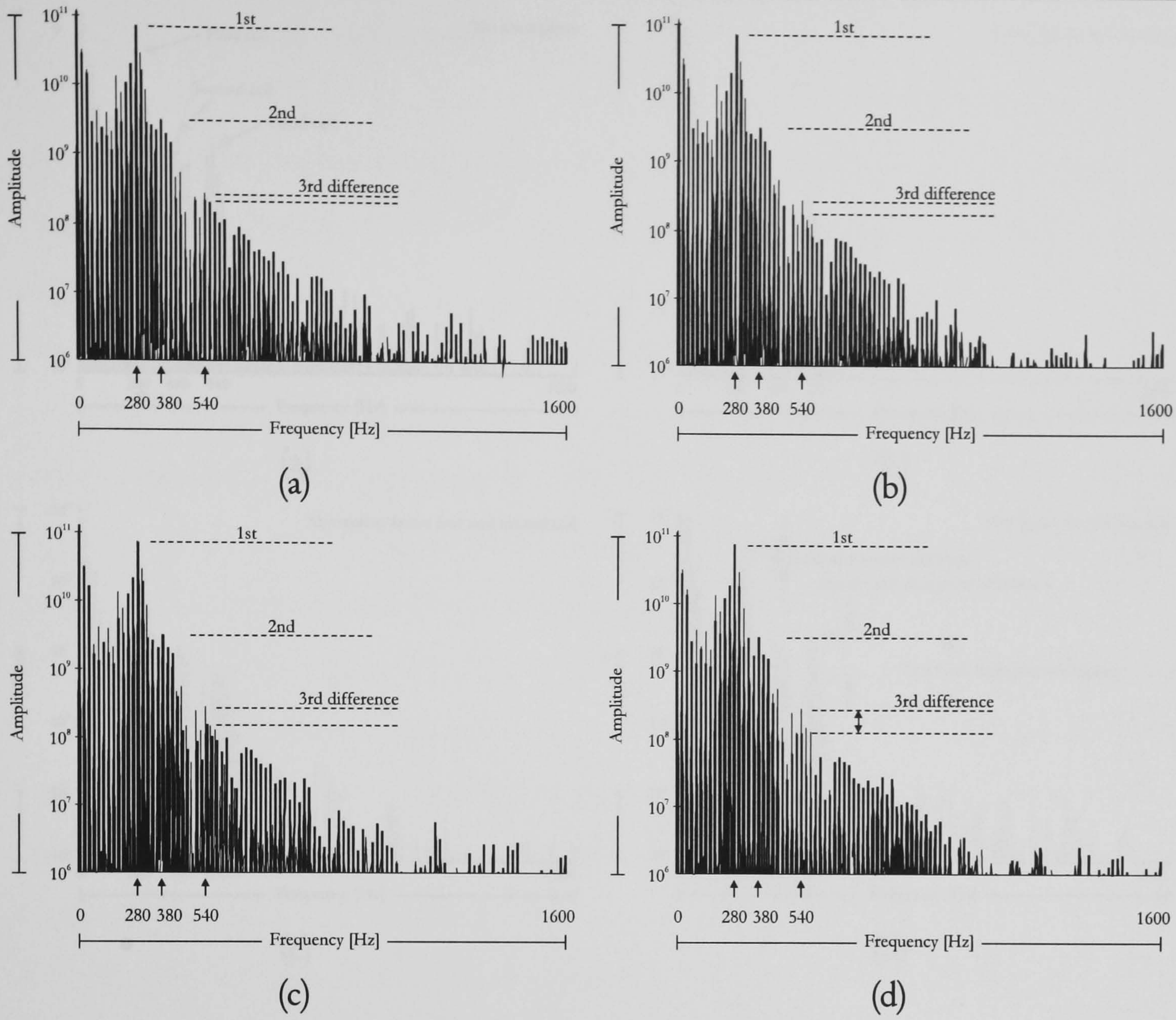

Figure 8.16: *Change in power spectrums due to the absorption increase in the third cell: (a) 8% absorption, (b) 16% absorption, (c) 24% absorption and (d) 32% absorption*

In next experiments we successively introduced single microscope slides in sensing units. First the slide is inserted in the first cell, then in the second cell and finally in the last cell. In each step the power spectrum is recorded. All power spectrums are presented in Figure 8.17.

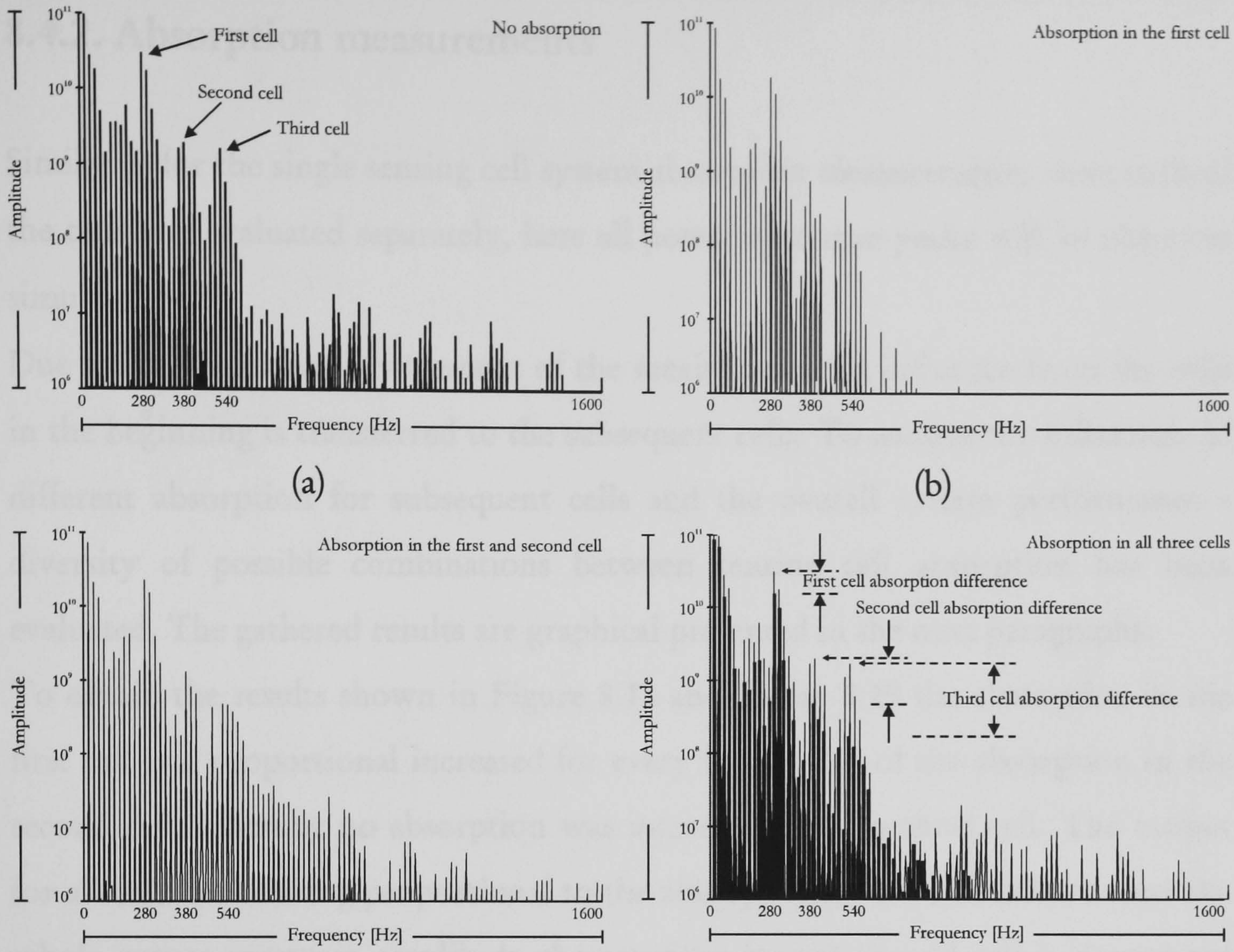

Figure 8.17: *Power spectrum of the FMCW Coherence addressed system: (a) without absorption; (b) microscope slide inserted in the first cell; (c) additional microscope slide inserted in the second cell; (d) one microscope slide in each cell and comparison with the spectrum without absorption*

In Figure 8.17a all three beat frequencies are clearly visible. After a microscope slide is inserted in the first cell the amplitude for all three power spectrum peaks is reduced proportional to the absorption caused (Figure 8.17b). Similar the amplitude of the second and third beat peak is reduced after the next slide is inserted in the second cell (Figure 8.17c). The final spectrum is obtained after one slide has been inserted in each cell. In Figure 8.17d also the difference between the power spectrum without absorption and the power spectrum with absorption present in each cell is indicated.

8.4.2. Absorption measurements

Similar as for the single sensing cell system absorption measurements, were each of the cells was evaluated separately, here all power spectrum peaks will be observed simultaneously.

Due to the successive arrangement of the sensing cells the influence from the cells in the beginning is transferred to the subsequent cells. To analyse the influences of different absorption for subsequent cells and the overall system performance a diversity of possible combinations between sensing cell absorption has been evaluated. The gathered results are graphical presented in the next paragraphs.

To obtain the results shown in Figure 8.18 and Figure 8.19 the absorption in the first cell was proportional increased for every fixed value of the absorption in the second cell, whereby no absorption was introduced to the third cell. The output for all cells is declining proportional to the absorption in the first cell whereas the whole power spectrum amplitude characteristic for the second cell is downward shifted according to the fixed values of the absorption in second cell. Because of the zero absorption in the third unit the third output just follows the second one.

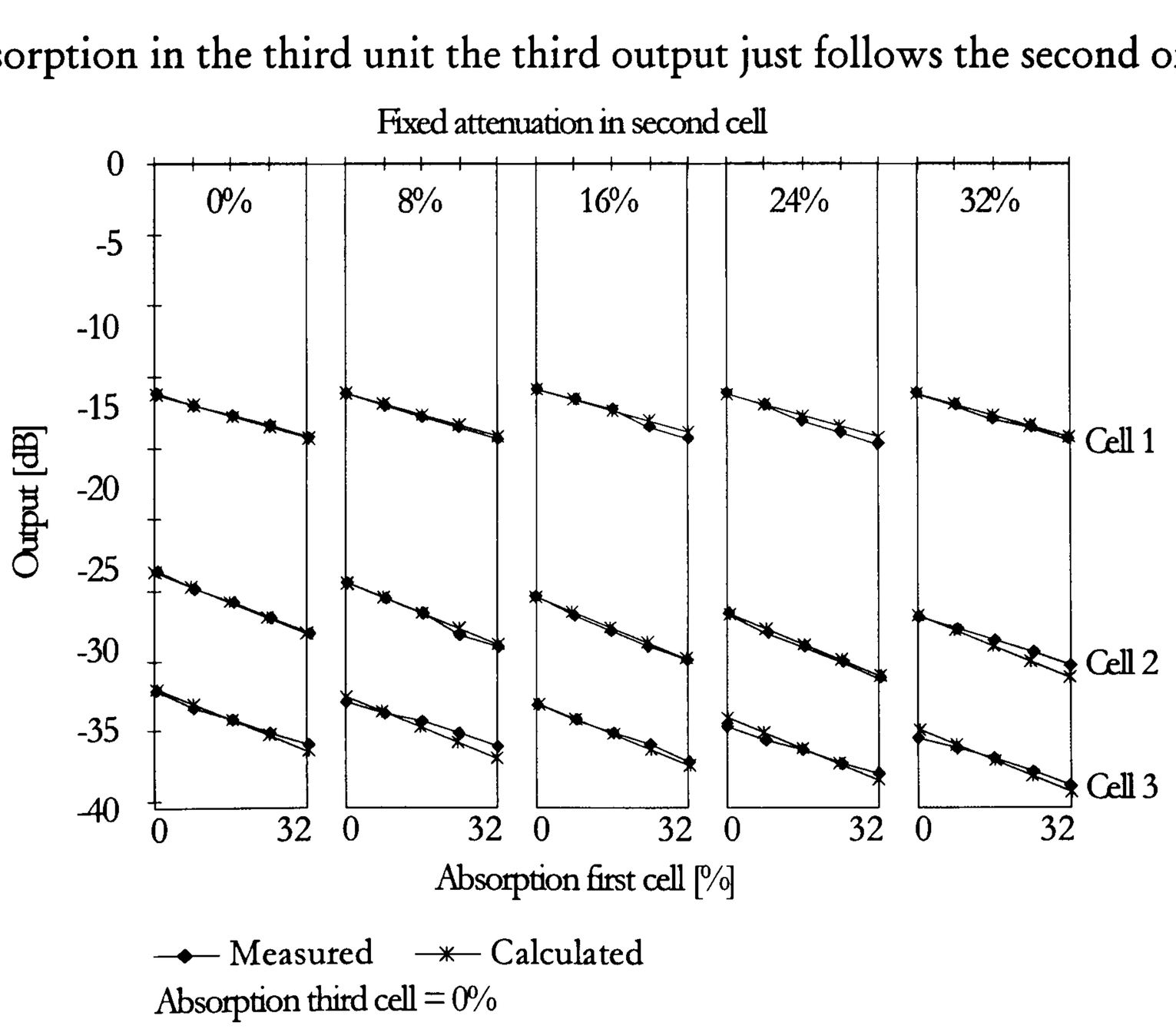

Figure 8.18: *Absorption in the second cell held at fixed values shown*

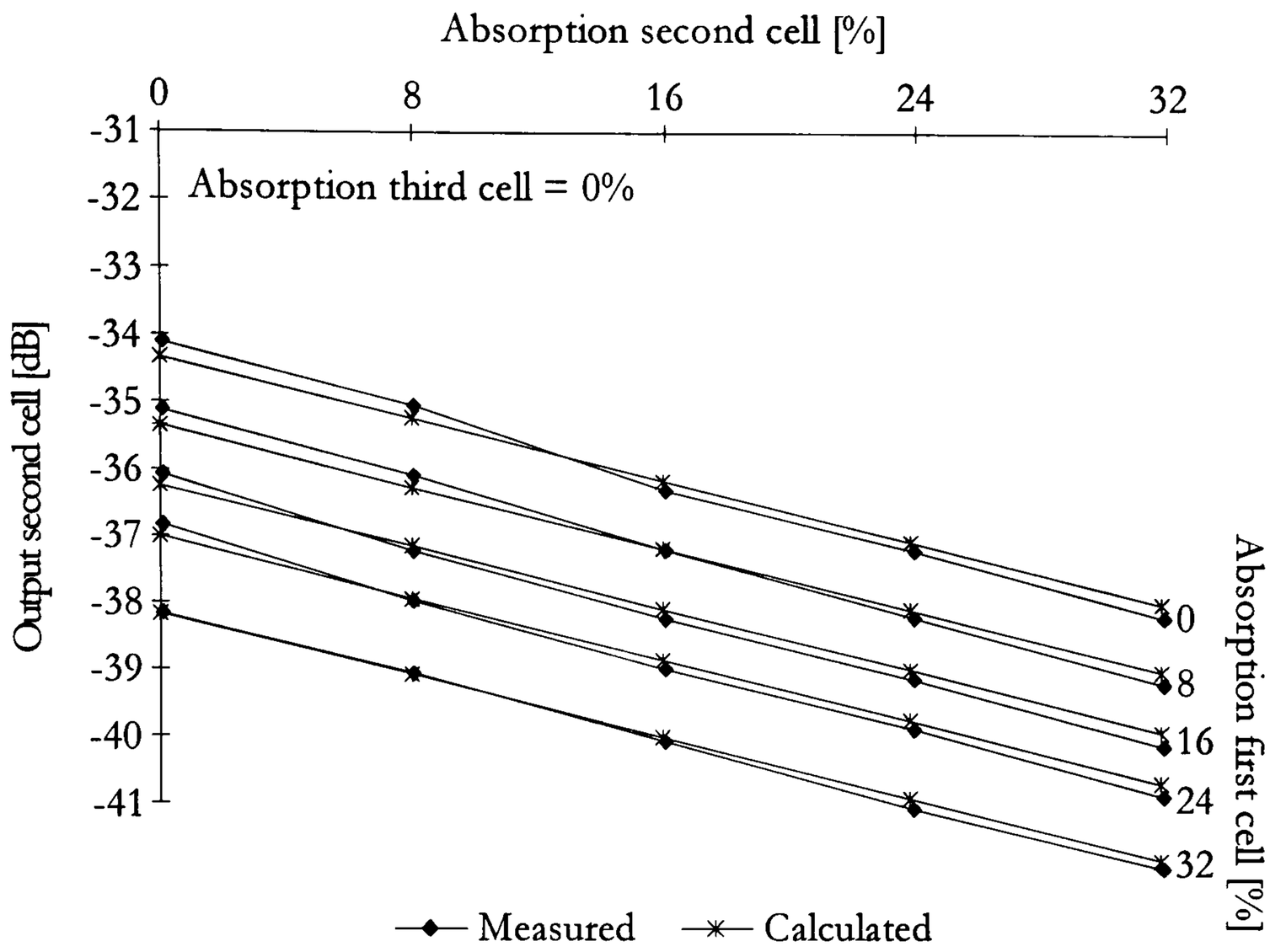

Figure 8.19: *Output change for second cell due to absorption for different values of first cell absorption*

Similar results presented in Figure 8.20 and Figure 8.21 are obtained if the absorption in the first cell is proportional increased and the absorption in the third cell is held at different fixed values. Since no extra absorption is introduced in the second cell, the ration between first and second cell outputs remains constant and a linear regression of the third cell with increased absorption is present. As indicated using the dot-line curve, in the third cell output two influences are superimposed. First is the influence of the absorption in the first cell and second the measured absorption for the third cell.

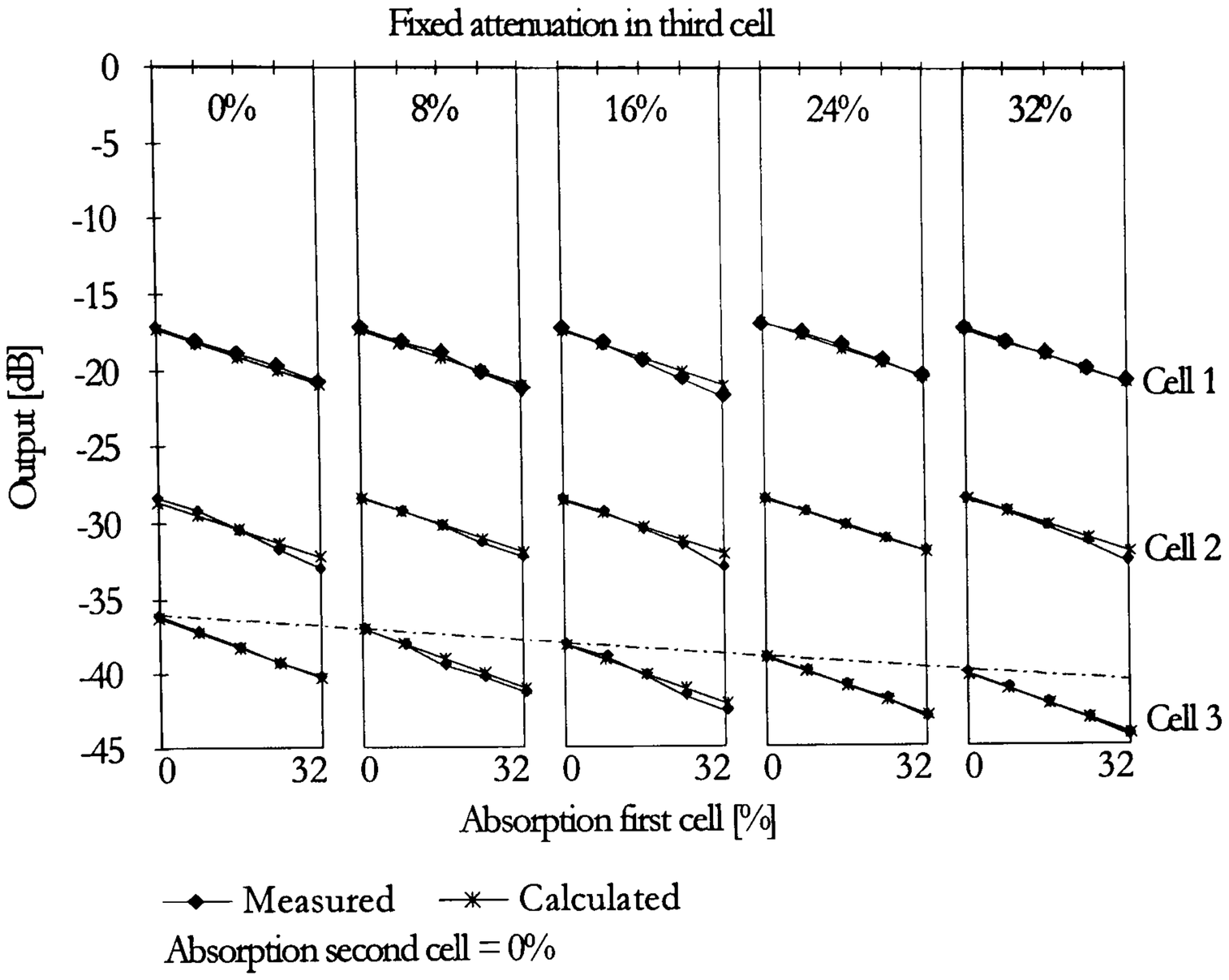

Figure 8.20: *Absorption in the third cell held at fixed values shown*

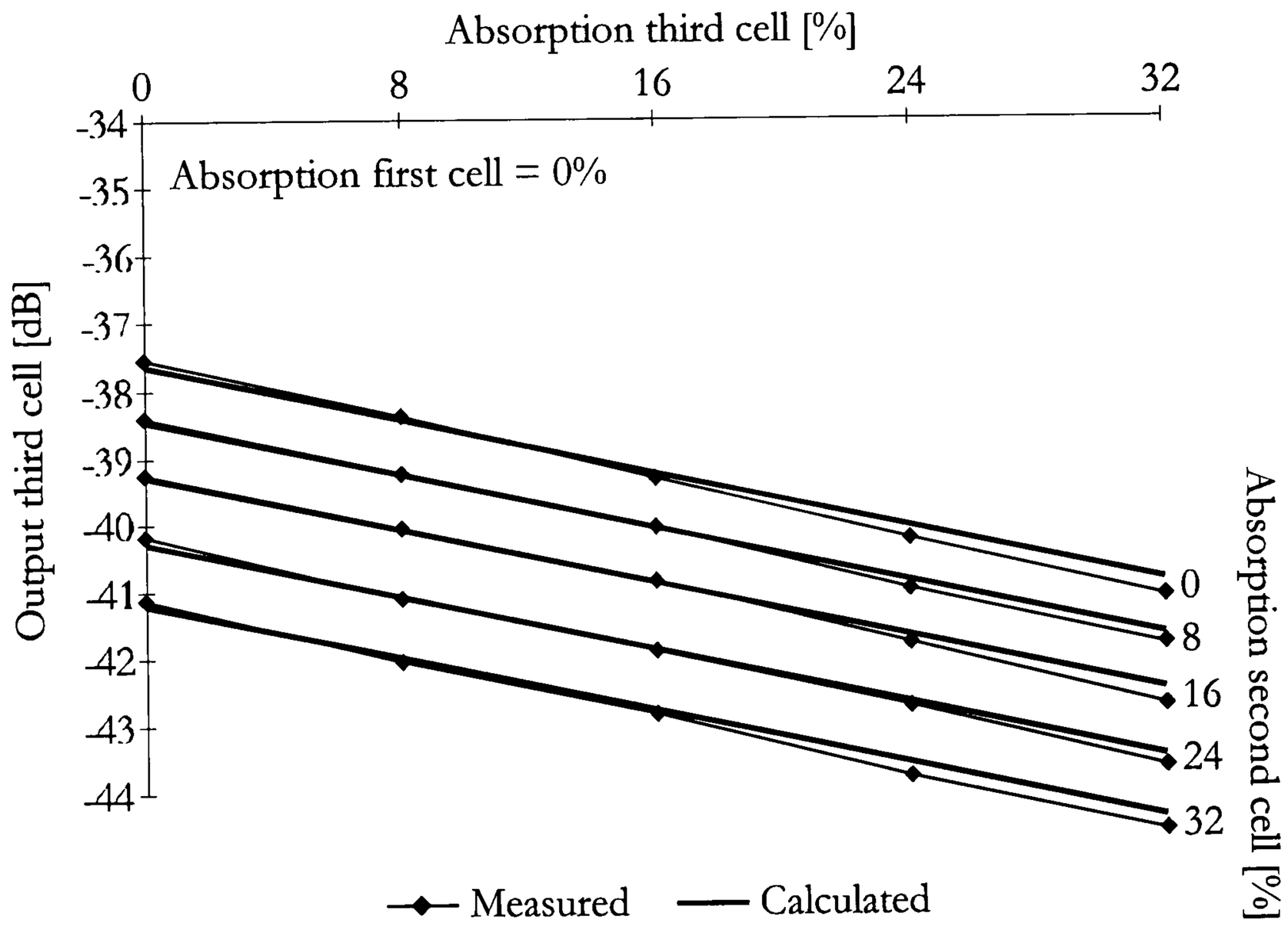

Figure 8.21: *Output change for third cell due to absorption for different values of second cell absorption*

In the last series of experiments for absorption measurement a proportional increase of absorption for the third cell and absorption at fixed values for the first cell has been introduced. The results are shown in Figure 8.22.

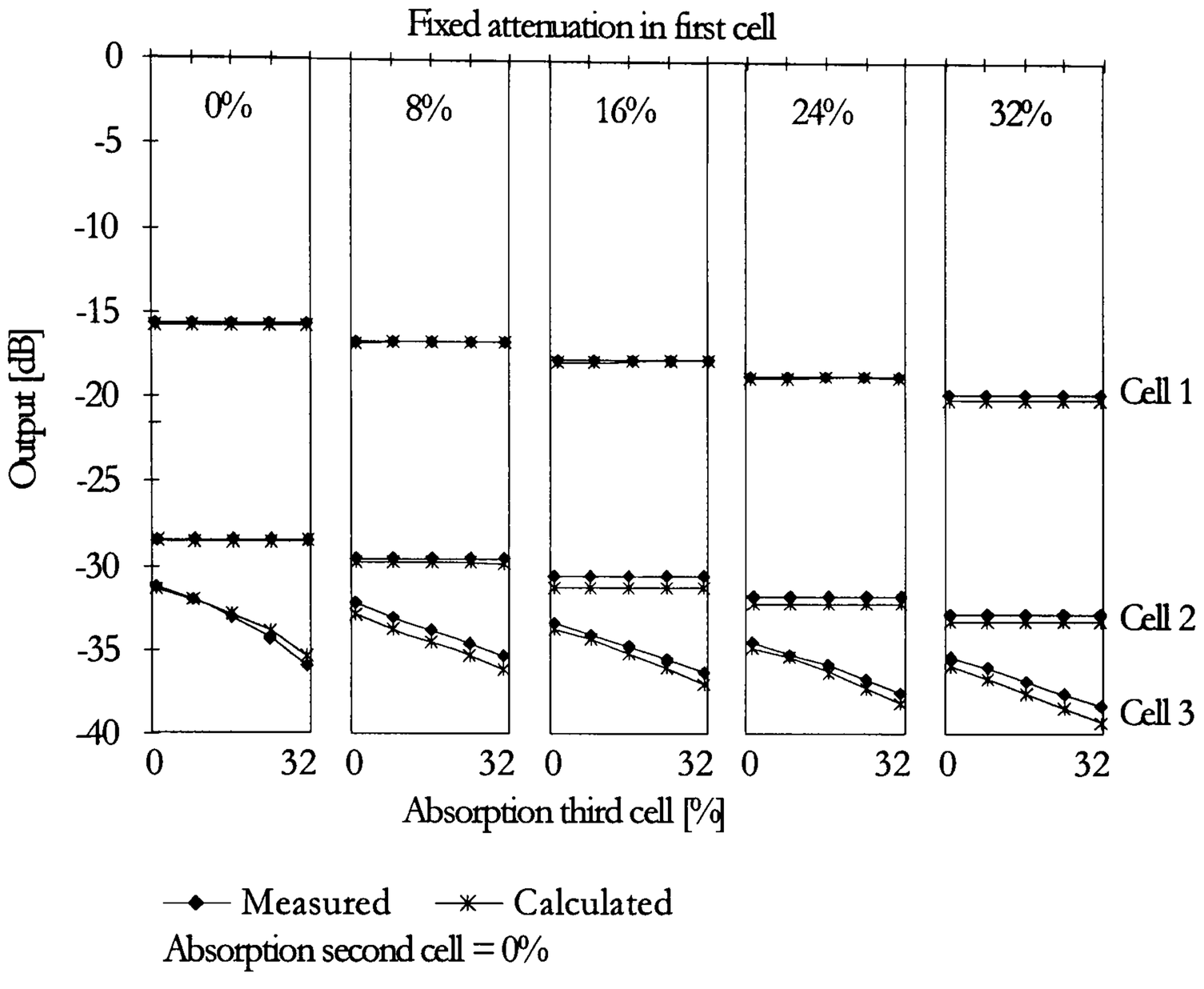

Figure 8.22: *Absorption in the first cell held at fixed values shown*

The increase of the fixed absorption in the first cell causes a step like response for the first and consequently second unit. The output of the third cell declines proportional to the absorption introduced as expected. Without regard to preceding cells the sensitivity in each sensing unit is approximately the same, and it is mostly influenced by the length of the cell.

8.5. Summary and Conclusion

In this chapter the proposed approach for addressing quasi-distributed interferometric absorbance sensors using coherence addressing and the FMCW method has been experimentally evaluated. Coherence addressing of the cells using

FMCW is achieved by the interferometric mixing of two signals originating from each cell. We have performed experimental verification of the proposed addressing mechanism and shown how different sensing cells can be addressed and how the information about the measurand can be acquired. In doing this we found that the output of a sensing unit is inversely proportional to the absorption measured. According to the signal loss due to the cell construction and the available space in the frequency domain defined by the coherence length of the source effectively 10 to 15 sensing units could be arranged is series. In order to eliminate the mutual influence between cells do to the serial configuration individual power spectrum peaks are identified and assigned to the sensing cells at the beginning of the measuring process.

When performing measurements of power spectrum amplitudes at appropriate beat frequencies a tracking technique is used to collect the individual values (since during the initial set-up of the system approximate values of the beat frequencies are stored, it is much easier to determine the beat amplitude through operation of the system). After all cells are scanned the individual absorption value is calculated using previous calculations starting with the first cell.

The problem associated with the use of optical switches which was present with the FMCW Reference arm addressing method does not appear with the FMCW Coherence Addressing method. The cells are addressed directly through their beat frequencies and the appropriate power spectrum in the frequency domain. Therefore no optical switching is necessary, while more sophisticated post signal processing is required.

The system is essentially insensitive to outside perturbations (compared to the interferometer related problems associated with the separated reference arm within the FMCW Reference arm method), since apart from the cell length, both reflected beams from each cell travel the same path and experience the same perturbations.

The feasibility of the proposed method was demonstrated using three open path microoptic cells connected in series. One of the possible application areas for the introduced quasi-distributed absorption based measurements is a distributed gas detection system, especially for methane. Here sensitivity levels below the lower explosive level of methane would be achievable, enabling a serial arranged methane gas detection system.

Further experimental results regarding specific system parameters and system application will be presented in next sections.

9. Full characterisation of system performance

In the previous chapter extended absorption measurement for individual cells and the assembled quasi distributed system have been accomplished. To fully characterise the coherence addressed quasi-distributed absorption based system implementing the FMCW method we have to determine additional system performance parameters, i.e. dynamic range, resolution, stability, the influence of disturbances, etc. This parameters will be examined in the next subsections.

9.1. Dynamic range

We define the dynamic range for the coherence addressed quasi-distributed absorption based sensor system as the range of absorption which could be measured expressed in decibels.

The dynamic range for an individual cell was determined by observing the difference between the power spectrum amplitude at a given beat frequency when

no absorption is introduced and when absorption filters with different levels of absorption are inserted inside the measuring cell. The absorption filters ranged from 1.1dB to 16dB of absorption.

First, the range of absorption which could be measured was determined for each cell separately and the results are presented in Figure 9.1.

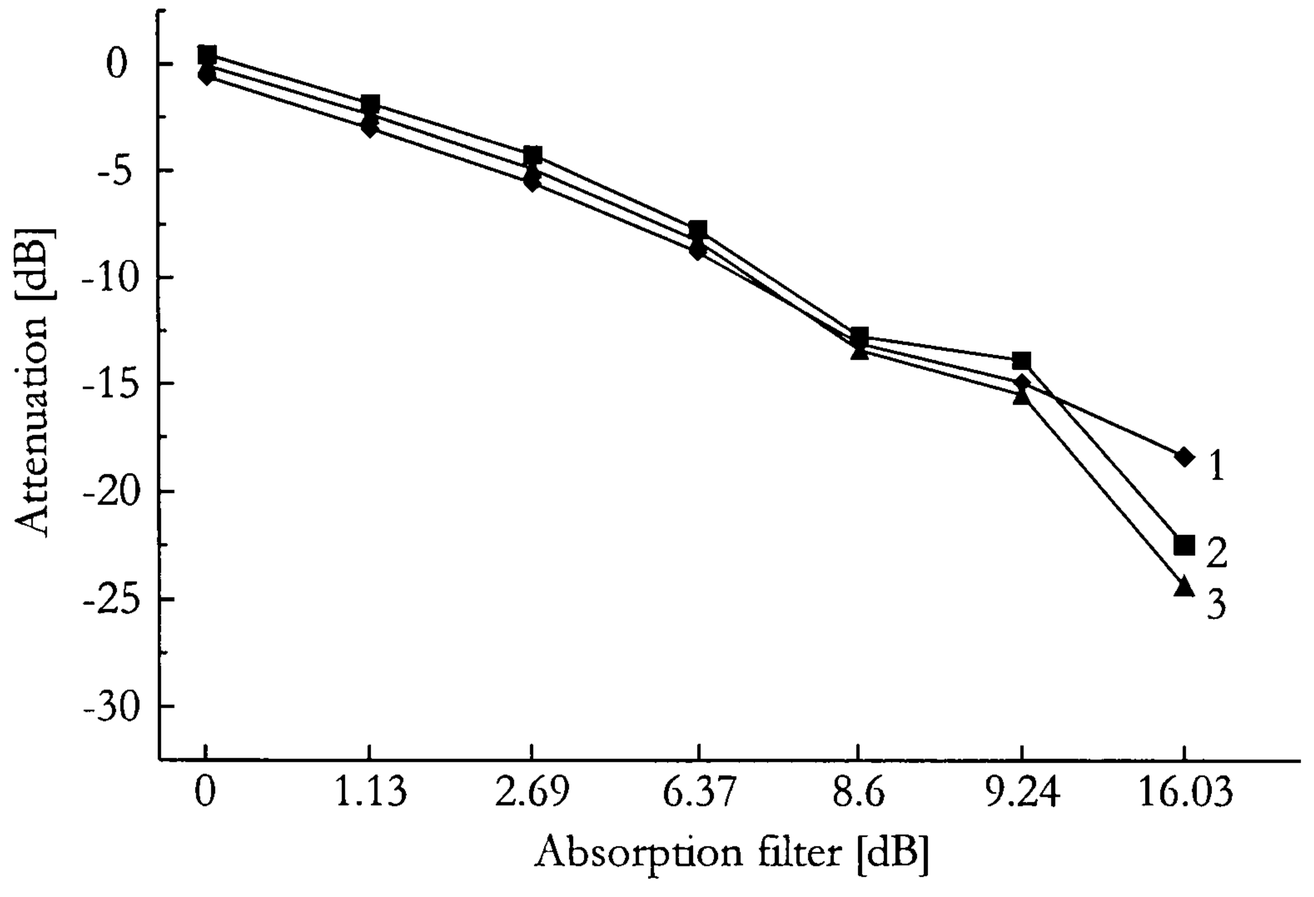

Figure 9.1: *Dynamic range measurement for individual cells*

The curves 1,2 and 3 represent the output of the cells in the presence of the absorption filter. The aim was to find the highest absorption value which could be detected implementing an individual cell. As seen from the Figure 9.1 individual curves cover the output range up to 25dB (something less for the first cell which is probably a consequence of the cell assembling stage). According to that, the sensor systems dynamic range for each of the three cells was measured to be approximately 20dB if the cells were observed individually.

Secondly, the cells were connected into the quasi-distributed configuration and the dynamic range experiments were repeated. During the connecting procedure also the difference between the output power spectrums without absorption present and the output power spectrum with the highest absorption able to resolve has been recorded. The power spectrum differences for individual beat frequencies for

the first, second and third cell are shown in Figure 9.2a, Figure 9.2b and Figure 9.2c.

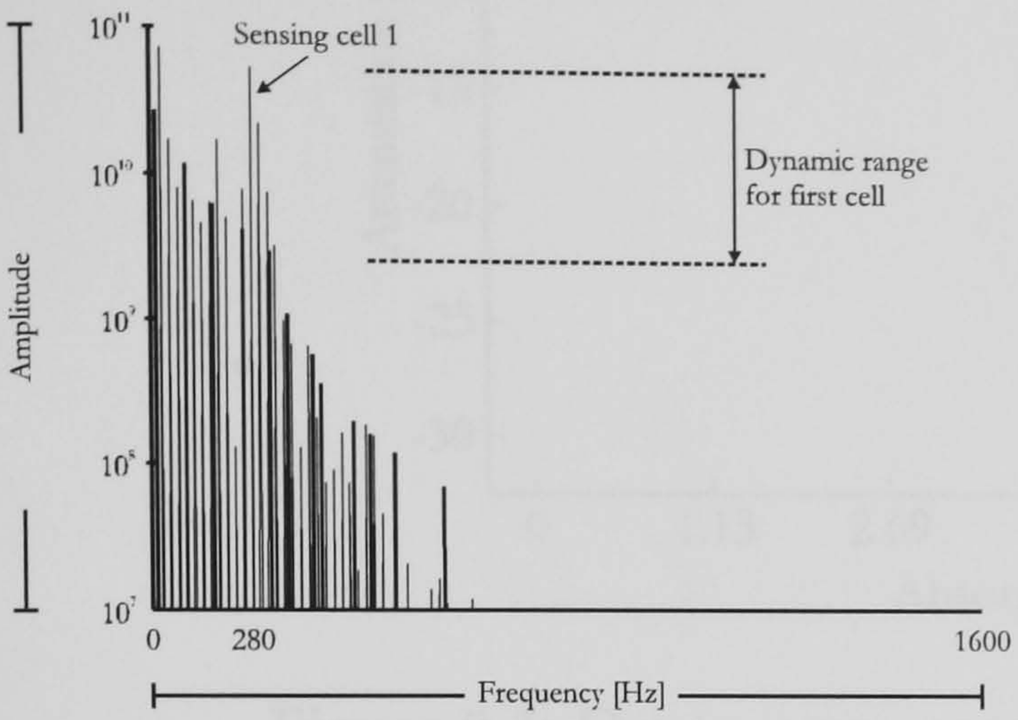

(a)

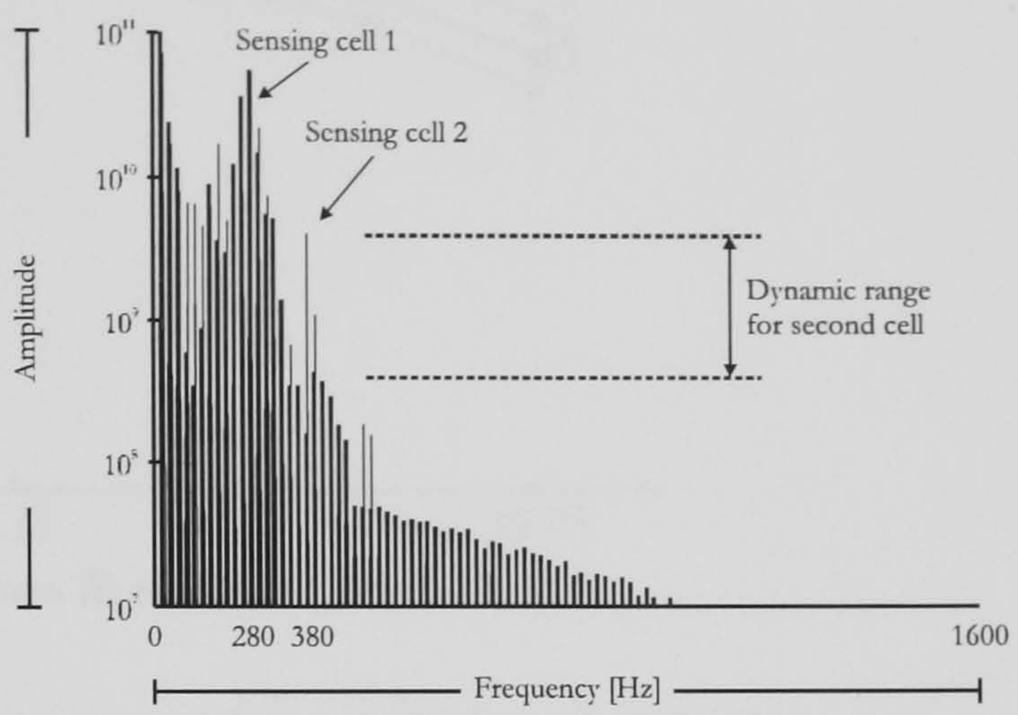

(b)

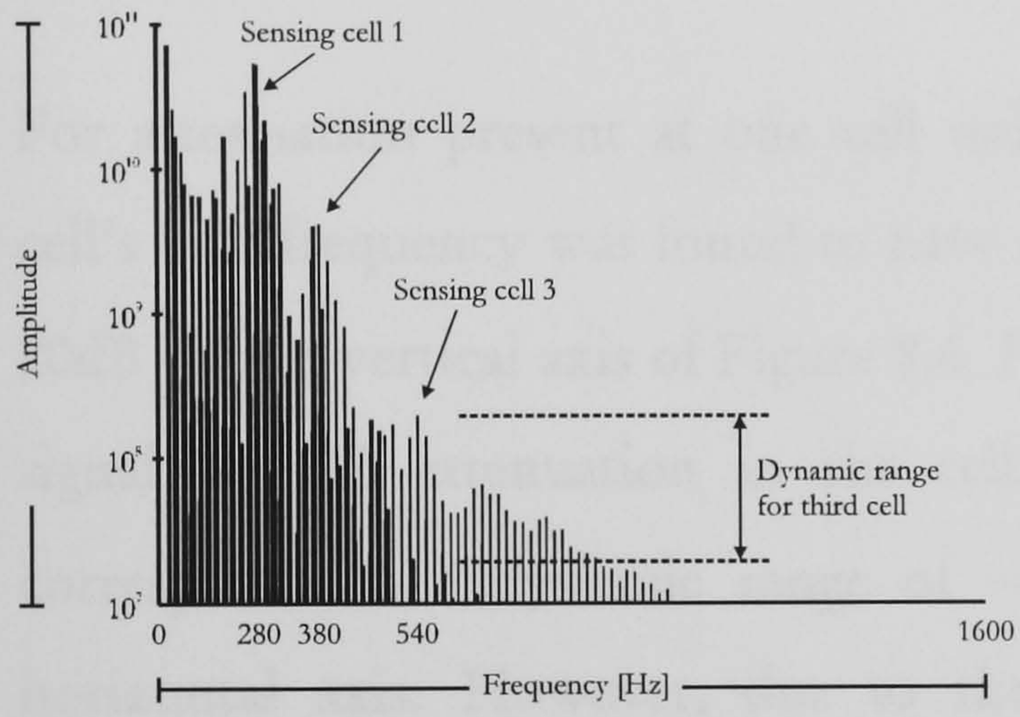

(c)

Figure 9.2: *Dynamic range measurement for individual sensing cells and the corresponding power spectrum change: (a) first cell, (b) second cell and (c) third cell*

After the system has been assembled absorption element were successively placed into each cell in order to determine the maximum to which the cell could respond. The gathered results are presented in Figure 9.3.

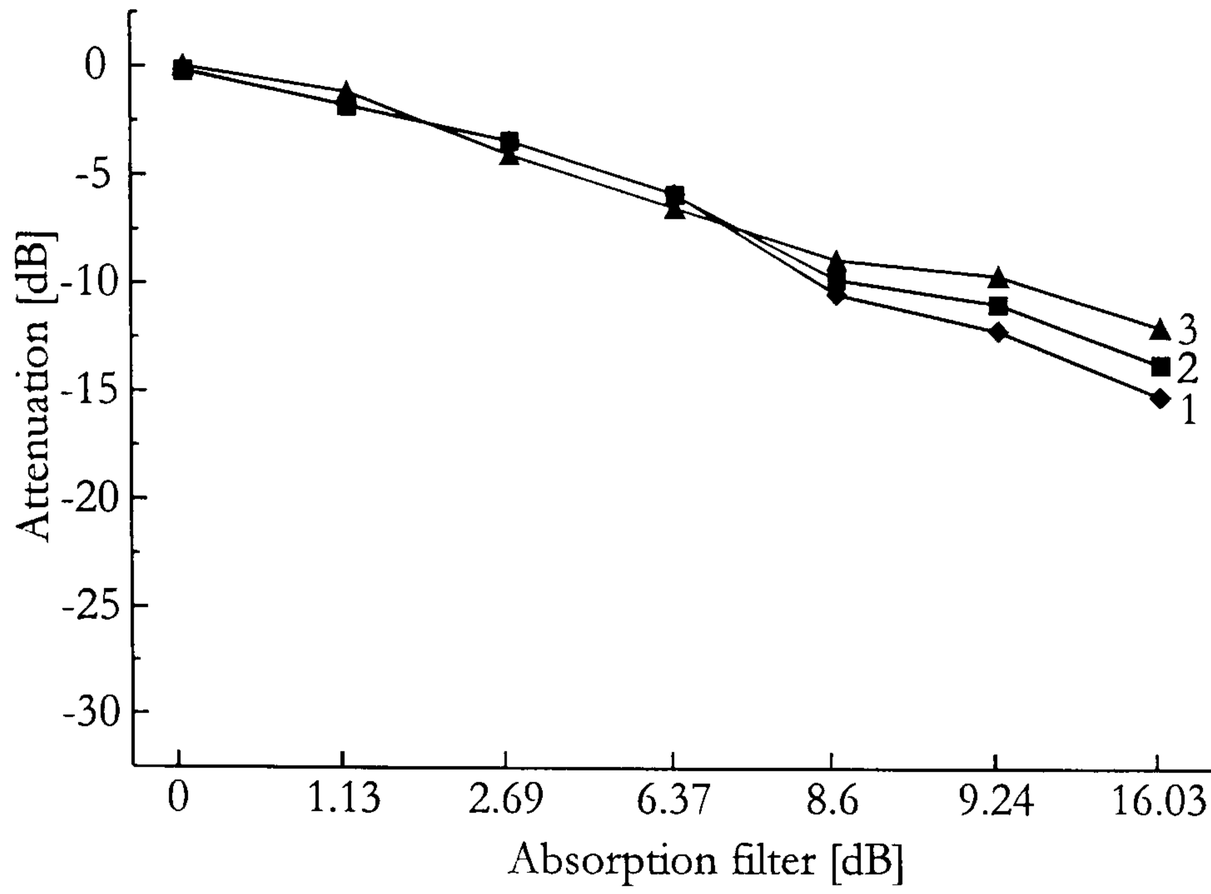

Figure 9.3: *Dynamic range measurement for multiple cell system*

For attenuation present at one cell only, the power spectrum amplitude at the cell's beat frequency was found to have a measurable range of 20dB, i.e. a range of 20dB on the vertical axis of Figure 8.6. From Figure 8.6, where the slope is ~2.5dB signal per dB attenuation in the cell, a range of 20dB on the vertical axis corresponds to a dynamic range of ~8dB in attenuation measurement on the horizontal axis. However, due to the serial arrangement of the system, the available dynamic range of any individual cell is reduced when attenuation is present at earlier cells in the fibre line. For example if the first two cells have an attenuation present of ~0.3dB, then the dynamic range of the third cell is reduced to ~6.8dB.

9.2. Stability

Another very important property of a sensor or sensing system is its output signal time stability. During the evaluation of coherence addressed quasi-distributed absorption sensors by the FMCW method the output time stability for individual cells as well as for the composed system has been measured. Figure 9.4 shows the output time stability for the first sensing unit.

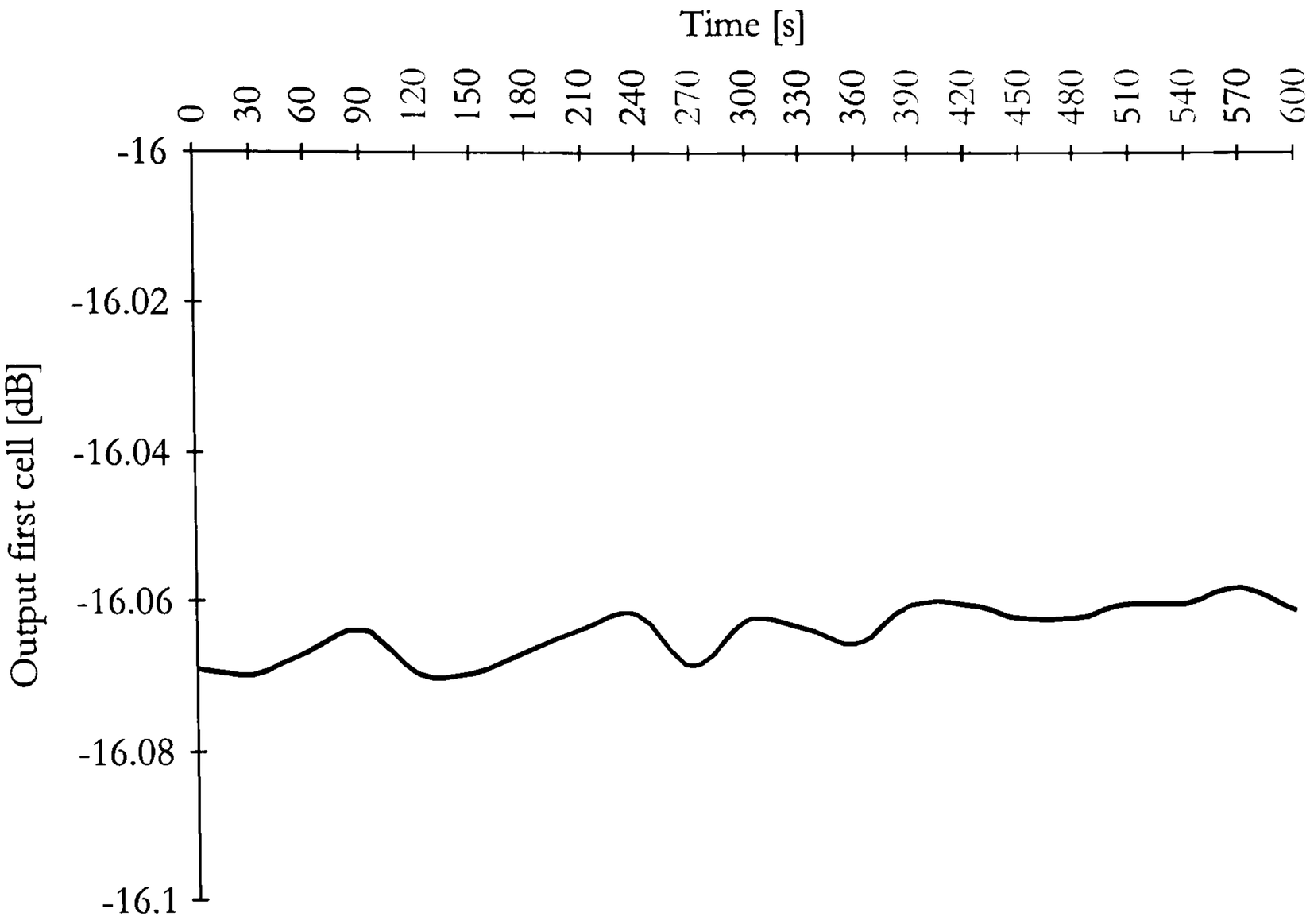

Figure 9.4: *Output time stability for the first sensing unit*

During the observed time period the mean value of the output was -16.064dB with a standard deviation of 0.0034dB, which means that the output distribution is almost negligible spread around the mean value. According to this stable and time independent measurements can be accomplished.

The time stability of the output signal for the second cell is shown in Figure 9.5.

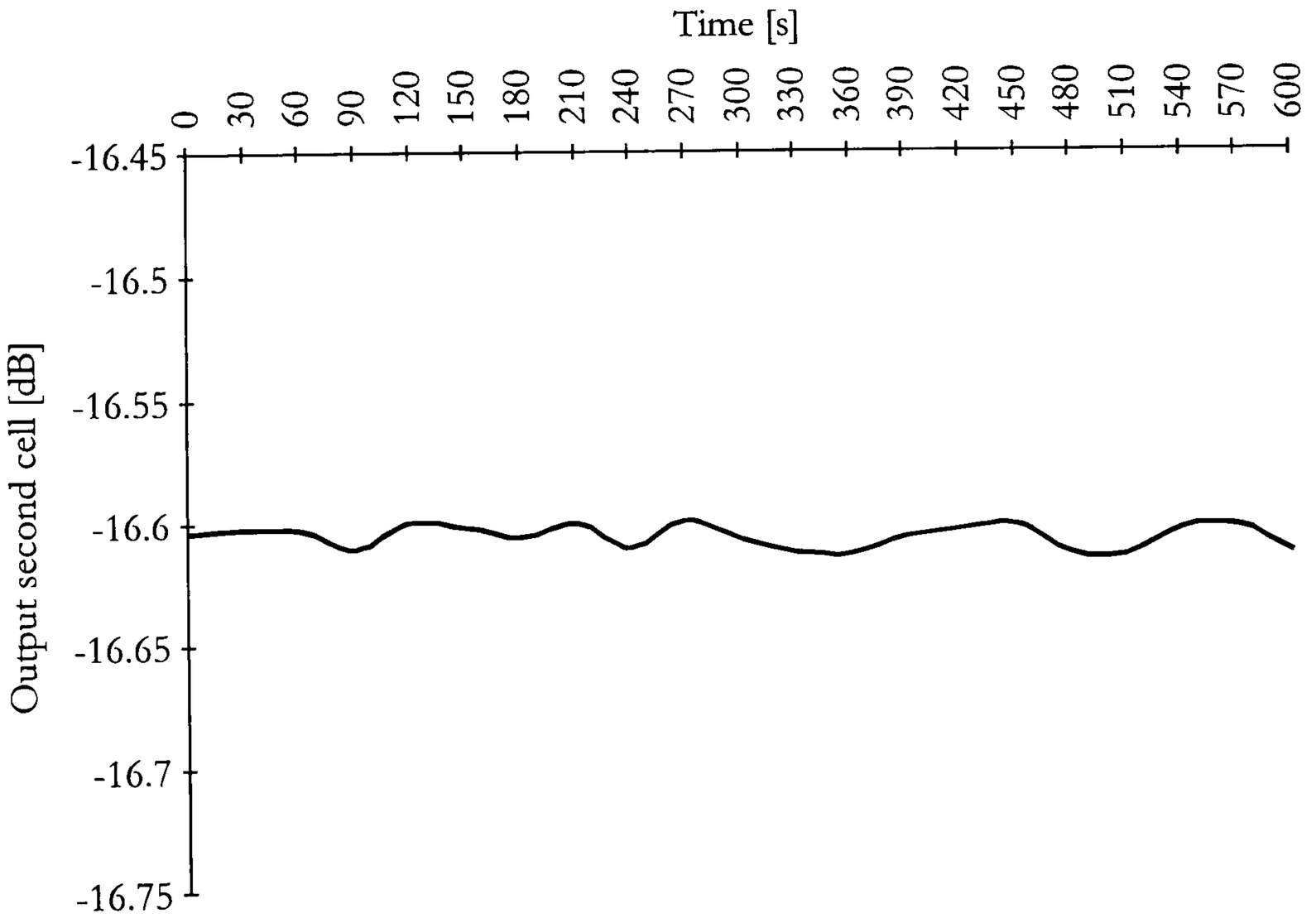

Figure 9.5: *Time stability of the second cell output*

The mean value of the output when the second cell is observed individually is -16.606dB. Since the standard deviation is 0.00509dB the variation of the output signal is negligible and the measured signal is constant with time.
Finally also the time stability of the output signal for the third cell has been observed. During a 10min interval the values of the power spectrum amplitude at the beat frequency have been recorded and are shown in Figure 9.6.

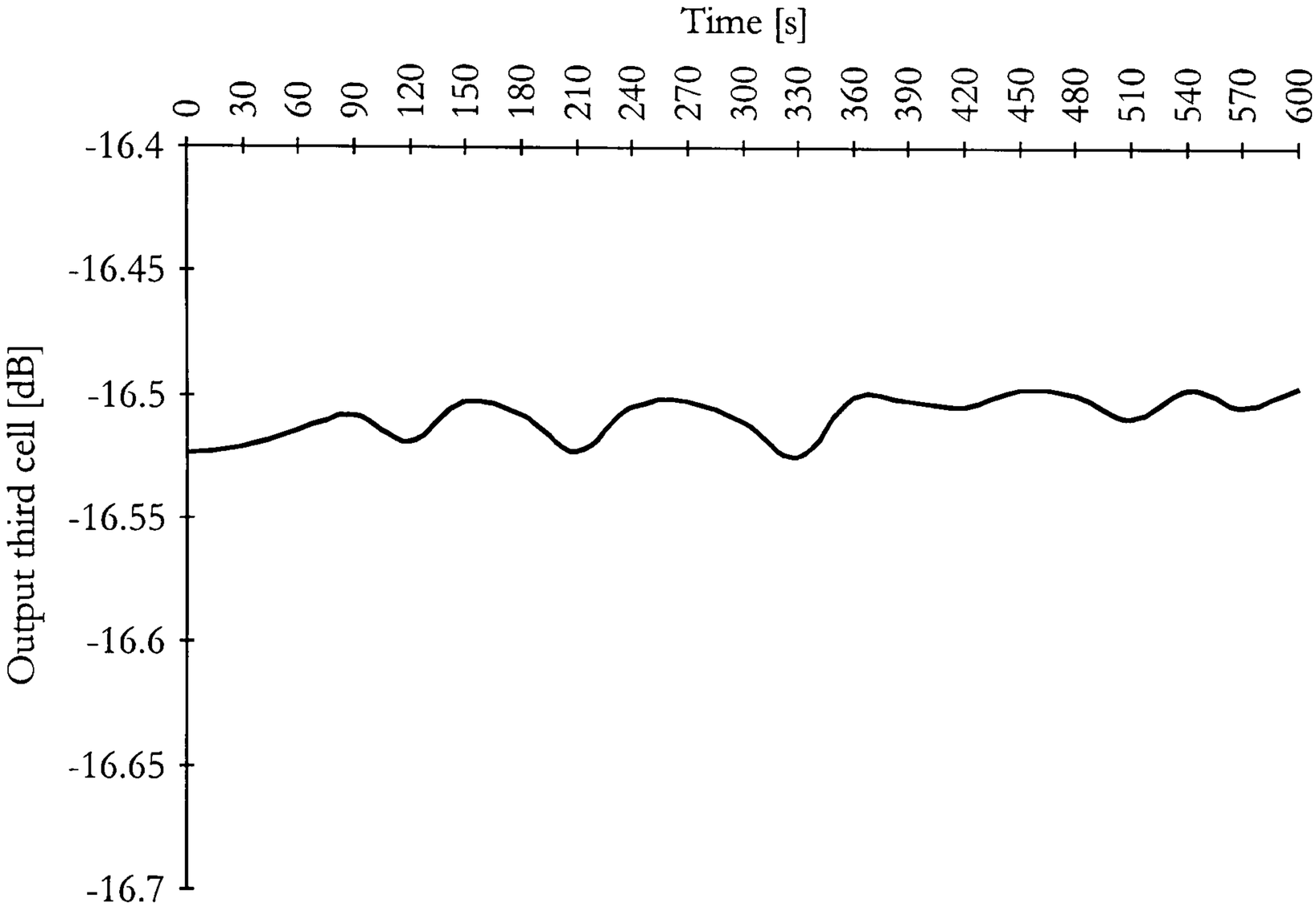

Figure 9.6: *Time stability of the third cell output*

The third cell output mean value has been recorded as -16.5046dB and the standard deviation is 0.00882dB. The variations of the individual output signals for sensing cells are negligible and the measured signals is constant with time.

In the same manner as for individual cells the amplitude time stability of individual power spectrum beat frequencies has been observed for the connected system. During a 10min interval the values of the power spectrum amplitude for each sensing beat frequency have been recorded, whereby no additional absorption has been introduced into the system. The results are shown in Figure 9.7.

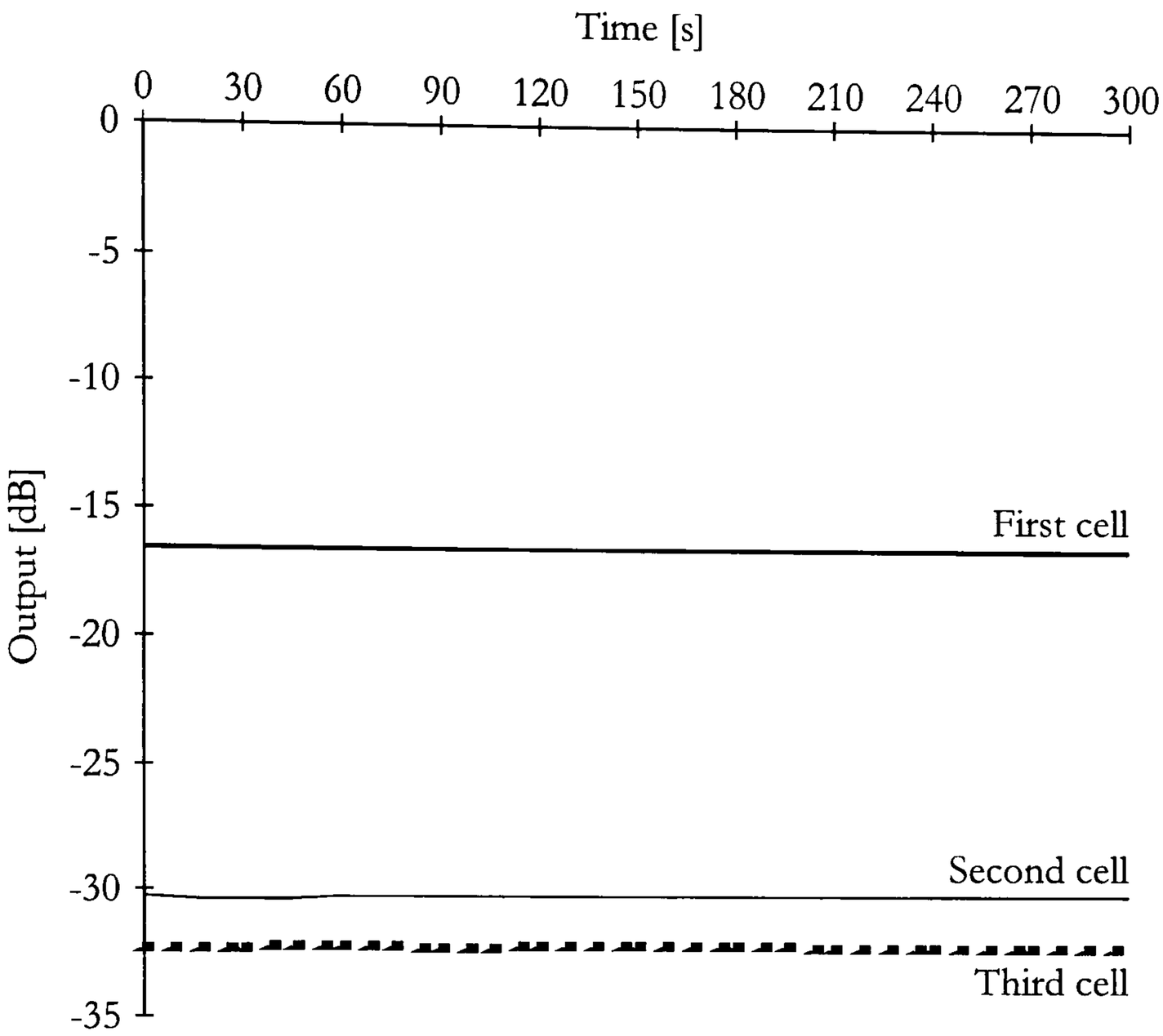

Figure 9.7: *Output stability of the coherence addressed quasi distributed system*

9.3. Resolution

For determination of system resolution, the noise level of the measurement was observed to be less then ~0.03dB. Hence a resolution of ~0.01dB can be estimated. If methane concentration measurements are supposed for the coherence addressed quasi distributed absorption system the resolution limited concentration measurements depend on the lengths of the cells used. Since measuring cell lengths of less then 20mm are not appropriate for this type of gas absorption measurements due to very low absorption coefficients, in worst case the resolution limited concentration we can detect is about $23*10^3$ ppm. For cell lengths of more than 40mm the concentration which could be detected is less then $10*10^3$ ppm. Even if we consider the worst case resolution limited concentration detection, the measured value is still located below our initial goal of detecting 50% of the lower explosion level concentration of methane in air.

9.4. Temperature and fibre bend influence

For many interferometer applications temperature changes are crucial to the system performance, since they cause drift or change in the output which is not related to the parameter to be measured.

In order to evaluate the proposed coherence addressed quasi distributed measuring system we heated the fibre at different locations (the lead in fibre before the coupler, after the coupler and the connecting fibre between the cells) using a laboratory gas burner. During the heating process the change in the power spectrum amplitude at the beat frequencies corresponding to the individual sensing unit has been observed. We found out that the temperature has a negligible influence on the sensing system. Without regard to the location of the temperature influence, the power spectra did not experienced any change and remained stable. The output stability of the system has been already shown in Figure 9.7.

The second disturbance which could influence the performance of the system are macro and micro bends of the lead in fibre, or the fibre which is connecting the sensing units. The system has been tested on macro bends by bending the fibre by hand and on micro bends by pressing the fibre with a sharp object. Both bending mechanisms cause a minor change in the power spectrum amplitudes. The amplitude drop is mainly due to the micro bend attenuation, since the macro bend effect is almost negligible. Basic precautions for avoiding or suppressing microbend effects is to use a fibre optic cable designed to minimise microbend effects, and/or to shield the fibre from harsh mechanical influences.

9.5. Crosstalk experiments

In order to verify the crosstalk analysis which has been presented in chapter 6 an experiment has been initiated to accomplish the evaluation.

The cross interference due to a short connecting fibre (near or less than the coherence length of the source) was tested using just one microoptic cell. Since the results regarding the mutual influence of multiple cells are very similar to the result obtained with only one cell we have decided to evaluate just a single cell. With multiple cell testing we would have to destroy many fibre-capillary joints, but were limited with the number of capillaries due to the expenses of the project. For the experiment we have gradually decreased the fibre length of the second fibre-capillary connection, while we observed the time response and the appropriate power spectrum. A typical time response without cross interference being present is shown in Figure 9.8.

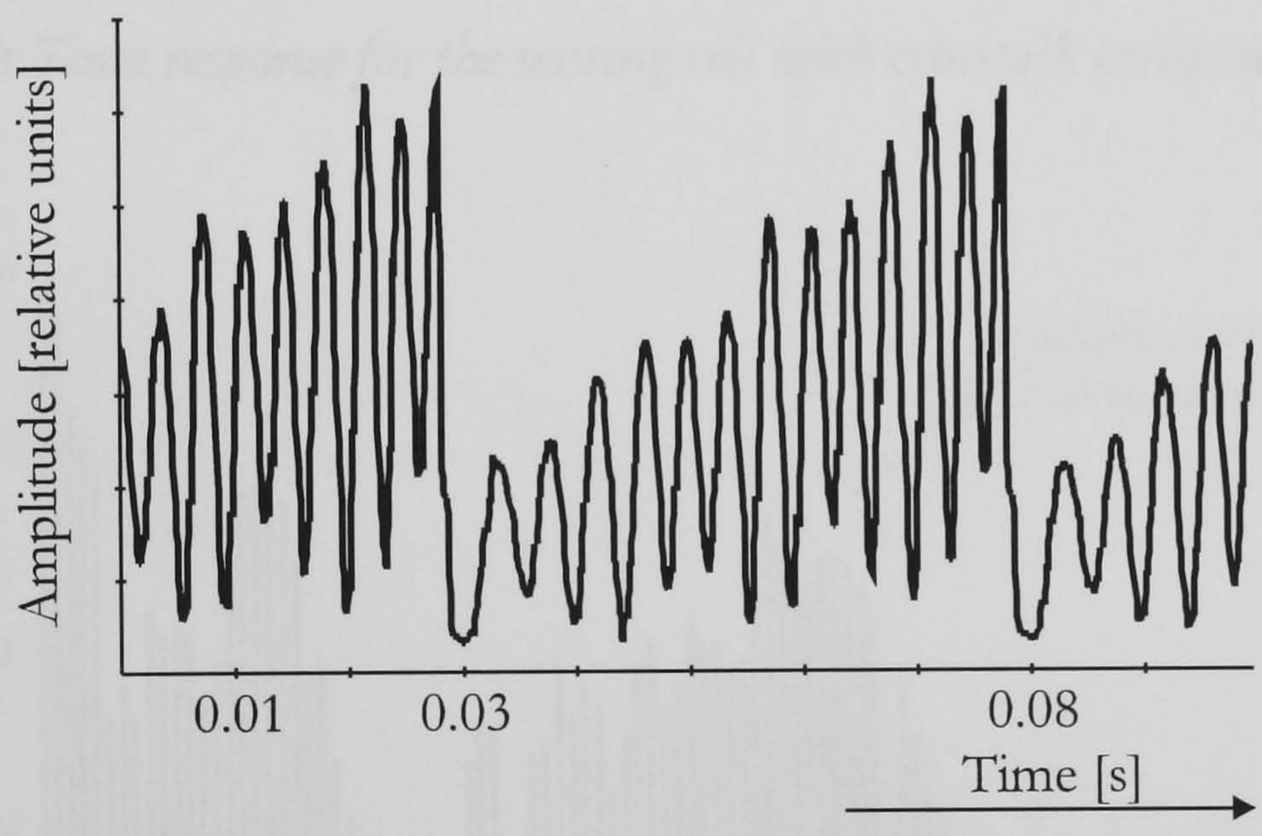

Figure 9.8: *Time response for the sensing cell without high frequency crosstalk components*

In this case the fibre length of the second fibre-capillary connection has been a few meters. This is much more than the coherence length of the source and therefore no backreflection induced cross interference has been observed.

After the fibre length has been reduced down to a few ten centimetres first signs of additional high frequency components could be observed (the coherence length of the source is approximately 40cm). When the length of the fibre is further reduced to 20cm the cross interference components become clearly visible. The time

response for this particular case is shown in Figure 9.9 and the appropriate power spectrum in Figure 9.10.

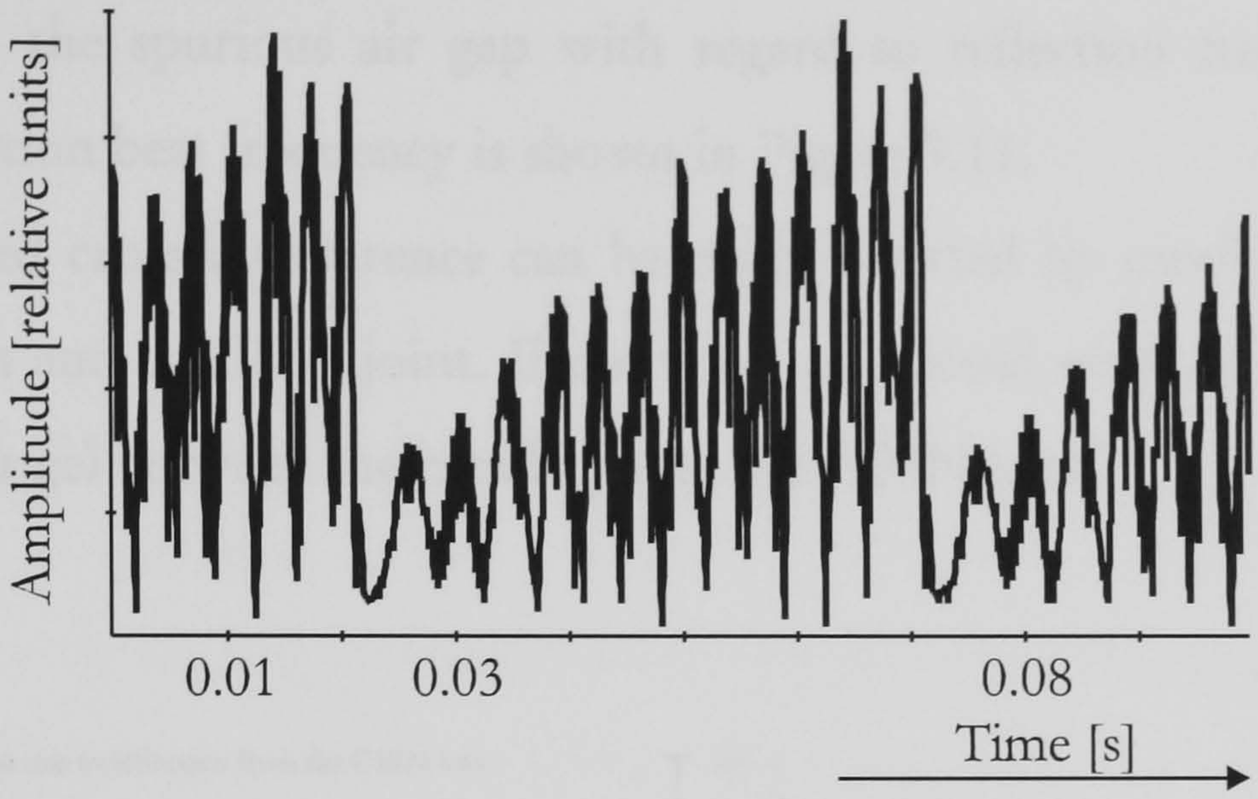

Figure 9.9: *Time response for the sensing cell with crosstalk components present*

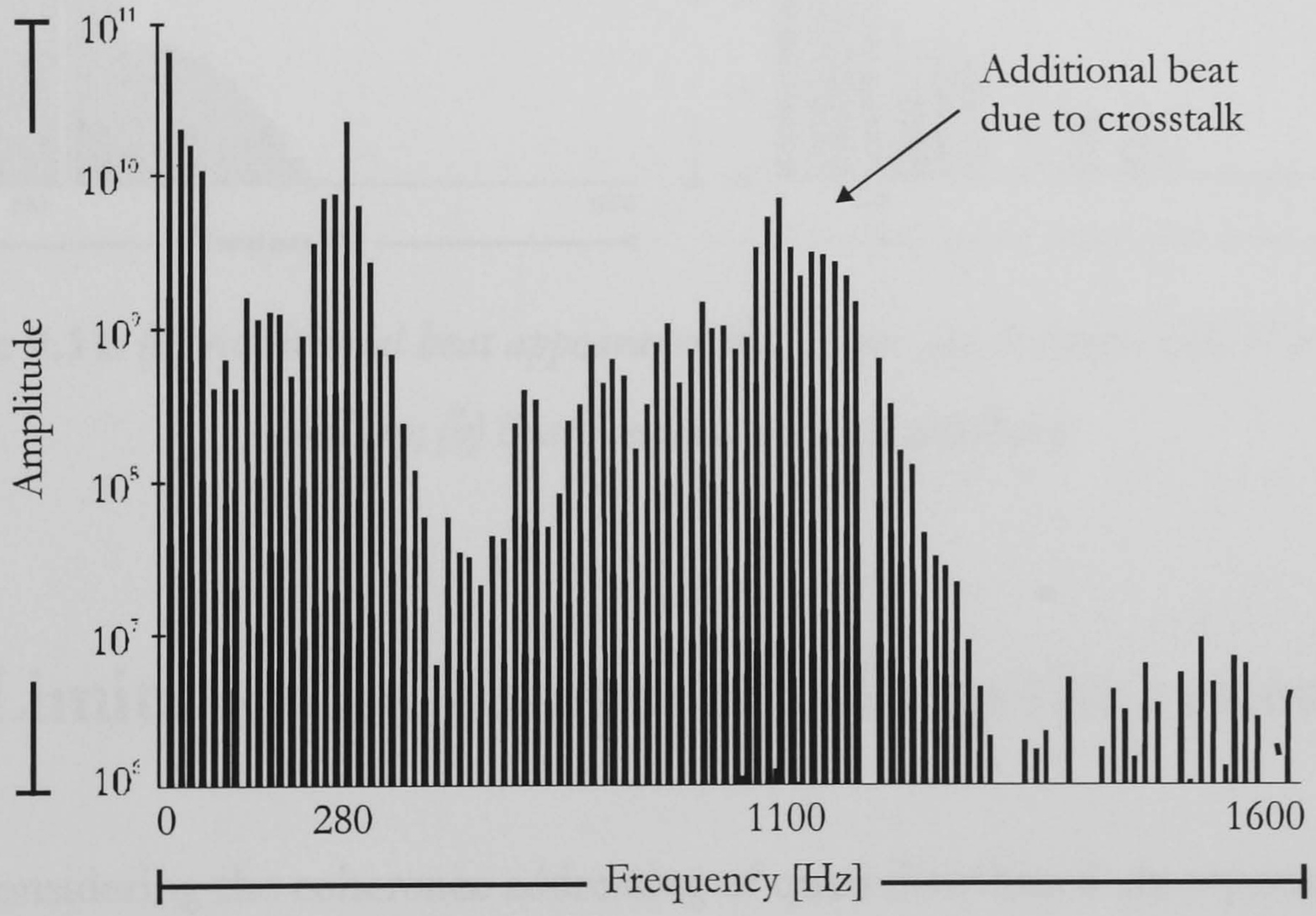

Figure 9.10: *Power spectrum with additional beat frequency due to crosstalk*

Due to the spurious reflection from the end of the fibre which is connected to the second capillary an additional beat frequency around 1100Hz is observed. Since the connecting pieces between successive sensing units are expected to be at least a few meters the problem of spurious reflection induced crosstalk could be ignored.

Cross interference noise is also induced by air gaps between the capillary and the GRIN lens. A comparison between the power spectrum with the main beat frequency and the spurious air gap with regard to reflection from the second capillary reflection beat frequency is shown in Figure 9.11.

Air gap induced cross interference can be easily omitted by careful alignment of the GRIN lens and capillary joint. If necessary one could even apply some index matching oil or gel between the capillary and the GRIN lens.

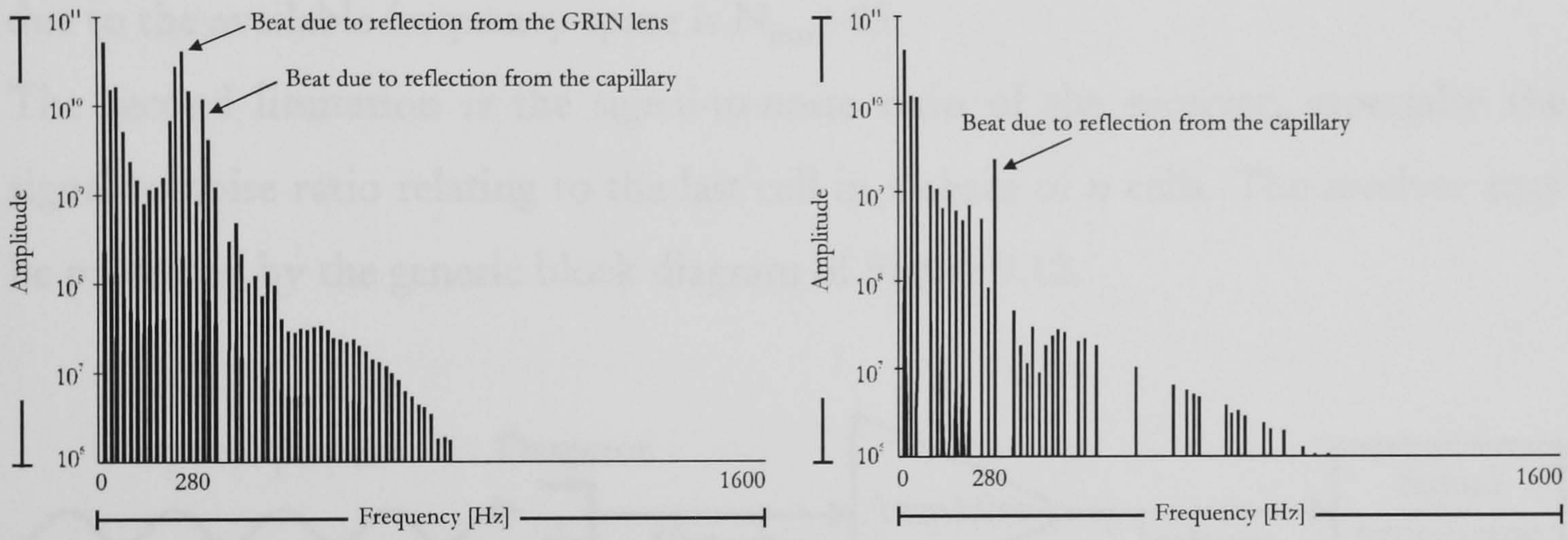

Figure 9.11: *(a) Additional beat appearance due to air gap between GRIN lens and capillary; (b) Beat frequency due to capillary*

9.6. Limitation on number of cells in the system

When considering the coherence addressing of quasi-distributed absorption sensors by the FMCW method the maximum number of sensors is limited by two factors: the available space in the frequency domain and the signal to noise ratio.

The available space in the frequency domain is limited by the coherence length of the source. To distinguish between different beat frequencies in the power spectrum at the detector, every sensing unit should have its own unique optical

path difference. With increase in coherence length of the source, the number of sensing cells each with a unique length can be increased. The maximum number of sensors N_{maxf} due to the available frequency space is:

$$N_{\text{maxf}} = \frac{\omega_c}{\Delta\omega} \tag{9.1}$$

where ω_c is the maximum beat frequency (with a source coherence length of 20cm, ω_c~1700Hz), and $\Delta\omega$~20Hz is the minimum resolvable difference between two beat frequencies. According to system parameters the maximum number of sensors due to the available frequency space is N_{maxf}~85.

The second limitation is the signal-to-noise ratio of the receiver, especially the signal-to-noise ratio relating to the last cell in a chain of *n* cells. The receiver may be presented by the generic block diagram of Figure 9.12.

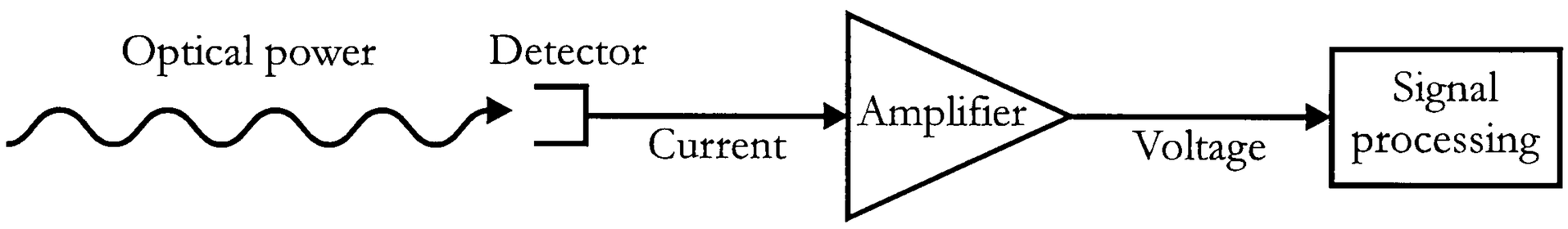

Figure 9.12: *Block diagram of receiver*

The photodiode converts the received optical power into an electrical current, and the next requirement is the transformation of this current into an amplified voltage signal. As in all fibre-optoelectronics systems is at this point, the receiver input where the signal level is weakest, that the signal-to-noise ratio is determined and the system performance level established. In practice the need for a certain minimum signal-to-noise ratio sets a lower limit on the acceptable level of received optical power.

To calculate the signal-to-noise ratio relating to the last cell we need to obtain the signal level from the last cell and also the receiver noise level. In general the

receiver noise consists of amplifier noise, dark current noise, shot noise and thermal noise.

From the analysis given by Gowar [9.1] we can write a general expression for the rms signal-to-noise ratio both, the PIN photodiode and transimpedance amplifier in our system as:

$$\frac{S}{N} = \frac{\Re P_{incident}}{\sqrt{\left\{V_{AMP}^2\left[\frac{1}{R^2} + \frac{4\pi^2}{3}B^2C^2\right] + I_{AMP}^2 + 2e\left(\Re P_{rec} + i_d\right) + \frac{4kT}{R}\right\}B}} \tag{9.2}$$

the denominator in the above expression consists of (i) amplifier voltage and current noise, (ii) shot and dark current noise and (iii) thermal noise respectively. Here

B is the bandwidth,

T is the temperature; T~300 K,

e is the electronic charge; e = 1.6 10^{-19} Coulomb,

k is the Boltzmann's constant; k = 1.3810^{-23} J/K and

$\Re$ is the Photodiode responsivity ($\Re$~0.9 A/W).

V_{AMP} and I_{AMP} are the voltage and current noise figures for the amplifier (input stage only). Typical values are: $V_{AMP} \approx 4nV/\sqrt{Hz}$, $I_{AMP} \approx 10fA/\sqrt{Hz}$, C is the effective input capacitance combining the effects of diode capacitance and amplifier capacitance (C~10pF). i_d is the dark current (~0.3nA).

The effective resistance R in the thermal noise term and amplifier noise term are the combined effects of the PIN diode effective resistance which is approximately equal to the feedback resistor in the transimpedance stage (for large input resistance of the amplifier):

$$\frac{1}{R} = \frac{1}{R_{AMP}} + \frac{1}{R_{FEEDBACK}} \tag{9.3}$$

Since our bandwidth requirements are very modest (5kHz) comparison of the various terms in the denominator (9.2) shows that shot noise limited detection may be readily achieved. Because the dark current $i_d << \Re P_{incident}$ we have the conditions for shot noise limited detection $P_{incident}$~mW levels as follows:

$$\frac{4kT}{R} << 2e\Re P_{rec}$$

$$I_{AMP}^2 << 2e\Re P_{rec} \Rightarrow I_{AMP} << 1.8pA/\sqrt{Hz}$$

$$V_{AMP}^2\left[\frac{1}{R^2}+\frac{4\pi^2}{3}B^2C^2\right] << 2e\Re P_{rec}$$

Under the shot noise limited detection the SNR term (9.2) is simplified to:

$$\frac{S}{N} = \frac{\Re P_{incident}}{\sqrt{2e\Re P_{rec}B}} \tag{9.4}$$

For the FMCW coherence addressed system the output light intensity I_{out_1} for the first sensing cell is calculated by taking the first order correlation of the total optical field (see Chapter 5 equation (5.20)), where the time variable is limited to one pulse of the beat frequency:

$$I_{out\_1} \propto r_{11}^2(A+Bt)+r_{21}^2t_{11}^2t_{11}'^2(A+Bt)e^{-\alpha_1C_14L_1}+ \tag{9.5}$$
$$2r_{11}r_{21}t_{11}t_{11}'(A+Bt)e^{-\alpha_1C_12L_1}\cdot\cos\left(\frac{2\pi}{\lambda_0}\left(\frac{2n_eL_1}{\lambda_0}\right)(\lambda_0+\Delta\lambda)\right)$$

To calculate the SNR for the FMCW coherence addressed system and determine the limitation for the number of cells in the system we can compute the signal levels as follows. By neglecting the amplitude change due to modulation ($A+Bt$ is constant) and assuming $e^{-\alpha CL} \sim (1-\alpha CL)$ from the third term in equation (9.5) the amplitude of the beat signal returning from cell 1 is approximately:

$$I_{beat\_1} \approx 2r_{11}^2\left(1-r_{11}^2\right)\left(1-\alpha_{m1}C_1L_1\right)\Re P_{incident} \tag{9.6}$$

where $P_{incident}$ is the incident power.

The amplitude of the beat signal returned form cell *n* is reduced because the incident and returning beams have to pass through the preceding cells each with a transmission factor of t_i^2 (Figure 9.13). Assuming that all cells have a similar throughput transmission of t^2 (~0.92) and a GRIN lens reflectance r^2 (0.04) then

$$I_{beat\_n} \approx \left[\left(t^2\right)^{2(n-1)}\right]2r^2\left(1-r^2\right)\left(1-\alpha_{mn}C_nL_n\right)\Re P_{incident} \tag{9.7}$$

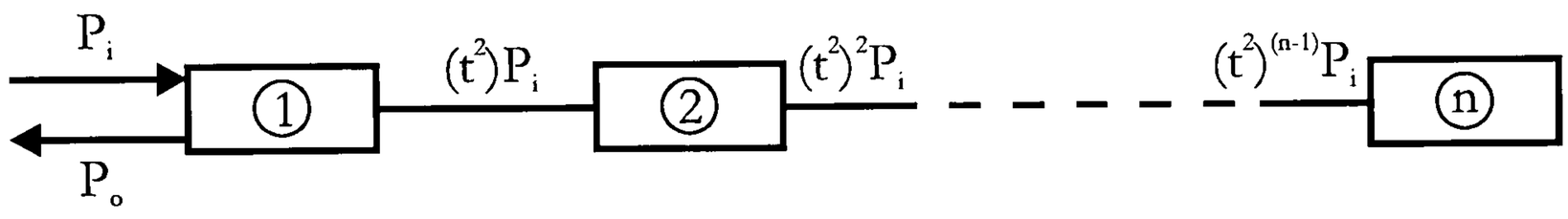

Figure 9.13: *Reduction in power through cells*

From equation (9.7) the reduction in the beat signal caused by absorption is:

$$\Delta I_{beat\_n} \approx A\Re P_{incident}\left[\left(t^2\right)^{2(n-1)}\right]2r^2\left(1-r^2\right) \tag{9.8}$$

where A is the absorbance ($A=\alpha_m CL$) and $r^2=0.04$.

Since the system is shot noise limited we can calculate the signal-to-noise ratio for the absorption signal from cell *n* according to equation (9.4) as:

$$\frac{S}{N} = \frac{A\Re P_{incident}\left[\left(t^2\right)^{2(n-1)}\right]2r^2\left(1-r^2\right)}{\sqrt{2e\Re P_{rec}B}} \tag{9.9}$$

where $\Re$ is the photodiode responsivity (~0.9 A/W), B is the bandwidth (5kHz) and P_{rec} is the total power received by the photodiode.

In the worst case with a large number of sensors in the system, we assume that all the incident power is reflected back to the receiver and so, taking into account the 50:50 coupler, $P_{rec}=0.5P_{incident}$. Under this equation (9.9) simplifies to:

$$\frac{S}{N}=\frac{A\Re\sqrt{P_{incident}}\cdot 2r^2\left(1-r^2\right)\left(t^2\right)^{2(n-1)}}{\sqrt{e\Re B}} \tag{9.10}$$

When expressing the signal-to-noise ratio in dB (9.10) becomes:

$$10\log\frac{S}{N}=10\left\{\begin{array}{l}\frac{1}{2}\log\left(P_{incident}\right)+\log\Re-\frac{1}{2}\log\left(e\Re B\right)+\log A+\\ \log\left[2r^2\left(1-r^2\right)\right]+2(n-1)\log\left(t^2\right)\end{array}\right\} \tag{9.11}$$

With this assumptions and substituting the values for the parameters, the worst case shot-noise-limited SNR is:

$$\begin{aligned}SNR&=\left[10\left\{-1.65-4.57\cdot10^{-2}+7.57+\log A-1.11-0.072(n-1)\right\}\right]dB\\ &=\left[10\left\{4.76-0.072(n-1)+\log A\right\}\right]dB\\ SNR&=\left[47.6-0.72(n-1)+10\log A\right]dB\end{aligned} \tag{9.12}$$

Equation (9.12) predicts that we can still detect an absorbance of ~10^{-3} in the last cell at a SNR of ~5dB, for the maximum cell number, n=20.

From practical construction considerations, we do not anticipate to have more than ~20 cells in a system. The above results show that there should not be any problems in regard to either the available space in the frequency domain or in the signal-to-noise levels.

9.7. Summary and conclusions

With the FMCW Coherence addressing mechanism the common interferometer associated problems were negligible. Because both reflections from the sensing cell travel through the identical optical fibre slight deformations or temperature changes cause the same optical path change for both signals and no change in the output interference is observed. Without regard to the location of the temperature influence, the power spectra changed less than the noise level. Both bending mechanisms cause less than 0.05dB change in the power spectrum amplitudes. The amplitude drop is mainly due to the micro bend attenuation, since the macro bend effect is almost negligible. Since a temperature controlled and current stabilized source is used, variations in source intensity are minimized, and in addition, a reference source power level can be extracted from the input coupler and used for feedback control of the source power.

The system is essentially insensitive to the polarisation state because, apart from the cell length, both reflected beams from each cell travel the same path and experience the same perturbations.

Although the selection of different optical path differences, i.e. cell lengths enables the separation between sensor signals in the frequency domain, it does not completely ensure their separation from "cross terms" which are the result of undesired interference between any two optical paths associated with more that one sensor in a system. The experimental investigation of crosstalk sources and their influence on the performance of the system complies with the analytical investigation presented in previous chapters. To avoid crosstalk between successive sensors it is necessary to make sensors incoherent with each other by introducing long connecting fibre lengths between sensing units which are much greater then the coherence length of the source. Due to non perfect alignment of the GRIN lens relative to the capillary air gap reflections could result in crosstalk. However this can be very easily omitted by the use of index matching gel or oil.

The efficiency of the system to detect gas concentration on various positions along the optical fibre can be comprehended from the dynamic range, resolution properties and signal-to-noise ratio. Consideration of the available space in the frequency domain and the signal to noise ratio indicates that systems containing 20 serial sensing units are feasible.

One of the possible applications for the system is in measurement of gas concentration such as methane. The sensitivity level which is useful in practice (for methane alarm systems) is detection below the Lower Explosive Level (LEL: 5% methane in air). For example, to detect 50% of the LEL and assuming a methane absorption coefficient[3] of $\alpha_m = 0.25 cm^{-1} atm^{-1}$ for the (weak) near IR lines around 1665nm, the system has to detect an attenuation of 0.27dB or 6% change in the power spectrum amplitude for an individual sensing unit of length 5cm. The experimental results presented (where the system has been evaluated using similar absorption values of ~8%, but with a broadband absorber) indicate that the proposed system is feasible for quasi-distributed gas detection. However because the methane gas absorption line-width is ~5GHz then appropriate adjustment of the scan range and sweep time would be necessary. Although the current system has been evaluated using a scan range of 90GHz, the scan range can easily be reduced to ~5GHz while maintaining the same beat frequencies by reducing the sweep period from 0.05s to ~3ms.

References

[9.1] J. Gowar, "Optical Communication Systems ", Prentice Hall International, UK, 1993

10. Specific application of the system for absorption line measurement

For specific applications of the FMCW coherence addressed system for quasi distributed trace gas monitoring, the system has to cope with narrow band gas absorption lines.

In the previous chapters, the method for coherence addressing of quasi-distributed sensors by the FMCW method has been confirmed using broadband absorbers. With broadband absorbers we suppose that the absorption coefficient is constant over the whole scanning range, where the scan is defined as the range of source wavelength due to the sawtooth modulation of the source. In order to model narrow band absorption where the absorption line width is less than the FMCW scan, we will replace the constant value of the absorption coefficient for the wide band case, with an absorption line described using the Lorentzian function.

10.1.Effect on system performance of having a narrow band absorber

The basic difference between a wide band and narrow band absorber is shown in Figure 10.1. Whereas the wide band absorber has a constant value of the absorption coefficient over the scanning range of wavelengths, the narrow band absorption line can be described as a Lorentzian function.

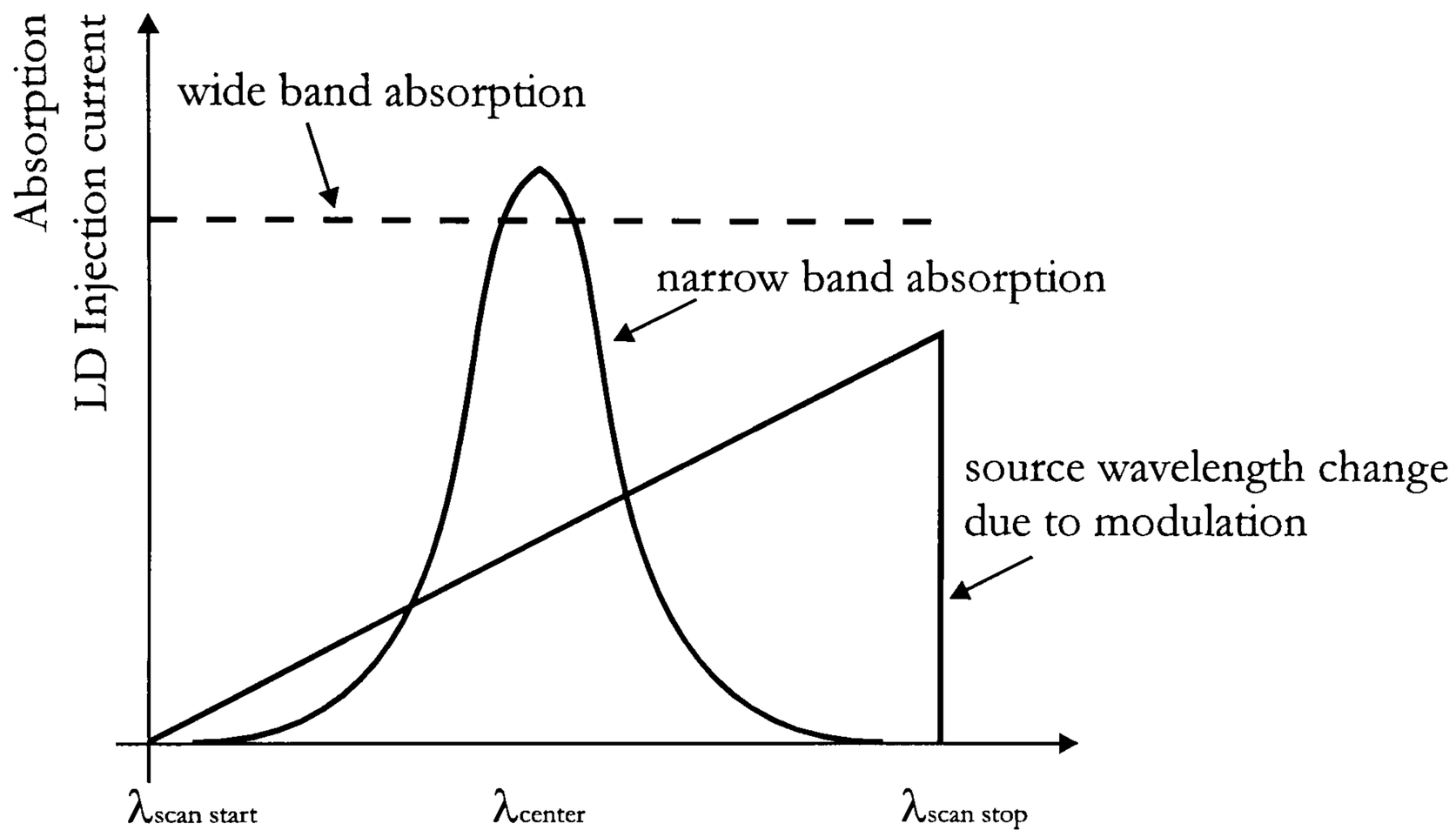

Figure 10.1: *Comparison between wide band and narrow band absorption during sawtooth source modulation*

The value of the narrow band absorption coefficient over the scanning range as a function of wavelength or wavenumber, $\nu = 1/\lambda$ can be described as:

$$\alpha(\nu) = \frac{\alpha_m}{\left\{\left(\frac{\nu - \nu_0}{\gamma}\right)^2 + 1\right\}} \tag{10.1}$$

where α_m is the absorption at the line centre, ν_0 is the wavenumber at the line centre and γ is the line-halfwidth [1].

To simulate specific application of the system, all absorption coefficients in equation (5.23) will be replaced with the narrow band absorption coefficient $\alpha(\nu)$. Considering previous experiments the wavelength scan range due to source modulation is 0.7nm or approximately 120GHz in the frequency domain. To analyse the effects of introducing a narrow band absorber, three distinctive narrow band absorption lines with half-linewidths of 500MHz, 2.5GHz and 5GHz will be used. A general representation of Lorentzian function including half-linewidth γ is shown in Figure 10.2.

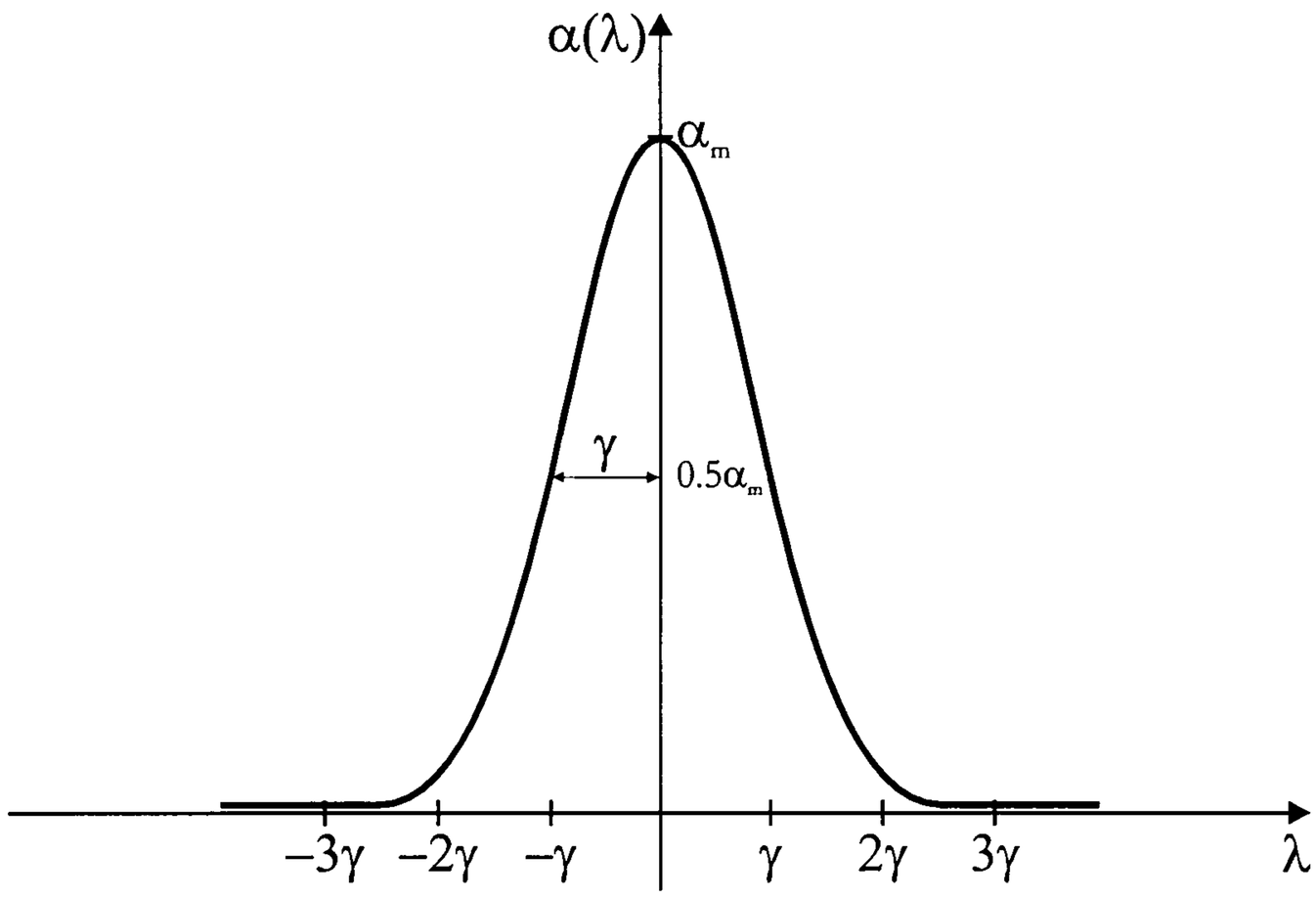

Figure 10.2: *General Lorentzian narrow band absorption line with line-halfwidth* γ

The first absorption line is very narrow and will serve here to demonstrate the effect of ultra narrow absorption bands, whereas the second and third absorption lines are chosen to represent pressure-broadened trace gas absorption lines. The second absorption line is approximately similar to methane (Methane has half-linewidth of ~2.5GHz; full width ~5GHz).

10.1.1. Single cell performance with a narrow band absorber

In the first set of calculations, the influence of narrow band absorption on the single cell system setup is evaluated. The absorption has been increased from 0% to

1% in steps of 0.2% and the power spectrum beat amplitude has been recorded. Figure 10.3 presents the comparison between system output characteristics for the narrow band absorption lines.

As expected, the sensitivity of the system decreases when the linewidth is reduced. Since the interval during the wavelength scan in which absorption occurs is shortened, the level of absorption is reduced and hence the gradient of the output characteristics is decreased. We can represent this effect by observing the cross-section between the absorption line and the sawtooth modulation signal as presented in Figure 10.4.

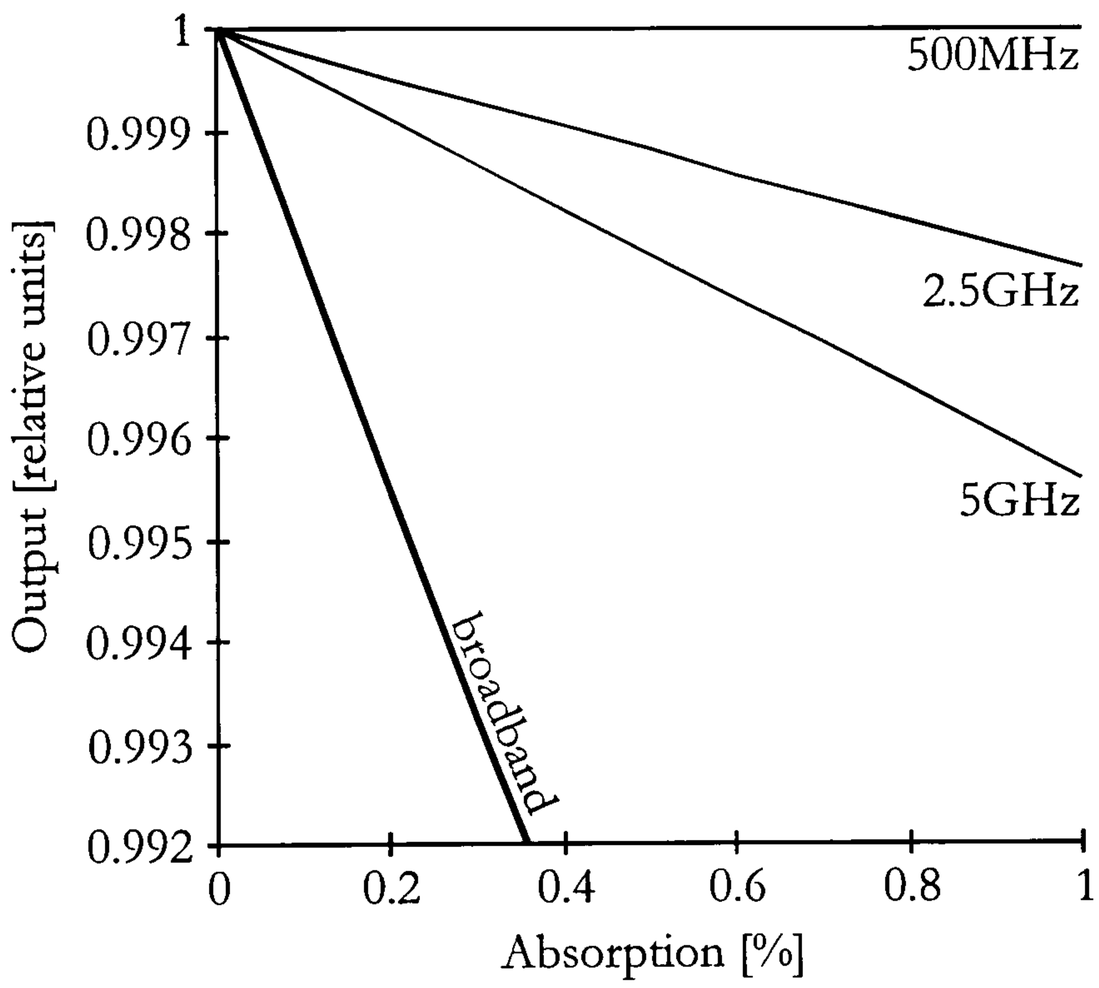

Figure 10.3: *Output characteristics for single cell FMCW coherence addressing system using three different narrow band absorption lines. Half linewidths γ shown on graph; broadband absorber shown for comparison*

Examination of Figure 10.3 shows that, for example a linewidth of 2.5GHz reduces the absorption by a factor of ~7.5 compared to the broadband case.

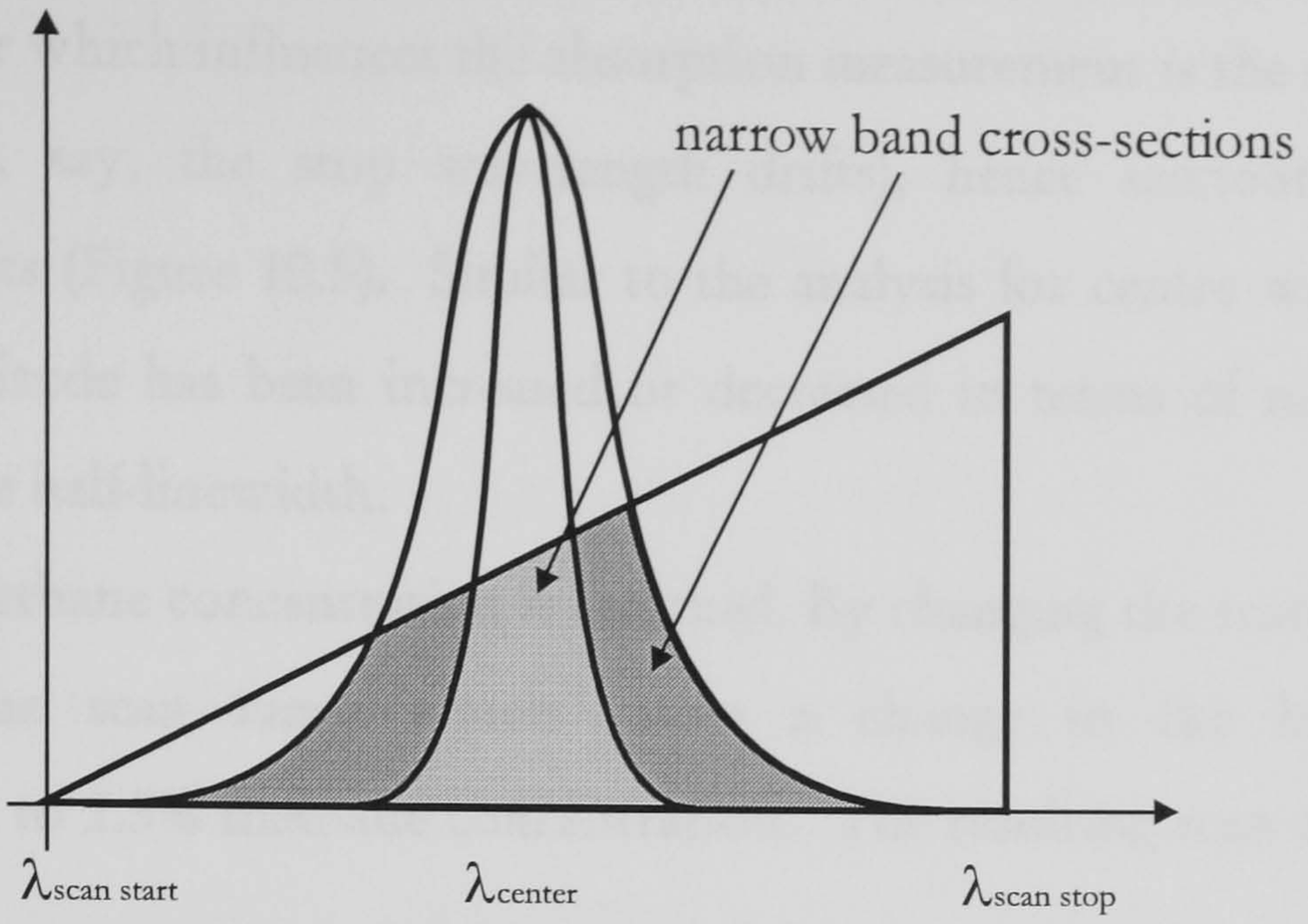

Figure 10.4: *Cross-section between the absorption spectrum and modulation signal*

A factor which can affect the measurement accuracy of the system is drift of the centre laser wavelength in relation to the (fixed) absorption line due to temperature changes.

In order to determine the required source wavelength stability and hence the temperature stability, we have performed a calculation where the centre laser wavelength has been shifted left or right from the absorption line centre and the change in beat amplitude observed. The centre wavelength has been increased or decreased in terms of multiples of the absorption line half-linewidth assuming a 5cm sensing cell.

Without absorption present the centre laser wavelength drift had no influence on the system. If absorption is present inside the sensing cell, the drift causes a reduction in the measured signal. For example, if we assume that we have 5% methane (the LEL) in the cell, then a shift of the central wavelength by $\pm 3.5\gamma$ would result in a signal reduction so that the apparent concentration would be 2.5%

For smaller shifts of the central wavelength, for example if the wavelength is stabilised within $\pm\gamma/2$ then the resulting relative error for methane concentration measurements is ~0.36%.

Another factor which influences the absorption measurement is the scan amplitude drift (so that, say, the stop wavelength drifts), hence sawtooth modulation amplitude drifts (Figure 10.5). Similar to the analysis for centre wavelength drift the scan amplitude has been increased or decreased in terms of multiples of the absorption line half-linewidth.

Again a 5% methane concentration is assumed. By changing the scan amplitude we determined the scan range which causes a change in the beat amplitude corresponding to 2.5% methane concentration. The resulting scan amplitude drift is $\pm 7.8\gamma$.

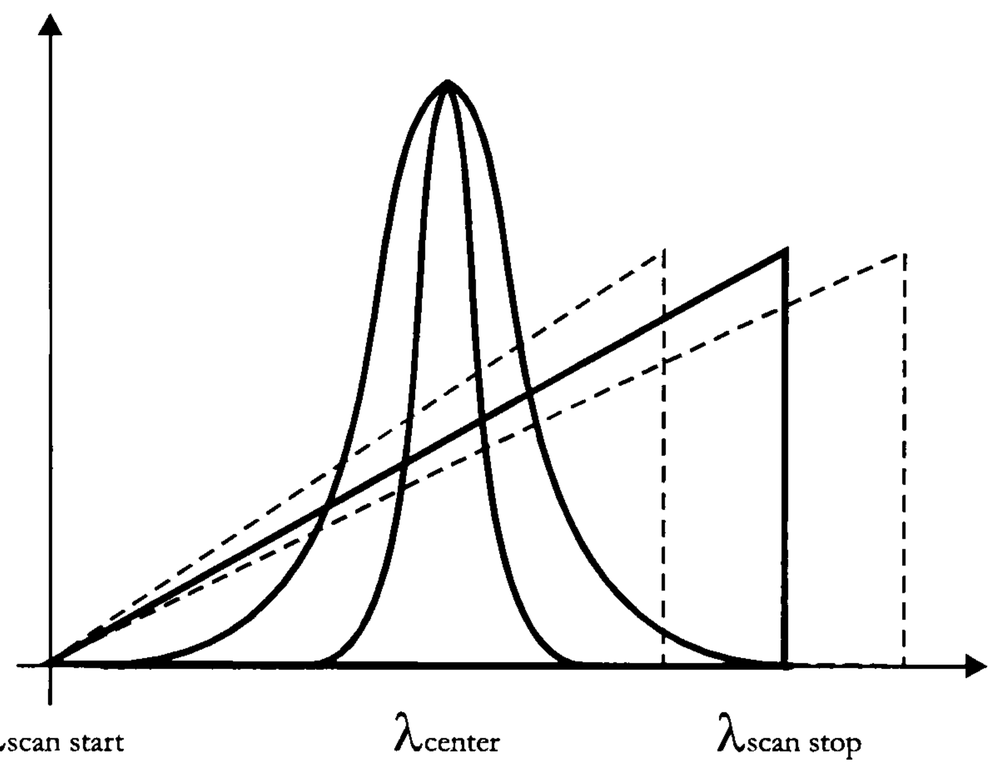

Figure 10.5: *Change in overlap between absorption spectra and scan due to scan amplitude drift*

Thus if we compare the effects of centre wavelength drift and scan amplitude drift, the centre wavelength drift is much more influential (approximately double the effect).

Finally the measured beat amplitude is additionally influenced by the discrete Fourier transform. Although the output value should be independent of any shifts of the central laser wavelength or scan amplitude if there is no narrow band absorber in the cell, we could still observe some changes.

The explanation lies in the discrete Fourier transform and non infinite time limits. As we already explained in the third chapter, when the limits of the Fourier Integral approach infinity the Fourier transform and the corresponding power spectrum give a series of discrete frequencies centred around the beat frequency. If the limits are not infinite the discrete peaks become narrow bands.

In our case when the central wavelength or scan amplitude changes the beat frequency changes and hence the beat in the power spectrum is shifted for a very small amount. Since we have finite time intervals this corresponds to a changed value of the beat amplitude. With infinite short sampling (continuous sampling) this would not cause problems since our initial amplitude would shift to left or right keeping the same value. However since we do not sample continuously we do not observe the whole power spectrum but only discrete values. If the shift of the beat frequency is not large enough to fall into the next discrete frequency value (this is the usual case) we do not observe the shifted peak but see a change in the initial beat. This problem can be minimised by using instrumentation with high sampling rates over long sampling intervals.

10.1.2.Multiple cell performance in having a narrow band absorber

In the second set of simulations the influence of narrow band absorption on a multiple cell system has been studied. For three different narrow band absorption spectrums the outputs of three microoptic sensing cells have been recorded. We have gradually increased the absorption from 0% to 1% in steps of 0.2% in each sensing unit simultaneously. Figure 10.6(a,b,c) presents the individual output characteristics for 500MHz, 2.5GHz and 5GHz absorption spectrum half-linewidths respectively.

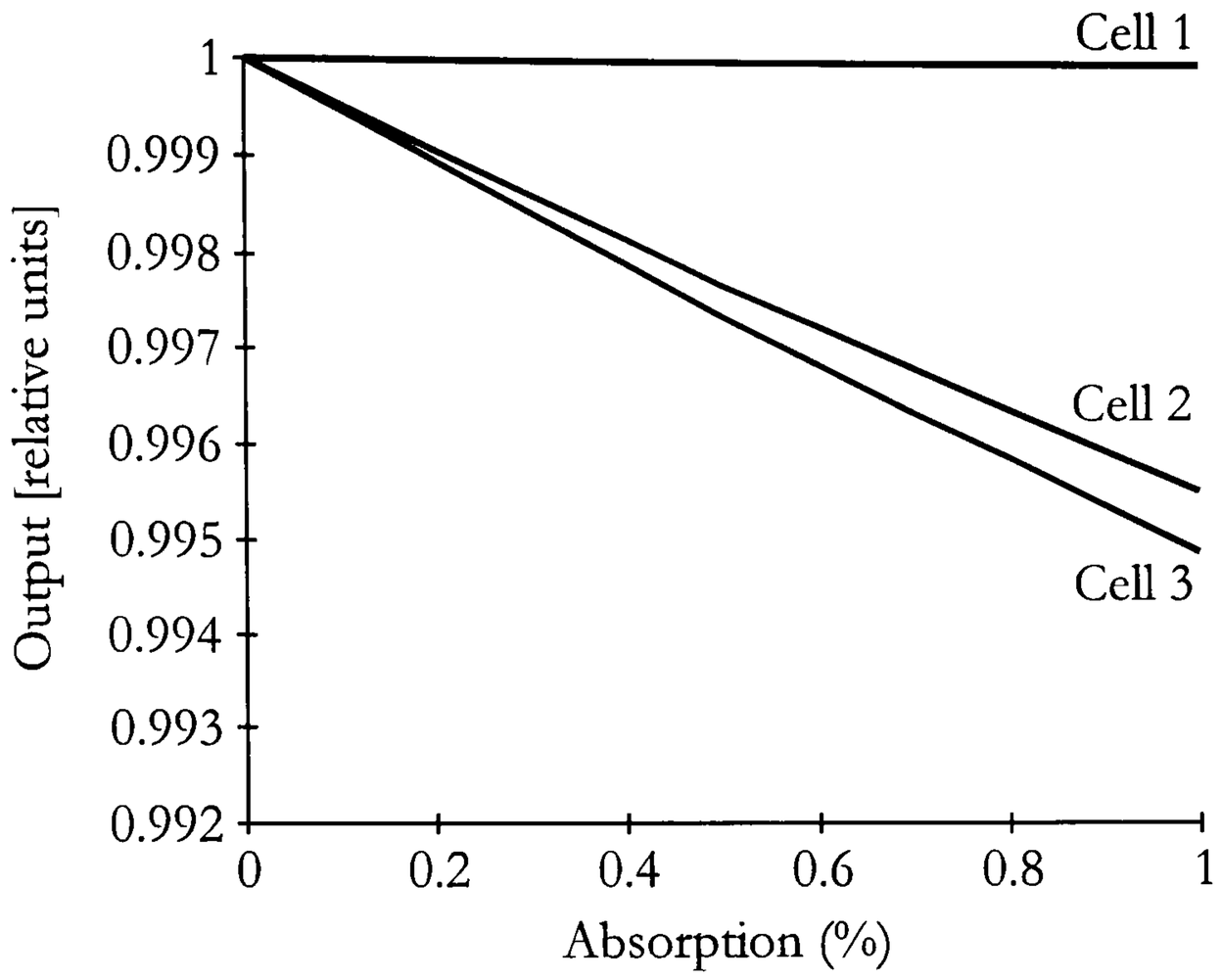
Cell 1
Cell 2
Cell 3
1
0.999
0.998
0.997
0.996
0.995
0.994
0.993
0.992
Output [relative units]
0
0.2
0.4
0.6
0.8
1
Absorption (%)

(a)

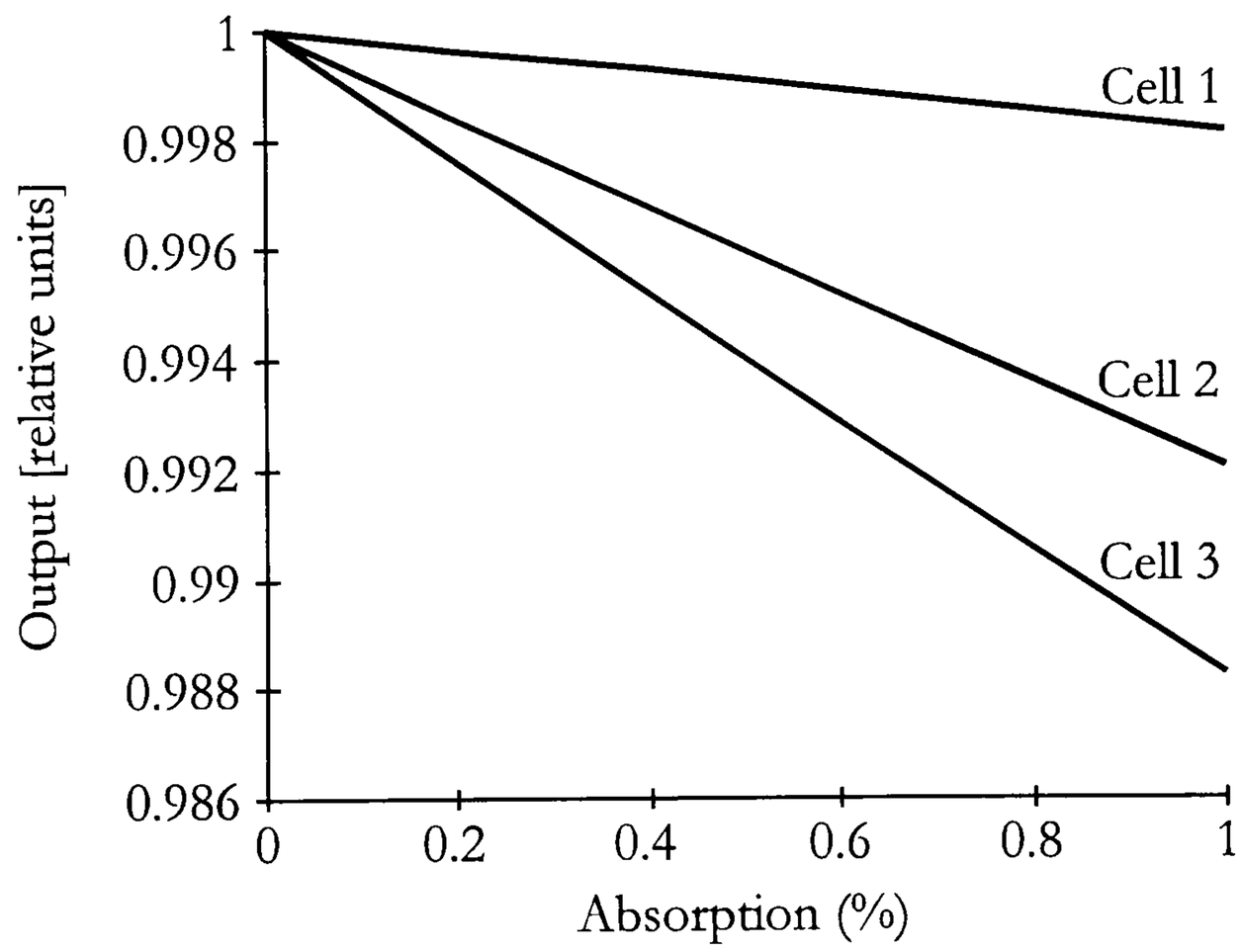
Cell 1
Cell 2
Cell 3
1
0.998
0.996
0.994
0.992
0.99
0.988
0.986
Output [relative units]
0
0.2
0.4
0.6
0.8
1
Absorption (%)

(b)

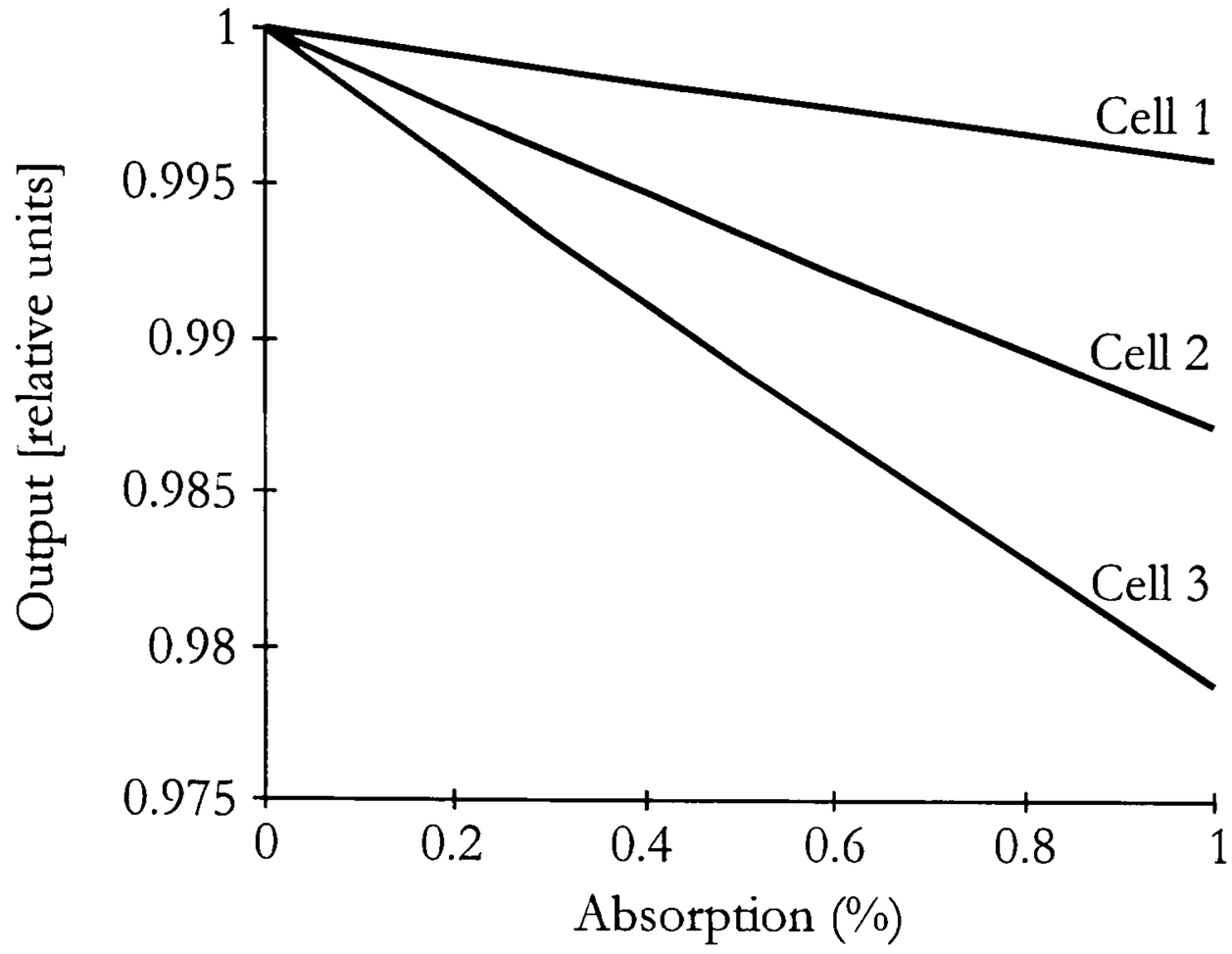

(c)

Figure 10.6: *Output characteristics for multiple unit system: (a) 500MHz, (b) 2.5GHz and (c) 5GHz absorption half-linewidth*

One can observe that in the case of very narrow absorption spectrums (500MHz) the absorption induced decline of the first output cell is negligible compared to the second and third cell. This can be explained by the short interval in which the absorber absorbs during the wavelength scan. Because of the serial arrangement of the system the second and third cell experience higher absorption values even with very narrow absorption spectrums, and therefore the output is reduced as expected. For absorption linewidths of all other intermediate levels similar output characteristics would be observed. The decay rate of individual sensing units outputs is increasing proportional to the increase of the absorption half-linewidth.

A possibility to further increase the absorption is to reduce the scanning range of wavelengths and therefore increase the cross-section between the absorption line and the sawtooth modulation signal. Two different scan ranges are considered here. The first is a scan of $\Delta\lambda_{max}$= 0.7nm (124GHz) corresponding to previous broadband results and the second is a reduced range of 0.1nm (17GHz). The outputs of three microoptic sensing cells have been recorded for both scan ranges

while the absorption has been gradually increased from 0 to 1% in steps of 0.2% in the last sensing cell with no absorbance in cells one and two. Figure 10.7 presents the third cell output characteristics for two typical trace gas half-linewidths, i.e. 2.5GHz and 5GHz in comparison with broadband absorption.

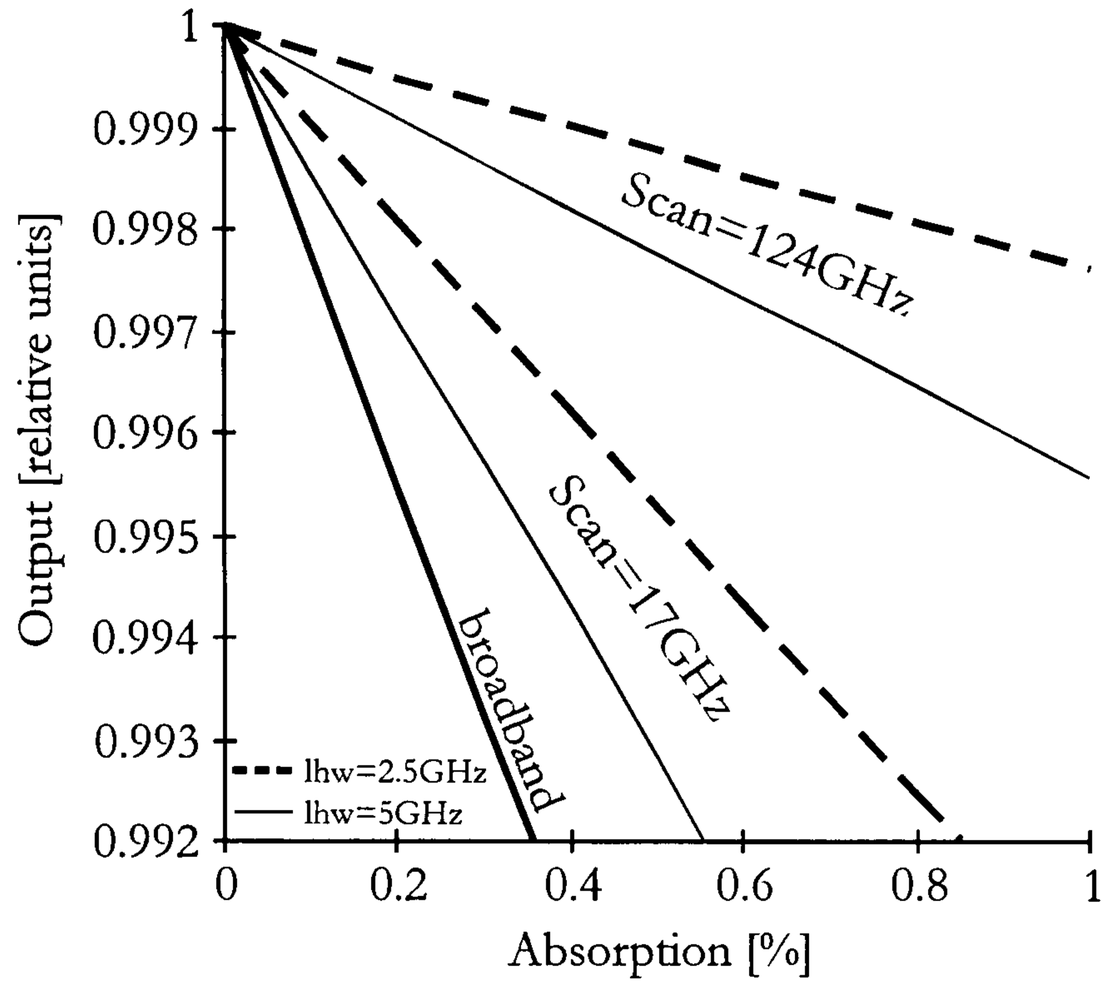

Figure 10.7: *Third cell output characteristics for typical trace gas half-linewidths when reducing the scan range and comparison with broadband absorption*

A consequence of the scanning range reduction is the shift of the beat frequencies to lower values. However this can be compensated by increasing the modulation frequency (reducing T) of the ramp. For example to maintain the same beat frequency when the scan range is reduced from 124GHz to 17GHz the sweep period has to be reduced from 50ms to 6.75ms.

In the narrow band case, the important factor is the ratio of scan range to linewidth. According to the results in Figure 10.7 the slope of the output characteristics for the 17GHz scan is ~0.95dB signal per dB attenuation in the cell for 2.5GHz half-linewidth. Here the ratio of scan range to linewidth is 3.4. Comparing this with the broadband (simulation) results (~2.5 dB signal per dB cell attenuation with a scan range of 124 GHz), the sensitivity is only reduced by a factor of ~2.6.

Similar as with the single cell system we evaluated the influence of the central laser wavelength and scan amplitude drift using the 2.5GHz methane line-halfwidth as a typical narrow absorption line. All three outputs are observed simultaneously.
For a multiple cell system the maximum central wavelength and scan amplitude drift is determined by the shortest sensing cell. (The longer the cell, the smaller the error in determining the concentration since C = Absorbance/αL). Hence with a shortest cell length of 5cm, similar figures apply, namely, $\pm 3.5\gamma$ for the centre wavelength drift and $\pm 7.8\gamma$ for scan amplitude drift.
For narrow band multiple sensor systems, the frequency of the source should be stabilised within ranges determined by centre wavelength drift and scan amplitude drift. Using the 2.5GHz absorption line the source should be stabilised within ~± 8.868GHz. This correspond to the absorption spectra half-linewidth/wavelength change ratio of ~0.282.

10.2. Increasing the absorption with the use of a dummy cell

An examination of equation (5.23) reveals another way of improving the sensitivity which in fact applies to both broad-band and narrow-band absorbers.
Since the beat signal from, say, the third cell makes a double pass through the preceding cells, but only has an effective path length of one pass in the third cell (see beat term in equation 5.23), the sensitivity may be increased by using the beat signal from the next cell to measure the absorption in the preceding cell. In such a system, the last cell would be a dummy cell (no absorption) to provide the measurement for the second last cell. For example, for a single cell system one would use 2 cells with second cell being the dummy. Using the usual equations for the beat signal from the two cells and assuming as usual that $e^{-A} \sim (1-A)$, where A=

$\alpha_m CL$, the beat signal from each cell will be reduced due to absorption by the following factors:

$$\text{beat}_1 \rightarrow 1\text{-}A_1 \qquad (10.2)$$

$$\text{beat}_2 \rightarrow 1\text{-}2A_1\text{-}A_2$$

However with the second cell a dummy cell ($A_2=0$) we can measure absorption in the first cell from the beat signal in the second cell with twice the sensitivity compared with the first beat signal. The influence on the third cell output characteristics for 2.5GHz half-linewidth is shown in Figure 10.8 (the absorbtion has been gradually increased from 0 to 1% in steps of 0.2% in the last sensing cell with no absorbance in cells one and two).

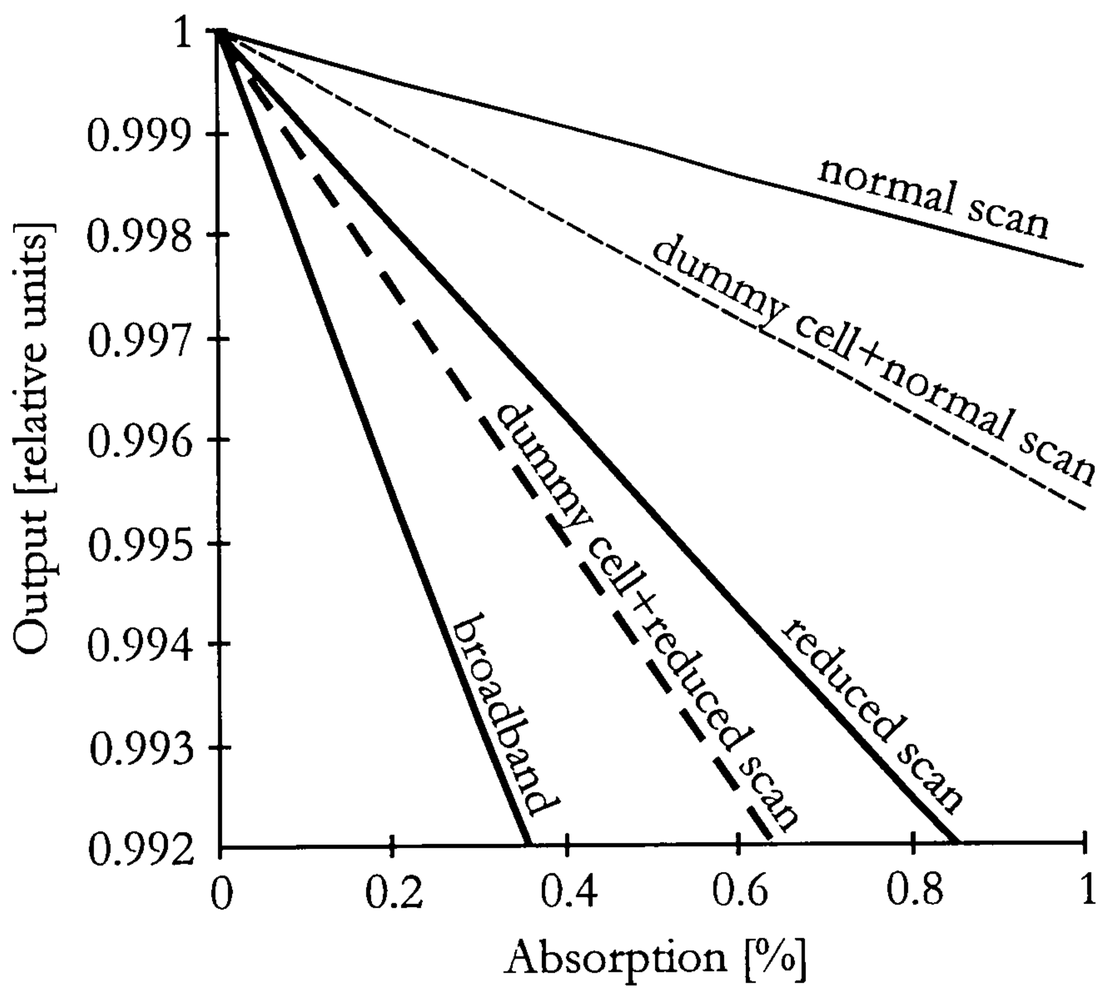

Figure 10.8: *Increase of the absorption with the introduction of a dummy cell*

10.3. Signal to noise ratio and the influence of the narrow band absorber on the number of cells in the system

In order to check the simulations, and also to calculate the signal to noise ratio in the next section, we now derive an analytic expression for the effect of the narrow band absorber. The linear scan of the source frequency (or wavenumber ν) can be described by the relation:

$$\nu = \nu_1 + \Delta\nu\left(\frac{t}{T}\right) \tag{10.3}$$

where ν_1 is the starting wavenumber and $\Delta\nu$ is the scan range.

As the source is scanned through the absorption line, the output intensity of the beat signal will vary in accordance with equation (10.1). What we actually measure is the time average of the beat signal so we can define an equivalent time-averaged absorption as:

$$\alpha_{eq} = \frac{1}{T}\int_0^T \alpha(\nu)dt \tag{10.4}$$

Substituting the scan equation (10.3) into the Lorentzian function equation (10.1) and performing the integral of equation (10.4) we obtain:

$$\alpha_{eq} = \alpha_m \frac{\arctan(\xi)}{\xi} \tag{10.5}$$

where $\xi=\Delta\nu/2\gamma$ and we have assumed that the scan is symmetric about the absorption line centre. Equation (10.5) predicts that for $\xi=3.4$, $\alpha_{eq}=\alpha_m/2.6$, in agreement with the results in Figure 10.7.

According to results presented in chapter 9.6 shot noise limited detection can be readily achieved. Under shot noise limited detection, the worst case SNR is approximately:

$$\frac{S}{N}=\frac{\left(\alpha_{eq}CL\right)\Re\sqrt{P_{incident}}\cdot 2r^2\left(1-r^2\right)\left(t^2\right)^{2(n-1)}}{\sqrt{e\Re B}} \tag{10.6}$$

where α_{eq} is obtained from equation (10.5), $\Re$ is the photodiode responsivity (~0.9A/W), $P_{incident}$ is the incident optical power on the system, B is the bandwidth (5kHz) and e is the electronic charge.

For a typical narrow band absorber like methane (with absorption line-halfwidth of ~2.5GHz) and source incident power of ~0.5mW and substituting the values for the parameters, the SNR is:

$$SNR=\left[47.6-0.72(n-1)+10\log\left(\alpha_{eq}CL\right)\right]dB \tag{10.7}$$

Equation (10.7) predicts that we can still detect methane concentrations of 10% of the LEL in the last cell of ~5cm length at a SNR of ~5 dB for the maximum cell number n=23 if a reduced scan (17GHz) is implemented. For the large scan range (124GHz) the number of cells where we can still detect 10%LEL in the last cell is reduced to n=12.

10.4.Specific system applications

A specific system application is distributed gas concentration measurements (or detection) of gases such as methane. In practice (for methane alarm systems) detection below the Lower Explosive Level (LEL - 5% methane in air) should be

considered. For example, for 10% of the LEL and assuming a methane absorption coefficient [1] of $\alpha_m = 0.25 cm^{-1} atm^{-1}$ for the (weak) near IR lines around 1665nm with half-linewidths of ~2.5GHz, the calculated absorbance, A=0.006 for a 5cm path-length sensor cell (or equivalently 0.027dB). The results in Figure 2 indicate that detection of this level is well within the system capability for the 17 GHz scan range. Also, experimental results from the broad-band absorption system indicate that a resolution in cell attenuation measurements of 0.01dB can be attained. Hence for the narrow band case where sensitivity is reduced by a factor of 2.6, we can expect to resolve down to typically 10%LEL provided the ratio of scan range to absorption linewidth is < 3.4. With the additional implementation of a last dummy cell the sensitivity could be doubled and we expect to resolve ~5%LEL.

10.5.Summary

We have demonstrated the feasibility of the coherence addressed FMCW method for narrow band absorbers. Generally when narrow band absorbers are introduced one can expect that the system performance is reduced. The extent to which the narrow band absorption effects the system depends greatly on the ratio between scan range and linewidth. Reducing this range to unity consequently increases system performance towards broadband absorption.

By simultaneously reducing the scan range and sweep frequency the narrow band absorption can be effectively enhanced. Compared to broadband absorption the performance is reduced, however distributed detection of an absorbance of ~ 6×10^{-3} (equivalent to ~ 10% of LEL for methane) is feasible. The results show that there should not be any problems in regard to either the available space in the frequency domain or in the signal-to-noise levels for systems with up to ~20 cells.

In order to determine the laser source wavelength stability two different wavelength drifts have been investigated: centre laser wavelength drift and scan amplitude drift. For single cell regime the ratio between the absorption spectra half-linewidth and wavelength change is ~0.282 for 2.5GHz half-linewidth. For

multiple cell systems the requirements for the wavelength source stability are determined by the shortest cell in the system and are approximately the same.

To avoid the central laser wavelength drift in relation to the (fixed) absorption line the source temperature must be held constant, whereas the laser injection current modulation should maintain the modulation depth (current scan start, current scan stop and amplitude of the modulating signal). To control the centre wavelength within $\pm 3.5\gamma$ (considering a typical laser diode temperature induced wavelength change of 0.1nm/°C) the temperature should stabilised within ±0.5°C. This temperature stabilisation is feasible, since the thermoelectric heater/cooler is usually implemented together with the leasing structure on the same substrate and therefore extremely good thermoconductance, hence response time and stability between the thermoelectric cooler and the laser diode is achieved. To keep the scan amplitude drift below the $\pm 7.8\gamma$ limit and using a typical laser diode current induced wavelength change of 0.05nm/mA the current amplitude should be controlled within ±1.1mA.

References

[10.1] G. Stewart, A. Mencaglia, W. Philip, W. Jin, "Interferometric Signals in Fiber Optic Methane Sensors with Wavelength Modulation of the DF Laser Source", Journal of Lightwave technology, Vol. 16, No. 1, January 1998

11. Signal processing and Calibration system

In this chapter the signal processing and calibration system for the coherence addressed quasi distributed absorption based sensing system will be presented. The signal processing and calibration unit should perform all necessary signal processing operations including the Fourier transformation and post signal processing. Since the signal processing system is built around a micro controller unit, a description of the micro controller hardware structure and appropriate software for the controller and personal computer will be presented.

11.1. Hardware configuration

The basic set-up of the micro controller is presented in Figure 11.1.

The micro controller unit includes the following components:

- power transformer and AC/DC converter

PAGE

MISSING

IN

ORIGINAL

- micro controller board
    - Hitachi H8/510 controller chip
        * 8 16-bit registers
        * 5 8-bit registers
        * 10MHz clock
        * 4 channel 10bit AD converter (13.4µs)
        * 56 I/O pins (seven 8-bit slots)
        - 64K ROM/EPROM
        - 64K STATIC RAM
        - RS232 interface using the MAX232 chip
- PIN diode (light detector) with transimpedance amplifier
- display
- four key keypad

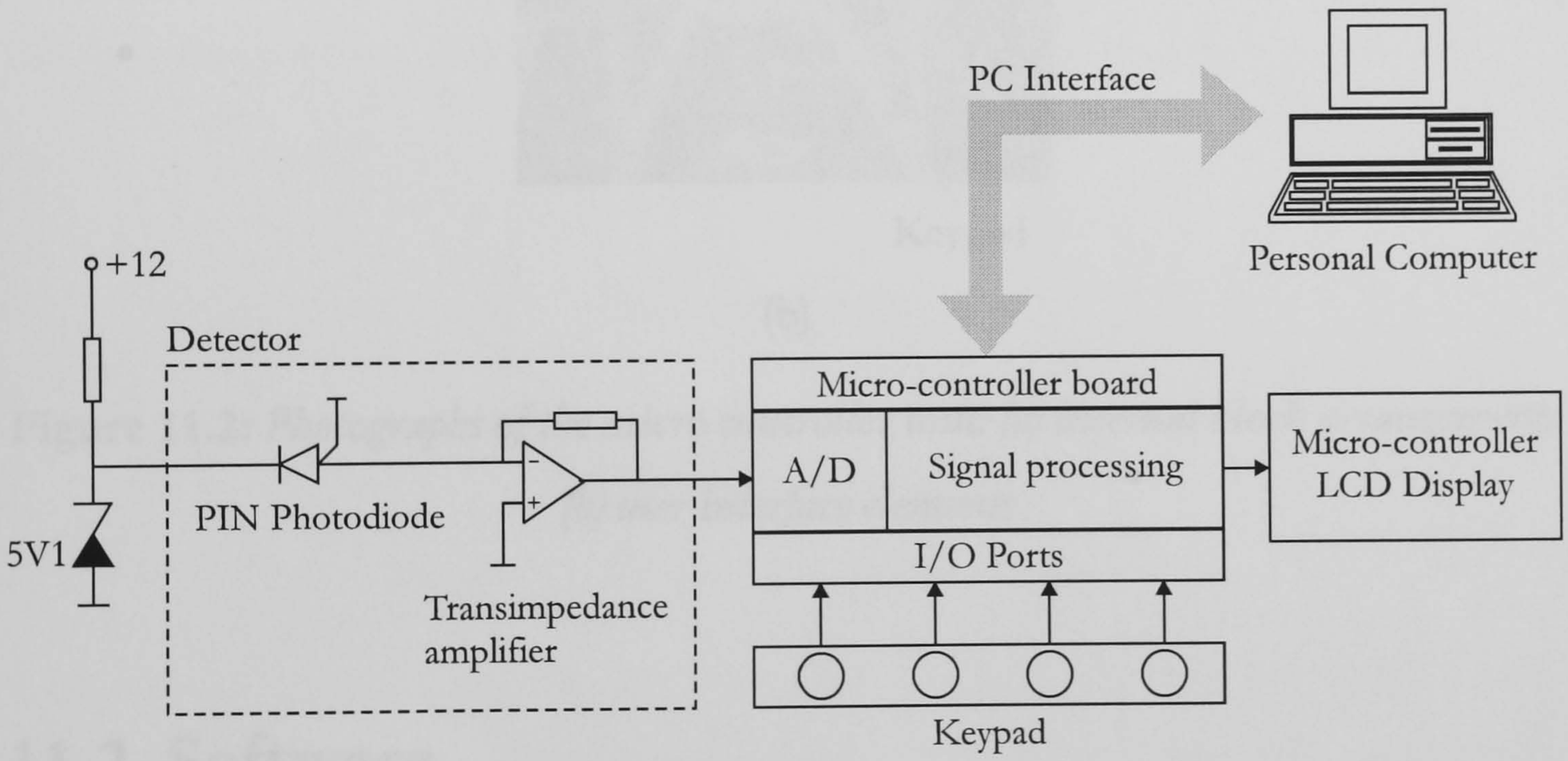

Figure 11.1: *Structure of the micro controller unit*

Photographs of the unit are presented in Figure 11.2.

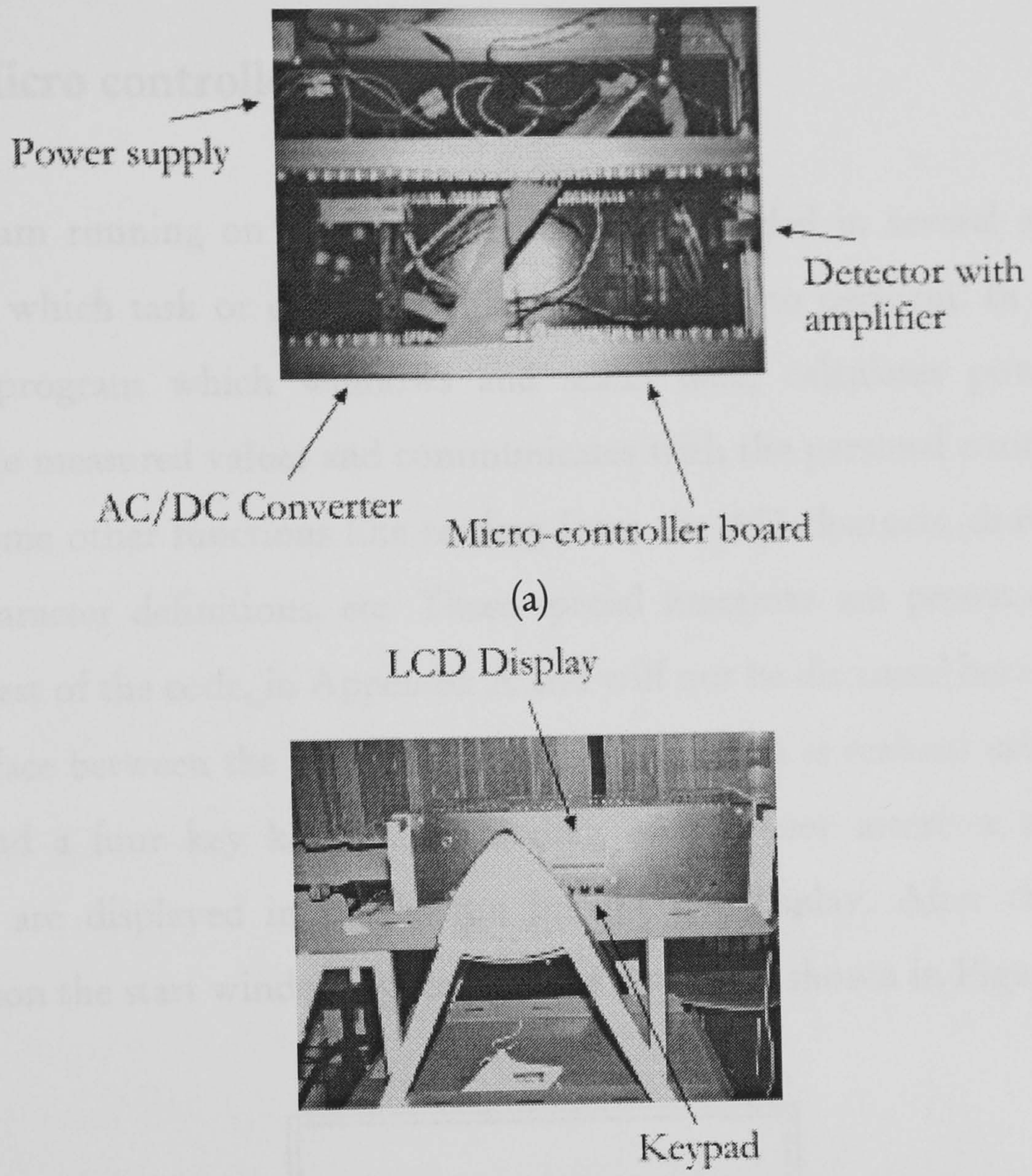

Figure 11.2: *Photographs of the micro controller unit: (a) internal block arrangement; (b) user interface elements*

11.2. Software

The programs which have been written to enable the signal analysis of the coherence addressed quasi distributed sensing system can be divided into two categories. First the software which supports the micro controller and second the spectral analyser program for the personal computer. All software code is written in standard C programming language and the code listings are given in Appendix

A and Appendix B for the controller program and personal computer program respectively.

11.2.1. Micro controller program

The program running on the micro-controller is divided in several subroutines, depending which task or operation the controller has to perform. In addition to the core program which windows and scales data, calculates power spectra, displays the measured values and communicates with the personal computer, there are also some other functions like reading from the AD channels, drawing on the screen, character definitions, etc. These special functions are presented, together with the rest of the code, in Appendix A and will not be discussed here.

The interface between the user and the micro-controller is realised using the LCD display and a four key keypad. Depending on the user interface tree the key functions are displayed in the button line of the display. After the hardware initialisation the start window appears on the display as shown in Figure 11.3.

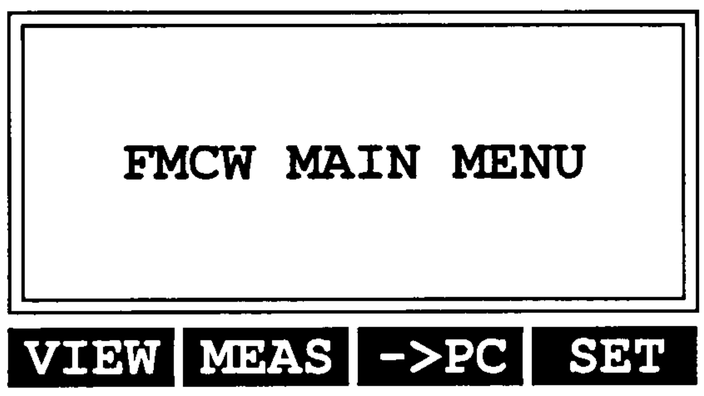

Figure 11.3: *Main micro-controller window*

The user may choose from one of the subroutines and jump into the **VIEW MENU**, **MEASUREMENT MENU** and **TRANSFER TO PC MENU**, whereas the **SET MENU** is currently not utilised but could be applied for some initial parameter settings. By pressing the key beneath the highlighted text displayed on the LCD, the program jumps into one of the submenus/subroutines. One can return to a higher level by using the **UP** key.

In the **VIEW MENU** we can observe the signal from the detector in time domain or the appropriate power spectrum. To display the time domain signal the values

from the analog to digital conversion are first stored then scaled to fit in the displayed window and finally displayed on the LCD.

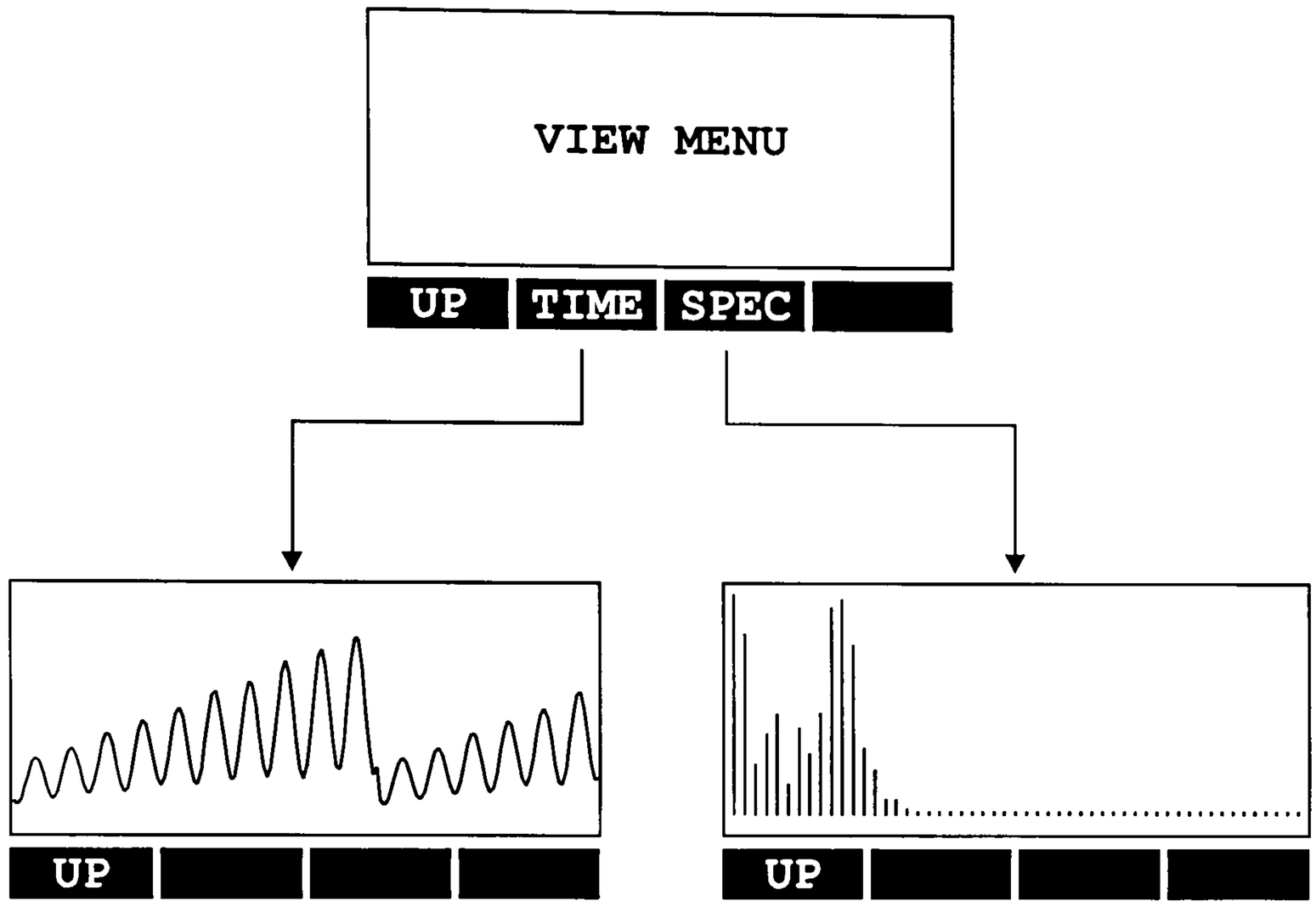

Figure 11.4: *View display window and sub-windows*

To view the power spectrum of the measurement system the data is first windowed using Welch, Hanning or Barttlet window. After that a 512 point Fast Fourier Transform is calculated. The resulting power spectrum is presented on the LCD. The window hierarchy for the **VIEW MENU** is shown in Figure 11.4.

If the **MEASUREMENT MENU** is selected one may further choose to measure an individual cell and then decide which one, or ones may perform a multiple measurement and measure all cells simultaneously. In either case the output (or absorption) value for a particular unit together with a bar graph indicating the beat amplitude is presented. The measurement display window hierarchy is shown in Figure 11.5.

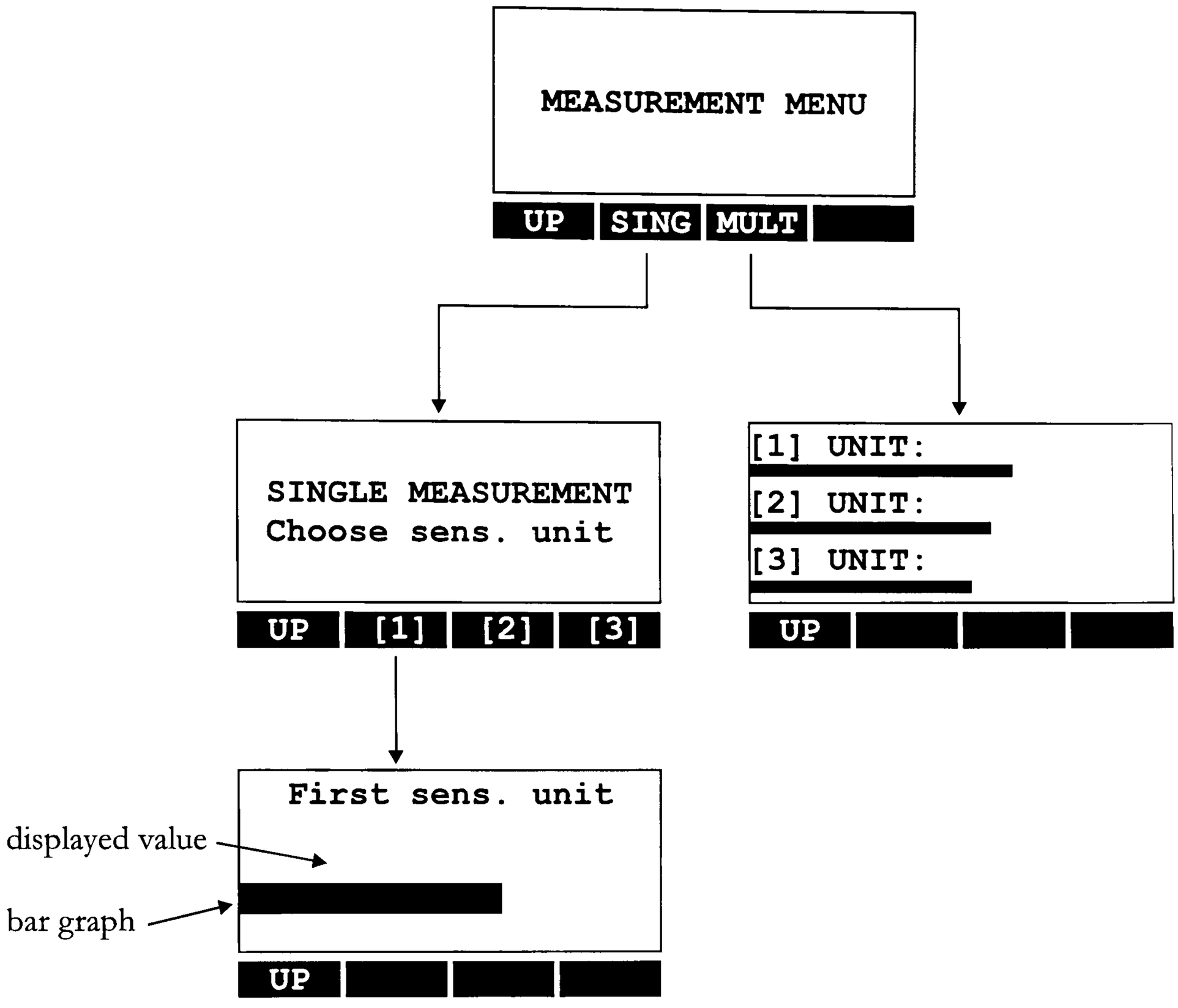

Figure 11.5: *Measurement display window and sub-windows*

Finally the **TRANSFER TO PC MENU** is used to transmit data from the micro-controller to the personal computer. First a handshake between the controller and computer is performed by transmitting and receiving special tokens, and after the personal computer program has switched to the graphics mode 1024 unit data packages are transmitted to the personal computer. As shown in Figure 11.6 the communication is established after the **START** button has been pressed. The communication with the personal computer is interrupted after an abort token has been received from the computer, and the controller returns to the **H8->PC MENU**.

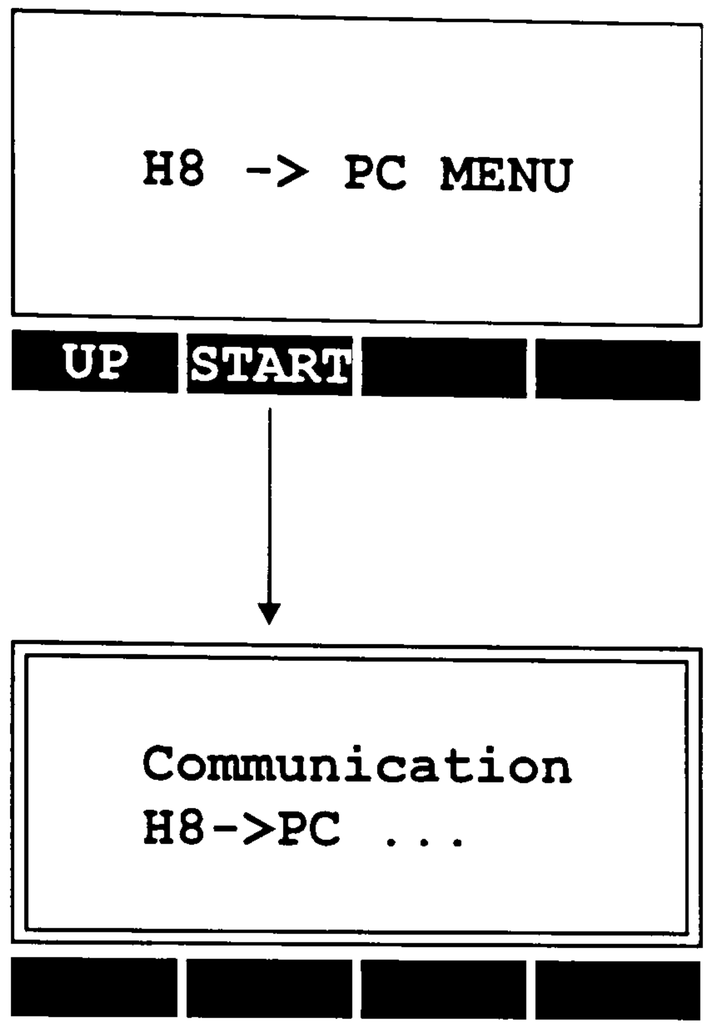

Figure 11.6: *Communication with the personal computer window*

11.2.2. Personal computer program

The software for the personal computer (PC) was written with the aim to present the power spectrum and the beat frequencies for the sensing cells with the appropriate absorption values on a large high resolution display. Additionally, due to its high computational power, the PC enables higher refresh rates of the spectrum to be displayed and more points in the FFT to be calculated.

After the measured signal has been converted from analogue to digital format, using the micro-controller board, data is transmitted to the PC. First a handshake between the micro-controller and the PC is performed to assure that both are ready to transmit and/or receive data. Then packages of data arrays with a length of 1024 units are transmitted to the PC.

The program on the PC first performs Welch, Hanning or Barttlet data windowing and then calculates the 1024 point Fast Fourier Transform. The resulting power spectrum is presented in the upper half of the screen with additional beat frequency and peak amplitude markings. In the lower half of the screen, the measured and windowed signal in the time domain are presented.

The markers corresponding to the power spectrum peaks are first presented using the initial input frequency values, but can be moved during operation by means of the computer keyboard.

The C-code for the PC program is given in Appendix B.

11.3. Absorption measurements using the micro controller and the personal computer

For absorption measurements using the micro-controller and the PC, the Spectrum Analyser and detector within the coherence addressed quasi distributed system are replaced by the micro-controller unit and the PC respectively.

To perform the evaluation of the changed system microscope slides are inserted inside the cells and the power spectrum changes are observed on the computer display. The initial power spectrum window capture is presented in Figure 11.7.

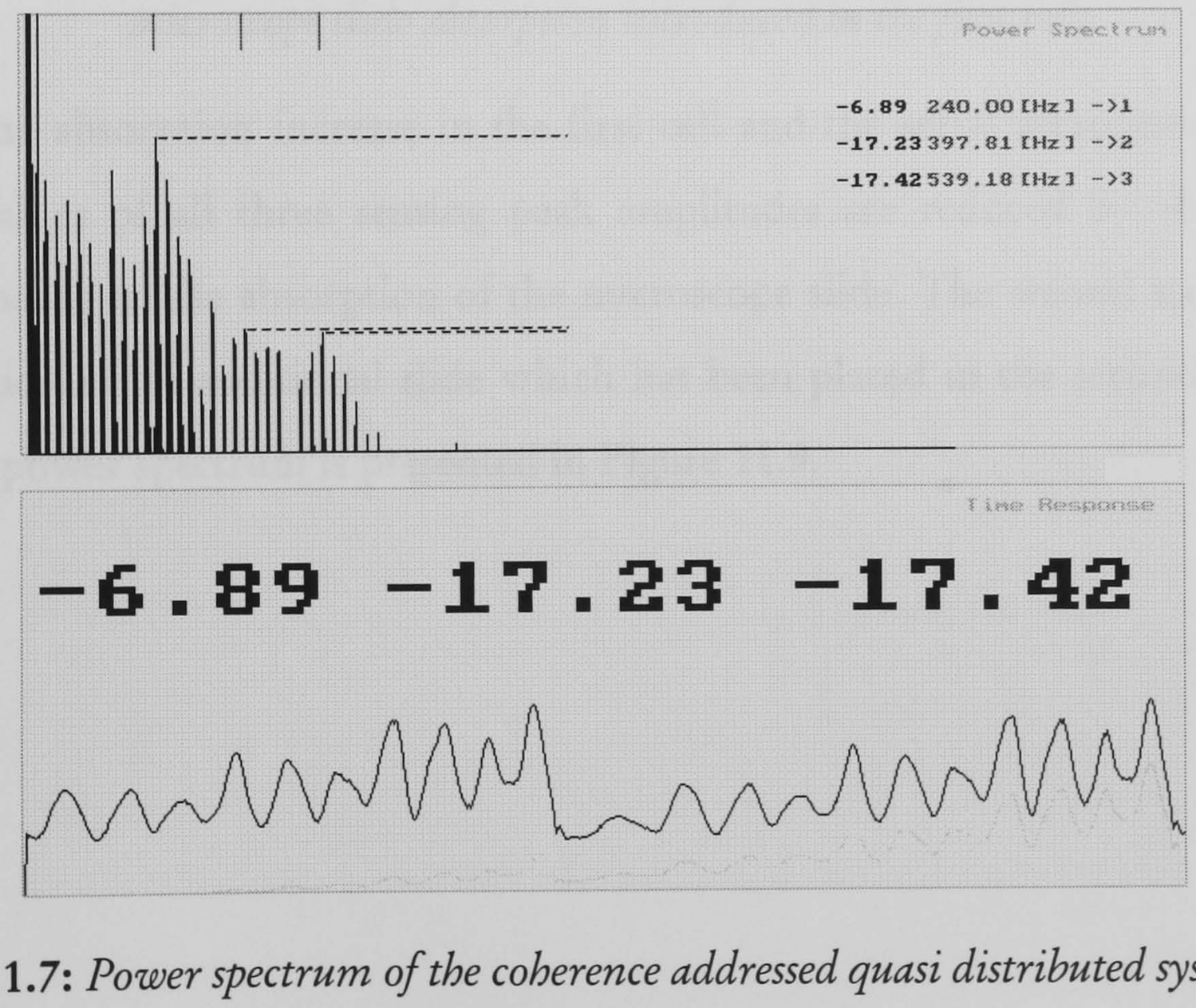

Figure 11.7: *Power spectrum of the coherence addressed quasi distributed system when no additional absorption is introduced*

All three power spectrum peaks are clearly visible and the corresponding amplitude value expressed in dB is also presented in the lower (time response) half

of the screen using large characters. In the next step a microscope slide is introduced into the first cell and the response is shown in Figure 11.8.

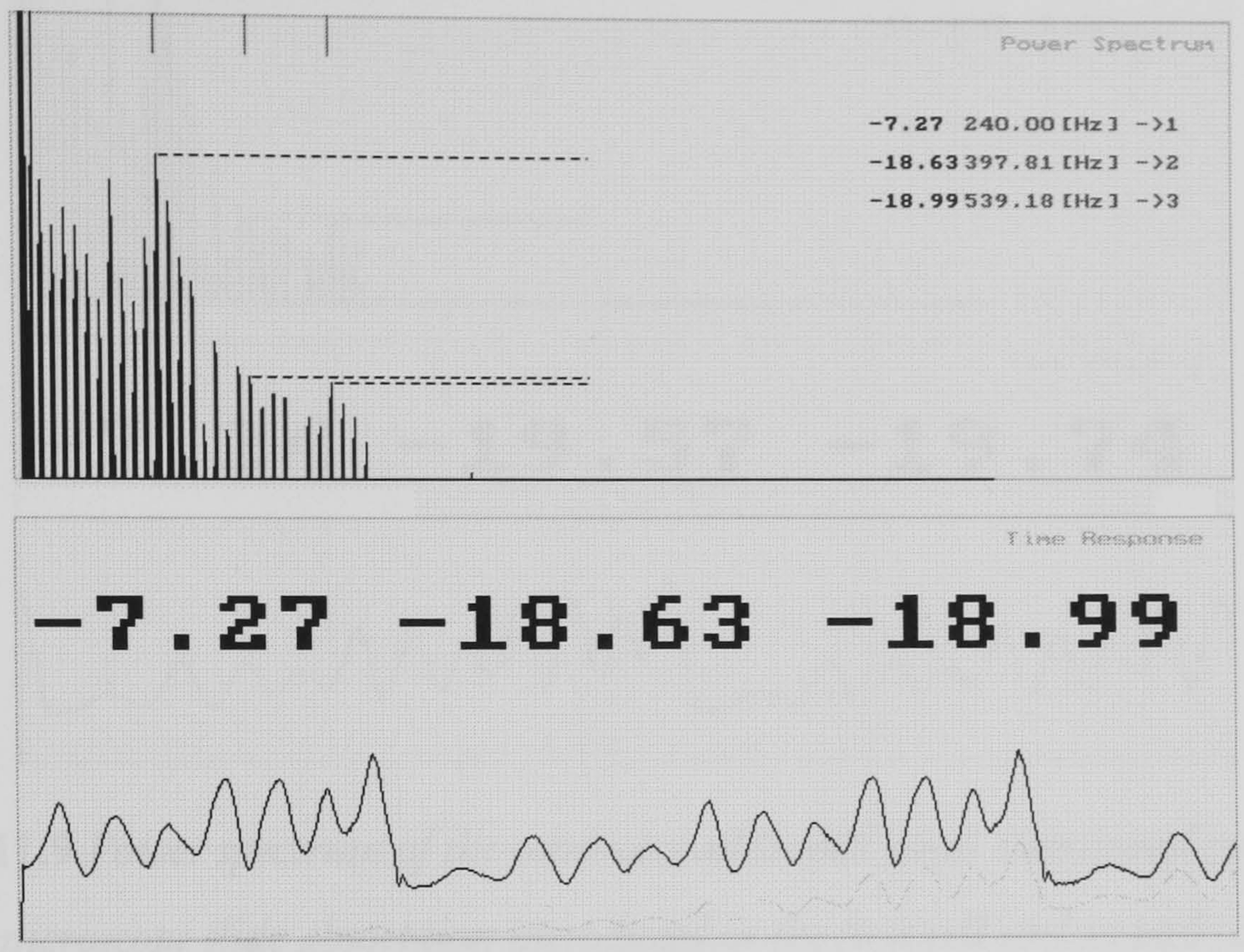

Figure 11.8: *Power spectrum of the coherence addressed quasi distributed system with microscope slide absorption introduced in the first cell*

Due to the absorption increase in the first cell and the serial arrangement of the system values of all three sensing peak amplitudes are reduced by the amount corresponding to the absorption of the microscope slide. The second step was the introduction of an additional slide which has been placed in the second cell. The resulting power spectrum is presented in Figure 11.9.

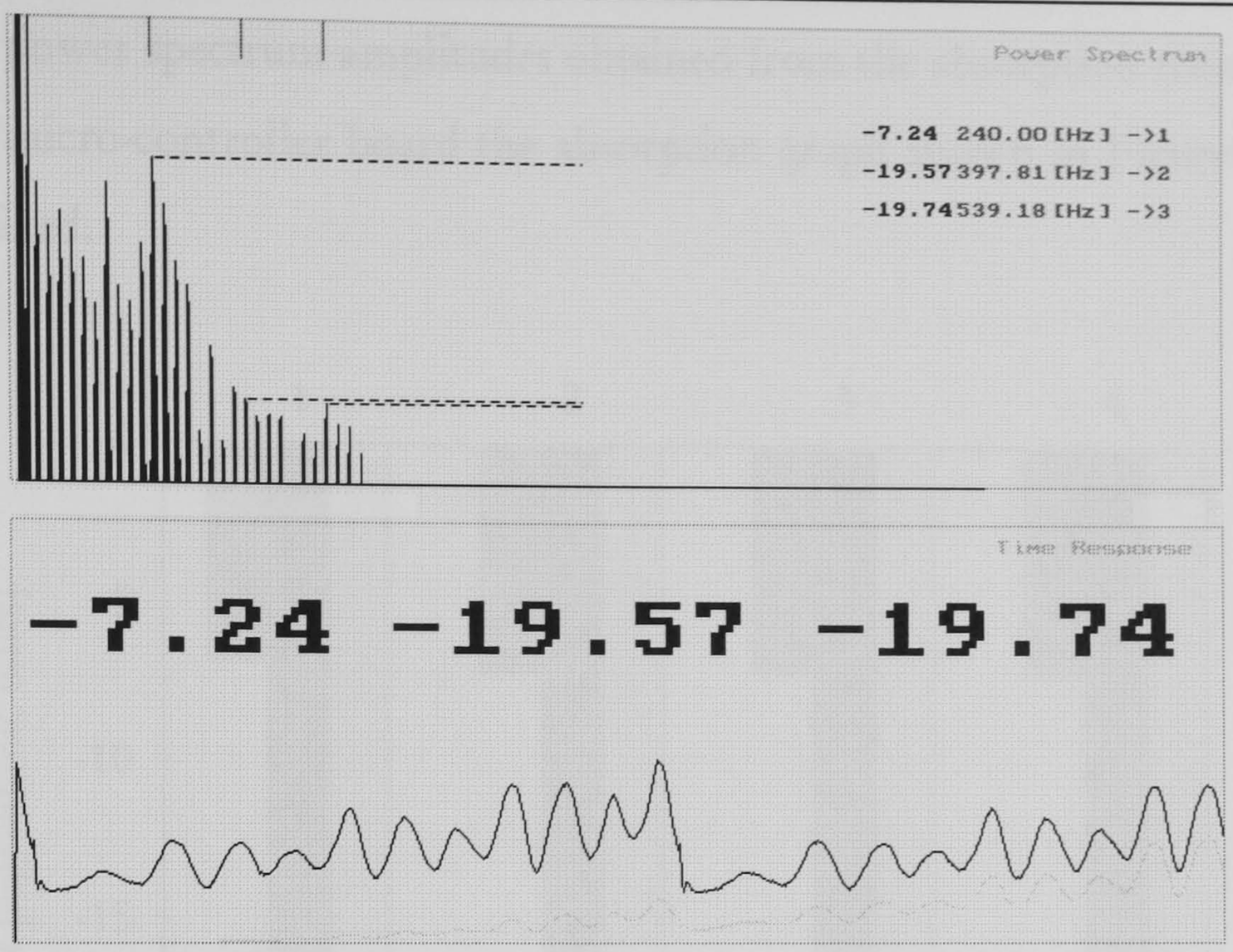

Figure 11.9 *Power spectrum of the coherence addressed quasi distributed system with microscope slide absorption introduced in the first cell and second cell*

For the final experiment an additional microscope slide was introduced in the last cell. The resulting power spectrum is shown in Figure 11.10.

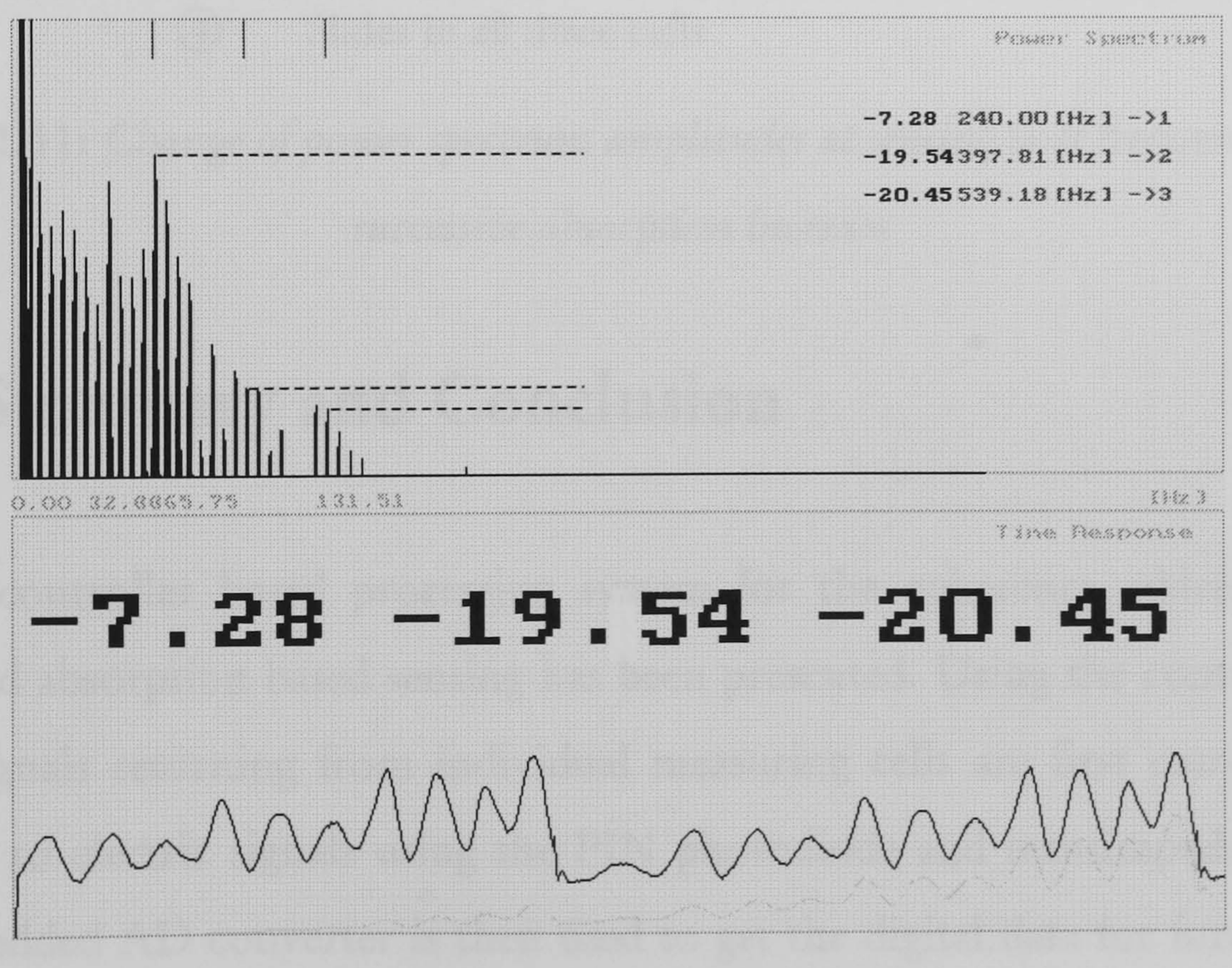

Figure 11.10 *Power spectrum of the coherence addressed quasi distributed system with microscope slide absorption introduced in the first cell, second cell and third cell*

From the power spectrum amplitudes obtained from the absorption measurements using the micro-controller board the absorption graph shown in Figure 11.11 has been obtained.

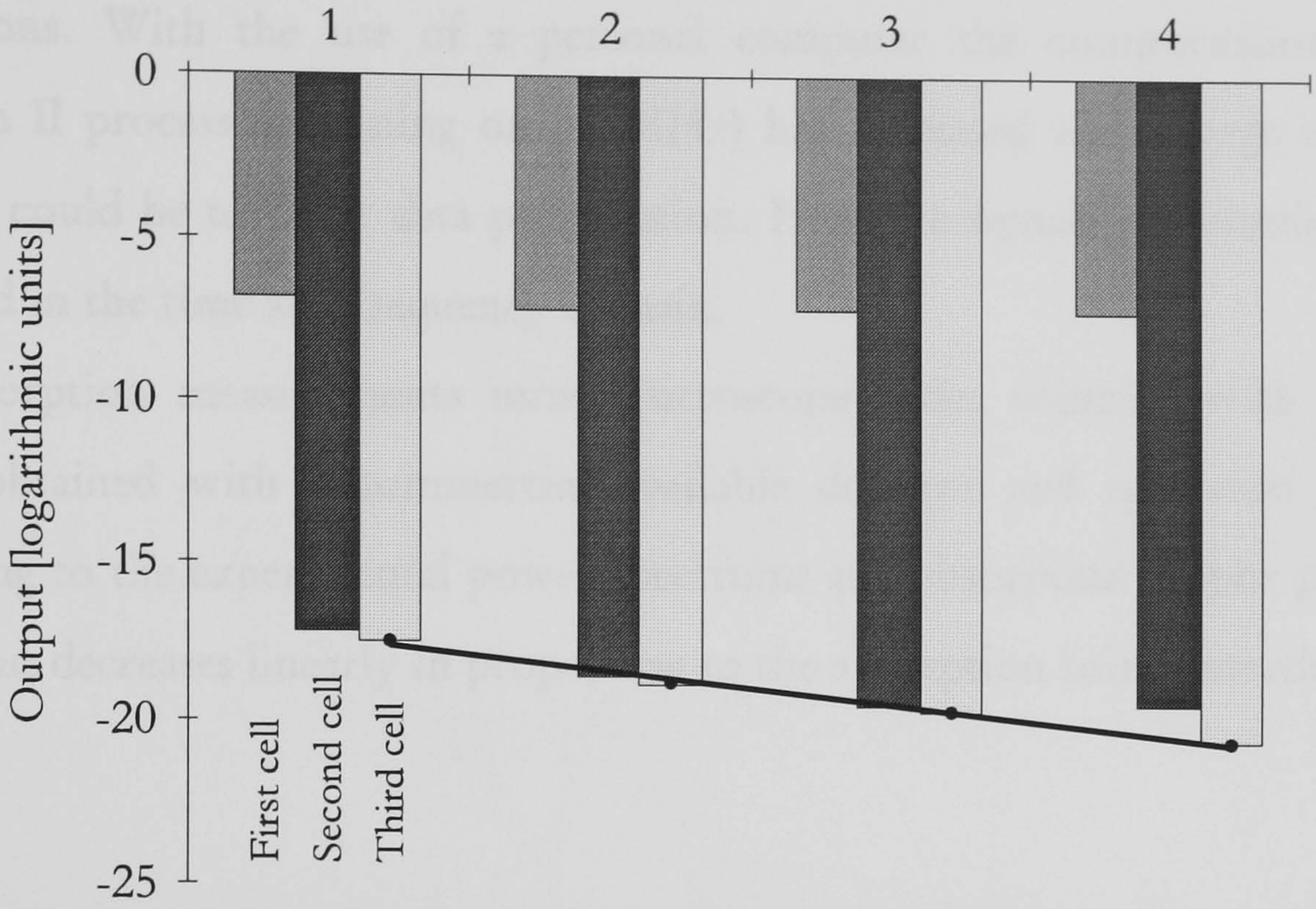

Figure 11.11: *Change of power spectrum amplitudes at sensing beat frequencies due to successive absorption increase*

11.4. Summary and Conclusion

A micro-controller based processing system for the coherence addressed quasi distributed absorption based sensing has been presented. Using the controller unit optical signals returning from individual measuring cells are first converted and amplified to electric signals using the PIN photodiode and transimpedance stage. The embedded AD converter is then used to get the digital data for further signal processing. With a small graphics LCD display and a four key keypad, a simple and effective menu driven user interface has been implemented. Due to the limited computational power of the controller the power spectrum calculation has proven

to be time consuming. Although the power spectrum of the measured signals with its distinctive beat frequencies can be presented, the refresh rate is in order of 10s. Because of that an additional program for a personal computer has been written. Both programs include the same core algorithm for Fast Fourier Transform calculations. With the use of a personal computer the computational power (Pentium II processor running on 350MHz) has increased and a large computer monitor could be used for data presentation. Here the signals are simultaneously presented in the time and frequency domain.

The absorption measurements using microscope slides coincide with previous results obtained with a commercial available detector and spectrum analyser. According to the experimental power spectrums and absorption graphs presented, the output decreases linearly in proportion to the absorption being introduced.

12. Analysis of Quasi-Distributed Optical Sensors Combining RF Modulation with the FMCW Method

In previous chapters, we have analysed and demonstrated an optical sensor system for quasi-distributed measurement of absorption for application in trace gas detection in the near-IR. The system is based on the Frequency-Modulated Continuous Wave (FMCW) method in which beat frequencies are used to identify individual sensing units along a length of optical fibre. In this chapter, we show how the sensitivity of such a system can be improved by combining the FMS method with the FMCW scheme. We first present the mathematical analysis for a single cell system and then demonstrate the feasibility of the method for multiple cell systems.

12.1.Introduction

The basis for a number of sensitive spectroscopic detection methods is the ease with which the diode lasers can be wavelength-modulated. Using a DFB laser system, high-sensitivity detection of a number of important gases, including methane, carbon dioxide, carbon monoxide, etc. can be obtained [12.1],[12.2]. The simplest way to employ diode lasers for chemical sensing is to directly measure the absorption spectrum from the transmitted laser power through the absorption feature as a function of wavelength. However, direct absorption measurement is limited since it requires detection at almost DC frequencies where detector and laser background noise are high [12.3]. To overcome this problem, a number of modulation techniques have been developed. They can be roughly divided into two categories, i.e. wavelength modulation spectroscopy and frequency modulation spectroscopy, distinguished by the frequency of the modulation.

Because of the available technology, techniques that use low modulation frequency were implemented first and are usually referred as wavelength modulation spectroscopy (WMS) [12.4]. Here the laser diode injection current is sinusoidally modulated as the laser wavelength is tuned through an absorption line. In general one recovers signals at the first and second harmonics of the modulation frequency and for weak absorption the signals are proportional to the concentration of the absorbing medium.

The second related spectroscopic method is frequency modulation spectroscopy (FMS) [12.5], first introduced in the early 1980. In FMS the laser is modulated at much higher frequencies than normally used in WMS, typically in the radio-frequency range. In frequency space, the modulated-laser electric field consists of a carrier frequency, which is the natural emission frequency of the diode laser, and side bands displaced from the carrier by integral multiples of the modulation frequency. When light is square-law detected in a photodiode each of the sidebands

mixes with the carrier to generate a signal at the modulation frequency. Modulation and detection are performed in the RF region because the intensity noise in diode lasers is at minimum and high signal-to-noise ratios can be achieved.

FMS and WMS are actually two limiting cases of the same technique. They are distinguished by the frequency of modulation (low for WMS and high for FMS) and the modulation depth (high for WMS and low for FMS). In FMS the modulation index of the laser is small, but the ratio of the modulation frequency to the absorption linewidth is large; the absorption feature of interest is probed by a singe isolated sideband. In WMS the ratio of the modulation frequency to the absorption line is small, but the modulation index is large. As the result the absorption feature is probed with a large number of sidebands. WMS offers moderate sensitivity and simple detection electronics, FMS provides maximum sensitivity at the expense of requiring RF technology.

The third method is a simple variation of the FMS: two-tone-frequency-modulation spectroscopy (TTFMS) [12.6],[12.7],[12.8],[12.9]. The method requires diode-laser modulation at two distinct radio frequencies with detection at the difference between the two applied frequencies. This method offers the advantage that arbitrarily large modulation frequencies can be applied to the laser to maximise the differential absorption experienced by the sidebands, but detection at the lower beat frequency allows the use of relatively low bandwidth detectors and demodulation techniques.

12.2.Principle of the combined FMS and FMCW methods

The proposed system is illustrated in Figure 12.1. Absorption measurements are made using a series of open-path micro-optic cells constructed from GRIN lenses,

with each cell of differing length. Somewhat similar to two tone frequency modulation spectroscopy, we apply a double modulation on the laser output. First the laser diode injection current is sawtooth modulated, providing a linear scan over a certain frequency/wavelength range. Secondly the laser output is externally modulated at radio frequencies. At a micro-optic cell, the two glass/air interfaces give rise to two back-reflected signals directed to the detector. Due to the time delay between the two back-reflections, we obtain two RF modulated waves which are being scanned through the wavelength range, but which differ in frequency by a fixed amount, namely, the beat frequency, ω_b, as determined from the time delay (proportional to the cell length and unique for each cell). These waves are coherently mixed, detected and displayed on the spectrum analyser.

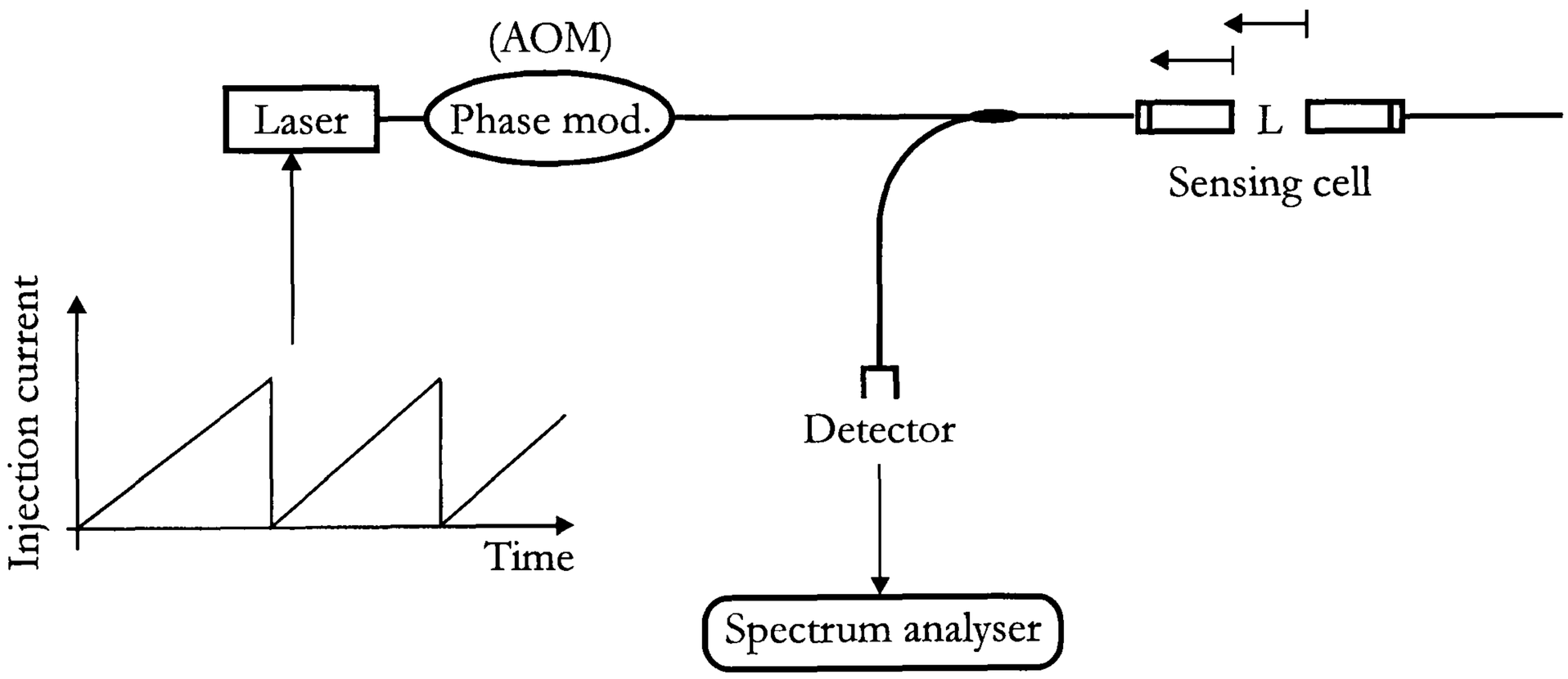

Figure 12.1: *Arrangement for frequency modulation spectroscopy using microoptic sensing cell*

Because each of the back-reflected waves are also rf-modulated at ω_m (low modulation index), each contains, approximately, single upper and lower sidebands. As we will show (see Figure 12.3), we can arrange matters so that only one of these sidebands is attenuated by the narrow band absorber (gas absorption line). With this condition, an imbalance is created and a new signal, proportional

to the absorbance, appears in the output spectrum at the difference frequency $(\omega_m-\omega_b)$.

12.3.Mathematical model of the absorption sensor combining RF modulation with the FMCW method

We will first derive the mathematical model for the proposed method for a single micro-optic sensing cell.

After the light beam $E_0e^{j\omega t}$ leaves the modulator (see Figure 12.1), its electric field amplitude is given by [8]:

$$E_{out}(t) = E_{in}e^{j\omega_0 t}\sum_{n=-\infty}^{\infty} J_n(\beta)e^{jn\omega_m t} \tag{12.1}$$

where β is the modulation index and is a function of modulation power. The effect of the phase modulator is to produce an infinite set of sidebands spaced at integral multiples of modulation angular frequency ω_m from the carrier frequency ω_0. Each sideband has an amplitude that is proportional to $J_n(\beta)$. For practical purposes β is usually less than one and only the carrier and first pair of sidebands have significant amplitudes:

$$J_0(\beta)\approx 1 \text{ and } J_{\pm 1}(\beta)\approx \pm\frac{\beta}{2} \tag{12.2}$$

The output electrical field therefore consists of three frequency components:

$$E_{out}(t) \cong E_{in} e^{j\omega_0 t} \cdot \left[1 + \frac{\beta}{2} e^{j\omega_m t} - \frac{\beta}{2} e^{-j\omega_m t} \right] \tag{12.3}$$

$$= E_{in} e^{j\omega_0 t} + E_{in} \frac{\beta}{2} e^{j(\omega_0+\omega_m)t} - E_{in} \frac{\beta}{2} e^{j(\omega_0-\omega_m)t}$$

If we now consider our microoptic sensing cell with two reflections arising from the glass/air interfaces we get two reflected signals E_1 and E_2 (Figure 12.2).

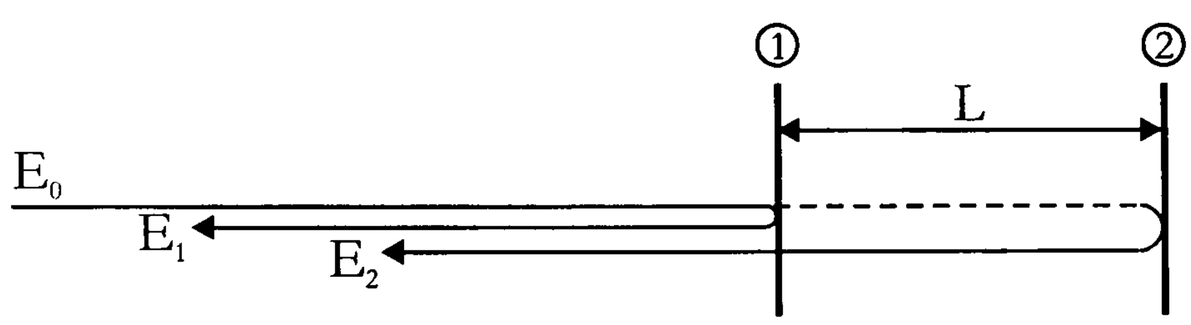

Figure 12.2: *Signal reflections from the microoptic sensing cell*

Due to the sawtooth injection current modulation of the source, the output signal from the cell, for each frequency component ω has the form:

$$E_{out} = E_0 \left\{ r_1 e^{j\omega t} + r_2 tt' e^{j(\omega t+\psi+\Delta\psi)} \right\} \tag{12.4}$$

where r_1, r_2 are reflection and t, t' transmission coefficients at the glass to air interfaces. Changes of the output light amplitude due to modulation are neglected.

With the three frequency components arising from the rf-modulation according to (12.3), the total field returning from the cell is:

$$E_{out} = E_0 \left\{ \begin{array}{l} r_1 e^{j\omega_0 t} + r_1 \frac{\beta}{2} e^{j(\omega_0+\omega_m)t} - r_1 \frac{\beta}{2} e^{j(\omega_0-\omega_m)t} + \\ r_2 tt' e^{j(\omega_0 t+\psi+\Delta\psi)} + r_2 tt' \frac{\beta}{2} e^{j\left((\omega_0+\omega_m)t+\psi^+ +\Delta\psi^+\right)} - r_2 tt' \frac{\beta}{2} e^{j\left((\omega_0-\omega_m)t+\psi^- +\Delta\psi^-\right)} \end{array} \right\} \tag{12.5}$$

here ω_m is the modulation frequency. The dynamic phase shifts are wavelength dependent:

$$\psi = 2\pi \frac{2n_e L}{\lambda_0}; \qquad \psi^+ = 2\pi \frac{2n_e L}{\lambda_0^+}; \qquad \psi^- = 2\pi \frac{2n_e L}{\lambda_0^-} \tag{12.6}$$

$$\Delta\psi = 2\pi \frac{2n_e L\Delta\lambda}{\lambda_0^2}; \Delta\psi^+ = 2\pi \frac{2n_e L\Delta\lambda}{\lambda_0^{+2}}; \Delta\psi^- = 2\pi \frac{2n_e L\Delta\lambda}{\lambda_0^{-2}}$$

where $\Delta\lambda$ is the wavelength change due to sawtooth modulation, n_e is the refractive index, and λ_0^+ and λ_0^- are the appropriate wavelengths for the $(\omega_0+\omega_m)$ and $(\omega_0-\omega_m)$ components respectively:

$$\frac{1}{\lambda^+} = \frac{\omega_0+\omega_m}{2\pi c} = \frac{\omega_0}{2\pi c} + \frac{\omega_m}{2\pi c} = \frac{1}{\lambda_0} + \frac{1}{\lambda_m} \tag{12.7}$$

$$\frac{1}{\lambda^-} = \frac{\omega_0-\omega_m}{2\pi c} = \frac{\omega_0}{2\pi c} - \frac{\omega_m}{2\pi c} = \frac{1}{\lambda_0} - \frac{1}{\lambda_m}$$

since

$$\frac{1}{\lambda_0} >> \frac{1}{\lambda_m} \Rightarrow \frac{1}{\lambda^+} \approx \frac{1}{\lambda_0} \text{ and } \frac{1}{\lambda^-} \approx \frac{1}{\lambda_0} \tag{12.8}$$

With this assumptions (12.5) modifies to:

$$E_{out} = E_0 \left\{ \begin{array}{l} r_1 e^{j\omega_0 t} + r_1 \frac{\beta}{2} e^{j(\omega_0+\omega_m)t} - r_1 \frac{\beta}{2} e^{j(\omega_0-\omega_m)t} + \\ r_2 tt' e^{j(\omega_0 t+\psi+\Delta\psi)} + r_2 tt' \frac{\beta}{2} e^{j((\omega_0+\omega_m)t+\psi+\Delta\psi)} - r_2 tt' \frac{\beta}{2} e^{j((\omega_0-\omega_m)t+\psi+\Delta\psi)} \end{array} \right\} \tag{12.9}$$

Since the sawtooth modulation ramp can be described as $\lambda=\lambda_0+\Delta\lambda_{max}t/T$ where T is the period of the ramp, we have $\Delta\psi=\omega_b t$ where ω_b is the beat frequency for the cell given by:

$$\omega_b = \frac{4\pi n_e L \Delta\lambda_{max}}{\lambda_0^2 T} = \left(\frac{2n_e L}{c}\right)\left(\frac{\Delta\omega_{max}}{2\pi}\right)\omega_{ramp} \qquad (12.10)$$

where $\Delta\omega_{max}$ is the scan range in terms of frequency and ω_{ramp} is the ramp frequency.

Equation (12.9) thus has 6 components in the frequency domain as illustrated in Figure 3. The 6 components are fixed in relation to each other, but are scanned over the frequency range of the sawtooth modulation ramp, namely, $\Delta\omega = \left(\frac{2\pi c}{\lambda_0^2}\right)\Delta\lambda_{max}$.

Suppose we now have a narrow-band absorber in the cell, such as a trace gas with a near-IR absorption line, with half linewidth, γ (γ typically a few GHz for pressure-broadened lines).

Since the first 3 components in equation (12.9) correspond to reflections from the first interface in the cell they do not experience absorption. However, provided that $\omega_m >> \gamma$, we can adjust the central laser frequency and limit the scan range so that only one of the remaining 3 components experiences absorption, as shown in Figure 3. If we choose one of the sidebands, then when absorption is present in the cell, we create an imbalance so that a new frequency component appears in the output whose amplitude is proportional to the absorbance. Here we choose the $(\omega_0+\omega_b-\omega_m)$ component, because mixing in the output with the ω_0 component gives rise to a signal component at $(\omega_m-\omega_b)$. We can then chose system parameters so that ω_b and ω_m are similar, which means that the $(\omega_m-\omega_b)$ frequency can be observed by low frequency detection equipment. Also, as can be seen from Figure 12.3, with $(\omega_m-\omega_b)$ small, the central laser frequency is approximately adjusted to the absorption line centre. (This does need to be exact because the laser wavelength is scanned over a range greater than the absorption line width).

With the assumption that only the $(\omega_0+\omega_b-\omega_m)$ component is attenuated, equation (12.9) becomes:

$$E_{out} = E_0\left\{\begin{array}{l} r_1 e^{j\omega_0 t} + r_1\frac{\beta}{2}e^{j(\omega_0+\omega_m)t} - r_1\frac{\beta}{2}e^{j(\omega_0-\omega_m)t} + \\ r_2 tt' e^{j(\omega_0 t+\psi+\Delta\psi)} + r_2 tt'\frac{\beta}{2}e^{j((\omega_0+\omega_m)t+\psi+\Delta\psi)} \\ -r_2 tt'\frac{\beta}{2}e^{-2\alpha_a CL}e^{j((\omega_0-\omega_m)t+\psi+\Delta\psi)} \end{array}\right\} \tag{12.11}$$

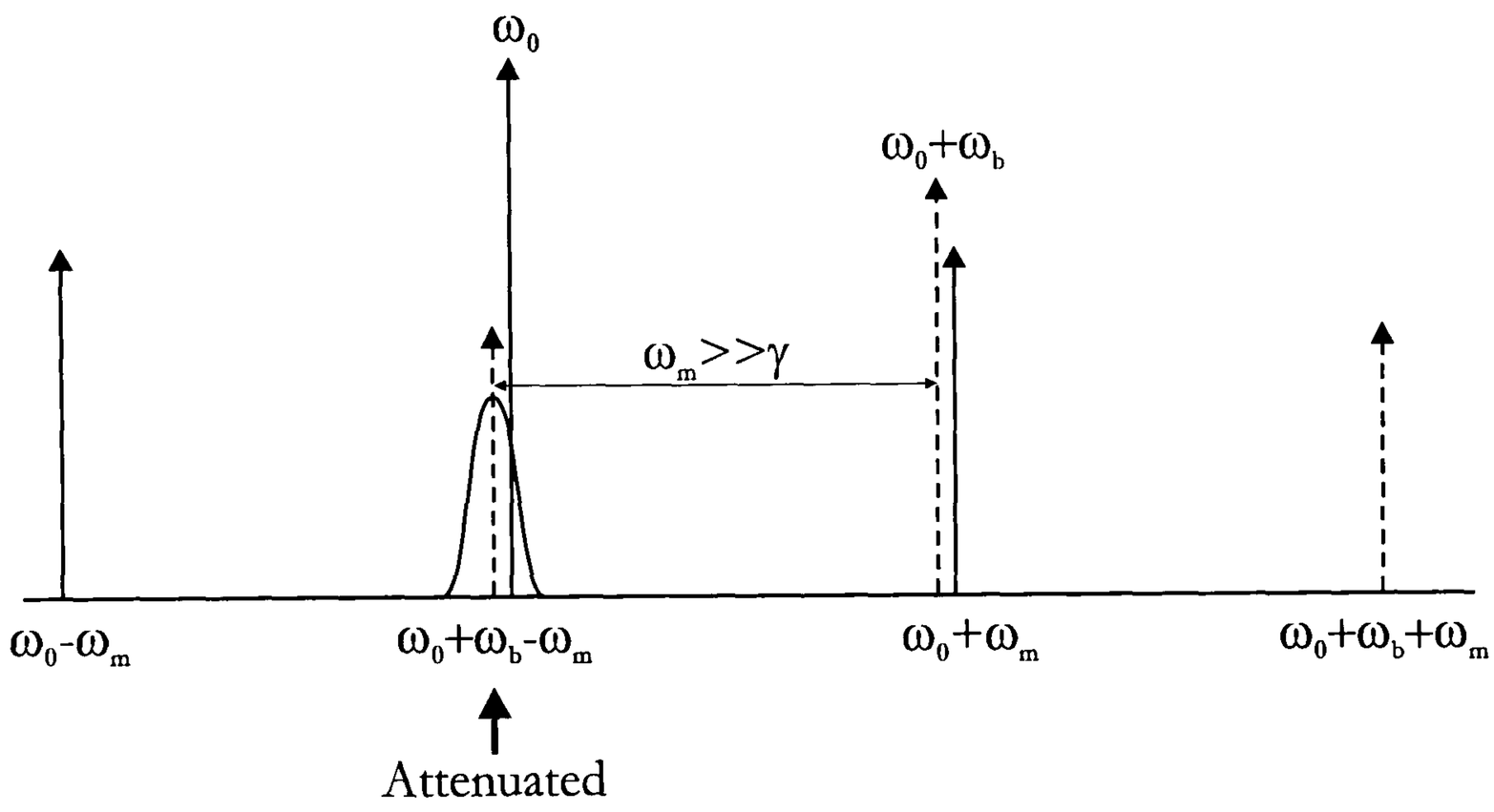

Figure 12.3: *Frequency components described by equation (12.9)*

Assuming small absorbance:

$$e^{-2\alpha_a CL} \cong 1-2\alpha_a CL = 1-\alpha CL = 1-A \tag{12.12}$$

where α_a is the amplitude attenuation coefficient, $\alpha = 2\alpha_a$ is the intensity coefficient, A is the absorbance and with $r_1=-r_2$ and tt'~1, equation (12.11) becomes:

$$\frac{E_{out}}{r_1 E_0} \approx \left\{ \begin{array}{l} e^{j\omega t} + \frac{\beta}{2} e^{j(\omega+\omega_m)t} - \frac{\beta}{2} e^{j(\omega-\omega_m)t} - e^{j(\omega t+\psi+\Delta\psi)} - \frac{\beta}{2} e^{j((\omega+\omega_m)t+\psi+\Delta\psi)} \\ + \frac{\beta}{2}(1-A) e^{j((\omega-\omega_m)t+\psi+\Delta\psi)} \end{array} \right\} \tag{12.13}$$

The total output light intensity is calculated by taking the first order correlation of the total electrical field (E_{out}/r_1E_0):

$$r_1^2 I_0 \cdot \left\{ \begin{array}{l} e^{j\omega_0 t} + \frac{\beta}{2} e^{j(\omega_0+\omega_m)t} - \frac{\beta}{2} e^{j(\omega_0-\omega_m)t} - e^{j(\omega_0 t+\psi+\Delta\psi)} - \frac{\beta}{2} e^{j((\omega_0+\omega_m)t+\psi+\Delta\psi)} \\ + \frac{\beta}{2}(1-A) e^{j((\omega_0-\omega_m)t+\psi+\Delta\psi)} \end{array} \right\} \times \tag{12.14}$$

$I \approx$

$$\left\{ \begin{array}{l} e^{-j\omega_0 t} + \frac{\beta}{2} e^{-j(\omega_0+\omega_m)t} - \frac{\beta}{2} e^{-j(\omega_0-\omega_m)t} - e^{-j(\omega_0 t+\psi+\Delta\psi)} - \frac{\beta}{2} e^{j((\omega_0+\omega_m)t+\psi+\Delta\psi)} \\ + \frac{\beta}{2}(1-A) e^{-j((\omega_0-\omega_m)t+\psi+\Delta\psi)} \end{array} \right\}$$

$$I \approx r_1^2 I_0 \cdot \left\{ \begin{array}{l} 2 + \frac{\beta^2}{4}(A^2+2A^2+4) + \left[-\frac{\beta^2}{2} - \frac{\beta^2}{2}(1-A) \right] (\cos 2\omega_m t - \cos(\psi+\Delta\psi)) + \\ \frac{\beta^2}{2}(1-A)\cos(2\omega_m t - \psi - \Delta\psi) + \frac{\beta^2}{2}\cos(2\omega_m t + \psi + \Delta\psi) \\ -2\cos(\psi+\Delta\psi) - \beta A \cos(\omega_m t - \psi - \Delta\psi) + \beta A \cos(\omega_m t) \end{array} \right\} \tag{12.15}$$

Since β is small, $\beta^2 \approx 0$ and with $\Delta\psi = \omega_b t$, equation (12.15) simplifies to

$$I \approx r_1^2 I_0 \cdot \left\{ 2 - 2\cos(\omega_b t + \psi) + \beta A \cos(\omega_m t) - \beta A \cos((\omega_m - \omega_b)t - \psi) \right\} \tag{12.16}$$

where I_0 is the incident intensity. As can be seen from equation (12.16), a new frequency component, proportional to the absorbance, A, appears at $(\omega_m-\omega_b)$. As we discuss later, each cell in a multi-cell system has a different value of ω_b so the absorbance of a cell is monitored through its unique $(\omega_m-\omega_b)$ component. Although

we assumed equal reflectivities for the cell interfaces ($r_1 = -r_2$), this is not necessary to the final results since the terms arise from the mixing of components from both interfaces. The method also offers an advantage compared to two-tone-frequency modulation spectroscopy, since only one phase modulator (one of the more expensive parts in the system) is used, whereas detection at the lower frequency ($\omega_m - \omega_b$) allows the use of relatively low bandwidth detectors and demodulation techniques.

In the above analysis, the $(\omega_0 + \omega_b - \omega_m)$ sideband was assumed to experience a constant absorbance A. This would only be true if the laser wavelength scan range is very small, much less than the absorption linewidth. In practice, to prevent the need for precise tuning of the laser wavelength to the absorption line centre, the sawtooth ramp will scan the $(\omega_0 + \omega_b - \omega_m)$ sideband through the absorption line, and the output amplitude of the $(\omega_m - \omega_b)$ signal will vary in accordance with the absorption lineshape function. For this case, what we observe at the output is the time average of the $(\omega_m - \omega_b)$ signal, so we define an equivalent time-averaged absorption coefficient as:

$$\alpha_{eq} = \frac{1}{T}\int_0^T \alpha \, dt \tag{12.17}$$

where, as before, T is the period of the sawtooth ramp.

The sawtooth ramp is described by: $\omega = \omega_1 + \Delta\omega_{max}(t/T)$ and if we consider a Lorentzian function for the absorption line:

$$\alpha(\nu) = \frac{\alpha_m}{1 + \left(\frac{\omega - \omega_0}{\gamma}\right)^2} \tag{12.18}$$

We obtain:

$$\alpha_{eq} = \alpha_m \frac{\tan^{-1}(\xi)}{\xi} \tag{12.19}$$

where α_m is the absorption at the line centre, $\xi = \Delta\omega_{max}/2\gamma$ and we have assumed that the scan is symmetric about the absorption line centre, ω_0.

Hence we can use an equivalent absorbance $A = \alpha_{eq}CL$ in equation (12.16) to obtain the output signal in term of the ratio ξ of scan range to linewidth.

We noted earlier that we need $\omega_m >> \gamma$ for the absorber to affect the $(\omega_0 + \omega_b - \omega_m)$ sideband only. There is also a limitation on the maximum scan range. With reference to Figure 12.3, the nearest component (reflected from the second cell interface) that could come under the absorption line is the $(\omega_0 + \omega_b)$ component if the scan is too large. To prevent this, we need $(1/2)\Delta\omega_{max} << (\omega_m - \gamma)$

In summary we can list the requirements as follows:

- $(\omega_m - \omega_b)$ small to give low detection frequency
- central laser wavelength set, approximately, to the absorption line centre
- $\Delta\omega_{max} << 2(\omega_m - \gamma)$ say, $\Delta\omega_{max} \sim 2(\omega_m - 2\gamma)$
- $\omega_m >> \gamma$ say $\omega_m \sim 4\gamma$
- $\Delta\omega_{max}$ as small as possible, consistent with suitable beat frequencies, to maximise α_{eq}

As an example, consider methane gas with the Q6 absorption line in the near-IR at 1665.5nm with half linewidth (angular frequency), $\gamma \sim 2\pi \times 2.5\text{GHz}$ and $\alpha_m \sim 0.25\text{cm}^{-1}\ \text{atm}^{-1}$ [12.2]. To satisfy the above criteria we typically need $\omega_m \sim 2\pi \times 10\text{GHz}$ and $\Delta\omega_{max} \sim 2\pi \times 10\text{GHz}$. We chose ω_b close to ω_m to give a low detection

frequency, $(\omega_m - \omega_b)$, and from equation (12.10) the required ramp frequency is: $\omega_{ramp} = 0.3\omega_b$ for a 5cm cell. Also the equivalent absorbance, $A = \alpha_{eq} CL$, can be calculated from equation (12.19) as $0.55\alpha_m$ CL, giving a value of 3.4×10^{-2} for 5% methane in a 5cm cell (Lower Explosive Level, LEL, is 5% for methane). With a modulation index of $\beta \sim 10\%$, and $r^2 \sim 4\%$, then from equation (12.16), the intensity of the $(\omega_m - \omega_b)$ signal is $\sim 1.4\times10^{-4} I_0$ for the LEL methane concentration, where I_0 is the incident light intensity.

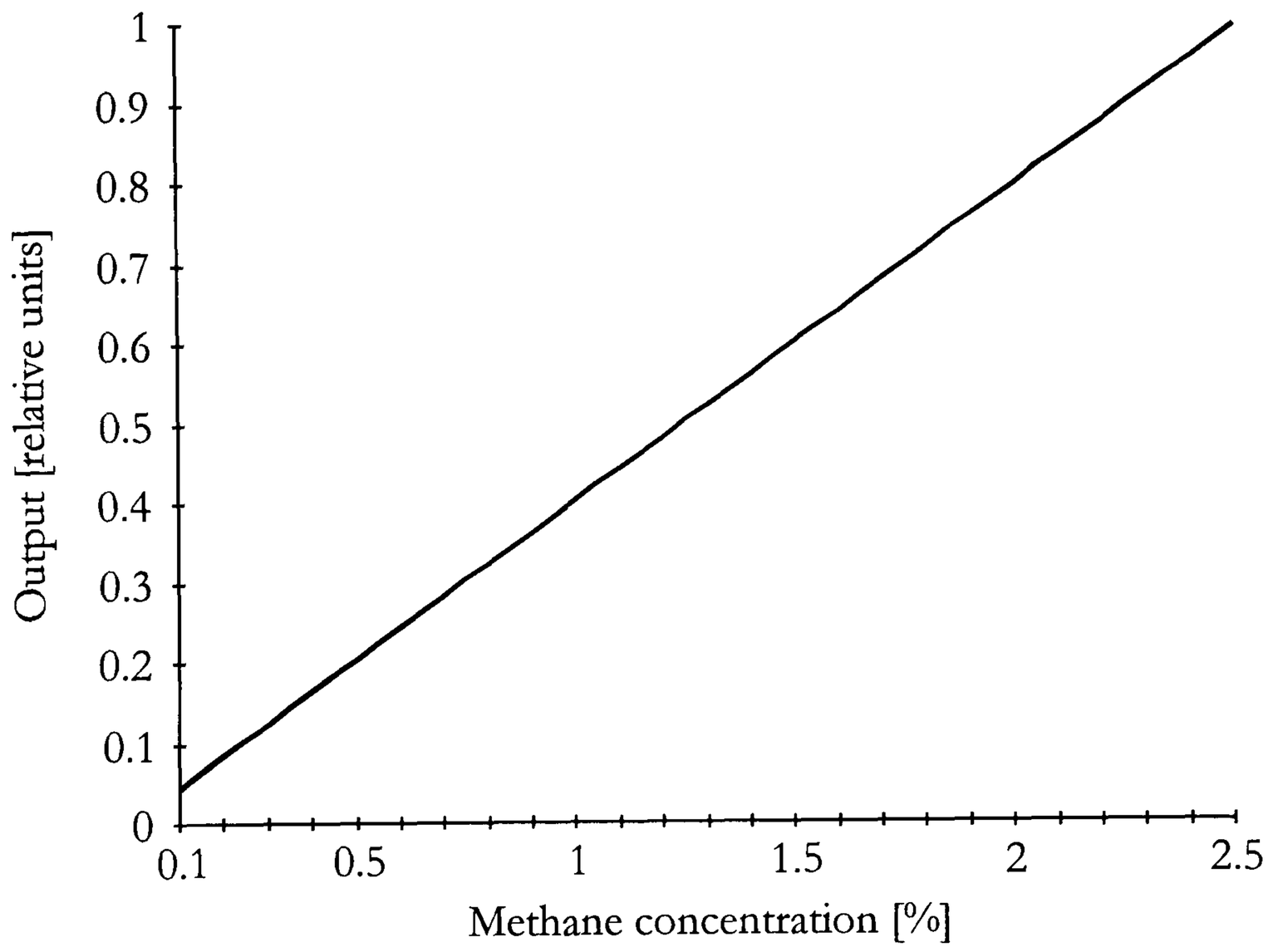

Figure 12.4: *Output versus methane concentrations for the absorption sensor combining RF modulation with the FMCW method*

With the system combining the RF modulation and FMCW method the slope of the output characteristics is 3.54dB per % of methane concentration or 49.8dB change per dB of attenuation (Figure 12.4). Compared with the coherence addressing differential absorption technique this is approximately 50 times better.

12.4.Multiple Cell Systems

The combined FMS/FMCW method can be applied for two basic multiple cell arrangements, parallel and serial, as illustrated in Figure 12.5.

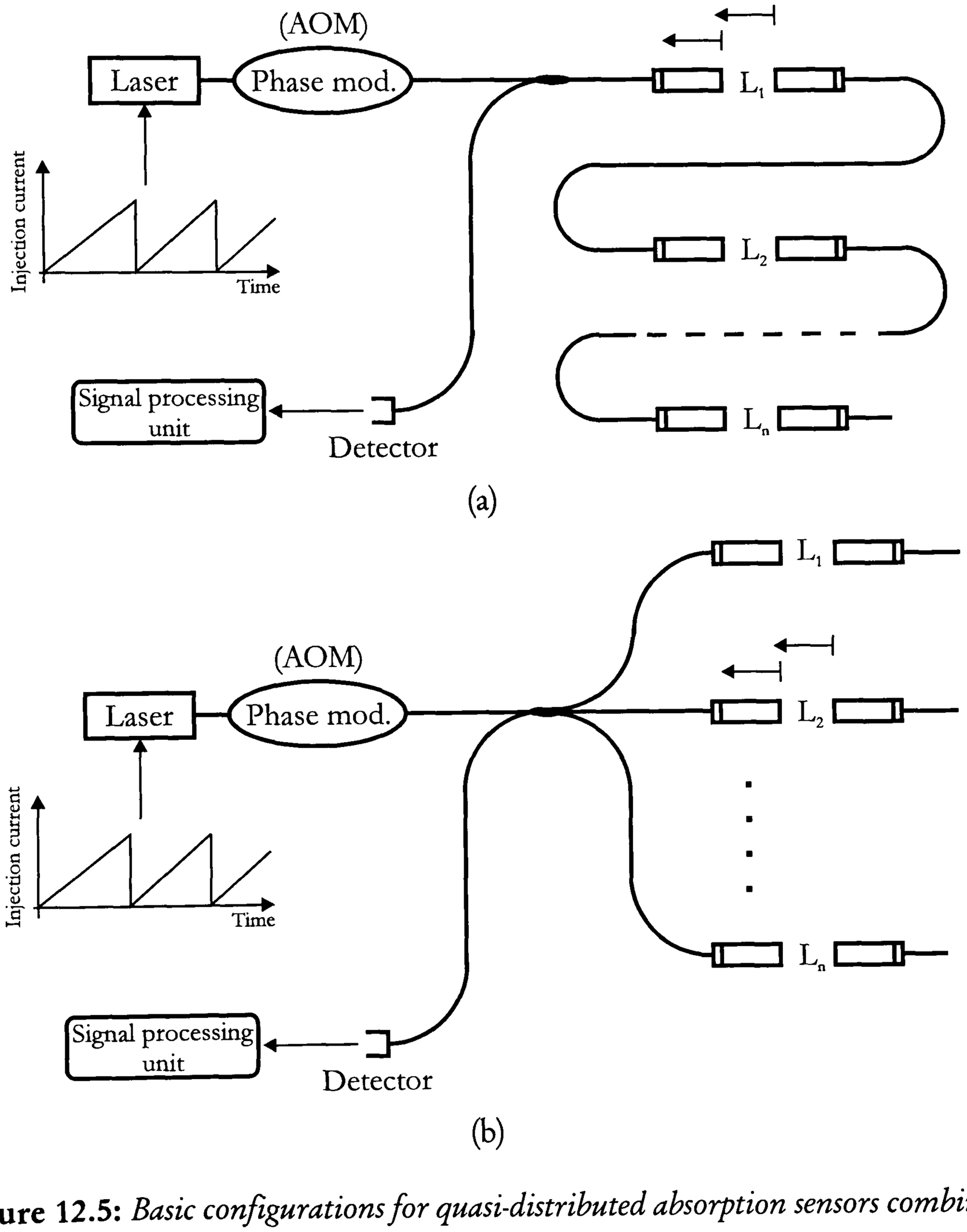

Figure 12.5: *Basic configurations for quasi-distributed absorption sensors combining RF modulation with the FMCW method; (a) serial, (b) parallel*

Similar to the single cell system, we assume that only the $(\omega_0+\omega_{bi}-\omega_m)$ components are attenuated by the absorption feature, where ω_{bi} is the individual beat frequency for each sensing unit. According to equation (12.10), in order to change the beat frequencies for different cells we have to influence either the length of the cell, the sawtooth modulation frequency or the wavelength change due to modulation. The simplest way to discriminate multiple cells is to use different sensing lengths, and we can estimate the range of cells lengths possible as follows.

As we discussed earlier, we set the central laser frequency ω_0 to approximately the absorption line centre. Then from Figure 3, it follows that we need: $|\omega_{bi}-\omega_m|<\gamma$ for the scan to sweep the $(\omega_0+\omega_{bi}-\omega_m)$ component through the absorption line. Hence:

$$\left(1-\frac{\gamma}{\omega_m}\right)<\frac{\omega_{bi}}{\omega_m}<\left(1+\frac{\gamma}{\omega_m}\right) \tag{12.20}$$

Since ω_{bi} is proportional to the cell length L_i we can write:

$$\frac{\omega_{bi}}{\omega_m}=\frac{L_i}{L_m} \tag{12.21}$$

where L_m is the cell length for $\omega_b = \omega_m$

So the maximum allowed range of cell lengths is $L_i = L_m\left[1\pm{}^{\gamma}\!/_{\omega_m}\right]$ giving detection frequencies $(\omega_m-\omega_{bi})$ in the range $0\rightarrow\gamma$. For the typical figures given earlier for methane, $\gamma/\omega_m=0.25$, so $L_i=5\pm1.25$cm. However, to ensure detection is at low frequency values, the range of lengths used would be considerably restricted.

We can get round this problem by using different sawtooth modulation frequencies for different cells. The cell is still assigned using the length, but the beat frequency and hence detection frequency is modified using the frequency of the sawtooth modulation. Thus each sensing unit is characterised by two parameters, the length of the cell and the appropriate sawtooth modulation frequency. There are two major outcomes using the modified scheme. First we can employ more cells in the system and at the same time we can reduce the detection frequencies even below 10MHz, which additionally simplifies the detection electronics. Depending on the possibility to generate different sawtooth modulation frequencies, the number of cells can be greatly increased.

12.5.Summary and conclusions

To improve the performance of a quasi distributed sensing system when detecting absorption features with a narrow absorption spectrum, we have proposed and implicated a method which combines frequency-modulation spectroscopy with the FMCW method. A full analysis has been given with methane detection as an example. The method offers the advantage of very good discrimination with high sensitivity, since a new component appears in the power spectrum whose amplitude is proportional to the absorbance. Each cell in a multiple cell system produces a unique spectral component for quasi-distributed measurements.

References

[12.1] W. Jin, "Performance analysis of a time-division-multiplexed fiber-optic gas-sensor array by wavelength modulation of a distributed-feedback laser," Applied Optics, Vol. 38, No. 25, pp. 5290-5297, 1999

[12.2] G. Stewart, A. Mencaglia, W. Philp, W. Jin, "Interferometric Signals in Fibre Optic Methane Sensors with Wavelength Modulation of the DFB Laser Source," Journal of Lightwave Technology, Vol. 16, No. 1, pp. 43-53, 1998

[12.3] H.C. Sun, E.A. Whittaker, Y.W. Bae, C.K. Ng, V. Patel, W.H. Tam, S. McGuire, B. Singh, B. Gallois, "Combined wavelength and frequency modulation spectroscopy: a novel diagnostic tool for materials processing," Applied Optics, Vol. 32, No. 6, pp. 885-893, 1993

[12.4] J.M. Supplee, E.A. Whittaker, W. Lenth, "Theoretical description of frequency modulation and wavelength modulation spectroscopy," Applied Optics, Vol. 33, No. 27, pp. 6294-6302, 1994

[12.5] G.C. Bjorklund, "Frequency-modulation spectroscopy: a new method for measuring weak absorptions and dispersions," Optics Letters, Vol. 5, No. 1, pp. 15-17, 1980

[12.6] D.T. Cassidy, J. Reid, "Harmonic Detection with Tunable Diode Lasers - Two-Tone Modulation," Applied Physics, Vol. B, No. 29, pp. 279-285, 1982

[12.7] D.E. Cooper, R.E. Warren, "Two-tone optical heterodyne spectroscopy with diode lasers: theory of line shapes and experimental results," J. Opt. Soc. Am., Vol. B 4, No. 4, pp. 470-480, 1987

[12.8] G.R. Janik, C.B. Carlisle, T.F. Gallagher, "Two-tone frequency-modulation spectroscopy," J. Opt. Soc. Am., Vol. B 3, No. 8, pp. 1070-1074, 1986

[12.9] V.G. Avetisov, P. Kauranen, "Two-tone frequency-modulation spectroscopy for quantitative measurements of gaseus species: theoretical, numerical, and experimental investigation of line shapes," Applied Optics, Vol. 35, No. 24, pp. 4705-4723, 1996

13. Conclusions

In the thesis *"Application of the FMCW method to quasi-distributed absorption sensors"*, we have introduced and evaluated different methods for addressing quasi distributed sensor units. By combining coherence addressing and the frequency modulated continuous wave method (FMCW) to distinguish between different sensing units arranged in series, five different addressing mechanisms have been presented:

- Coherent FMCW with reference arm addressing
- FMCW with coherence addressing
- Forward FMCW
- FMCW White light reference arm addressing
- FMCW White light coherence addressing

For all addressing schemes theoretical models have been derived. According to simulation results two approaches have been initially experimentally investigated, i.e. "reference arm addressing" and "coherence addressing". Results indicate

substantial advantages of the coherence method, especially considering interferometer stability and noise due to environmental influences. Consequently further experimental analysis has focused on FMCW coherence addressing.

The feasibility of the proposed method was demonstrated using a three cell microoptic sensor system. In general, the experimental and simulation results are in agreement. To take into account the mutual influence between cells due to the serial configuration, a calibration process at the beginning is necessary. Here individual power spectrum peaks are identified and assigned to the sensing cells. Considerations on the available space in the frequency domain and the signal to noise ratio indicate that systems containing 20 serial sensing units are feasible. To avoid crosstalk between successive sensors it is desirable to make sensors mutually incoherent. This is achieved by long connecting fibre lengths between sensing units which are much greater then the coherence length of the source. The common interferometer associated problems were negligible. Because both reflections from the sensing cell travel through the identical optical fibre, slight deformations or temperature changes cause less than 0.05dB change in the power spectrum amplitudes. Since a stabilised source is used variations in source intensity are minimised. If necessary, a reference source power level could be extracted from the input coupler and used for feedback control of the source power.

Further we have investigated the influence of the absorption spectrum linewidth on system performance. We observe that the sensitivity is reduced proportional to the decrease of the absorption half-linewidth. To compensate for that, one can increase the absorption by reducing the scanning range of wavelengths and therefore increase the cross-section between the absorption line and the sawtooth modulation signal. As a consequence the beat frequencies shifts to lower values, however this can be compensated by increasing the modulation frequency (reducing T) of the ramp. The important factor which determines the performance of the system when using narrow band absorbers is the ratio between scan range

and absorption linewidth. For a 2.5GHz absorption half-linewidth and using a 17GHz scan a ~0.95dB signal drop per dB attenuation in the cell is achieved. Here the ratio of scan range to linewidth is 3.4. Compared to broadband absorption the performance is reduced, however distributed detection of an absorbance of ~ 6×10^{-3} (equivalent to ~ 10% of LEL for methane) is feasible.

In order to additionally improve the sensitivity we have presented a theoretical analysis of a new scheme based on combining the (FMCW) technique with frequency modulation spectroscopy (FMS). Both single and multiple cell systems were evaluated, using methane detection as an example. The laser diode injection current is sawtooth modulated to provide a linear scan of the output over a certain frequency/wavelength range and the output is also externally modulated at radio frequencies. By arranging for only one sideband of the modulation to be attenuated by the absorption feature, a new signal, proportional to the absorbance, appears in the output spectrum at a frequency corresponding to the difference between the rf-modulation frequency and the beat frequency of a cell. This allows the use of relatively low bandwidth detectors and demodulation techniques. The resulting output characteristics experienced a 3.54dB change per % of methane concentration or 49.8dB change per dB of attenuation. This is approximately 50 times more as with narrow band absorbers using the initial FMCW coherence addressed system.

To further reduce the detection frequencies even below 10MHz and at the same time employ more cells in the system one can apply different sawtooth modulation frequencies for different cells. The cell is still assigned using the length, but the beat frequency and hence detection frequency is modified using the frequency of the sawtooth modulation. Thus each sensing unit is characterised by two parameters, the length of the cell and the appropriate sawtooth modulation frequency. The method combining the FMCW technique with frequency modulation spectroscopy is highly sensitive and applicable to a variety of other chemical species with narrow absorption lines, such as in trace gas analysis.

Possible application of the system includes quasi-distributed trace gas detection of gases such as methane (refineries, coal mines, etc.). Using FMCW coherence addressing 10%LEL methane detection in systems with 20 serial connected measuring units could be achieved. In addition to trace gas detection other quantities could be observed by proper modifications of the microoptic cell. Here the space between both GRIN lenses is filled with a transparent sol-gel whose transparency is changing depending on temperature, pH, humidity, etc.

Plans for the future include the construction of the experimental system combining the (FMCW) technique with frequency modulation spectroscopy (FMS) and its evaluation and implementation. Two approaches could be investigated. First the single point sensor designed for low concentration measurements and second, quasi-distributed trace-gas concentration measurements.

Appendix A - Relation between quantities used to describe absorption

In the thesis we are using different quantities to describe absorption (through different absorption cell lengths, different concentrations of the absorption feature, or different αC factors). In this appendix a brief summary of relations between those quantities and their explanation is given.

The absorption of light of incident intensity I_0 by a concentration, C, of a chemical or gas is described by the Beer-Lambert law:

$$I = I_0 e^{-\alpha_m LC} = I_0 e^{-2\alpha_i LC}$$

where α_i is the amplitude attenuation coefficient and L is the cell length. The absorbance (A) is defined as:

$$A = 2\alpha_i CL$$

and the dB attenuation is calculated according to

$$\text{dB attenuation} = 4.34A$$

Through the thesis the absorption in percent is defined as:

$$absorption\,[\%] = \frac{I_0 - I}{I_0} \cdot 100 = \left[1 - e^{-A}\right] \cdot 100$$

for small absorbance values absorption in percent is equal to:

$$absorption\,[\%] = A \cdot 100$$

The concentration C of a chemical or gas is given either by percent per volume unit or in parts per million:

$$ppm = \left[\frac{C[\%]}{100}\right] \cdot 10^6$$

Appendix B - Micro controller program

```
/*****************************************************************************/
/*****************************************************************************/
/**          FREQUENCY MODULATED CONTINUOUS WAVE INTERFEROMETRY             **/
/**                                PhD                                      **/
/**                Miha Zavrsnik                                            **/
/** Hardware:    - H8/510 10 MHz - EMU v1.0 board (100ns memory)            **/
/**              - piggy back expansion  v1.0 (LCD,keyboard)                **/
/*****************************************************************************/
/**                        Last update: 11.11.1999                          **/
/*****************************************************************************/
/*****************************************************************************/
/*                             programe fmcw3.c                              */

#include <ioh8510.h>
#include <stdio.h>
#include <math.h>

#define PI 3.14
#define BEAT1 260
#define BEAT2 400
#define BEAT3 560
#define FREQ 14.3

void send();
char recive();
void nacin1();
void nacin2();
void fft ();
void line();
void cls_line();
void lcd_init();
void cls_lcd();
void cls_put();
void rectangle();
```

```
void set_x1();
void set_y1();
void status_read();
void lcd_write_1();
char lcd_read_1();
void set_x2();
void set_y2();
void lcd_write_2();
char lcd_read_2();
void put_pixel();
void bar();
void slim_bar();
void del_slim_bar();
void block();
void text();
void textin();
int getkey();
void kursor();
void kroznica();
void delilnik();
unsigned int adc_a();
long int faza();

/************************* Definiranje fontov ***********************/
const char chartable[93][7]={
                        {0x00,0x00,0x00,0x00,0x00,0x00,0x00},   /*   */
                        {0x00,0x00,0x00,0x5f,0x00,0x00,0x00},   /* ! */
                        {0x00,0x00,0x03,0x00,0x03,0x00,0x00},   /* " */
                        {0x00,0x14,0x7f,0x14,0x7f,0x14,0x00},   /* # */
                        {0x00,0x04,0x2a,0x7f,0x2a,0x10,0x00},   /* $ */
                        {0x00,0x44,0x20,0x10,0x08,0x44,0x00},   /* % */
                        {0x00,0x36,0x49,0x49,0x4e,0x30,0x48},   /* & */
                        {0x00,0x00,0x04,0x03,0x00,0x00,0x00},   /* ' */
                        {0x00,0x00,0x00,0x3e,0x41,0x41,0x00},   /* ( */
                        {0x00,0x41,0x41,0x3e,0x00,0x00,0x00},   /* ) */
                        {0x00,0x24,0x18,0x7e,0x18,0x24,0x00},   /* * */
                        {0x00,0x08,0x08,0x3e,0x08,0x08,0x00},   /* + */
                        {0x00,0x00,0x00,0x80,0x60,0x00,0x00},   /* , */
                        {0x00,0x08,0x08,0x08,0x08,0x08,0x00},   /* - */
                        {0x00,0x00,0x00,0x00,0x40,0x00,0x00},   /* . */
                        {0x00,0x40,0x20,0x10,0x08,0x04,0x00},   /* / */
                        {0x00,0x3e,0x51,0x49,0x45,0x3e,0x00},   /* 0 */
                        {0x00,0x00,0x42,0x7f,0x40,0x00,0x00},   /* 1 */
                        {0x00,0x42,0x61,0x51,0x49,0x46,0x00},   /* 2 */
                        {0x00,0x21,0x41,0x45,0x4b,0x31,0x00},   /* 3 */
                        {0x00,0x18,0x14,0x12,0x7f,0x10,0x00},   /* 4 */
                        {0x00,0x27,0x45,0x45,0x45,0x39,0x00},   /* 5 */
                        {0x00,0x3c,0x4a,0x49,0x49,0x30,0x00},   /* 6 */
                        {0x00,0x01,0x71,0x09,0x05,0x03,0x00},   /* 7 */
                        {0x00,0x36,0x49,0x49,0x49,0x36,0x00},   /* 8 */
                        {0x00,0x06,0x49,0x49,0x29,0x1e,0x00},   /* 9 */
                        {0x00,0x00,0x00,0x14,0x00,0x00,0x00},   /* : */
                        {0x00,0x00,0x80,0x64,0x00,0x00,0x00},   /* ; */
                        {0x00,0x08,0x14,0x22,0x41,0x00,0x00},   /* < */
                        {0x00,0x14,0x14,0x14,0x14,0x14,0x00},   /* = */
                        {0x00,0x00,0x41,0x22,0x14,0x08,0x00},   /* > */
                        {0x00,0x02,0x01,0x59,0x09,0x06,0x00},   /* ? */
                        {0x00,0x3e,0x41,0x5d,0x5d,0x0e,0x00},   /* @ */
                        {0x00,0x7e,0x09,0x09,0x09,0x7e,0x00},   /* A */
                        {0x00,0x7f,0x49,0x49,0x49,0x36,0x00},   /* B */
                        {0x00,0x3e,0x41,0x41,0x41,0x22,0x00},   /* C */
                        {0x00,0x7f,0x41,0x41,0x22,0x1c,0x00},   /* D */
                        {0x00,0x7f,0x49,0x49,0x49,0x41,0x00},   /* E */
                        {0x00,0x7f,0x09,0x09,0x01,0x01,0x00},   /* F */
                        {0x00,0x3e,0x41,0x49,0x49,0x3a,0x00},   /* G */
                        {0x00,0x7f,0x08,0x08,0x08,0x7f,0x00},   /* H */
                        {0x00,0x00,0x41,0x7f,0x41,0x00,0x00},   /* I */
                        {0x00,0x20,0x40,0x41,0x3f,0x01,0x00},   /* J */
                        {0x00,0x7f,0x08,0x14,0x22,0x41,0x00},   /* K */
                        {0x00,0x7f,0x40,0x40,0x40,0x40,0x00},   /* L */
                        {0x00,0x7f,0x02,0x04,0x02,0x7f,0x00},   /* M */
                        {0x00,0x7f,0x04,0x08,0x10,0x7f,0x00},   /* N */
                        {0x00,0x3e,0x41,0x41,0x41,0x3e,0x00},   /* O */
```

```
{0x00,0x7f,0x09,0x09,0x09,0x06,0x00},    /* P */
{0x00,0x3e,0x41,0x41,0x51,0x3e,0x40},    /* Q */
{0x00,0x7f,0x09,0x19,0x29,0x46,0x00},    /* R */
{0x00,0x26,0x49,0x49,0x49,0x32,0x00},    /* S */
{0x00,0x01,0x01,0x7f,0x01,0x01,0x00},    /* T */
{0x00,0x3f,0x40,0x40,0x40,0x3f,0x00},    /* U */
{0x00,0x1f,0x20,0x40,0x20,0x1f,0x00},    /* V */
{0x00,0x3f,0x40,0x3c,0x40,0x3f,0x00},    /* W */
{0x00,0x63,0x14,0x08,0x14,0x63,0x00},    /* X */
{0x00,0x07,0x08,0x70,0x08,0x07,0x00},    /* Y */
{0x00,0x61,0x51,0x49,0x45,0x43,0x00},    /* Z */
{0x00,0x00,0x00,0x7f,0x41,0x41,0x00},    /* [ */
{0x00,0x04,0x08,0x10,0x20,0x40,0x00},    /* \ */
{0x00,0x41,0x41,0x7f,0x00,0x00,0x00},    /* ] */
{0x00,0x04,0x02,0x01,0x02,0x04,0x00},    /* potenca */
{0x00,0x40,0x40,0x40,0x40,0x40,0x00},    /*  _ */
{0x00,0xff,0xff,0xff,0xff,0xff,0x00},    /* nedef. */
{0x00,0x20,0x54,0x54,0x38,0x40,0x00},    /* a */
{0x00,0x7f,0x44,0x44,0x44,0x38,0x00},    /* b */
{0x00,0x38,0x44,0x44,0x44,0x00,0x00},    /* c */
{0x00,0x38,0x44,0x44,0x44,0x7f,0x00},    /* d */
{0x00,0x38,0x54,0x54,0x54,0x18,0x00},    /* e */
{0x00,0x08,0x7e,0x09,0x01,0x02,0x00},    /* f */
{0x00,0x18,0xa4,0xa4,0xa4,0x78,0x00},    /* g */
{0x00,0x7f,0x08,0x04,0x04,0x78,0x00},    /* h */
{0x00,0x00,0x44,0x7d,0x40,0x00,0x00},    /* i */
{0x00,0x40,0x80,0x80,0x7d,0x00,0x00},    /* j */
{0x00,0x7f,0x10,0x28,0x44,0x00,0x00},    /* k */
{0x00,0x41,0x7f,0x40,0x00,0x00,0x00},    /* l */
{0x04,0x78,0x04,0x78,0x04,0x78,0x00},    /* m */
{0x00,0x7c,0x08,0x04,0x04,0x78,0x00},    /* n */
{0x00,0x38,0x44,0x44,0x44,0x38,0x00},    /* o */
{0x00,0xf8,0x24,0x24,0x24,0x18,0x00},    /* p */
{0x00,0x18,0x24,0x24,0x24,0xf8,0x00},    /* q */
{0x00,0x7c,0x08,0x04,0x04,0x08,0x00},    /* r */
{0x00,0x08,0x54,0x54,0x54,0x20,0x00},    /* s */
{0x00,0x00,0x04,0x7f,0x44,0x40,0x00},    /* t */
{0x00,0x3c,0x40,0x40,0x40,0x3c,0x00},    /* u */
{0x00,0x1c,0x20,0x40,0x20,0x1c,0x00},    /* v */
{0x00,0x3c,0x40,0x30,0x40,0x3c,0x00},    /* w */
{0x00,0x44,0x28,0x10,0x28,0x44,0x00},    /* x */
{0x00,0x1c,0xa0,0xa0,0xa0,0x7c,0x00},    /* y */
{0x00,0x44,0x64,0x54,0x4c,0x44,0x00},     /* z */
{0x00,0xff,0xff,0xff,0xff,0xff,0x00},     /* nedef.*/
{0x00,0x00,0x00,0xff,0x00,0x00,0x00}      /* | */
};


/*int vredm1=0;*/

main()

{
int i,k,k1,k2,x, prava;
int vredm11=0, vredm12=0, vredm13=0;
int ad0, vrh, vrhpom[128], vrhm1=0, pom;
int data[129];
int temp[320];
char msg[100];

float input_real[512], input_imag[521];
float window,max_spec;
int max_index;

long int podatek;
char j1,j2,j3;    /* receive, transmitt flags */

int j=0,ii,jj, index1, index2, index3;
float a,y;

P5DDR=0x0f;
P6DDR=0xdf;
```

```
lcd_init();     /* inicializacija lcd-a */
cls_lcd();      /* brisanje displaya */


/************************* Zacetni izpis na display-u ******************************/
textin(15,10,"FERI-LEOSS '98");
text(12,30,"F M C W");
text(12,45,"-------");
rectangle(0,0,127,63);rectangle(2,2,125,61);
/***********************************************************************************/

text(85,48,"ini..");

glavni:
        k1=0;
        cls_lcd();
        index1=BEAT1/FREQ+1;
        index2=BEAT2/FREQ+1;
        index3=BEAT3/FREQ+1;
        text(18,25,"FMCW MAIN MENU");
        line(0,55,125,55);
        rectangle(0,0,125,52);rectangle(2,2,123,50);
        textin(0,56,"View|Meas|->PC|Set");


k=getkey();

/***********************************************************************************/

if(k==1)          /* View time and frequency domain */
{

view_menu:


    cls_lcd();
text(25,25,"VIEW MENU");
textin(0,56," UP |Time|Spec|   ");


k1=getkey();

if (k1==1) goto glavni;

if (k1==2)    /* time */
 {
   cls_lcd();
   pom=0;
   textin(0,56," UP |    |    |    ");
   while((P5DR&0x10)==0x10)     /* dokler ni 1. tipka (izhod) pritisnjena */
    {
     pom=54;
     for (i=0; i<128; i++)
      {
       ad0=adc_a();
       y=((float)4.92/(float)1023)*ad0;
       vrhpom[i]=(int) (64-y*54/4.92);
      }
     cls_lcd();
   textin(0,56," UP |    |    |    ");
   for (i=0; i<128; i++)
    {
     /*pom=pom%127;*/
     line(i,pom,i+1,vrhpom[i]);
     pom=vrhpom[i];
     sprintf(msg,"%5.2f",y);text(35,50,msg);
     printf("\n\r Vhod AD0= %2.5f ",y);
    }
```

```
      }
    k1=getkey();
    goto view_menu;
  }

if (k1==3)     /* view spectrum */
 {
   cls_lcd();
   pom=0;
   textin(0,56," UP |    |     |     ");
   while((P5DR&0x10)==0x10)      /* while not first key-(UP) pressed */
    {
      for (j=1; j<=512; j++) /* 512 data sampling for fft */
        {
          ad0=adc_a();
          /*input_real[j]=((float)4.92/(float)1023)*ad0;*/
          input_real[j]=ad0;
          input_imag[j]=0;

        }

          for (j=1; j<=512; j++) /* 512 data windowing */
           {
               /*window=1-((j-0.5*256)/(0.5*256)*(j-0.5*256)/(0.5*256));*/   /*   Welch
window */
                window=(1-cos(2*PI*(j-1)/512));      /* Hanning window */
               /* window=1-fabs((j-0.5*512)/(0.5*512)); /* Barttlet window */

               input_real[j]=window*input_real[j];


           }


          fft(input_real, input_imag, 512); /* do fft on sample data  */


          max_spec=0;
          max_index=0;
          for (j=511; j<=512; j++) /* max searching */
             {
              if (input_real[j]>max_spec)
                { max_spec=input_real[j];
                  max_index=j;
                }
              }
          printf("\n\r Max spec= %2.5f [%d]",max_spec,max_index);



          /*-------------------------------------------------
           Do log scale
          -------------------------------------------------*/
          for (j=1; j<=512; j++)
             {
               input_real[j]=20*log10(max_spec/input_real[j]);
               if ( input_real[j]>50 )
                 {
                   input_real[j]=50;
                 }
             }
          /*-------------------------------------------------*/


          cls_lcd();
          textin(0,56," UP |    |     |     ");

          sprintf(msg,"%2.2f",input_real[index1]);text(90,0,msg);
          sprintf(msg,"%2.2f",input_real[index2]);text(90,8,msg);
          sprintf(msg,"%2.2f",input_real[index3]);text(90,16,msg);
```

```
/*-------------------------------------------------
 Draw Power Spectrum
-------------------------------------------------*/
for (i=1; i<=128; i++)
{
 line(i,50,i,(int)(input_real[i]));  /* 50- */
 printf("\n\r Spec out= %2.5f ",input_real[i]);
}

 line(index1*2,0,index1*2,10);      /* mark first peak */
 line(index2*2,0,index2*2,10);      /* mark second peak */
 line(index3*2,0,index3*2,10);      /* mark third peak */
/*-------------------------------------------------*/

} /* end while not first key pressed */
      k1=getkey();
      goto view_menu;
     }


}

/*****************************************************************************/

if(k==2)          /* Measurement */
{

meas_menu:


    cls_lcd();
    text(8,25,"MEASUREMENT MENU");
    textin(0,56," UP |Sing|Mult|   ");


    k1=getkey();

if (k1==1) goto glavni;  /* back to main menu */

if (k1==2)     /* single measurement */
 {
   single:
   cls_lcd();

   text(2,25,"SINGLE MEASUREMENT");
   text(2,32,"Choose sens. unit");
   textin(0,56," UP | 1 | 2  | 3  ");

   k2=getkey();
        if (k2==1) goto meas_menu;
        if (k2==2)     /* first unit */
          {
            cls_lcd();
            pom=0;
            text(0,0,"First sensing unit");
            text(0,8,"Delta T[%]=");
            textin(0,56," UP |   |    |    ");

            while((P5DR&0x10)==0x10)          /*  dokler  ni  1.  tipka  (izhod)
pritisnjena */
                  { ad0=adc_a();
                    y=((float)4.92/(float)1023)*ad0;
                    vrh=(int) (65-30*y*sin(pom));
                    /*pom=pom%128;*/

                    for (ii=0; ii<100; ii++)
                    bar(3,vrh,vrhm1);

                    pom++;
                    vrhm1=vrh;
                    sprintf(msg,"%d",vrh);text(100,8,msg);
```

```
                printf("\n\r Vhod AD0= %d ",vrh);
              }
            }

    k1=getkey();
    goto single;
  }

if (k1==3)          /* multiple measurement */
 {
    cls_lcd();
    text(0,0,"[1] Unit:");
    text(0,16,"[2] Unit:");
    text(0,33,"[3] Unit:");

    textin(0,56," UP |    |     |    ");
    del_slim_bar(1);
    del_slim_bar(3);
    del_slim_bar(5);
    while((P5DR&0x10)==0x10)     /* while not first key-(UP) pressed */
     {
        for (j=1; j<=512; j++) /* 256 data sampling for fft */
         {
           ad0=adc_a();
           /*input_real[j]=((float)4.92/(float)1023)*ad0;*/
           input_real[j]=ad0;
           input_imag[j]=0;
         }

       for (j=1; j<=512; j++) /* 256 data windowing */
          {
             /*window=1-((j-0.5*256)/(0.5*256)*(j-0.5*256)/(0.5*256));*/ /* Welch
window */
             window=(1-cos(2*PI*(j-1)/512));    /* Hanning window */
             /*window=1-fabs((j-0.5*512)/(0.5*512)); /* Barttlet window */

           input_real[j]=(input_real[j]*window); /* window  */
          }

     /*------------------99-01-28 13:32------------------
      Do FFT on sample data
     ----------------------------------------------------*/
      fft(input_real, input_imag, 512);
     /*----------------------------------------------------*/

    max_spec=0;
    max_index=0;
    for (j=511; j<=512; j++) /* max searching */
       {
        if (input_real[j]>max_spec)
          { max_spec=input_real[j];
            max_index=j;
          }
        }
    printf("\n\r Max spec= %2.5f [%d]",max_spec,max_index);



    /*----------------------------------------------
     Do log scale
    ----------------------------------------------*/
    for (j=1; j<=512; j++)
       {
         input_real[j]=20*log10(max_spec/input_real[j]);
         if ( input_real[j]>50 )
           {
             input_real[j]=50;
           }
       }
    /*----------------------------------------------*/
```

```
sprintf(msg,"%2.2f",input_real[17]);text(70,0,msg);
sprintf(msg,"%2.2f",input_real[28]);text(70,16,msg);
sprintf(msg,"%2.2f",input_real[38]);text(70,33,msg);

vrh=(int)input_real[19];
slim_bar(1,vrh,vredm11);
vredm11=vrh;

vrh=(int)input_real[30];
slim_bar(3,vrh,vredm12);
vredm12=vrh;

vrh=(int)input_real[40];
slim_bar(5,vrh,vredm13);
vredm13=vrh;

/*line(i,50,i,(int)(50-input_real[i]/4));*/ /* no log10 scale */
/* line(2*i,50,2*i,(int)(50-100*input_real[i]));   /* log10 scale */

 /*sprintf(msg,"%5.2f",y);text(35,50,msg);*/

 printf("\n\r----------------------------------");
 for(j=16; j<21; j++)
  {
   printf("\n\r Spec out= %2.5f| %d ",input_real[j],j);
  }
 for(j=30; j<41; j++)
  {
   printf("\n\r Spec out= %2.5f| %d ",input_real[j],j);
  }
 printf("\n\r++++++++++++++++++++++++++++++++++");



/*  vrh=(int) (65-6*y*sin(pom));
            pom++;
            sprintf(msg,"%d",vrh);text(70,0,msg);
            slim_bar(1,vrh,vredm11);
            vredm11=vrh;*/

          }
        k1=getkey();
        goto meas_menu;
      }


}
/*****************************************************************************/

if(k==3)          /* Microcontroller to PC */
{

pc_menu:


    cls_lcd();
    text(20,25,"H8 -> PC MENU");
    textin(0,56," UP |Start|    |    ");


k1=getkey();

if (k1==1) goto glavni;

if (k1==2)
 {

   cls_lcd();
      rectangle(0,0,127,47);rectangle(2,2,125,44);
```

```
   text(21,20,"Communication");text(35,36,"H8->PC...");


pom=0;
textin(0,56," UP |    |    |    ");

j1=recive();
if (j1==(char)65) /* flag from PC to start transmission */
  {
   send((char)0xff);send('g');   /* switch to PC graphics mode */
   j2=recive();
   sprintf(msg,"%d",j2);text(50,10,msg);
   if (j2==(char)0xff)
   {
    while((j3=recive())==(char)0xff)      /* until PC is working */
     {
       for (i=0; i<2048; i++) /* sample 2048 values */
         {
          ad0=adc_a();
          temp[i]=ad0;
         }
        for (i=0; i<2048; i++) /* send 2048 values */
          {
          /*y=((float)4.92/(float)1023)*ad0;*/
          nacin2((int)temp[i]);


          /*nacin1((long)podatek);*/          /* send data to PC */
          pom++;                            /* increment counter */
         }
       pom=0;
      } /* end while */

     } /* end if 0x00 flag */
    } /* end if (char)65 flag from PC */
  /*k1=getkey(); */
  goto pc_menu;
 }

if (k1==3)
     {
       cls_lcd();
       textin(0,56," UP |    |    |    ");
       while((P5DR&0x10)==0x10)      /* dokler ni 1. tipka (izhod) pritisnjena */
        { ad0=adc_a();
          y=((float)4.92/(float)1023)*ad0;
          vrh=(int) (32-2*y*sin(pom)+10);
          pom=pom%128;
          line(pom,32,pom+1,vrh);
          pom++;
          sprintf(msg,"%5.2f",y);text(35,50,msg);
          printf("\n\r Vhod AD0= %2.5f ",y);

        }
       k1=getkey();
       goto pc_menu;
     }


}

/*****************************************************************************/

if(k==4)              /* Set Menu */
{

set_menu:


    cls_lcd();
    text(20,25,"SET MENU");
    textin(0,56," UP |Zero|    |    ");
```

```
k1=getkey();

if (k1==1) goto glavni;

if (k1==2)
 {
   cls_lcd();
   pom=0;
   textin(0,56," UP |    |     |     ");
   while((P5DR&0x10)==0x10)     /* dokler ni 1. tipka (izhod) pritisnjena */
    { ad0=adc_a();
      y=((float)4.92/(float)1023)*ad0;
      vrh=(int) (32-2*y*sin(pom));
      pom=pom%128;
      line(pom,32,pom+1,vrh);
      pom++;
      sprintf(msg,"%5.2f",y);text(35,50,msg);
      printf("\n\r Vhod AD0= %2.5f ",y);

    }
   k1=getkey();
   goto set_menu;
 }

if (k1==3)
 {
   cls_lcd();
   textin(0,56," UP |    |     |     ");
   while((P5DR&0x10)==0x10)     /* dokler ni 1. tipka (izhod) pritisnjena */
    { ad0=adc_a();
      y=((float)4.92/(float)1023)*ad0;
      vrh=(int) (32-2*y*sin(pom)+10);
      pom=pom%128;
      line(pom,32,pom+1,vrh);
      pom++;
      sprintf(msg,"%5.2f",y);text(35,50,msg);
      printf("\n\r Vhod AD0= %2.5f ",y);

       }
      k1=getkey();
      goto set_menu;
     }


}

/*while(1)
{
k=getkey();
if(k==1) {
      cls_lcd();
      kroznica(60,30,30);
      while(1)
      {
      cls_lcd();
      adc();
      }
      } */
/*if(k==2)          {         cls_lcd();         text(0,30,"Ovo          ni          drugi
del");text(0,56,"[kos][tex][pos]");}*/
/*if(k==3)                    {                  cls_lcd();                  line(0,0,127,63);
line(0,63,127,0);text(0,56,"[kos][tex][pos]");}*/
/*if(k==4) { cls_lcd(); line(60,60,60,10); line(0,0,127,0); }*/

}

/********************** Port 6 (control) ****************************/
/*                                                                  */
/* Port 6:    D7    D6    D5    D4    D3    D2    D1    D0         */
/*            0     0     0     cs2   cs1   e     r/w   d/i        */
/*                                                                  */
```

```
/*************************************************************/

/****************** Rutine za lcd prikazovalnik ******************/

/******************* inicializacija ********************************/

void lcd_init()
{
int i;
/*P6DDR=0xdf;*/
P3DDR=0xff;          /* port 3 output (v njega vpisujemo) */

P6DR=0xc0;           /* reset porta 6 */
/*for(i=1;i<20000;i++);*/
P6DR=0xd8;    /* cs1=1, cs2=1 */
P3DR=0x3f;    /* display ON */
P6DR=0xdc;    /* se enable=1 */
P6DR=0xd8;    /* enable=0 */

/* dolocitev startne linije displaya */

P3DR=0xc0;     /* display start line */
P6DR=0xdc;    /* se enable=1 */
P6DR=0xd8;

}
/****************** set page X (cs1) ****************************/

void set_x1(data)
char data;
{
char bf;
P3DDR=0x00;      /* port 3 bomo brali */
do
{
 P6DR=0xea;
 P6DR=0xee;
 bf=P3DR;
 P6DR=0xea;
}
while((bf&0x80)!=0);  /* preverimo bussy in ce je, ponavljamo */
P3DDR=0xff;      /* v port 3 vpisujemo */

P6DR=0xe8;
P3DR=0xb8+(data&0x07);    /* vpis X-te strani */
P6DR=0xec;    /* enable=1 */
P6DR=0xe8;    /* enable=0 */
}

/******************** set page X (cs2) ****************************/

void set_x2(data)
char data;
{
char bf;
P3DDR=0x00;
do
{
 P6DR=0xd2;
 P6DR=0xd6;
 bf=P3DR;
 P6DR=0xd2;
}
while((bf&0x80)!=0);
P3DDR=0xff;

P6DR=0xd0;
P3DR=0xb8+(data&0x07);    /* vpis X-te strani */
P6DR=0xd4;    /* enable=1 */
P6DR=0xd0;    /* enable=0 */
}

/******************* set Y address (cs1) ************************/
```

```
void set_y1(data)
char data;

{
char bf;
P3DDR=0x00;
do
{
 P6DR=0xea;
 P6DR=0xee;
 bf=P3DR;
 P6DR=0xea;
}
while((bf&0x80)!=0);
P3DDR=0xff;
P6DR=0xe8;    /* cs1=1, cs2=0 */
P3DR=0x40+(data&0x7f);    /* vpis Y vrednosti */
P6DR=0xec;    /* enable=1 */
P6DR=0xe8;    /* enable=0 */
}

/******************** set address Y (cs2) ********************************/

void set_y2(data)
char data;
{
char bf;
P3DDR=0x00;
do
{
 P6DR=0xd2;
 P6DR=0xd6;
 bf=P3DR;
 P6DR=0xd2;
}
while((bf&0x80)!=0);
P3DDR=0xff;
P6DR=0xd0;   /* cs1=0, cs2=1 */
P3DR=0x40+(data&0x7f);   /* vpis Y vrednosti */
P6DR=0xd4;   /* enable=1 */
P6DR=0xd0;   /* enable=0 */
}

/******************** branje statusa ************************/

void status_read()
{
char bf;
P3DDR=0xff;
do
{
 P6DR=0xda;
 P6DR=0xde;
 bf=P3DR;
 printf("\n\rStatus=%x",bf);
 P6DR=0xda;
}
while((bf&0x80)!=0);
}

/***************** vpis podatkov na display (cs1) ***************************/

void lcd_write_1(data)
char data;
{
char bf;
P3DDR=0x00;
do
{
 P6DR=0xea;
```

```
 P6DR=0xee;
 bf=P3DR;
 P6DR=0xea;
}
while((bf&0x80)!=0);
P3DDR=0xff;          /* vpis v port 3 */

P6DR=0xe8;           /* cs1=1, cs2=0 */
P6DR=0xe9;           /* d/i=1, r/w=0 */
P6DR=0xed;           /* se enable */
P3DR=data;           /* vpis vrednosti "data" na display */
P6DR=0xe8;           /* enable=0 */


}

/******************** vpis podatkov na display (cs2) ************************/

void lcd_write_2(data)
char data;
{
char bf;
P3DDR=0x00;
do
{
 P6DR=0xd2;
 P6DR=0xd6;
 bf=P3DR;
 P6DR=0xd2;
}
while((bf&0x80)!=0);
P3DDR=0xff;


P6DR=0xd1;   /* cs1=0, cs2=1, d/i=1, r/w=0 */
P6DR=0xd5;   /* se enable */
P3DR=data;   /* vpis vrednosti "data" na display */
P6DR=0xd0;   /* enable=0 */
}

/******************** branje podatkov z displaya (cs1) ************************/

char lcd_read_1()
{
char bf,x;
P3DDR=0x00;
do
{
 P6DR=0xea;
 P6DR=0xee;
 bf=P3DR;
 P6DR=0xea;
}
while((bf&0x80)!=0);

P6DR=0xeb;      /* cs1=1, cs2=0, r/w=1, d/i=1 */
P6DR=0xef;      /* se enable */
x=P3DR;         /* branje vrednosti s porta 3*/
P6DR=0xe8;
return(x);
}

/********************** branje podatkov z displaya (cs2) ******************/

char lcd_read_2()
{
int i,x;
char bf;
P3DDR=0x00;

do
{
 P6DR=0xd2;
```

```
 P6DR=0xd6;
 bf=P3DR;
 P6DR=0xd2;
}
while((bf&0x80)!=0);
P6DR=0xd0;

P6DR=0xd3;  /* cs1=0, cs2=1, d/i=1, r/w=1 */
P6DR=0xd7;  /* se enable */
x=P3DR;
P6DR=0xd3;   /* enable=0 */
return(x);
}

/********************** cls rutina ********************************/

void cls_lcd()
{
char j;
int i;
for(j=0x00;j<0x08;j++)
{
 set_x1(j);
 set_x2(j);
 set_y1(0x00);
 set_y2(0x00);
 for(i=0;i<64;i++)
  {
   lcd_write_1(0x00);
   lcd_write_2(0x00);
  }
}
}

/************************** put_pixel rutina ********************************/

void put_pixel(x,y)
char x,y;
{
int hi,lo;
char tocka,data1,data;
 if(x<64)
 {
   lo=y%8;
   tocka=0x01;
   tocka=tocka<<lo;
   set_x1(y/8);
   set_y1(x);
   data1=lcd_read_1();      /* dummy read */
   data=lcd_read_1();       /* real read */
   set_y1(x);
   lcd_write_1(tocka|data);
 }
 else
 {
   x-=64;
   lo=y%8;
   tocka=0x01;
   tocka=tocka<<lo;
   set_x2(y/8);
   set_y2(x);
   data1=lcd_read_2();      /* dummy read */
   data=lcd_read_2();       /* real read */
   set_y2(x);
   lcd_write_2(tocka|data);
  }
}



/*****************************************************************************/
/*                          FFT transfrom                                    */
```

```
/*****************************************************************************/

void fft (ar,ai,dolzina)
 float ar[],ai[];
 int dolzina;
 {


        /* deklaracije spremenljivk */

        int n, n2, a, c, d, f, g, h, j, seg;
        float b,e,k,l,n1,co,si,mean_sq_power, rms;
        int m,p,q,r,s,t,u,w,z;



        n=dolzina;

        n1=log10(n)/log10(2);



        n2=1; /* 1 - fft, -1 - invfft */

        a=n;
        b=2*PI/n;

        for (c=1; c<=n1; c++)
              {
               d=a;
               a=a/2;
               e=0;

               for (f=1; f<=a; f++)
                    {
                     co=cos(e);
                     si=sin(e)*n2;
                     e=e+b;
                     u=1;

                     for (g=d; g<=n; g=u*d)
                           {
                            u++;
                            h=g-d+f;
                            j=h+a;
                            k=ar[h]-ar[j];
                            l=ai[h]-ai[j];
                            ar[h]=ar[h]+ar[j];
                            ai[h]=ai[h]+ai[j];
                            ar[j]=co*k+si*l;
                            ai[j]=co*l-si*k;
                           }
                    }

         b=2*b;
        }

        m=1;
        p=n/2;
        q=n-1;

        for (r=1; r<=q; r++)
         {
                if (r> (m-0.1)) goto label1;

                k=ar[m];
                l=ai[m];
```

```
                ar[m]=ar[r];
                ai[m]=ai[r];
                ar[r]=k;
                ai[r]=l;

                label1: s=p;

                label3: if (s> (m-0.1)) goto label2;

                m=m-s;
                s=s/2;

                goto label3;

                label2: m=m+s;
        }
                for (w=1; w<=n; w++)
                 {

                        mean_sq_power=ar[w]/n*ar[w]/n+ai[w]/n*ai[w]/n;

                        ar[w]=5*sqrt(mean_sq_power);

                 }


                /* outtextxy(0, maxy/2+10,"0");
                 outtextxy(64, maxy/2+10,"160");
                 outtextxy(128, maxy/2+10,"320");
                 outtextxy(256, maxy/2+10,"640");
                 outtextxy(512, maxy/2+10,"1280 [Hz]");*/



} /* fft */

/************************ Line ***************************************/

void line(x1,y1,x2,y2)
int x1,y1,x2,y2;
{
 int a,b,y,n,xx;
 if(x1>x2)
   {
       xx=x1; x1=x2; x2=xx; xx=y1; y1=y2; y2=xx;
   }


 a=y2-y1;
 b=x2-x1;

 if(b==0)
 {
    if(y1>y2) { xx=y1; y1=y2; y2=xx;}
    for(n=y1;n<=y2;n++) put_pixel(x1,n);
   return;
  }
    if(a==0)
    {
     if(x1>x2) {xx=x1; x1=x2; x2=xx;}
     for(n=x1;n<=x2;n++) put_pixel(n,y1);
   return;
    }
   for(n=x1;n<x2;n++)
   {
     put_pixel(n,(int)((float)(((float)a*(float)(n-x1))/(float)b)+(float)y1));
   }
if(y1>y2)
```

```
    {
        xx=y1; y1=y2; y2=xx; xx=x1; x1=x2; x2=xx;
    }

    for(n=y1;n<y2;n++)
    {
      put_pixel((int)((float)(((float)b*(float)(n-y1))/(float)a)+(float)x1),n);
    }

}
/************************Cls_Line ************************************/

void cls_line(x1,y1,x2,y2)
int x1,y1,x2,y2;
{
 int a,b,y,n,xx;
 if(x1>x2)
   {
       xx=x1; x1=x2; x2=xx; xx=y1; y1=y2; y2=xx;
   }

a=y2-y1;
b=x2-x1;

if(b==0)
{
   if(y1>y2) { xx=y1; y1=y2; y2=xx;}
   for(n=y1;n<=y2;n++) cls_put(x1,n);
  return;
 }
   if(a==0)
   {
    if(x1>x2) { xx=x1; x1=x2; x2=xx;}
    for(n=x1;n<=x2;n++) cls_put(n,y1);
  return;
   }
  for(n=x1;n<x2;n++)
  {
    cls_put(n,(int)((float)(((float)a*(float)(n-x1))/(float)b)+(float)y1));
   }
 if(y1>y2)
   {
       xx=y1; y1=y2; y2=xx; xx=x1; x1=x2; x2=xx;
   }

   for(n=y1;n<y2;n++)
   {
     cls_put((int)((float)(((float)b*(float)(n-y1))/(float)a)+(float)x1),n);
   }


}

/************************** Text rutina ************************************/

void text(x,y,string)        /* izpise dolocen text na doloceno lokacijo*/
int x,y;
char *string;
{
int n,j,nn,jj;
 if(x<64)
{
  set_x1(y/8);
  set_y1(x);
    for(n=0;n<strlen(string);n++)
    {
      for(j=0;j<7;j++)
       {
        lcd_write_1(chartable[(string[n]-32)][j]);
        if(++x>63) goto poz;
       }
    }
```

```
}
else
{
  x-=64;
  set_x2(y/8);
  set_y2(x);
  for(n=0;n<strlen(string);n++)
  {
   for(j=0;j<7;j++) lcd_write_2(chartable[(string[n]-32)][j]);
  }
}
return;
poz:
     x-=64;j+=1;
     set_x2(y/8);
     set_y2(x);
     for(nn=n;nn<strlen(string);nn++)
     {
       for(jj=j;jj<7;jj++) lcd_write_2(chartable[(string[nn]-32)][jj]);
       j=0;
     }
   return;
}

/************************* Text rutina (inverzni izpis)**********************/

void textin(x,y,string)         /* izpise dolocen text na doloceno lokacijo*/
int x,y;
char *string;
{
int n,j,nn,jj;
 if(x<64)
 {
   set_x1(y/8);
   set_y1(x);
     for(n=0;n<strlen(string);n++)
     {
      for(j=0;j<7;j++)
       {
        lcd_write_1(~chartable[(string[n]-32)][j]);
        if(++x>63) goto poz;
       }
     }

}
else
{
  x-=64;
  set_x2(y/8);
  set_y2(x);
  for(n=0;n<strlen(string);n++)
  {
   for(j=0;j<7;j++) lcd_write_2(~chartable[(string[n]-32)][j]);
  }
}
return;
poz:
     x-=64;j+=1;
     set_x2(y/8);
     set_y2(x);

     for(nn=n;nn<strlen(string);nn++)
     {
       for(jj=j;jj<7;jj++) lcd_write_2(~chartable[(string[nn]-32)][jj]);
       j=0;
     }
   return;
}
/************************* Clear put_pixel ******************************/

void cls_put(x,y)
```

```
int x,y;

{
int lo,tocka;
char data;
if(x<64)
{
   lo=y%8;
   tocka=0x01;
   tocka=tocka<<lo;
   set_x1((char)(y/8));
   set_y1((char)x);
   data=lcd_read_1();      /* dummy read */
   data=lcd_read_1();       /* real read */
   if((data&tocka)!=tocka)
   set_y1((char)x);
   lcd_write_1((char)((data|tocka)-(char)tocka));
 }
 else
 {
   x-=64;
   lo=y%8;
   tocka=0x01;
   tocka=tocka<<lo;
   set_x2((char)(y/8));
   set_y2((char)x);
   data=lcd_read_2();      /* dummy read */
   data=lcd_read_2();       /* real read */
   set_y2((char)x);
   lcd_write_2((char)((data|tocka)-(char)tocka));

  }
}

/****************************** Pravokotnik *********************************/

void rectangle(x_left,y_left,x_right,y_right)
int x_left,y_left,x_right,y_right;
{
line(x_left,y_left,x_right,y_left);
line(x_left,y_right,x_right,y_right);
line(x_left,(y_left+1),x_left,(y_right-1));
line(x_right,(y_left+1),x_right,(y_right-1));
}


/************************** Bar routine ***************************************/
/* dol - pomik v vrsticah navzdol                                             */
/* vrednost - vrednost, ki se izrisuje                                        */
/* vredm1 - stara vrednost                                                    */
/* 0xff - pisanje 8 pikslov navpicno                                          */
/* 0x00 - brisanje 8 pikslov navpiŸno                                         */
/* 0x3c - pisanje sredinskih stirih pikslov navpicno                          */
/* 0xc3 - brisanje sredinskih stirih pikslov navpicno                         */
/******************************************************************************/

void bar(dol,vrednost,vredm1)
int dol,vrednost,vredm1;

{
  int n,razlika;
     set_x1(dol);
     set_x2(dol);
     set_y1(0);lcd_write_1(0xff);


if((vrednost<64)&&(vredm1<64))
 {
  razlika=vrednost-vredm1;
  if(vrednost>vredm1)
   {
```

```
        set_y1((char)(vredm1));
        for(n=0;n<razlika;n++)  lcd_write_1(0xff);
      }
    else
      {
       set_y1((char)(vrednost));
       for(n=0;n>razlika;n--) lcd_write_1(0x00);
      }
       set_y2(0x00);
       for(n=0;n<64;n++) lcd_write_2(0x00);

    }

if((vrednost>=64)&&(vredm1>=64))
{
 razlika=vrednost-vredm1;
  if(vrednost>vredm1)
   {

      set_y2((char)(vredm1-64));
      for(n=0;n<razlika;n++)  lcd_write_2(0xff);
   }
     else
     {
      set_y2((char)(vrednost-64));
      for(n=0;n>(razlika-1);n--) lcd_write_2(0x00);
     }
      set_y1(0x00);
      for(n=0;n<64;n++) lcd_write_1(0xff);


}

if((vrednost<64)&&(vredm1>=64))
{
      set_y1((char)(vrednost));
      for(n=0;n<(63-vrednost);n++) lcd_write_1(0x00);

           set_y1((char)(63));
           lcd_write_1(0x00);

           set_y2((char)(0x00));
           for(n=0;n>(64-vredm1);n--)  lcd_write_2(0x00);


    }

    if((vrednost>=64)&&(vredm1<64))
    {
           set_y1((char)(vredm1));
           for(n=0;n>(vredm1-63-1);n--)  lcd_write_1(0xff);

           set_y2((char)0x00);
           for(n=0;n<(vrednost-64);n++) lcd_write_2(0xff);
    }


}
/************************** Slim_Bar routine ********************************/
/* dol - pomik v vrsticah navzdol                                           */
/* vrednost - vrednost, ki se izrisuje                                      */
/* vredm1 - stara vrednost                                                  */
/* 0x3c - pisanje sredinskih stirih pikslov navpicno                        */
/* 0xc3 - brisanje sredinskih stirih pikslov navpicno                       */
/****************************************************************************/

void slim_bar(dol,vrednost,vredm1)
int dol,vrednost,vredm1;

{
```

```
 int n,razlika;

    set_x1(dol);
    set_x2(dol);
    set_y1(0);lcd_write_1(0x3c);



if((vrednost<64)&&(vredm1<64))
 {
  razlika=vrednost-vredm1;
  if(vrednost>vredm1)
   {

      set_y1((char)(vredm1));
      for(n=0;n<razlika;n++)  lcd_write_1(0x3c);
   }
  else
    {
     set_y1((char)(vrednost));
     for(n=0;n>razlika;n--) lcd_write_1(0x00);
    }
     set_y2(0x00);
     for(n=0;n<64;n++) lcd_write_2(0x00);

  }

if((vrednost>=64)&&(vredm1>=64))
{
 razlika=vrednost-vredm1;
 if(vrednost>vredm1)
  {

     set_y2((char)(vredm1-64));
     for(n=0;n<razlika;n++)  lcd_write_2(0x3c);
  }
    else
    {
     set_y2((char)(vrednost-64));
     for(n=0;n>(razlika-1);n--) lcd_write_2(0x00);
    }
     set_y1(0x00);
     for(n=0;n<64;n++) lcd_write_1(0x3c);


}

if((vrednost<64)&&(vredm1>=64))
{
     set_y1((char)(vrednost));
     for(n=0;n<(63-vrednost);n++) lcd_write_1(0x00);


     set_y1((char)(63));
     lcd_write_1(0x00);

     set_y2((char)(0x00));
     for(n=0;n>(64-vredm1);n--)  lcd_write_2(0x00);


}

  if((vrednost>=64)&&(vredm1<64))
  {
       set_y1((char)(vredm1));
       for(n=0;n>(vredm1-63-1);n--)  lcd_write_1(0x3c);

       set_y2((char)0x00);
       for(n=0;n<(vrednost-64);n++) lcd_write_2(0x3c);
  }


}
```

```
/************************** Del_slim_Bar routine ******************************/
/* dol - pomik v vrsticah navzdol                                             */
/******************************************************************************/

void del_slim_bar(dol)
int dol;

{
 int n;

     set_x1(dol);
     set_x2(dol);
     set_y1(0);lcd_write_1(0x3c);

     set_y1((char)(0));
       for(n=0;n<63;n++)  lcd write 1(0x00);
     set_y2((char)(0));
       for(n=0;n<63;n++)  lcd_write_2(0x00);
}



/************************** Getkey routine ************************************/

int getkey()
{
 int i;
 char val,a,vale1;

 do
 {
   val=P5DR;
   val=~val;
   val>>=4;
  }
 while(!val);                    /* ce tipka ni pritisnjena, cakaj */
/* for(i=0;i<1000;i++);*/
 i=1;
 while((val>>=1)!=0) i++;     /* ugotovi stevilko tipke (i) */
 do
 {
  val=P5DR;
  val=~val;
  val>>=4;
 }
 while(val!=0);                  /* cakaj, dokler ni tipka spuscena */
 return(i);
}


/************************** Kroznica ******************************************/

void kroznica(x,y,r)
int x,y,r;
{
 float a,x1,y1;
 int x2,y2;
 for(a=0.1;a<=6.4;a=a+0.1)
 {
   y1=r*sin(a);
   x1=r*cos(a);
   x2=x+x1;
   y2=y+y1;
   put_pixel(x2,y2);
   line(x,y,x2,y2);
   }
}

/************************** Delilnik frekvence ********************************/
void delilnik()
{
```

```
int i,j,n;
char value;

/***************************** PORT 5 *********************************/
/*                                                                    */
/*    P57       P56      P55      P54      P53      P52      P51      P50   */
/*                                                                    */
/*    T4        T3       T2       T1      CLEAR     X1       X0       LE   */
/*                                                                    */
/**********************************************************************/

P3DDR=0xff;                  /* postavitev, za vpisovanje v vse tri vhode */
/*P6DDR=0xdf;*/

P6DR=0xc0;                   /* postavitev cs1=cs2=0 za display */
P5DR=0x01;                   /* LE=1 (na LATCH-u) */
P3DR=0x19;                   /* vrednost, z katero delimo osnovno frekvenco */

P5DR=0x08;                   /* postavitev CLEAR=1 na 4040 */
for(i=0;i<100;i++);          /* pocakamo na reset */
  for(i=0;i<2;i++)           /* postavimo fazno razliko */
   {
    P5DR=0x00;               /* x1=x0=0 */
    P5DR=0x04;               /* x1=1  x0=0 */
   }
  P5DR=0x06;                  /* odpremo oba stevca 4040 (x1=x0=1) */
}

/************************** A/D pretvornik ******************************/

unsigned int adc_a()
{
unsigned int x,w,i;
float a=0;
char msg[100];

AD_ADCSR=0x08;   /* 08 */
BSC_AR3T=0xFF;

   AD_ADCSR=0x20;
   while(((int)AD_ADCSR & (0x0080))==0);
   x=AD_ADDRA;
/* AD_ADCSR=0x08; to vrstico lahko izpustim*/
   x>>=6;

   /*y=((float)4.92/(float)1023)*x;*/

/*   printf("\n\r ADC: %d => %7.5f",x,y);*/


   /*for(w=0;w<1000;w++);*/
   return(x);
}

/************************** Merjenje fazne razlike **************************/

/*****************************  PORT 4 *********************************/
/*                                                                      */
/*      P47     P46     P45     P44     P43     P42     P41     P40     */
/*                                                                      */
/*       -       -       -      cf   40103(7) 40103(6) smer   Q2(ready) */
/*                                                                      */
/************************************************************************/

long int faza()
{
int val1,val3;
unsigned int val2;
long int val;

float sval;
char cf,qd;
```

```
cf=0;

 P3DDR=0x00;
/* P6DDR=0xdf;*/
 P4DDR=0xfc;

 P4DR=0x14;                          /* peroida branja 04=100 pulzov */

  P6DR=0xc0;                         /* OE1=OE2=1 */
   qd=P4DR;
   if((qd&0x01)==1)                     /* ce je Q2(ready)=1 */
   {
    P6DR=0x80;                          /* OE1=0, OE2=1 */
    val1=P3DR;                          /* prebere vrednost z prvega stevca */
    P6DR=0x40;                          /* OE1=1, OE2=0 */
    val3=P3DR;                          /* prebere vrednost z drugega stevca */
    P6DR=0xc0;
    val2=val3<<8;
    val=val1|val2;                    /* skupni sestevek */
    P4DR=0x04;                        /* postavi Q2(ready)=0*/
    P4DR=0x14;
   }
/*    send((char)val1);*/
/*    send((char)val3); */

   if((qd&0x02)==2) { val=-val; /*send('n');*/ }
 /*  else send('p');*/
  /* printf("\n\r Faza= %ld",val);*/
return(val);
}

/************************** Rutine za serijski kanal ************************/


/***************************** RX rutina ************************/
char recive()

{
  char i;
  while(!((SCI1_SSR)&0x40));
  i=SCI1_RDR;
  SCI1_SSR=((SCI1_SSR)&0xbf);
  return(i);
 }



/***************************** TX rutina ************************/
void send(i)
char i;
{
  while(!((SCI1_SSR)&0x80));
  SCI1_TDR=i;
  SCI1_SSR=((SCI1_SSR)&0x7f);
}

/*************************1. nacin posiljanja ********************************/
/************************* 4 8 bitna stevila  ********************************/
void nacin1(vnos)
long int vnos;
{
char podatek,i;
  for(i=0;i<4;i++)
  {
   podatek=(char)(vnos&0x00ff);
   send((char)podatek);
   vnos>>=8;
  }
}

/*************************2. nacin posiljanja ********************************/
/************************* 2 8 bitna stevila  ********************************/
```

```
void nacin2(vnos)
int vnos;
{
char podatek,i;

  for(i=0;i<2;i++)
  {
   podatek=(char)(vnos&0x00ff);
   send((char)podatek);
   vnos>>=8;
  }
}


/***************** inicializacijska  rutina **********************/
void setup_sci()
{
SCI1_SCR=0xc0; /* disable SCI */
SCI1_SMR=0x4;  /* 8N1 */
SCI1_BRR=7;    /* Baud_rate=38400 */
SCI1_SCR=0x3C; /* enable SCI, disable interrupts */
}

/****************** get line vt100 ****************************/

int get_line(pozicija)
char *pozicija;

{
char znak;
int i;

i=0;
do {
        znak=recive();
        if((znak==8)&&(i>0))
                        { i--;
                          send(8);
                          send(32);
                          znak=8;
                        }
        else pozicija[i++]=znak;
        send(znak);
      } while((znak!=13)&&(znak!=10)&&(i<78));
pozicija[--i]=32;
pozicija[i++]=0;
return(i);
}

int putchar(i)
int i;
{ send(i);
  return(1);
  }

int getchar()
{ int i;
  i=recive();
  send(i);
  if(i==13) i=EOF;
  return(i);
 }
```

Appendix C - Personal Computer program

```
#include <string.h>
#include <stdio.h>
#include <conio.h>
#include <FCNTL.h>
#include <io.h>
#include <stdlib.h>
#include <dos.h>
#include <graphics.h>
#include <mem.h>
#include <math.h>
#include "comm.h"
//#include "mdef.h"


#define IER  0x02F9
#define LCR  0x02FB
#define MCR  0x02FC
#define LSR  0x02FD
#define MSR  0x02FE
#define DLL  0x02F8
#define DLM  0x02F9
#define DATA 0x02F8

#define TXBUFF 1024
#define RXBUFF 25000
#define DBUFF  32768


#define POLJE 2048
#define FREQ 3.28767123
#define PI 3.14

ASYNC port;
       int rcode, ste=0;
```

```
        long  y1=0,x[3];
        long val,vsota,sred_vred,sens;
        //int  podatek,podatekm1=0;


unsigned int nn;
         int n,st, key;
         int k, isign, maxx, maxy;
         int cbf1, cbf2, cbf3; /* constant for beat freq = BEAT FREQ /13.51 */
         float beat1=240, beat2=400, beat3=540;

         unsigned long mmax, m, j, istep, i;
         double        wtemp, wr, wpr, wpi, wi, theta;
         float         tempr, tempi, tmax, amp_max, amp_min;


void talk(void);
void contin();
void nicla();



/*************************************************************************/
// sprejmna rutina, caka dokler ne pride byte rutina
/*************************************************************************/

char rx(ASYNC *port)
{
                int rxch;
                while (((rxch = async_rx(port)) & B_RXEMPTY));
                rxch&= (0xff);
                return(rxch);
}

/*************************************************************************/
// oddajna rutin, ce je buffer poln se zatakne in caka, da je vsaj eden byte
// prost
/*************************************************************************/

void tx(ASYNC *port,char c)
{
        while(async_txfree(port)<1);
        async_tx(port,c);
}


/*************************************************************************/
/*                          FFT transfrom                                */
/*************************************************************************/

void fft (float ar[], float ai[], int dolzina)
{


         /* deklaracije spremenljivk */
         //double ar[POLJE], ai[POLJE];
         int n, n2, a, c, d, f, g, h, j, seg;
         float b,e,k,l,n1,co,si,mean_sq_power, rms;
         int m,p,q,r,s,t,u,w,z;
         char msg2[10];

         n=dolzina;



         n1=log10(n)/log10(2);
```

```
n2=1; /* 1 - fft, -1 - invfft */

a=n;
b=2*PI/n;

for (c=1; c<=n1; c++)
       {
        d=a;
        a=a/2;
        e=0;

        for (f=1; f<=a; f++)
              {
               co=cos(e);
               si=sin(e)*n2;
               e=e+b;
               u=1;

               for (g=d; g<=n; g=u*d)
                     {
                      u++;
                      h=g-d+f;
                      j=h+a;
                      k=ar[h]-ar[j];
                      l=ai[h]-ai[j];
                      ar[h]=ar[h]+ar[j];
                      ai[h]=ai[h]+ai[j];
                      ar[j]=co*k+si*l;
                      ai[j]=co*l-si*k;
                     }
               }

 b=2*b;
}

m=1;
p=n/2;
q=n-1;

for (r=1; r<=q; r++)
 {
       if (r> (m-0.1)) goto label1;

       k=ar[m];
       l=ai[m];

       ar[m]=ar[r];
       ai[m]=ai[r];
       ar[r]=k;
       ai[r]=l;

       label1: s=p;

       label3: if (s> (m-0.1)) goto label2;

       m=m-s;
       s=s/2;

       goto label3;

       label2: m=m+s;
 }

for (w=1; w<=n; w++)
 {

       mean_sq_power=ar[w]/n*ar[w]/n+ai[w]/n*ai[w]/n;

       ar[w]=5*sqrt(mean_sq_power);
```

```
                        //line((w+1), maxy/2-1, (w+1), maxy/2-2*temp[w]);
//                      printf("\t%f\t%f\n", w-1, ar[w]/n, ai[w]/n);
                    }

                  /*    for (w=1; w<=3; w++)
                    {
                        printf("\t%f\n", temp[w]);
                    }*/
} /* fft */



/*****************************************************************************/
/*                              MAIN                                         */
/*****************************************************************************/

void main(void)

{


        char k1,l,i,tipka,d;
        int val1,val3;
        unsigned int val2;


        /* request auto detection */
        int gdriver = DETECT, gmode, errorcode;
        int val4[2], maxkk;
        int i1,kk,a,v1,j1,val1,val13,val14[4],n1,val1m1,kon,pom1,pom2;

        float window;

        float fir[7], spec_max, spec_min=0, avarage,avarage_old=0, abs_max;
        int max_counter;

        float input_real[POLJE], input_imag[POLJE];
        float temp[POLJE/4];


        char *msg,msg1[10],jj,znak;
        long val5,ii;


        int maxx, maxy;
        int dolzina;

        int podatek, podatekm1=0;



        //printf("\n %d",cbf1);

        printf("\n H8 -> PC Program start");
        getch();

        // inicializacija serijskega kanala
        AllocRingBuffer(&port, RXBUFF, TXBUFF,0);
        printf("\n Alloc OK");

        rcode = async_open(&port, COM2, "38400N81");
```

```
if (rcode != R_OK)
 {
  printf("\nSerial port initialization failed, exit code = %d", rcode);
  exit(rcode);
 }

printf("\n Koncana alokacija");
tx(&port,(char)65);     /* send (char)65 flag to H8 for communication start*/
printf("\n (char)65 flag transmitted to H8");
getch();

k1=rx(&port);             /* get flag from H8 */
printf("\n Got flag from H8");
getch();

if(k1==(char)0xff) l=rx(&port);

if(l=='g')
 {
  printf("\n Switch to graphics mode");
  getch();

  /* initialize graphics and local variables */
  initgraph(&gdriver, &gmode, "");

 /* read result of initialization */
 errorcode = graphresult();
 if (errorcode != grOk)
   {
    printf("Graphics error: %s\n", grapherrormsg(errorcode));
    printf("Press any key to return to shell:");
    getch();
    return;

   }

 kon=1;
 pom1=0;
        tx(&port,(char)0xff);
        cleardevice();

        maxx=getmaxx();
        maxy=getmaxy();



        abs_max=0;

  while(!kbhit())

   {

        tx(&port,(char)0xff);
        setcolor(WHITE);



/*****************************************************************/
/*                    data transfer from H8 to PC                */
/*                    data is in data[..]                        */
/*****************************************************************/

        input_real[0]=0;
        input_imag[0]=0;

        for (kk=1; kk<=POLJE; kk++)
         {

           /*for(i=0;i<4;i++) { val4[i]=(int)rx(&port);val4[i]&=(int)0xff;}
```

```
temp[kk]=(float)((long)val4[0]|(long)((long)val4[1]<<8)|(long)((long)val4[2]<<16)|(lo
ng)((long)val4[3]<<24));*/

            for(i1=0;i1<2;i1++) { val4[i1]=(int)rx(&port);val4[i1]&=(int)0xff;}
            //data[kk]=(float)( (int)val4[0]| (int)((int)val4[1]<<8) );

            input_real[kk]=(float)( (int)val4[0]| (int)((int)val4[1]<<8) );
            input_imag[kk]=0;


          }


          cleardevice();
          setlinestyle(SOLID_LINE, 1, 1);
/*****************************************************************/
/*                        Draw time response                     */
/*****************************************************************/

        podatekm1=480;
        setcolor(WHITE);
        for (kk=1; kk<=POLJE; kk++)
         {
           podatek=(int)(480-input_real[kk]/10);
           //sprintf(msg1,"%ld",podatek);
           //outtextxy(30,8*kk,msg1);



           line(kk, podatekm1, kk+1 , podatek);
           podatekm1=podatek;

         }
/*****************************************************************/
/*                        Data windowing                         */
/*****************************************************************/

      /*
         podatekm1=480;
         setcolor(RED);

         for (kk=1; kk<=POLJE; kk++)
                {
                  window=1-((kk-0.5*POLJE)/(0.5*POLJE)*(kk-0.5*POLJE)/(0.5*POLJE));  /*
Welch window */
                 //window=0.5*(1-cos(2*PI*(kk-1)/POLJE)); /* Hanning window */
                 //window=1-fabs((kk-0.5*POLJE)/(0.5*POLJE)); /* Barttlet window */

        /*              input_real[kk]=input_real[kk]*window;
                 podatek=(int)(480-input_real[kk]/10);

                 line(kk, podatekm1, kk+1 , podatek);
                 podatekm1=podatek;

                }

/*****************************************************************/
/* Rectangular window FIR filter

Filter type: BP
Passband: 450 - 550 Hz
Order: 6
Transition band: 1227 Hz
Stopband attenuation: 21 dB

Coefficients:

a[0] =       0.0553083
a[1] =       0.132358
```

```
   a[2] =       0.199386
   a[3] =       0.225895
   a[4] =       0.199386
   a[5] =       0.132358
   a[6] =       0.0553083

/*****************************************************************************/


fir[0] =-5.41208e-010;
fir[1] =-0.00498425;
fir[2] =0.0249379;
fir[3] =0.960093;
fir[4] =0.0249379;
fir[5] =-0.00498425;
fir[6] =-5.41208e-010;

/*
for (kk=1; kk<=POLJE-6; kk++)
 {


  input_real[kk]=fir[0]*input_real[kk]+fir[1]*input_real[kk+1]+
                 fir[2]*input_real[kk+2]+fir[3]*input_real[kk+3]+
                 fir[4]*input_real[kk+4]+fir[5]*input_real[kk+5]+
                 fir[6]*input_real[kk+6];


 }

*/


/*****************************************************************/
/*       Segmenting samplet data to four segments and avareging the fft   */
/*****************************************************************/


          podatekm1=480;
          setcolor(RED);

          for (kk=1; kk<=POLJE; kk++)
                 {
                    //window=1-((kk-0.5*POLJE)/(0.5*POLJE)*(kk-0.5*POLJE)/(0.5*POLJE));
/* Welch window */
                  window=0.5*(1-cos(2*PI*(kk-1)/POLJE)); /* Hanning window */
                  //window=1-fabs((kk-0.5*POLJE)/(0.5*POLJE)); /* Barttlet window */


                  input_real[kk]=input_real[kk]*window;
                  podatek=(int)(480-input_real[kk]/10);

                  line(kk, podatekm1, kk+1 , podatek);
                  podatekm1=podatek;

                 }



           /* fft of the segment */
           fft(input_real, input_imag, POLJE);

           /* save output to temp[] */

           for (kk=1; kk<=POLJE; kk++)
              {
                temp[kk]=input_real[kk];

              }

           /* Find amp_max and amp_min to scale graph */
```

```
amp_max=0;
amp_min=1000;
for (kk=10; kk<=POLJE; kk++)
   {
     if (temp[kk]>amp_max) amp_max=temp[kk];
     if (temp[kk]<amp_min) amp_min=temp[kk];

    }
/* Logarithimc scale inside amp_max and amp_min */
for (kk=10; kk<=POLJE; kk++)
   {
     temp[kk]=100*log10(amp_max/temp[kk]);
     if (temp[kk]>239) temp[kk]=239;

    }
```

```
/*****************************************************************************/
/*                          Draw spectrum and other data                     */
/*****************************************************************************/

        /* rectangle in upper half of the screen */

        setcolor(8);
        line(0, 0, maxx, 0);
        line(maxx, 0, maxx, maxy/2);
        line(0,0,0,maxy/2);
        line(0,maxy/2, maxx, maxy/2);


        outtextxy(520,8,"Power Spectrum");


        line(0, maxy/2+20, maxx, maxy/2+20);
        line(0, maxy/2+20, 0, maxy);
        line(0, maxy, maxx, maxy);
        line(maxx, maxy, maxx, maxy/2+20);

        outtextxy(520,maxy/2+28,"Time Response");


        sprintf(msg1,"%2.2f",0*FREQ);
        outtextxy(0, maxy/2+10,msg1);
        sprintf(msg1,"%2.2f",(int)10*FREQ);
        outtextxy(40, maxy/2+10,msg1);
        sprintf(msg1,"%2.2f",20*FREQ);
        outtextxy(80, maxy/2+10,msg1);
        sprintf(msg1,"%2.2f",40*FREQ);
        outtextxy(160, maxy/2+10,msg1);
        outtextxy(600, maxy/2+10,"[Hz]");



        /*************************************/
        /* Draw spectrum in the upper window */
        /*************************************/

        for (kk=3; kk<=512; kk++)
                {
                 setcolor(9); /* 9  blue */

                 line((kk+1),239,(kk+1),temp[kk] );/* log10 scale */

                }
         /*************************************/

        //avarage=0.5*(spec_max+spec_min);
        /*avarage+=temp[38];

        //sprintf(msg1,"%2.2f",avarage_old);
```

```
//outtextxy(542,28,"Output");
//outtextxy(542,36,msg1);


max_counter++;
if (max_counter>4)
  {

    abs_max=temp[38];
    max_counter=0;
  //  outtextxy(300,170,"reset");
    avarage_old=0.2*avarage;
    avarage=0;
  }

line (540,20,620,20);
line (540,20,540,100);
line (540,100,620,100);
line (620,20,620,100);



  /*
  for (kk=20; kk<=POLJE/8; kk++)
    {

    if (temp[kk]>spec_max) { spec_max=temp[kk]; maxkk=kk; }

    }
  */

/*************************************************/
/* Change of line mark parameters using keyboard */
/*************************************************/


if(kbhit()){
          key = getch();
                if(key == '1')  beat1=beat1+FREQ;          // 1
                else if(key == 0x21)  beat1=beat1-FREQ;    // Shift 1
                else if(key == '2')  beat2=beat2+FREQ;     // 2
   else if(key == 0x22)  beat2=beat2-FREQ;    // Shift 2
   else if(key == '3')  beat3=beat3+FREQ;     // 3
   else if(key == 0x23)  beat3=beat3-FREQ;    // Shift 3
/*  }
   if(key == '2')
    {
     key = getch();
         if(key == '+')  cbf2=cbf2++;
         else if(key == '-')  cbf1=cbf2--;
    }
   if(key == '3')
    {
     key = getch();
         if(key == '+')  cbf3=cbf3++;
         else if(key == '-')  cbf3=cbf3--;
    }    */

  else if(key == 0x1b ) goto label1;
 //      else if(key == 0x31)   regulator = 1;
 //      else if(key == 0x32)   regulator = 2;
 //      else if(key == 0x33)   regulator = 3;
          }

/* constants for beat frequency */
  cbf1=beat1/FREQ;
  cbf2=beat2/FREQ;
  cbf3=beat3/FREQ;

  /*************************************/
  /* sprintf(msg1,"%2.2f",beat1);
   outtextxy(2, 350,msg1);
```

```
   sprintf(msg1,"%d",cbf1);
   outtextxy(2, 370,msg1);

   sprintf(msg1,"%d",cbf2);
   outtextxy(2, 390,msg1);
  /*****************************************/

/*******************/
/* First peak data */
/*******************/
   setlinestyle(SOLID_LINE, 1, 1);
   settextstyle(DEFAULT_FONT, HORIZ_DIR, 4);
   sprintf(msg1,"%2.2f",-temp[(cbf1)]/10);
   setcolor(WHITE);
   outtextxy(10,300,msg1);
   settextstyle(DEFAULT_FONT, HORIZ_DIR, 1);
   outtextxy(450,50,msg1);
    setcolor(10);
    sprintf(msg1,"%2.2f",cbf1*FREQ); //*FREQ
    outtextxy(500,50,msg1);
    outtextxy(550,50,"[Hz] ->1");


    line ((cbf1),0,(cbf1),20);     /* vertical line to mark peak */

    /* horizontal line to mark peak */
    setcolor(WHITE);
    setlinestyle(DASHED_LINE, 1, 1);
    line((cbf1), temp[(cbf1)], 300, temp[(cbf1)]);


/*********************/
/* Second peak data */
/*********************/
    setlinestyle(SOLID_LINE, 1, 1);
    settextstyle(DEFAULT_FONT, HORIZ_DIR, 4);
    sprintf(msg1,"%2.2f",-temp[(cbf2)]/10);
    setcolor(WHITE);
    outtextxy(200,300,msg1);
    settextstyle(DEFAULT_FONT, HORIZ_DIR, 1);
    outtextxy(450,70,msg1);

    setcolor(10);
    sprintf(msg1,"%2.2f",cbf2*FREQ); //*FREQ
    outtextxy(500,70,msg1);
    outtextxy(550,70,"[Hz] ->2");


    line ((cbf2),0,(cbf2),20);     /* vertical line to mark peak */

    /* horizontal line to mark peak */
    setcolor(WHITE);
    setlinestyle(DASHED_LINE, 1, 1);
    line((cbf2), temp[(cbf2)], 300, temp[(cbf2)] );

/*******************/
/* Third peak data */
/*******************/
    setlinestyle(SOLID_LINE, 1, 1);
    settextstyle(DEFAULT_FONT, HORIZ_DIR, 4);
    sprintf(msg1,"%2.2f",-temp[(cbf3)]/10);
    setcolor(WHITE);
    outtextxy(425,300,msg1);
    settextstyle(DEFAULT_FONT, HORIZ_DIR, 1);
    outtextxy(450,90,msg1);
    //printf("%2.2f\n",spec_max);
    setcolor(10);
    sprintf(msg1,"%2.2f",cbf3*FREQ); //*FREQ
    outtextxy(500,90,msg1);
    outtextxy(550,90,"[Hz] ->3");
    //printf("%d\n",maxkk);
```

```
            line ((cbf3),0,(cbf3),20);      /* vertical line to mark peak */

            /* horizontal line to mark peak */
            setcolor(WHITE);
            setlinestyle(DASHED_LINE, 1, 1);
            line((cbf3), temp[(cbf3)], 300, temp[(cbf3)]);

        } /* end while */

label1:
    tx(&port,(char)0x00);
    closegraph();
    //printf("\n PC -> H8 signal za konec");
    //getch();

    }

     async_close(&port);
     printf("\n\r konec");

    }
```

Appendix D - Publications related to the PhD Thesis

In this appendix we would like to present PhD thesis related publications accepted and/or submitted to scientific journals and presented on international and national conferences and technical meetings:

Scientific Journals

1. Miha Završnik, George Stewart, "Coherence addressing of quasi-distributed absorption sensors by the FMCW method," Journal of Lightwave Technology, Vol. 18, No. 1, pp. 57-65, January 2000

2. Miha Završnik, George Stewart, "Theoretical analysis of a quasi-distributed optical sensor system using FMCW for application to trace gas measurement," submitted to Photonics Technology Letters (PTL #7645)

3. Miha Završnik, George Stewart, "Analysis of Quasi-Distributed Optical Sensors Combining RF Modulation With the FMCW Method," submitted to Optical Engineering (OE #200022)

Conferences

4. Miha Završnik, George Stewart, "Coherence addressing of quasi-distributed absorption sensors by the FMCW method," Smart Structures and Materials 1999, Sensor Phenomena and Measurement Instrumentation for Smart Structures and Materials, Proceedings SPIE, Vol. 3670, pp. 304-310, 1-4 March 1999, Newport Beach, USA

5. Miha Završnik, George Stewart, "Characterization and Application of FMCW Coherence Addressed Quasi-Distributed Absorption Sensors," Smart Structures and Materials 2000, Sensor Phenomena and Measurement Instrumentation for Smart Structures and Materials, Proceeding SPIE not jet available, 5-9 March 2000, Newport Beach, USA

6. Miha Završnik, Denis Đonlagic, George Stewart, "Koherencno naslavljanje kvazi porazdeljenih absorpcijskih senzorjev z uporabo frekvencne modulacije laserske diode", Proceedings of the 8th Electrotechnical and Computer Science Conference ERK'99, 23. - 25. september 1999, Portoroz, Slovenija. Ljubljana: IEEE Region 8, Slovenian IEEE section, 1999, Vol. A, pp. 545-548

7. Miha Zavrsnik, George Stewart, "System for addressing of quasi-distributed absorption based gas sensors," Power Engineerig, VIII. International Expert meeting, pp. C:203-211, 11-13 May 1999, Maribor Slovenia

8. Miha Završnik, George Stewart, Denis Đonlagic, "Diferencna absorpcijska detekcija s pomocjo frekvenène modulacije laserske diode Zbornik 1.

konference "Avtomatizacija v industriji in gospodarstvu, p. 142-145, Maribor, april 1999

9. Miha Završnik, Denis Đonlagiæ, George Stewart, "Porazdeljene optiène meritve z uporabo frekvenène modulacije laserske diodee," Proceedings of the 7th Electrotechnical and Computer Science Conference ERK'98, p. A: 525-528, Portoroz, September 1998